UNVERSITY OF SHEFFIELD

TIME-DEPENDENT ANALYSIS OF CONTINUOUS PRECAST PRESTRESSED CONCRETE BEAMS

by

MOHD. SALEH JAAFAR, B.Sc., M.Sc.

A thesis submitted to the University of Sheffield

for the degree of Doctor of Philosophy

in the Faculty of Engineering

September 1997

To

My parents

wife and children

ABSTRACT

A literature survey on the subject of construction, analysis and design of precast prestressed concrete beams made continuous has been conducted from which various methods of achieving continuity between the precast units have been identified. A need to re-evaluate the analysis and design of such structures has been established with special emphasis on the time-dependent aspects.

An extensive evaluation of the time-dependent properties of concrete and the time-dependent behaviour of reinforced and prestressed concrete structures has been conducted. The evaluation used widely accepted methods of prediction for the material properties and four different analytical procedures for the behaviour of the structures.

In a preliminary evaluation of the material properties, the methods of prediction based on the CEB78, CEB90 and ACI recommendations have been compared. This was followed by a more extensive parametric study of the factors affecting the material properties of plain concrete using the CEB90 recommendations. In a preliminary evaluation of the analytical procedures for structures subject to varying stress, the time-dependent behaviour of reinforced concrete sections using the Effective Modulus Method (EMM), Rate of Creep Method (RCM), Age-adjusted Effective Modulus Method (AEM) and Superposition Method (SSM) have been compared. This was followed by a more extensive evaluation of the factors affecting time-dependent behaviour of simply supported prestressed concrete beams using the AEM method.

An evaluation of the parameters affecting the time-dependent behaviour of continuous precast prestressed concrete beams has been conducted using the SSM method which was based on a finite element analysis of prestressed concrete structures using the commercially available package, ADAPT. Both the AEM and ADAPT analyses have been compared against each other, and verified satisfactorily against a large number of experimental results. A special procedure to include cracked section properties has also been included into ADAPT analysis and it was found to improve time-dependent predictions of cracked reinforced concrete beams. Using the available features in ADAPT, the evaluation of continuous precast prestressed concrete beams has been extended to members connected using other methods of achieving continuity.

Based on this study, several recommendations have been made on the treatment of the methods of prediction for the material properties and for the analysis of structures under varying state of stress, and on the analysis and design of continuous precast prestressed beams using unstressed reinforcement to provide continuity.

CONTENT

		Page
ACKNOWLEDGEMENT		i
INDEX OF FIGURES		ii
INDEX OF TABLES		viii
NOTATION		xi
Chapter 1: INTRODUCTION		1
1.1	State of the Art	1
1.2	Statement of the Problem	5
1.3	Object of the Present Investigation	6
Chapter 2: LITERATURE REVIEW		8
2.1	Introduction	8
2.2	Development of Continuity Connection in Precast Prestressed Bridge Beams.	9
2.2.1	Methods of achieving continuity	9
2.2.1.1	Bolts and welded connections	9
2.2.1.2	Connection using ordinary reinforcing steel	11
2.2.1.3	Tied-deck slab connection	12
2.2.1.4	Locally separated deck slab connection	12
2.2.1.5	Connection using post-tensioned steel	15
2.2.1.6	Connection using splicing of pretensioned strands	17
2.2.2	Advantages and disadvantages of each method	17
2.3	Experimental and Analytical Studies for Precast Beams Made Continuous	20
2.3.1	Experimental investigations	20
2.3.1.1	Connection using ordinary reinforcing bars	20
2.3.1.2	Other methods of achieving continuity	27
2.3.2	Analytical investigations	31

2.3.2.1 Continuous precast prestressed concrete beams 32
2.3.2.2 Other related analytical work 37
2.4 Discussion 43

Chapter 3: PREDICTION METHODS FOR TIME-DEPENDENT BEHAVIOUR OF CONCRETE STRUCTURES 46

3.1 Introduction 46
3.2 Classification of Concrete Deformation 47
3.2.1 Elastic strain 47
3.2.2 Shrinkage 48
3.2.3 Creep 48
3.3 Creep and Shrinkage Predictions of Concrete 50
3.3.1 Formulation according to CEB-FIP Model Code for Concrete Structures, 1978 (CEB78) 52
3.3.1.1 Creep 52
3.3.1.2 Shrinkage 54
3.3.2 Formulation according to the American Concrete Institute Committee 209 (ACI209, 1982) 55
3.3.2.1 Creep 55
3.3.2.2 Shrinkage 57
3.3.3 Formulation according to CEB-FIP Model Code 1990 (CEB90) 58
3.3.3.1 Creep 58
3.3.3.2 Shrinkage 60
3.4 Relaxation of Prestressing Steel 61
3.5 Time-dependent Analysis of Concrete Structures 62
3.5.1 The effective modulus method 62
3.5.2 The age-adjusted effective modulus method 63
3.5.3 Rate of creep method 65
3.5.4 Principle of superpositi6on and step-by-step method 67

5.5 Brief Comparison Between CEB90 and ACI 189

Chapter 6: ORDINARY CROSSHEADS FOR CONTINUITY 215

6.1 Introduction 215

6.2 Behaviour under Short Term Loads 216

6.3 Time-dependent Analysis 219

6.3.1 Creep and Shrinkage Effects 219

6.3.2 Effects of Differential Shrinkage 226

6.4 Comparisons with Current Design Method 228

6.5 Effects of Cracked Insitu Crossheads on Sagging Restraint Moments 231

Chapter 7: NON-CONVENTIONAL METHODS FOR CONTINUITY 245

7.1 Introduction 245

7.2 Continuity using Prestressing Steel 245

7.3 Continuity using Forced Support Settlement 250

7.4 Further Evaluations on the Use of Post-tensioned Deck Slabs for Continuity 252

7.5 Further Evaluations on the Use of Forced Support Settlement for Continuity 255

Chapter 8: CONCLUSIONS AND RECOMMENDATIONS FOR FURTHER WORK 265

8.1 Conclusions 265

8.2 Recommendations for Further Work 271

References 273

Appendices 282

ACKNOWLEDGEMENTS

This dissertation is based on a research work undertaken in the Department of Civil and Structural Engineering at the University of Sheffield under the supervision of Professor Peter Waldron. The author cannot thank him enough for the interest he has shown and the supervision he has provided in spite of a very busy schedule of his own. The author is indeed indebted for his useful suggestions and constructive criticisms he provided throughout this study.

The author is grateful for the opportunity to pursue this study to the Universiti Putra Malaysia who provided financial assistance to cover both tuition and boarding fees.

Without the love and support of my wife and family, this study would have not been possible. Their support is greatly appreciated.

INDEX OF FIGURES

Number	Title	Page
1.1	Long term effects of simple precast prestressed beams made continuous	7
2.1	Method of achieving continuity using bolts and welded connection	10
2.2	Methods of achieving continuity using ordinary reinforcing steel in deck slab across intermediate piers	13
2.3	Tied-deck slab connection	14
2.4	Locally separated deck slab	14
2.5	Continuity of single prestressed concrete beams using post-tensioned steel	16
2.6	Connection of precast beams using splicing of the pretensioned strands technique	19
2.7	Test set-up to study the effectiveness of the continuity method using ordinary reinforcing bar under short term flexural loads	24
2.8	Elevation and cross section of a shear test	25
2.9	Positive moment connections tested under short term loads	26
2.10	Use of pretensioned concrete rods to replace ordinary reinforcing bars for negative moment reinforcement (Burn, 1966)	30
2.11	Classification for connection rigidity according to Suter (1981)	40
3.1	Nominal and true elastic strains under constant load	49
3.2	Shrinkage deformation of an unloaded specimen	50
3.3	Creep deformation of a concrete specimen under constant load, imposed at time t_o	50
3.4	Creep of concrete due to constant stress and gradually applied stress	65
3.5	Parallel creep curves assumed in the rate of creep method	66
3.6	Principles of superposition of concrete strains	66
3.7	Step-by-step method for continuously varying stress	68
3.8	Strength and elastic modulus development predicted by ACI	68

3.9	Comparisons for creep strains	79
3.10	Comparisons for shrinkage strains	79
3.11	Comparisons for total strains	79
3.12	Comparisons for elastic strains	80
3.13	Comparisons between nominal and actual strain under increasing elastic modulus	80
3.14	Total time-dependent deformation for different steel contents (Chouman, 1990)	81
3.15	Total time-dependent deformation for plain concrete	82
3.16	Total time-dependent deformation for 0.63% steel content	82
3.17	Total time-dependent deformation for 1.74% steel content	83
3.18	Total time-dependent deformation for 4.47% steel content	83
4.1	Transformed section and initial strain distribution for reinforced and prestressed sections	90
4.2	Time-dependent actions and deformations	94
4.3	A typical composite section of precast prestressed beam and cast insitu slab	95
4.4	Basis of analysis for cracked prestressed concrete sections	96
4.5	Idealised moment curvature diagram to account for tension stiffening	98
4.6	Time-dependent change of strain and curvature for cracked sections	99
4.7	Basis of beam element formulation for ADAPT	104
4.8	Prestress tendon relaxation model	105
4.9	Modelling bonded reinforcement in ADAPT	105
4.10	Model used for computer implementation of cracked sections	106
4.11	Comparison of deflections between elastic analysis and ADAPT for homogenous section	109
4.12	Comparisons of deflections between elastic analysis and ADAPT for composite section	109

4.13	Four different models considered to account for bonded non-prestressing steel	112
4.14	Comparison between Model 1 of ADAPT analysis and experimental results (from Chouman, 1990) for sections with different degrees of reinforcement	113
4.15	Comparisons between experimental results and ADAPT analyses for sections reinforced with 1.62% steel	114
4.16	Comparisons between experimental results and ADAPT analyses for sections reinforced with 4.47% steel	114
4.17	Comparisons between AEM and ADAPT analyses with experimental result for prestressed beams from Breckenridge (1964)	124
4.18	Comparisons between AEM and ADAPT analyses with experimental result for prestressed beams from Hutton (1966)	124
4.19	Comparisons between AEM and ADAPT analyses with experimental result for prestressed beams (A_s=0) from Chouman (1990)	125
4.20	Comparisons between AEM and ADAPT analyses with experimental result for prestressed beams (A_s=1.3%) from Chouman (1990)	125
4.21	Experimental and model prediction for reinforced concrete beams using uncracked stiffness	126
4.22	Experimental and model prediction for prestressed concrete beams using uncracked stiffness	126
4.23	Experimental and model prediction using cracked sections using cracked stiffness	126
4.24	Comparisons between experimental and computer models for continuous composite beams (Mattock *et al*, 1961)	127
5.1	Volume to surface area ratio for different precast sections	143
5.2	Creep of plain concrete under different combinations of parameters yielding maximum and minimum total deformations	143
5.3	Effect of age at loading (t_o) on creep characteristics of plain concrete	144
5.4	Effect of concrete strength (f'_c) on creep characteristics of plain concrete	145
5.5	Effect of average relative humidity (RH) on creep characteristics of plain concrete	146

5.6	Effect of volume to surface area ratio (*V/S*) on creep characteristics of plain concrete	147
5.7	Shrinkage of plain concrete under combinations of parameters yielding maximum and minimum deformations	148
5.8	Development of shrinkage under combinations of parameters yielding maximum and minimum shrinkage	148
5.9	Effect of f'_c on shrinkage characteristics of plain concrete under combinations of parameter yielding maximum and minimum deformation	149
5.10	Effect of *RH* on shrinkage characteristics of plain concrete under combinations of parameters yielding maximum and minimum deformation	150
5.11	Effect of *V/S* on shrinkage characteristics of plain concrete under combinations of parameters yielding maximum and minimum deformation	151
5.12	Ratio of shrinkage for *V/S*=50mm and 140mm under any combination of other parameters	152
5.13	Time-dependent deformations of reinforced concrete sections subject to a combination of parameters yielding maximum deformation	164
5.14	Time-dependent deformations for reinforced concrete sections under a combination of parameters yielding minimum deformation	165
5.15	Effect of reinforcement on creep and shrinkage of reinforced sections subject to combinations of parameters yielding maximum and minimum deformation	166
5.16	Effect of stress on creep characteristics of plain and reinforced concrete sections	167
5.17	Time-dependent stresses in concrete and steel for reinforced sections under a combination of parameters yielding maximum deformation	168
5.18	Time-dependent stresses in concrete and steel for reinforced sections under a combination of parameters yielding minimum deformation	169
5.19	The effect of creep and shrinkage on time-dependent stress in steel reinforcement under the combination of parameters yielding maximum deformation	170

5.20	A comparison between span/depth ratio and flexural rigidity to deflections due beam selfweight (SW) and superimposed live load (SLL)	199
5.21	Time-dependent camber for sections *T10*, *M10* and *SY6* with maximum recommended span subject to four different combinations of parameters	200
5.22	Time-dependent camber for sections *Y8* and *U12* with maximum recommended span subject to four different combinations of parameters	201
5.23	Camber of prestressed section with maximum recommended span.	201
5.24	Effect of bottom non-prestressed steel on sections with maximum and minimum flexibility subject to the combination of f'_c and *RH* yielding maximum deformation	202
5.25	Effect of top non-prestressed steel on sections with maximum and minimum flexibility subject to the combination of f'_c and *RH* yielding maximum deformation	203
5.26	Effect of top and bottom non-prestressed steel on sections with maximum and minimum flexibility subject to the combination of f'_c and *RH* yielding minimum deformation	204
5.27	Time-dependent camber for sections *T10*, *M10* and *SY6* with maximum recommended span subject to four different combinations of parameters and a reduced level of prestress	205
5.28	Time-dependent camber for sections *Y8* and *U12* with maximum recommended span subject to four different combinations of parameters and a reduced level of prestress	206
5.29	Camber of prestressed section with maximum recommended span subjected to the higher and the reduced initial stress	206
5.30	Effect of age at loading on the camber under combinations of parameters yielding maximum and minimum deformation	207
5.31	Effect of age at loading on stresses at the bottom fibre under the combinations of parameters yielding maximum and minimum deformation	208
5.32	Time-dependent camber and deflection due to selfweight, prestressing and shrinkage actions considered separately	209
5.33	Creep and shrinkage properties for different sections	210
5.34	Rate of increase in deflection and camber due selfweight, prestressing and shrinkage actions considered separately	211

5.35	Comparison for time-dependent deflections between combined and separate analyses	211
5.36	Comparison of time-dependent material characteristics according to CEB90 and ACI for section SY6	212
5.37	Comparison of time-dependent material characteristics according to CEB90 and ACI for section T10	213
5.38	Comparison of time-dependent camber/deflection for unloaded beams of sections SY6 and T10	213
6.1	Element mesh used for composite beams	233
6.2	General tendon layout for pretensioned steel in precast beams	233
6.3	Bending moments (kNm) in the region of an internal support in the absence of live load (Clark, 1997)	234
6.4	Development of shrinkage and its differential strain	235
7.1	Three different prestressing profiles evaluated to counter hogging stress over the support	257
7.2	Effects of differential support settlement in a continuous beam on the development of forces (Ghali, 1986)	258
7.3	Typical reduction in the induced force due to the action of creep	259

INDEX OF TABLES

Number	Title	Page
3.1	Curing factors for different curing conditions	58
3.2	Probability of agreement between predictive models given by ACI-209 and experimental data (Branson, 1977)	70
3.3	A summary of statistical evaluations of creep and shrinkage model given by CEB78 and CEB90 (CEB Bulletin No. 199, 1990)	70
3.4	Strength and elastic modulus development according to CEB78	73
3.5	Strength and elastic modulus development according to ACI-209	73
3.6	Strength and elastic modulus development according to CEB90	74
3.7	Ratio of strength and elastic modulus values at different ages to 28 day values for all strength ranges	74
4.1	Comparisons between different computer codes for time-dependent analysis of prestressed concrete structures	88
4.2	Stress at top and bottom fibres of a composite section	110
4.3	Experiments on the time-dependent behaviour of reinforced and prestressed concrete beams	119
4.4	Statistical evaluation of long term deflections of prestressed concrete beams	120
4.5	Statistical evaluation of long term deflections of reinforced concrete beams using uncracked stiffness	121
4.6	Statistical evaluations of long term deflections of reinforced concrete beams using cracked stiffness	122
4.7	Statistical evaluations to characterise the error over the whole loading duration	123
5.1	Summary of creep properties for t_o=3 days (combinations 1-8) and 28 days (combinations 9-16)	141
5.2	Effects of curing duration on short and long term shrinkage for V/S= 50mm	142
5.3	Summary of shrinkage properties under combinations of parameters yielding maximum and minimum deformations	142

5.4	Microstrain values in reinforced concrete sections under combinations of parameters yielding maximum deformations	160
5.5	Microstrain values in reinforced concrete sections under combinations of parameters yielding minimum deformations	161
5.6	Stresses in steel under combinations of parameters yielding maximum deformations	162
5.7	Stresses in concrete under combinations of parameters yielding maximum and minimum deformations	163
5.8	A summary of sections used for the evaluation of time-dependent behaviour of simple flexural members	192
5.9	A summary of the instantaneous stress, deflection and prestressing force required for each section used in the time-dependent analysis	192
5.10	Summary of time-dependent analysis for sections with the maximum recommended span under four different conditions	193
5.11	Summary of analysis on the effect of bottom non-prestressed steel for sections *T10* and *SY6* under combinations of f'_c=30 and *RH*=40% (Combination 1)	194
5.12	Summary of analysis on the effect of top non-prestressed steel for sections *T10* and *SY6* under combinations of f'_c=30MPa and *RH*=40% (Combination 1)	195
5.13	Summary of analysis on the effect of top and bottom non-prestressed steel for sections *T10* and *SY6* under combinations of f'_c=60MPa and *RH*=90% (Combination 4)	196
5.14	Summary of analyses on the effect of initial stress level for sections *T10* and *SY6* under Combinations 1 (f'_c=30MPa and *RH*=40%) and 4 (f'_c =60MPa and *RH*=90%)	197
5.15	Summary of simple prestressed beam analyses using CEB90 and ACI predictions for material characteristics and AEM method for time-dependent analyses for sections *T10* and *SY6*	198
6.1	Components of elastic stresses in simply supported beams constructed using propped or unpropped procedure at mid-span (Node 6)	236
6.2	Components of elastic stresses for two-span beams constructed using three different sequences of construction using narrow insitu crossheads	237

6.3	Components of elastic stresses for two-span beams constructed using three different sequences of construction using wide insitu crossheads	238
6.4	Prestressing at mid-span and end beams to satisfy initial and service limiting stress requirements according to o BS5400	239
6.5	Summary of the restraint moments (kNm) at the intermediate support	240
6.6	Stresses at the bottom (σ1) and top (σ4) fibres of the insitu crossheads at the intermediate support resulting from restraint moments	241
6.7	Restraint moments and concrete stresses at the interface between precast beams and insitu crossheads	242
6.8	Restraint moments (kNm) and the corresponding stress (MPa) over the intermediate support due to differential shrinkage	243
6.9	Comparisons of restraint moments (kNm) and the corresponding stresses (MPa) determined from PCA method and ADAPT analyses	243
6.10	Effects of cracked insitu crossheads on time-dependent restraint moments and stresses	244
7.1	The required level of prestressing to satisfy zero concrete tensile stress conditions under superimposed live loads	260
7.2	A summary of results from short term and time-dependent analyses for sections T10 made continuous using post-tensioned steel	261
7.3	Calculations for the instantaneous reduction in centre support reaction and stress due to forced differential settlement of the central support	262
7.4	Comparison between stresses due to forced support settlement of 0.3% of span length and those from superimposed live loads	263
7.5	Actions and stresses for different sequences and methods of construction for beams with Profile A tendons	264

NOTATION

The principal symbols used in Chapter 3 and 4 are as follows. Other symbols are defined in the text.

A	Transformed area of concrete
$\overline{A}_c$	Age-adjusted concrete area
A_c	Area of concrete section
A_{ct}	Cracked concrete section
A_{ps}	Area of prestressing steel
A_s	Area of non-prestressing steel
B	First moment of area of transformed section from top fibre
$\overline{B}_c$	Age-adjusted first moment of concrete area from top fibre
β_{xx}	General symbols for creep and shrinkage coefficients
$\beta_{xx}(t)$	General symbols for creep and shrinkage coefficients at time t
$\chi(t,t_o)$	Ageing coefficient at time t for member loaded at time t_o
$\Delta\varepsilon_c(t,t_o)$	Change in creep strain at time t for member loaded at time t_o
$\Delta\varepsilon_o(t)$	Change in creep strain at the top fibre at time t
$\Delta M(t)$	Increment in bending moment at time t
$\Delta N(t)$	Increment in axial force at time t
d_p	Distance of prestressing steel from top fibre
d_s	Distance of non-prestressed steel from top fibre
$\Delta\sigma(t)$	Change in stress at time t
$\Delta\psi(t)$	Change in curvature at time t
ε	Strain
ε_c	Creep strain
$E_c(t)$	Elastic modulus of concrete at time t
$\varepsilon_c(t,t_o)$	Creep strain at time t for member loaded at time t_o
ε_e	Elastic strain
$E_e(t)$	Effective elastic modulus of concrete at time t
$\varepsilon_e(t)$	Elastic strain at time, t
ε_i	Initial strain in concrete at any fibre

ε_{oi}	Initial strain at top fibre
ε_p	Eccentricity of prestressing steel
E_p	Elastic modulus of prestressing steel
E_s	Elastic modulus of non-prestressed steel
$\overline{E}_e$	Age-adjusted effective elastic modulus of concrete
$\varepsilon_{sh}(t,t_s)$	Shrinkage strain at time t after curing duration t_s
ε_{shu}	Ultimate shrinkage strain
ε_{si}	Initial strain in non-prestressed steel
ε_{so}	Basic shrinkage coefficient
$f_c(t)$	Cylinder strength of concrete at time t
$\phi(t,t_o)$	Creep coefficient at time t for member loaded at time t_o
f_{pe}	Effective stress in prestressing steel
f_{pi}	Initial stress in prestressing steel
f_{pu}	Ultimate strength in prestressing steel
f_{py}	Yield stress in prestressing steel
ϕ_u	Ultimate creep coefficient
I	Second moment of area of transformed section from top fibre
I_c	Age-adjusted second moment of concrete area from top fibre
I_{ct}	Second moment of area for cracked section
k'_1, k'_2, k'_3 *etc*	Coefficients that represent correction factors to compute shrinkage strains according to ACI
k_1, k_2, k_3 *etc*	Coefficients that represent correction factors to compute creep coefficients according to ACI
m	Modular ratio
M_a	Applied bending moment
M_i	Initial bending moment
N_i	Initial axial force
r	Radius of gyration
RH	Relative humidity
σ	Stress
$\sigma(t)$	Stress at time, t
σ_i	Initial stress in concrete
σ_o	Applied stress at time t_o

V/S	Volume to surface area ratio
y	Distance from top fibre
y_b	Distance from bottom fibre to the centroid of uncracked section
y_c	Depth of cracked neutral axis
y_{ct}	Centroid of cracked section from top fibre
ψ_i	Initial curvature

CHAPTER ONE

INTRODUCTION

1.1 State of the Art

The use of precast prestressed concrete beams in bridge construction has been widespread mainly due to simplicity in design and construction and the economic advantages they offer. Standardised sections with factory controlled quality has played a major role in cutting the construction cost. Until recent times, their popularity had risen steadily with up to 75% of total motorways and trunk-road bridges in the UK being constructed from precast prestressed beams (Srikandan, 1989). But their use has generally been restricted to single span construction. The system is simple to design and construct, but is not without problems. Leaks and corroded joints that come with this simple form of construction have posed severe maintenance problems for many bridge authorities.

The inherent problems associated with expansion joints have revived the call for jointless or integral bridges. Bressey in 1933 (Tilly, 1993) had recommended the use of such systems for bridge superstructures, but this was not generally accepted at that time. This was possibly due to factors such as uncertainties in differential settlement and the economy of using standard beams with simple spans. But the trend of constructing jointless bridges has been gaining momentum in the USA where many states have used this concept to a large degree since early 1980s. Initial concern of large stresses which

could be developed especially for long and multi-span bridges were not proven to be serious (Loveall, 1985). The use of jointless bridges became a primary response by bridge engineers in the USA to overcome joint related problems. Burke (1990) reports that by 1980, 87% of transportation departments in the USA had routinely used continuous construction in short and medium span bridges compared to 2% in 1930.

The calls for such a form of construction has gathered similar momentum in the UK (Kumar, 1986, Paterson, 1993 and Taylor, 1993). A recent survey by the Department of Transport (DTp) confirmed that leakage in the expansion joints of bridge decks contributes more than any other element to deck and substructure corrosion damage (Pritchard and Smith, 1991). It was reported that 75% of 200 bridges surveyed suffered joint leakage. The authorities have recognised the importance of continuous construction by introducing new requirements for all new road bridges to be joint free (Pritchard and Smith, 1993).

Time-dependent deformation for this type of structure is very complex and depends on many design parameters. The inherent difficulty associated with the design of this type of structure has been identified as the uncertainty in determining the redistribution of time-dependent deformation due to the restraining effect provided by the continuity joints (Figure 1.1). In a simple unloaded prestressed beam, creep of concrete due to prestressing results in additional camber with time, while concrete shrinkage and relaxation of the prestressing steel reduce the prestressing force and thus the camber. The selfweight of the beam and any permanent load causes the member to deflect downwards, which increases with time due to the action of creep. If the upward deflection from the prestressing force is greater than the downward deflection due to the combined actions of shrinkage, relaxation and the beam's selfweight, the beam will continue to camber. If two adjacent beams are made continuous with a rigid connection, the beam at the intermediate support is restrained from rotating and, as a result, positive restrained bending may occur. Due to the many different combinations of loading, material and structural properties and the possible sequences of construction, the levels of the hogging or sagging restraint moment and their significance at the intermediate support require lengthy calculation for each different combination.

Earlier investigations into the levels of the restraint moment have not provided designers with more specific guidelines. A study by Mattock *et al* (1960) was the only experimental investigation to date that directly address the problem of predicting the level of the restraint moment at the intermediate support for precast prestressed beams made continuous using ordinary reinforcing steel within the deck slab over the intermediate support. This experimental programme was followed by a few analytical investigations by Mattock *et. al* (1961), Suttikan (1978), and the National Co-operative Highway Research Program (NCHRP), USA (NCHRP, 1985). The studies have only resulted in general design guidelines which make bridge designers aware of the presence of the restraint moment.

These general design guidelines have led to different design practices amongst bridge designers and they may not all necessarily be conservative. A survey conducted by the National Co-operative Highway Research Program, USA (NCHRP, 1985) revealed that US bridge designers take many different approaches in designing such structures. Many designers do not consider time-dependent effects on continuous precast prestressed beams at all. They simply provide "standard reinforcement" for continuity based on their design experience. In the UK, some have suggested that the restraint moments are not significant, hence it is sufficient that the calculations for their values assume that the structures are made continuous when the precast beams are at 100 days of age (Hambly and Nicholson, 1992). It has also been suggested that the interactions between creep and differential shrinkage that cause sagging and hogging restraint moment respectively may cancel out each other.

At present, due to the uncertainty of the level of the sagging restraint moment that could develop at the intermediate support, some have also suggested the need to provide reinforcing steel at the bottom section of the insitu cross heads, known as positive reinforcement (Hambly, 1992 and Clark, 1997). The reinforcement is provided to carry the tensile stress that may develop at the bottom fibre of the insitu cross heads due to the restrained sagging moment.

The provision of ordinary reinforcing steel across deck slabs over the intermediate piers is the most common practice adopted to provide continuity. This reinforcement is provided only to satisfy the ultimate strength requirement which is calculated in the same way as for conventionally reinforced concrete sections. This method of achieving continuity may satisfy Classes 3 or 2 for bridges designed according to BS5400, but the requirement for zero tensile stress under service loads for Class 1 bridges cannot be satisfied. The superimposed live loads that are applied to continuous beams cause tensile stresses at the top fibre of the insitu cross heads to occur. Depending on the load levels and the structural properties of the precast beams made continuous, the tensile stresses may cause the insitu cross heads to crack. Thus, full continuity is inevitably reduced. The level of tensile stress may increase if a hogging restraint moments (instead of sagging, as generally expected) develops at the intermediate support due to the time-dependent effects.

The possible cracks that may develop at the insitu crossheads, either as a result of the time-dependent effects or the superimposed live loads, not only does not satisfy the Class 1 requirement, but also does not fully address the initial concern with respect to durability in the support region. Clearly there is a need to look into different alternatives for achieving continuity between the precast units to address both the durability problem and the tensile stress requirements of BS5400 for Class 1 structures.

Many different methods of achieving continuity have been proposed (see Chapter 2). The use of prestressing over the intermediate support has been suggested to ensure that tensile stresses do not develop at the top fibre of the insitu crossheads over the intermediate support as well as providing full continuity between the precast beams. Investigations for such continuity methods have generally evaluated the performance of the structures under short term loads where they were shown to perform satisfactorily up to the ultimate load (Campbell and Batchelor, 1977, Jayanandanan, 1988 and Rodriguez, 1990). The performance of such structures under time-dependent effects needs to be established.

The provision of prestressing over the support, as mentioned above, provides the required precompression stress at the top fibre of the insitu cross heads at the intermediate support. It is also possible to provide the required precompression by adjusting the height of supports. Since the precompression stresses which occur at the top of the insitu crossheads reduce due to creep effects after continuity has been established, the performance of such continuity methods under time-dependent effects will also need to be evaluated.

1.2 Statement of the Problem

The use of precast prestressed simply supported beams has been widely applied to construction of road and highway bridges. The durability problems associated with this form of construction have prompted the call for jointless or integral form of construction for road bridges. The application of precast prestressed beams for continuous construction is becoming more important since the Department of Transport (DTp) requires that all new road and highway bridges to be joint-free.

There is a lack of guidance on design aspects of this type of structure especially with respect to its time-dependent effects. BS5400: part 4 (1990) provides general guidelines and adopts a design procedure which was initially proposed by the Portland Cement Association (USA). The procedure was essentially derived from the work done by Mattock *et al* in 1960s which involved two half-scale structural tests of two-span continuous precast prestressed beams. For simplicity, it was assumed that the time-dependent effects due to the prestressing force acted independently to those of other loads such as the beam selfweight and the insitu slabs. A more rigorous investigation is required in order to predict the restrained moments that may develop at the insitu crossheads. Evaluations of structures consisting of many different combinations of materials and structural properties as well as sequences of construction need to be conducted so that better design guidelines may be produced.

There is also a need to evaluate alternative continuity methods if the Class 1 bridges designed according to BS5400 are considered. Since the service condition is an

important design considerations for prestressed concrete structures, the evaluations of such the continuity methods need to take the time-dependent effects into account.

1.3 Object of the Present Investigation

The need to build continuous or integral prestressed bridges and the inadequacy of the recommendations pertaining to these members with respect to time-dependent effects require further research. Using an analytical tool, this study was set to serve the following objectives:

1) To evaluate and verify an analytical tool that is suitable for this investigation.

2) To study and determine the factors affecting time-dependent effects of simple prestressed beams with or without non-prestressed reinforcement.

3) To determine the levels of time-dependent restraint moment developed at the intermediate support for structures using ordinary reinforcement over the crossheads to provide the continuity connection.

4) To evaluate the elastic and time-dependent performance of other form of continuity for this type of structure.

5) To recommend a design approach for evaluating the time-dependent effects of continuous precast prestressed beams.

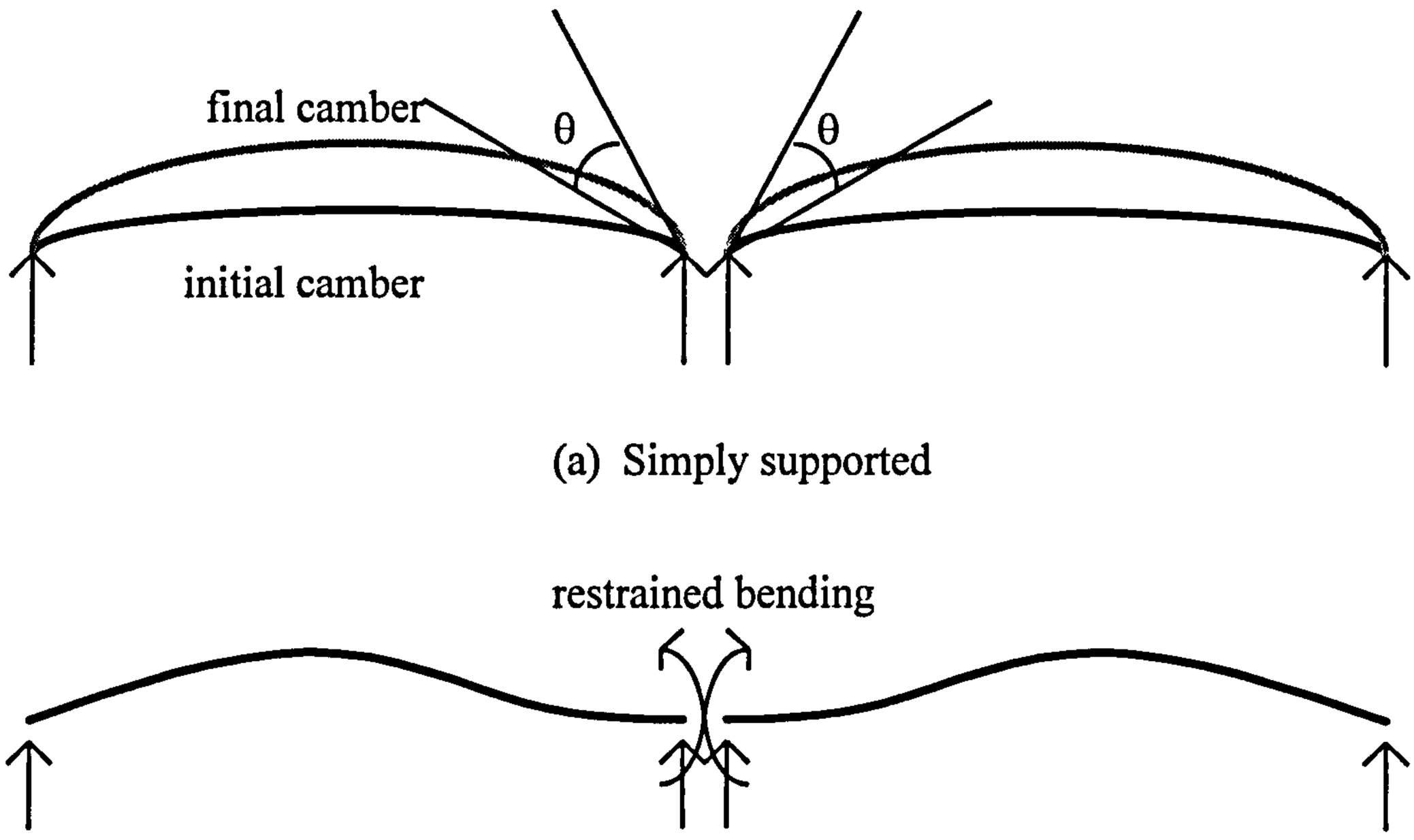

Figure 1.1: Long term effects of simple precast prestressed beams made continuous

CHAPTER TWO

LITERATURE REVIEW

2.1 Introduction

Continuous beams are structurally more efficient than simply supported beams. They are more rigid (flexurally), thus able to carry more loads, or for equivalent loads and sectional properties, they can extend to longer spans. The efficient use of continuous beams in prestressed concrete bridges, however, has largely been overshadowed by simplicity in design and construction of simply supported beams. Accordingly, most multi-span precast prestressed concrete bridges constructed in the UK and USA have consisted of a series of simple spans.

A considerable amount of research to investigate and confirm structural efficiency of continuous beams made of precast prestressed concrete beams has been carried out in the USA (Mattock *et al*, 1961 and Kaar *et al* 1960) and UK (Kajfasz *et al*, 1963) for more than 30 years. But it has not been sufficient to encourage a wider use of such a system. Interest in constructing continuous precast prestressed concrete beams, however, has only been recently renewed both in the USA (Burke, 1990) and the UK (Pritchard, 1993) due to persistent durability problems caused by joint leakage in simply supported systems.

In 1990, the Transport and Road Research Laboratory (TRRL) UK, commissioned a consultant to carry out a survey on the existing methods of achieving continuity for precast beams and to evaluate their performance with respect to durability. The survey listed five different methods of achieving continuity that have been constructed in the UK (TRRL Contractor Report 247, 1991). Evaluations of 20 of the constructed bridges that represented the five methods of achieving continuity indicated that they were all effective in preventing surface water from penetrating the bridge decks and substructure (TRRL Contractor Report 294, 1991).

The analysis and design aspects of such systems are understandably more complex compared to the simply supported system. The renewed interest in continuous systems, however, has prompted this study to understand further the behaviour of this type of structure. A literature survey has been conducted to facilitate this investigation in which an historical development of continuity methods has been compiled and experimental and analytical work carried out to date are reported in this Chapter.

2.2 Development of Continuity Connection in Precast Prestressed Concrete Beams.

2.2.1 Methods of achieving continuity

In addition to the methods presented in the TRRL reports, a wider and more current search of methods of achieving continuity between precast prestressed concrete beams has been conducted and is summarised in this section.

2.2.1.1 Bolts and welded connections

Bishop (1962) proposed a method by which precast prestressed concrete beams may be connected to bring about continuous action under dead and live load. It was proposed that a connection using embedded bolts and steel plates as shown in Figure 2.1 be used to achieve this effect. The method requires all beams to be erected as simple spans and one of the end beams (at the first support) is jacked upward to a distance as shown in the figure. The beams are then connected by welding together the plates which have been embedded into the ends of the top and bottom flanges of the precast beams. The jacked

end is then lowered to the support after the connection is secured. The process is repeated as required according to number of spans involved.

The connection requires a lot of bolts (up to 40 in one connection) and welding of the endplates. The connection is not very suitable for structures subjected to cyclic loading such as bridges due to possible fatigue in the welded connection. It also requires high precision to position bolts and endplates properly, and the exposed steel plates and bolts may reduce durability of the structures significantly.

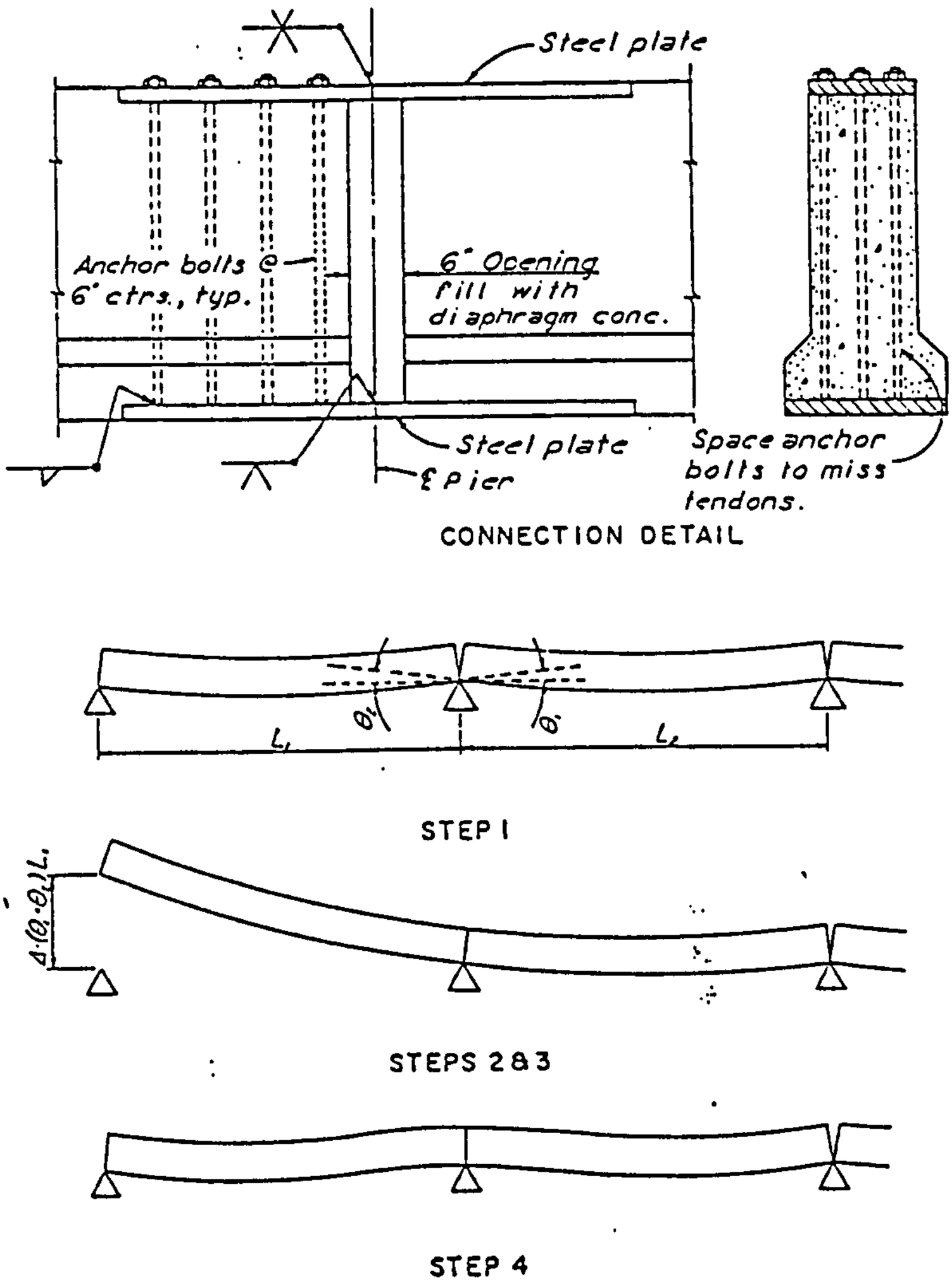

Figure 2.1: Method of achieving continuity using bolts and welded connections (Bishop, 1962)

2.2.1.2 Connection using ordinary reinforcing steel

This is by far the most popular method chosen by bridge designers in order to establish continuity between precast prestressed concrete beams. This method makes use of ordinary steel reinforcement which is placed within deck slabs over intermediate supports. The reinforcement is designed to transfer the resultant hogging moments due to the effects of restraint or external loading from superimposed dead and live loads. The method can be divided into three variants that are known as wide insitu crossheads, narrow insitu crossheads and integral crossheads cast in two stages (Pritchard, 1991 and 1993).

The wide insitu crosshead uses precast beams normally shorter than the span between supporting piers (Figure 2.2a). The beams are supported on temporary supports and the wide insitu crosshead is cast around the ends of adjacent precast beams with an embedment length of about one meter. The crossheads are supported on a single row of bearings set centrally on the piers. This form of continuity is most widely used in the UK with about 20 such bridges having been constructed with spans ranging from 12 to 35m.

The narrow insitu crosshead method is used when precast beams are long enough to be erected between supporting piers (Figure 2.2b). The crossheads are narrow, and precast beams are supported on two separate bearings on the same pier head. There are seven such bridges that have been constructed in the UK (Pritchard and Smith, 1991 and Srikandan, 1989).

The third variant using ordinary reinforcement is called the integral crosshead cast in two stages (Figure 2.2c). An insitu crosshead is first cast over the pier to support the precast beams and an insitu joint is then cast in the second stage to form a completely continuous structure. Four bridges have been built using this method in the UK (Pritchard and Smith 1991).

Early investigations on this method indicated that positive moment connection, i.e. reinforcing bars at the bottom of the insitu crossheads, was required at the supporting piers to resist sagging moments caused by the creep and shrinkage effects in the precast beams or the sagging moments due to live loads applied to a remote span. The positive moment connection may be provided in the form of ordinary reinforcement protruding out from the bottom flanges of the precast beams.

2.2.1.3 Tied-deck slab connection

Tied-deck slab connection (Figure 2.3) was developed during the UK Standard Bridge exercise of the 1970's (Pritchard, 1991). The bridge decks are designed and constructed in the conventional multi-span simply supported manner. Long reinforcement dowels are incorporated at the mid-depth of slab to tie the slab together over the pier. The dowels are sleeved and hence debonded from the surrounding slab over a short length over the pier to permit slab rotation.

2.2.1.4 Locally separated deck slab connection

Kumar (1988) proposed a simple continuity method called 'locally separated deck slab continuity'. Details of this connection are shown in Figure 2.4. In this method, the connection itself is confined to the deck slab only. The slab is expected to flex to accommodate the rotations of the simply supported deck beams erected in the conventional multi-span manner. Flexural rotation of the slab is permitted by separating the deck from the precast beams for a length of about 1.5m by a layer of compressible material. It offers great advantages in the ease of construction and also allows greater tolerance to support settlement compared to the full continuity provided by full depth crossheads. Eight such bridges have been constructed in the UK including the 5-span, 110m long River Frome Bridge, with the approval of the DTp (Kumar, 1993).

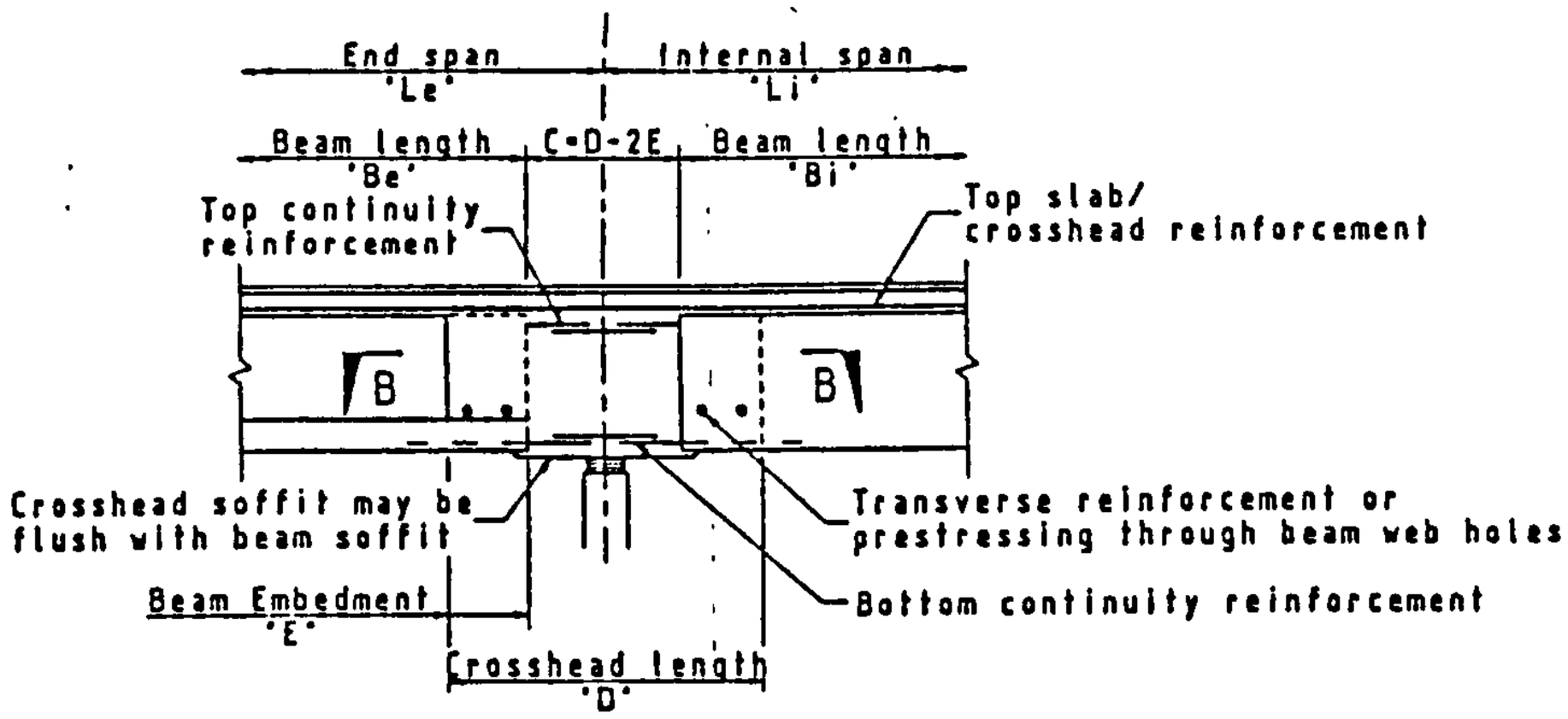

(a) Wide in-situ crosshead

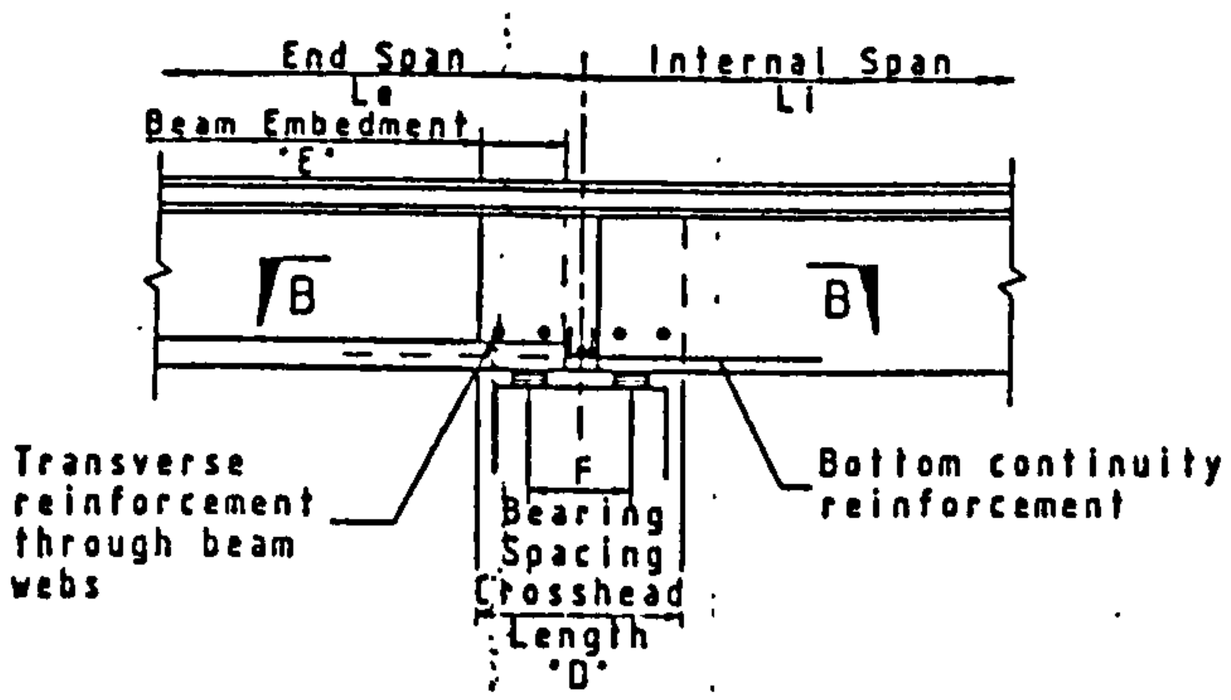

(b): Narrow in-situ crosshead

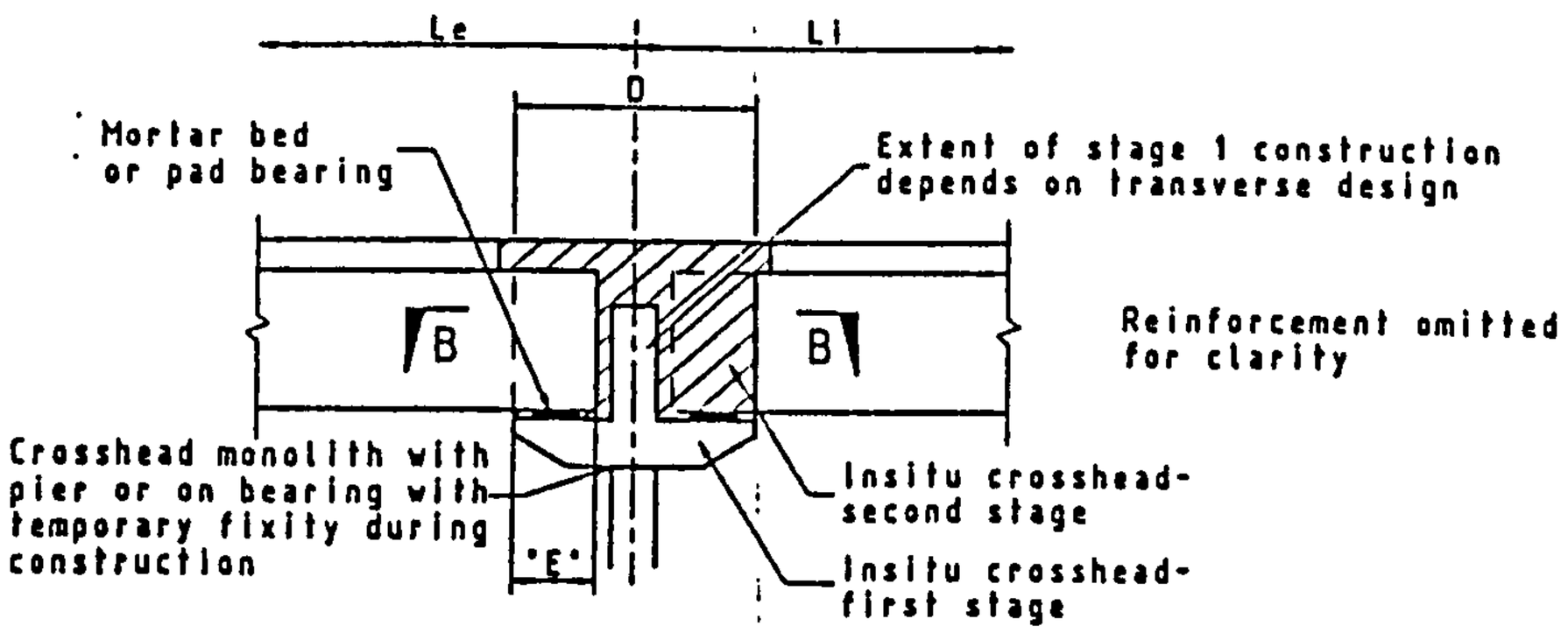

(c) Crossheads cast in two stages

Figure 2.2: Methods of continuity using ordinary reinforcing steel in deck slab across intermediate piers (Pritchard, 1991)

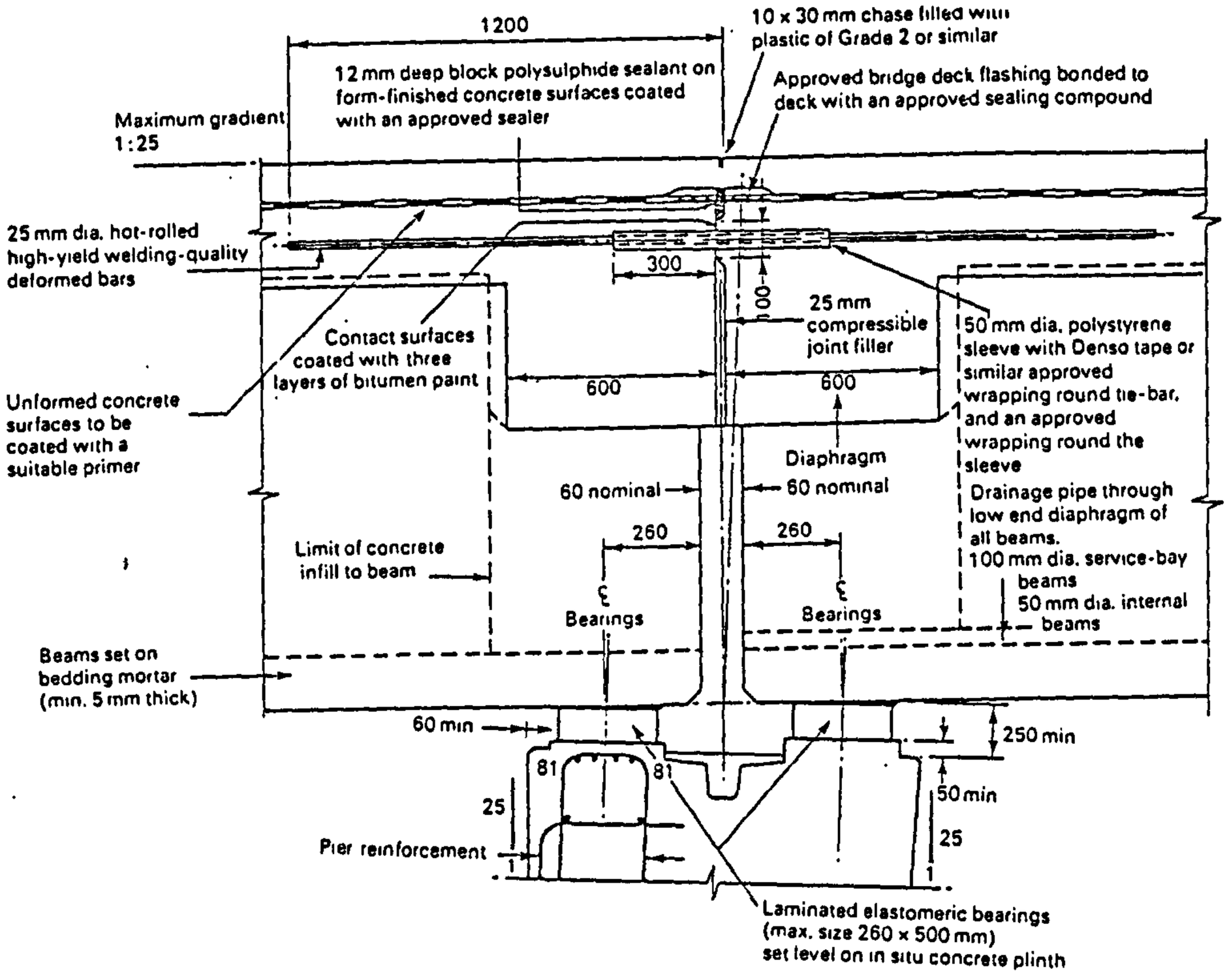

Figure 2.3: Tied-deck slab connection (Kumar, 1986, Courtesy G Maunsell & Partners, London)

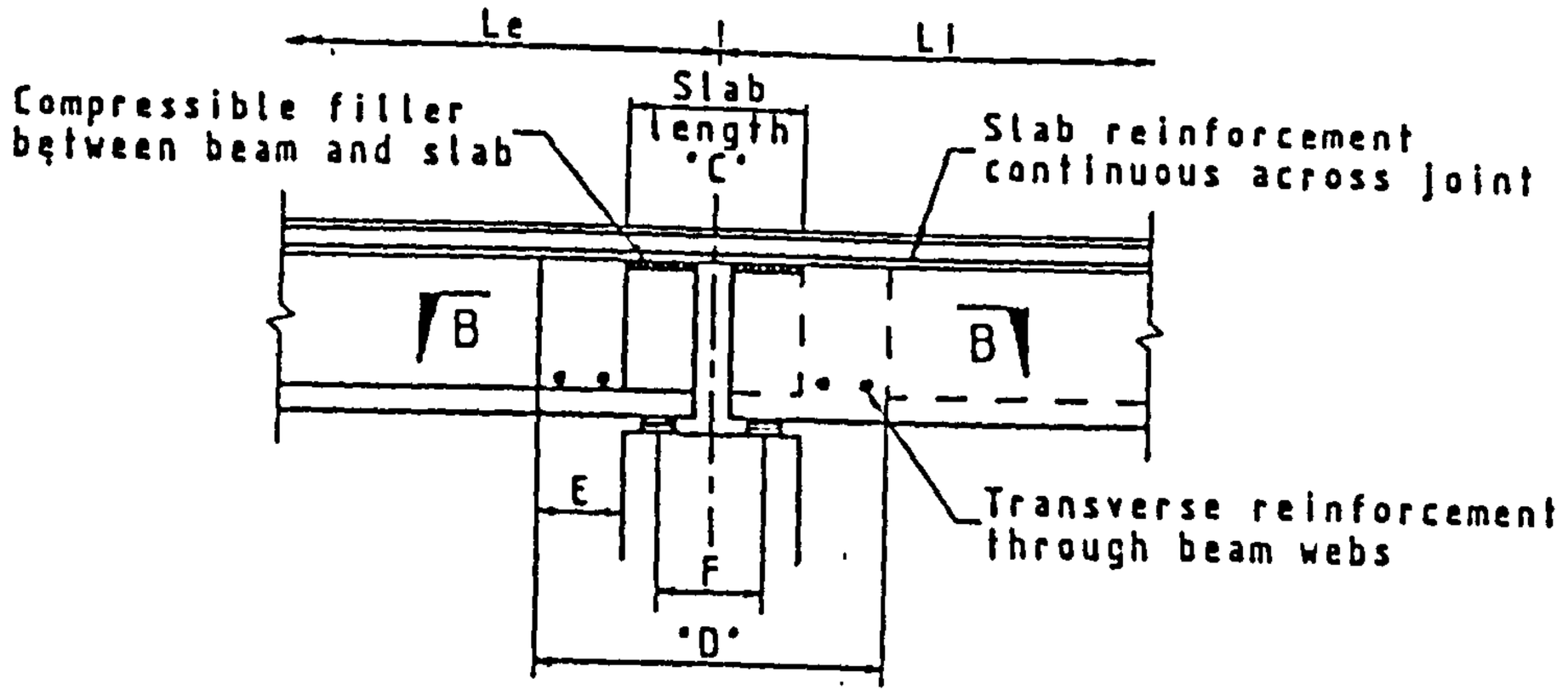

Figure 2.4: Locally separated deck slab (Pritchard, 1991)

2.2.1.5 Connection using post-tensioned steel

Simple precast beams can be made continuous by the provision of prestressing over the intermediate support. Prestressing is carried out either over the whole beam length (overall post-tensioning) or just over the pier (Figure 2.5). In overall post-tensioning, precast beams can either be cast on site as simple beams which have tendon ducts for the subsequent post-tensioning operation, or use standard precast prestressed beams with prestressing being supplied between the beams. In the case of using standard factory produced precast sections, the case may be considered to be similar to externally post-tensioned beams. Two or three short span beams may be post-tensioned from end to end. Tendon couplers may need to be used if the bridge span is too long, to avoid a significant loss of prestressing force due to friction. Coupling of tendons are made either over the pier or at the points of contra-flexure (Tadros *et al*, 1993). This form of construction has been used in the USA and Germany (Grant, 1966 and Seible, 1986).

For local post-tensioning over the pier, the prestressing steel extends up to one quarter span and is used to counter the hogging moment normally present at the intermediate supports due to live loads. The pre-compression in this area will ensure that the connection remains crack free under service load, hence maintaining full stiffness of the structural member across the joints.

This method of connection may also be able to relieve the stress due to the beam's own self weight in the mid-span region. This is quite an important characteristic of this method because dead load can predominate in the service load range (Gee, 1987). The possible reduction of mid-span stress may result in the use of fewer pretensioned wires. Standard precast beams may be used for this form of construction with minor modification to accommodate the amount of shear connectors and reinforcement especially at beam ends.

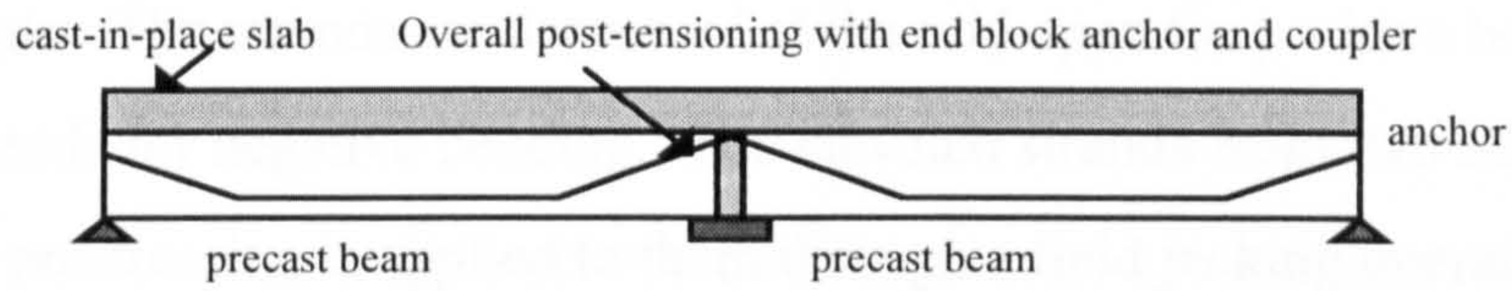

(a) beams are post-tensioned the whole beam length

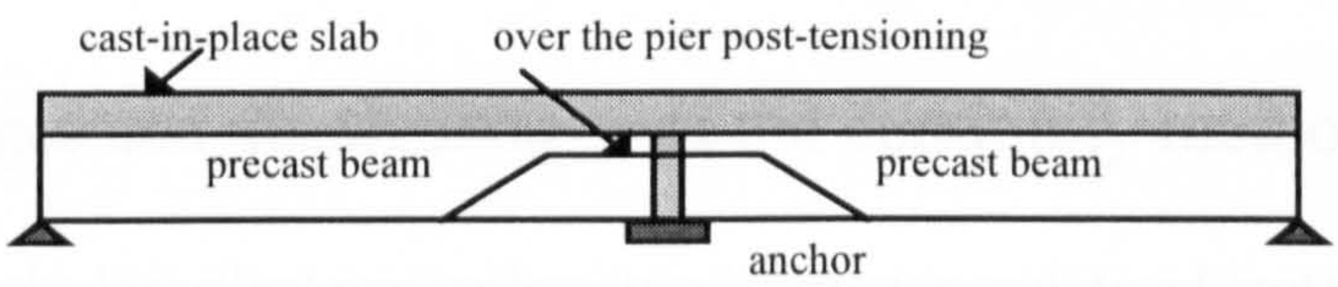

(b) beams are connected using 'cap cables' over the support

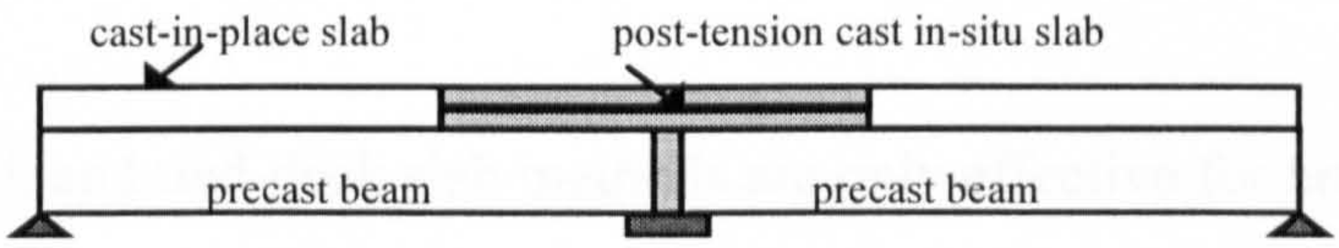

(c) beams are connected using straight post-tesnioned steel

Figure 2.5: Continuity of single presstressed concrete beams using post-tensioned steel

2.2.1.6 Connection using splicing of pretensioned strands

A team from the University of Nebraska, USA has recently proposed a splicing technique of pre-tensioned strands to establish continuity between simple precast beams (Tadros *et al*, 1993). In this system, the same strands are used for positive and negative bending moments. The strands are depressed at the mid-span for positive bending and elevated at the ends for negative bending. The elevated strands from two adjacent units are spliced and prestressing is applied to them through a field jacking operation at the interior supports. The splicing operation is shown in Figure 2.6. This system has successfully been tried for pedestrian and cycle bridges in Nebraska, USA (Ficenec *et al*, 1993).

2.2.2 Advantages and disadvantages of the continuity methods

Each of the methods described earlier has its advantages and disadvantages. The choice depends on many considerations such as the availability of precast beams, the bridge length, layout and function, and also the availability of construction and design expertise that may affect the overall economy if one method is chosen over the other.

The separated deck and tied-deck slab methods are only effective for horizontal connection. No hogging moment is expected over the piers and design is basically similar to that for conventional simply supported beams. Extra consideration, however, is required for the separated slab deck connection where the thin connecting slab must properly account for end rotations of simple beams.

Connection using ordinary reinforcement across the joints within the deck slab is the simplest form of construction to achieve a degree of continuity. This form of continuity does not require more skilled workers than those already with the experience of constructing conventional simply supported bridges. Besides the provision of the positive moment connection, the system does not call for any change in the current form of producing precast beams. The method, however, requires additional effort in the design stage if it is to account for restraint moment caused by the actions of creep and differential shrinkage. The assumption of full continuity for live load is highly

questionable for this method of continuity as the stiffness at the joints will greatly reduce once cracks start to appear at the top fibre of the insitu crossheads under service load, or at the bottom fibre of the insitu crossheads due to the time-dependent effects. Analysis assuming uncracked stiffness under service loads will, therefore, overestimate negative bending moment at the supports and underestimate sagging moment at the mid-spans. The possibility of cracks occurring at the top slab of the crossheads due to service loads also presents potential durability problems.

Continuity methods using prestressing offers the better form of continuity because full continuity is guaranteed under full service load. It addresses both potential durability problem as well as ensuring full rigidity of the continuous members. The use of strand couplers for long prestressing steel, however, may be critical as possible loss of prestressing force may concentrate at the couplers if corrosion occurs around them. A bridge survey in Germany (Seible, 1986) indicated that, for this type of connection, severe cracking occurred in the regions of strand coupling and many tendons had ruptured in its vicinity. It was observed that of all beams incorporating post-tensioned steel to form structures into continuous members, 66% of the beams with coupling joints had severe cracking problem as opposed to 20% of continuous beams without coupling joints.

For multiple span bridges where the use of strand couplers is inevitable, use of local prestressing over the piers is more attractive as it requires a simpler prestressing operation. Compared to continuity with ordinary steel over the insitu crossheads, the prestressed solution has the advantage that the joint is more rigid and crack-free under service loads. The disadvantage of this method is that it requires extra cost for construction, although it may prove to be economical in the long run. Special care is required during post-tensioning because the loss of prestress may be significant due to the use of relatively short prestressing tendons. A temporary ban on the use of post-tensioned beams for all UK bridges since 1990 (DTp, 1992) has also probably dampened enthusiasm for the application of this method. It is believed that after the temporary ban is lifted (New Civil Engineer, 1996), this method of construction will

become an attractive alternative for bridge engineers to overcome joint leakage problem and improve durability of concrete bridges.

For continuity provided by splicing of the built in strands, several benefits can be realised including the efficient use of strands and eliminating the need for end blocks, anchorage zone reinforcement, widening of webs to accommodate ducts and the grouting of ducts. However, the system apparently needs major changes in the precasting process as large modification to the profile of the beam and wire draping are required. The system is very difficult to construct and the splicing operation requires highly skilled workers to ensure proper connection is established. Further development and assessment of the system is believed to be continuing by the team at the University of Nebraska, USA.

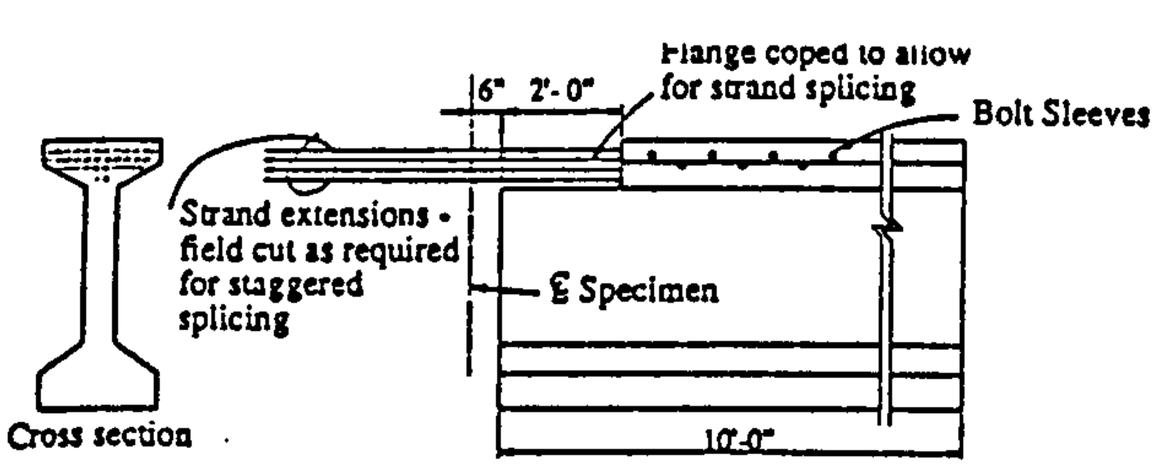

a) Precast girder, side view

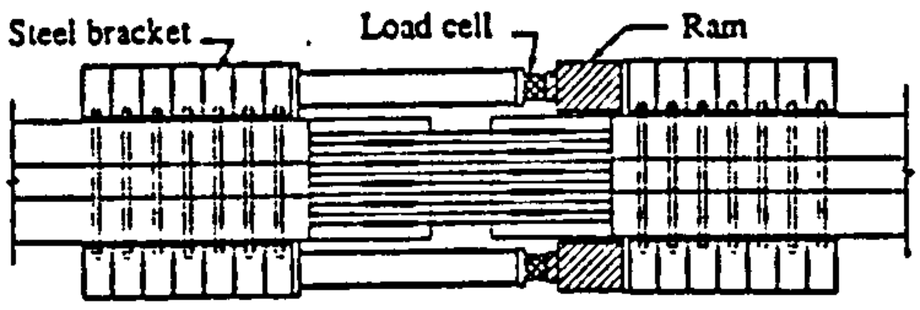

c) Jacking operation, top view

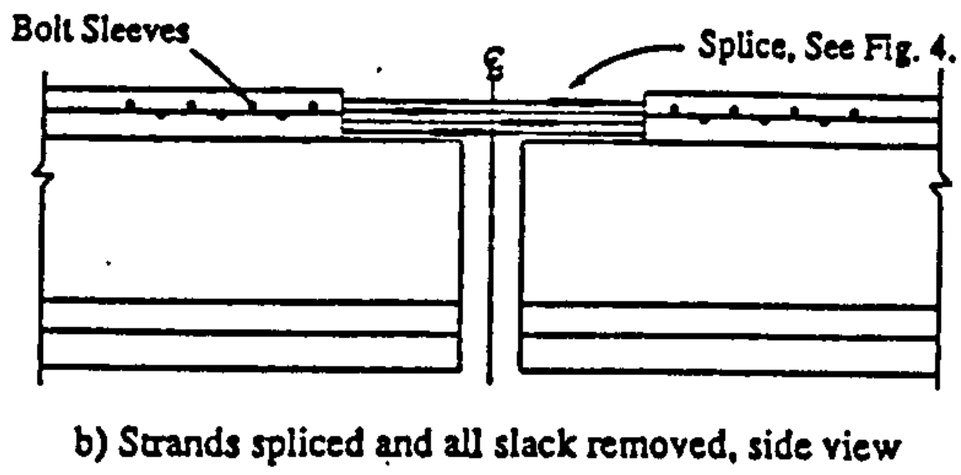

b) Strands spliced and all slack removed, side view

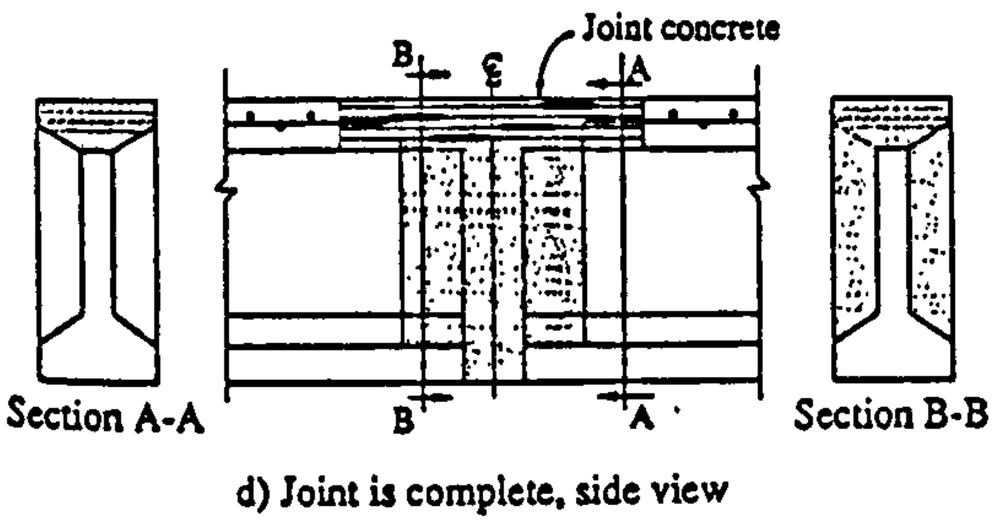

d) Joint is complete, side view

Figure 2.6: Connection of precast beams using splicing of the pretensioned strands technique (Tadros *et al* 1993)

2.3 Experimental and Analytical Studies for Continuous Precast Prestressed Concrete Beams

2.3.1 Experimental investigations

2.3.1.1 Connections using ordinary reinforcing bars

The first extensive experimental research program on continuous precast prestressed concrete beams was carried out by the Portland Cement Association (PCA) Laboratory, USA in early 1960's (Mattock *et al*, 1960 and Kaar *et al*, 1961). The comprehensive program included:

(a) A feasibility study of establishing continuity between precast beams,

(b) Horizontal shear connection tests between precast beams and cast in situ slab decks,

(c) Flexural tests on continuous beams made of precast units,

(d) Shear tests on continuous beams made of precast units,

(e) Creep and shrinkage studies of continuous beams made of precast units, and

(f) A test on a half-scale highway bridge continuous over two spans.

The series of tests conducted by the PCA were only for precast prestressed concrete beams that were made continuous using ordinary reinforcing steel in the insitu deck slabs across the intermediate support. The reinforcing bars were expected to transfer negative bending moment arising from the superimposed live loads across the continuity connection. In the first series of the experiments, fifteen half-scale composite beams comprising of 22 inches (558.8mm) deep precast I-beams and 24x3inches (610x76mm) cast insitu slabs were tested under negative bending over a central support and a 2-point load system (Figure 2.7). The tests examined the flexural behaviour of the structure at ultimate and the degree of continuity provided by the negative moment connection (reinforcing bar in the deck slab).

The tests showed that such a continuity method was sound under short term loads up to the ultimate load. Although the concrete strength of the concrete forming the diaphragm (between the two connected members) was about 2,000psi (13.8MPa) lower than that for the precast beams, the results showed that the failure at ultimate occurred away from the diaphragm in all tests. The failure at ultimate, therefore, involved the precast unit which means that the presence of the compressive prestress in the ends of the precast units may need to be considered in the analysis of the composite section at ultimate. However, this approach was recommended for only for a highly reinforced sections (greater than 2.49%). For sections containing less than 1.5% reinforcing bar and the precompression stress due to the prestressing is less than $0.4f'_c$, it is recommended that the presence of the prestressing force is neglected. Section analysis using a rectangular stress block as for conventionally reinforced concrete structures can therefore be applied in such cases.

The degree of continuity for such a connection was found, as expected, to be less than that of an uncracked homogeneous continuous beam. Observed values of the negative bending started to deviate from those predicted by the elastic theory as soon as cracks appeared over the support. The continuity moment continued to drop to 66% of the uncracked value when loaded to twice the value of the service load and remained the same until cracks appeared at the mid-span.

Subsequent tests for shear failure had also been conducted on another fifteen half-scale model composite beams consisting of the same I-beam, but where the slab dimension was increased to 39x3inches (991x76mm). The beams tested were single span with a tied-down cantilever at one end (Figure 2.8). The results showed that, of the fifteen beams, no beam failed in shear in the connection between the precast beams. Thirteen of the beams had shear failures in the precast beams, one had flexural failure in the precast beam and one had failure at the interface between the precast beams and slabs. Another series of similar tests conducted in the UK by Sturrock (1974) using wider crossheads showed that there was no difficulty in providing shear reinforcement in the crossheads in order to ensure flexural failure in the beams, rather than shear failure in the connection or crosshead.

For structures consisting or three of more spans, positive moment can occur at the interior supports for certain patterns of live load. Hence, subsequent tests on the performance of the beams connected using ordinary reinforcing bars in the deck slab under positive bending moment were also carried out. Positive moment reinforcement (located towards the bottom of the beams) protruded out of the ends of the precast beams and was connected at the diaphragm. Two types of connection were investigated i.e. welded and hook connections (Figures 2.9). The test result indicated that the welded connection performed satisfactorily under service and ultimate loads. As for the hook connection, it performed less satisfactorily where the bar ruptured at the bend before the yield strength could be developed. It was suggested, however, that the bar connection could perform better if the inside radius of the hook was not less than the bar diameter (Mattock and Kaar, 1960).

A further experimental program was set up to examine the behaviour of the structure under long term loads. The study attempted to evaluate the influence of creep deformation of the precast beam due to the applied prestressing force and the dead weight of the beam and of differential shrinkage between the precast beam and the insitu deck slab, on the long term continuity behaviour of this type of continuous beam. Two 2-span half scale models of continuous beams were observed for two years. The two beams were identical in all particulars, except one incorporated a positive moment connection at the interior support while the other did not. The beams were pretensioned with at total of 28 prestressing wires, two of which were located at the top and the remaining 26 were positioned towards the bottom of the beams. The pretensioned wires were released at 7 or 8 days after casting with a total prestressing force of 175,000 lbs (778.4kN). Once erected, a series of concrete blocks were hung from the beams in order to simulate the actual stress of the prototype beams under selfweight. Details of the beam section were similar to those tested under shear failure (Figure 2.8) and the positive moment connection used was as shown in Figure 2.9b. Measurements were made of the long term variations in reactions and deflections. At the end of the observation period, the beams were loaded to failure to ascertain if the actions of creep and shrinkage had affected the ultimate strength of the beams.

Results of the long term reaction showed that there was an increase in the centre support reaction immediately after the slab formwork was stripped. This increase continued reaching its peak for both beams after about 30 days, after which there was a continuous reduction of the centre support reactions. It should be noted that an increase in the centre support reaction corresponds to a negative restraint moment, and likewise, a decrease in the reaction corresponds to positive restraint moment at the centre support. The results clearly indicated that the behaviour of the beams at the initial stage was dominated by the action of differential shrinkage which was later overtaken by the actions of creep. Both beams developed final positive restraint moment at the centre support with the beam provided with the positive moment connection yielding larger values at the end of the observation period. Cracks were visible for the beam without the positive moment connection after 337 days, after which the reactions of the beam remained almost constant. The reactions for the beam which incorporated the positive moment connection continued to increase to the last day of the observation period. The final (2 year) moment was observed to be 18.2kip-ft (24.7kNm) which represented about 32% of the design service load negative moment at the support. Subsequently a load test of the beams to failure indicated that the actions of creep and shrinkage had not affected the ultimate load capacity of the beams.

It should be noted that these are the only reported tests carried out to date in which the level of restraint moment in continuous precast prestressed concrete beams was measured. The tests highlighted an important long term feature of such structures where the levels of restraint moment developed at the centre support could be sufficiently large to cause cracking at the insitu diaphragm. The presence of cracking at the bottom of the diaphragm may reduce the effectiveness of the continuity as a result of which the analysis of the structure under live load cannot assume full continuity until the cracks are closed. That such a high level of restraint moment can be developed in the absence of the live load need to recognised so that proper design specifications can be outlined. There are a myriad combinations of material, structural configurations, environmental conditions and construction sequences that may affect the level of the restraint moment, and it is difficult as well as expensive to run more experiments of this nature to ascertain

the level of the restraint moment under different combinations. Reliable analytical predictions are therefore required to help bridge designers to predict the levels of the restraint moment with reasonable accuracy for a given set of conditions. Although the test series has revealed an important aspect of the time-dependent behaviour of such structures, it is by no mean comprehensive enough to generalise other similar form of structures but subject to different combinations of conditions. The results of these tests, however, have become the reference point of all subsequent analytical that has attempted to predict the time-dependent behaviour such structures.

It should be acknowledged that the form of continuity using ordinary reinforcing steel across the deck slab offers the simplest form of construction as well as offering some of the advantages of continuity. However, the system cannot avoid the development of tensile stresses or possibly cracks in the deck slab due to the application of live loads. This could result in less durable structures and cause the joint to lose some of its stiffness. Some researchers, therefore, have suggested and tested several alternative techniques of construction which ensure crack free structures.

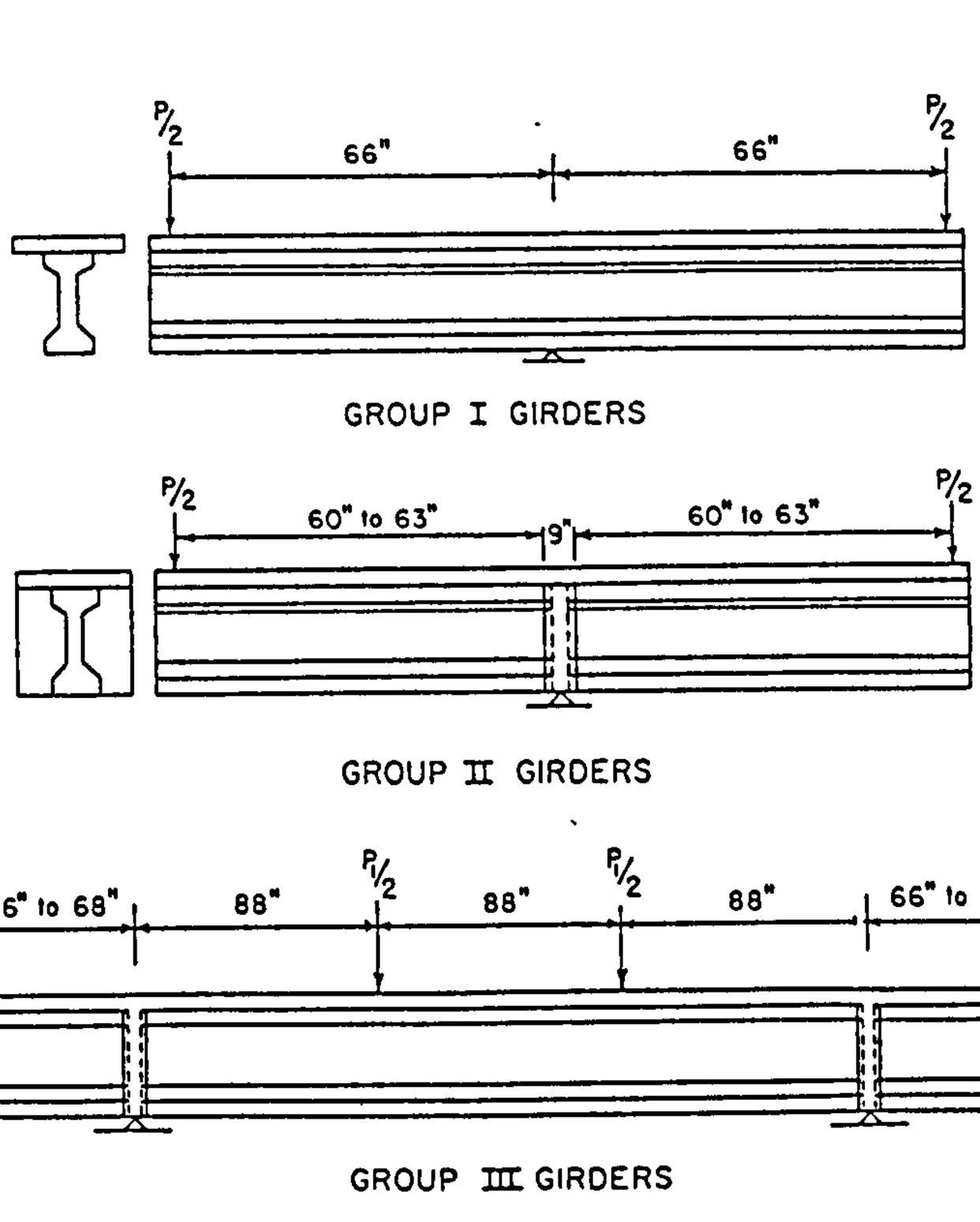

Figure 2.7: Test set-up to study the effectiveness of producing continuity using ordinary reinforcing bars under short term flexural loads (Kaar *et al*, 1960)

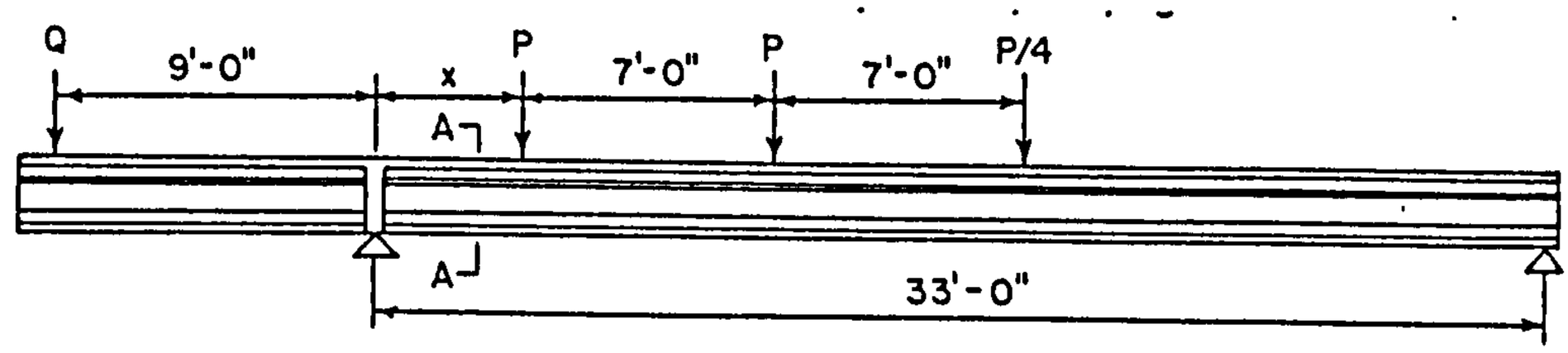

Elevation of Typical Girder

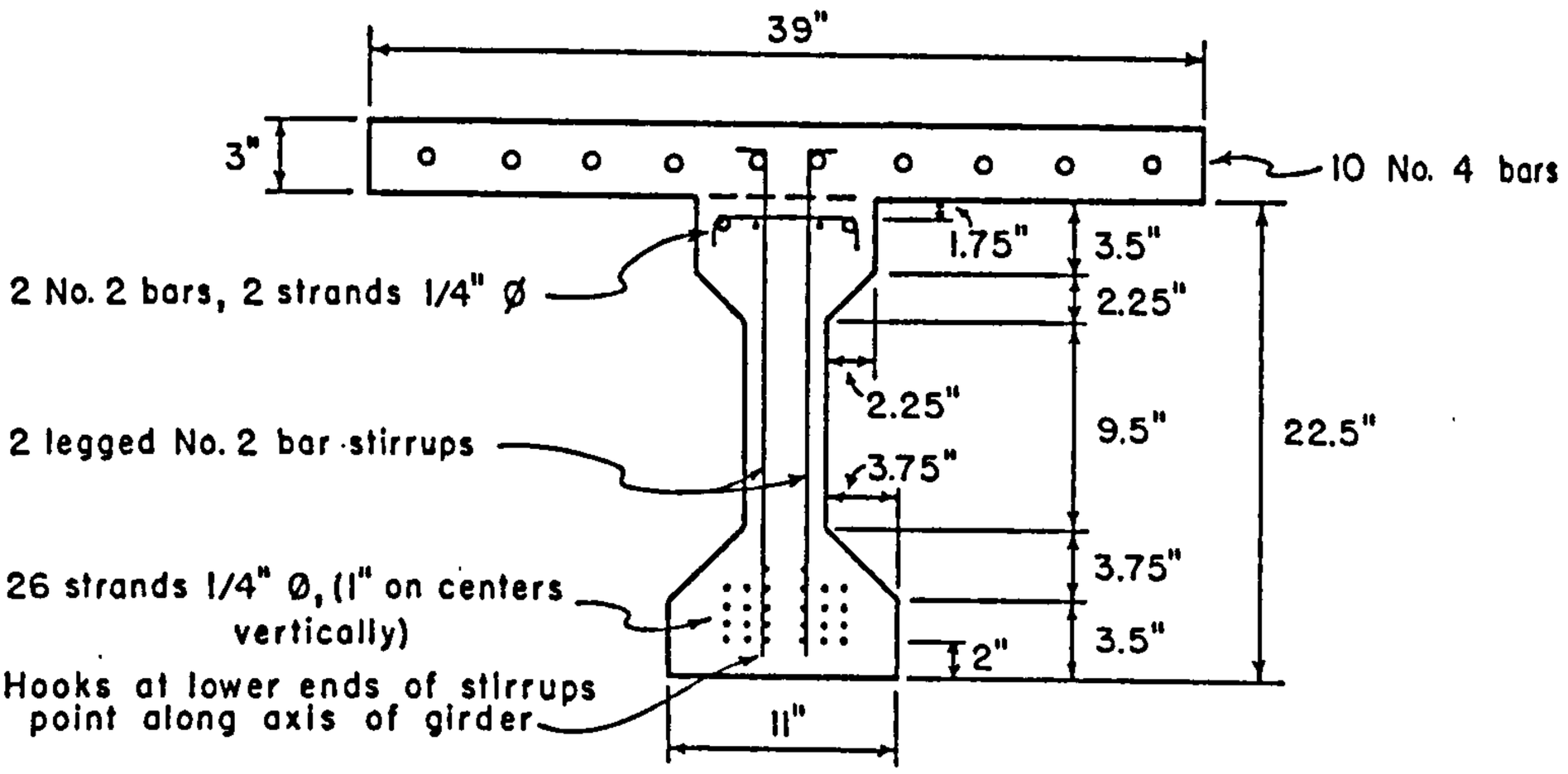

Section A-A

Fig. 1 — Elevation and Cross-Section of a Typical Test Girder.

Figure 2.8: Elevation and cross-section of a shear test (Mattock *et al*, 1960)

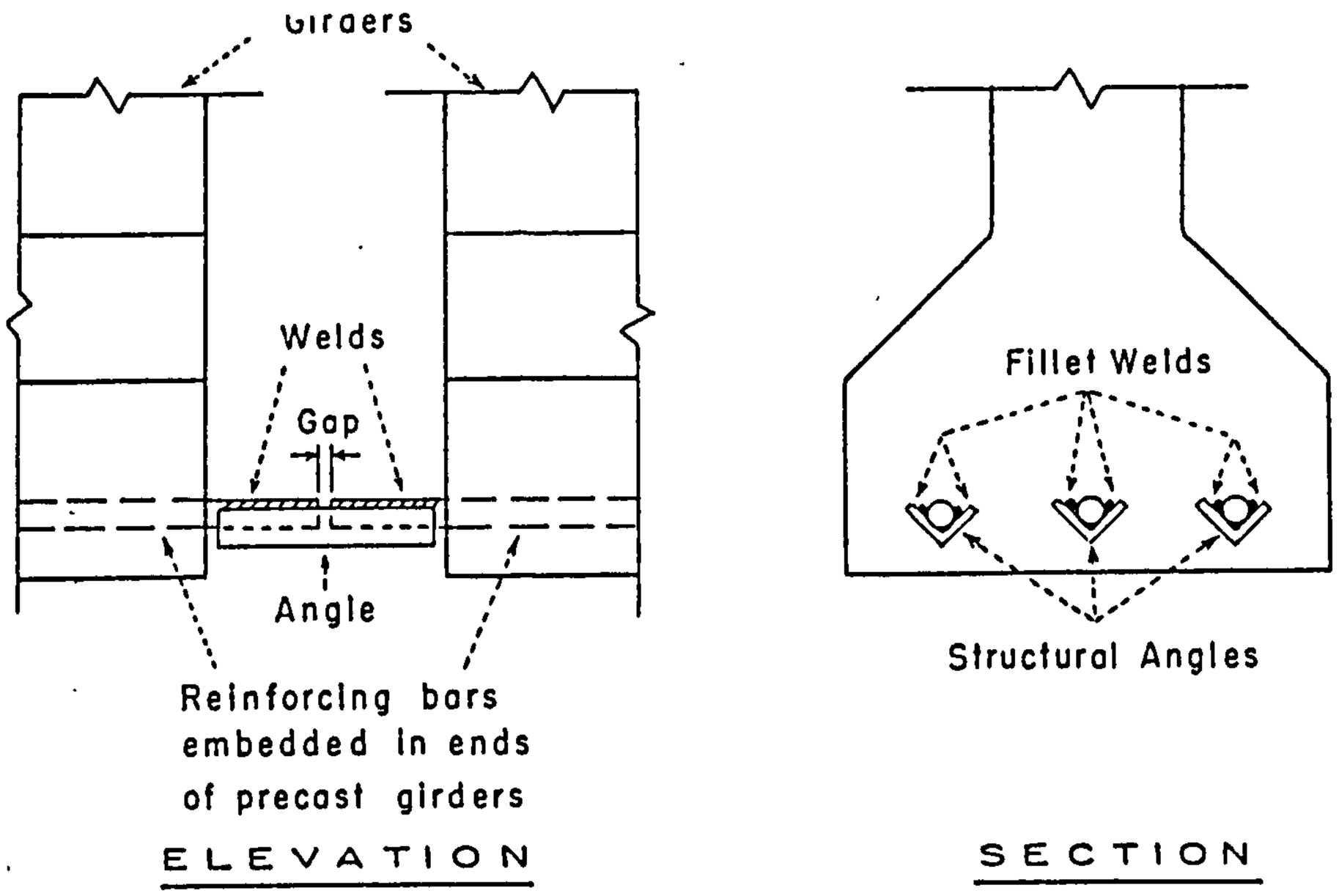

(a) Welded connection for positive moment connection

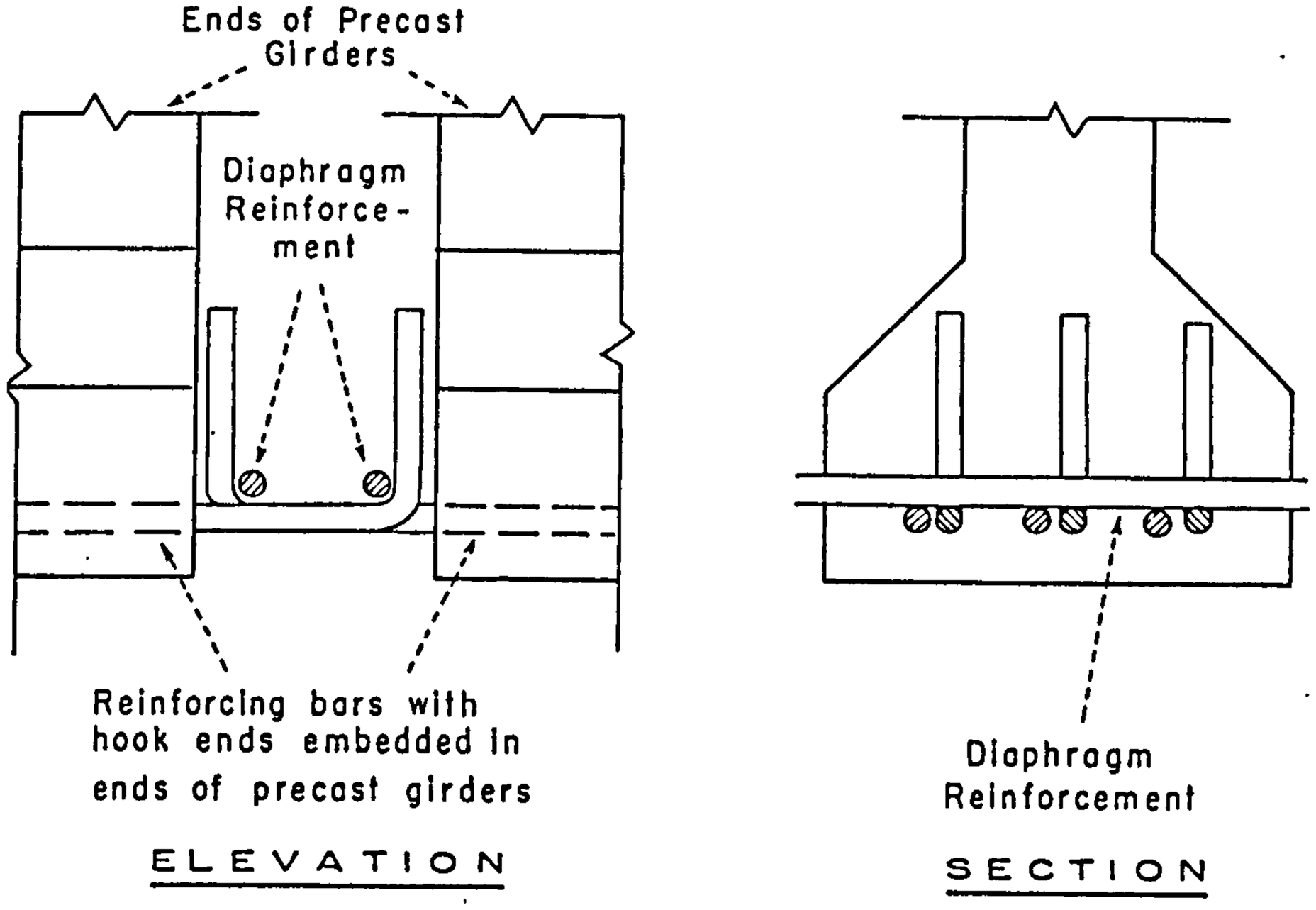

(b) Hook connection for positive moment reinforcement

Figure 2.9: Positive moment connections tested under short term loads (Mattock *et al*, 1960)

2.3.1.2 Other methods of achieving continuity

There have been several reported experiments on other more effective methods of achieving continuity to overcome the limitations of using ordinary reinforcing bars.

To improve the joint properties of such structures, Burns (1966) has proposed the use of pretensioned precast concrete rods to replace the reinforcing bars as reinforcement for negative bending moments. Each rod was of 2x2inches (50.8x50.8mm) in cross section and contained a single pretensioned wire (Figure 2.10). The ease of construction is similar to that of using the ordinary bars. Slab sections reinforced by the rods over the support were expected to behave as partially prestressed concrete sections. Cracks in the slab are delayed due to the presence of the prestressed rods, considering perfect bond exists between the rods and the cast insitu slab. If the applied live loads are such as to cause the slab and the rods to crack, the presence of the pretensioned wires in the rods were expected to close the cracks once the live loads were removed. A series of tests involving five specimens arranged either as double cantilevers or on two-span beams showed that the beams reinforced with pretensioned rods improved the cracking behaviour of the beams. The beams containing the rods showed first cracks at 50% of the ultimate load, compared with 25% for the beams containing the ordinary bar reinforcement. Another experiment by Shaikh and Branson (1970) had shown similar performance for this type of beam detail. This type of connection detail has successfully been used in a bridge construction in Canada (Lin and Burns, 1981).

Experiments to assess the effectiveness of using post-tensioned steel to convert a series of simply supported members into a continuous structure have been conducted by several researchers. Campbell and Batchelor (1979) tested a 1/3.47 scale direct model of a prototype bridge structure of *U* sections. The beam comprised of four pretensioned concrete troughs which were erected in series with the aid of temporary supports and subsequently made continuous by longitudinal post-tensioning after a situ deck had been cast.

The construction sequence of the model was the same as that specified for the prototype. The beam was tested under service and ultimate loads. Theoretical response under the service load was estimated from an elastic analysis which took into account the variation in section properties, but assumed uniform elastic modulus for the concrete over the entire length of the beam. The maximum measured deflection under this service load was 83% of the theoretical value. The ultimate load test gave failure load of the beam to be 20% more than its predicted capacity. The study indicated that such a structure performed satisfactorily under service and ultimate loads and that its behaviour could be safely predicted by the elastic methods of analysis.

A similar method of producing continuity was also investigated by Rodrigues (1990). Continuity was achieved by a concordant post-tensioned tendon, which passed through the precast beams in a duct. The duct rose and entered the cast in place slab at the support. The main objective of the study was to examine the redistribution of bending moments at loads close to failure. Seven, two-span continuous beams were tested for this purpose.

Beam reactions and deflections were recorded at all incremental loads. It was observed that deflections, curvatures and support reactions showed linear behaviour in the early phase of loading. The deviation from the elastic theory generally increased for load levels higher than the cracking load. The maximum deviation from the elastic theory did not necessarily occur at the highest levels of loading. The test results indicated that most of the beams had the maximum deviation of support reactions for loads around 40-60% of the failure loads. The experiment showed that full redistribution took place. It was proposed that the amount of redistribution could be determined from a comparison between the actual value of the maximum load and the value given by theoretical calculations based on the elastic theory. The experiment was very useful and indicated that full continuity and sufficient rigidity can be obtained up to failure load. It was, however, limited only to cases of beams with concordant tendons.

Jayanandanan (1989) tested a series of precast beams made continuous using prestressed deck slabs. Three 1/3 scale model of *M8* beams were tested to achieve flexural mode of

failure and a further eight were tested to achieve shear mode of failure. The deck slabs had three different degrees of prestress: zero, partial and fully prestress. The tests showed that both the partial and full prestressed slabs remained uncracked under full service load, but similar non-prestressed deck slabs cracked under one third of the service load. The results showed that the system had great promise for complete elimination of cracks under full service load.

The provision of prestressing force in the deck slab is also likely to have a beneficial effect on the distribution of moments along the span due to the beam's selfweight by redistribution to other parts of the structure. The effect on internal redistribution of the existing stresses, however, could not be observed and analysed because the test was set up in such a way that the beam was statically determinate. For the same reason, possibly useful information on the rotational capacity of each slab at the intermediate support under ultimate loads was also unavailable. It would certainly be of interest to know the magnitude of the stress in the precast beam being relieved by the provision of a prestressing force in the deck slab.

Composite construction, either between cast insitu slabs and precast beams or between cast insitu slabs and steel beams, has long been recognised as an economical means of resisting positive moments, but it is not structurally effective in areas of negative moment area due to concrete cracking. Similar forms of construction using prestressed deck slabs but with steel beams has been carried out by some other researchers such as Kennedy and Grace (1982), Basu *et al* (1987), Saadatmanesh *et al* (1989) and Ayyub *et al* (1992). Tests of such structures have generally shown that the provision of prestressing in the slab over the support increased the cracking load and maintained the stiffness of the beams. Cracks could effectively be eliminated under service load and stresses in the tension flange of the steel beams at mid-span could be reduced. It has been shown that prestressing in the deck slab over the intermediate support increased the load carrying capacity of composite beams by about 20%, Basu *et al* (1987).

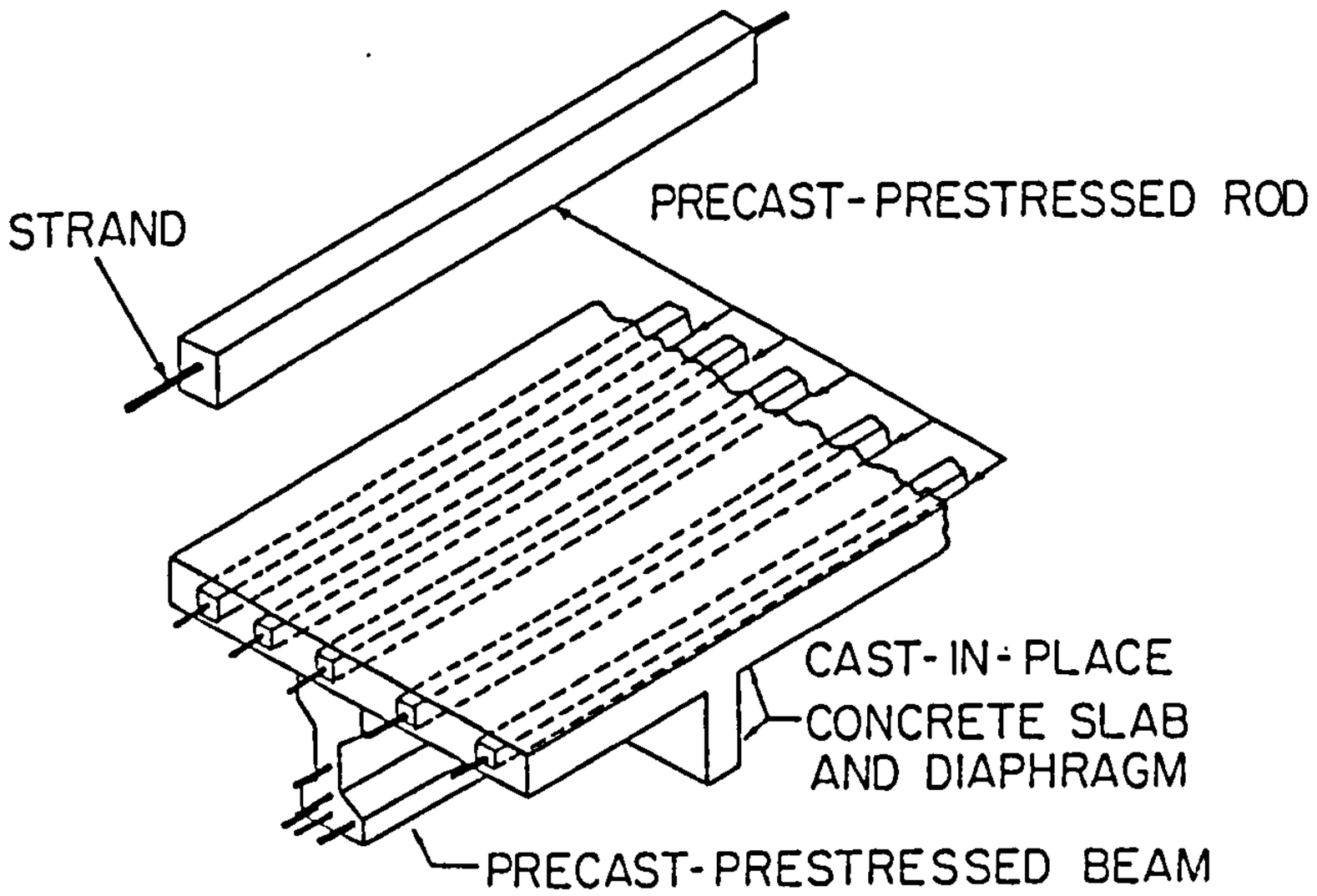

Figure 2.10: Use of pretensioned concrete rods to replace ordinary reinforcing bars for negative moment reinforcement (Burn, 1966)

2.3.2 Analytical investigations

Physical testing of prototype structural elements is often a preferred method of investigating the actual behaviour of structures under a given set of conditions because it provides physical observation as well as numerical results. However, if it is not possible to conduct experiments on prototype structures due to physical, economic or practical considerations, physical or analytical modelling can and has been adopted to simulate the actual behaviour of the prototype structures. Physical modelling has its own strengths and limitations. Sufficient work has been carried out on the elastic and post-elastic response of physical models to lend credibility to structural models subjected to instantaneous loads. Even then, the physical model should be as large as possible and it has been suggested that no particular problems producing unpredictable size effects exists for models of up to a scale ratio 1:4 (Noor and Boswell, 1992).

Analytical modelling also has its own strengths and limitations. However, with an increasing volume of knowledge with respect to material properties and structural behaviour of concrete structures, it is possible to develop analytical models that are able to predict the behaviour of structures subjected to special conditions by incorporating the relevant existing knowledge. This is further helped by the increasing availability of micro-computers where complex and lengthy calculations can be carried out at a high speed. The results of analytical predictions supported in parts by physical evidence have become one of the most important tools that help engineers understand the behaviour of many complex structures.

Analytical studies conducted on continuous precast prestressed concrete beams are accordingly reviewed in this section. Special emphasis is given to the time-dependent aspects of the studies. Since limited analytical work has been conducted on the long term behaviour of this type of structure, more general but relevant analytical work on time-dependent predictions of prestressed concrete structures are also reviewed.

2.3.2.1 Continuous precast prestressed concrete beams

The experimental evidence presented in an earlier section showed that substantial levels of sagging (positive) restraint moment can be developed at the support causing cracking at the bottom of the diaphragm. Complimenting the PCA experimental programme, an analytical procedure was proposed by Mattock (1961) to predict the restraint moment at the intermediate support due to the actions creep and shrinkage. It was proposed that moments at the support due to prestress and dead loads should be calculated as if the prestress and the dead loads had been applied to the continuous beam, not to the individual spans. This calculation may use any conveniently available elastic analysis for statically indeterminate structures. Mattock suggested that the prestress moment at each section should be based on the prestress force and the distance from the point of the prestress force to the centroid of the full composite section. The moments obtained by this analysis are then multiplied by a correction factor, $(1-e^{-\phi})$. ϕ is creep coefficient calculated from the time the continuity is made, not from the time the beams were pretensioned. The resulting moments are then considered as the restraint moments at the support after continuity is established.

The same procedure was also suggested to predict the restraint moment due to the action of differential shrinkage. Uniform moment due to the differential shrinkage was also assumed to be applied to the continuous beam and conventional elastic analysis for indeterminate structures may be used to compute the support moment due to this action. The moment due to the differential shrinkage, M_s, is given by,

$$M_s = \varepsilon_s E_{cs} A_{cs} \left(e_2' + t/2\right) \qquad \ldots(2.1)$$

where

ε_s	=	differential shrinkage strain
E_{cs} and A_{cs}	=	Elastic modulus and area of slab concrete
$(e'_2+t/2)$	=	distance between mid-depth of slab and centroid of composite section

The moment at the support resulting from Equation 2.1 is then multiplied by a factor $\left(\frac{1-e^{-\phi}}{\phi}\right)$, where ϕ is as previously defined. This method of analysis was later officially published by the PCA (Freyermuth, 1969) complete with design examples. This method is now known as the PCA Method (NCHRP, 1985).

It should be noted that the multipliers introduced by the method were derived from the rate of creep method. Derivation of the method has been described in great detail by Mattock (1961) and the summary of the derivation has also been presented by Clark (1981). The simplicity of the method, and probably because there are few other practical choices available, has made it the most popularly adopted method in current design practice (NCHRP, 1985; Clark, 1983 & 1997; Hambly and Nicholson, 1990 & 1992).

The PCA method mentioned above made some underlying assumptions that designers using it should be made aware of. The effects of the superposition of the prestressing moment and that due to the dead loads are not a true reflection of the actual behaviour of the structure. While superposition can often be used correctly for structures under short term loads, its application for predicting long term behaviour is highly questionable. This is because there is a continuous change in the interaction between the prestressing and the dead load moments, hence there is a continuous change in the state of the stress in the concrete. Since the creep phenomenon itself is stress dependent, ignoring the change in the stress is not strictly correct and can inflate the effects caused by the prestressing moment. Increased values of the prestressing moment will subsequently increase the values of the long term positive restraint moment at the support. Depending on the section along the beam being considered i.e. either the section at the mid-span or at the support, overestimating the positive restraint moment may not be conservative.

Overestimating the positive restraint moment at the support is not conservative as the compressive stress at the top fibre of the insitu crossheads may be correspondingly overestimated. By adding this compressive stress component to that from a subsequent

short term analysis for the applied live loads (causing tensile stress at the same fibre) may actually underestimate the resultant tensile stress. Overestimating the positive restraint moment will overestimate the tensile stress at the bottom fibre of the precast beams at mid-span. This requires a greater provision of pretensioned steel in the precast beams resulting in a conservative design.

Another feature by the method requiring careful consideration is in the use of the creep coefficients in the multipliers. Creep coefficients are merely predicted quantities whose value may vary greatly depending on the source of their derivation. It is, however, important to note that different derivations for the creep coefficient exist. ACI-209 (1982), for example, defines the creep coefficient as the ratio between creep strain at time *t* to the elastic strain at the time of stress application. On the other hand, the CEB-78 and CEB-90 codes define the creep coefficient as the ratio between creep strain at time *t* to the elastic strain as if the stress is applied at 28 days (see Chapter 3). Clearly the creep coefficients determined by the CEB definitions are numerically higher than those of the ACI-209 for structures loaded at concrete ages less than 28 days.

A more realistic analytical model incorporating the continuous change in the state of stress has been introduced by Suttikan (1978). He developed a computer program called PBEAM to analyse both time-dependent response and strength in continuous precast prestressed concrete beams. The beams were assumed to be straight in their original condition with a cross section having a vertical axis of symmetry through which loads were statically applied. The beams were idealised as straight lines and modelled as a series of *discrete elements* connecting members at nodal points in a time-step analysis using cracked section properties

The procedure divides time into small time intervals in which the responses are determined as if they are independent of time. The model computes the instantaneous response of continuous precast beams, and the response is then modified to obtain time-dependent values. The ACI-209 predictions for strength, elastic modulus, creep and shrinkage were adopted to predict the time-dependent characteristics of concrete, and the rate of creep method and superposition method of creep analysis under variable

stress were adopted to compute the creep strains. Results from the procedure were compared with the experimental values by Mattock *et al* (1960). It was found that the time dependent response of the analytical procedure resulted in error of only 21% when compared with the measured response. Based on this relatively good agreement with the experimental results, it was suggested that the program be used to carry out a parametric study to further investigate the behaviour of continuous precast prestressed beams under short and long term loads. This was achieved under the National Co-operative Highway Research Program (NCHRP), USA (NCHRP Report 322, 1985).

Comparisons of the restraint moments between the PBEAM and those of the PCA method suggested that the PCA method clearly yielded greater values of restraint moment. Using the same examples as those given in the design procedure of the PCA method (Freyermuth, 1969), the PCA method was shown to yield almost similar values of restraint moment when the continuity was assumed to be established at early ages (17 days). When the continuity was considered to be established at 37 days, the PCA method yielded values of restraint moment about 2.5 times greater. Greater differences were further observed when continuity at 67 days was considered where the PCA method yielded a sagging restraint moment of 302kip-ft (409.4kNm), whereas the PBEAM actually yielded a hogging restraint moment of 333kip-ft (451.4kNm). Despite the potential use of the PBEAM to handle complex analyses accounting for time-dependent effects, the study, however, acknowledged that it was difficult to use. It is also not very clear whether the effects of debonded tendons near the end beams can be accommodated by PBEAM.

A further computer program called BRIDGERM was developed within the NCHRP which was considered to be more user friendly. The complexity of the calculation used in the PBEAM program by considering cracked section properties was simplified by the BRIDGERM program which considered the uncracked state of the structures for the long term analysis. The program, however, adopted the PCA method to predict the time-dependent restraint moment the difference being that BRIDGERM considered the presence of the precast beam supports which are not removed after the establishment of the continuity for thin diaphragm.

Several recommendations with respect to the time-dependent behaviour of continuous precast prestressed beams were made based on the parametric study by the NCHRP. It was suggested that the degree of continuity in the connection for live loads could vary between nearly zero to 100 percent, depending on the material and the age when the continuity was established. The nearly zero continuity case relates to diaphragms fully cracked at the bottom fibres and the 100% continuity case represents the uncracked diaphragm. Cracks at the bottom section of the diaphragm occurred for beams connected at early age (17 days), and the continuity cannot be considered in the analysis for the subsequent application of live loads as long as these cracks remain open. Despite the calculations suggesting high values of positive restraint moment at the support causing cracking of the diaphragm, the report strongly recommended that positive moment reinforcement should not be used. It was argued that although the presence of the positive reinforcement increased the effects of continuity for the live loads (assuming the cracked condition is achieved under long term effects), it also increased the positive restraint moments at the supports, hence also throughout the span. Therefore, it was argued that the increase in positive moment within the span due to the application of live loads by not providing the positive reinforcement in the diaphragm is virtually balanced by the increased positive restraint moments should reinforcement be provided.

The recommendations given by the NCHRP still leave a great deal of uncertainty on the treatment of beams with respect to the effects of the restraint moment at the intermediate support due to long term effects. It is still unclear how different levels of sagging restraint moment affect the continuity of structures under live loads. If zero continuity is assumed, the structure is designed as simply supported for the live loads. Hence, no benefit of continuity is realised in the design. As it is, designers are still required to calculate the levels of the restraint moment at the support. Since both the PBEAM and the BRIDGERM programs are not commercially available, designers have to resort to the PCA method for the calculation of the restraint moment to estimate the value for each structure subject to different conditions.

2.3.2.2 Other related analytical work

It has been noted earlier that the time-dependent response of a prestressed concrete member is very complex. It depends on a lot of parameters including time-dependent properties of the materials, geometry of the structure, loading arrangements, levels of prestressing, methods and sequences of prestressing and structural configuration. The actions of creep and differential shrinkage of composite sections and the continuity of the precast members further complicate the problem of analysis under the long term effects. Although the creep and shrinkage actions may not affect the ultimate load capacity of the members, they may greatly affect the serviceability criteria of the members such as deflection and cracking which are important in many cases. Several analytical studies have been conducted using computer methods in an attempt to understand the complexity of the behaviour and to help predict the performance of such structures at service.

Early computer methods to predict time-dependent behaviour of simple prestressed concrete beams can be traced to the work by Corley, Sozen, and Siess (Suttikan, 1978). They developed a numerical step-by-step method based on the rate of creep and the superposition methods to estimate deformation under variable stress. The stress-strain relationships of the prestressing steel and concrete were assumed to be linear and the creep of concrete was proportional to the stress level at the time under consideration. Time was divided into several intervals of interest and the stress conditions and curvatures at any section along the beam at the ends of each time steps were calculated based on the stress conditions and curvatures of those sections up to the beginning of the corresponding time step. Deflections of the beam were calculated by integrating the curvatures along the span length.

Dilger (1982) proposed a method to analyse creep for uncracked beams that made use of the ageing coefficient developed by Bazant (1972) to calculate creep transformed sectional properties. With these properties, time-dependent stresses and deformation and statically indeterminate forces were determined by quasi-elastic analysis. The method is particularly useful for composite members or members with multiple layers of reinforcement.

A step-by-step procedure has been adopted to carry out time-dependent analysis of composite and non-composite beams by Ghali (1986), Teng (1991) and Abdul Karem and Tadros (1993). This procedure is very attractive as it enables the use of any structural analysis procedure and evaluates the required time-dependent deformations using any constitutive relations. It reduces the time-dependent problem of prestressed beams into a series of instantaneous response problems. It uses the initial strain concept i.e. the strain that is independent of the changes in strain during a certain time interval. The stress at each interval is calculated in terms of the stress increment that has occurred in the preceding interval.

Ghali (1986) further proposed a unified procedure for serviceability design of prestressed and reinforced concrete structures. The procedure derived equations based on equilibrium and section compatibility and accounted for instantaneous and time dependent changes in concrete, ordinary steel and prestressing steel. This avoided the need to compute prestress losses separately because the losses could be obtained as by-products of the analysis. Accuracy in the predictions of stress and strain in the prestressing steel, ordinary steel and concrete is always guaranteed through equilibrium of forces. The analysis assumed that applied bending moments had been computed (taken as input data), and no changes in section stiffness were taken into consideration. The analysis was general in that it could use any creep prediction method. The analysis, however, suggested the use of the age-adjusted effective modulus method to compute the time-dependent increment of creep strains to account for the sections under variable stress.

Abdel Karem and Tadros (1993) developed a computer program to evaluate stresses in concrete and steel at any cross section in a statically indeterminate composite beam or plane frame. The program was written specifically for beams made continuous using splicing of prestressing tendons, but the concept can be applied to any multistage construction procedure. The analysis takes into account time dependent and composite effects of the precast beams and cast-in-situ slab and adopt the superposition method for determining constitutive relation. The procedure uses the creep and shrinkage model

suggested by the CEB-FIP and ACI-209 and does not take the change in section properties with time into consideration.

The theoretical predictions of instantaneous and time dependent deformation of continuous precast beams described above assume an idealised structural system. They assume that precast beams are transformed from simple to fully continuous after the insitu connection has been established. This assumption is acceptable as long as there is no cracking over the support. For members in which continuity is achieved by the provision of prestressing, the assumption is valid for the major part of the loading range. But for members for which continuity is achieved using ordinary reinforcement in the deck slab, the assumption of full continuity may overestimate the negative bending over the support and underestimate the positive bending in the mid-span. This assumption will also underestimate deflections of members which is also undesirable.

Suter (1981) in his report on the design of a continuous structure made up of precast units argued that current approaches of structural analysis neglect possible discontinuity of deformations at joints. It is known that the discontinuity could reduce the value of negative moment at the support by a factor of two. In the report, it is suggested that depending on joint types, the moment over the support will vary from zero to its full value. It is proposed that these discontinuities can be modelled by a spring whose coefficient depends on the length and type of connection. The connections were classified as flexible, medium rigid, rigid and very rigid. The flexible connection was obtained by having hooks or lapped bar, the medium rigid was obtained by having unstressed steel bar within insitu concrete over the intermediate support, the rigid connection was obtained through welding of the ordinary reinforcing bars and the very rigid connection was obtained through prestressing (Figure 2.11). In view of the accompanying tests that were carried out, it was suggested that the proposed spring coefficient was applicable for sections with maximum depth of only 400mm. It was proposed that the construction of deeper beams for bridges by means of prefabricated members should adopt a quasi-rigid connection by means of prestressing or heavy reinforcement over the support.

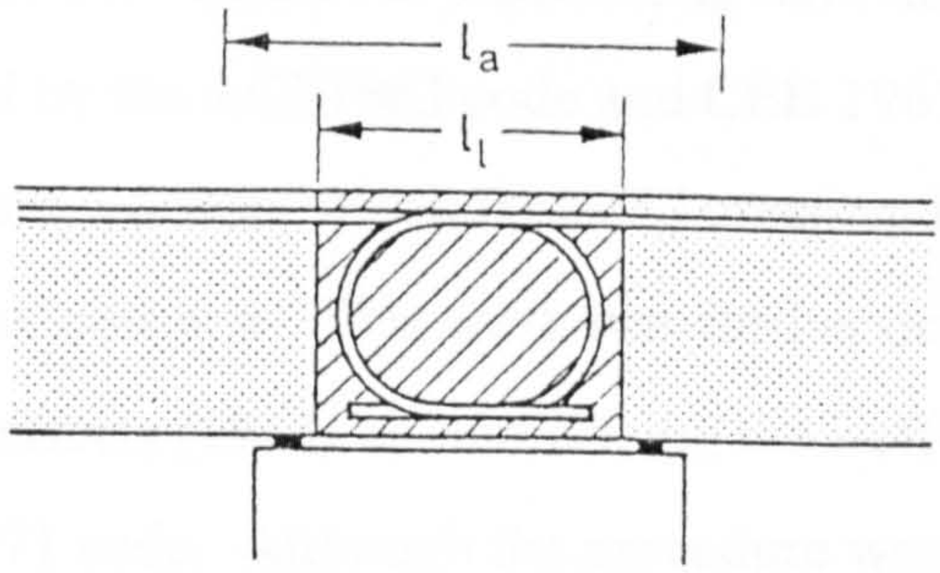

(a) Flexible connection (hooks)

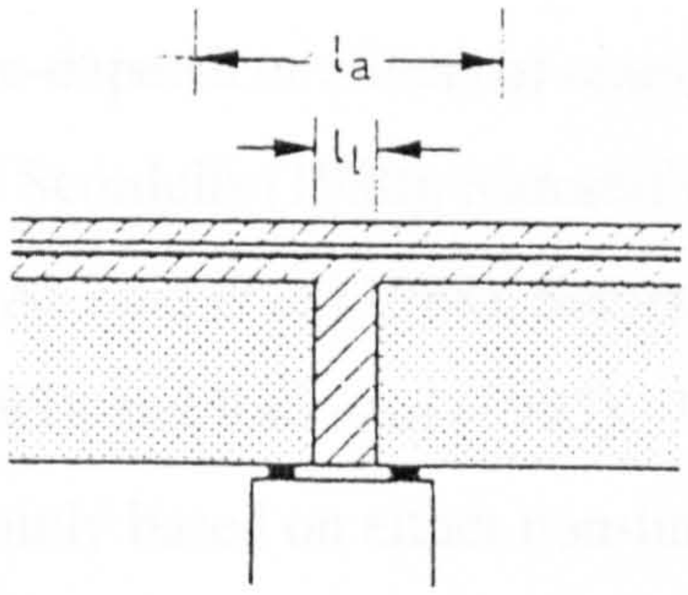

(b) Medium rigid connection (reinforcing bar across intermediate support)

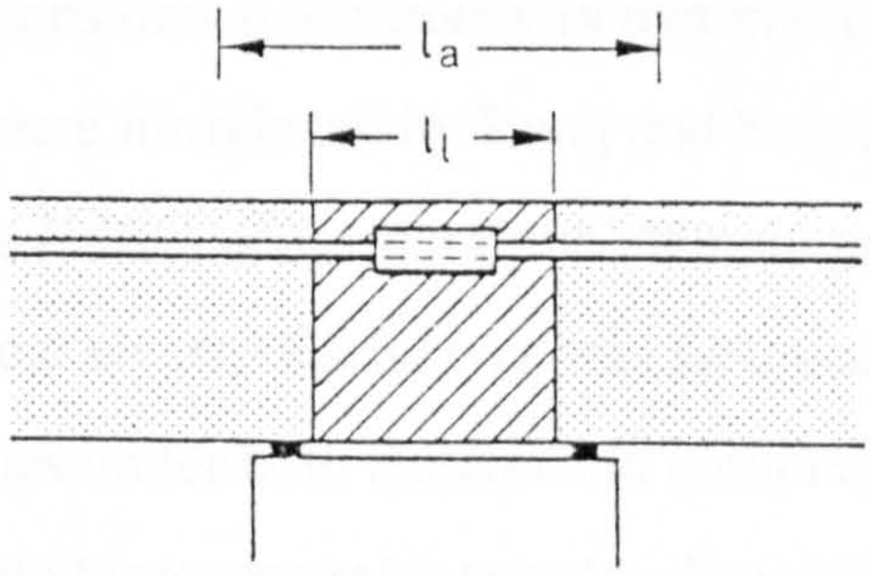

(c) Rigid and very rigid (welding or prestressing)

Figure 2.11: Classification for connection rigidity according to Suter (1981)

The analytical procedures described above only consider uncracked section properties. Cracked sections present another level of complexity in developing analytical predictions especially with the requirement to predict the time-dependent response.

Early analytical procedures developed for the long term deformation of cracked concrete structures only referred to conventional reinforced concrete members. Theoretical work by Yu and Winter (1960), and Gesund (1962) led to the use of a simple multiplier

applied to the instantaneous deformation to predict long term deformation. A similar approach was also adopted by the ACI 1963 code and CEB 1961. Branson and Ozell (1961) introduced a time-step concept which included creep and shrinkage and varying values of elastic modulus of concrete. This work was further developed by Branson to include tension stiffening effects (1963) by introducing the I-effective method which led to adoption by the ACI 1971 code. Although the procedure was only initially meant for reinforced concrete structures, Shaikh and Branson (1971) suggested that it could be used for cracked prestressed structures as well.

Direct theoretical work on time-dependent effects of cracked prestressed concrete structures are due to Kang and Scordelis (1980), Moustafa (1986), Inomata (1987), Gilbert (1988), Ghali (1988), Al-Zaid *et al* (1988), Samra (1989), Rao and Jayaraman (1989), Teng and Branson (1993), and Rao *et al* (1993). The procedures suggested by respective researchers were mainly based on either non-linear analysis, Branson's I-effective method, or the direct equilibrium and strain compatibility method.

Non-linear analysis which considers nonlinearity in material properties, section geometry and time effects were introduced by Kang and Scordelis (1980) and Moustafa (1986). Kang and Scordelis (1980) adopted a finite element approach which divides concrete sections into discrete layers. Each layer was assumed to carry tension up to its tensile strength. Creep values under both tension and compression were considered to be equal, and time was divided into several intervals. The method of superposition and the step-by-step procedure for computing time-dependent strains were adopted in the analyses. Time-step forward integration was performed and increments of displacement and strain were added successively. Equilibrium equations were updated at each step taking into account material and geometric nonlinearity.

Moustafa (1986) suggested a general and a very rigorous method of analysis that handled homogenous or composite sections under cracked or uncracked conditions. The procedures were derived considering nonlinearity of the concrete material in which time effects were included through the use of residual strain concepts. The program also adopted the superposition method and step-by-step procedure to compute the time-

dependent increments of the concrete strains. The generality of the method allowed the use of different time-dependent material predictions for creep and shrinkage.

The I-effective method that was initially introduced for cracked reinforced concrete structures (Branson and Ozell, 1963) was further developed by Teng and Branson (1993) to include prestressed concrete sections. The method extended the initial work which was based on the empirical formula for effective stiffness calculations of cracked prestressed concrete sections by introducing time stepping in its formulation. The method has been subjected to verification from various experiments (Teng, 1991). It was therefore, considered to be more acceptable compared to the CEB procedure for calculating cracked section stiffness where it is obtained by interpolation between the stiffness of uncracked sections to those of the fully cracked sections (Ghali, 1986).

Analytical methods derived from the basis of direct equilibrium and strain compatibility equations have been adopted by many investigators. The procedure assumes that initial stress at time to is known. The stress at any time t and at any layer of a section can then be given in terms of the initial stress, the change of stress and the neutral axis at any t. Both the changes in the stress and the neutral axis are unknown, but can be solve using the concept of strain compatibility and equilibrium of forces. Inomata (1987) has used a this concept and has assumed the non-coincidence of the levels of zero stress and strain. A fifth order solution was presented to compute the neutral axis locations of cracked prestressed beams. Rao and Jayaraman (1989) used a similar approach to Inomata, and reasserted the need to assume non-coincidence of zero stress and strain planes. They presented a third degree polynomial equation for solving the neutral axis locations.

Ghali and Favre (1986) also adopted equilibrium of forces and strain compatibility approach with the additional inclusion of applied normal forces. They did not include stiffening effects in the formulation but suggested the use of interpolation coefficients as given by the CEB procedure to estimate the cracked section stiffness. Application of the same principal has also been used by Al-Zaid *et al* (1988) and Gilbert (1988).

2.4 Discussion

Experimental evidence for continuous precast prestressed concrete beams using different methods of achieving continuity described in the previous sections suggests that such structures perform satisfactorily under short term service and ultimate loads. The structural behaviour of such members under service loads can be safely estimated using conventional method of elastic analysis. For precast members made continuous using ordinary reinforcing bars, the analysis at ultimate can also use the conventional analytical procedure where the plastic hinge formation or ductility of the section dictates the amount of elastic moment to be distributed to other parts of the structure. For members which use prestressed steel over the intermediate support, the analysis of the members at ultimate has to consider the contribution of secondary moments.

Review of the literature indicates that the contribution of the secondary moments at failure is still subject to ongoing debate. Lin and Thornton (1972), Scholz (1990), Wyche *et al* (1992) and Cohn and Lounis (1993) suggested that, if elastic moments are used for the calculation of the ultimate moment, then the secondary moment shall be included in the calculation. This is based on the view that full ductility cannot be achieved in prestressed concrete sections, hence the parasitic moments due the prestressed steel in continuous beams (or for that matter the secondary moments due to other effects such as support settlement) can still be present at ultimate.

Other researchers, however, have taken the view that full plasticity can be considered for prestressed concrete structures. Huber (1986) and Harajli and Hijazi (1991) conducted studies to evaluate the ultimate load carrying capacity of prestressed concrete members using plastic theory. It was assumed that structures always had sufficient ductility and no other form of failure occurred prior to collapse. They concluded that, since sufficient ductility is assumed to occur in prestressed members, the secondary moments disappear at the ultimate condition.

The difference in opinions regarding the treatment of secondary moments at ultimate are reflected by three different codes of practice (Wyche *et al*, 1992). The Australian code AS3600 treats the secondary moment due to prestressing at ultimate similar to other

secondary effects due to settlement, creep, shrinkage and temperature. It allows for 20-30% redistribution of the elastic moment where there is sufficient ductility. The American code ACI-89 suggests that all factored moments due to dead and live loads are redistributed depending on section ductility. The maximum percentage of redistribution allowed is 20%. The secondary moment due to prestressing force is then added to the adjusted moment without any factor. BS5400 treats secondary moments in a similar way as the Australian code, except it does not allow redistribution for members with cross sections exceeding 1200mm deep.

Despite the ongoing debate on the treatment of the secondary moments due to prestressing in continuous concrete beams, there is ample evidence to show that continuous precast prestressed concrete beams perform satisfactorily under short term service and ultimate loads and their behaviour can be predicted with reasonable accuracy using elastic theory. However, little experimental evidence exists for the long term effects of such structures, and merits further work. Since service load criteria are often important in concrete bridge design, more information on the long term service performance is needed.

Despite the lack of experimental data on the long term behaviour of continuous precast prestressed beams, an increasing amount of information on the long term behaviour of simply supported reinforced or prestressed concrete beams is readily available in literature. Information obtained for the simply supported beams is naturally vital in order to understand the behaviour of continuous beams. Since actual experiments of continuous precast prestressed beams could prove to be difficult and costly, this information can also be used to develop analytical methods that extend the predictions of the long term behaviour of prestressed simply supported concrete beams to statically indeterminate structures.

This review shows that there is still a gap in knowledge in predicting the restraint moment at the intermediate support for continuous structures made of precast prestressed concrete beams. The simplistic analytical method developed by the PCA over 30 years ago is still effectively used by current bridge designers. With subsequent

developments of time-dependent methods of analyses for prestressed concrete structures, the PCA method requires a second look. New procedures in structural analyses which incorporate the latest knowledge in creep and shrinkage predictions as well making full use of modern computer technology may be used to supplement the limited experimental work which exist or is likely to be carried out for this type of structure.

A large number of time-dependent analyses of prestressed concrete structures using computer methods have been developed of late. Most of the new computer programs adopt either the age-adjusted method and step-by-step procedure or the superposition method and step-by-step procedure for calculating time-dependent strains. Accordingly, there is probably little to separate between any modern computer programs dealing with the time-dependent analyses of prestressed concrete structures other than their ease of use.

CHAPTER THREE

PREDICTION METHODS FOR TIME-DEPENDENT ANALYSIS OF CONCRETE STRUCTURES

3.1 Introduction

In a simply supported reinforced concrete beam, the selfweight of the beam and any permanent load causes the member to deflect downwards, which increases with time due to the action of creep. If prestressing is introduced in the beam, the prestressing force and its eccentricity may cause the beam to camber. The action of creep due to the prestressing results in additional camber with time, while concrete shrinkage and relaxation of the prestressing steel reduce the prestressing force, and thus the camber. If the actions for the upward deflection are greater than those for the downward deflection, the beam will continue to camber with time. And if two adjacent simply supported beams are made continuous with a rigid connection, the beams at intermediate support are restrained from rotating and as a result, positive restraint bending moment may develop at the intermediate support.

Time-dependent behaviour of continuous precast prestressed concrete beams clearly depends on their creep and shrinkage characteristics. The effects of creep and shrinkage

on the time-dependent response of such structures depends not only on the properties of the materials, but also on the geometry of the structure, the amount of prestressing force in the precast sections, the method of achieving continuity over the intermediate supports, the sequence of construction and the age of the precast beams when continuity is established. The magnitude of restraint moment should be determined by considering the complex interactions between these factors. Different combinations of these factors may produce either positive or negative restraint moment. Both the magnitude and the direction of the restraint moment must be accurately assessed for each combination of these factors. However, it should be noted that the accuracy of such an analysis cannot be better than the individual predictions of creep, shrinkage and relaxation of the constituent materials.

This chapter presents the various methods available for the predictions of creep and shrinkage of concrete and relaxation of prestressing steel along with their effects in the time-dependent analysis of prestressed concrete structures.

3.2 Classification of Concrete Deformation

The three basic important deformations occurring due to changes in material characteristics, environmental and loading conditions are, instantaneous elastic deformation, creep and shrinkage deformation. For concrete under constant load and temperature, the total strains may be expressed as the sum of the instantaneous, creep and shrinkage strains.

3.2.1 Elastic strain

The instantaneous strain occurs immediately upon application of stress. It depends on the magnitude of the stress and the Young's modulus of concrete E_c, which is a function of the concrete age. At any time t, the instantaneous elastic strain, $\varepsilon_e(t)$, may be expressed as a function of stress, $\sigma(t)$ and elastic modulus, $E_c(t)$ which is given by

$$\varepsilon_e(t) = \frac{\sigma(t)}{E_c(t)} \qquad \ldots(3.1)$$

The elastic modulus increases with time at a decreasing rate. When the applied stress is constant, the instantaneous strain obtained from the above equation gradually decreases as the value of the elastic modulus increases. This is called true instantaneous strain which is usually less than the nominal instantaneous strain (Figure 3.1).

3.2.2 Shrinkage Strain

Shrinkage of concrete occurs due to its volumetric change even when it is free from externally imposed stress and temperature changes. The change in volume is generally attributed to the loss of free water to the atmosphere, the hydration process itself and the process of carbonation with chemicals in the surrounding environment. Figure 3.2 shows a general deformation of concrete due to shrinkage.

Some of the most important variables that affect shrinkage of concrete are:

(1) Aggregates: aggregates provide restraint against deformation of cement paste due to shrinkage. Generally, higher aggregate content in a concrete mix will result in less shrinkage.

(2) Water-cement ratio: shrinkage is directly proportional to the water content in a mix because an increase in the volume of water increases the potential for shrinkage.

(3) Member size and shape: drying takes place at a faster rate nearer to the surface than it does at the core of the member. This results in non-uniform shrinkage with the relatively moist inner core acts as a restraint (Hansen *et al,* 1966). Generally, small or narrow specimens have higher shrinkage.

(4) Ambient relative humidity: higher ambient relative humidity results in a smaller loss of free water to the atmosphere and hence lower shrinkage.

3.2.3 Creep strain

Figure 3.3 shows the deformation history of a concrete specimen under hygral equilibrium and a constant stress. When the stress is applied at time t_o, instantaneous elastic deformation occurs. As the time increases from t_o to t_i, an increase in

deformation occurs, although there is no shrinkage deformation. This increment of deformation with time is called creep. In the absence of shrinkage, creep is generally defined as that part of the total deformation which is in excess of the nominal instantaneous deformation. As the nominal instantaneous strain is always greater than the true elastic strain, creep may be defined as the deformation in excess of the true elastic deformation.

The magnitude of creep and its development with time are influenced by many factors, the most important of which are:

(1) Concrete strength: the greater the strength at the time of stress application, the less the ultimate creep deformation.

(2) Age at loading: younger concrete at the time of the application of stress will display greater creep deformation.

(3) Ambient relative humidity: creep deformation is inversely proportional to the ambient relative humidity

(4) Aggregates: bigger volumes of aggregate in a given concrete mix and higher elastic modulus of the aggregate display lower creep deformation.

(5) Stress: before the onset of internal cracking at 40-60% of the stress to strength ratio, creep is directly proportional to the stress. Creep increases non-linearly after the internal cracking.

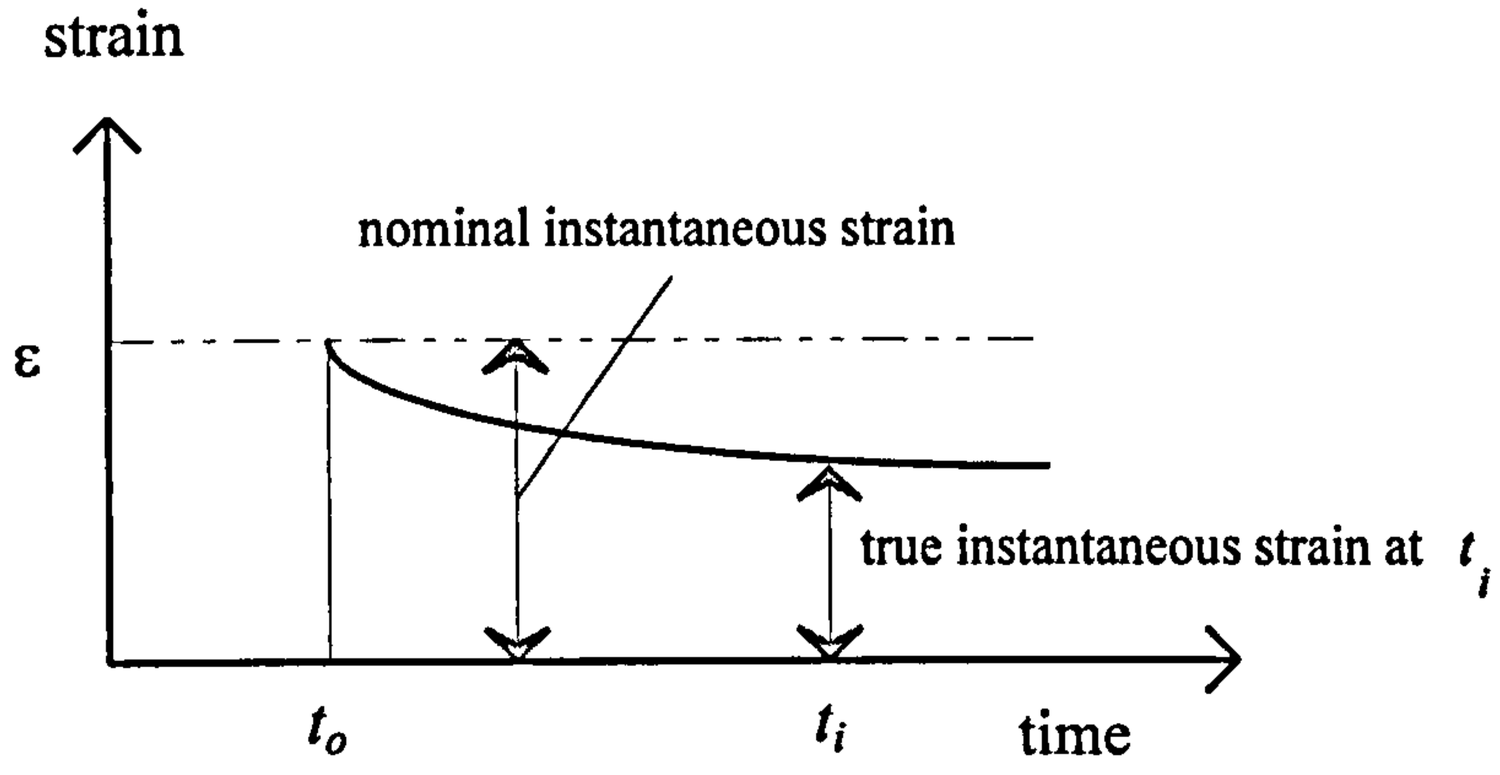

Figure 3.1: Nominal and true elastic strains under constant load

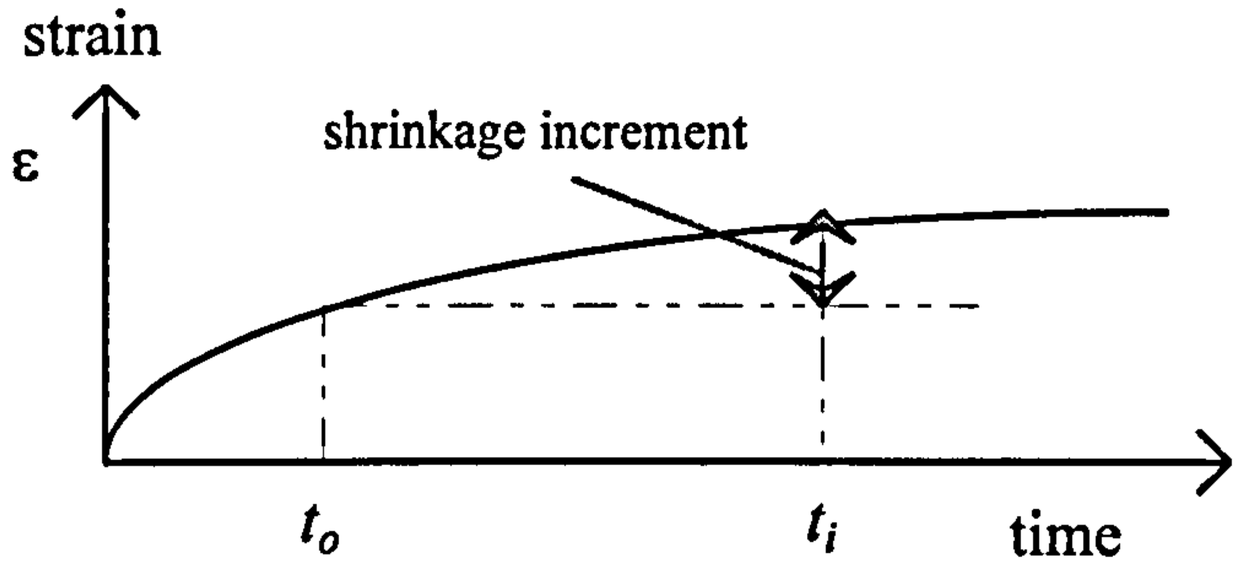

Figure 3.2 Shrinkage deformation of an unloaded specimen

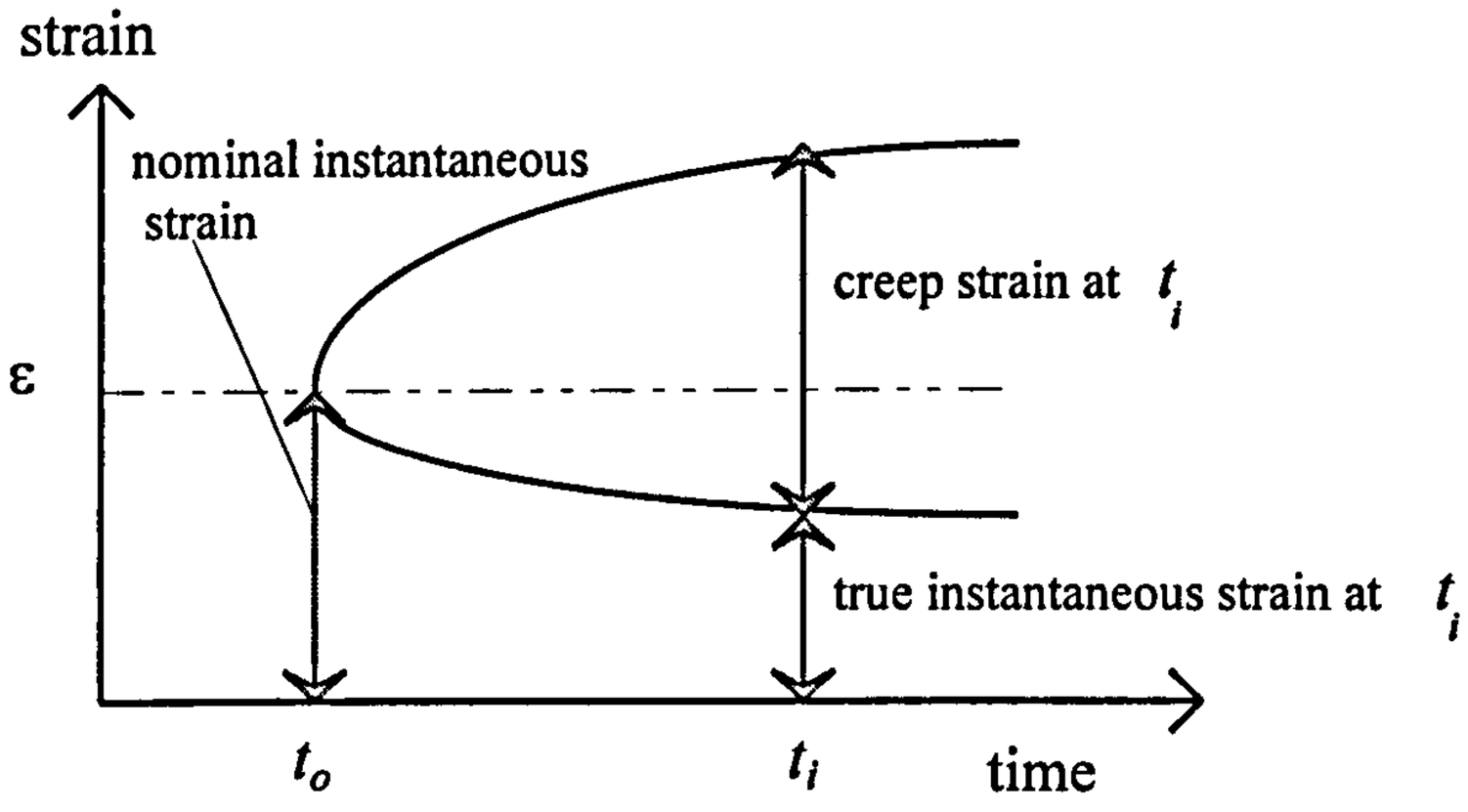

Figure 3.3: Creep deformation of a concrete specimen under constant load, imposed at time t_o

3.3 Creep and Shrinkage Predictions of Concrete

In order to accurately predict the effects of creep and shrinkage on concrete structures, two basic prerequisites are necessary. They are:

(1) Reliable data for creep and shrinkage properties of a given mix and conditions to which the structures are subjected.

(2) An analytical procedure for the inclusion of these material properties in structural analysis.

To obtain reliable data, laboratory tests may be carried out but this is not often practical.

The designers often have to resort to available models to predict these properties.

It has to be acknowledged that despite a long history of research in creep and shrinkage behaviour of concrete, it is still not possible to derive constitutive laws to completely describe its mechanisms. However, the huge amount of experimental data published in the literature makes it possible to describe the behaviour of concrete on a macro level. This enables researchers to formulate empirical models with varying degrees of complexity.

A creep model is generally represented by either a product or a summation function. Both CEB90 (CEB-FIP Model Code, 1990) and the ACI-209 (American Concrete Institute Committee 209, 1982) use a product function to describe creep taking age at loading as a major parameter. In ACI-209, this is then corrected by a function that describes creep development with time in which, relative humidity, consistency of fresh concrete, fine aggregate content, member size and air content are important considerations. The CEB90 approach is similar but mainly considers concrete strength, member size, and mean relative humidity. It is argued that it is more convenient to predict creep based on the four parameters contained in the CEB90 approach because they are readily known at a design stage. The mix constituents such as the water-cement ratio and the aggregate content are already considered in the prediction of the strength and the elastic modulus of concrete.

The summation function, as adopted by CEB78 (CEB-FIP Model Code for Concrete Structures, 1978) represents creep as summation of three creep components, that is rapid initial flow, delayed elastic strain and plastic strain. CEB78 models rapid initial flow using a logarithmic function (Equation 3.2a), but describes creep development with time in the form of delayed elasticity and plasticity using an exponential function (Equations 3.2b and 3.2c). The CEB78 model considers age at loading, member size, workability of fresh concrete and relative humidity in its formulation.

This study does not attempt to look into details of the many different models that describe these time-dependent properties. It does not seek to improve any of the predictive models. Rather it is more concerned with looking into the time-dependent effects in prestressed concrete structures. As is often noted, greater complexity in the

creep and shrinkage models does not always result in better or more accurate predictions. It is sufficient to include the three most common models referred to above as a basis for further investigation in this thesis. The three models used in this study are the results of a compromise between different schools of thought regarding the creep and shrinkage phenomena of concrete.

3.3.1 Formulation according to CEB-FIP Model Code For Concrete Structures, 1978 (CEB78)

3.3.1.1 Creep

CEB78 defines a creep coefficient as the ratio between creep strain at time *t* and the initial strain for a stress applied at 28 day. The creep coefficient can be estimated from

$$\phi(t,t_o) = \beta_a(t_o) + 0.4\beta_d(t,t_o) + \phi_f[\beta_f(t) - \beta_f(t_o)] \qquad ...(3.2)$$

The coefficient $\beta_a(t_o)$ represents the irreversible part of the deformation which is developed during the first few days after the load has been imposed (also called rapid initial flow) which is given by

$$\beta_a(t_o) = 0.4\left(1 - 0.2(\log t_o)\beta_{co} \geq 0\right) \qquad ...(3.2a)$$

$\beta_d(t,t_o)$ denotes a function corresponding to the development of delayed elastic strains which is given by

$$\beta_d(t-t_o) = 1 - e^{(-0.5(t-t_o)^{0.3})} \qquad ...(3.2b)$$

$\beta_f(t)$ represents a function corresponding to development with time of the delayed plasticity depending on notional member size, h_o.

$$\beta_f(t) = 1 - e^{(1-t^{\beta_{th}})} \qquad ...(3.2c)$$

where,

$$\beta_{th} = \frac{1}{15}\log\frac{25700}{h_o}, \text{ and} \qquad h_o = \frac{2A_c}{u} \text{ (mm)}$$

A_c is the cross sectional area of the structural member and u is the perimeter in contact with the atmosphere.

ϕ_f represents a basic flow coefficient which depends on ambient relative humidity, RH and is represented by

$$\phi_{f1} = 6.5 - 0.05RH \qquad \text{...(3.2d)}$$

Creep strain is given by

$$\varepsilon_c(t,t_o) = \frac{\sigma_o}{E_{c28}}\phi(t,t_o) \qquad \text{...(3.3)}$$

where E_{c28} is the elastic modulus of concrete at 28 days.

The modulus of elasticity at any time related to concrete strength is given by

$$E_c(t) = 9.5[f_c(t)]^{1/3} \text{ (GPa)} \qquad \text{...(3.4)}$$

where f_c(t) is compressive cylinder strength in MPa. The strength development of the concrete with age is expressed as

$$f_c(t) = 1.463\left(\frac{t^{0.73}}{t^{0.73}+5.27}\right)f_{c28} \text{ (MPa)} \qquad \text{...(3.4a)}$$

where f_{c28} is the strength of concrete at 28 days.

The above expression is suggested by Gilbert (1988) to represent the graph given by the CEB78.

3.3.1.2 Shrinkage

Shrinkage strains, $\varepsilon_{sh}(t,t_s)$ can be obtained from the following expression:

$$\varepsilon_{sh}(t,t_s) = \varepsilon_{so}[\beta_s(t-t_s) - \beta_s(t_o-t_s)] \qquad ...(3.5)$$

The value ε_{so} is a basic shrinkage coefficient which depends on ambient humidity. For a normal concrete and ordinary Portland cement and ambient relative humidity (*RH*) between 40 to 99 percent

$$\varepsilon_{so} = -0.00069\left(1-\left(\frac{RH}{100}\right)^3\right) \qquad ...(3.5a)$$

The value β_s is the coefficient that describes shrinkage development with time which is given by

$$\beta_s(t-t_s) = \left[\frac{\bar{t}}{0.018(h_o)^2+\bar{t}}\right]^{0.6} \qquad ...(3.5b)$$

where $\bar{t}$ is defined as duration of drying which is computed as $\bar{t} = t - t_s$ or $\bar{t} = t - t_o$.

Unless otherwise stated, Equations 3.2-3.5 are given by CEB Bulletin No.199 (1990). The expressions modify the original representation of the various coefficients in CEB78 which are represented by graphs and tables. The modification does not change the basic philosophy of the original CEB78 formulations. Representation of the coefficients using mathematical function is convenient for direct computation using computer codes.

3.3.2 Formulation according to the American Concrete Institute Committee 209, (ACI-209, 1982)

3.3.2.1 Creep

ACI-209 uses a combination of hyperbolic and power functions to represent a creep coefficient which is given by

$$\phi(t,t_o) = \frac{(t-t_o)^{0.6}}{10+(t-t_o)^{0.6}}\phi_u \qquad ...(3.6)$$

where the ultimate creep coefficient ϕ_u, is represented by

$$\phi_u = 2.35(k_1 k_2 k_3 k_4 k_6 k_7) \qquad ...(3.7)$$

Coefficients k_1 - k_7 represent empirical correction factors to account for different parameters that affect the magnitude of creep. The coefficient k_1 considers condition where the ambient relative humidity is greater than 40 percent and is given by

$$k_1 = 1.27 - 0.0067RH \qquad ...(3.7a)$$

The coefficient k_2 consider the age at loading, where for age at load application between one and 7 days, k_2 is given

$$k_2 = 1.13t_o^{-0.094} \qquad ...(3.7b)$$

For age greater than 7 days, k_2 is given by

$$k_2 = 1.25t_o^{-0.118} \qquad ...(3.7c)$$

The value k_3 considers the workability of concrete mix, measured by slump, sf (mm). It is given by

$$k_3 = 0.82 + 0.00264sf \qquad ...(3.7d)$$

The coefficient k_4 considers the factor due to shape and size of the specimen (measured by volume to surface area ratio, *V/S*) which is given by

$$k_4 = \frac{2}{3}\left[1 + 1.13e^{(-0.0213v/s)}\right] \qquad ...(3.7e)$$

The effect of fine aggregate content is represented k_6, which depends on the percentage of fine to total aggregate by weight (*F*). It is given by

$$k_6 = 0.88 + 0.0024F \qquad ...(3.7f)$$

The effect of air content, α (expressed in percentage of total volume) is represented by k_7

$$k_7 = 0.46 + 0.09\alpha \geq 1.0 \qquad ...(3.7g)$$

Creep strain is computed based on the strength and elastic modulus of concrete at the age of loading. Under constant stress (σ_o), the load-dependent strains are given by

$$\varepsilon(t) = \frac{\sigma_o}{E_c(t_o)}[1 + \phi(t, t_o)] \qquad ...(3.8)$$

The elastic modulus of elasticity at any time *t* depends concrete density, ρ (kg/m^3) and strength, f_c (MPa) which is given by

$$E_c(t) = 0.043\sqrt{\rho^3 f_c(t)} \ \text{(MPa)} \qquad ...(3.9)$$

Concrete strength depends on cement type and curing condition. For a concrete mix using ordinary cement and cured under steam condition, the strength is given by

$$f_c(t) = \frac{t}{1.0 + 0.95t} f_{c28} \ \text{(MPa)} \qquad ...(3.9a)$$

For a concrete mix using ordinary cement and cured under moist condition, the cylinder strength is given by

$$f_c(t) = \frac{t}{4.0 + 0.85t} f_{c28} \text{ (MPa)} \qquad ...(3.9b)$$

3.3.2.2 Shrinkage

ACI-209 uses a hyperbolic function to represent the shrinkage-time relationship. Shrinkage strain at any given time t is given by

$$\varepsilon_{sh}(t) = \frac{t - t_s}{35 + (t - t_s)} \varepsilon_{shu} \qquad \text{for moist cured} \qquad ...(3.10a)$$

$$\varepsilon_{sh}(t) = \frac{t - t_s}{55 + (t - t_s)} \varepsilon_{shu} \qquad \text{for steam cured} \qquad ...(3.10b)$$

where ε_{shu} is the ultimate shrinkage strain which depends on relative humidity, shape and size, slump, ratio of fine aggregate, air content and cement content.

$$\varepsilon_{shu} = 780 k_1' k_3' k_4' k_5' k_6' k_7' k_8 \qquad ...(3.11)$$

Correction factor due to relative humidity is given by Equations 3.9a and 3.9b, where RH is measured in percentage.

$$k_1' = 1.4 - 0.01RH \text{ , for } 40 \le RH \le 80 \qquad ...(3.11a)$$

or,

$$k_1' = 3.00 - 0.03RH \text{ , for } 80 > RH \le 100 \qquad ...(3.11b)$$

Correction factor due to slump is given by

$$k_3' = 0.89 + 0.00161sf \qquad ...(3.11c)$$

Correction factor due to size and shape factor (*V/S*) is given by

$$k_4' = 1.2e^{(-0.00472v/s)} \qquad ...(3.11d)$$

Standard curing duration for steam and moist cured concrete are 3 and 7 days, respectively. There is no correction factor for steam cured concrete, but for moist cured concrete, the correction factor due to curing duration other than 7 days can be obtained from Table 3.1. Correction factors due to percentage of fine to total aggregate (in weight, *F*) are given by Equations 3.11e and 3.11f.

Table 3.1: Curing factors for different curing duration

Moist curing duration (days)	1	3	7	14	28	90
k_5'	1.2	1.1	1.0	0.93	0.86	0.75

$$k_6' = 0.3 + 0.014F \text{ , for } F < 50\% \qquad ...(3.11e)$$

or,

$$k_6' = 0.9 + 0.02F \text{ , for } F \geq 51\% \qquad ...(3.11f)$$

Correction factors due to air and cement content (α and c) are given by Equations (3.11g) and (3.11h) respectively.

$$k_7' = 0.95 + 0.008\alpha \qquad ...(3.11g)$$

$$k_8' = 0.75 + 0.00061c \qquad ...(3.11h)$$

3.3.3 Formulation according to CEB-FIP model code 1990 (CEB90)

3.3.3.1 Creep

CEB90 utilises a complex combination of hyperbolic and power expressions to represent creep curves. Creep coefficient is given by

$$\phi(t,t_o)=\phi_o\beta_c(t-t_o) \qquad ...(3.12)$$

The coefficient ϕ_o is a notional creep and $\beta_c(t-t_s)$ is the coefficient to describe the development of creep with time after loading. Both quantities may be obtained from Equations 3.12a-3.12f.

$$\phi_o=\phi_{RH}\beta(f_{c28})\beta(t_o) \qquad ...(3.12a)$$

$$\phi_{RH}=1+\frac{1-0.01RH}{0.46(h_o/100)^{1/3}} \qquad ...(3.12b)$$

$$\beta(f_{c28})=\frac{5.3}{(f_{c28}/10)^{0.5}} \qquad ...(3.12c)$$

$$\beta(t_o)=\frac{1}{0.1+(t_o)^{0.2}} \qquad ...(3.12d)$$

$$\beta_c(t-t_o)=\left[\frac{t-t_o}{\beta_H+(t-t_o)}\right]^{0.3} \qquad ...(3.12e)$$

$$\beta_H=150\left\{1+\left(\frac{1.2RH}{100}\right)^{18}\right\}\frac{h_o}{100}+250\le 1500 \qquad ...(3.12f)$$

CEB90 defines creep coefficient as the ratio of creep strain to elastic strains at 28 days. For a constant stress applied at time t_o, creep strains are given by

$$\varepsilon_c(t,t_o)=\frac{\sigma_c(t_o)}{E_{c28}}\times\phi(t,t_o) \qquad ...(3.13)$$

where,

$$E_{c28}=2.15\times10^4\left(\frac{f_{c28}}{10}\right)^{1/3} \quad \text{(MPa)} \qquad ...(3.13a)$$

$$E_{ci}(t) = \exp\left\{s\left[1-\left(\frac{28}{t}\right)^{0.5}\right]\right\}^{0.5} E_{c28} \quad \text{(MPa)} \qquad \text{...(3.13b)}$$

$$f_c(t) = \exp\left\{s\left[1-\left(\frac{28}{t}\right)^{0.5}\right]\right\} f_{c28}. \quad \text{(MPa)} \qquad \text{...(3.13c)}$$

The value s in Equations 3.13b and 3.13c depends on the type of cement. It equals to 0.2 for rapid hardening high strength cement, 0.25 for normal hardening cement, and 0.38 for slowly hardening cement.

3.3.3.2 Shrinkage

Shrinkage strains are given by

$$\varepsilon_{cs}(t,t_s) = \varepsilon_{cso}\beta_s(t-t_s) \qquad \text{...(3.14)}$$

The value ε_{so} is a notional shrinkage coefficient and $\beta_s(t\text{-}t_s)$ is the coefficient that describes shrinkage development with time given by Equations 3.14a-d.

$$\varepsilon_{cso} = \varepsilon_s(f_{c28})\beta_{RH} \qquad \text{...(3.14a)}$$

where,

$$\varepsilon_s(f_{c28}) = \left[160 + 10\beta_{sc}\left(9-\frac{f_{c28}}{10}\right)\right]\times 10^6 \qquad \text{...(3.14b)}$$

and $\beta_{sc} = 4$ (slow cement), 5(ordinary cement), 8(rapid hardening cement).

The correction factor due to relative humidity is given by

$$\beta_{RH} = -1.55\left[1-\left(\frac{RH}{100}\right)^3\right] \quad \text{for } 99\% \geq RH \geq 40\%. \qquad \text{...(3.14c)}$$

Development of shrinkage with time is given by

$$\beta_s(t-t_s) = \left[\frac{t-t_s}{350(h_o/100)^2+(t-t_s)}\right]^{0.5} \qquad \text{...(3.14d)}$$

3.4 Relaxation of Prestressing Steel

Prestressing steel may be provided in several different forms, namely, wires, strands or bars. These may be produced by different processes, but all of them have a high elastic range which makes them suitable for prestressing. Different processes, however, produce different characteristics under high levels of sustained stress. These may generally be categorised as *stress-relieved* steel, which is also known as *normal-relaxation* steel, or *stabilised* steel, which is also known as *low-relaxation* steel (Hurst, 1988). Relaxation is defined as the phenomenon whereby the force required to maintain a highly stressed steel at a given elongation reduces with time.

Relaxation of steel is time-dependent and is negligible under small levels of initial stress. Normal-relaxation types of wire and strand can have around 8% relaxation loss under an initial stress of 70% of the ultimate. Low-relaxation types of wires and strand may typically have relaxation loss of about 2.5% under similar levels of initial stress (Hurst, 1988). It is always desirable to have experimental data on relaxation characteristics which are either obtained independently or supplied by the steel manufacturer. In the absence of these data, the time function for steel relaxation obtained from tests as suggested by Magura *et al* (1964) may be used. The following expression is slightly changed from the original expression given by Magura *et al* where the duration considered (t-t_o) has been changed from hours to days (Neville *et al*, 1983)

$$f_{pr}(t) = \frac{f_{pi}}{c}\left[\log_{10} 24(t - t_o)\right]\left(\frac{f_{pi}}{f_{py}} - 0.55\right) \qquad ...(3.15)$$

where f_{pi} = Initial stress, should be greater than $0.55f_{pu}$

f_{py} = $0.85f_{pu}$ for normal relaxation steel

= $0.9\,f_{pu}$ for low relaxation steel

c = 10 for normal relaxation steel

= 45 for low-relaxation steel

f_{pu} = ultimate strength of prestressing steel.

In prestressed concrete members, strain in the prestressing steel does not remain constant. The strain decreases due to creep and shrinkage of the concrete and this will have the effect of reducing the relaxation loss. Ghali and Trevino (1986) introduced a reduction coefficient χ_r to take this effect into consideration. For many practical cases, χ_r can be taken equal to 0.8, that is a 20% reduction in the loss due to relaxation (Collins and Mitchell, 1990).

3.5 Time-dependent Analysis of Concrete Structures

All predictive models for time-dependent material properties of concrete described in the Section 3.3 use plain concrete specimens subjected to constant stress as the basis of their formulations. However, reinforced and prestressed concrete structures do not contain plain concrete and are always subject to varying stresses. In conventional reinforced concrete structures, steel reinforcement provides restraining effect to concrete deformation causing the stress in the concrete to change. The varying stress in prestressed concrete structures is compounded by the loss of prestressing force due to creep and shrinkage of concrete and relaxation of prestressing steel.

This section reviews the four most common analytical procedures where the time-dependent material models are applied to structural problems. These four analytical procedures are the effective modulus method (EMM), age-adjusted modulus method (AEM), rate of creep method (RCM), and superposition method (SSM). Detailed discussions and comparisons of these methods and other available methods are available elsewhere [Gilbert (1988), Neville (1970), Rusch (1978), and Chiorino *et al* (1984)].

3.5.1. The effective modulus method (EMM)

The EMM states that creep is treated as delayed elastic strain and is taken into account simply by reducing the elastic modulus of concrete. The elastic modulus of concrete $E_c(t)$ is reduced to an effective modulus, $E_e(t)$ by the creep coefficient given by

$$E_e(t,t_o) = \frac{E_c(t_o)}{1+\phi(t,t_o)} \qquad ...(3.16)$$

For concrete where a constant stress applied at time t_o, total time-dependent strain is thus given by

$$\varepsilon(t,t_o) = \frac{\sigma(t_o)}{E_e(t,t_o)} + \varepsilon_{sh}(t) \qquad ...(3.17)$$

where $\varepsilon_{sh}(t)$ is shrinkage strain at any time t.

Equation 3.17 indicates that the creep strain depends on the current level of stress and is, therefore, independent of stress history. The method predicts that if the stress is entirely removed, the creep strain disappears indicating complete creep recovery which does not agree with experimental observations. The method may be good for concrete under constant stress or if the stress is first applied when the concrete is mature. However, the method is unsuitable for many practical cases in prestressed concrete structures where the concrete is normally stressed at an early age.

3.5.2 The age-adjusted effective modulus method (AEM)

An adjustment to the EMM to include the effect of ageing is introduced in the Age-adjusted Effective Modulus Method (AEM). The concept of the age-adjusted effective modulus is described in Figure 3.4 where a specimen is subject to two types of stress history. The first is a constant stress σ_o applied instantaneously at t_o; the second is a gradually applied stress $\sigma(t)$ that reaches full magnitude σ_o at time t_1. The creep strain at any time t greater than t_o produced by the instantaneously applied stress is always greater than that resulting from the gradually applied stress. This is due to ageing because a concrete loaded at an earlier age will result in greater creep deformation. Since the stress increment or decrement in reinforced or prestressed concrete structures are rarely instantaneous, the reduced creep deformation due to this effect needs to be considered. This reduction is introduced by a term called an ageing coefficient, $\chi(t,t_o)$.

The creep strain at time t due to gradually applied stress $\sigma(t)$ is given by

$$\varepsilon_c(t) = \frac{\sigma(t)}{E_c(t_o)}\chi(t,t_o)\phi(t,t_o) \qquad ...(3.18)$$

If an instantaneous stress σ_o is initially applied at t_o and then gradually reduced with time, the change in stress at any time t is given by

$$\Delta\sigma(t) = \sigma(t) - \sigma_o \qquad ...(3.18a)$$

The total strain, $\varepsilon(t)$ may be expressed as the sum of the strains produced by the initial stress (σ_o), the gradually applied stress increment or decrement ($\Delta\sigma$) and the shrinkage strain as given by

$$\varepsilon(t) = \frac{\sigma_o}{E_c(t_o)}[1+\phi(t,t_o)] + \frac{\Delta\sigma(t)}{E_c(t_o)}[1+\chi(t,t_o)\phi(t,t_o)] + \varepsilon_{sh}(t) \qquad ...(3.19a)$$

or,

$$\varepsilon(t) = \frac{\sigma_o}{E_e(t,t_o)} + \frac{\Delta\sigma(t)}{\overline{E}_e(t_o)} + \varepsilon_{sh}(t) \qquad ...(3.19b)$$

where $E_e(t,t_o)$ is the effective modulus from Equation 3.15 and $\overline{E}_e$ is the age-adjusted effective modulus which is given by

$$\overline{E}_e(t,t_o) = \frac{E_c(t_o)}{1+\chi(t,t_o)\phi(t,t_o)} \qquad ...(3.19c)$$

The ageing coefficients are determined from associated creep coefficients, hence factors affecting the ageing coefficients are similar to those for creep. Calculation of the coefficients can be very time consuming. However, based on parametric analysis, a simple expression for the coefficient has been adopted by the CEB-FIP Model Code 1990 (clause 5.8.4.3). The single expression takes the time at load application as the only parameter affecting the coefficient and it is given by

$$\chi = \frac{t_0^{0.5}}{1 + t_0^{0.5}} \qquad ...(3.19d)$$

Some researchers (Chiorino *et al* (1984), Ghali (1986) and Gilbert (1988)) have suggested that an ageing coefficient can be taken to be equal to 0.8 when the age of the first loading exceeds about 5 days and the final creep coefficients lie between 1.5 and 3.5. This covers most practical situations for prestressed concrete structures. Upper and lower limits of 0.9 and 0.6 have been suggested Gilbert (1988) the lower value relates to load application at younger ages. The method approaches the effective modulus method as the coefficient approaches unity. This can be the case if the load is applied to mature concrete.

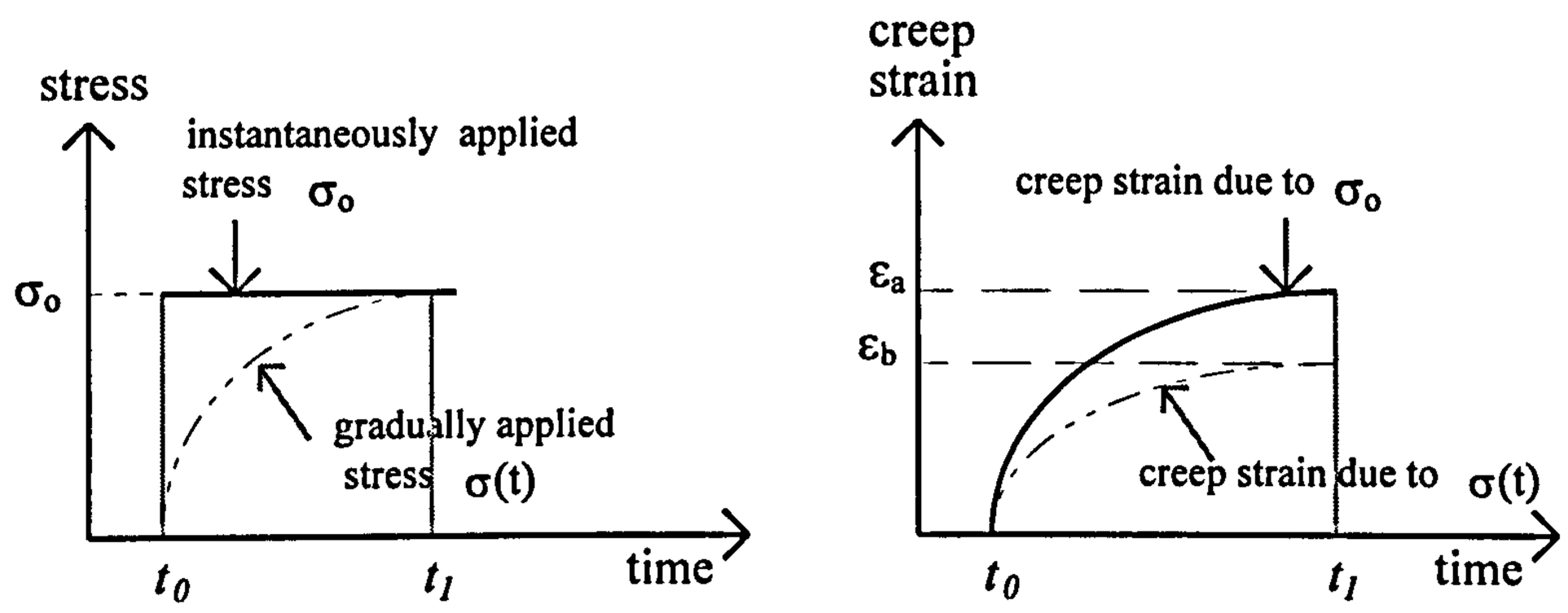

Figure 3.4: Creep of concrete due to constant stress and gradually applied stress

3.5.3 Rate of creep method (RCM)

The basic assumption of this method is that the rate of change of creep with time is independent of the age at loading. This means that the creep curves for the same concrete for loads applied at different ages are parallel. This assumption requires only a single creep curve to be used to calculate creep strains for any given stress history.

An example of this assumption is shown in Figure 3.5. For the parallel creep curves, the ordinates EF and CD are assumed to be equal any time t greater than t_1 in which CD=CF-AB. This may be expressed as

$$\phi(t,t_i) = \phi(t,t_o) - \phi(t_i,t_o) \qquad ...(3.20)$$

which indicates that a creep-time curve due to any stress applied at time t_i is completely defined by a single curve, $\phi(t,t_o)$. Therefore, the creep strain at any time t caused by a stress applied at time t_i is given by

$$\varepsilon_c(t,t_i) = \frac{\sigma_i}{E_c(t_o)}\phi(t,t_i) = \frac{\sigma_i}{E_c(t_o)}\left[\phi(t,t_o) - \phi(t_i,t_o)\right] \qquad ...(3.21)$$

The change in creep strain between any two times t_1 and t_2 after loading at t_i is given by

$$\Delta\varepsilon_c(t,t_i) = \varepsilon_c(t_2,t_i) - \varepsilon_c(t_1,t_i) = \frac{\sigma_i}{E_c(t_o)}[\phi(t_2,t_i) - \phi(t_1,t_i)] \qquad ...(3.22)$$

This method also assumes the shrinkage strain at any time t is related to creep coefficient, ϕ by the following expression:

$$\varepsilon_{sh}(t) = \frac{\varepsilon_{sh}(\infty)}{\phi(\infty,t_o)}\phi(t,t_o) \qquad ...(3.23)$$

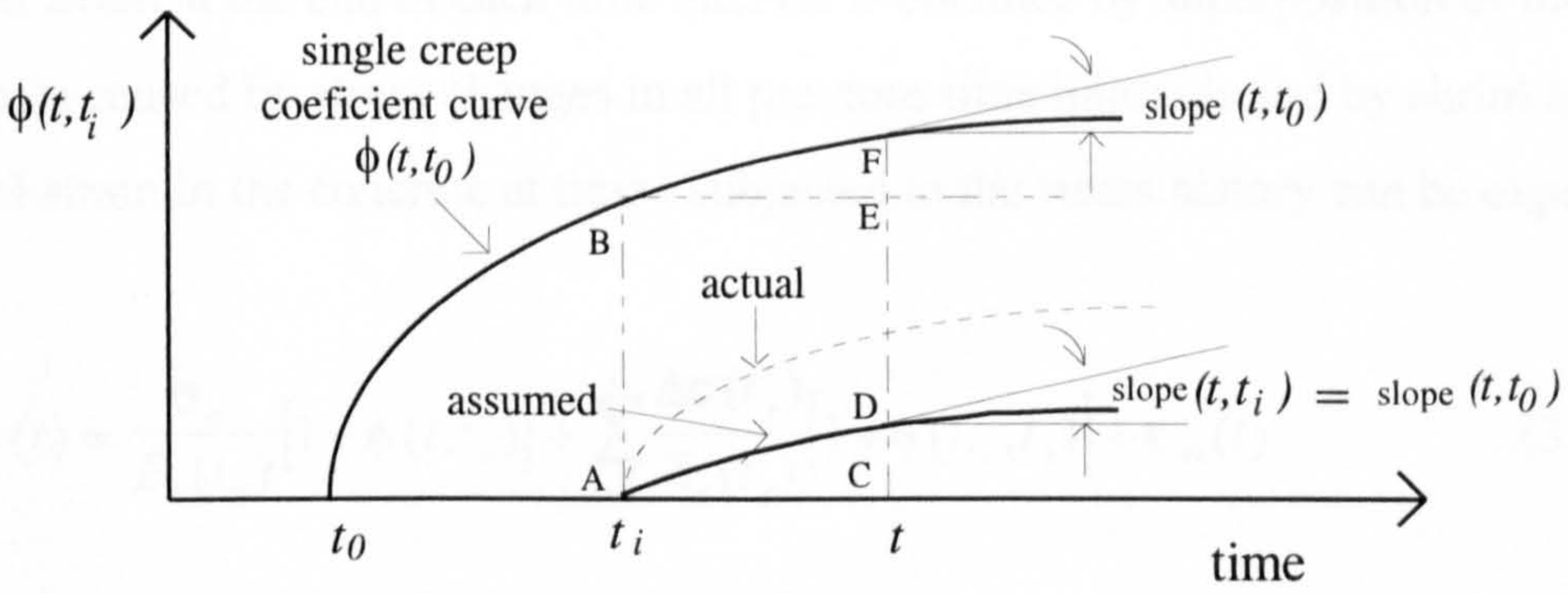

Figure 3.5: Parallel creep curves assumed in the rate of creep method (Gilbert, 1988)

3.5.4 Principle of superposition and step-by-step method (SSM)

The principle of superposition states that creep strains produced by a stress condition applied at time t is assumed to be unaffected by any other stress condition applied either earlier or later. It asserts that total strain at any given time is obtained by adding (or subtracting) independent strains caused by different stress histories and duration. This principle can be illustrated by Figure 3.6. Figures 3.6(a) and (b) show that there are two different creep curves for two stresses applied at two different times. If the two stresses are added, an increasing stress history develops and the creep curve produced by this is assumed to be equal to the sum of the creep curves produced by each stress increment acting independently, Figure 3.6(c). If the initial stress is reduced to an equal amount at t_2, a decreasing stress history develops and the creep due to the second stress is subtracted from the creep due to the initial stress as if the stresses acted independently.

Since stress increases or decreases gradually in practice, a step-by-step method has to be adopted in order to apply the principle of superposition. Figure 3.7 shows an example of a structure subjected to a gradually decreasing stress condition. In this example, time is divided into several intervals and the stress increment, $\Delta\sigma\ (t_i)$, which occurs during the i-th interval is assumed to be applied at the middle of that interval. The increments of instantaneous plus creep strain caused by $\Delta\sigma\ (t_i)$ are calculated at the end of each subsequent time interval using the appropriate elastic modulus and creep coefficients. The total strain at the end of each time interval is obtained by superposition of the strain increments caused by stress changes in all previous time intervals and by shrinkage. The total strain in the concrete at time t subjected to the stress history can be expressed as

$$\varepsilon(t) = \frac{\sigma_o}{E_c(t_o)}\left[1+\phi(t,t_o)\right] + \sum_{j=1}^{i}\frac{\Delta\sigma(t_j)}{E_c(t_j)}\left[1+\phi(t_{i+},t_j)\right] + \varepsilon_{sh}(t) \qquad \text{...(3.24)}$$

Equation (3.24) indicates that a large amount of data and computation is required where at each time step, the elastic modulus and creep coefficients have to be specified and previous stress history stored throughout the analysis. More accurate analysis also requires smaller time increments. This procedure is not convenient for manual calculation, but has been readily adopted in many computer analyses.

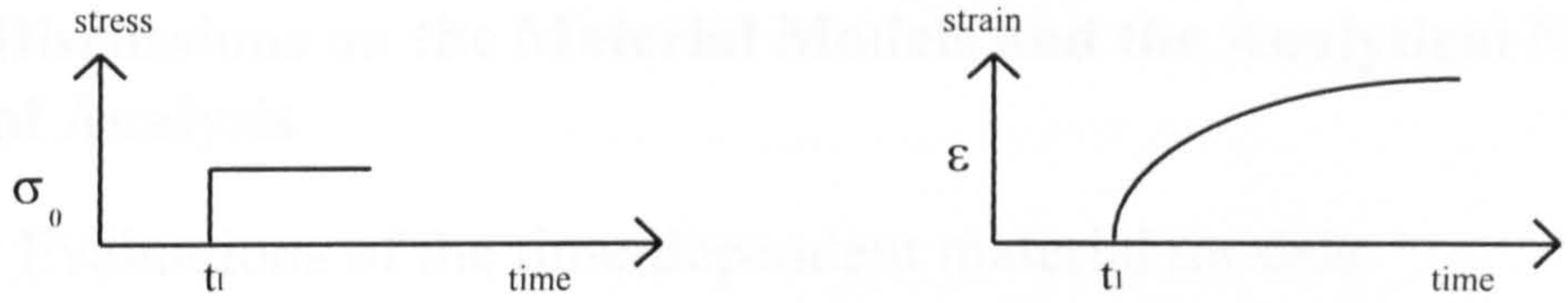

(a) creep strain due to stress applied at time t_1

(b) additional creep strain due to additional stress applied at time t_2

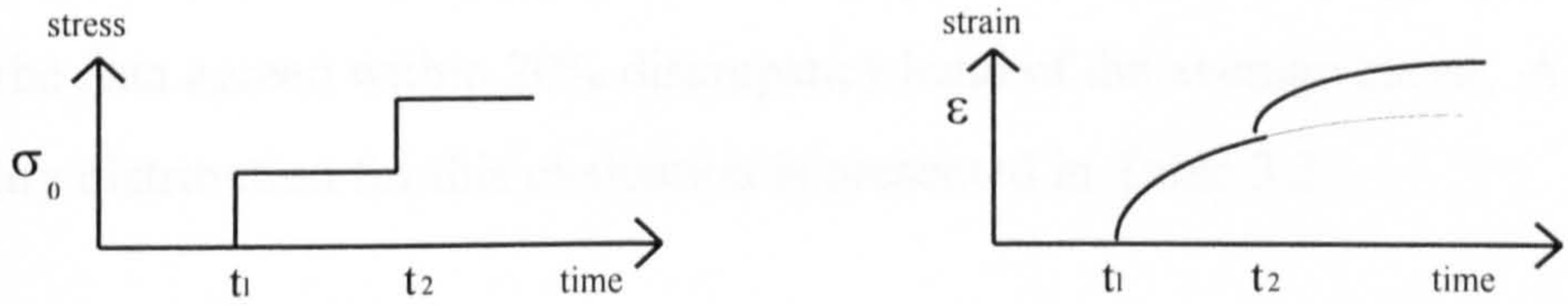

(c) resultant creep strain due to stress increasing stress history

(d) resultant creep strain due to decrasing stress history

Figure 3.6: The principles of superposition of concrete strains

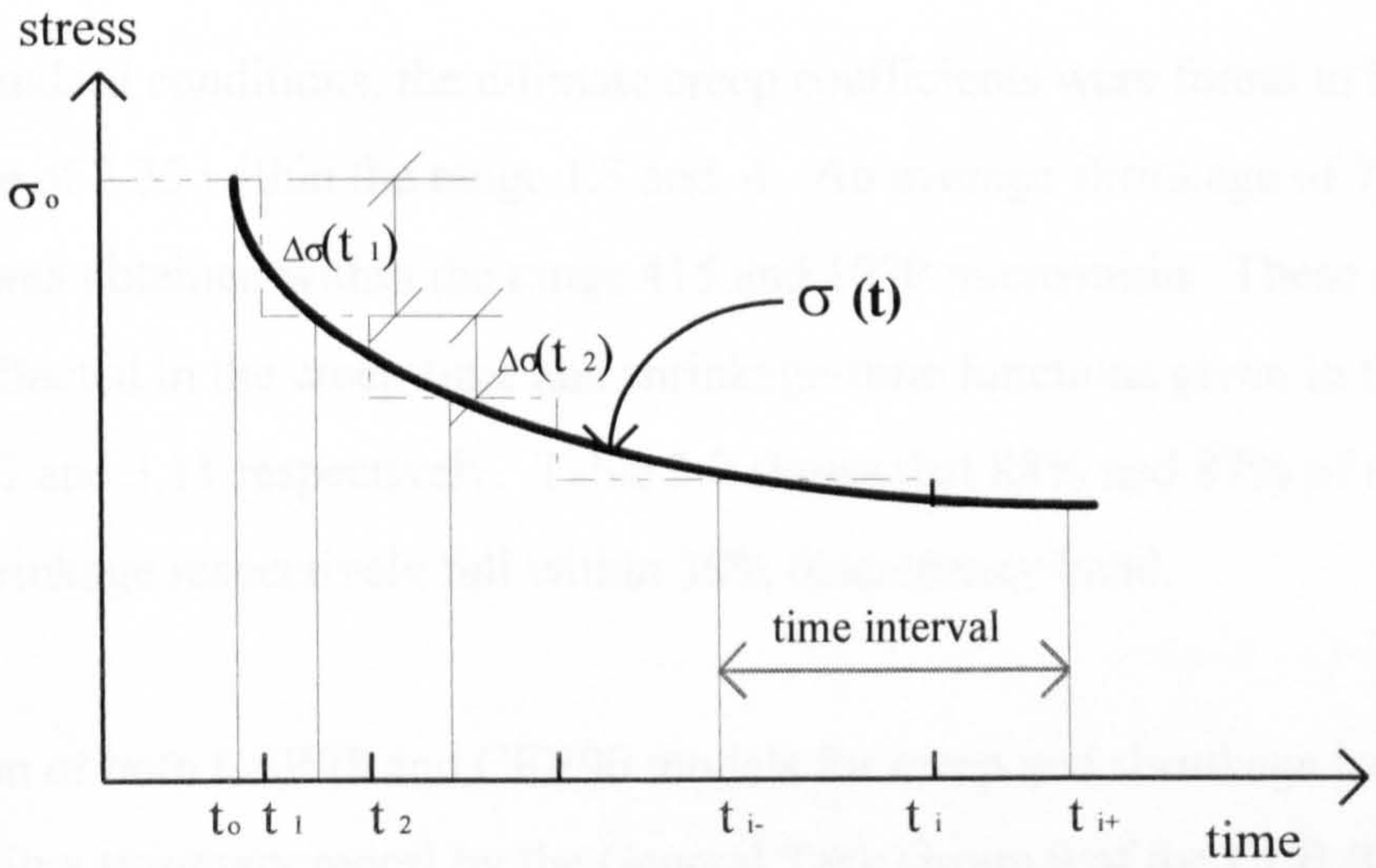

Figure 3.7: Step-by-step method for continuously varying stress

3.6 Discussions on the Material Models and the Analytical Methods of Analysis

3.6.1 Evaluations of the time-dependent material models.

The accuracy of the material models has been evaluated using a large number of experimental observations. The ACI model was empirically derived using a curve fitting technique where an average curve was adopted as the predictive model (Branson, 1977). In the case of the concrete strength and the elastic modulus, the average curves were evaluated against more than 250 specimens of concrete of different mixes and densities. It was found that 62% of the data agreed within 10% discrepancy band and 93% of the data agreed within 20% discrepancy band of the average curve. A detailed probability distribution for this evaluation is presented in Table 3.2.

Branson (1977) also obtained time-dependent creep and shrinkage models through curve fittings of the experimental results of a total of 470 creep and 356 shrinkage specimens. The ultimate creep and shrinkage values under 'standard conditions' were used as the basis of the creep-time and shrinkage-time functions. The standard conditions refer to circumstances where the concrete is subject to average ambient humidity of 40% or less, has an average thickness of 150mm and subject to loading age of 7 days for moist cured and 1-3 days for steam cured condition. Other 'non-standard conditions' were calculated using correction factors.

Under the standard conditions, the ultimate creep coefficients were found to have an average value of 2.35 within the range 1.3 and 4. An average shrinkage of 780 microstrain was obtained within the range 415 and 1070 microstrain. These average values are reflected in the creep-time and shrinkage-time functions given in the Equations 3.7 and 3.11 respectively. Table 3.2 shows that 88% and 87% of the data for creep and shrinkage respectively fall within 30% discrepancy band.

An evaluation of both CEB78 and CEB90 models for creep and shrinkage have been documented in a summary report by the General Task Group 9 of the CEB (CEB Bulletin No. 199, 1990). A statistical evaluation using a computerised data bank for creep and shrinkage was reported. A total of 150 experiments for creep and 167 for

shrinkage were used in the evaluation. The experimental data were scrutinised to meet specified conditions to ensure that they reflected a reasonable range of concrete compositions.

The accuracy of the prediction models were characterised by the $\overline{F}$ and $\overline{V}$ values, where $\overline{F}$ is an indication of overall error in the prediction and $\overline{V}$ corresponds to a mean coefficient of variation in the prediction. $\overline{F}$ is evaluated for a fixed time i.e. deformation after a fixed time of loading or drying, and $\overline{V}$ refers to the mean error over the entire duration of loading or drying. The statistical evaluation shows that both CEB models give better prediction for long term values compared to the prediction over the entire duration of loading (or drying). CEB90 represents a significant improvement over CEB78 in the errors associated with the prediction of shrinkage. A summary of this evaluation is tabulated in Table 3.3.

Table 3.2: Probability of agreement between predictive models given by ACI-209 and experimental data (Branson, 1977)

discrepancy band	Percentage of data agreeing within discrepancy band (%)			
	concrete strength, f_c (253 specimens)	elastic modulus, E_c (274 specimens)	creep (479 specimens)	shrinkage (356 specimens)
10%	62	62	34	32
20%	93	83	66	64
30%	97	95	88	87
40%	100	99	96	96
50%	100	100	99	99

Table 3.3: A summary of statistical evaluations of creep and shrinkage model given by CEB78 and CEB90 (CEB Bulletin No. 199, 1990)

Statistical values	CEB78		CEB90	
	creep	shrinkage	creep	shrinkage
$\overline{F}$ (%)	27.2	22.9	not given	19
$\overline{V}$ (%)	20.6	44.6	20.4	32.9

3.6.2 Numerical evaluation of the development of strength and elastic modulus.

The previous evaluations confirm that it is not possible to have an exact prediction of the time-dependent properties of concrete. Each model was evaluated against a different set of data but produces similar confidence levels for the accuracy of the predictions. Although the previous evaluations were carried out independently for the strength, creep and shrinkage properties, the following evaluations attempt to make numerical comparisons between the different code approaches. These are compared individually for strength, creep and shrinkage as well as for the combined effect.

To enable a comparison to be made between the models, a similar concrete composition is assumed. The mix composition and operating conditions assumed for this comparison are:

(a) Concrete density	= 2400 kg/m^3
(b) Cement content	= 350 kg/m^3
(c) Percentage of fine to total aggregate content	= 40%
(d) Air content	= 5%
(e) Slump of fresh concrete	= 50mm
(f) Moist curing duration	= 7 days
(g) Applied stress	= 5 MPa

Other conditions are varied to ascertain their effects on the concrete. Concrete design strength is varied from 30 MPa to 60 MPa, average relative humidity is varied between 40 to 90%, the age at stress application is varied from 3 to 100 days, and the volume to surface area ratio is varied between 50 to 125mm. These variations are assumed to represent the majority of the circumstances under which prestressed structures are used.

Results of the concrete strength and elastic modulus for the three different methods are tabulated in Tables 3.4-3.6. The results show that CEB78 and ACI-209 predict slower strength development compared to CEB90, but CEB78 gives the greatest long term strength at 36% more than the strength at 28 days. CEB90 gives the long term strength

of about 20% of the 28 day values compared to 15% by ACI-209. For the development of the elastic modulus, ACI gives the slowest rate where only 60% of the 28 day values are achieved on the third day, compared to 76% and 77% by CEB78 and CEB90 respectively.

The development of the elastic modulus is more directly related to concrete deformation where a lower modulus of elasticity corresponds to a higher initial strain for a given stress level. Hence, for a similar creep coefficient, total creep deformation will tend to be higher in concretes having a lower modulus of elasticity. The difference in the prediction of the elastic modulus development probably explains why the definition of creep coefficients are different for ACI-209 than for CEB78 and CEB90. CEB defines the creep coefficient as the ratio of creep strain to the elastic strain as if the stress is applied at 28 days, while ACI-209 defines the creep coefficient as the ratio of creep strain to the elastic strain at the age of stress application. Other conditions being similar, CEB90 is expected to give lower creep coefficients compared to CEB78 because it consistently gives higher values of the elastic modulus for all strength and age ranges. By definition, ACI is expected to produce the lowest creep coefficient for ages at loading less than 28 days because it predicts slower development of elastic modulus.

ACI-209 treats strength development differently between the moist cured and steam cured concrete. For precast prestressed structures where the concrete is steam cured and stress is applied at an early age, the strength development is closer to that of the CEB predictions. Figure 3.8 compares strength and elastic modulus development for concretes under moist and steam curing conditions. On the third day, the steam cured concrete attains an elastic modulus of 28.2 GPa as opposed to 21.6 GPa for the moist cured concrete. The difference in the elastic modulus prediction will have a direct effect on time-dependent deformation predicted by ACI. This difference becomes insignificant if stress is applied to the concrete after about 14 days because the predicted elastic modulus values are virtually identical after this age, Figure 3.8.

Calculations of the different strengths and their respective elastic modulus values also show that the strength and the elastic modulus at any given age are linear functions of the 28 day values (see Table 3.7). Given the 28 day values, the strength and elastic modulus can be predicted with reasonable accuracy. This linear relationship can be very useful where the strength and the elastic modulus development for any concrete strength can be defined by a single curve.

Table 3.4: Strength and elastic modulus development according to CEB78

age	$f_c(28)$=30 MPa		$f_c(28)$=40 MPa		$f_c(28)$=50 MPa		$f_c(28)$=60 MPa	
(days)	f_c(MPa)	E_c(GPa)	f_c(MPa)	E_c(GPa)	f_c(MPa)	E_c(GPa)	f_c(MPa)	E_c(GPa)
3	13.0	22.4	17.4	24.6	21.8	26.5	26.1	28.2
7	19.3	25.4	25.7	28.0	32.2	30.2	35.6	32.1
14	24.8	27.7	33.1	30.5	41.4	32.9	49.7	34.9
28	30.0	29.5	40.0	32.5	50.0	35.0	60.0	37.2
100	37.0	31.7	49.5	34.9	61.8	37.6	74.2	39.9
360	40.9	32.7	54.6	36.0	68.2	38.8	81.9	41.2

Table 3.5: Strength and elastic modulus development according to ACI-209

age	$f_c(28)$=30 MPa		$f_c(28)$=40 MPa		$f_c(28)$=50 MPa		$f_c(28)$=60 MPa	
(days)	f_c(MPa)	E_c(GPa)	f_c(MPa)	E_c(GPa)	f_c(MPa)	E_c(GPa)	f_c(MPa)	E_c(GPa)
3	13.7	18.7	18.3	21.6	22.9	24.2	27.5	26.5
7	21.1	23.2	28.1	26.8	35.2	30.0	42.2	32.8
14	26.4	26.0	35.2	31.0	44.0	33.6	52.8	36.8
28	30.2	27.8	40.3	32.1	50.4	35.9	60.4	39.3
100	33.7	29.4	44.9	33.9	56.2	37.9	67.4	41.5
360	34.8	29.8	46.4	34.5	58.1	38.5	69.7	42.2

Table 3.6: Strength and elastic modulus development according to CEB90

age	$f_c(28)$=30 MPa		$f_c(28)$=40 MPa		$f_c(28)$=50 MPa		$f_c(28)$=60 MPa	
(days)	f_c(MPa)	E_c(GPa)	f_c(MPa)	E_c(GPa)	f_c(MPa)	E_c(GPa)	f_c(MPa)	E_c(GPa)
3	17.9	24.0	23.9	26.4	29.9	28.4	35.9	30.2
7	23.4	27.4	31.2	30.1	38.9	32.4	46.7	34.5
14	27.0	29.4	36.1	32.4	45.1	34.9	54.1	37.1
28	30.0	31.0	40.0	34.1	50.0	36.8	60.0	39.1
100	33.7	32.9	45.0	36.2	56.2	39.0	67.5	41.4
360	35.9	33.9	47.9	37.4	59.9	40.2	71.9	42.8

Table 3.7: Ratio of strength and elastic modulus values at different ages to 28 day values for all strength ranges

Age	CEB78		ACI-209		CEB90	
(days)	$f_c(t)/f_c(28)$	$E_c(t)/E_c(28)$	$f_c(t)/f_c(28)$	$E_c(t)/E_c(28)$	$f_c(t)/f_c(28)$	$E_c(t)/E_c(28)$
3	0.43	0.76	0.45	0.67	0.60	0.77
7	0.64	0.86	0.70	0.83	0.78	0.88
14	0.83	0.94	0.87	0.97	0.90	0.95
28	1.00	1.00	1.00	1.00	1.00	1.00
100	1.23	1.07	1.11	1.06	1.12	1.06
360	1.36	1.11	1.15	1.07	1.20	1.09

3.6.3 Evaluation of the development of creep and shrinkage.

Figures 3.9-3.11 show comparisons for creep, shrinkage, and total time-dependent strains for the three models. The graphs represent concrete subjected to an applied stress of 5 MPa at 7 days, exposed to average relative humidity of 50%, moist cured for 7 days and with a volume to surface area ratio of 50mm. The elastic strains at the age of loading are 178, 198 and 146 microstrains for CEB78, ACI-209, and CEB90 respectively. The high initial strain given by ACI corresponds to the low elastic modulus at the time of loading which invariably results in a low creep coefficient. The corresponding creep coefficients at 1000 days after loading are 2.973, 1.538 and 3.171 for CEB78, ACI-209 and CEB90 respectively. The elastic strains at 28 days are more

uniform where CEB78, ACI-209 and CEB90 give the values of 158, 156, and 166 microstrains respectively.

The graphs show that the ACI model gives the highest estimates for shrinkage strains but the lowest estimates for creep strains. Both CEB models tend to give lower estimates for shrinkage strains but higher values for creep. However, total strains due to both of these effects plus the instantaneous strain are about the same for all three models. The difference between the maximum and minimum predictions for creep and shrinkage strains for the given conditions are equivalent to 29% and 18% of the maximum creep and shrinkage values. The difference between the maximum and minimum values is drastically reduced to 6.5% for total strain. This observation points to the fact that the models cannot completely predict all cases of creep and shrinkage deformation individually, but they can be accurate enough to predict total time-dependent deformation of plain concrete. This calculation also demonstrates that the elastic, creep and shrinkage components of deformation tend to compensate each other to arrive at a similar magnitude of total deformation. This is perhaps explained by the fact that creep is always measured as a strain in excess of the elastic and shrinkage strains.

The graphs also show that shrinkage is more dominant than creep at an early stage for the ACI model, while the CEB models predict creep and shrinkage to be similar during this same stage. This pattern continues with increasing age but at a decreasing rate. For long term deformations (calculated at 1000 days), ACI predicts that for this particular mix and conditions, the shrinkage strains form about 52% of the total deformation while creep strains form about 29%. The CEB78 model predicts shrinkage and creep to represent about 46% and 39% of the total deformation respectively. CEB90 gives almost equal values where shrinkage represents about 43% and creep represents about 41% of the total deformation. This observation is particularly important when the creep and shrinkage effects are evaluated on prestressed concrete members. As has already been discussed, creep due to prestressing effects produces the opposite deformation to that of shrinkage in flexural members.

As noted earlier, under an increasing elastic modulus of concrete, the actual elastic strain is always smaller than the nominal instantaneous value. This is particularly significant if the stress is applied at an early age, and the ACI prediction for strength development under moist conditions is used. Figure 3.12 shows the elastic strains are gradually decreasing with age, with ACI showing the largest reduction. This obviously has an effect on the prediction of creep which is always smaller than the actual creep strain. For the conditions given in Figure 3.13, the nominal creep strain given by ACI after 1000 days is 341 microstrain, but the actual creep strain is 448 microstrain. This indicates that the ACI model predicts creep to be about 25% less than the actual creep value. Similar patterns of instantaneous, creep and shrinkage deformations, albeit with varying proportion, are observed if the concrete is subject to different conditions such as design strength, relative humidity, age at loading, and volume to surface ratio. Further parametric analyses have been undertaken and are discussed in Chapter 5.

3.6.4 Evaluation of the time-dependent analysis of concrete structures.

The analytical methods described in Section 3.4 are linear approximations of non-linear problems. Several attempts to evaluate these linear approximations have been published. The Concrete Society (1973) published a technical report on creep of structural concrete in which a short evaluation of some analytical methods were made. The effective modulus method, rate of creep method and superposition method were compared against experimental results obtained from Ross (1958). The measured values were taken from two concrete specimens, one subject to variable stress in the form of a rising step function and the other in the form of a falling step function. The comparison showed that EMM overestimated both creep and creep recoveries, whereas the RCM underestimated both quantities. The SSM also overestimated both creep and creep recovery but to a lesser degree compared to the EMM.

In a more rigorous study, Bazant and Najjar (1987) carried out numerical comparisons of the effective modulus, age-adjusted, rate of creep, rate of flow (RFM), Levi's and Arutyunian's method of analysis. The comparisons were made with the superposition method which was considered to offer exact solutions. All methods were applied to solve a variety of different problems such as prestress loss, stress distribution and

deflections in composite beams, buckling deflections of a slender symmetrically reinforced concrete column, members subject to shrinkage only and cracked reinforced concrete beams. Overall, it was shown that the AEM was the most accurate method, while the EMM and RFM came next in accuracy. The AEM and EMM were considered the simplest methods of all because they reduced the creep problem into a simple elastic problem. Other methods were not only less accurate, they were also more complicated for manual calculation.

Comparisons with relatively recent experimental results (Choumann, 1990) are also presented here to provide general appreciation of each method of analysis. Concrete columns of 100x180mm cross section and 435mm long were subjected to a constant load 7 days after casting equivalent to a stress of 5 MPa. The sections contained varying degrees of reinforcement and were exposed to controlled relative humidity with the range 45-55%. The initial concrete stress is expected to decrease due to the restraining effect provided by the reinforcement, whereas plain sections will remain under a constant stress of 5 MPa throughout the experiment. Calculation for time-dependent deformation according to the EMM, RCM and AEM methods were determined after Gilbert (1988) and calculation according to the SSM method used a commercial computer codes, ADAPT (1993).

Figure 3.14 shows an example of the effect of reinforcement on time-dependent deformation of concrete under constant axial load (Chouman, 1990). The steel reinforcement not only restrains the concrete deformation, it also reduces the compressive stress in the concrete. Indeed, for highly reinforced concrete, it is possible to have resultant tensile stress in the concrete due to the combined action of creep and shrinkage. From the experiment it is clear that bonded reinforcement affects time dependent deformation of the concrete. For measurements after 8 months, the deformation for the section with 4.47% of reinforcement is about 50% less than that for the plain section.

Figures 3.15-3.18 show comparisons between different methods of analysis and the experimental results. For these particular specimens, all figures show that the SSM and AEM consistently give very good predictions of total time-dependent deformation of the concrete. EEM gives a very close approximation to AEM for lightly reinforced sections, but a larger margin is observed for specimens with a high reinforcement content. This is possibly due to the greater stress reduction in the concrete with a higher reinforcement content. For this experiment, RCM consistently gives lower estimate of total deformation.

It can be concluded that the AEM gives sufficient accuracy to determine time-dependent deformation of concrete structures for general application. When greater accuracy is required, a computer method using superposition and the step-by-step method can be used.

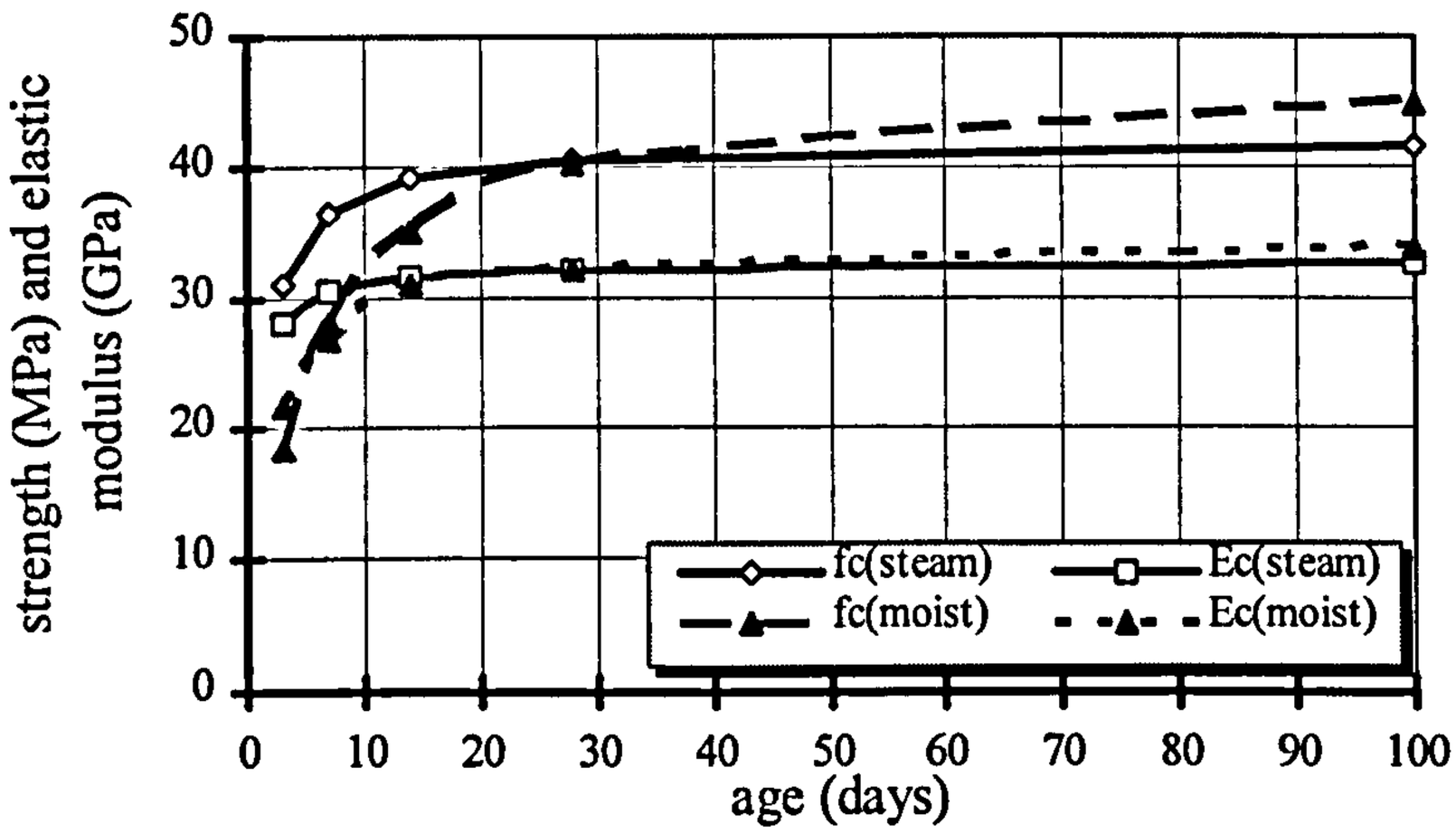

Figure 3.8: Strength and elastic modulus development predicted by ACI

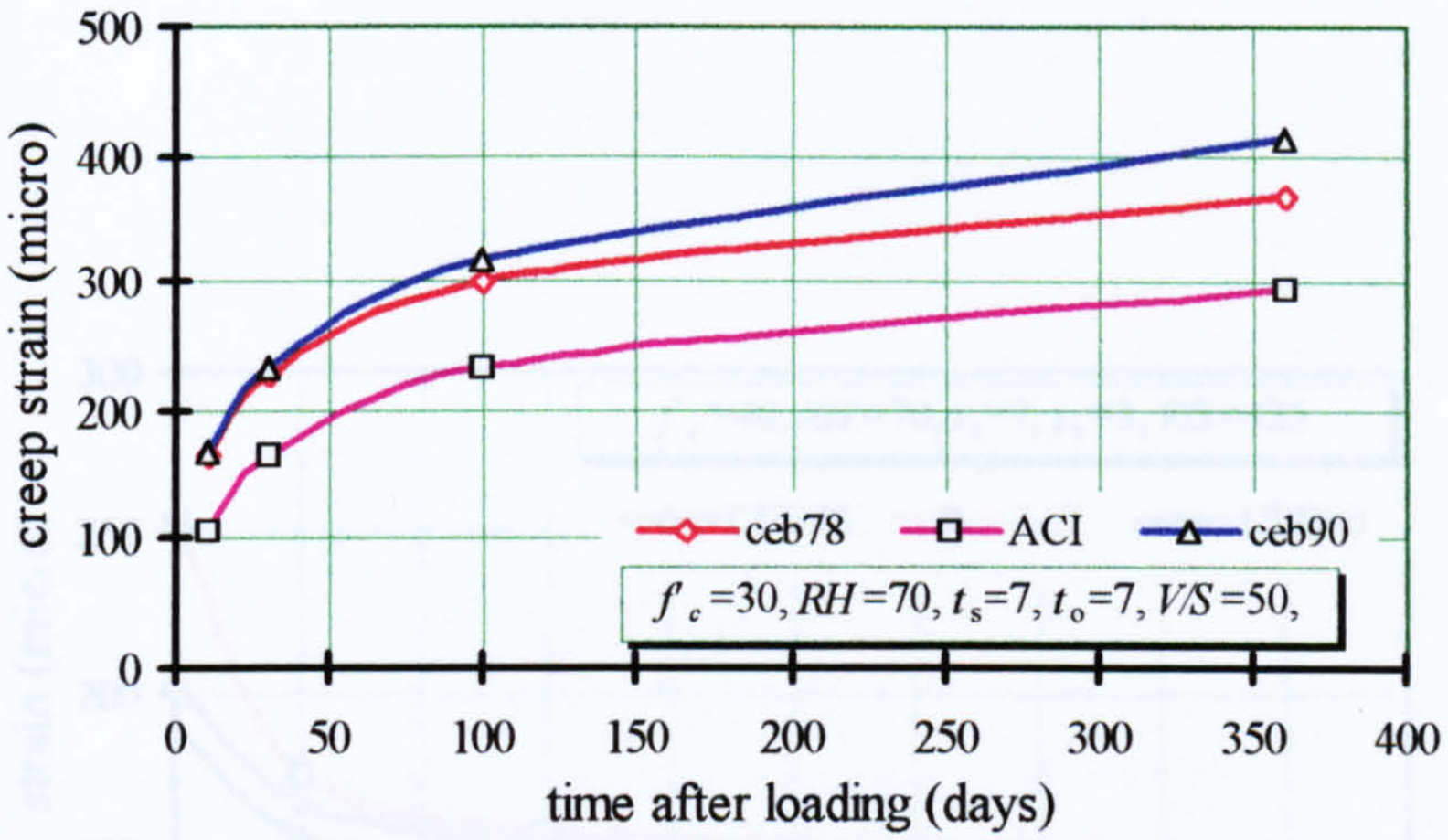

Figure 3.9: Comparisons for creep strains

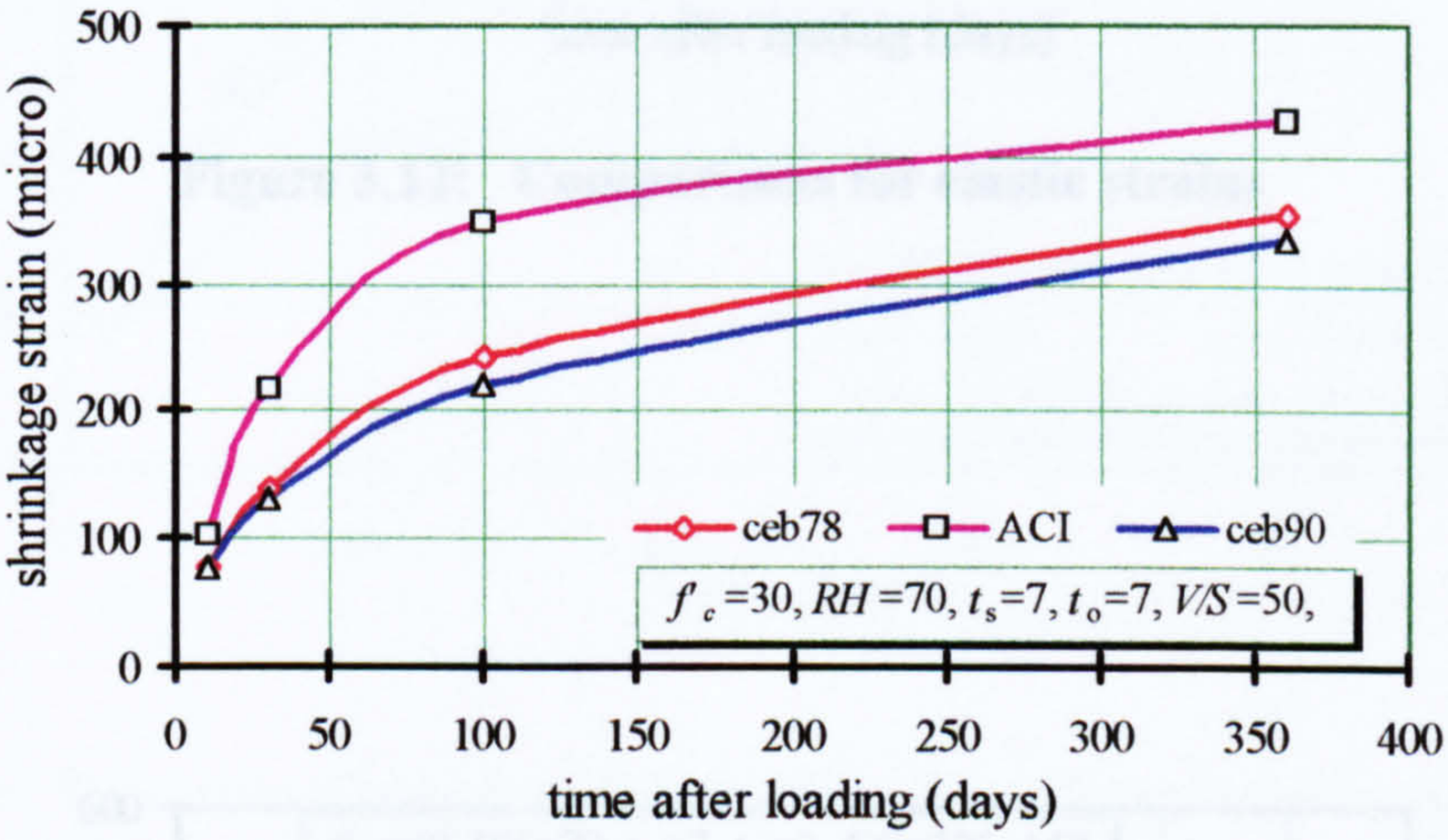

Figure 3.10: Comparisons for shrinkage strains

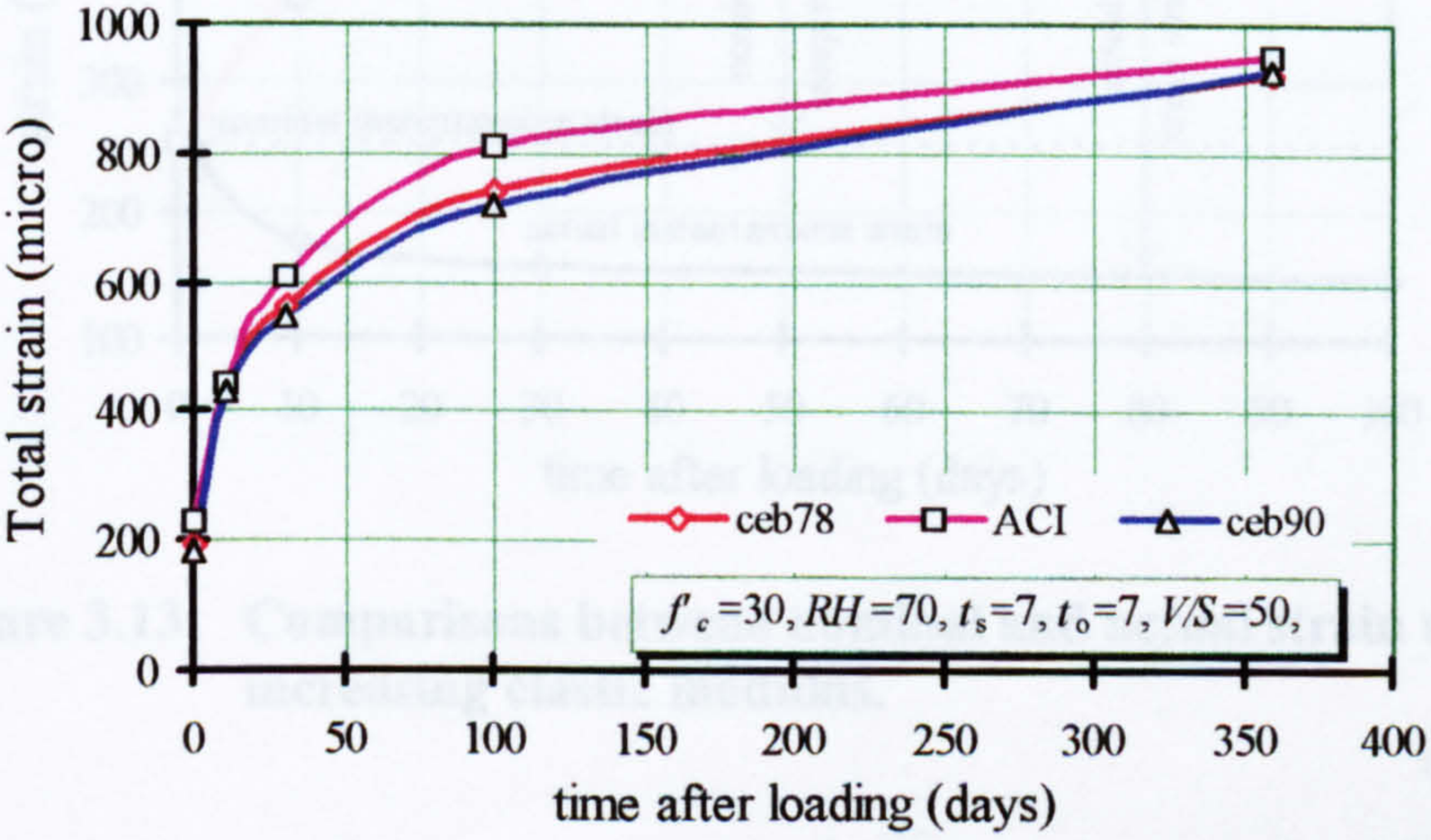

Figure 3.11: Comparisons for total strains

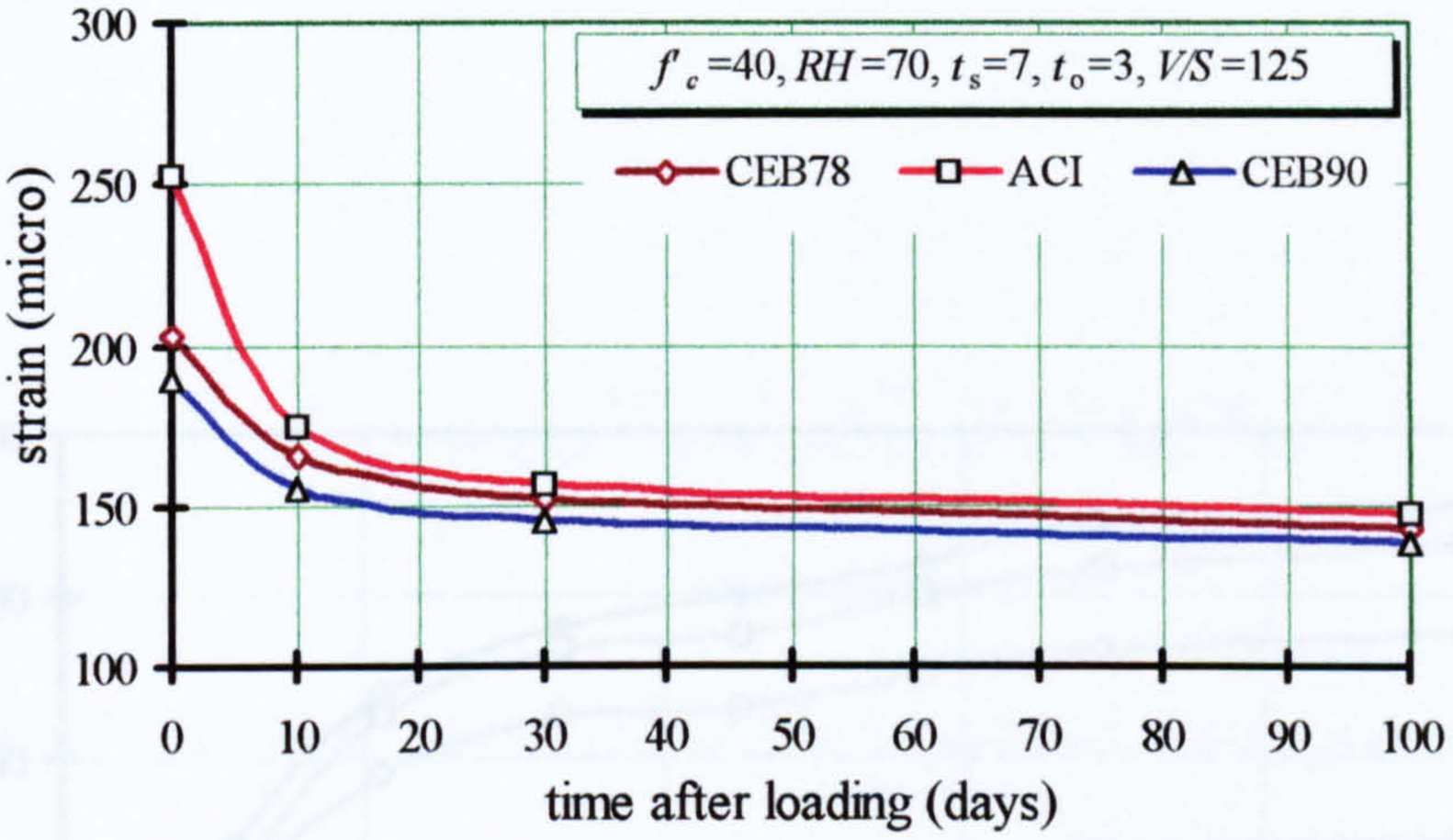

Figure 3.12: Comparisons for elastic strains

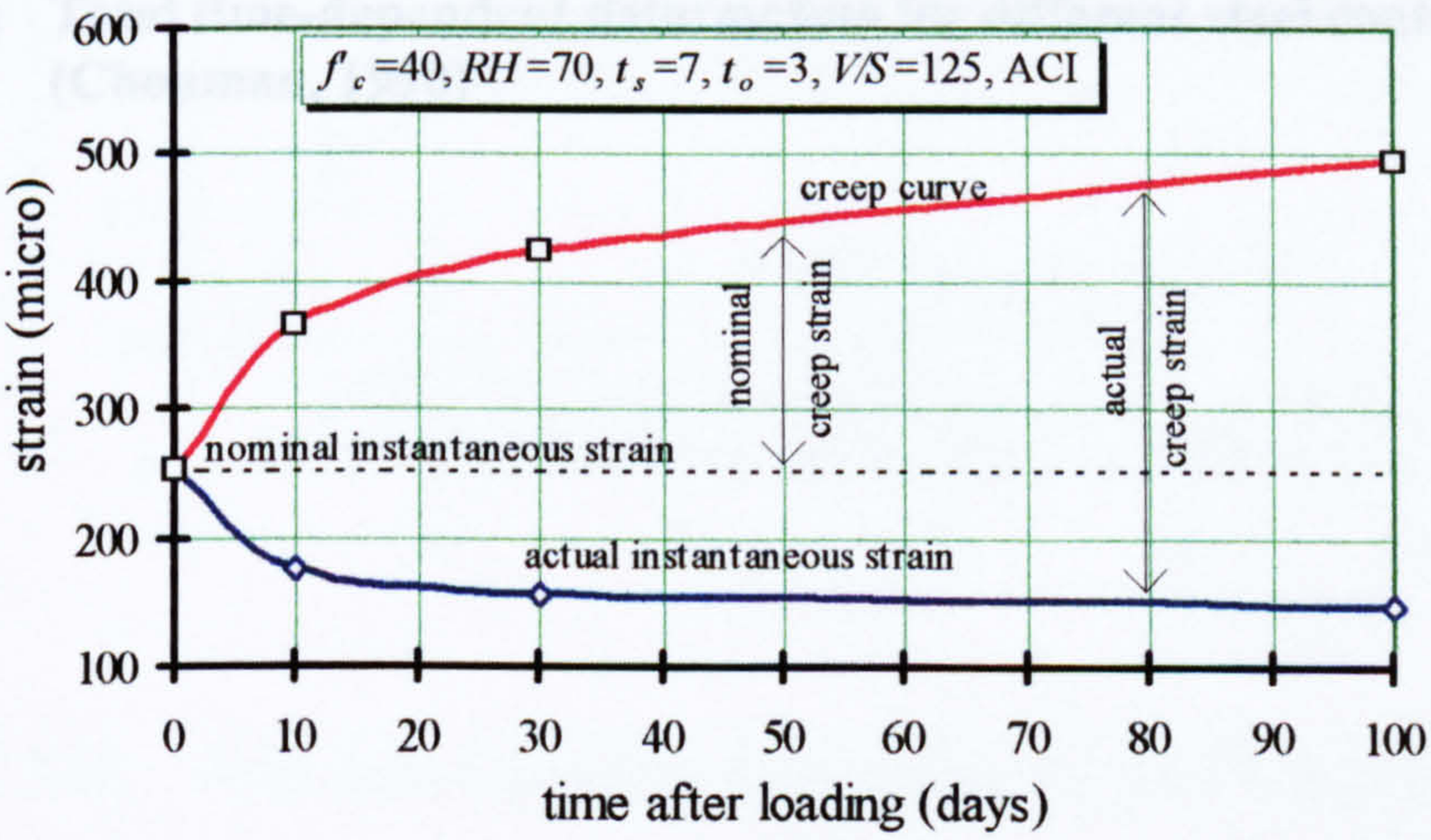

Figure 3.13: Comparisons between nominal and actual strain under increasing elastic modulus.

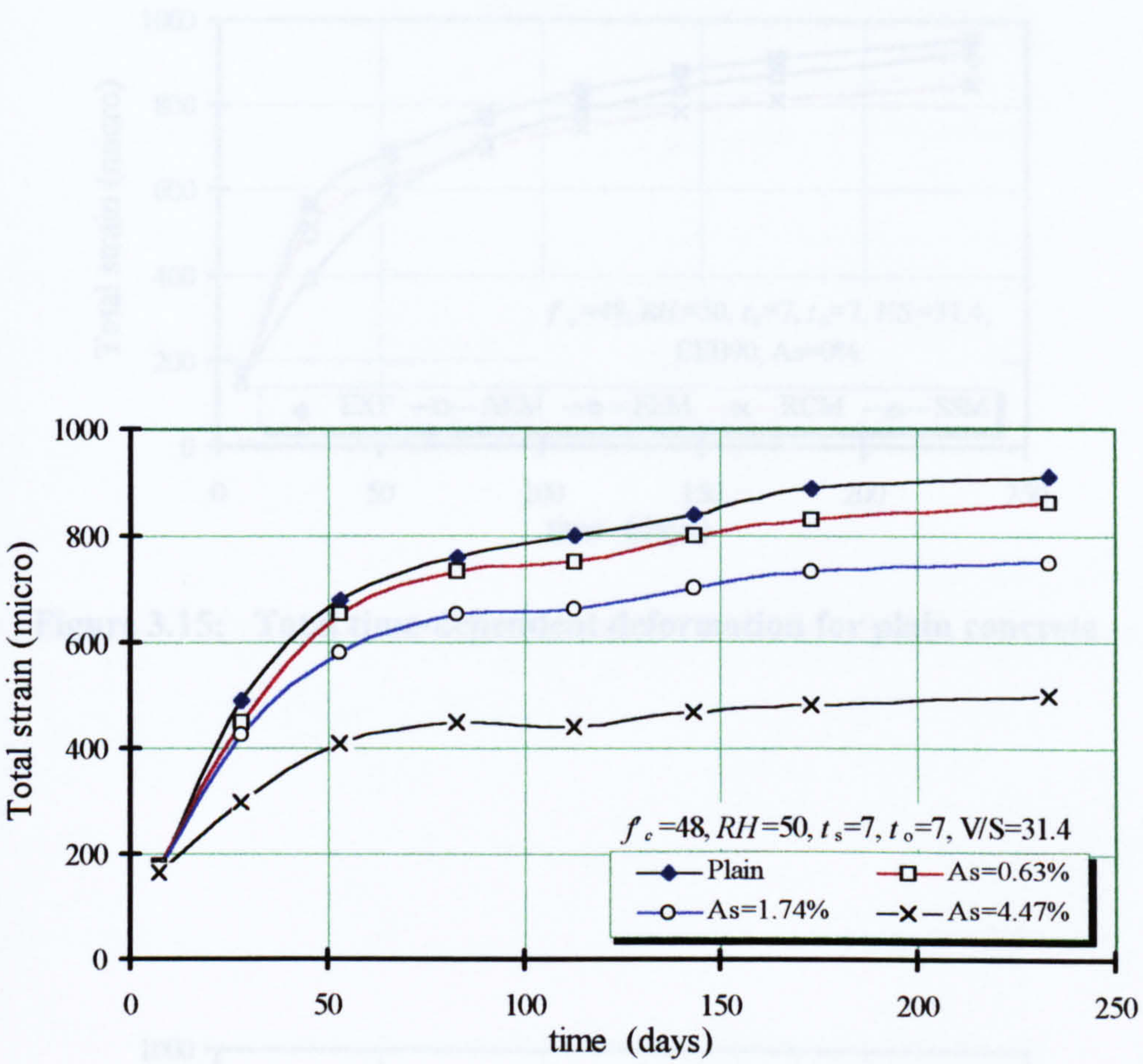

Figure 3.14: Total time-dependent deformation for different steel contents, (Chouman, 1990)

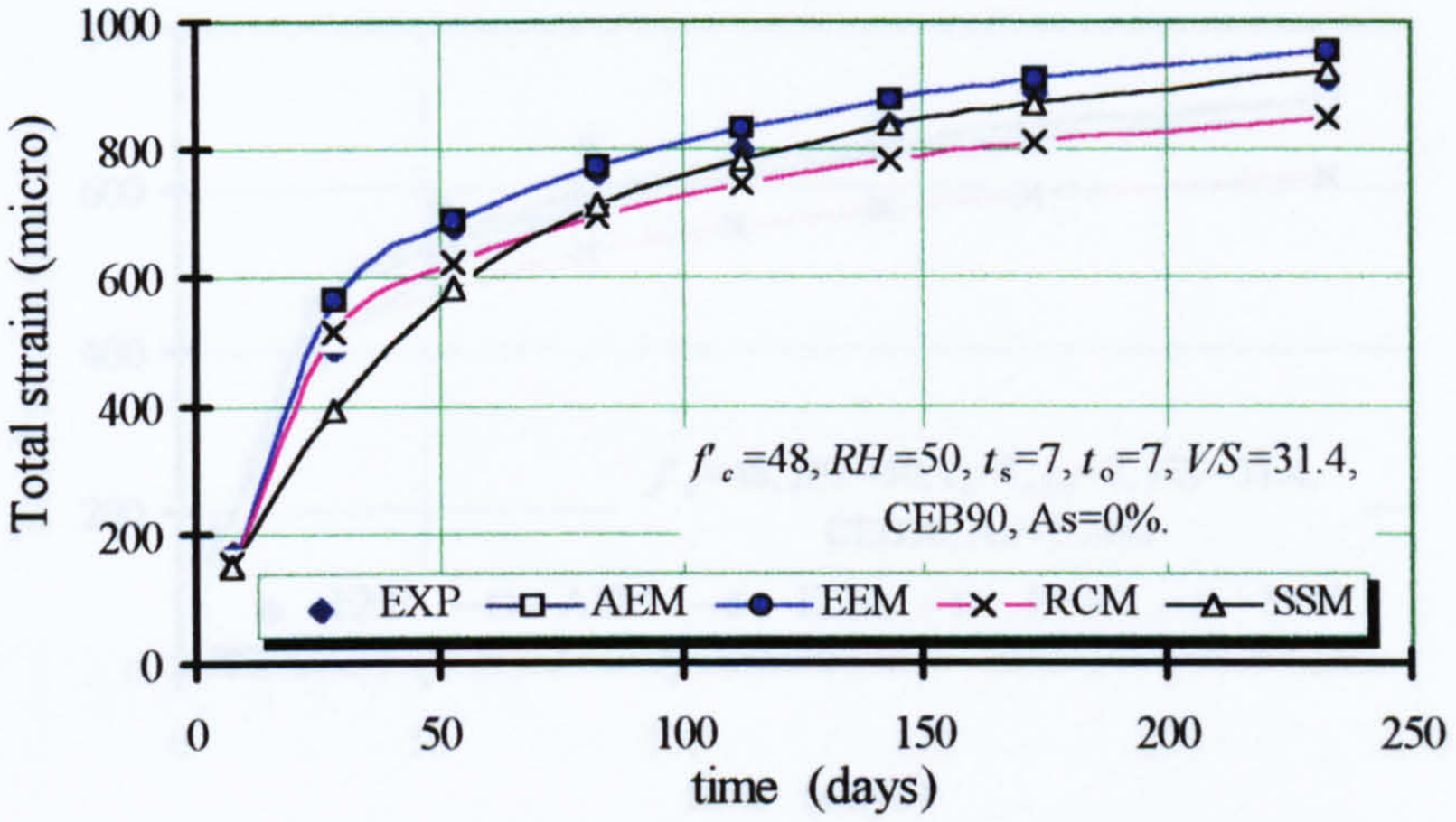

Figure 3.15: Total time-dependent deformation for plain concrete

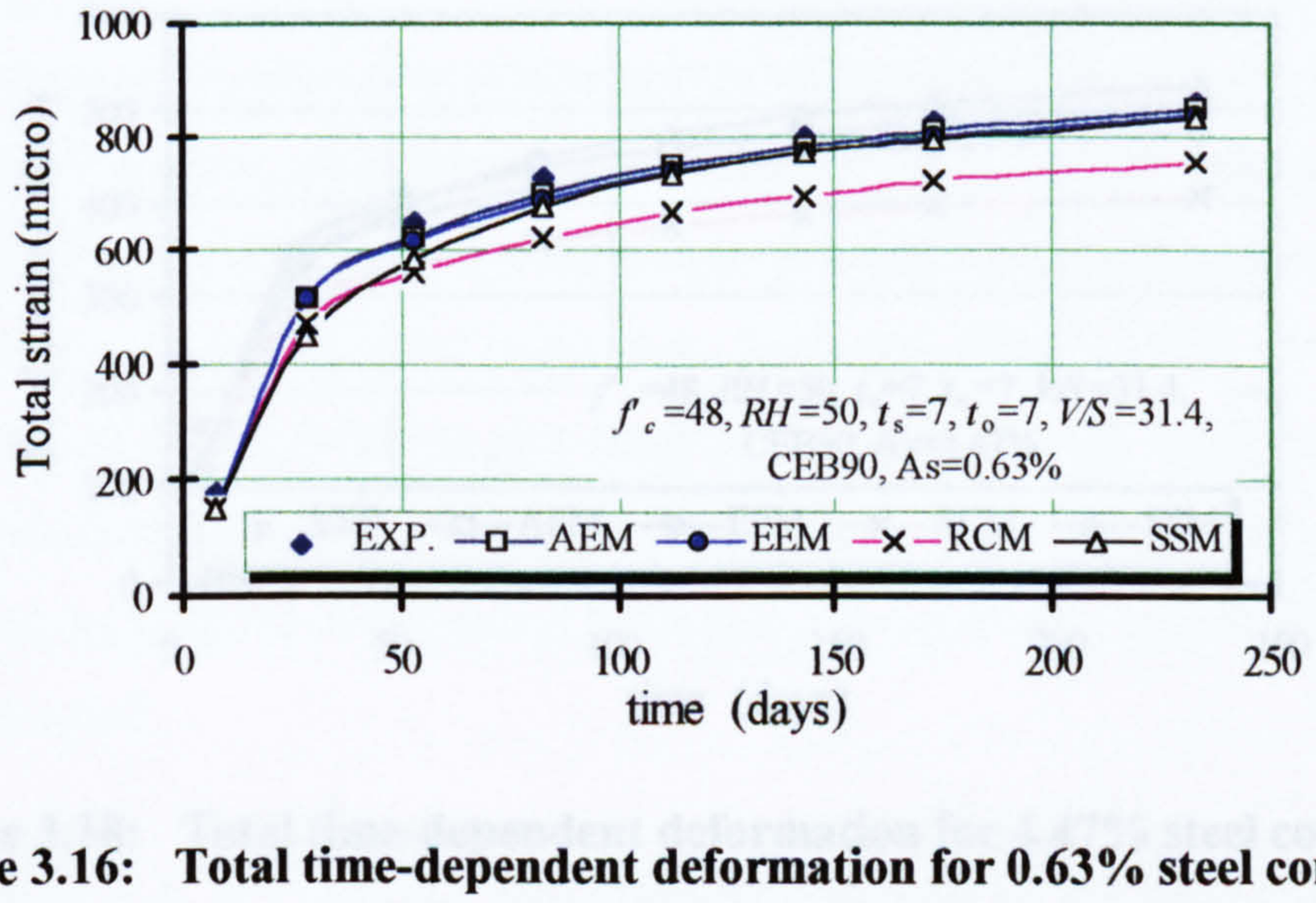

Figure 3.16: Total time-dependent deformation for 0.63% steel content

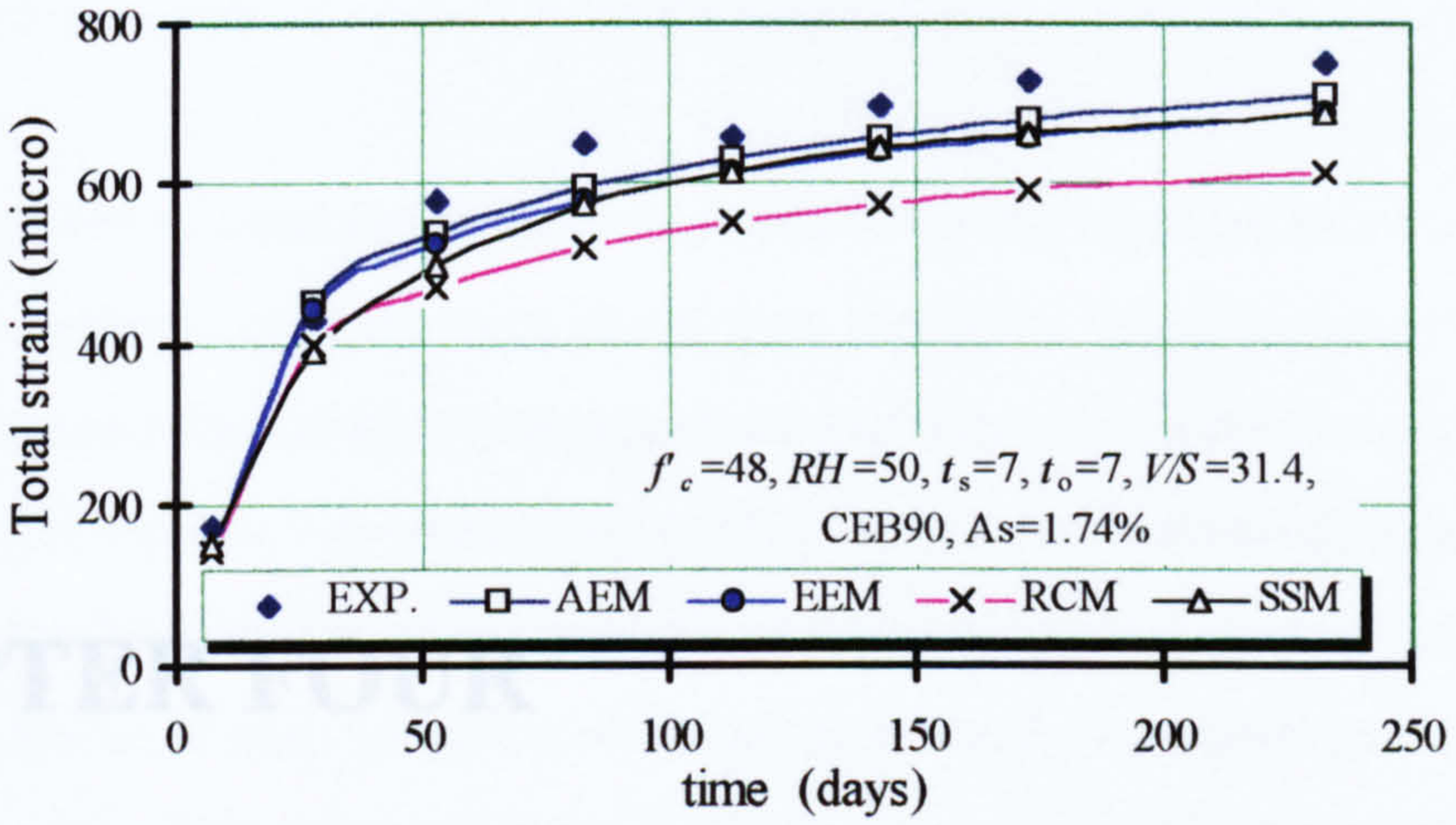

Figure 3.17: Total time-dependent deformation for 1.74% steel content

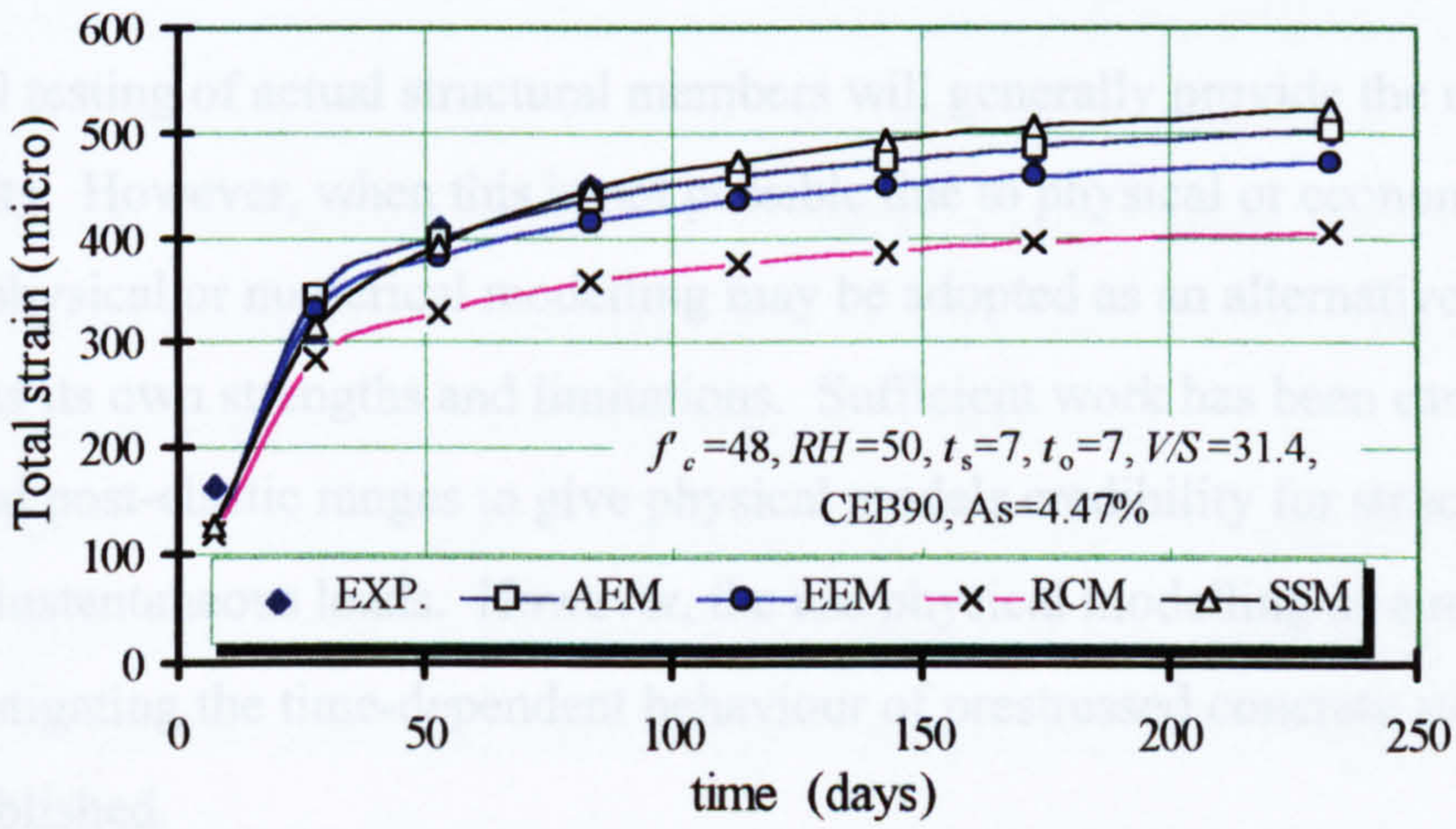

Figure 3.18: Total time-dependent deformation for 4.47% steel content

CHAPTER FOUR

COMPUTER MODELS FOR TIME-DEPENDENT DEFORMATION OF CONCRETE STRUCTURES

4.1 Introduction

Experimental testing of actual structural members will generally provide the most reliable results. However, when this is not possible due to physical or economic constraints, physical or numerical modelling may be adopted as an alternative. Physical modelling has its own strengths and limitations. Sufficient work has been carried out in the elastic and post-elastic ranges to give physical models credibility for structures subjected to instantaneous loads. However, the use physical modelling as a research tool for investigating the time-dependent behaviour of prestressed concrete structures is not well established.

Due to relatively high cost and time constraints for constructing and testing physical models, computer methods of analysis have been used by many investigators. Analytical methods adopted for this type of investigation include simple sectional analyses based on the basic concepts of strain compatibility and equilibrium or the more generalised approaches such as the finite element method. A review of the application

of these analytical procedures for the problem in hand has been discussed in Chapter 2. However, various computer codes that have been developed for this purpose are briefly discussed in this section.

Early development of specialised computer codes for time-dependent behaviour of prestressed concrete structures can be traced from the 1970s. Most of these codes were developed and used for numerical investigations and only a few were extended for commercial applications. Sinno and Furr (1972) used a combination of the rate of creep method and step-by-step procedure to develop a computer code to predict the time-dependent response of non-composite and composite simply supported pretensioned prestressed beams. The program assumed a linear stress-strain relationship for both the concrete and prestressing steel. The effects of ageing and relaxation of steel were not taken into consideration. The program was used to predict prestress loss and camber in pretensioned beams. Investigations for the effects of differential shrinkage and creep of the composite sections were also possible, but there was no provision to study the effects of external loads on the time-dependent deformation of the beam.

Program PBEAM was developed by Suttikan (1978) using a discrete element method. The program was specifically written to predict the instantaneous and time-dependent response of precast beams connected to form a continuous beam using ordinary negative reinforcement over the intermediate support. For the instantaneous analysis, the program was able to predict non-linear response up to the ultimate load. The discretised elements and sections were essential when non-linearity of stress-strain relationship of concrete and prestressing steel were used. Cracks were modelled by a spring in the discrete element and the non-linear stress-strain relationship across the depth of the section was modelled by the discretised sections. The program was verified using the experimental program by Mattock (1960) and was found to give predicted values within 21% of the experimental results.

Kang and Scordelis (1980) developed a computer code called PCFRAME to carry out instantaneous and time-dependent analysis of general reinforced and prestressed concrete frames. The program idealises structural frames into a series of one

dimensional line elements interconnected by joints. Each element is defined by a cross section which is discretised into multiple layers of concrete, reinforcing and prestressing steel. Each layer is defined by corresponding areas, local y co-ordinates and material properties. The program use the parabolic-linear Hognestad stress-strain law for concrete, multi-linear stress-strain law for prestressing steel and bi-linear stress-strain law for non-prestressing steel. Tension stiffening due to uncracked concrete is ignored. It accounts for time effects by adopting the superposition principle and step-by-step procedures. The ACI material model for time-dependent properties is used for the analysis. The program was satisfactorily verified using available experimental data. Tests by Lin (1955) on continuous prestressed beams subject to failure loads were used for non-linear analysis under instantaneous loads, and tests by Brackenridge (1964) on full scale simple prestressed beams were used for time-dependent analysis.

Teng and Branson (1991) developed another program for time-dependent analysis of cracked prestressed structures based on the assumption of progressive crack theory using the I-effective method (see Section 4.3). The code considers tension stiffening effects in the formulation, but is limited to a single span structure. The program compared well against experimental results on simple partially prestressed beams by Shaikh and Branson (1970). Tadros and Abdel Kareem (1993) developed another computer code based on the basic concepts of strain compatibility and equilibrium to carry out analysis of prestressed structures. The formulations are similar to that of Ghali (1988) where age-adjusted properties were used for the time analysis. The program was specifically developed to investigate time-dependent response of precast prestressed members being connected using the splicing technique (Chapter 2).

A commercial computer code, ADAPT (1993) has been written specifically to carry out analysis of prestressed concrete beams. The program idealises prestressed frames and discretises prestressing steel in a similar way as in PCFRAME. The finite element formulation based on one dimensional line elements and step forward integration to include time effects are also similar to that of PCFRAME. ADAPT, however, does not discretise sections into multiple layers of concrete and steel because it only considers

linear properties of the materials. This means that the stress and strain are also considered linear across the depth of the concrete section.

ADAPT introduces a new *SLAVE* element to enable modelling section with different material properties. Composite action between precast beams and a cast insitu slab or between concrete and steel can effectively be modelled using this element. The element ensures rigid connection where compatibility between connected joints is guaranteed.

Other more general computer codes for concrete structures such as ABAQUS and ANSYS, although more established for general applications in structural analysis, have no direct procedure for inclusion of prestressing. They require special manipulation for the analysis. Time-dependent properties of concrete and relaxation of prestressing steel are also not readily available.

Needless to mention, there are many other computer codes that have been developed and are continually coming into the market. It has not been possible to evaluate every one of these and each will come with its own strengths and weaknesses. It is, however, necessary to ensure that the selected code is capable of doing the work expected of it and there is sufficient opportunity for upgrading its capability where the code is lacking. Overall, analysis undertaken by ADAPT was found to be sufficient for the present investigation. Besides using the established numerical formulation, it has a high degree of flexibility to account for many different combination of construction and has sufficient built in elements for more flexible modelling of the types of structures to be investigated. Where ADAPT is lacking, such as in the time-dependent analysis of cracked sections, an interfacing program can be readily developed to overcome the problem. A summary of comparisons between the programs discussed are shown in Table 4.1 where only the names of principle investigators are quoted.

The following sections present formulations for manual calculation derived from the basic concepts of strain compatibility and equilibrium for uncracked and cracked conditions (Sections 4.2 and 4.3). This is referred as the classical method of analysis which is used to verify and complement the computer models given by ADAPT. Based

on the classical method of analysis, a series of computer programs for time-dependent analyses of reinforced concrete sections under axial loads and simply supported reinforced or prestressed concrete beams under flexural loads have been developed in this study using *Mathcad5.0* (1994). *Mathcad5.0* is a window based electronic sheet which contains a wide range of mathematical functions and is capable of carrying out complex numerical computations. The programs can adopt any of the creep and shrinkage prediction methods described in Chapter 3 and any of the three analytical procedures i.e. the EMM, RCM and AEM methods to compute time-dependent strains of reinforced and prestressed concrete sections.

Section 4.4 gives a general description, and the features and capabilities of ADAPT and the modelling techniques adopted to carry out the stated investigation. Manual calculations and computer models are methodically verified and compared in Section 4.5.

Table 4.1: Comparisons between different computer codes for time-dependent analysis of prestressed concrete structures.

Characteristic\Reference	Suttikan (1978)	Scordelis (1980)	Branson (1991)	Tadros (1993)	ADAPT (1993)
Non-linear concrete model	yes	yes	no	yes	no
Prestressing steel model	Magura	Magura	PCI	PCI	Magura
Concrete model	ACI	ACI	ACI	CEB78/ ACI	CEB78/ ACI
Structural analysis *	DEM	FEM	SM	SM	FEM
Time-dependent analysis	SSM/ RCM	SSM	SSM	SSM	SSM
Composite elements	2	no	2	2	2+
Number of span	2+	2+	1	2	2+
Cracked section	yes	yes	yes	no	no
Tension stiffening	no	no	yes	no	no
Non-linear support	yes	no	no	no	yes
Flexibility for different construction sequence	no	no	no	no	yes
Varied continuity connection	no	no	no	no	yes

**note: DEM = discrete element method, FEM = finite element method, SM = stiffness method*

4.2 Classical Method of Analysis

The procedures outlined in this section are similar to those of Ghali and Favre (1986) and Gilbert (1988).

4.2.1 Instantaneous deformation of concrete beams

Elastic analysis using transformed section is used to determine short and long term behaviour of reinforced or prestressed concrete structures. The method assumes that the section remains uncracked, one end is unrestrained in the axial direction, and the section remains plane. Figure 4.1 shows a concrete section under pure bending and prestress. The reinforcement is transformed into an equivalent concrete area using the modular ratio, m. Since a time dependent analysis will be carried out, the centroidal axis of a concrete section will change with time. Therefore, any arbitrary reference points may be chosen to calculate mechanical properties and stress-strains of the sections. For convenience, all section properties are calculated based on the top fibre as the reference level. From Figure 4.1, the strain at any point y on the section below the top surface is defined in terms of the top fibre strain, ε_{oi}, and the curvature, ψ_i.

Under instantaneous load, the strain (ε_i) and stress in concrete (σ_i) and steel (ε_{si}) at any point from the top fibre is defined as

$$\begin{aligned} \varepsilon_i &= \varepsilon_{oi} - y\psi_i \\ \sigma_i &= E_c\varepsilon_i = E_c(\varepsilon_{oi} - y\psi_i) \\ \varepsilon_{si} &= E_s(\varepsilon_{oi} - d_s\psi_i) \end{aligned} \qquad (4.1)$$

where E_c and E_s are the elastic modulus of concrete and steel respectively.

The resultant initial axial force N_i can be determined by integration of the stress block over the depth of the section. For reinforced concrete beams, N_i is zero but for prestressed beams, N_i equals the initial prestressing force P_i. In general,

$$N_i = \int \sigma_i dA = E_c\varepsilon_{oi}\int dA - E_c\psi_i\int y dA = E_c\varepsilon_{oi}A - E_c\psi_i B \qquad (4.2)$$

where A is the transformed section and B is the first moment of the transformed section about the top fibre. If the first moment about the top fibre is integrated over the depth of the section, the initial bending moment (M_i) can be determined. For reinforced concrete, M_i is equal to the applied bending moment (M_a) at the section; and for prestressed beams, $M_i = M_a - P_i d_p$, where d_p is the distance from top fibre to the centroid of the prestressing steel. M_i is given by

$$M_i = -\int \sigma_i y dA = -E_c \varepsilon_{oi} \int y dA + E_c \psi_i \int y^2 dA = -E_c \varepsilon_{oi} B + E_c \psi_i I \qquad (4.3)$$

where I is the second moment of inertia about the top fibre.

Rearranging Equations 4.2 and 4.3, the expressions for initial strain and curvature can be obtained in terms of the initial moment (M_i) and axial force (N_i):

$$\varepsilon_{oi} = \frac{BM_i + IN_i}{E_c(AI - B^2)} \qquad (4.4)$$

$$\psi_i = \frac{AM_i + BN_i}{E_c(AI - B^2)} \qquad (4.5)$$

Substituting Equations 4.4 and 4.5 into Equation 4.1, provides a general expression for the initial concrete stress at any point below the top fibre:

$$\sigma_i = \frac{(B - yA)M_i + (I - yB)N_i}{AI - B^2} \qquad (4.6)$$

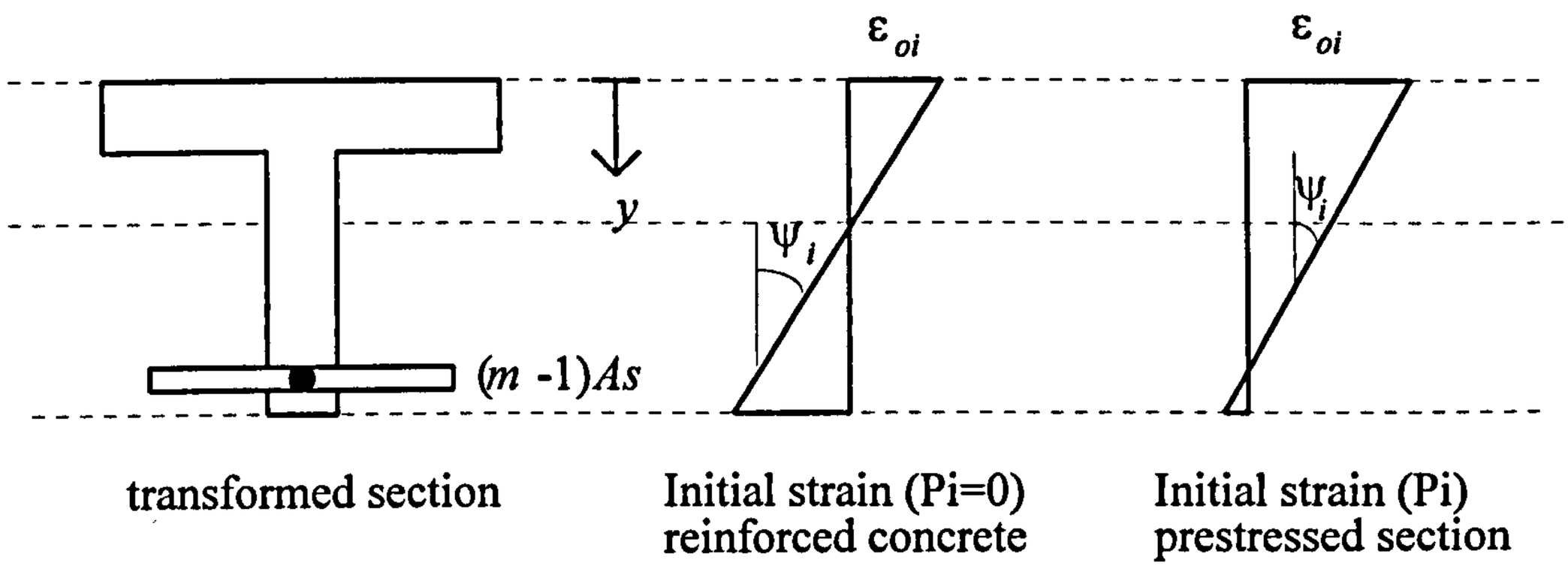

Figure 4.1: Transformed section and initial strain distribution for reinforced and prestressed sections

4.2.2 Time dependent deformation of simple beams

Time-dependent deformation of a concrete section is shown in Figure 4.2 where the total top fibre strain and curvature at any time *t* are given by

$$\varepsilon_o(t) = \varepsilon_{oi} + \Delta\varepsilon_o(t) \qquad \text{and} \qquad \psi(t) = \psi_i + \Delta\psi(t) \tag{4.7}$$

A *relaxation* procedure, which was first introduced by Bresler and Selna (1964), can be used together with the AEM to determine the strain and curvature increment for the concrete section. In this procedure, the total strain is held constant at any time interval. If the creep and shrinkage strains are changing, then the instantaneous strain must also change by an equal and opposite amount. This results in additional stress along the cross section, thus disturbing the internal equilibrium. An incremental axial force (ΔN) and bending moment (ΔM) must be applied to restore equilibrium.

Similar to Equations 4.4 and 4.5, the increments of top fibre strain and curvature produced by ΔN and ΔM may be obtained by

$$\Delta\varepsilon_{oi} = \frac{\bar{B}\Delta M_i + \bar{I}\Delta N_i}{\bar{E}_e(\bar{A}\bar{I} - \bar{B}^2)} \tag{4.8}$$

$$\Delta\psi_i = \frac{\bar{A}\Delta M_i + \bar{B}\Delta N_i}{\bar{E}_e(\bar{A}\bar{I} - \bar{B}^2)} \tag{4.9}$$

where, $\bar{E}_e$, $\bar{A}$, $\bar{B}$ and $\bar{I}$ are the age-adjusted effective elastic modulus, area, first moment of area and second moment of area about the top fibre. They are age-adjusted properties because ΔN and ΔM are gradually applied.

The restraining force necessary to prevent the deformation due to creep is given by

$$-\Delta N_{creep} = -\bar{E}_e\phi(A_c\varepsilon_{oi} - B_c\psi_i) \tag{4.10}$$

$$-\Delta M_{creep} = -\bar{E}_e\phi(B_c\varepsilon_{oi} - I_c\psi_i) \tag{4.11}$$

where A_c, B_c, and I_c refer to the concrete section only since it is only the concrete that is creeping. The restraining force to prevent the deformation due to shrinkage is given by

$$-\Delta N_{shrinkage} = -\overline{E}_e \varepsilon_{sh} A_c \tag{4.12}$$

$$-\Delta M_{shrinkage} = +\overline{E}_e \varepsilon_{sh} B_c \tag{4.13}$$

For prestressed section, the restraining force required to prevent reduced relaxation in the tendons is given by

$$-\Delta N_{relaxation} = \chi_r f_{pr} A_p \tag{4.14}$$

$$-\Delta M_{relaxation} = -\chi_r f_{pr} A_p d_p \tag{4.15}$$

where f_{pr} is the relaxation loss given in Equation 3.15, χ_r is a reduction coefficient for relaxation loss described in Section 3.4. The total restraining force is summation of the individual creep, shrinkage and relaxation components and is given by

$$-\Delta N = -\overline{E}_e[\phi(-A_c\varepsilon_{oi} + B_c\psi_i) - \varepsilon_{sh}A_c] + \chi_r f_{pr} A_p \tag{4.16}$$

$$-\Delta M = -\overline{E}_e[\phi(-B_c\varepsilon_{oi} + I_c\psi_i) - \varepsilon_{sh}B_c] - \chi_r f_{pr} A_p d_p \tag{4.17}$$

The loss of stress at any distance from the top fibre in the concrete due to relaxation and the change of stress which occurs due to application of ΔN and ΔM to restore equilibrium are given by

$$\Delta\sigma_{relax} = -E_e[\phi(\varepsilon_{oi} - y\psi_i) + \varepsilon_{sh}] \tag{4.18}$$

$$\Delta\sigma_{restore} = \overline{E}_e[\Delta\varepsilon_o - y\Delta\psi] \tag{4.19}$$

The actual change of stress that occurs during the time interval due to creep and shrinkage is the summation of Equations 4.18 and 4.19. The change in stress for non-prestressed and prestressed steel, is given by

$$\Delta\sigma_s = E_s(\Delta\varepsilon_o - d_s\Delta\psi) \tag{4.20}$$

$$\Delta\sigma_p = E_p(\Delta\varepsilon_o - d_p\,\Delta\psi) + \chi_r f_{pr} \tag{4.21}$$

These formulations are valid for all composite sections not only those incorporating of precast prestressed beams and cast in situ concrete slabs. However, for composite concrete beams, the elastic modulus of either the precast beams or the cast in situ slab can be chosen as a reference to compute the transformed properties. For a typical composite precast prestressed beam and cast in situ slab shown in Figure 4.3, new section properties to be used in the analysis are given by

$$A = \sum_{j=1}^{n} m_{cj} A_{cj} + \sum_{k=1}^{n} m_{sk} A_{sk} + \sum_{k=1}^{n} m_{pk} A_{pk} \tag{4.22a}$$

$$B = \sum_{j=1}^{n} m_{cj} A_{cj} d_{cj} + \sum_{k=1}^{n} m_{sk} A_{sk} d_{sk} + \sum_{k=1}^{n} m_{pk} A_{pk} d_{pk} \tag{4.22b}$$

$$I = \sum_{j=1}^{n} (m_{cj} I_{cj} + m_{cj} A_{cj} d_{cj}^2) + \sum_{k=1}^{n} m_{sk} A_{sk} d_{pkj}^2 + \sum_{k=1}^{n} m_{pk} A_{pk} d_{pkj}^2 \tag{4.22c}$$

where $m_{cj} = E_{cj} / E_{ref}$, $m_{sk} = E_{sk} / E_{ref}$, and $m_{pk} = E_{pk} / E_{ref}$, and n refers to the number of concrete, non-prestressing steel and prestressing layers. Strains at any distance from the reference level and the curvature due to instantaneous loads are as given by Equation 4.1. Similar to Equation 4.6, the stresses due to the instantaneous values N and M in the concrete and steel, and the incremental stress in the prestressing steel are given by

$$\begin{aligned} \sigma_{cj} &= E_{cj}(\varepsilon_{oi} - y\psi_i) \\ \sigma_{sk} &= E_{sk}(\varepsilon_{oi} - d_{sk}\psi_i) \\ \Delta\sigma_{pk} &= E_{pk}(\varepsilon_{oi} - d_{pk}\psi_i) \end{aligned} \tag{4.23}$$

The time-dependent change in the axial force and bending moment are similarly considered for the composite section and are as given by Equations 4.16 and 4.17. The

change in the axial force and bending moment due to creep, shrinkage and relaxation effects are given by Equations 4.24 and 4.25.

$$-\Delta N = -\sum_{j=1}^{n} \overline{E}_{ej}[\phi_j(A_{cj}\varepsilon_{oi} - B_{cj}\psi_i) + \varepsilon_{shj}A_{cj}] + \sum_{k=1}^{n} R_k k_k \qquad (4.24)$$

$$-\Delta M = -\sum_{j=1}^{n} \overline{E}_{ej}[\phi_j(-B_{cj}\varepsilon_{oi} + I_{cj}\psi_i) - \varepsilon_{sh}B_{cj}] - \sum_{k=1}^{n} k_k R_k d_p \qquad (4.25)$$

The change in axial strains, $\Delta\varepsilon_{oi}$, and curvature, $\Delta\psi_i$, are computed according to Equations 4.8 and 4.9 except A, B and I are age-adjusted properties where the modular ratio m in Equations 4.22 are replaced by $\overline{m}_{cj}$, $\overline{m}_{sk}$ and $\overline{m}_{pk}$ where $\overline{m}_{cj} = \overline{E}_{cj} / \overline{E}_{ref}$, $\overline{m}_{sk} = E_{sk} / \overline{E}_{ref}$, and $\overline{m}_{pk} = E_{pk} / \overline{E}_{ref}$. The change of stress at a point in the j-th concrete element at a depth y below the reference point is equal to the sum of the stress loss due to relaxation of the age-adjusted transformed section when creep and shrinkage are fully restrained, and the stress which results when ΔN and ΔM are applied to the cross sections. This change is given by

$$\Delta\sigma = -E_{ej}[\phi_j(\varepsilon_{oi} - y\psi_i) + \varepsilon_{shj} - (\Delta\varepsilon_o - y\Delta\psi)] \qquad (4.26)$$

The change in stress in any layer of non-prestressed steel, $\Delta\sigma_s$, and prestressing steel, $\Delta\sigma_{ps}$, are similar to that given by Equations 4.20 and 4.21.

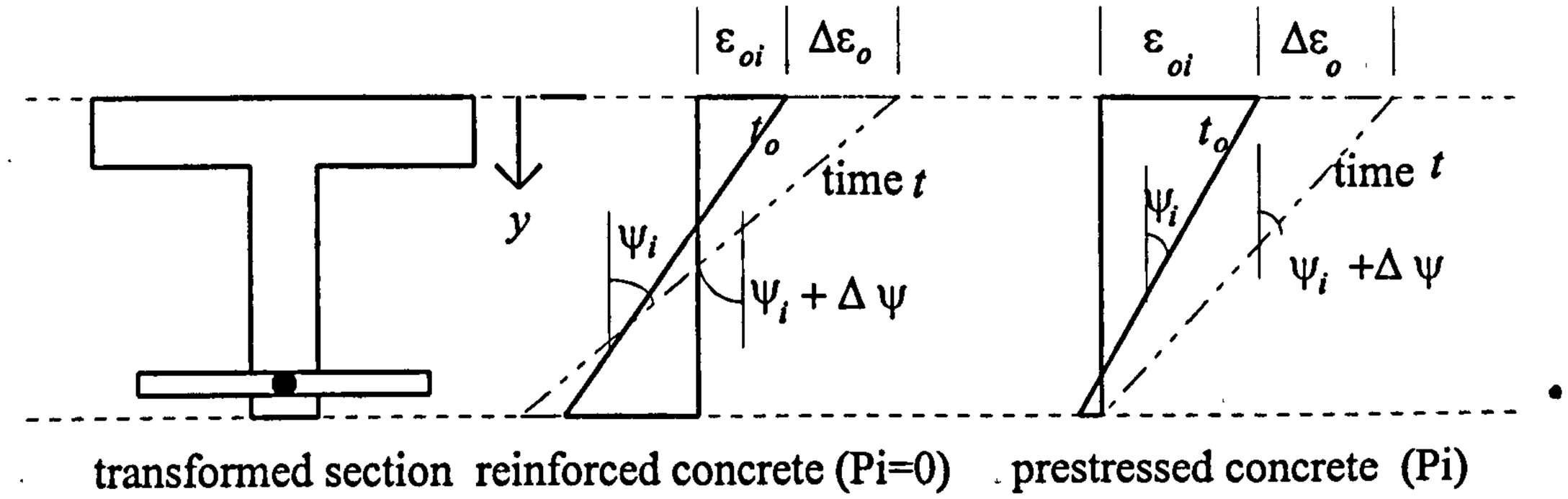

Figure 4.2: Time-dependent deformations for reinforced and prestressed concrete sections

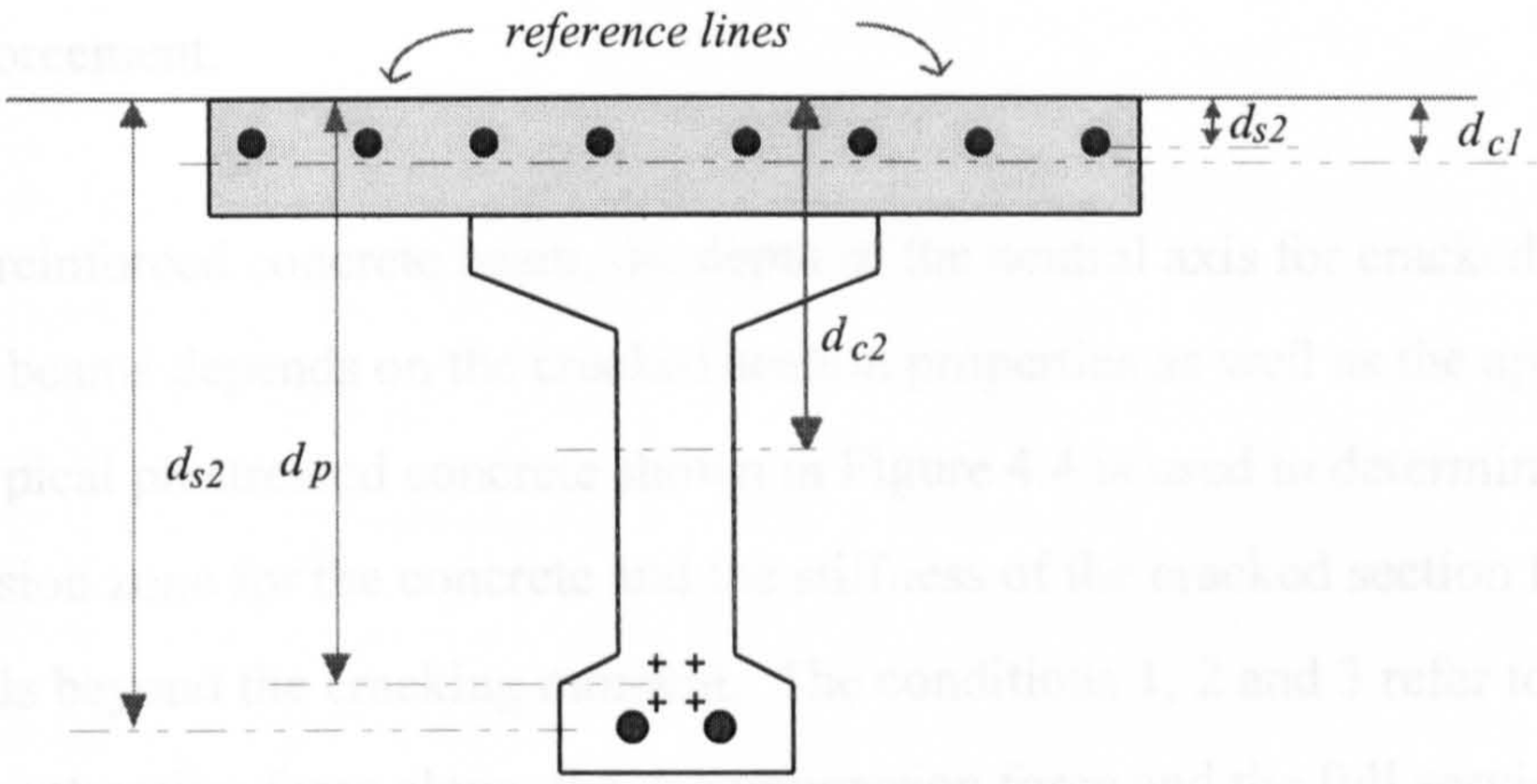

Figure 4.3: A typical composite section of precast prestressed beam and cast insitu slab

4.3 Considerations for Cracked Conditions

4.3.1 Cracked sections under instantaneous actions

Discussions presented in the preceding section assume that concrete remains uncracked throughout the analysis. This condition is generally applicable within a design practice where cracks are not allowed under service loads. However, for a more general design practice where cracks are encountered under service loads, as in the case of partially prestressed beams, the presence of cracks need to be considered in the analysis.

If cracks occur in the members, the tensile stress beyond the tensile strength of concrete may only be carried by steel reinforcement and section stiffness is greatly reduced. In between the cracks, concrete continues to carry tensile load, hence continues to contribute to member stiffness. In flexural members, the onset of cracking causes a sudden loss of stiffness and the short term moment-curvature relationship becomes non-linear.

In the classical elastic theory for a reinforced concrete beam, it can be shown that the depth of the neutral axis for the beam is section-dependent (Kong and Evans, 1975). It is assumed that the section is fully cracked up to the neutral axis and no tensile stress exist in the concrete below the axis. The section stiffness for the fully cracked section is

obtained by considering the remaining concrete under compression and the contribution of the reinforcement.

Unlike the reinforced concrete beam, the depth of the neutral axis for cracked prestressed beams depends on the cracked section properties as well as the applied loads. A typical prestressed concrete shown in Figure 4.4 is used to determine the depth of compression zone for the concrete and the stiffness of the cracked section for any service loads beyond the cracking moment. The conditions 1, 2 and 3 refer to sections under the prestressing force alone, the decompression force and the full service load respectively. The section will crack at its bottom fibre under condition 3 if the tensile stress exceeds the concrete modulus of rupture, σ_r.

An iterative procedure is required to determine the depth of the neutral axis for cracked section, and the stresses in concrete and the prestressing steel. The mechanical properties of the cracked section i.e. the cracked moment of inertia (I_{cr}) and new centroidal area for the cracked section are obtained once the position of the neutral axis (y_{cr}) has been determined. The procedure to obtain these properties can be obtained from any standard text book on prestressed concrete structure, such as that written by Nilson (1982).

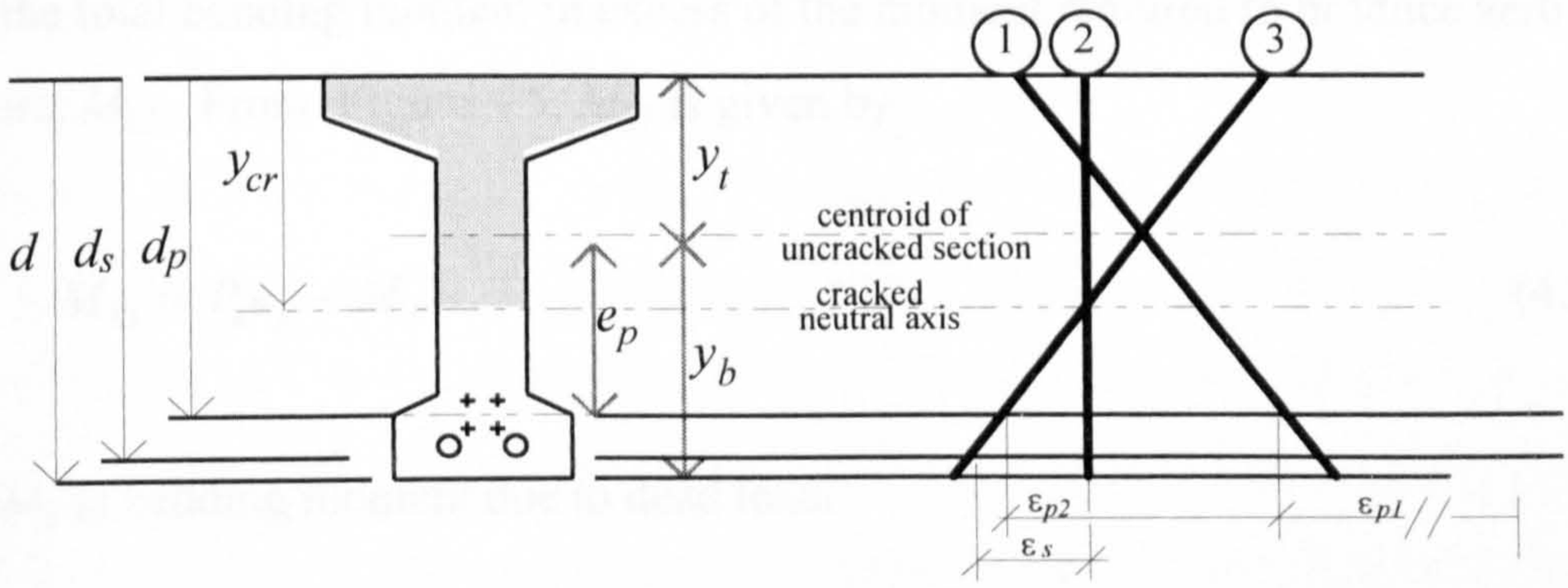

(a) Fully cracked section (b) Strains in three different loadings

Figure 4.4: Basis of analysis for cracked prestressed concrete sections

4.3.2 Effects of tension stiffening

The use of mechanical properties based on a fully cracked section as outlined in Section 4.3.1 will overestimate member deformation. If the stiffness of uncracked and fully cracked sections at any given load are considered as the upper and lower limit, the true stiffness of cracked section lies between these two limits. To account for stiffening effects due to uncracked sections, the I-effective method, as adopted by the ACI code, or interpolation procedure as adopted by the CEB, can be readily utilised. Both methods provide empirical estimates of stiffness in cracked concrete sections. The I-effective method which was developed by Branson and Trost (1982) suggests a unified expression for prestressed and non-prestressed sections for the effective stiffness which is given by

$$I_{ct}(t_i) = \left\{\frac{M_{cr}}{M_{L2}}\right\}^4 I_{ucr} + \left[1 - \left\{\frac{M_{cr}}{M_{L2}}\right\}^4\right] I_{cr} \leq I_{ucr} \tag{4.27}$$

where M_{cr} is the moment required to crack the section which is given by

$$M_{cr} = \frac{\sigma_r I_{ucr}}{y_b} + \frac{P_e I_{ucr}}{A_{ucr} y_b} \tag{4.27a}$$

M_{L2} is the total bending moment in excess of the moment required to produce zero curvature, M_{L1}. From Figure 4.5, M_{L1} is given by

$$M_{L1} = P_e e_p - M_d \tag{4.27b}$$

where M_d is bending moment due to dead load.

The effective depth of the centroidal axis for the cracked section, y_{ct} is given by

$$y_{ct}(t_i) = \left\{\frac{M_{cr}}{M_{L2}}\right\}^{2.5} y_{ucr} + \left[1 - \left\{\frac{M_{cr}}{M_{L2}}\right\}^{2.5}\right] y_{cr} \leq y_{ucr} \tag{4.28}$$

Fully cracked section properties I_{cr} and y_{cr} to be used in Equations 4.27 and 4.28 are obtained from the procedure mentioned in Section 4.3.1.

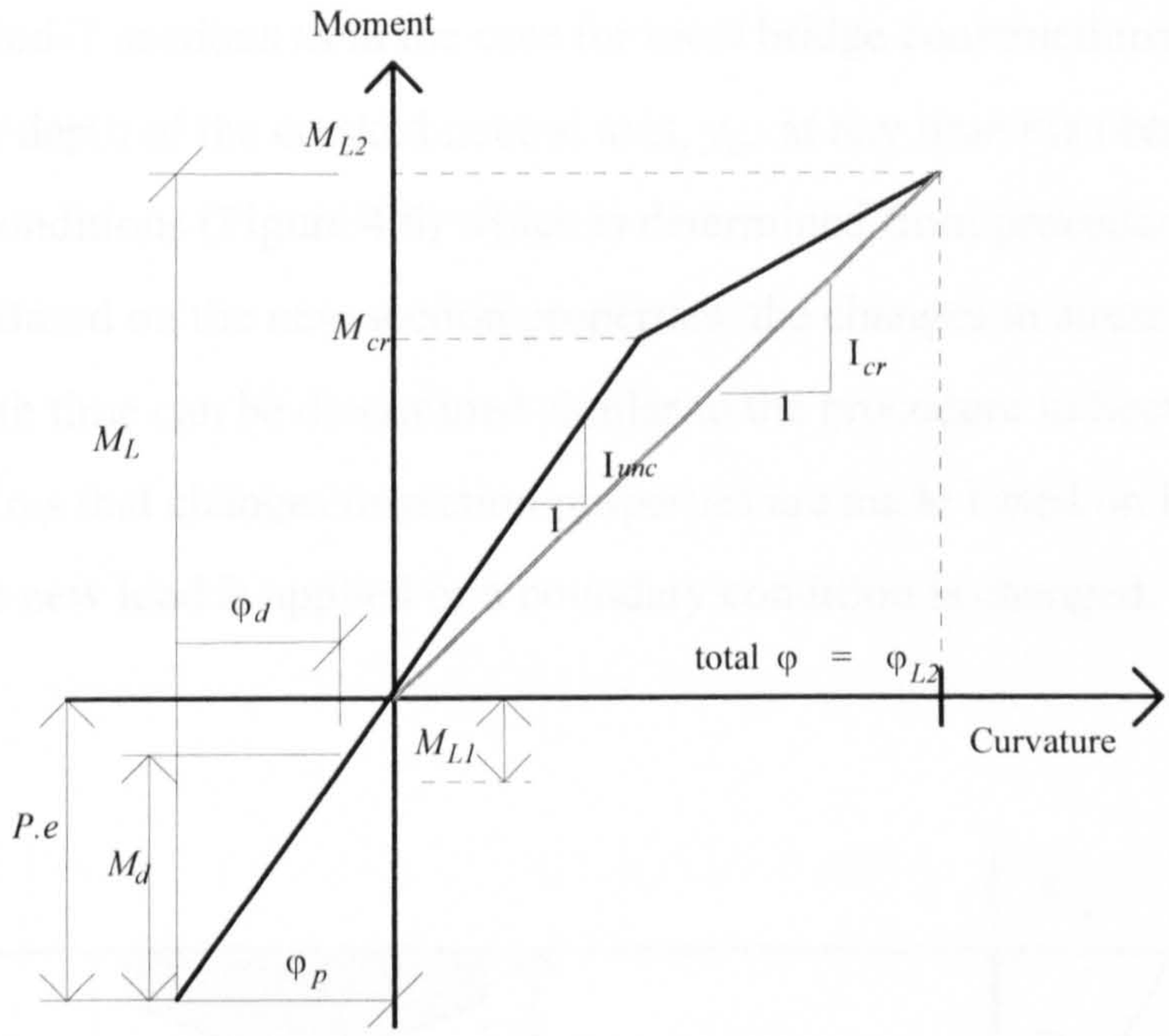

Figure 4.5: Idealised moment-curvature diagram to account for tension stiffening (Branson and Trost, 1982).

4.3.3 Cracked sections under time-dependent effects

In cracked concrete sections, it is assumed that only the concrete in the compression zone creeps and all tension is carried by the steel reinforcement. Creep causes a change in the neutral axis location as the strains increase in the compressive region of the concrete. In general, the depth of concrete under compressive stress increases as the depth of the neutral axis increases with time. An iterative numerical solution procedure is required to account accurately for this gradual change of section properties. The procedure requires the section properties after each time step be modified as the depth of the neutral axis changes.

For a given load, a constant depth of the neutral axis of cracked sections at any time interval is assumed as suggested by Ghali (1986) and Gilbert (1988). This assumption

was considered acceptable because the change in the total compressive force with time was found to be very small. The additional area under compressive stress is close to the neutral axis position where the stress and strain are approaching zero value. The adverse effect of this assumption is further reduced if flexural members comprise of *Y*, *M*, *U* and inverted-T sections as in the case for most bridge constructions. Using this assumption, the depth of the cracked neutral axis, y_{cr}, at any time t is obtained from the instantaneous conditions (Figure 4.6) which is determined from procedures described in Section 4.3.1. Based on the new section properties, the changes in stress and deformation with time can be determined similar to the procedure in Section 4.2. This procedure requires that changes in section properties are made based on instantaneous analysis when a new load is applied or a boundary condition is changed.

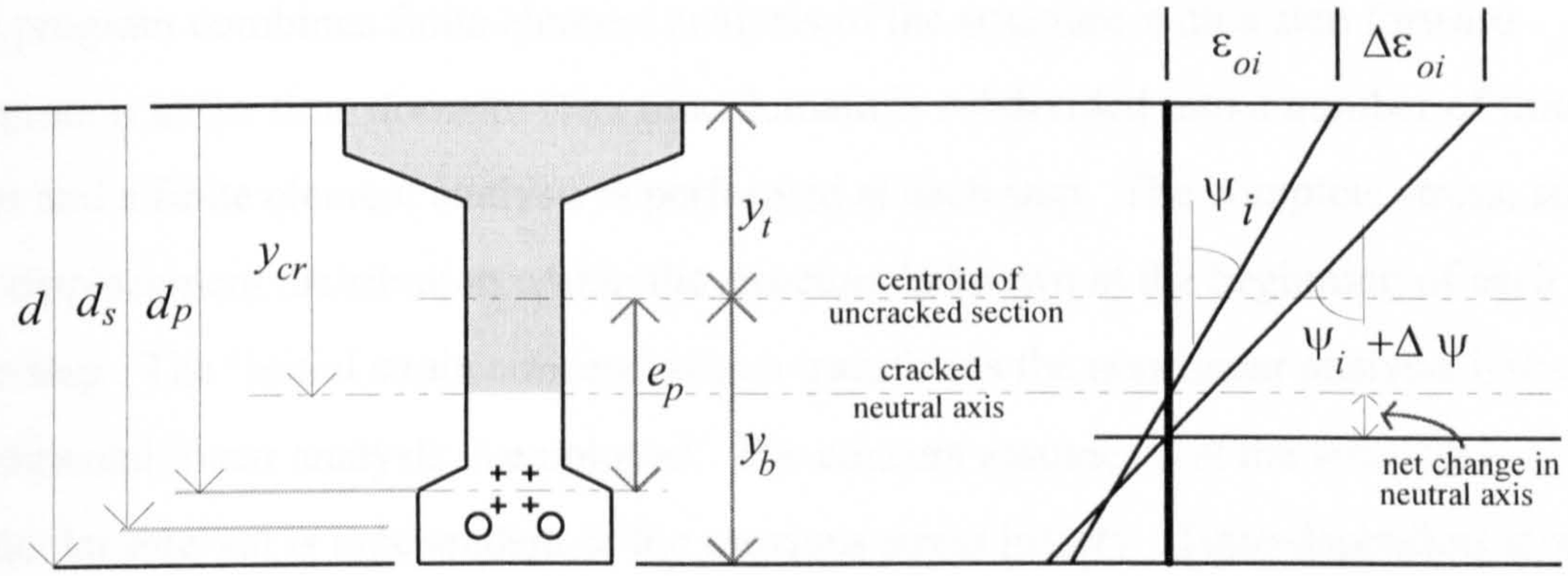

Figure 4.6: Time-dependant change of strain and curvature for cracked sections

4.4 Time-dependent Analysis Using Computer Models

4.4.1 General descriptions and capabilities of ADAPT (1993)

ADAPT models structural members as plane frame with global *X* and *Y* axes. Transitional displacements are considered in the *X* and *Y* directions and rotational displacements in the *Z* direction. Each element is defined by a constant section along its length and may be installed or removed from the structure at any solution step.

Composite action between different parts of the concrete and steel can be modelled using rigid connections (*SLAVE* element) between the elements. The rigid connection ensures compatibility of displacement at every node connected by it. The boundary conditions may be changed at any solution step to model the actual sequence used in the construction of continuous precast, prestressed concrete beams.

The program combines finite element analysis of the structure with a step forward integration in the time domain. The time domain is subdivided into a number of time steps and a finite element analysis is performed at each step. The complete stress, strain and displacement distribution within the structure is known at the beginning of each time step. The 'initial strain concept' which transforms the non-linear analysis into an incremental linear analysis is employed. The concept assumes that the strain at a particular interval is independent of the previous stress history. Time-dependent strain over the time step is considered as the initial loading for the finite element model and the total stress, strain and displacement due to this loading at the end of the time step are added to the values from the previous time step. The program considers all loads are gradually applied, hence the structural response due to instantaneously applied loads requires a zero length time step to be specified.

Equilibrium of forces is guaranteed at all time steps. Element stiffness may only be changed due to variations in elastic modulus with time, not due to cracking. Stress and strain are always considered to be linear at all times which is in line with linear creep theory for time-dependent analysis.

Implementation of prestressing operations at different stages can be modelled with great ease. Members can be stressed or de-stressed at any solution step using straight or curved tendon profiles. Prestressing steel can also be added or removed as and when required. The complete history of stress and deformation histories for concrete and prestressing steel at any solution step are reported to allow the serviceability conditions throughout the construction process as well as during the service life of the structure to be determined.

The program assumes a uniform distribution of nonprestressed steel throughout its analysis. Although this assumption may be acceptable for pretensioned members where the amount of bonded non-prestressed steel is nominal, the error can be significant if any section along the member contains a large area of bonded reinforcement. It was shown (Chapter 3) that there is a need to model the presence of bonded reinforcement properly due to their role in the time-dependent deformation and the transfer of stress from the concrete to the steel reinforcement. In the case of the structures being investigated in this research, large areas of bonded reinforcement is generally present at the intermediate support where continuity between precast units is established. This apparent limitation has been overcome by modelling the bonded reinforcement as an additional element acting compositely with the concrete element as shown in Section 4.4.3.

ADAPT also requires that a final creep coefficient and shrinkage be provided, and then determines the appropriate value at any time step according to either the ACI or CEB models. An additional program which considers different parameters (as described in Chapter 3) that affect the final creep and shrinkage has been written so that appropriate creep and shrinkage values for given conditions can be transferred to ADAPT.

Another limitation of ADAPT is that it only considers uncracked sections. In the case of a cracked section, the uncracked stiffness is assumed, hence deformation is underestimated. To overcome this problem, a further program can be developed to interface with ADAPT to check if cracked conditions occur and, if they are, new

stiffnesses based on cracked properties are calculated as described in Section 4.3. The new cracked stiffness is then fed into ADAPT for subsequent analysis.

4.4.2 Element formulations and material constitutive relationships

The beam element used by the program is based on the classical Bernouli-Euler beam theory where sections are assumed to remain plane and stress and strain relationships over the depth of the section are linear. Its stiffness matrix and load vectors only include axial and bending deformations. Time dependent strains included in the concrete constitutive model include ageing, creep, and shrinkage. The shrinkage strain may be uniform or vary linearly over the depth of each element. The creep and shrinkage strain increments contribute to the virtual work expression and are taken as the initial values in the load vector for the each time step. The ageing strain is a fictitious strain due to the change in the elastic modulus which does not contribute to the load vector but does enter the constitutive relationship.

The geometry of the beam element is defined by two nodes *I* and *J* located in the global *X* and *Y* plane and at the centroidal axis of the element (Figure 4.7a). The element cross section is defined by the local *y* and *z* plane and assumed constant over an element length (Figure 4.7b). The cross section must be symmetrical about the local *y* axis. Each element has six degrees of freedom where each end has two translations and one rotation (Figure 4.7c). The internal displacement fields (u_o and v_o) in the element are expressed in terms of the three independent local nodal displacements θ_I, θ_J and u_j (Figure 4.7d).

Prestressing steel is idealised by a system of linear prestressing segments which are connected at the nodes. Each tendon segment is assumed to be under uniform axial stress over its length. Initial prestressing forces are computed based on the actual jacking force at each tendon end. The calculation of initial prestressing force at each node may include the effects of instantaneous friction and anchorage slip loss encountered in post-tensioned beams. However, the loss due to elastic shortening in prestensioned beams must be determined prior to the analysis. Tendons are considered

to be perfectly bonded where displacement compatibility between prestressing steel segments and beam elements is enforced at the common nodes.

Relaxation loss of prestressing steel is computed based on the proposed equation by Magura *et al* (1964). The expression assumes that strain remains constant over any given time interval. However, since the stress history due to other loss mechanisms and external loading changes over time, the program introduces an additional procedure to incorporate the changing values in the stress history as proposed by Hernandez and Gamble (1975). The procedure assumes that all non-relaxation changes in tendon force occur at the ends of the time steps as shown in Figure 4.8.

Detailed description and theoretical formulations are presented in the manual (ADAPT, 1993).

4.4.3 Considerations for bonded reinforcement

ADAPT is primarily designed for fully prestressed members where the presence of bonded non-prestressed steel is assumed to be nominal and uniformly distributed over the section. In this study, the presence of both component of bonded reinforcement is to be properly accounted for because their effect on the time-dependent deformation could be significant. The steel provides a restraining effect for continuous deformation due to creep and shrinkage where the resulting tensile stress could reach yielding point for the steel.

The non-prestressing reinforcement can be modelled as separate elements which are connected to the respective concrete elements through rigid *SLAVE* elements (Figure 4.9). The rigid connection is necessary to model perfect bond between the concrete and the steel elements. This model has the advantage of accommodating un-symetrically reinforced sections. Verification of this model through comparisons with published experimental results and the classical method of analysis are presented in Section 4.5.

4.4.4 Computer implementation for cracked sections

ADAPT only produces approximate solutions for cracked sections because it assumes full uncracked stiffness of the members. A special procedure where cracked sections are accounted for is required in order to produce a more realistic analysis.

The computer implementation for cracked sections adopted here uses the described in Section 4.3 where tension stiffening effects are also taken into consideration . An instantaneous structural analysis is carried out prior to the time-dependent analysis for every change in boundary conditions or when an additional load is applied. This is to ensure that proper sectional stiffness is being used for the subsequent ADAPT analysis. If cracked sections are encountered, a procedure for modelling the cracked section is then implemented in which the centroidal axis of the uncracked section is maintained as the reference line for the new finite element model. New section properties for cracked sections are determined with values between the uncracked and fully cracked sections. The new cracked stiffness is calculated with respect to the centroidal axis of cracked section as shown in Figure 4.10. The suitability of such a procedure is verified against published experimental results (Section 4.5.4).

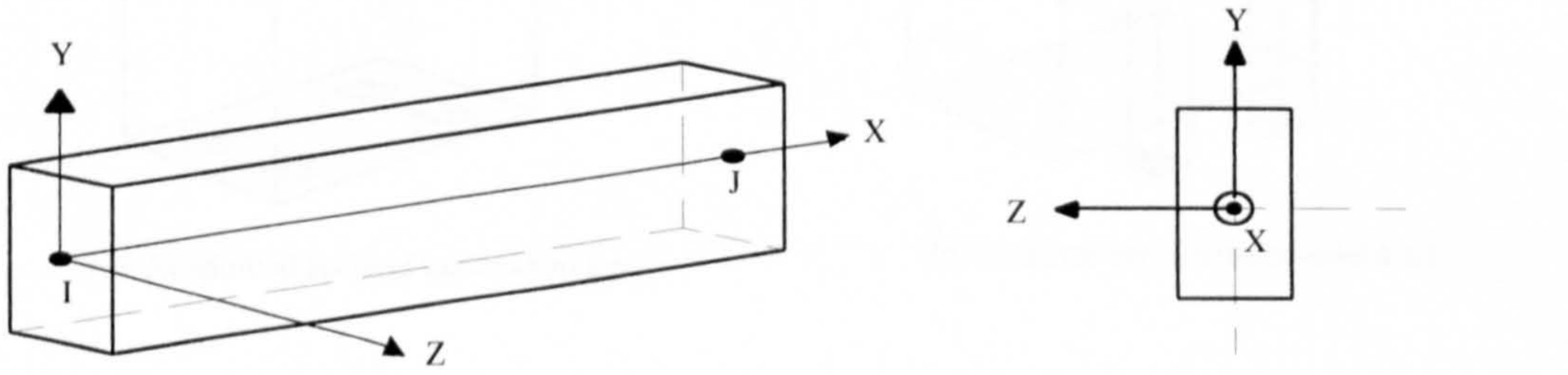

(a) Beam element local coordinate system

(b) cross section

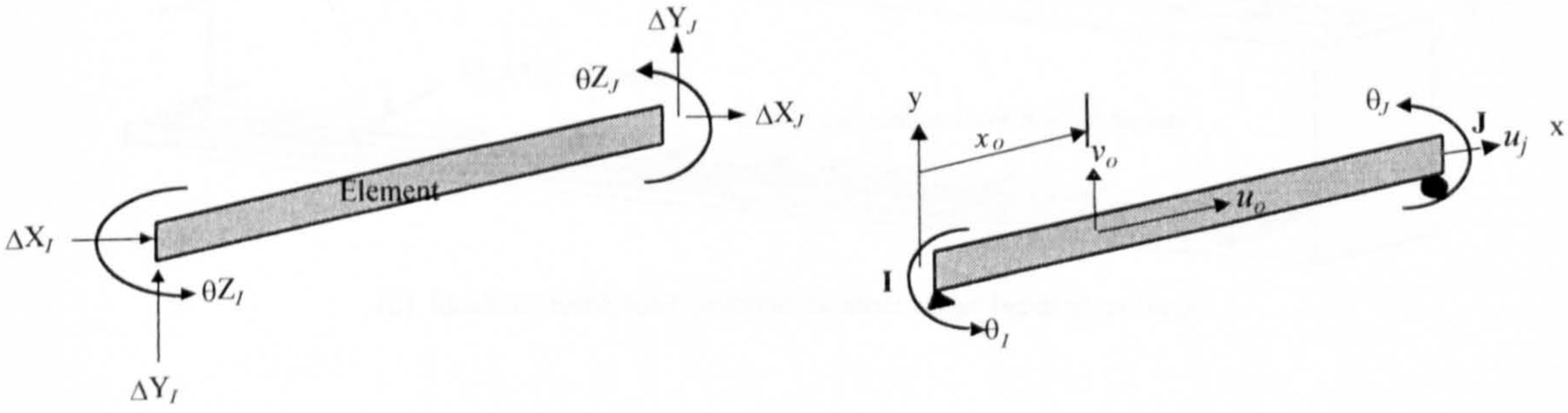

(c) Global displacement and degrees of freedom

(d) Local displacement and degrees of freedom

Figure 4.7: Basis of beam element formulation for ADAPT (1993)

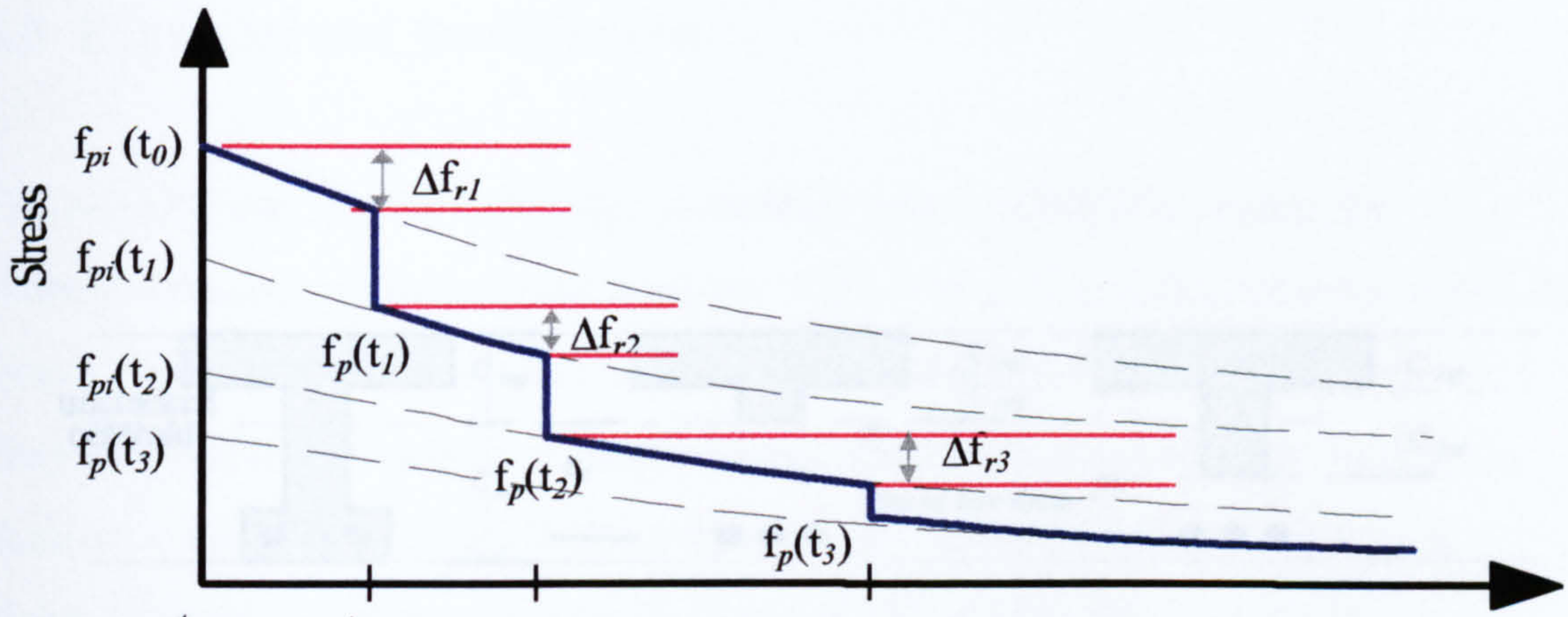

Figure 4.8: Prestress tendon relaxation model (ADAPT 1993)

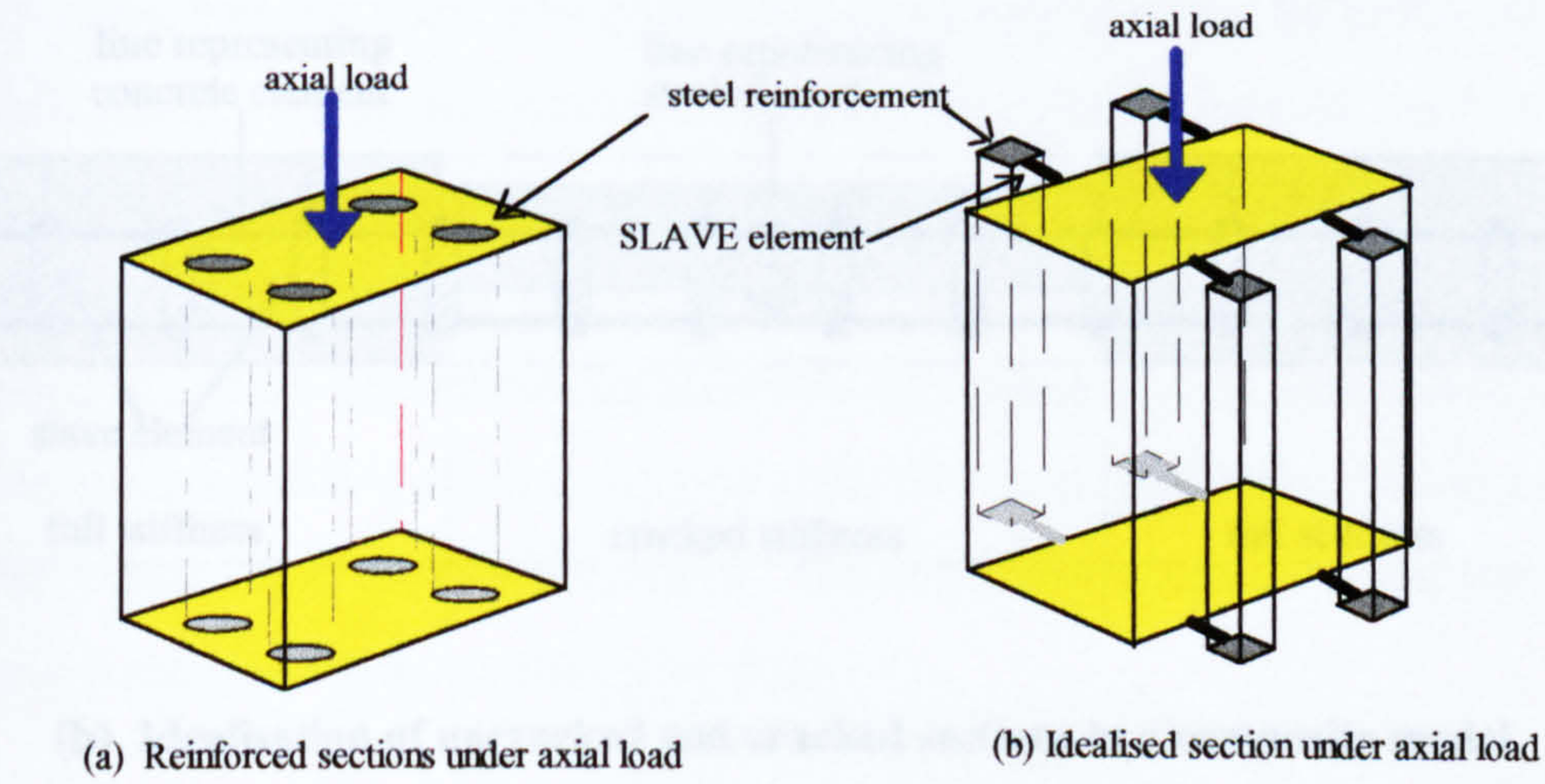

(a) Reinforced sections under axial load

(b) Idealised section under axial load

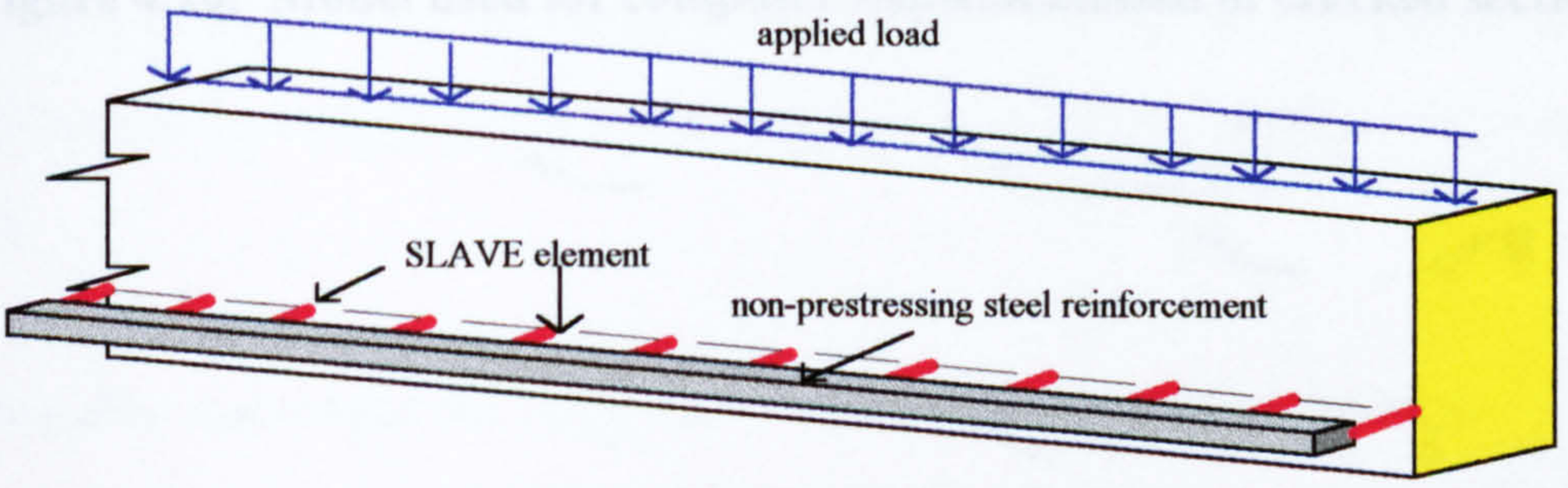

(c) Idealised reinforced concrete member under bending moment

Figure 4.9: Modelling bonded reinforcement in ADAPT

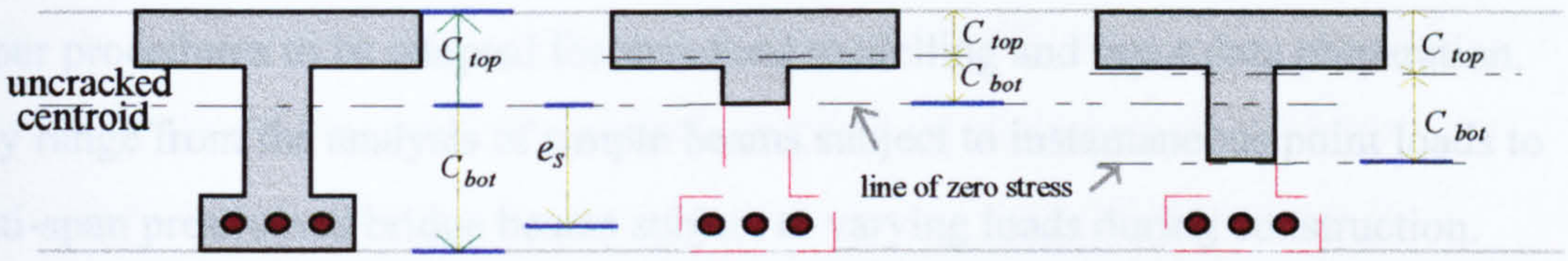

(a) section definition used for ADAPT modelling

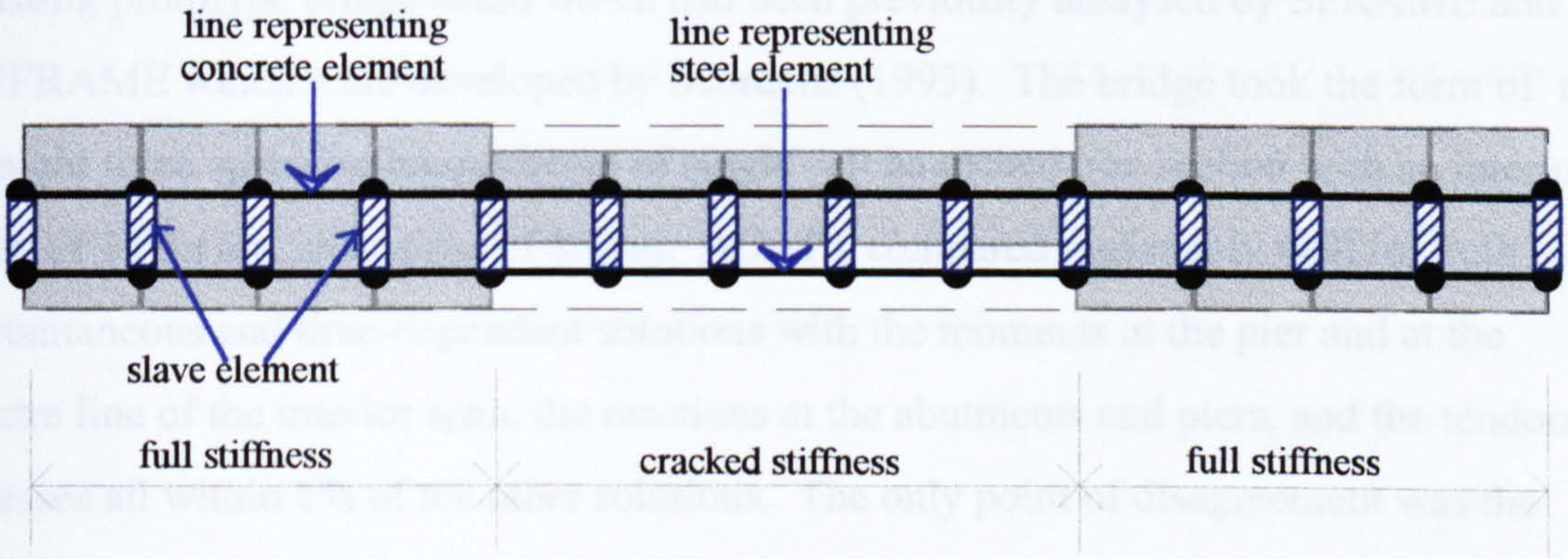

(b) Idealisation of uncracked and cracked sections in a composite model

Figure 4.10: Model used for computer implementation of cracked sections.

4.5 Examples and Verifications

The ADAPT user manual (1993) has presented various example problems for instantaneous and time-dependent analyses of structures. The examples demonstrate the proper procedures to be adopted for structural modelling and input data preparation. They range from the analysis of simple beams subject to instantaneous point loads to multi-span prestressed bridge beams subject to varying loads during construction. These examples are also used to verify the accuracy of ADAPT.

All simple beam analyses compared well with the results given by the calculations according the elastic beam theory. The analysis for incrementally constructed beams was compared with that of other existing computer codes. This analysis used an existing prototype bridge beam which had been previously analysed by SFRAME and PCFRAME which were developed by Scordelis (1993). The bridge took the form of a straight three span continuous beam of single cell haunched box section with an interior span of 137m and side spans of 86.9m. ADAPT compared reasonably well for both instantaneous and time-dependent solutions with the moments at the pier and at the centre line of the interior span, the reactions at the abutments and piers, and the tendon stresses all within 1% of the other solutions. The only point of disagreement was the centre span deflection where results differed by 11%.

Further verifications needed to be carried out in the following areas before confirming the accuracy of ADAPT for the forthcoming analyses. Firstly, an acceptable maximum element length for each structural model needs to be established for the following reasons:

(a) The manual did not verify the solutions for structures subjected to instantaneous uniformly distributed loads. Structural members subjected to a uniformly distributed loads are sensitive to the element size because the input loads in ADAPT are transformed into equivalent point loads applied at the end nodes.

(b) Composite structures i.e. structures comprising of two or more different materials form part of this study. The use of *SLAVE* element only guarantees the compatibility of the different components where they are connected.

Secondly, manipulation of the built-in functions in ADAPT such as the use of *SLAVE* elements for modelling the contribution of bonded reinforcement to time-dependent deformation need to be verified. Finally, the additional part of the analysis that considers cracked sections for instantaneous and time-dependent deformation will also need to be verified.

This section attempts to define the suitability of the computer model to be used as a research tool in this investigation. Homogenous and composite prestressed members under instantaneous uniformly distributed loads are compared with the classical elastic analysis. The presence of bonded reinforcement and its contribution to the composite action in structural members and the effects of cracked sections on structural deformation are verified through comparisons with laboratory investigations and the manual calculations using classical methods of analysis.

4.5.1 Element size

A series of analysis using ADAPT for simple monolithic and composite beams subjected to various forms of uniformly distributed loading have been carried out. Element length to depth ratios of 4.4 and 0.88 that represented typical large and small elements respectively were used to establish the effects of element size for different loading conditions. Resulting deflections and stresses due to symmetrical or un-symmetrical loading covering the whole or part of the beam were observed. The results showed significant differences in the solutions of the two element sizes.

A suitable element size needs to be established to ensure that the minimum number of elements is used consistent with the desired level of accuracy. To do this, the beams tested by Mattock *et al* (1960) was employed. The same beam was used later for the time-dependent analysis of continuous composite beams. This was based on the geometry of which were half-scale models of bridge beams with a full scale span of

20m. The span-depth ratio of the beam was 17.5 which is typical for road bridge members. The beam was subjected to a uniformly distributed load of 3.9kN/m. Results of the computer models for deflection are compared with those from an elastic analysis as shown in Figures 4.11 and 4.12. The accuracy of the deflections calculated by ADAPT have improved from 95% for an element length to depth ratio of 4.4 to 99.5% for an element length to depth ratio of 1.75. This is the case for both homogenous and composite sections.

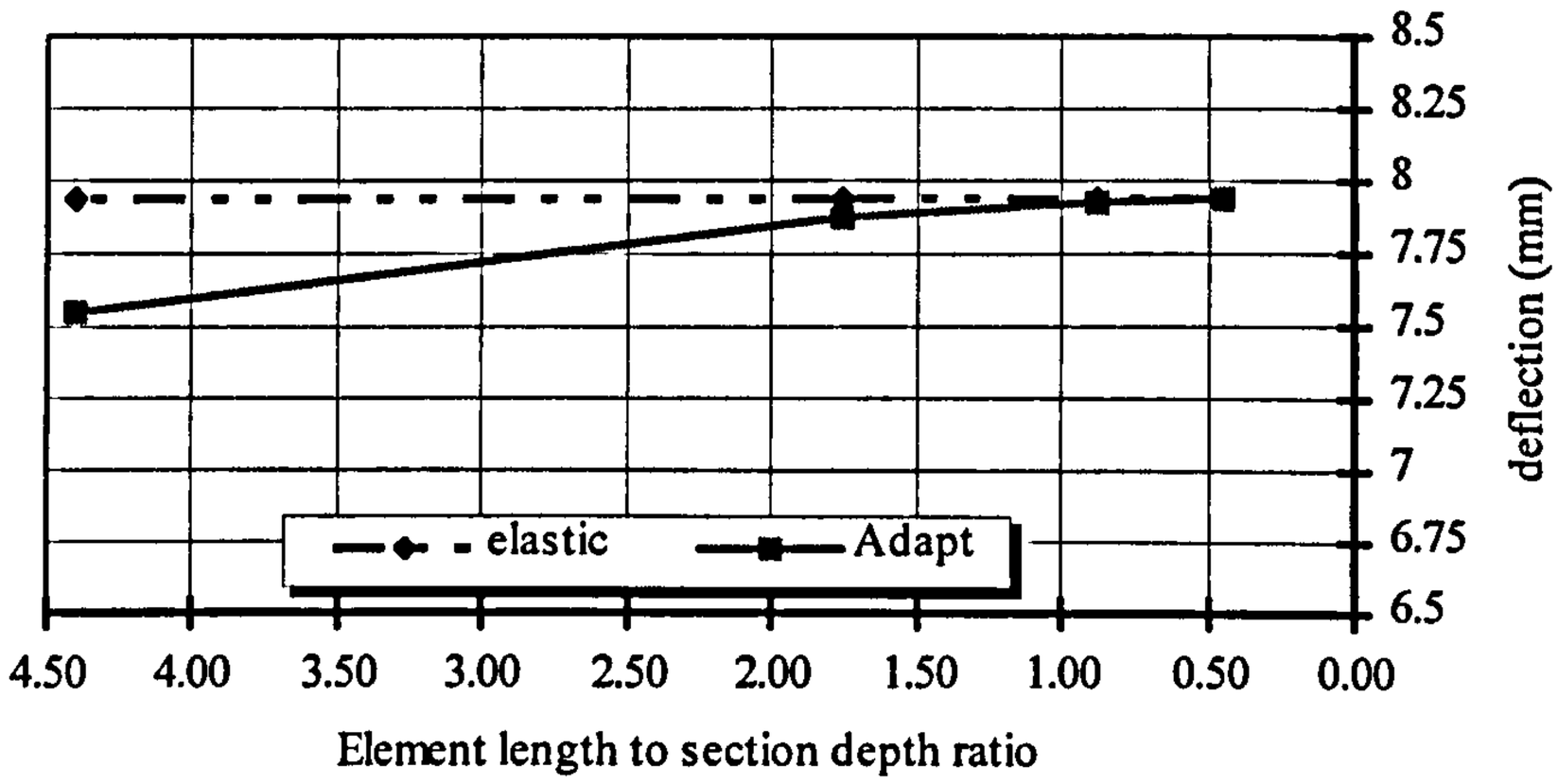

Figure 4.11: Comparisons of deflection between elastic and ADAPT for homogenous section

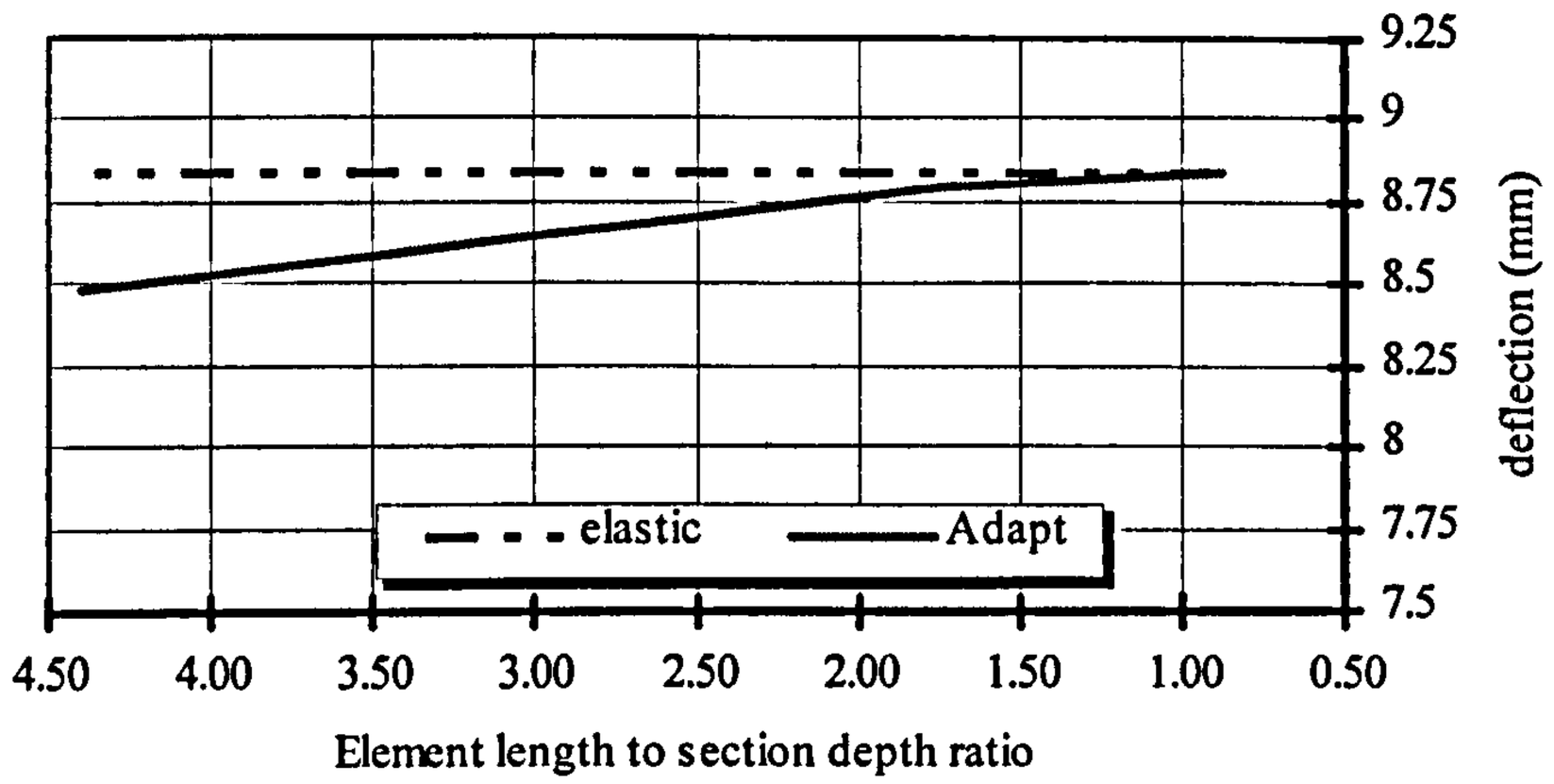

Figure 4.12: Comparisons of deflection between elastic and ADAPT for composite section

The magnitude of concrete stress is also comparable to that determined by elastic analysis. Table 4.2 shows that the stresses at the bottom and top fibres of the precast beam (σ_1 and σ_2) and the cast in situ slab (σ_3 and σ_4) are comparable between ADAPT and the elastic analysis when the element length to depth ratio is smaller than 1.75. Based on the deflection and stress solutions obtained by ADAPT it is therefore concluded an element length to depth ratio of 1.75 or less will give sufficient accuracy for any further analysis to be carried out in this project.

Table 4.2: Stress at top and bottom fibres for a composite section.

Element length to depth ratio	Stress under UDL (MPa) manual calculations				Stress UDL (MPa) ADAPT analyses			
	σ_1	σ_2	σ_3	σ_4	σ_1	σ_2	σ_3	σ_4
4.4	-7.06	7.74	0.41	0.61	7.14	7.96	0.32	0.565
1.75	-7.06	7.74	0.41	0.61	7.08	7.78	0.395	0.602
0.88	-7.06	7.74	0.41	0.61	-7.07	7.75	0.40	0.607

4.5.2 Time-dependent deformation of reinforced concrete sections.

A series of tests to investigate time-dependent deformations carried out by Chouman (1990) was used to verify the technique for modelling bonded reinforcement in concrete sections as described in Section 4.4.3. The gross concrete area of the section was 1.80×10^4 (mm^2) and the reinforcing steel content ranged from zero to 4.47%. The rectangular sections were subjected to a constant axial load of 90kN 7 days after casting and kept under ambient relative humidity of about 50%.

Four different possible analytical models for reinforced sections were tried. Model 1 neglected totally the presence of the bonded reinforcement. The gross sectional area of the concrete was subjected to the axial load which yielded an equivalent stress of 5MPa. Model 2 took into account the presence of bonded reinforcement by considering a transformed sectional area. The area of the reinforcement was multiplied with a

modular ratio of 6.7. For a similar axial load of 90kN and for the section reinforced with 4.47% of reinforcing steel, the initial stress to which the transformed section was subjected was calculated to be 3.85MPa. Both Models 1 and 2 represented monolithic sections (only the elastic modulus of concrete affected the time-dependent analysis) subjected to constant axial stress. Model 3 was chosen to represent the bonded reinforcement as a separate component but acting compositely with the concrete section under axial load. Actual areas of the reinforcement were used accordingly and the elastic modulus of the reinforcement were included in the analysis. Model 4 transformed the steel areas into equivalent concrete areas using the same modular ratio of 6.7 as in Model 2, but treating them as a separate component acting compositely with the concrete sections, as in Model 3. Details of each model are shown in Figure 4.13.

Since ADAPT does not have the facility to specify steel sections, an equivalent concrete strength (f'_c) of 1565 MPa was specified for the reinforcement in Model 3 in order to produce the actual elastic modulus of steel (200 MPa). This was calculated based on the formula of the elastic modulus of concrete adopted in ADAPT as given by Equation 4.29.

$$E_c = 2400^{1.5}(0.043)\sqrt{f'_c} \quad \text{(MPa)} \tag{4.29}$$

Comparisons of the total deformations between the experimental results and these models are shown in Figures 4.14 and 4.15.

Figure 4.14 shows a comparison between Model 1 and the experimental results for sections reinforced with 0.0, 0.63, 1.62 and 4.47% of reinforcing steel. Results of the analysis assuming the gross section (Model 1) indicate that ADAPT predicted the time-dependent deformations reasonably well for the sections without reinforcement and with 0.63% reinforcement. At 233 days, Model 1 underestimated the experimental results by 6 and 0.5% for the sections with 0.0 and 0.63% steel respectively. For the section reinforced with 1.62% steel, Model 1 overestimated the time-dependent deformation by 14%. Greater overestimation was calculated (71%) for the section reinforced with 4.47% steel. The overestimation of the deformations were due to the simplifying

assumption in Model 1 that the reinforcing steel did not affect the deformation. It can be seen that sections reinforced with about 1.0% or greater steel need to consider the presence of the reinforcement when the time-dependent deformations are calculated.

Comparisons of the total deformation for sections reinforced with 1.62 and 4.47% steel in Figures 4.15 and 4.16 indicate that both Model 3 and 4 are suitable for the analyses. The analyses using both models yielded results within 10% of the experimental values. Model 2 improved on the results from Model 1 where the overestimations of the deformation were reduced from 14 to 10% for the section reinforced 1.62% steel and from 71 to 56% for the section reinforced with 4.47%.

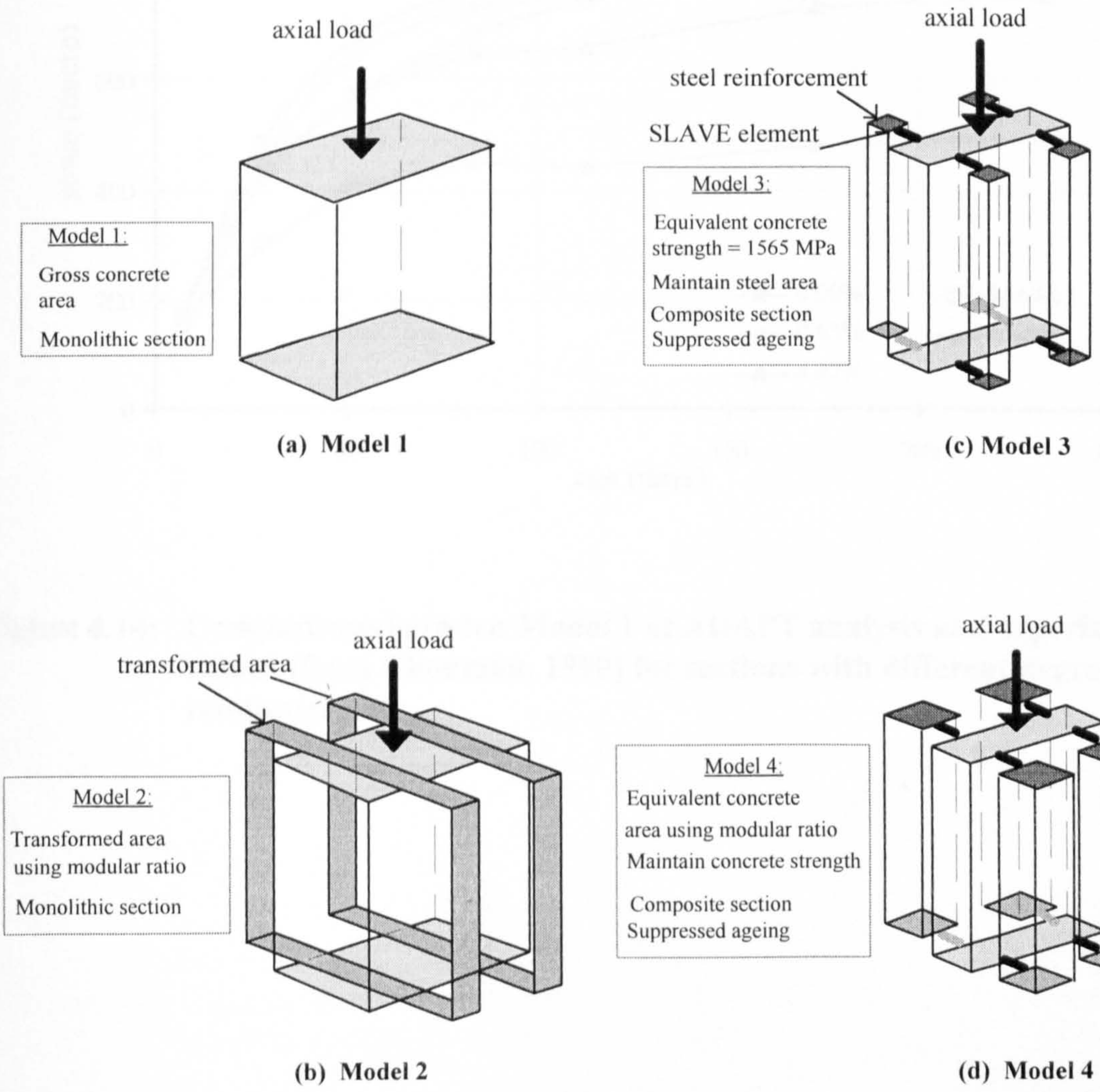

Figure 4.13: Four different models considered to account for bonded non-prestressing steel

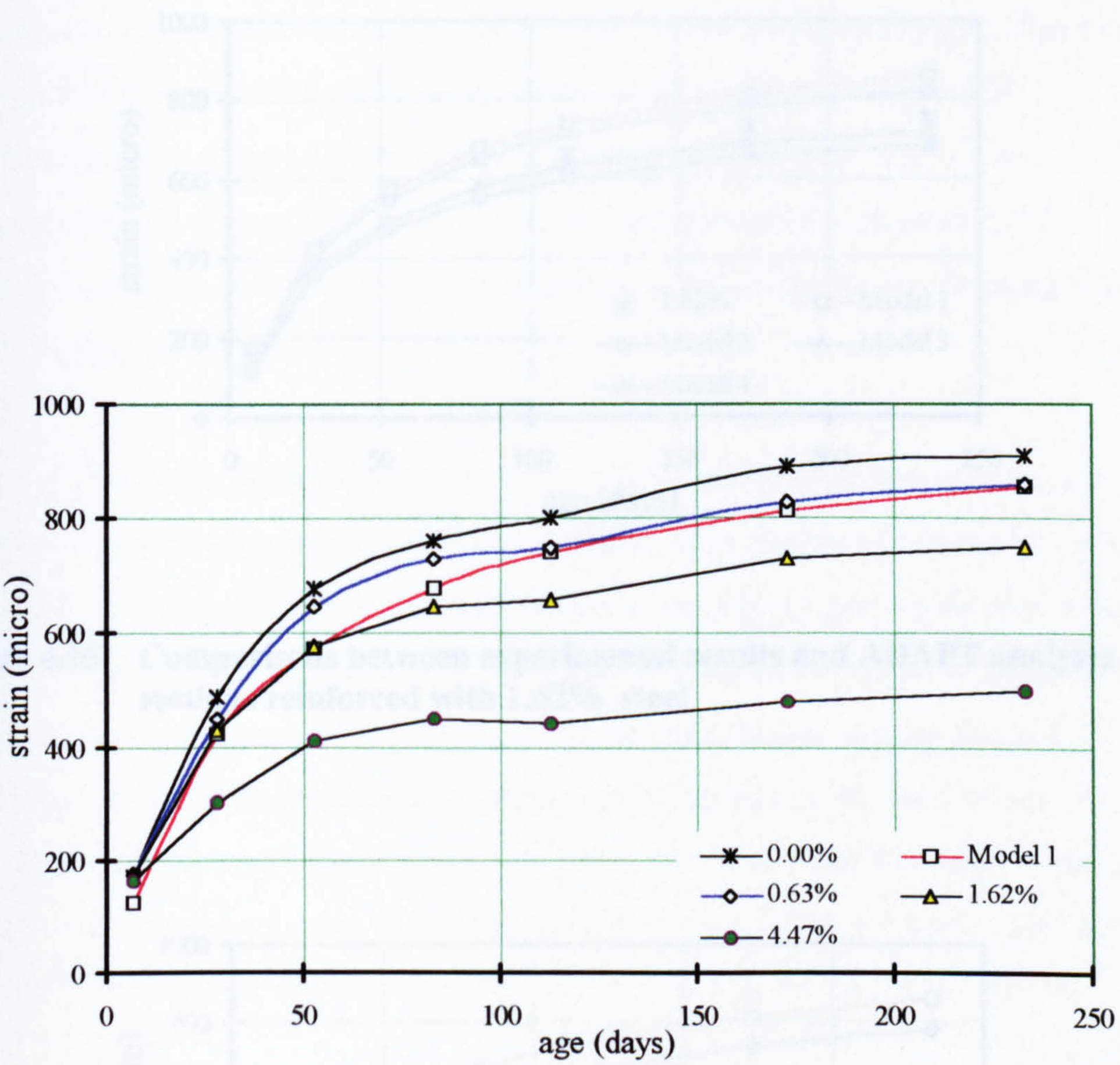

Figure 4.14: Comparisons between Model 1 of ADAPT analysis and experimental results (from Chouman, 1990) for sections with different degrees of reinforcement

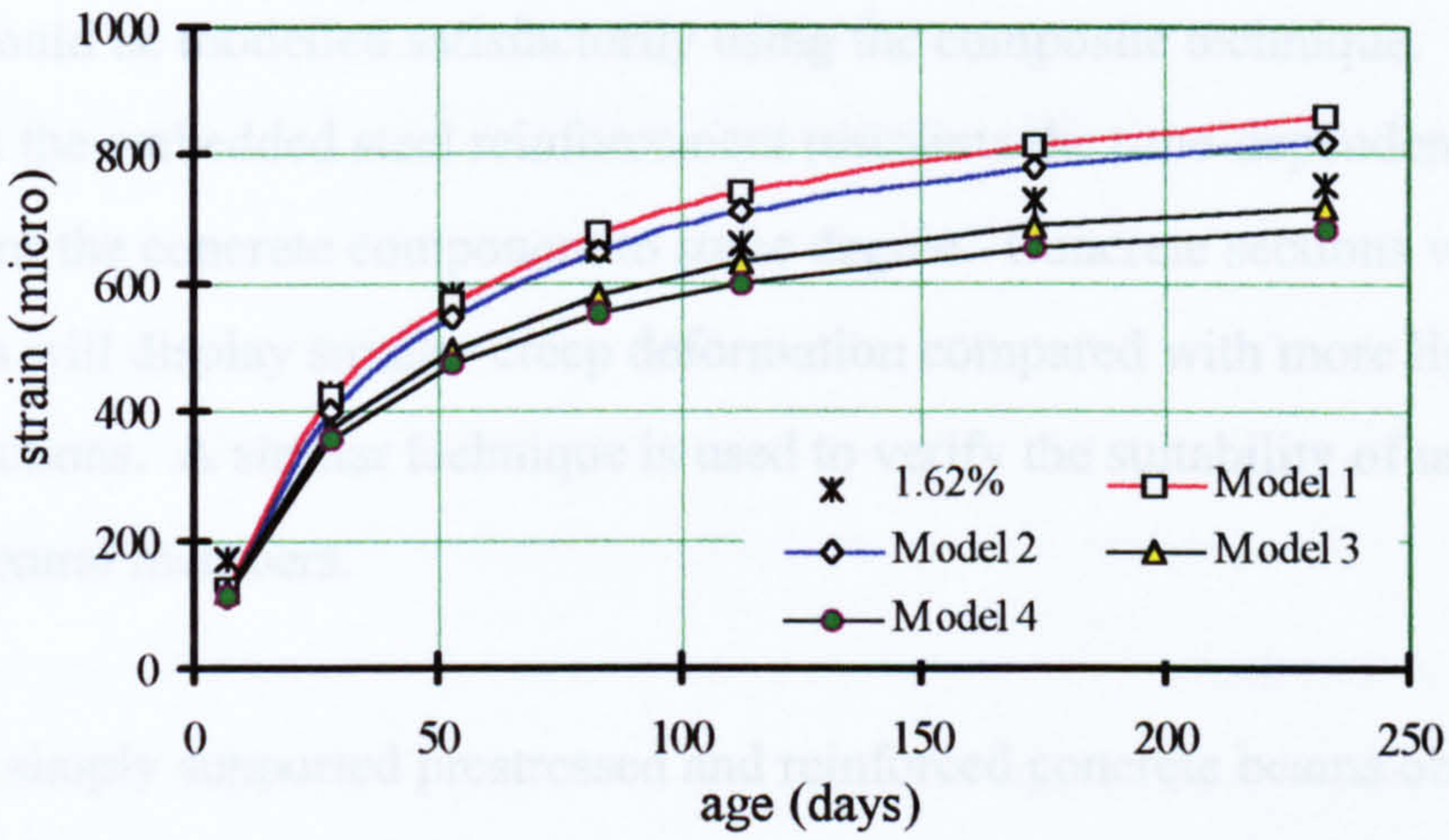

Figure 4.15: Comparisons between experimental results and ADAPT analyses for sections reinforced with 1.62% steel

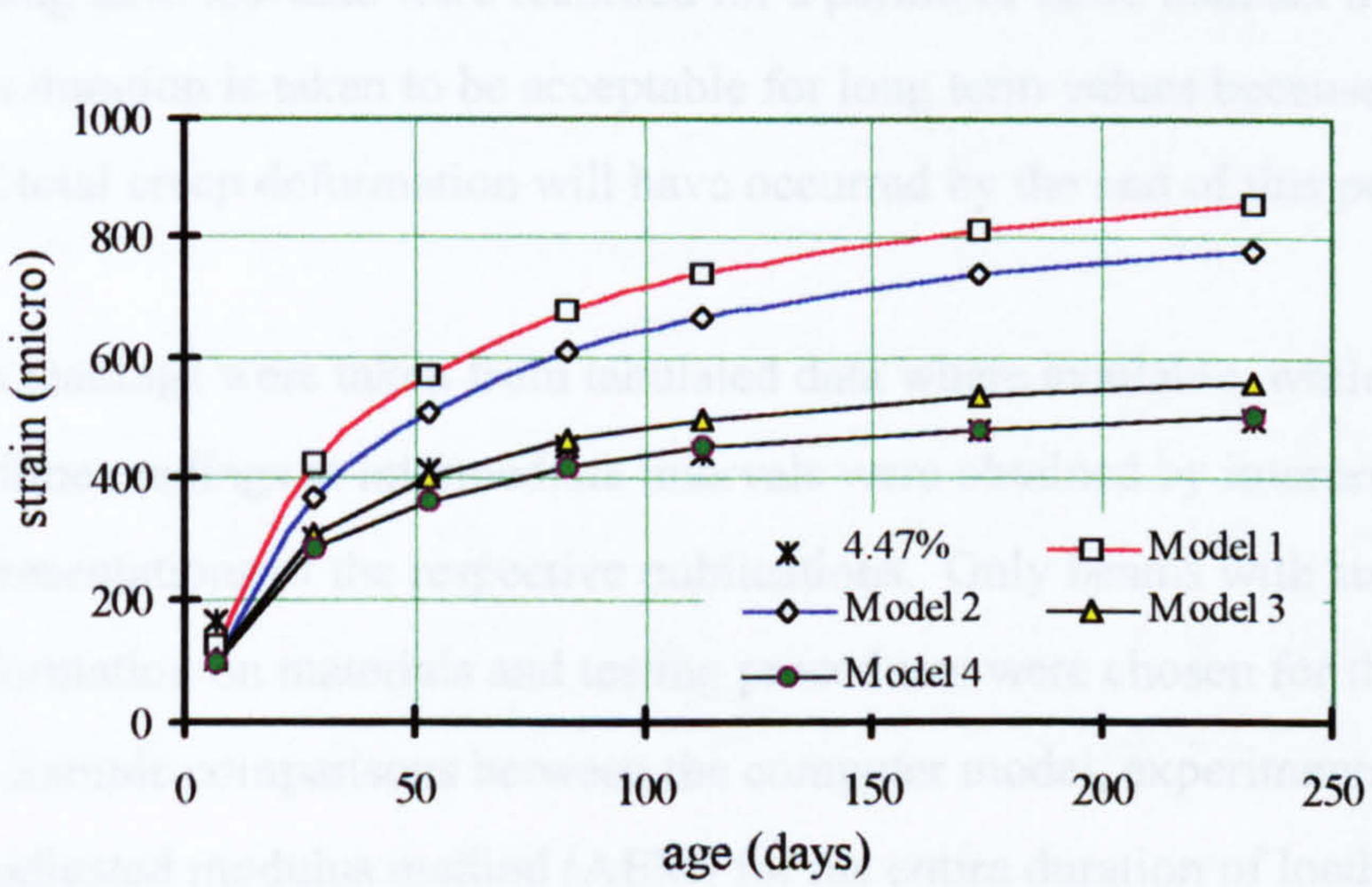

Figure 4.16: Comparisons between experimental results and ADAPT analyses for sections reinforced with 4.47 % steel

4.5.3 Time dependent deformation of simple flexural members

The previous section has shown that a reinforced concrete section subjected to constant axial stress could be modelled satisfactorily using the composite technique. This model confirms that the embedded steel reinforcement restraints the time-dependent deformation of the concrete component to some degree. Concrete sections with higher steel contents will display smaller creep deformation compared with more lightly reinforced sections. A similar technique is used to verify the suitability of using such a model for flexural members.

A total of 77 simply supported prestressed and reinforced concrete beams obtained from 9 different research projects from the USA, UK and Australia have been used to verify the model. A summary of the experimental details and their respective sources is shown in Table 4.3, with detailed descriptions and experimental data are given in Appendix A. Thirty four of these tests were of prestressed beams subjected to various loading conditions. Eight of the prestressed specimens were full size prestressed bridge beams. Most of the long term test data were recorded for a period of more than six months after loading. This duration is taken to be acceptable for long term values because the greater proportion of total creep deformation will have occurred by the end of this period.

All long term readings were taken from tabulated data where available, while deformation-time readings at intermediate intervals were obtained by interpreting the graphical representations of the respective publications. Only beams with sufficient published information on materials and testing procedures were chosen for this comparison. Sample comparisons between the computer model, experimental results and the age-adjusted modulus method (AEM) for the entire duration of loading are shown by Figures 4.17-4.20. The graphs show that the model produces good correlation with the experiments and the AEM method.

A similar approach to the statistical procedure used to evaluate the CEB creep and shrinkage models has been adopted here to establish the suitability of the computer model for structural members under flexural actions. The evaluation of the CEB material model was based on 16 different published experiments on creep and shrinkage

(CEB Bulletin No. 199, 1990). Accordingly, the number of experiments available here for flexural members are deemed to be sufficient for this evaluation.

To characterise the accuracy of the prediction models, a mean error ($\overline{X}$), standard deviation of the errors (Δ), and systematic overestimates or underestimates ($\overline{m}_i$) for the prediction of long term values have been evaluated. Summaries of this evaluation for long-term predictions for prestressed and reinforced beams are given in Tables 4.4 and 4.5 respectively. Calculated deformations obtained for this evaluation are based on uncracked member stiffnesses. A coefficient of variation ($\overline{V}_i$) which characterises the error over the entire duration for a given experiment has also been evaluated. Detailed formulae for these statistical values are presented in Appendix B.

Tables 4.4 and 4.5 show individual error and the ratio between calculated and experimental results (m_i). From these values, $\overline{X}$, Δ and $\overline{m}_i$ are evaluated. The results show that the model gives better predictions for prestressed beams than for reinforced concrete beams. For long term values of deflection, the model gives m_i=1.07 for prestressed beams as compared to $\overline{m}_i$=0.5 for reinforced concrete beams. The mean error and standard deviation of the error are 21.2mm and 45.7mm respectively for reinforced concrete beams. The model yielded poor predictions for reinforced concrete sections because deflections due to the full stiffness of the sections were assumed even after cracking. Individual errors showed that the deflections were underestimated between 64 to 30% of the experimental values. Figure 4.21 also shows that almost all the experimental long term deflections are outside the 20% band of the predicted values.

For prestressed beams, only two were subjected to loads greater than the cracking loads i.e. beams *181a* and *150%SL*. Cracked prestressed beams do not seem to suffer from gross underestimation of the deflections which were predicted to be within 16% of the experimental results. The mean error and standard deviation of error for long term deflection are at 2.25mm and 5.09mm respectively. This shows that the model can predict the long term deformation for prestressed beams very well. Long term

deflections for all simply supported prestressed beams were found to be within the 20% band of the predicted values (see Figure 4.23)

The long term prediction of cracked beam deflections improves to an acceptable level when the procedure for cracked sections, as outlined in Section 4.4.4, is implemented (see Table 4.6). An average values of stiffness between the uncracked and fully cracked sections was used to ascertain their effects on the predicted values. The average estimate of the long term deflection ratio improves from 0.5 to 0.94, the mean error improves from 21.2mm to 10.7mm, and the standard deviation of errors decreases from 45.7mm to 21.4mm. Figure 4.24 shows that the majority of the cracked beams analysed using this procedure fall within the 20% band of the experimental results. Combining the predictions for the long term values of all the specimens, the mean estimate ($\overline{m}_i$) is obtained at 1.02, or the average error in the predictions is only 2.2%.

To characterise the mean error over the entire duration of loading, $\overline{V}_i$ has been evaluated. A total of 21 specimens comprising of cracked and uncracked beams were available for this evaluation. Their individual values are presented in Table 4.8. The variation coefficients of the individual specimens range between 4.71% for beam *GLR1,2* to 287.8% for beam *1P-2R*. However, 16 of the specimens have variation coefficients of 25% or less and the mean variation coefficient for all specimens is 13.4%.

Results from the statistical evaluation show that the predictions given by the computer model predict the long term values much better than the intermediate values. The mean error in the long term values is 2.2% compared to 13.4% for the intermediate values. However, the values of the variation coefficients are still within acceptable accuracy, because the values for the CEB material model are also within this range (CEB Bulletin No.199, 1990).

4.5.4 Time-dependent deformation of continuous composite beams

Published experimental results for time-dependent behaviour of continuous precast prestressed composite beams are rare. A widely referred to experiment of such a structure is used to verify the computer model. The experiment was carried out by Mattock *et al* (1961) in the PCA Laboratory, USA in which the time-dependent change in the centre support reaction of a two span continuous composite beam was observed. The beams were half-scale models of typical bridge members. They were pretensioned at the age of 7 days and a uniformly distributed load was applied at the age of 9 days to simulate the actual stress under prestress and selfweight of the prototype beams. The beams were made continuous using conventional reinforcing steel in the deck slab over the intermediate support at the age of 30 days. The change in the centre support reaction was continuously monitored for two years.

The techniques adopted in the previous section to model simply supported flexural members are extended to ascertain their applicability for continuous precast prestressed composite beams. Beside the structural modelling, the beams were also modelled for their construction sequences. The results shown in Figure 4.24 for two sets of beams indicate that the model can be used to monitor time-dependent behaviour of such beams. Similar models can be used in further parametric analyses to quantify the behaviour of different structural configurations and construction sequences (see Chapter 6).

Table 4.3: Experiments on the time-dependent behaviour of reinforced and prestressed concrete beams

Researchers	Beam description	No. of beams	t_o and/or t_l	Span /Depth	Loading pattern and Duration	Experimental data
Washa and Fluck (USA-1948)	Simple span reinforced concrete beams with different sizes of rectangular cross sections	30	t_l= 14	20-70	UDL up to 910 days	deflections of cracked section
Yu and Winter (USA-1960)	Simple reinforced concrete beam spans = 4.27m and 6.09m, T-cross section, total depth = 305mm and 152mm	6	t_l= 30	14, 20 and 30	UDL up to 180 days	deflections
Cottingham, *et al* (USA-1961)	Simple prestressed beams of 6.09m span. Rectangular beam section - 133mm x 254mm.	3	t_o = 3 t_l= 60	24	50,75 and 100 % of design loads	strains and deflections
Breckenridge *et al* (USA- 1964)	Full size beam of 12.19m long simple span. Post-tensioned I-beams, 609.6mm deep	8	t_o = 9 t_l= 22	20	1/4 PL 0, 50,100 and 150% of SL	deflections and losses
Hutton, SG *et al* (USA-1966)	3.05m. simple prestressed, partially prestressed and reinforced rectangular sections, 152mm x 127mm	4	t_o= 7	24	under self-weight over 143 days	deflections and concrete strains
Shaikh and Branson (USA-1970)	4.57m prestressed and partially prestressed simple rectangular beams 152mm x 203mm	10	t_o= 7	22.5	Self-weight up to 172 days	camber
Bakos SL, *et al* (Aus. -1982)	Simple and 2-span reinforced concrete beams - with 100mm x 150mm rectangular sections	4	t_l= 28 t_l= 23	27-29	2-point loads up to 2000 days	deflections
Al-Khaja, W.A (UK-1986)	2.7m simple prestressed beams of rectangular and I-section	6	t_o = 8 t_l= 8	15	selfweight and point service load	strains, deflections and losses
Choumann, MM(UK- 1990)	2.7 m simple span partially prestressed beams, rectangular cross section	3	t_o= 8 t_l= 8	15	selfweight and point service load	strains and deflections

Note: t_o is the age at transfer and t_l=age at load application. UDL = Uniformly Distributed Load, PL = Point Load, SL=Service Load

Table 4.4: Statistical evaluation of long term deflections of prestressed concrete beams

Principal Investigator	Beam	Time (day)	Exp.(mm) [2]	Comp.(mm) [3]	Error,X (mm) [3-2]	m_i [3]÷[2]
Al-Khaja	ngi/c1	180	2.6	3	0.4	1.15
Al-Khaja	ngi/c1	365	2.76	3.1	0.34	1.12
Al-Khaja	ngr/c1	180	2.32	2.65	0.33	1.14
Al-Khaja	ngr/c1	365	2.45	2.8	0.35	1.14
Al-Khaja	ngi/c2	180	3.3	3.1	-0.2	0.94
Al-Khaja	ngi/c2	365	3.51	3.3	-0.21	0.94
Branson	I-1	172	12.8	15.1	2.3	1.18
Branson	I-3	172	10.4	13.3	2.9	1.28
Branson	II-2	140	5.5	7.7	2.2	1.40
Branson	II-3	140	4.7	6.5	1.8	1.38
Branson	III-1	124	12	15.5	3.5	1.29
Branson	III-2	124	11.1	13.6	2.5	1.23
Branson	III-3	124	8.3	11.8	3.5	1.42
Branson	IV-1	123	8.5	9.2	0.7	1.08
Branson	IV-2	123	7.9	9.4	1.5	1.19
Branson	IV-3	123	5.7	6.2	0.5	1.09
Cottingham	181a	270	20.3	17	-3.3	0.84
Cottingham	181b	270	10.9	11.1	0.2	1.02
Cottingham	181c	270	6.1	5.6	-0.5	0.92
Hutton	3P-0R	120	11.9	10.6	-1.3	0.89
Hutton	2P-1R	120	2	5.4	3.4	2.70
Hutton	1P-2R	120	2	0.52	-1.48	0.26
Breckenridge	173UL	180	31.8	34.4	2.6	1.08
Breckenridge	173UL	360	34.3	35.9	1.6	1.05
Breckenridge	50% SL	180	12.7	17	4.3	1.34
Breckenridge	50% SL	360	16.5	17.3	0.8	1.05
Breckenridge	100%SL	180	45.7	43	-2.7	0.94
Breckenridge	100%SL	360	49.5	44.9	-4.6	0.91
Breckenridge	150% SL	180	75.3	68.9	-6.4	0.92
Breckenridge	150% SL	360	86.3	72.6	-13.7	0.84

Table 4.5: Statistical evaluation of long term deflections of reinforced concrete beams using uncracked stiffness.

Principal investigator	Beam	Time (day)	Exp. (mm) [2]	Comp.(mm) [3]	Error, X (mm) [3-2]	m_i [3]÷[2]
Hutton	0P-3R	120	8.9	3.2	-5.7	0.36
Yu	A-2	180	33	16.2	-16.8	0.49
Yu	B-2	180	25.4	13.9	-11.5	0.55
Yu	C-2	180	21.6	12.1	-9.5	0.56
Yu	D-2	180	34.3	19.2	-15.1	0.56
Yu	E-2	180	15.2	7.4	-7.8	0.49
Yu	F-2	180	43.2	29.6	-13.6	0.69
Washa	A1,A4	900	10.2	7.1	-3.1	0.70
Washa	B1,B4	900	27.7	9.6	-18.1	0.35
Washa	C1,C4	900	39.9	17.3	-22.6	0.43
Washa	D1,D4	900	15.7	6.4	-9.3	0.41
Washa	E1,E4	900	64.5	21.9	-42.6	0.34
Washa	A2,A5	900	16.5	11.2	-5.3	0.68
Washa	B2,B5	900	40.1	14.9	-25.2	0.37
Washa	C2,C5	900	57.1	26.8	-30.3	0.47
Washa	D2,D5	900	18.8	9.9	-8.9	0.53
Washa	E2,E5	900	79.2	32.4	-46.8	0.41
Washa	A3,A6	900	27.7	18.9	-8.8	0.68
Washa	B3,B6	900	59.9	25.2	-34.7	0.42
Washa	C3,C6	900	93	45.8	-47.2	0.49
Washa	D3,D6	900	30.7	16.8	-13.9	0.55
Washa	E3,E6	900	122	52.2	-69.8	0.43

Table 4.6: Statistical evaluations of long term deflections of reinforced concrete beams using cracked stiffness.

Principal investigator	Beam	Time (day)	Exp.(mm) [2]	Comp.(mm) [3]	Error, X (mm)[3-2]	m_t [3]÷[2]
Hutton	0P-3R	120	8.9	3.2	-5.7	0.36
Yu	A-2	180	33	28.9	-4.1	0.88
Yu	B-2	180	25.4	25.4	0.0	1.0
Yu	C-2	180	21.6	22.8	1.2	1.06
Yu	D-2	180	34.3	31.1	-3.2	0.91
Yu	E-2	180	15.2	14.0	-1.2	0.92
Yu	F-2	180	43.2	42.8	-0.4	0.99
Washa	A1,A4	900	10.2	12.6	2.4	1.23
Washa	B1,B4	900	27.7	21.7	-6.0	0.78
Washa	C1,C4	900	39.9	53.8	13.9	1.35
Washa	D1,D4	900	15.7	19.8	4.1	1.26
Washa	E1,E4	900	64.5	37.6	-26.9	0.59
Washa	A2,A5	900	16.5	18.1	1.6	1.10
Washa	B2,B5	900	40.1	27.8	-12.3	0.69
Washa	C2,C5	900	57.1	59.7	2.6	1.04
Washa	D2,D5	900	18.8	22.0	3.2	1.17
Washa	E2,E5	900	79.2	53.7	-25.5	0.68
Washa	A3,A6	900	27.7	28.4	0.7	1.02
Washa	B3,B6	900	59.9	38.5	-21.4	0.64
Washa	C3,C6	900	93	69.1	-23.1	0.74
Washa	D3,D6	900	30.7	25.5	-5.2	0.83
Washa	E3,E6	900	122	84.1	-37.9	0.69
Bakos	1B1	520	25.0	23.4	-1.6	0.94
Bakos	1B2	520	8.5	6.8	-1.7	0.8

Table 4.7: Statistical evaluations to characterise the error over the whole loading duration.

Principal investigator	Beam	Duration (days)	S_i	$\bar{Y}_i$	V_i
Al-Khaja	NGI/C1	365	0.38	2.21	17.00
Al-Khaja	NGR/C1	365	0.34	1.96	17.18
Al-Khaja	NGR/C2	365	0.32	2.64	12.13
Chouman	GNR1,3	360	40.63	424.29	9.58
Chouman	GLR1,0	360	67.35	592.86	11.36
Chouman	GLR1,2	360	22.61	480.00	4.71
Cottingham	181a	270	4.28	17.75	24.10
Cottingham	181b	270	2.60	10.35	25.08
Cottingham	181c	270	1.51	5.88	25.63
Hutton	3P-0R	120	1.68	10.00	16.77
Hutton	2P-1R	120	0.82	3.96	20.74
Hutton	1P-2R	120	1.64	-0.57	-287.83
Breckenridge	173UL	360	8.15	25.20	32.36
Breckenridge	173(50%)	360	7.22	10.26	70.41
Breckenridge	173(100%)	360	3.05	-9.99	-30.54
Breckenridge	173(150%)	360	7.13	-28.17	-25.31
Washa	A-2	900	3.03	23.59	12.87
Washa	B-2	900	3.10	17.40	17.83
Washa	C-2	900	2.67	15.81	16.89
Washa	D-2	900	2.76	25.27	10.92
Washa	E-2	900	1.09	11.00	9.93
Washa	F-2	900	2.31	31.74	7.27

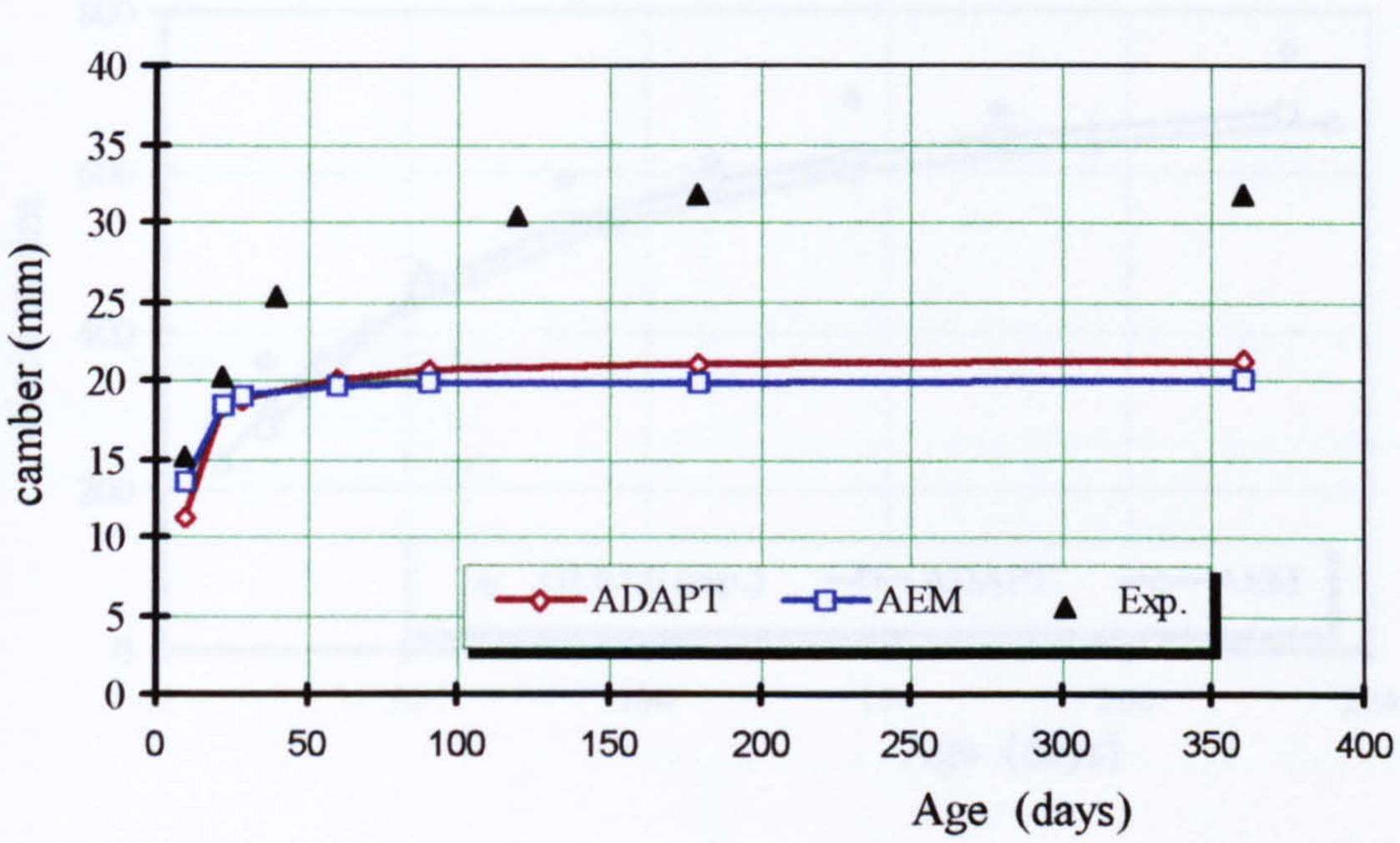

Figure 4.17: Comparisons between AEM and ADAPT analyses with experimental result for prestressed beams from Breckenridge (1964)

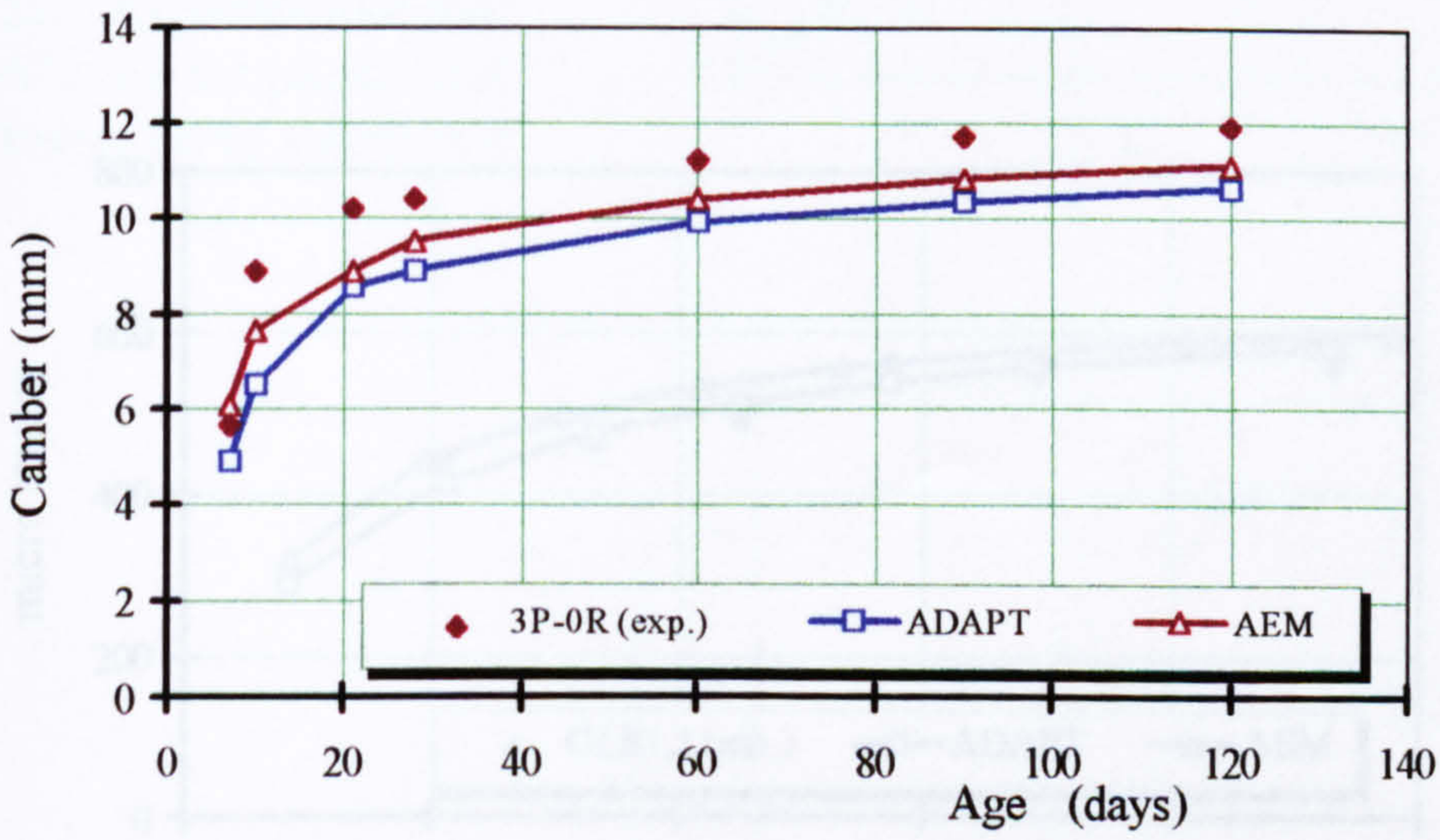

Figure 4.18: Comparisons between AEM and ADAPT analyses with experimental result for prestressed beams from Hutton (1966)

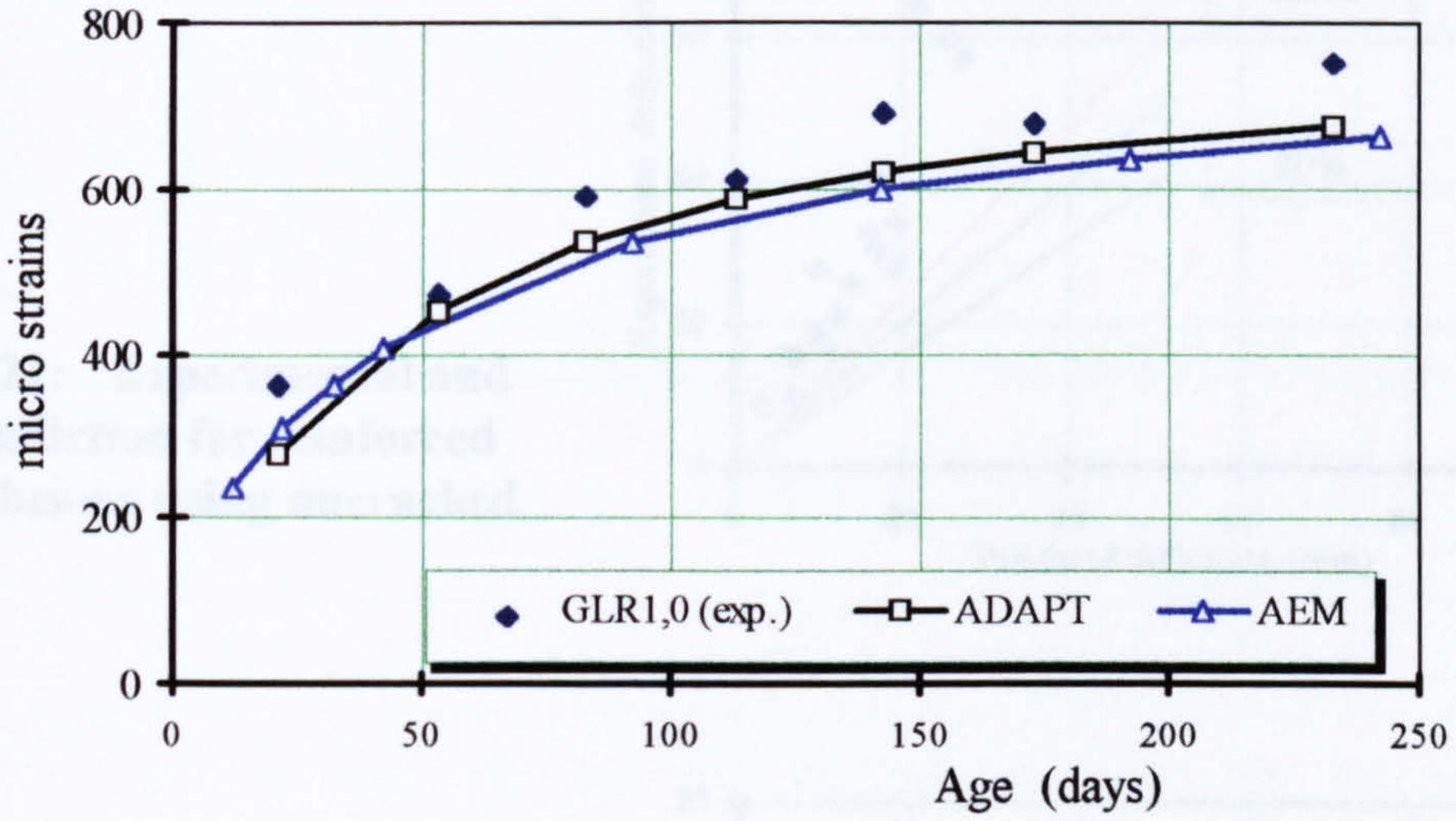

Figure 4.19: Comparisons between AEM and ADAPT analyses with experimental result for prestressed beams (A_s=0) from Chouman (1990)

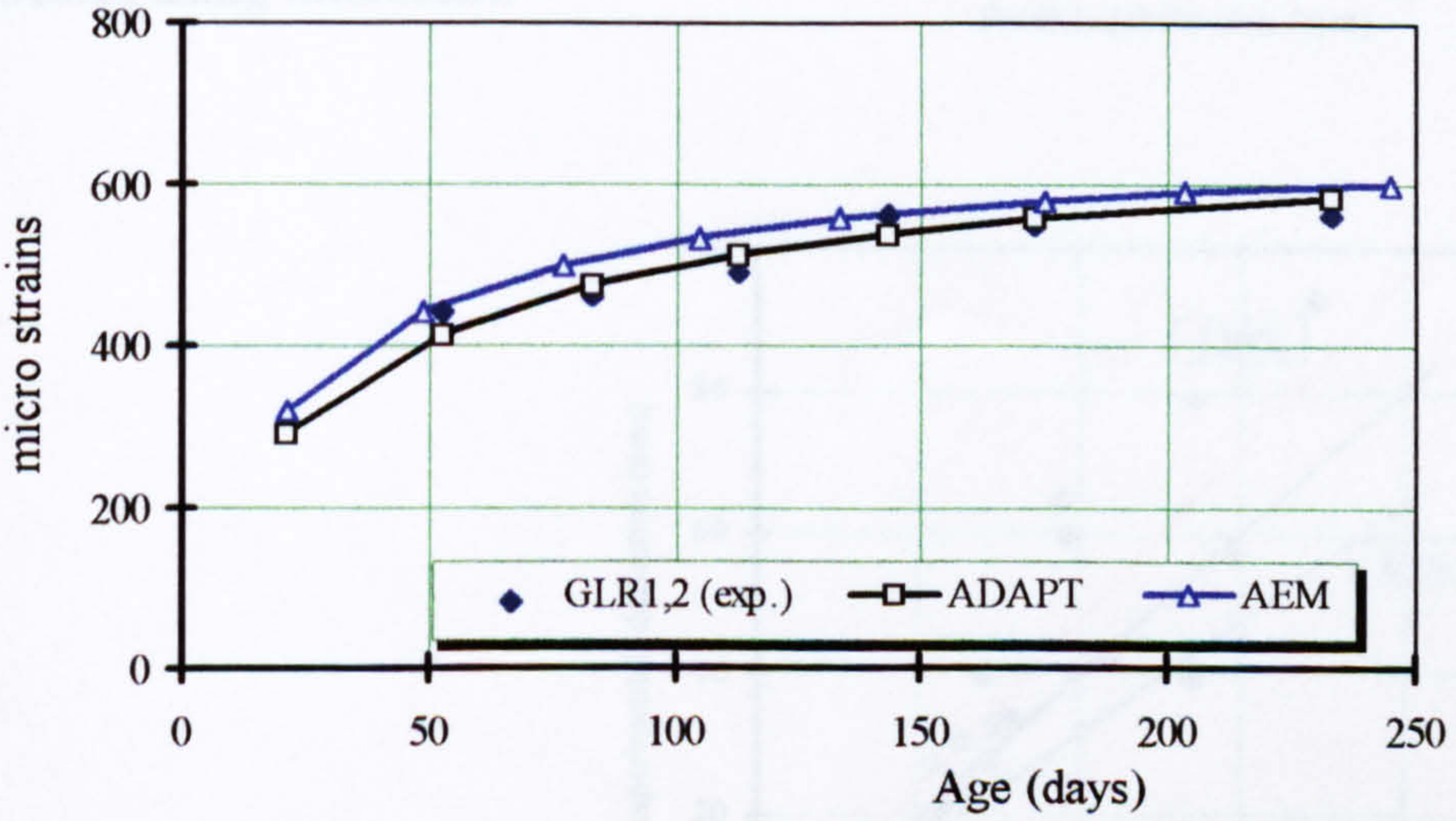

Figure 4.20: Comparisons between AEM and ADAPT analyses with experimental result for prestressed beams (A_s=1.3%) from Chouman (1990)

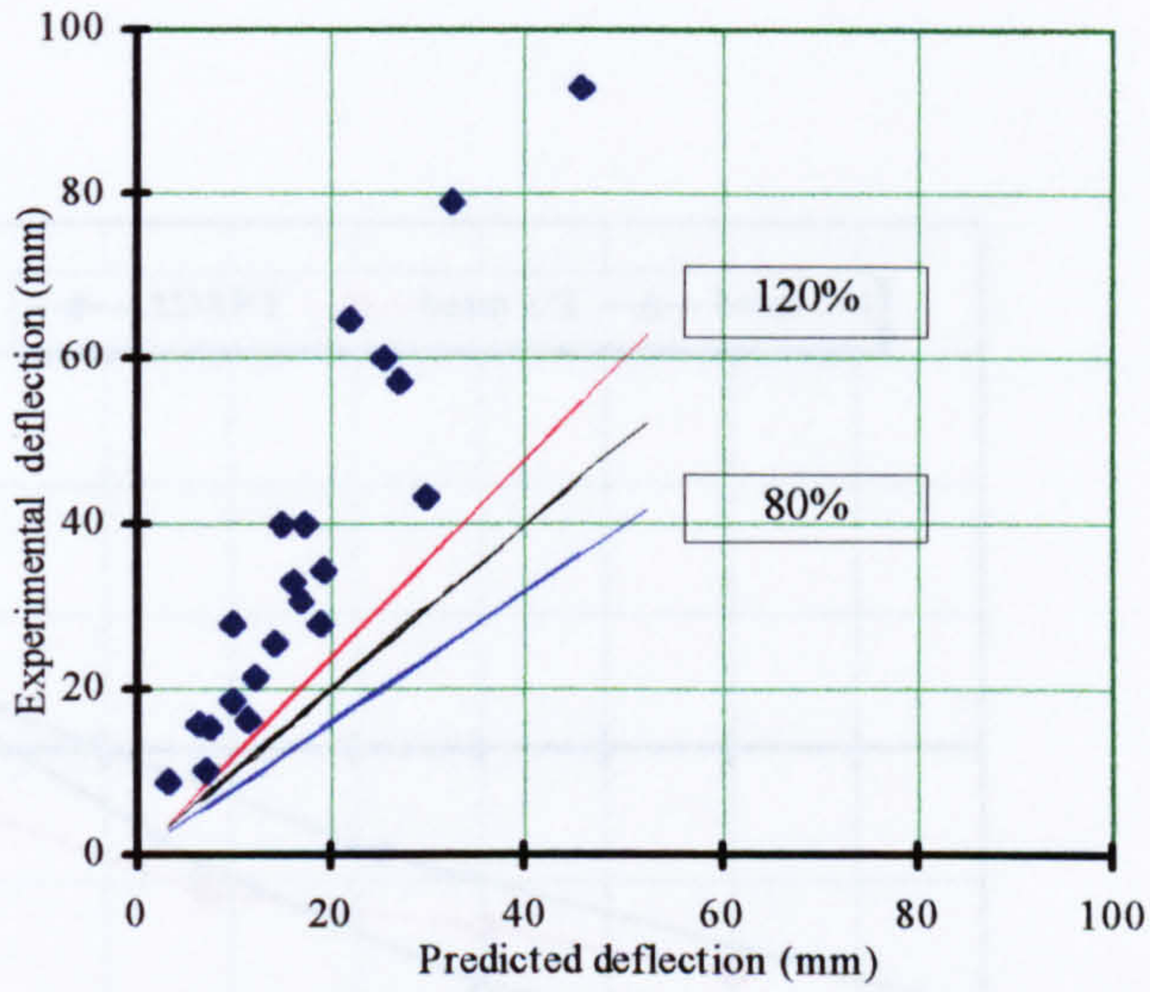

Figure 4.21: Experimental and model prediction for reinforced concrete beams using uncracked stiffness

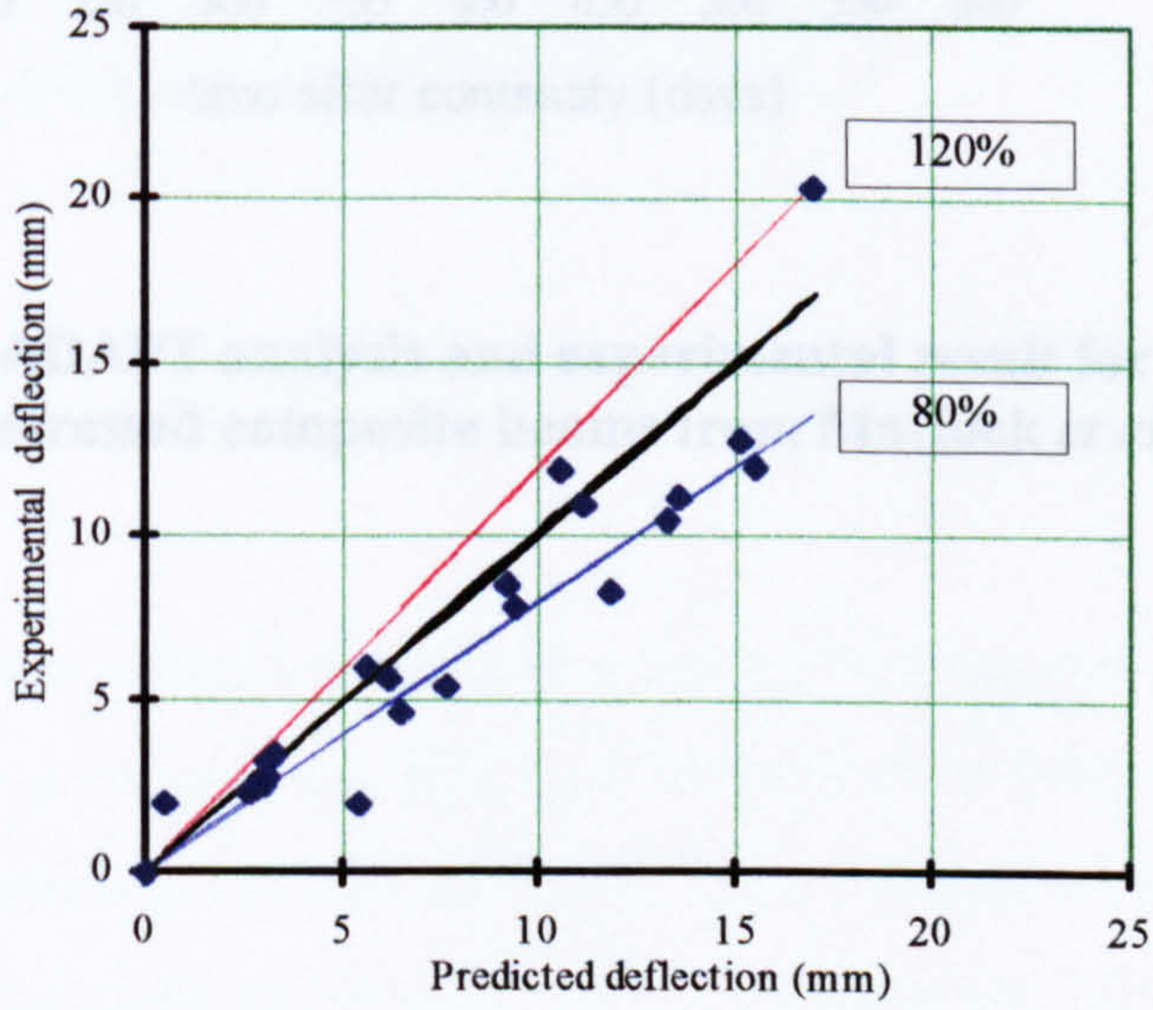

Figure 4.22: Experimental and model prediction for prestressed concrete beams using uncracked stiffness

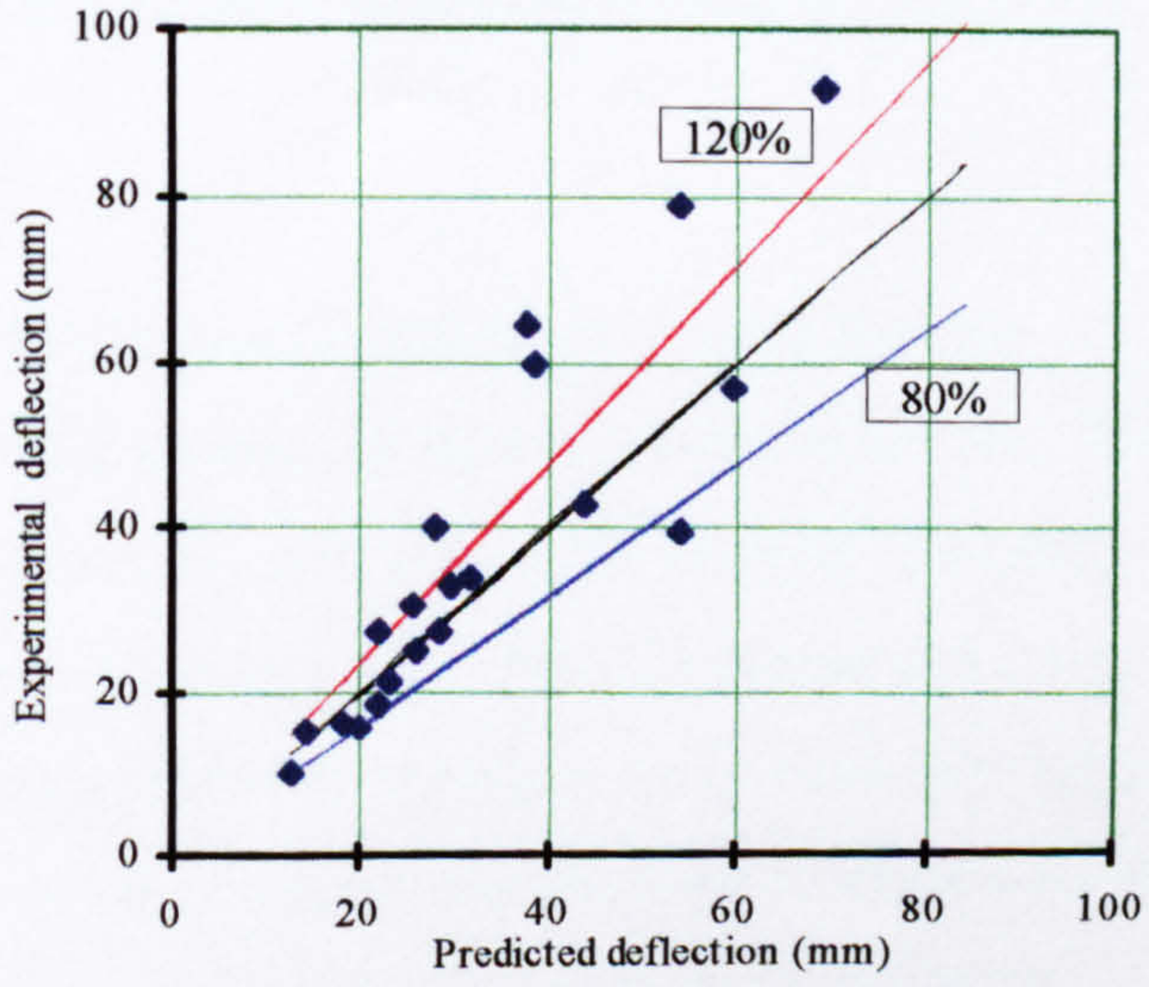

Figure 4.23: Experimental and model prediction for reinforced concrete beams using cracked stiffness

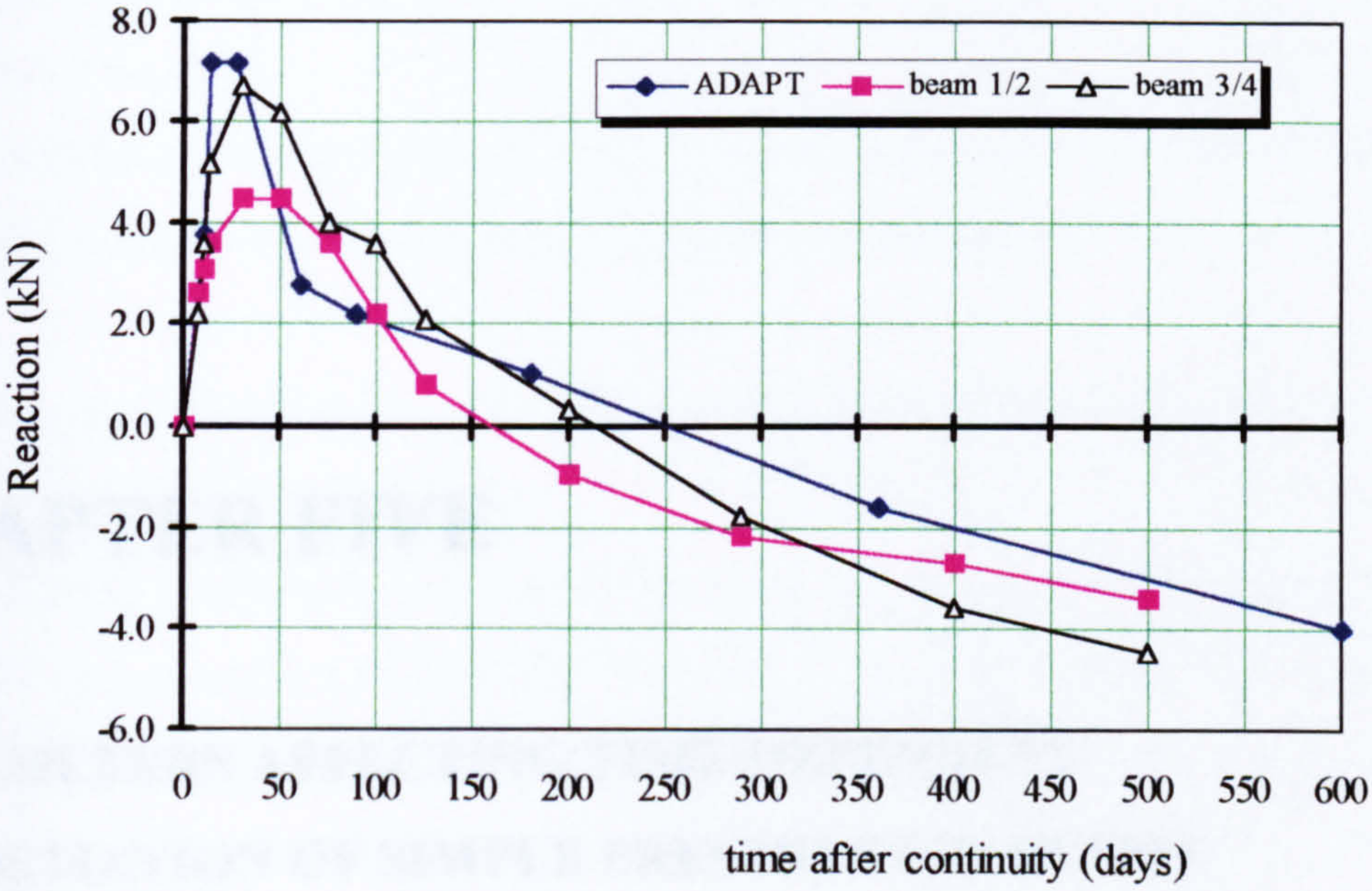

Figure 4.24: Comparisons between ADAPT analysis and experimental result for continuous precast prestressed composite beams from Mattock *et al* (1961)

CHAPTER FIVE

PARAMETERS AFFECTING TIME-DEPENDENT DEFORMATION OF SIMPLE PRESTRESSED BEAMS

5.1 Introduction

The literature survey presented earlier has indicated that, despite voluminous research on creep and shrinkage of concrete, it has not been possible to develop a deterministic prediction method to account for the various parameters affecting them. The available methods can describe creep and shrinkage phenomena under given circumstances only at macroscopic level. The predictive methods discussed in Chapter Three showed that each method can at best predict within 20% of the experimental results to which they are being compared.

This chapter attempts to ascertain the significance of each parameter on the time-dependent response of plain and reinforced concrete using numerical evaluations. This is done by first evaluating the influence of each parameter on the material response using the predictive methods described in Chapter Three. The development of creep and shrinkage strains with time under many different conditions have been calculated and from these values observations are made to characterise the degree of influence of each parameter. It should be noted that these parameters are directly or indirectly

correlated to produce unique creep and shrinkage properties for a given condition. Using a statistical technique, it may be possible to have a simplified single function to describe the relationship between these parameters.

Further evaluations are then carried out for structures subjected to axial stress only, and followed by the parametric evaluation for simple flexural members.

5.2 Parameters Affecting the Time-dependent Properties of Concrete

Parametric evaluations have been carried out for a range of practical cases using the predictive method given by CEB90 for creep and shrinkage of the concrete. The method was selected because it only requires parameters that are readily known at the design stage and has been satisfactorily compared with experimental results. The other reason for using CEB90 is that it defines the creep coefficient as the ratio of creep strain to elastic strain at 28 days. The ACI method defines creep coefficient as the ratio of creep strain to elastic strain on the day the load is applied. In the case of precast prestressed beams, the members are normally stressed as early as three days and, since the value of elastic modulus is directly related to the elastic strain, an accurate prediction of the elastic modulus results in a more accurate prediction of the elastic strain (thus, the creep coefficient). It was shown in Chapter Three that the elastic modulus is better predicted for concrete aged more than 21 days, hence, the creep coefficient as defined by CEB90 is more reliable.

Also from a practical point a view, the conditions considered in this evaluation represent typical conditions which the structures will be subjected to in actual construction practice for road bridges. The variations considered in the concrete design strength (f'_c), curing duration (t_s), age at loading (t_o), volume to surface area ratio (V/S) and average relative humidity (RH) are also taken within the ranges which are encountered in practice. The range of the variations adopted for this evaluation is 30-60MPa for concrete strength, 3-28 days for curing duration and age at loading, 50-140mm for volume to surface area ratio, and 40-90% for the average relative humidity. The range for the volume to surface area ratio was obtained from a study of the standard precast

sections which are currently being used for road bridges. The sections considered are the inverted *T*, *M*, *Y*, *SY*, *I* and *U* beams. The highest volume to surface area ratio is given by the *Y* section which ranges between 114mm for the *Y1* to 135mm for the *Y8* sections, and the smallest volume to surface area ratio is given by the *Inverted-T* sections which ranges between 50mm for *T10* section to 58mm for *T1* section. The variations in the volume to surface area ratios for all other sections are shown in Figure 5.1

Based on these parameters, the magnitude of concrete creep and shrinkage and their development with time for concrete under a total of more than 150 different conditions were calculated. Creep and shrinkage characteristics were then evaluated based on these values.

5.2.1 Creep of plain concrete

A general observation of the calculated creep strains indicate that creep is at a maximum when the combined parameters produce a condition such that the values of t_o, *RH*, *V/S* and f'_c are at a minimum. Conversely minimum creep is obtained when the maximum values of t_o, *RH*, *V/S* and f'_c are used. These conditions are considered as the upper and lower limits for creep that are generally encountered in practice. The values of creep for different conditions are shown by Figure 5.2.

An overall evaluation for creep shows that there is a very significant variation for any given precast section as indicated in Figure 5.2 and Table 5.1. It is clear that for any given section, the difference between the possible maximum and minimum creep is very significant. For example, for sections having *V/S*=50mm, creep of concrete with f'_c=30MPa, loaded at 3 days and exposed to 40% *RH* was calculated to have a 10,000-day value at 835 microstrain. Creep for a similar section but having f'_c=60MPa, loaded at 28 days and exposed to 90% *RH* was calculated to be only 160 microstrain.

To evaluate the degree of significance for each of these parameters in the calculation of creep, a summary for different combinations of these conditions that represent the upper

and lower bounds for each parameter is shown in Table 5.1. The summary shows the values of creep coefficient and strain, total strain and the ratio of creep to total strain for each given condition. The calculated strain under any condition is directly proportional to the level of applied compressive stress and a constant values of at 5MPa has been used here for all calculations. Figures 5.3-5.6 show creep strains and their development with time under these conditions.

The following evaluations of each parameter consider three aspects: (i) its effect on the magnitude of creep, (ii) its percentage of total deformation, and (iii) its effect on creep development.

5.2.1.1 Effect of age at loading

The effect of age at loading on creep properties is compared for concrete loaded at 3 and 28 days as given by combinations of parameters 1-8 and 9-16 respectively in Table 5.1. Its effect on time-dependent creep, the percentage of creep to total deformation and the rate of creep increase are shown in Figures 5.3.

Creep strains due to different ages at loading were evaluated by comparing between pairs of similar conditions. The results from Table 5.1 show that, for any given combination of parameters, the 28 and 10,000 day creep values for concrete loaded at 3 days are always greater than those for the same concrete loaded at 28 days. The ratios of creep strains between combinations 1 and 9 at 28 and 10,000 days were both evaluated to be 1.52. This value remains constant for all other corresponding combinations of parameters i.e. combinations 2 and 10, 3 and 11, *etc*. This shows that concrete loaded at 3 days displays 52% more creep than concrete loaded at 28 days at any time after loading under any corresponding combinations of parameters. The constant ratio also indicates that a concrete loaded at any age can be determined from a single curve at any age at loading. For example, if a creep-time curve for a given condition has already been obtained for t_o=7, the creep-time curve at other ages can be determined using a constant scaling factor.

A comparison between combinations 1 and 9 shows that, for concrete loaded at 3 days, creep represents 52.2% and 51.1% of the total deformation at 28 and 10,000 days respectively compared to 42.1% and 39.7% for the same concrete loaded at 28 days. This means that concrete loaded at 3 days represents 10.1% and 11.1% more creep to the total deformation than the same concrete loaded at 28 days. Under the combination of parameters that produce the minimum total deformation (combinations 8 and 16), creep of concrete loaded at 3 days represents 31.0 and 49.3% of the total deformation (at 28 and 10,000 days respectively) compared to 23.0 and 39.0% for concrete loaded at 28 days. This indicates that, under the combination of parameters yielding minimum deformations, concrete loaded at 3 days represent an additional of 8.0 and 10.3% (at 28 and 10,000 days respectively) of the total deformation than concrete loaded at 28 days. A comparison of other corresponding conditions consistently shows that under any given combination of parameters, concrete loaded at 3 days represents about 10% more of the 10,000 days total deformation than the same concrete loaded at 28 days.

A comparison between the calculated values combinations 8 and 9 presented in Table 5.1 and Figure 5.3(b) shows that, concretes with the combination of parameters yielding minimum deformation, but loaded at 3 days (combination 8) have levels of creep expressed as a percentage of total deformation than for those having the combination of parameters yielding maximum deformation, but loaded at 28 days (combination 9). This indicates that all concretes loaded at three days display greater levels of creep expressed as a percentage of total deformation than concretes loaded at 28 days, regardless of the combination of the parameters.

Figure 5.3(c) shows that the rate of creep development is not affected by age at loading. For a given combination of parameters, the rate of creep development for concrete loaded at 3 days is similar to that for the same concrete loaded at any other day.

5.2.1.2 Effect of concrete strength

To evaluate the effect of concrete strength on creep deformation, comparisons were made between combinations 1 and 5, 2 and 6, *etc.* (Table 5.1). Time-dependent creep, its percentage of total deformation and its rate of increase are shown in Figures 5.4.

Comparisons for creep strains and coefficients show that under corresponding combinations of parameters, concretes with 30MPa strength display greater creep strain and coefficients than those with 60MPa strength. It should be noted that concrete strength affects the creep coefficient and level of strain differently. From the formulation given by CEB90, the creep coefficients are only directly related to concrete strength, not to the elastic modulus. The creep strain, however, is directly related to the elastic modulus which is affected by the concrete strength. Comparisons for the creep coefficients show that for any corresponding combination of parameters, concretes with a characteristic strength of 30MPa display creep coefficients 41% greater than those for concretes with a characteristic strength of 60MPa at any time after loading.

A comparison of the magnitude of creep given by combinations 1 and 5 shows that 30MPa concretes display 78% more creep deformation than similar 60MPa concretes at any times after loading. This value remains constant for other corresponding combinations of parameters. This shows that creep of any concrete is proportional to that for concrete of a specified characteristic strength subject to similar a combination of parameters.

Table 5.1 shows that under combination 1, creep represents 52.2% and 51.1% of the total deformation at 28 and 10,000 days respectively, compared to 45.5% and 45.8% for combination 5. This indicates that under a given combination of conditions, concrete with a strength of 30MPa represents 6.7% and 5.3% more creep expressed as a percentage of the total deformation than similar concrete with a characteristic strength of 60MPa. Comparisons between other corresponding conditions show that the average difference in the percentage of creep to the final total deformation is about 6 %.

Figure 5.4(c) shows that for any combination of parameters, the characteristic strength of concrete does not affect creep development with time. This indicates that, for any given condition, the rate of creep development with time of a given concrete is constant regardless of its characteristic strength.

5.2.1.3 Effect of average relative humidity (*RH*).

The effects of *RH* on the creep characteristics were evaluated by comparing between combinations 1 and 2, 3 and 4, *etc*. Creep development with time, its percentage of total deformation and its rate of increase are shown in Figures 5.5.

A comparison between creep strains shows that, concretes exposed to lower value of *RH* displays greater creep at any time after loading. For the combination of parameters yielding maximum deformation, concretes subjected to 40% *RH* (combination 1) display 2.46 and 1.92 times greater creep strain than the same concretes at 90% *RH* (combination 2), at 28 and 10,000 days respectively. Slightly lower values were observed under the combination of parameters yielding minimum deformation where concretes subject to 40% *RH* (combination 15) display 2.40 and 1.74 times greater creep strain than similar concretes at 90% *RH* (combination 16), at 28 and 10,000 days respectively. Comparisons for all other corresponding combinations indicate some degree of interdependence between the *RH* values and the *V/S* ratios. Concretes with the minimum *V/S* ratio (50mm) consistently display 146 and 92% more creep at 40% *RH* than that at 90% *RH* at 28 and 10,000 days respectively. Concretes with the maximum *V/S* ratio (140mm) display 140 and 74% (at 28 and 10,000 days respectively) more creep at 40%*RH* than concretes with similar sections but subjected to *RH*=90% .

Comparisons between corresponding combinations consistently show that creep of concrete subjected to 40% *RH* forms a greater percentage of the total deformation at 28 days, but a smaller percentage at 10,000 days. This is apparently related to the deformation due shrinkage where its rate of development is directly related to the combination of *RH* and *V/S* values. Figure 5.5(b) shows that the effect of *RH* on the creep expressed as a percentage of the total deformation changes after about 500 and 5,000 days for the combinations of parameters yielding maximum and minimum deformation respectively.

Figure 5.5(c) shows that the rate of creep development is greater for concretes subject to 40% *RH* than that at 90% *RH* under both combinations of parameters yielding maximum and minimum deformation.

5.2.1.4 Effect of volume to surface area ratios (*V/S*).

The effects of volume to surface area ratios were evaluated through comparisons between combinations 1 and 3, 2 and 4, *etc*. Figures 5.6 show the effects of *V/S* on creep deformation, its percentage of the total deformation and its rate of development with time.

A comparison of creep strains for concretes having different *V/S* ratios shows that, under a given combination, a smaller *V/S* ratio displays greater creep strain at both 28 and 10,000 days. Calculations for combinations 1 and 3 showed that concretes having *V/S*=50mm display 38.6 and 20% more creep strain at 28 and 10,000 days respectively than those having *V/S*=140mm. These values were constant for all other corresponding combinations with *RH*=40%. In any combination of parameters when *RH*=90%, concretes with *V/S*=50mm display 35.5 and 9% more creep strain at 28 and 10,000 days respectively than those with *V/S*=140mm. This observation indicates that the effect of the *V/S* ratio on creep is related to *RH*. For any given *RH*, creep for a given *V/S* ratio is proportional to the creep for a section with another *V/S* ratio, regardless of the combination of other parameters.

Concretes having the maximum *V/S* ratio (140mm) display creep which formed 54.2 and 48.5% of the total deformation at 28 and 10,000 days respectively compared with those with the minimum *V/S* ratio (50mm) where the percentages were 52.2 and 51.1%. This results in a difference of about 2% for sections having the maximum and minimum *V/S* ratios. The difference was observed to be less significant under the average relative humidity of 90%, Figure 5.6(b). Figures 5.6(c) shows that under a given combination of parameters, concretes with smaller *V/S* ratios undergo creep deformation at a faster rate compared to those with higher *V/S* ratios.

5.2.2 Shrinkage of plain concrete

The CEB90 prediction for shrinkage stipulates that there are four main parameters to affect shrinkage of plain concrete. These parameters are the curing duration (t_s), compressive strength properties (f'_c), average relative humidity (*RH*) and the volume to

surface area ratio (*V/S*). The degree of significance of these parameters on the shrinkage of plain concrete were evaluated using several sets of conditions that represent typical high and low values of the four parameters. As for creep, shrinkage of concrete is at a maximum for a combination of parameters that have minimum values of f'_c, *RH* and *V/S*, and at a minimum when the maximum values of f'_c, *RH* and *V/S* are used. The difference between these conditions for shrinkage is shown in Figure 5.7.

5.2.2.1 Effect of curing duration

A summary of shrinkage strain for concrete having *V/S*=50mm, but cured for two different durations (t_s = 3 or 28 days), having different characteristic strength (f'_c = 30 or 60MPa), and subject to two different relative humidities (*RH* = 40 or 90%) is shown in Table 5.2.

The table shows that shrinkage values are similar under all corresponding combinations of parameters at both28 and 1,000 days after curing. For example, concretes with f'_c=30MPa and *RH*=40% were calculated to have a shrinkage of 182 and 574 microstrain at 28 and 1,000 days after curing respectively (combinations 17 and 19). This indicates that the curing duration does not affect the magnitude of concrete shrinkage under a given combination of parameters.

Table 5.2 (Column [3]) also shows that shrinkage development is not affected by curing duration. The table shows that for *V/S*=50mm, the ratio of 28 to 1,000 day shrinkage remains at 0.32 under all combinations of parameters. This is further shown in Table 5.3 where the ratio of 28 to 10,000 days shrinkage for concretes with *V/S*=140mm remains at 0.11 under all possible combinations of parameters. Figure 5.8 also indicates that the rate of shrinkage development is only affected the volume to surface area ratio.

Further evaluations for parameters affecting shrinkage of plain concrete did not therefor consider the variation in curing duration. A summary of the calculations for shrinkage under different possible combinations of the three other parameters that were expected to display typical high and low values of shrinkage is shown in Table 5.3. The following evaluations for the effects of f'_c, *RH* and *V/S* have been based on this table.

5.2.2.2 Effect of concrete strength

Figure 5.9 shows the effect of the concrete characteristic strength on shrinkage under combinations of parameters yielding maximum and minimum deformations. To evaluate the effect of concrete strength on shrinkage of plain concrete, comparisons were made between combinations 25 and 27, 26 and 28 *etc.*

From Table 5.3 it can be seen that, under any given combination of parameters, concretes with f'_c =30MPa consistently display about 50% more shrinkage strain than those 60MPa strength. This percentage remains nearly constant at any age after curing. This indicates that, similar to creep strain, shrinkage strain for concrete of any strength is proportional to the shrinkage strain for concrete of a given strength.

A comparison of shrinkage expressed as a percentage of the total deformation at 28 and 10,000 days indicates that concrete strength has no significant effect. Under the combination of parameters yielding maximum deformation, concretes with f'_c=30MPa (combination 25) develop shrinkage strains that represent 25 and 40% of the total deformation at 28 and 10,000 days respectively compared to 26 and 43% for with f'_c=60MPa (combination 27). Similarly, under the combination of parameters yielding minimum deformation, concretes with f'_c =30MPa (combination 30) develop shrinkage strains that represent 7.7 and 30% of the total deformation at 28 and 10,000 days respectively compared to 7.3 and 31% for concretes with f'_c =60MPa (combination 32). Similar patterns were observed under all other conditions.

5.2.2.3 Effect of average relative humidity

The effects of *RH* on shrinkage of concrete are shown in Figures 5.10. The effects of *RH* were evaluated by comparisons between combinations 25 and 26, 27 and 28 *etc.* (Table 5.3).

The ratio between the two shrinkage strains of all corresponding combinations shows that concretes at *RH*=40% displays shrinkage strains about 3.5 times greater than those at 90%*RH*. This indicates that, for the range of the values of the parameters considered

in this evaluation, *RH* has a more significant effect on shrinkage than concrete strength. The near constant ratio between the shrinkage strains of two concretes having similar parameters, but exposed to different humidities may also lead to a more simplified prediction of shrinkage. The shrinkage of concrete for any combination of parameters i.e. f'_c, *V/S* and t_s exposed to an average relative humidity is proportional to a similar concrete exposed to a specified *RH*.

A comparison of shrinkage strains at 28 and 10,000 days for any given combination of parameters shows that *RH* has very little effect on shrinkage development. Table 5.3 (Column 5) shows that under combination 27, (*V/S*=50, *RH*=40%) shrinkage strain at 28 days was calculated to represent about 28% of the 10,000 days shrinkage, compared to concrete under combination 28 (*V/S*=50, *RH*=90%) where the value is 27%. A comparison of other corresponding conditions shows similar effects (see Figure 5.8).

Figure 5.11 and columns 6 and 7 of Table 5.3 show that *RH* has a very significant effect on the percentage of shrinkage to total deformation which is apparently related to the *V/S* ratio. Concretes with *V/S*=50mm (combinations 25-28) show that shrinkage of concrete at 40% *RH* represent about 25 and 40% of the total deformation at 28 and 10,000 days respectively compared to 15 and 25% at *RH*=90%. The percentages of shrinkage to total deformation were calculated to be about 17 and 50% at 28 and 10,000 days respectively under combinations 29 and 31 (*V/S*=140mm, *RH*=40%) compared to about 8 and 30% for combinations 30 and 32 (*V/S*=140mm, *RH*=90%). The trends indicate that, under any combination of parameters, concretes subjected to *RH*=40% develop shrinkage that represent about 40-50% of the total deformation of plain concrete subject to a moderately constant stress of 5MPa.

5.2.2.4 Effect of volume to surface area ratio

The effect of the *V/S* ratio on shrinkage can be observed from Figure 5.7 where it can be seen that the volume to surface area ratio does not affect the final shrinkage of concrete, but it does affect its development with time very significantly. A comparison between combinations 25 and 29, 26 and 30 *etc.* from Table 5.3 shows that concrete with a higher *V/S* ratio displays slower shrinkage development since the ratio of 28 to 10,000

day shrinkage for *V/S*=50mm was calculated to be 28% compared to 11% for concrete with *V/S*=140mm.

Shrinkage of concrete for any given strength with any *V/S* ratio is proportional to shrinkage of similar concrete with a specified *V/S* ratio. Figure 5.12 shows that there is only a single curve that defines the ratio of shrinkage for a given concrete with *V/S*=50 and 140mm at any time up to the final shrinkage. The ratio decreases in the long term where the ratio is expected to reach unity.

5.2.3 Implications of these observations

Based on the parameters evaluated in the previous sections, it should be noted that, in practical terms, the age at loading, curing duration and the sectional properties represented by the volume to surface area ratios are known rather more precisely than the actual concrete strength and the average relative humidity. Therefore, the concern of potential inaccuracies for creep and shrinkage predictions of concrete therefore lie specifically with these two parameters.

The previous evaluation suggests that creep may be underestimated by about 78% if a characteristic strength of 60MPa is assumed whereas the actual characteristic strength is 30MPa. Shrinkage may be underestimated by about 50% if the same assumption applies. The possible underestimation of creep and shrinkage is even greater due to the average relative humidity. The evaluation has shown that creep of concrete at 40% *RH* could be 90% higher than the creep of similar concrete at 90% *RH*, whereas shrinkage of concrete is about 3.5 times greater over the same *RH* range.

The difference in the long term creep for the typical upper and lower bounds of f'_c and *RH* were calculated to be 366 (combinations 1 and 5) and 401 (combinations 1 and 2) microstrain respectively. These are equivalent to 73.2 and 80.2 microstrain per unit stress for the difference in f'_c and *RH* respectively. In terms of stress loss in the prestressing steel for prestressed structures, these values may be translated into a total loss due to creep of about 146MPa and 160MPa respectively (assuming a stress level in the concrete of 10MPa and an elastic modulus of the prestressing steel of 200GPa).

Similar calculations for the maximum difference in the loss of stress due to long term shrinkage were calculated to be 42MPa and 93MPa for f'_c and RH respectively.

The previous evaluations also showed that each different combination of parameters results in unique values of creep and shrinkage strains. However, several consistent patterns that correlate these values were observed. These are:

(a) Creep of concrete loaded at any given age under any corresponding condition is proportional to creep of a similar concrete loaded at another age. Rate of creep development is independent of age at loading under any given combination of parameters.

(b) Creep of concrete of any characteristic strength is proportional to the creep of concrete at a specified characteristic strength. Rate of creep development under any condition is independent of the concrete characteristic strength.

(c) The effect of the average relative humidity on creep is directly related to the volume to surface area ratio.

(d) Curing duration neither affects the shrinkage magnitude (after curing) nor its development.

(e) Shrinkage strain of concrete having f'_c=30MPa is always 50% greater than that for f'_c =60MPa under any corresponding condition, and the concrete strength does not affect shrinkage development.

(f) Under any corresponding combination of parameters, shrinkage strain of concrete exposed to 40% RH is always about 3.5 times greater than that exposed to 90% RH. The average relative humidity does not significantly affect shrinkage development.

(g) The volume to surface area ratio does not affect the final shrinkage of concrete, but it does affect its development with time. Every V/S value has its unique shrinkage development curve, even though all other parameters are the same.

These observations indicate that despite a high degree of variability in the magnitude of creep and shrinkage due to a large possible combination of conditions, there is a possibility of having a simplified expression for creep and shrinkage. This can help designer to predict creep and shrinkage of plain concrete under any given condition by considering fewer parameters.

Table 5.1: Summary of creep properties for t_o=3 days (combinations 1-8) and 28 days (combinations 9-16)

Comb	t_o	f'_c	V/S	RH	ϕ_{28} [1]	ϕ_{100000} [2]	ε_{cr28} [3]	$\varepsilon_{cr10000}$ [4]	ε_{to28} [5]	$\varepsilon_{to10000}$ [6]	[1]÷[2]	[3]÷[5]	[4]÷[6]
1	3	30	50	40	2.312	5.178	373	835	715	1634	0.446	0.522	0.511
2	3	30	50	90	0.939	2.69	151.5	434	364	767	0.349	0.416	0.566
3	3	30	140	40	1.668	4.294	269	692	496	1427	0.388	0.542	0.485
4	3	30	140	90	0.693	2.464	112	397	291	712	0.281	0.385	0.558
5	3	60	50	40	1.635	3.662	209	469	459	1024	0.446	0.455	0.458
6	3	60	50	90	0.664	1.902	85	243	248	485	0.349	0.343	0.501
7	3	60	140	40	1.18	3.036	151	389	323	901	0.389	0.467	0.432
8	3	60	140	90	0.49	1.742	63	223	203	452	0.281	0.310	0.493
9	28	30	50	40	1.52	3.404	245	549	582	1348	0.446	0.421	0.397
10	28	30	50	90	0.617	1.768	99.6	285	308	618	0.349	0.323	0.461
11	28	30	140	40	1.097	2.822	177	455	399	1189	0.389	0.444	0.383
12	28	30	140	90	0.455	1.619	73.4	261	248.3	575	0.281	0.296	0.454
13	28	60	50	40	1.075	2.407	137.5	308	383	864	0.447	0.359	0.356
14	28	60	50	90	0.437	1.25	55.9	160	215	402	0.350	0.350	0.398
15	28	60	140	40	0.775	1.996	99.2	255	268	767	0.388	0.370	0.332
16	28	60	140	90	0.322	1.145	41	146.5	178	375.5	0.281	0.230	0.390

Table 5.2: Effects of curing duration on short and long term shrinkage for *V/S*= 50mm

Conditions	t_s	f'_c	*RH*	ε_{sh28} [1]	ε_{sh1000} [2]	[1]÷[2] [3]
17	3	30	40	182	574	0.32
18	3	30	90	52.6	166	0.32
19	28	30	40	182	574	0.32
20	28	30	90	52.6	166	0.32
21	3	60	40	122	387	0.32
22	3	60	90	35.4	112	0.32
23	28	60	40	122	387	0.32
24	28	60	90	35.4	112	0.32

Table 5.3: Summary of shrinkage properties under combinations of parameters yielding maximum and minimum deformations.

Comb.	*f'c*	*V/S*	*RH*	ε_{sh28} [1]	$\varepsilon_{sh10000}$ [2]	ε_{to28} [3]	$\varepsilon_{to10000}$ [4]	[1]÷[2] [5]	[1]÷[3] [6]	[2]÷[4] [7]
25	30	50	40	182	656	715	1634	0.28	0.25	0.40
26	30	50	90	53	190	364	767	0.28	0.14	0.25
27	60	50	40	122	442	459	1024	0.28	0.26	0.43
28	60	50	90	35	128	248	485	0.27	0.14	0.26
29	30	140	40	67	591	399	1189	0.11	0.168	0.50
30	30	140	90	19	171	248	575	0.11	0.077	0.30
31	60	140	40	45	398	268	767	0.11	0.168	0.52
32	60	140	90	13	115	178	376	0.11	0.073	0.31

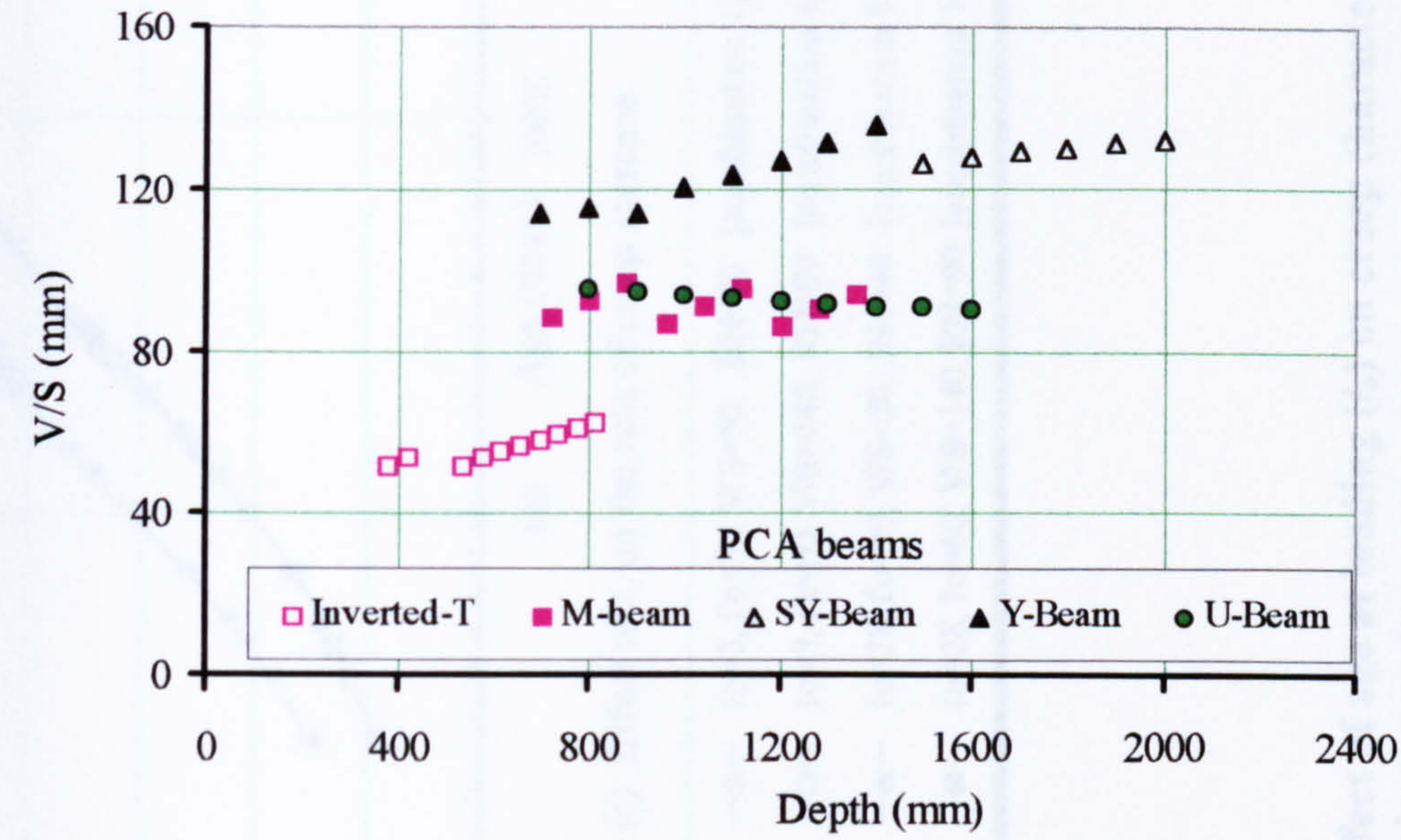

Figure 5.1: Volume to surface area ratio for different precast sections

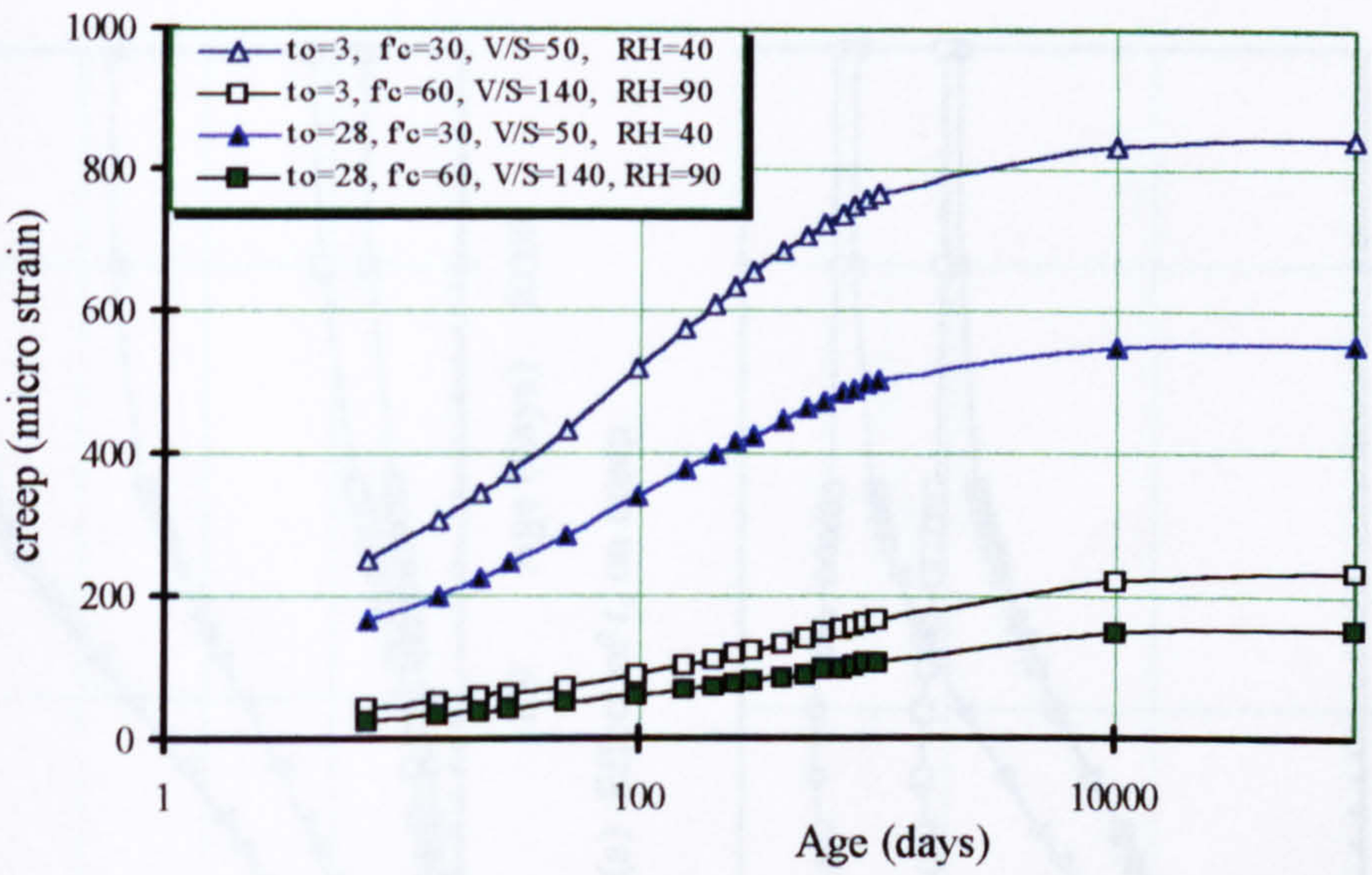

Figure 5.2: Creep of plain concrete under different combinations of parameters yielding maximum and minimum total deformations

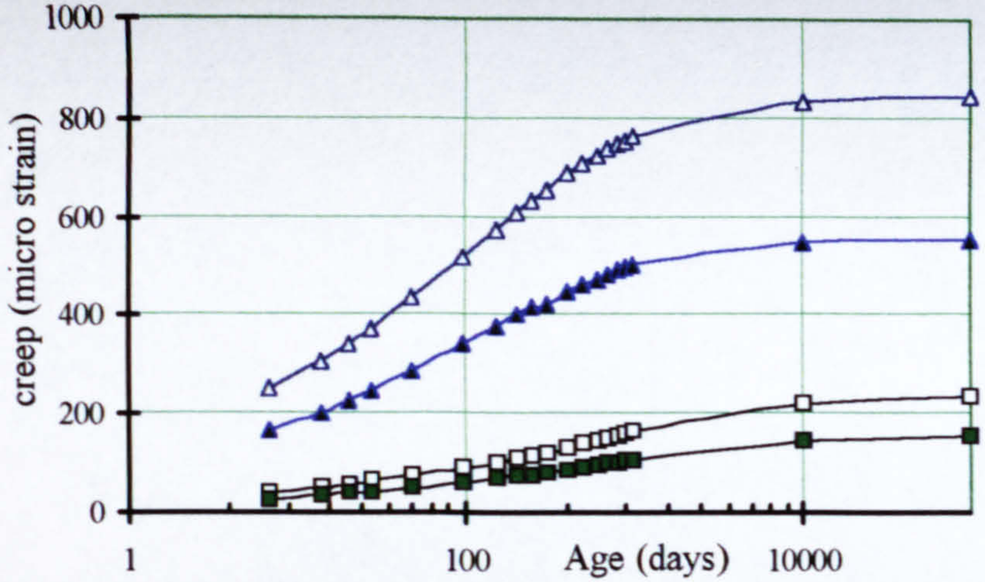

(a) Effect of t_o on creep

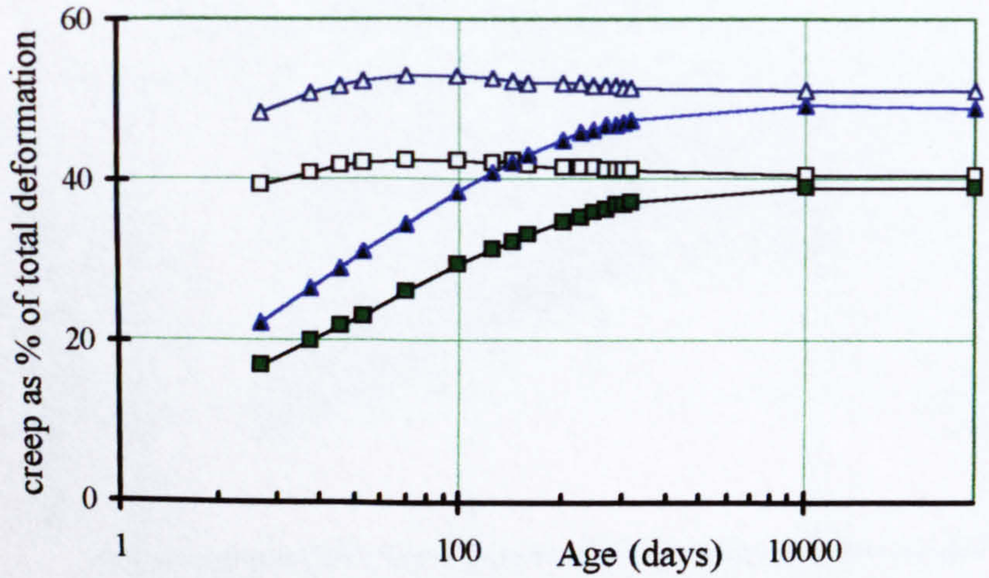

(b) Effect of t_o on creep as a percentage of total deformation

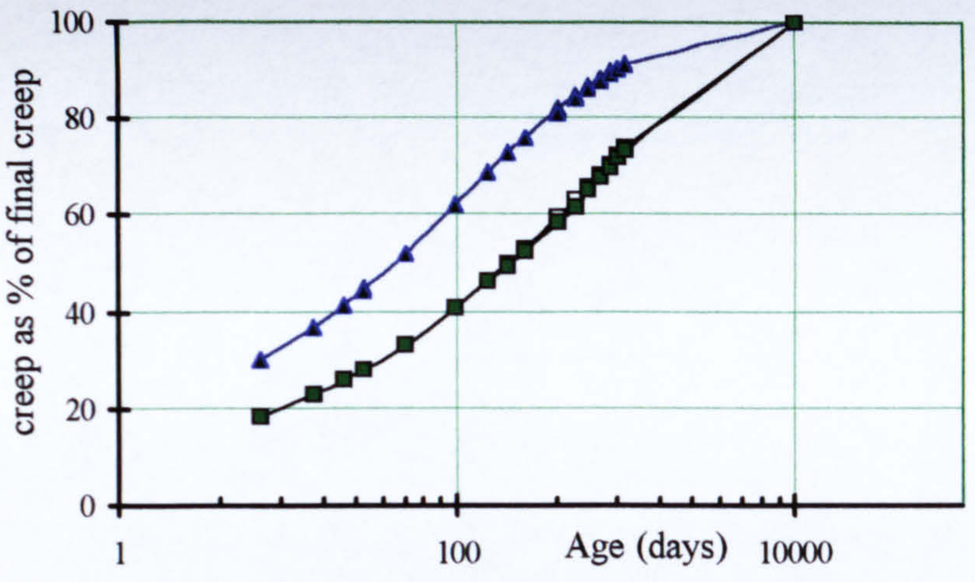

(c) Effect of t_o on the rate of creep increase

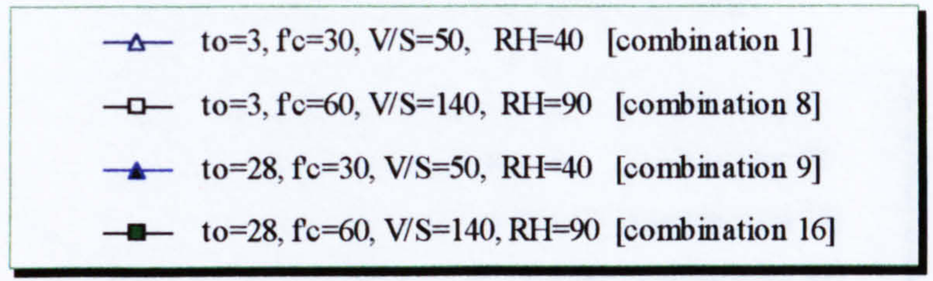

Figure 5.3: Effect of age at loading (t_o) on creep characteristics of plain concrete

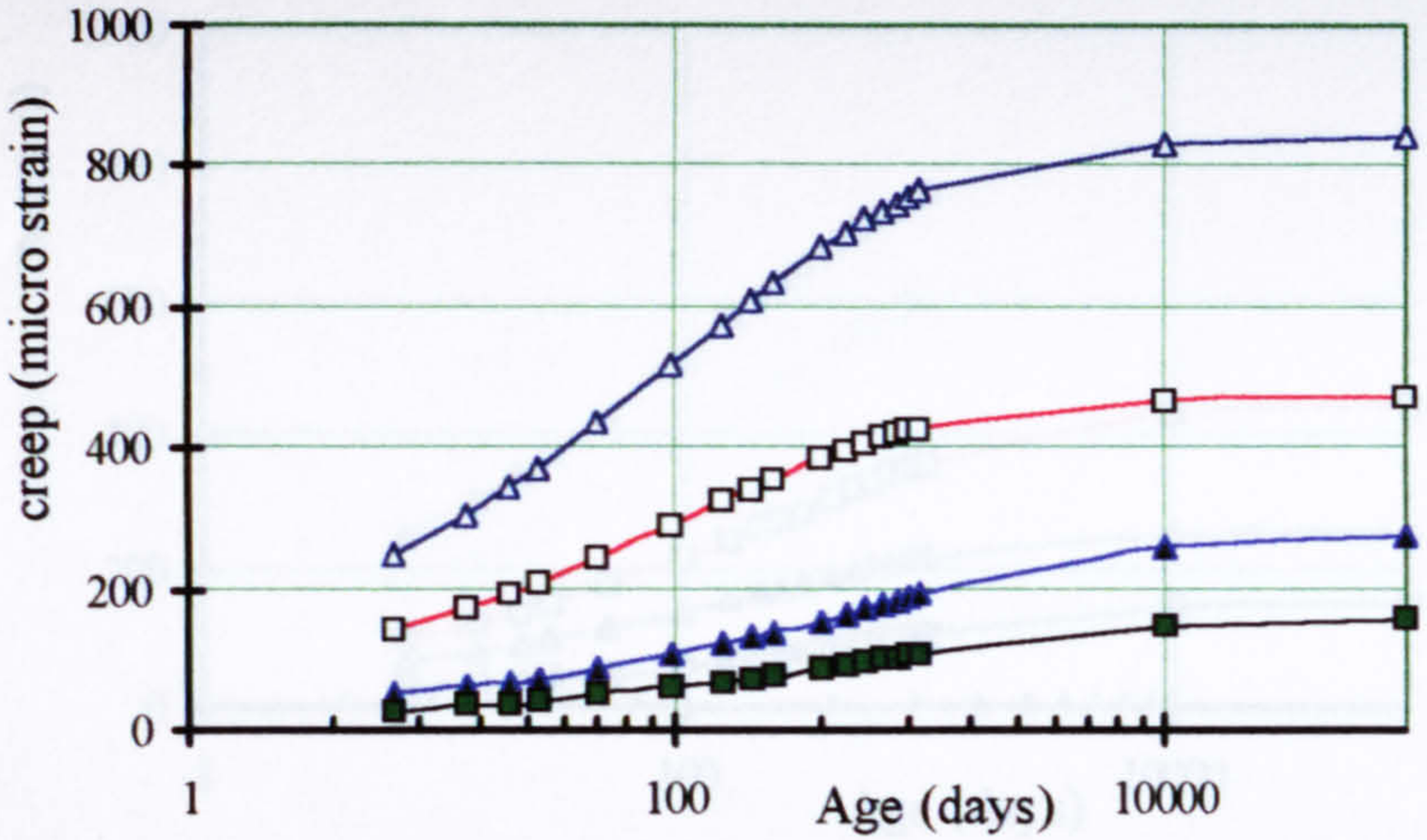

(a) Effects of f'_c on creep

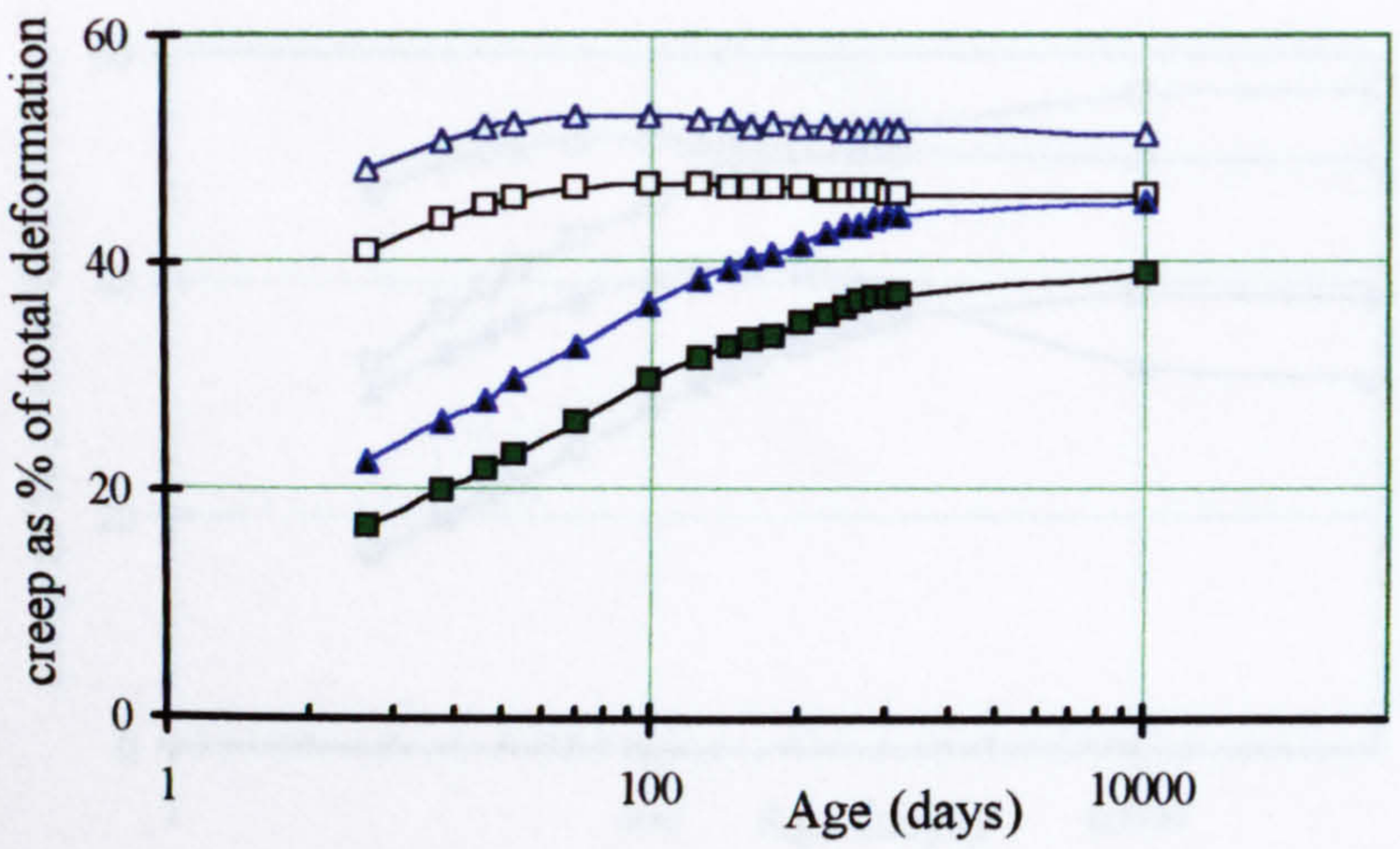

(b) Effects of f'_c on creep as a percentage of total deformation

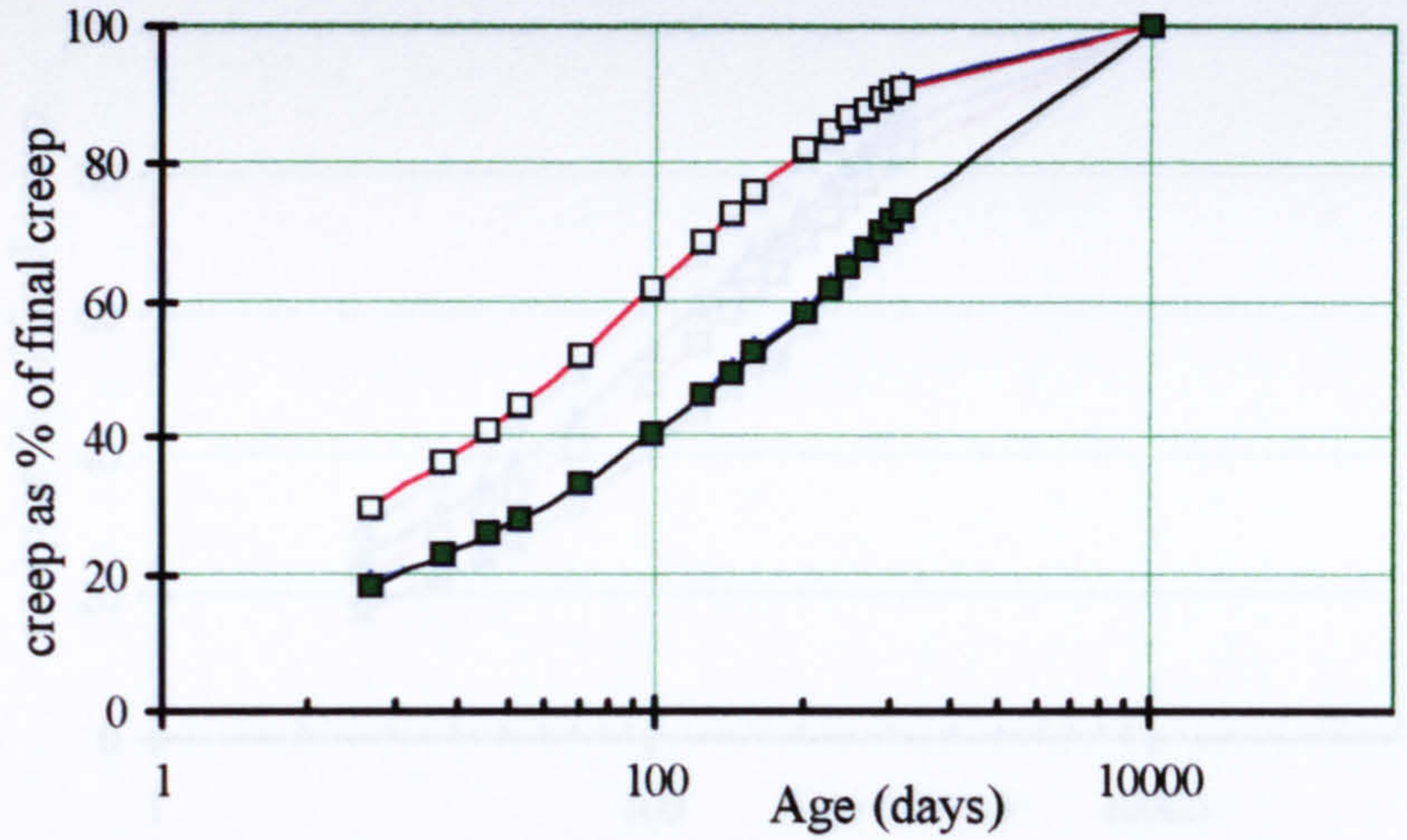

(c) Effects of f'_c on the rate of creep increase

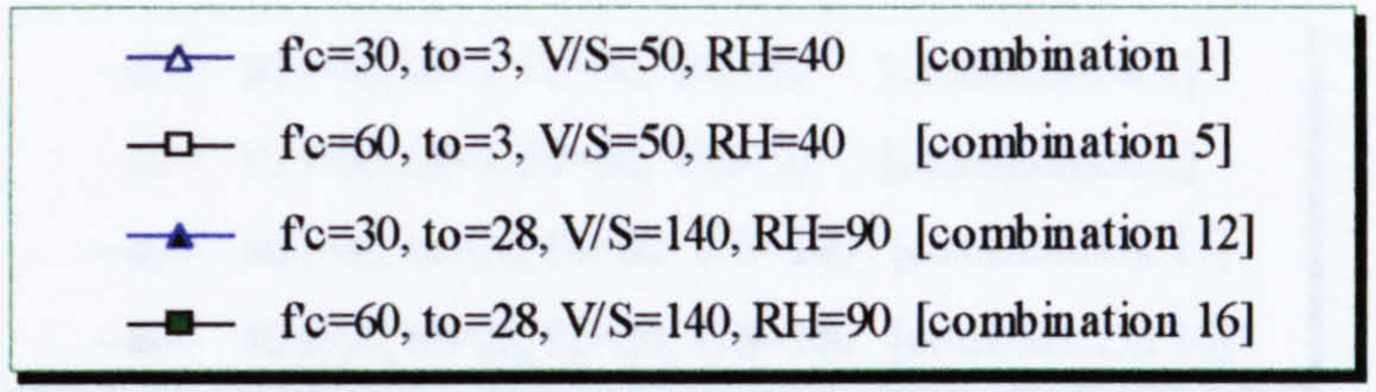

Figure 5.4: Effect of concrete strength (f'_c) on creep characteristics of plain concrete.

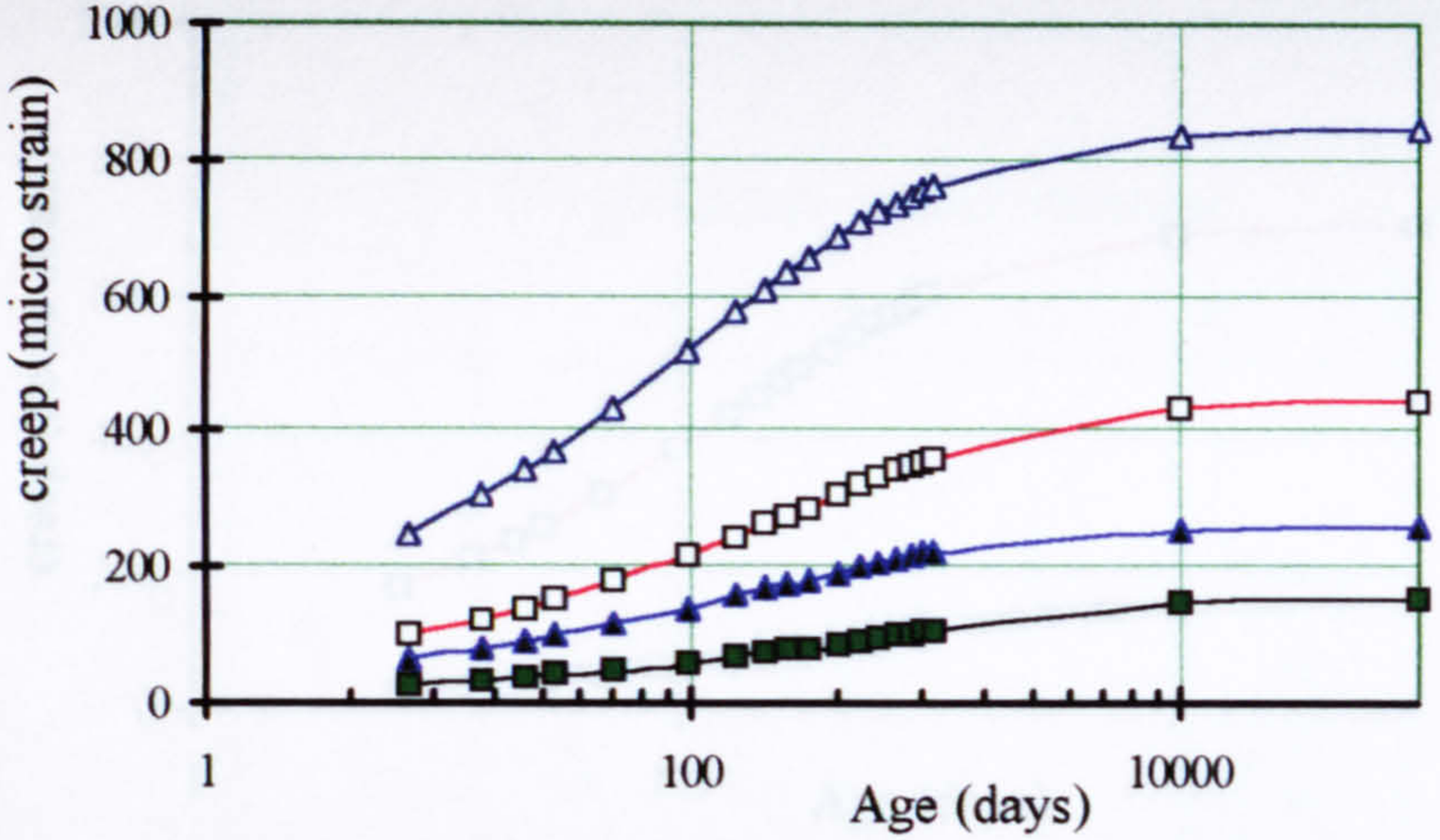

(a) Effect of *RH* on creep

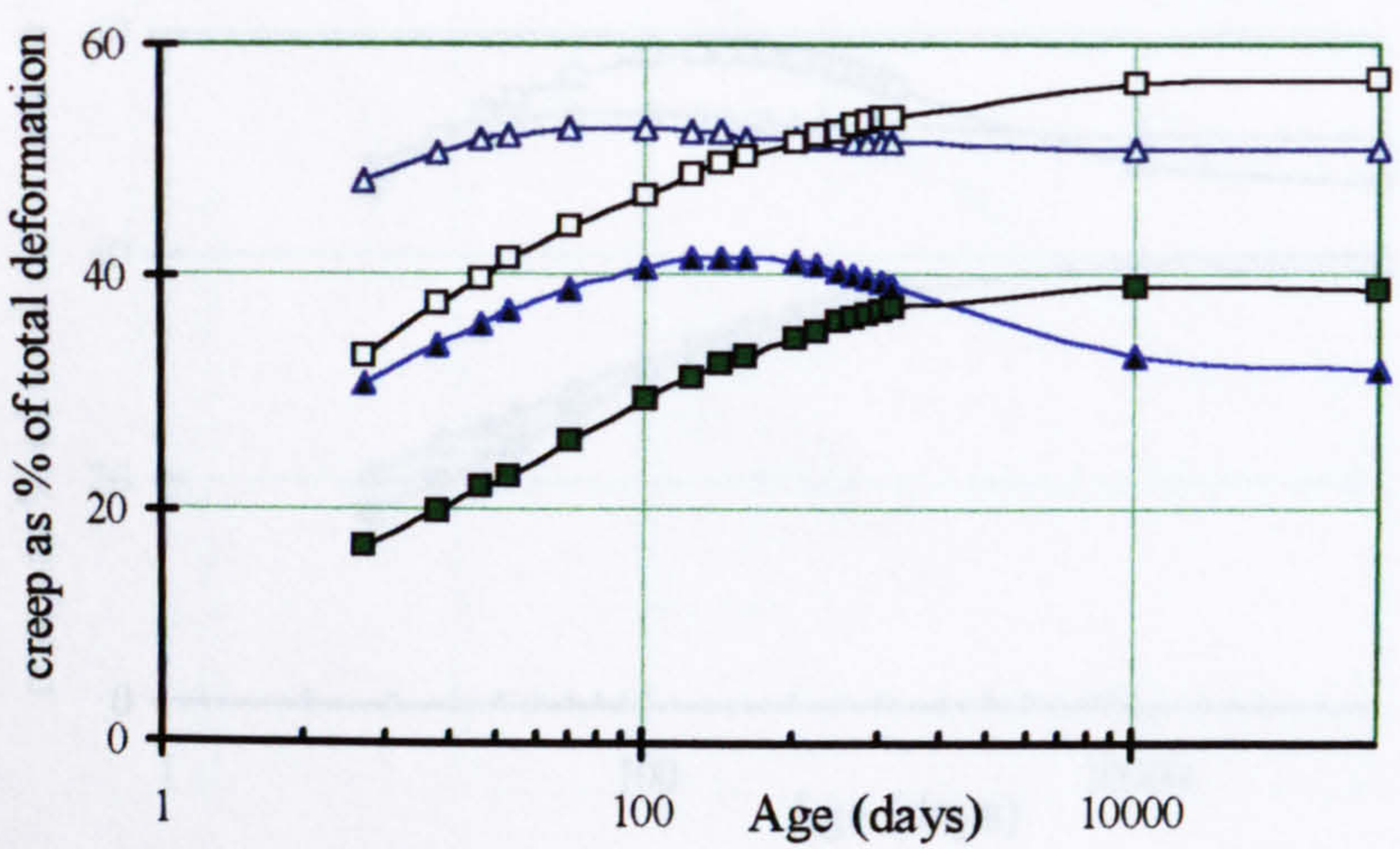

(b) Effect of *RH* on creep as a percentage of total deformations

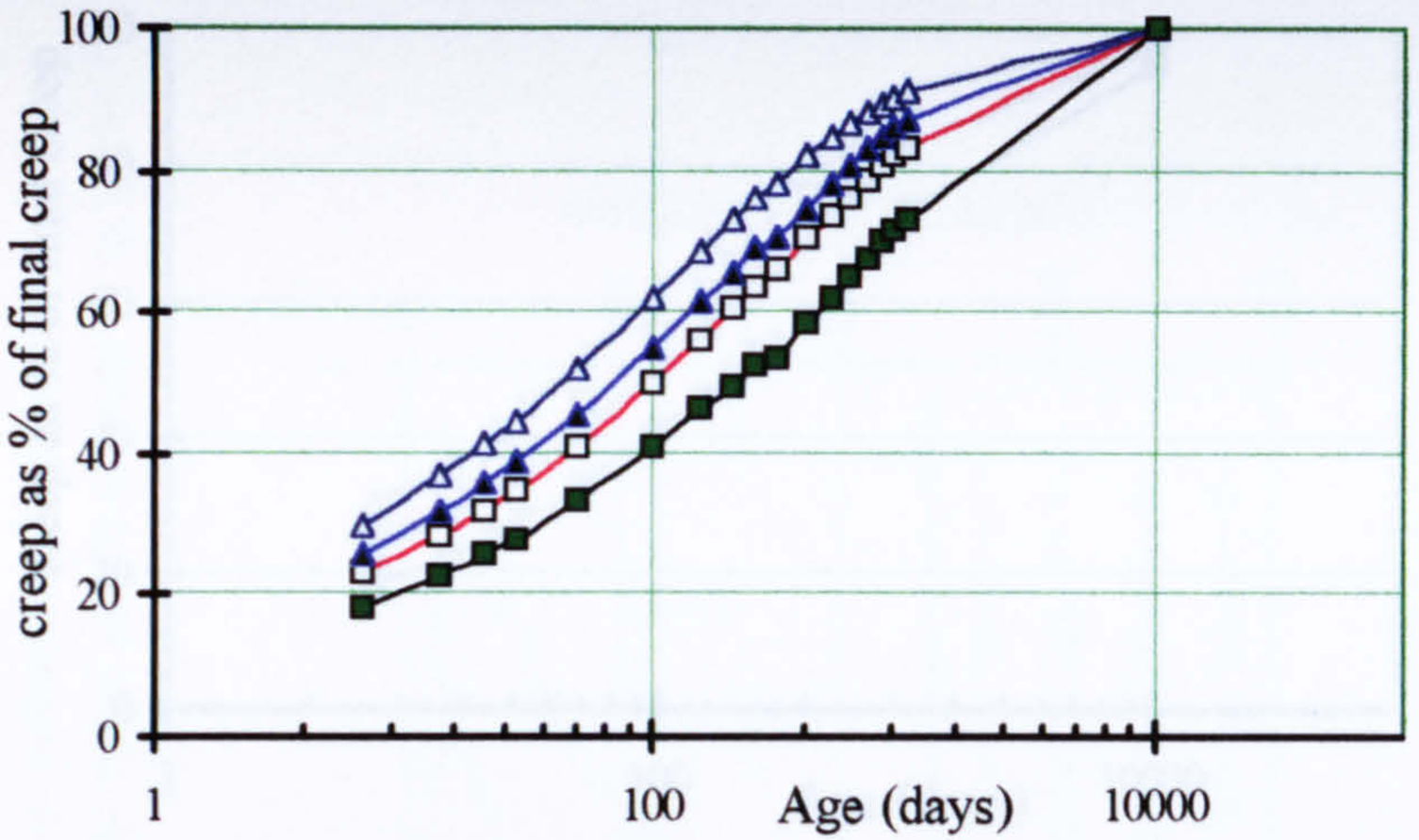

(c) Effect of *RH* on the rate of creep increase

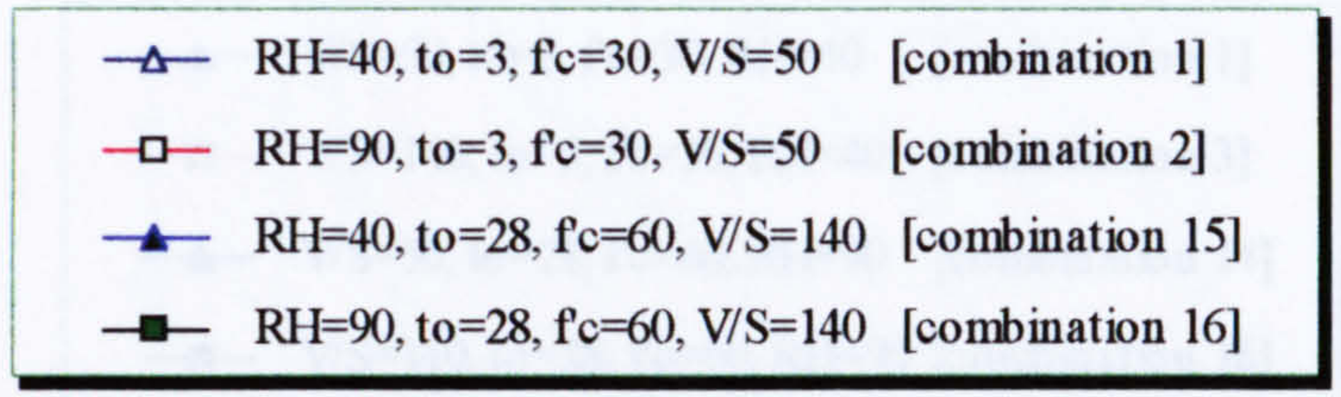

Figure 5.5: Effect of average relative humidity (*RH*) on creep characteristics of plain concrete

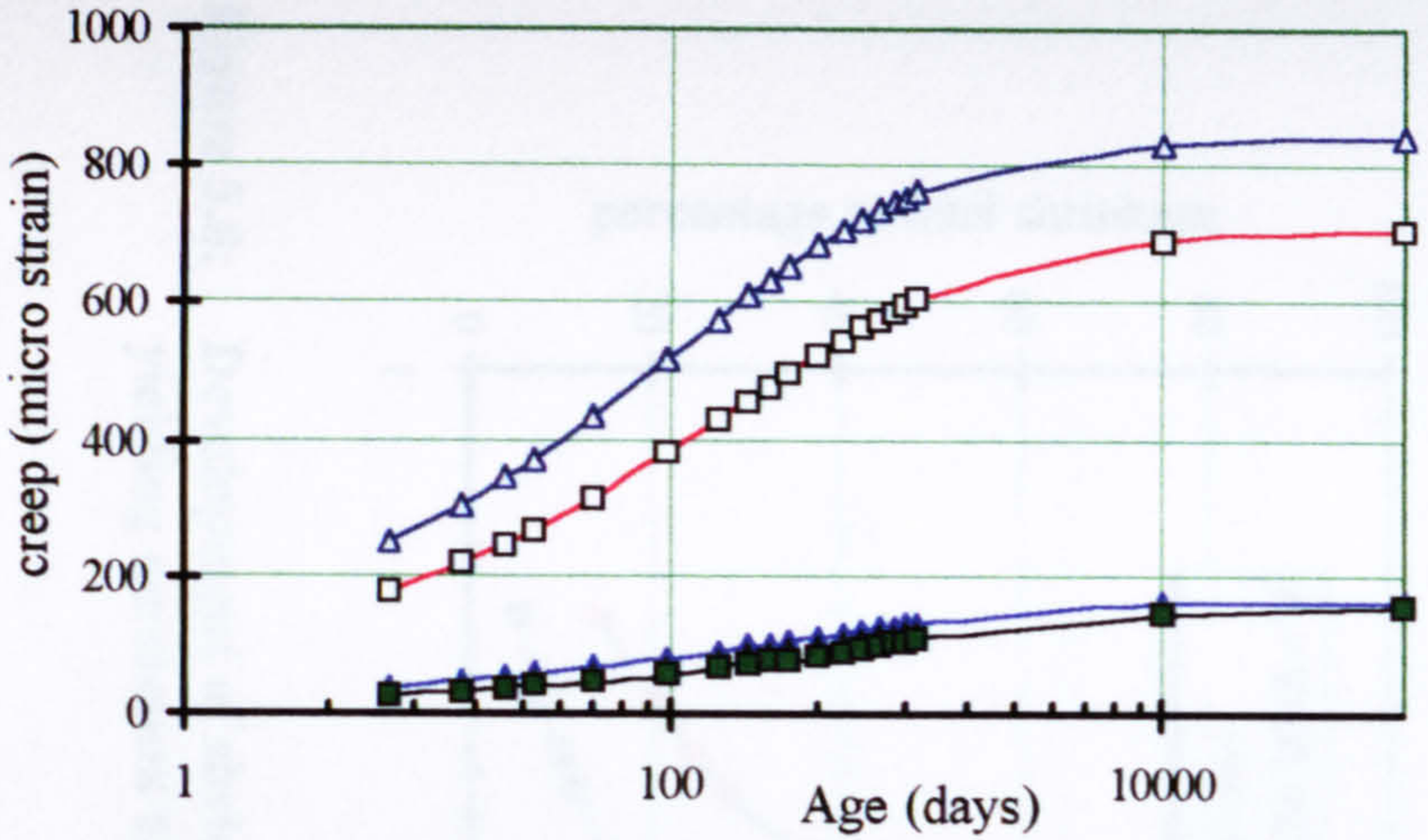

(a) Effect of *V/S* on creep

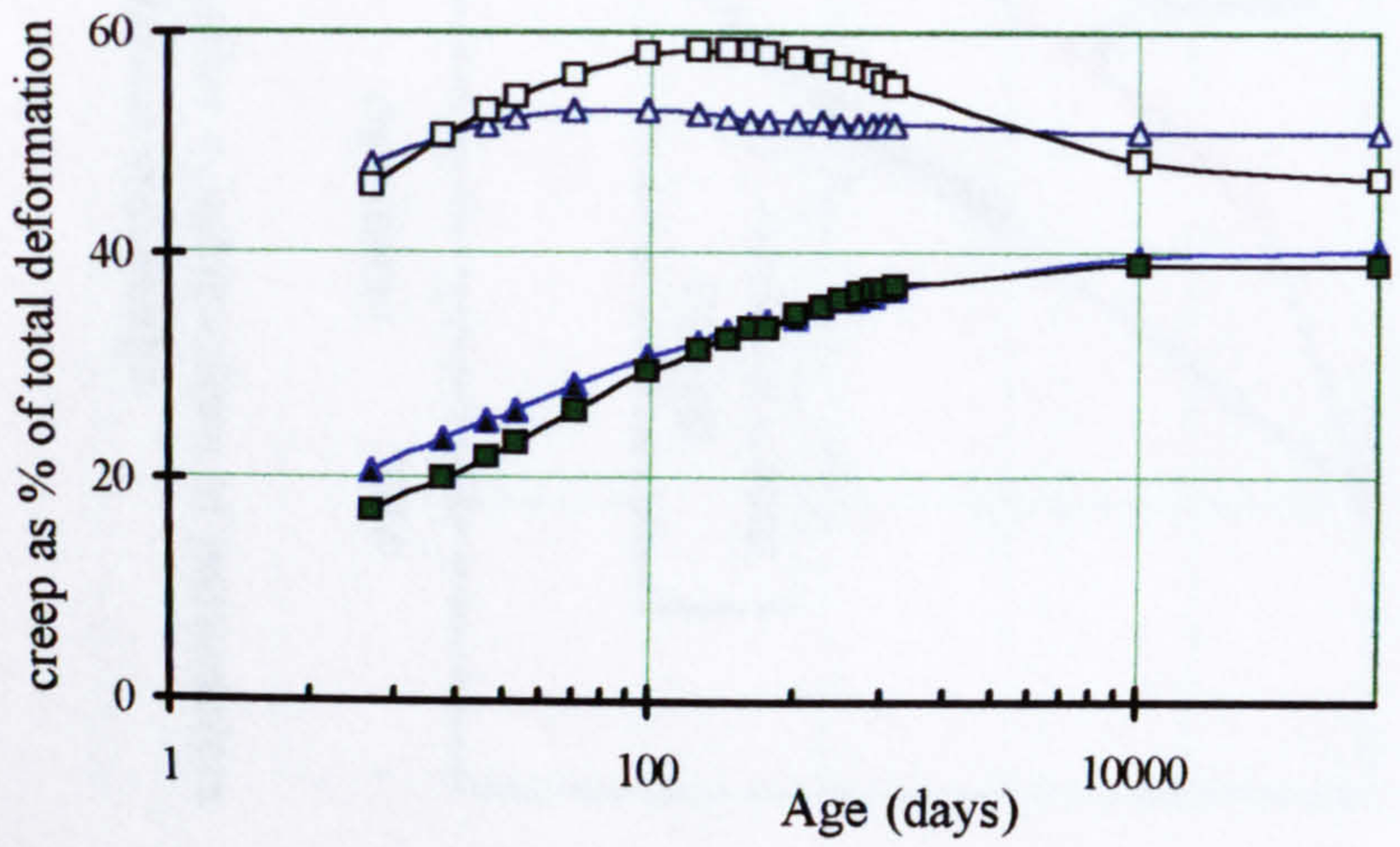

(b) Effect of *V/S* on creep as a percentage of total deformations

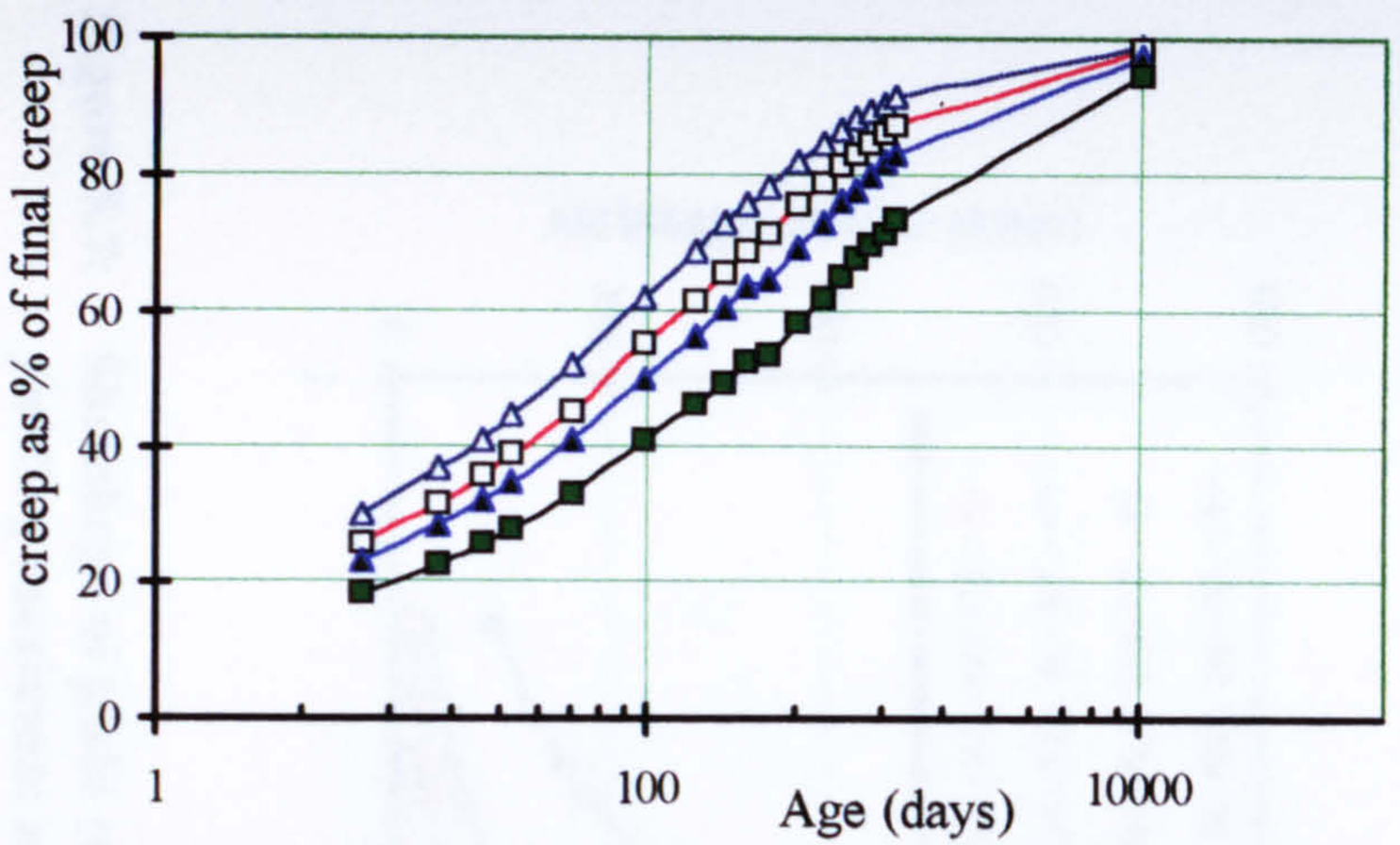

(c) Effect of *V/S* on the rate of creep increase

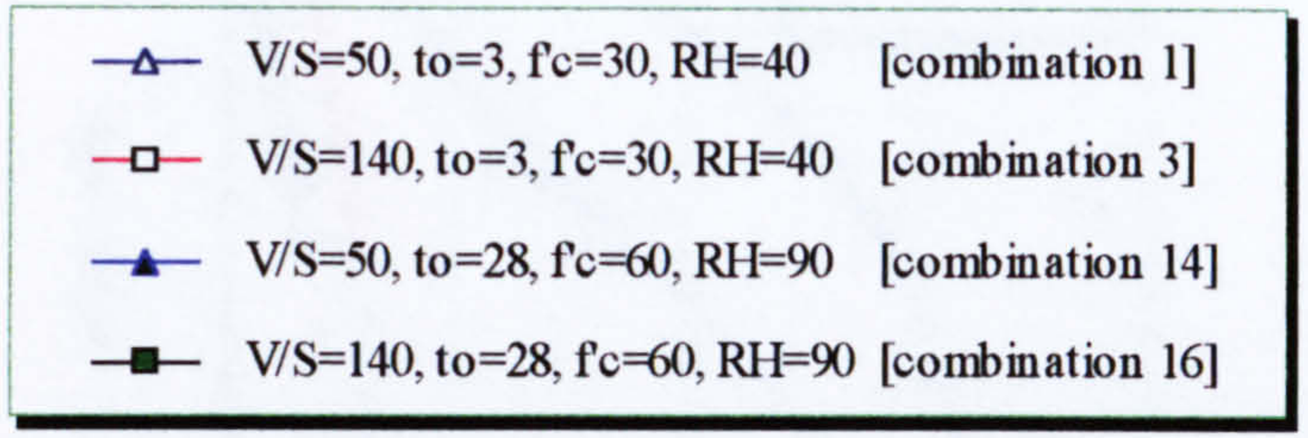

Figure 5.6: Effect of volume to surface area ratio (*V/S*) on creep characteristics of plain concrete

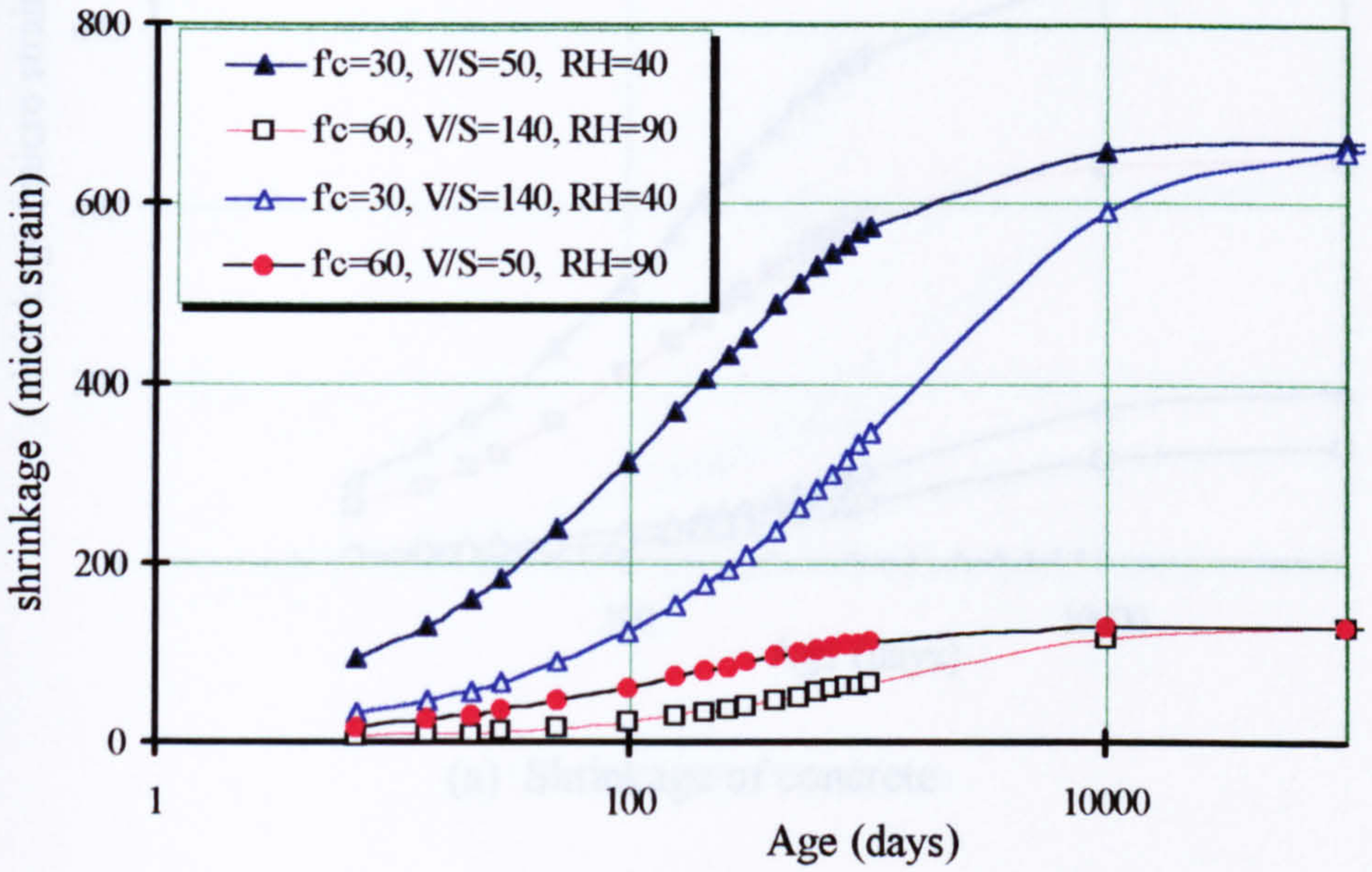

Figure 5.7: Shrinkage of plain concrete under combinations of parameters yielding maximum and minimum deformations.

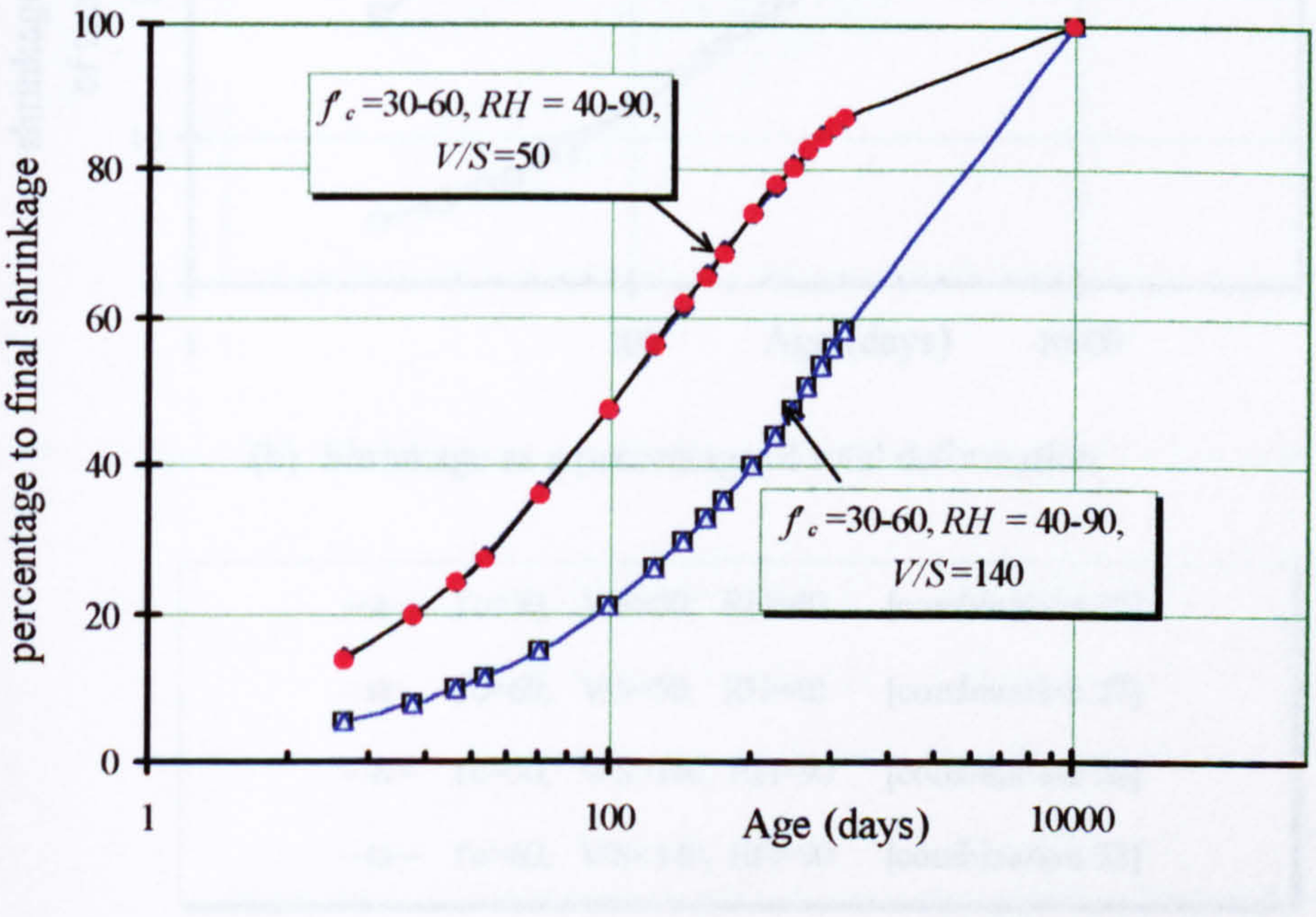

Figure 5.8: Development of shrinkage under combinations of parameters yielding maximum and minimum shrinkage.

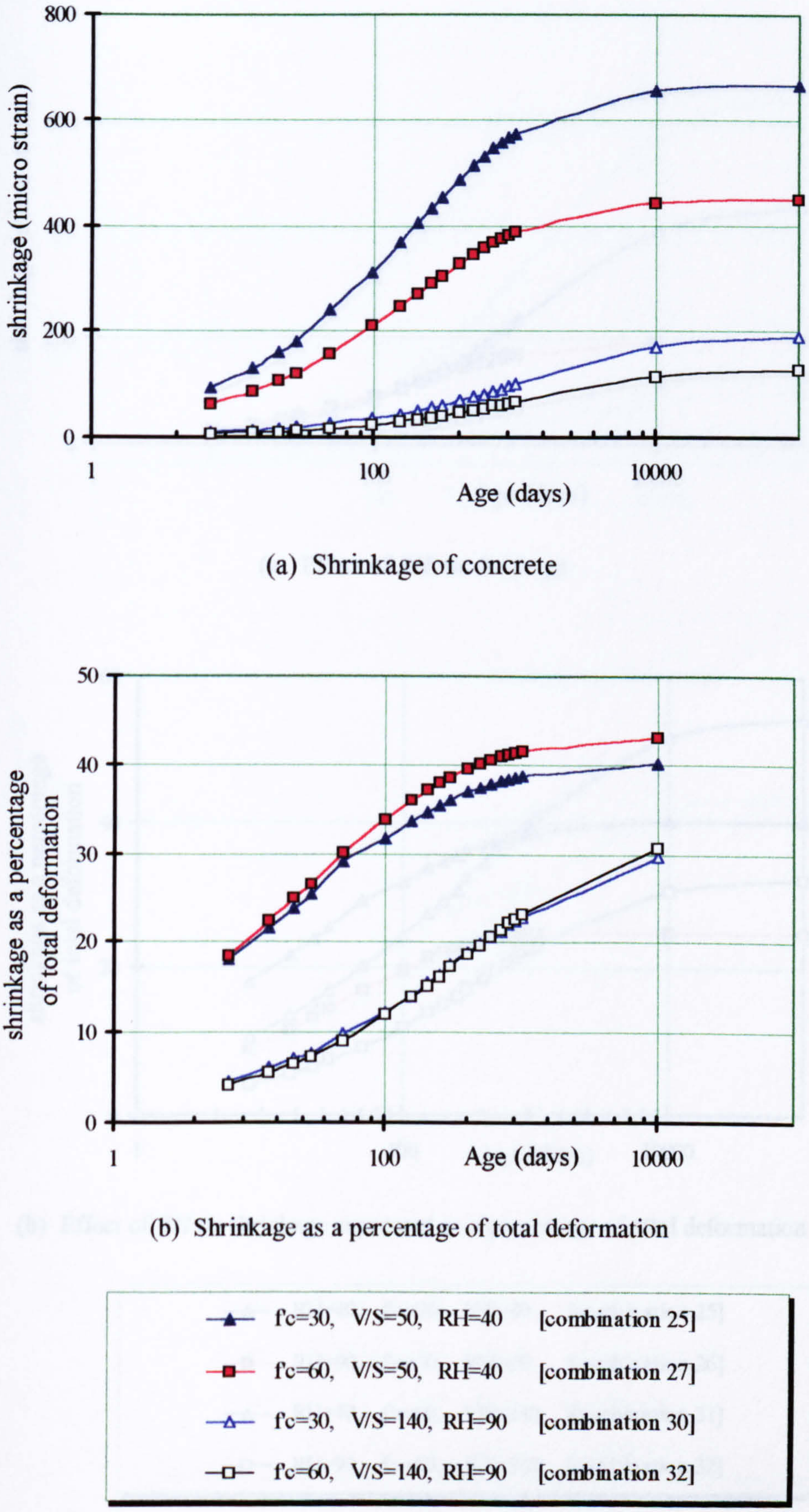

(a) Shrinkage of concrete

(b) Shrinkage as a percentage of total deformation

Figure 5.9: Effect of f'_c on shrinkage characteristics of plain concrete under combinations of parameter yielding maximum and minimum deformation

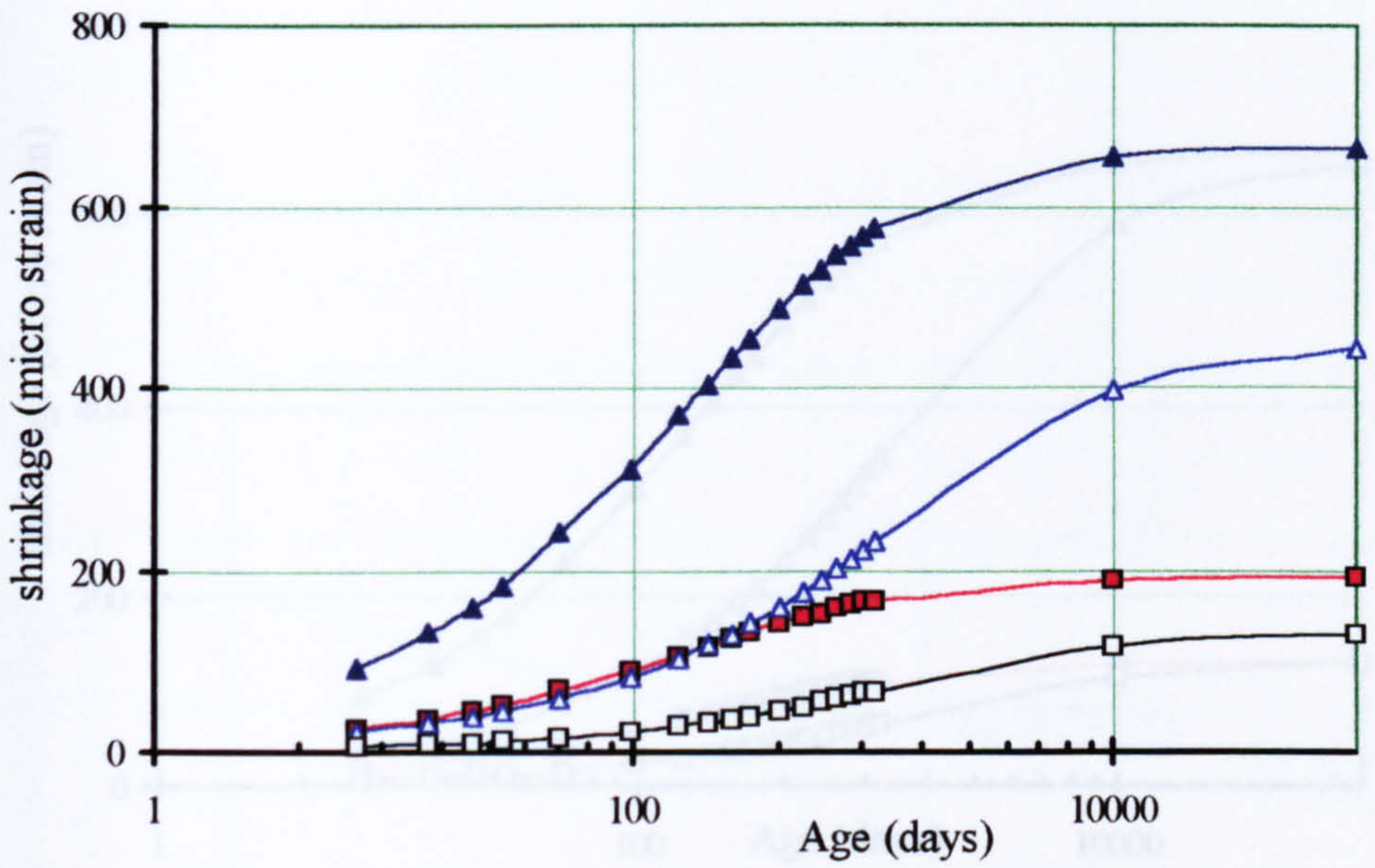

(a) Effect of *RH* on shrinkage

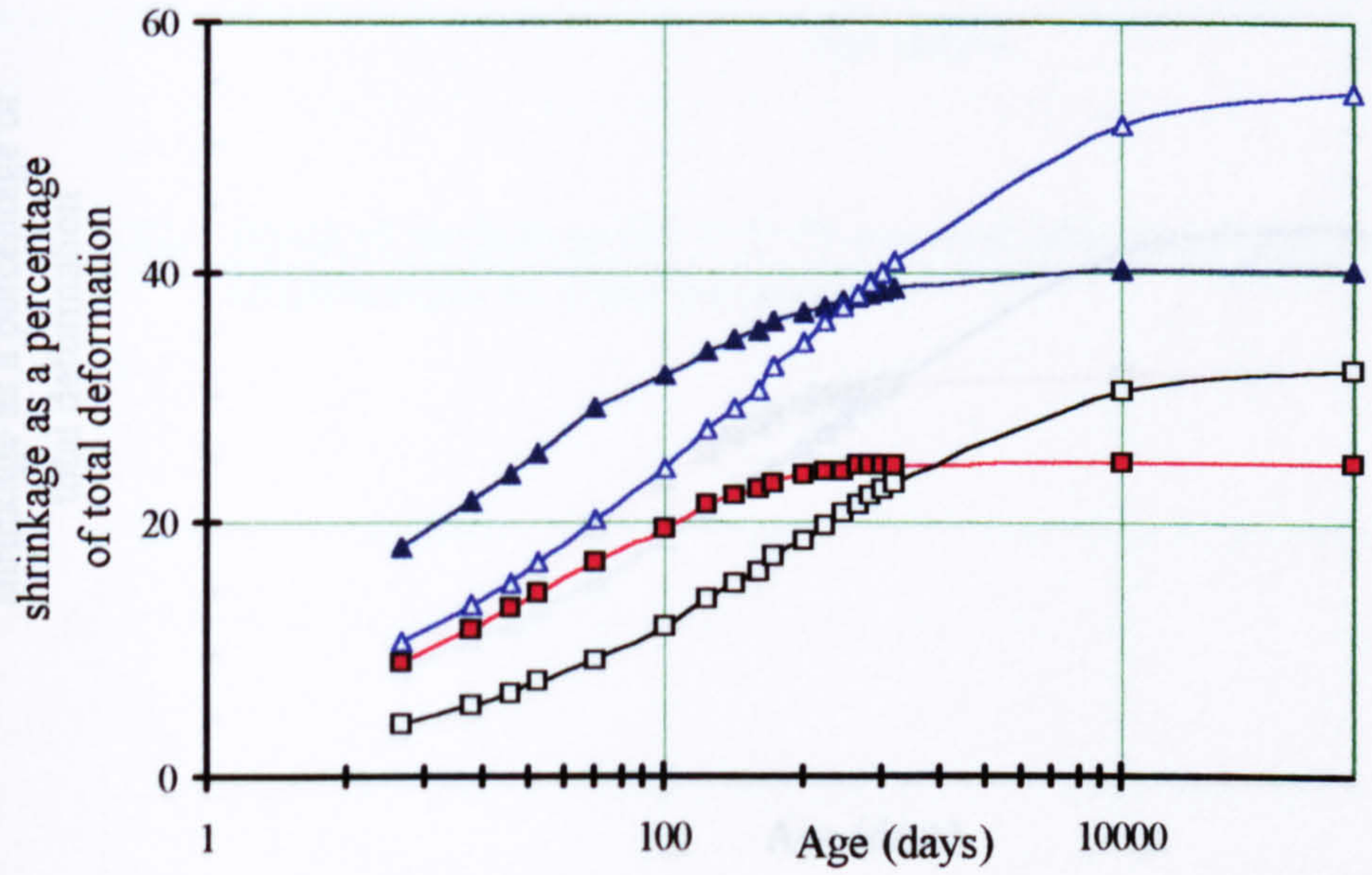

(b) Effect of *RH* on shrinkage expressed as a percentage of total deformation

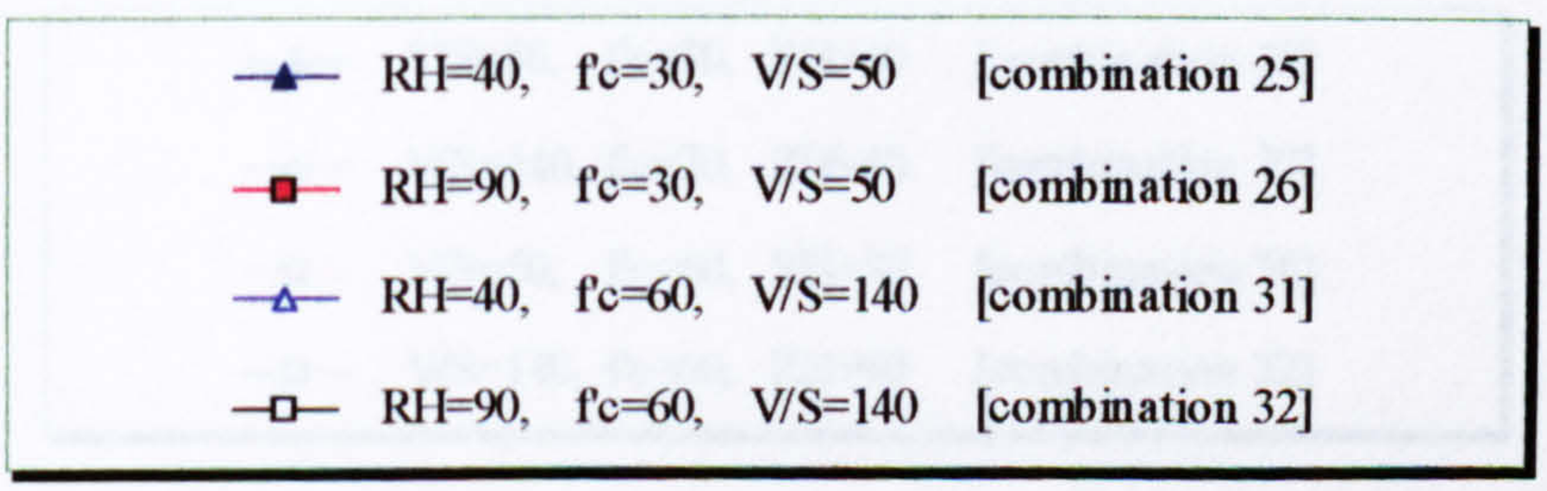

Figure 5.10: Effect of *RH* on shrinkage characteristics of plain concrete under combinations of parameters yielding maximum and minimum deformation

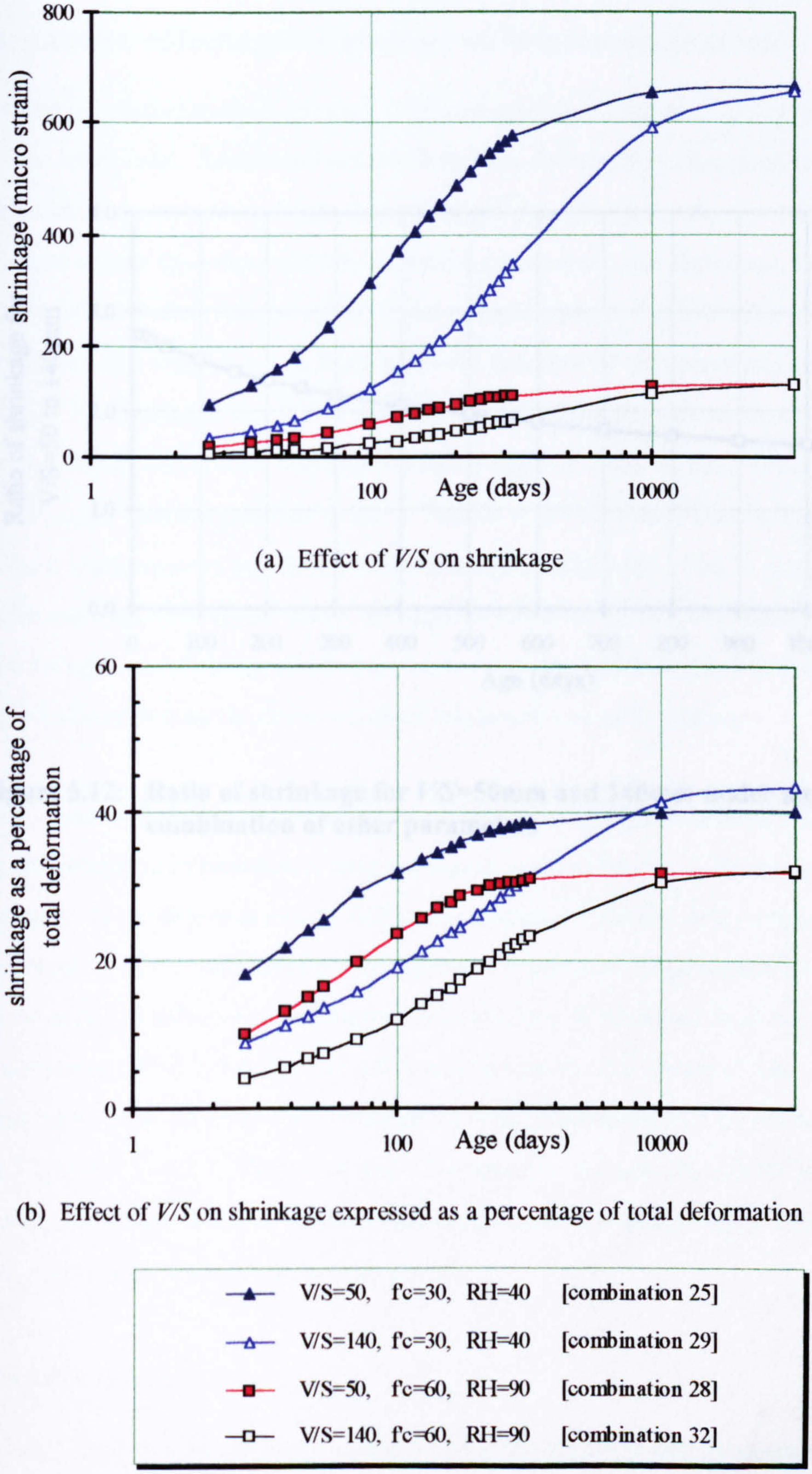

(a) Effect of *V/S* on shrinkage

(b) Effect of *V/S* on shrinkage expressed as a percentage of total deformation

Figure 5.11: Effect of *V/S* on shrinkage characteristics of plain concrete under combinations of parameters yielding maximum and minimum deformation

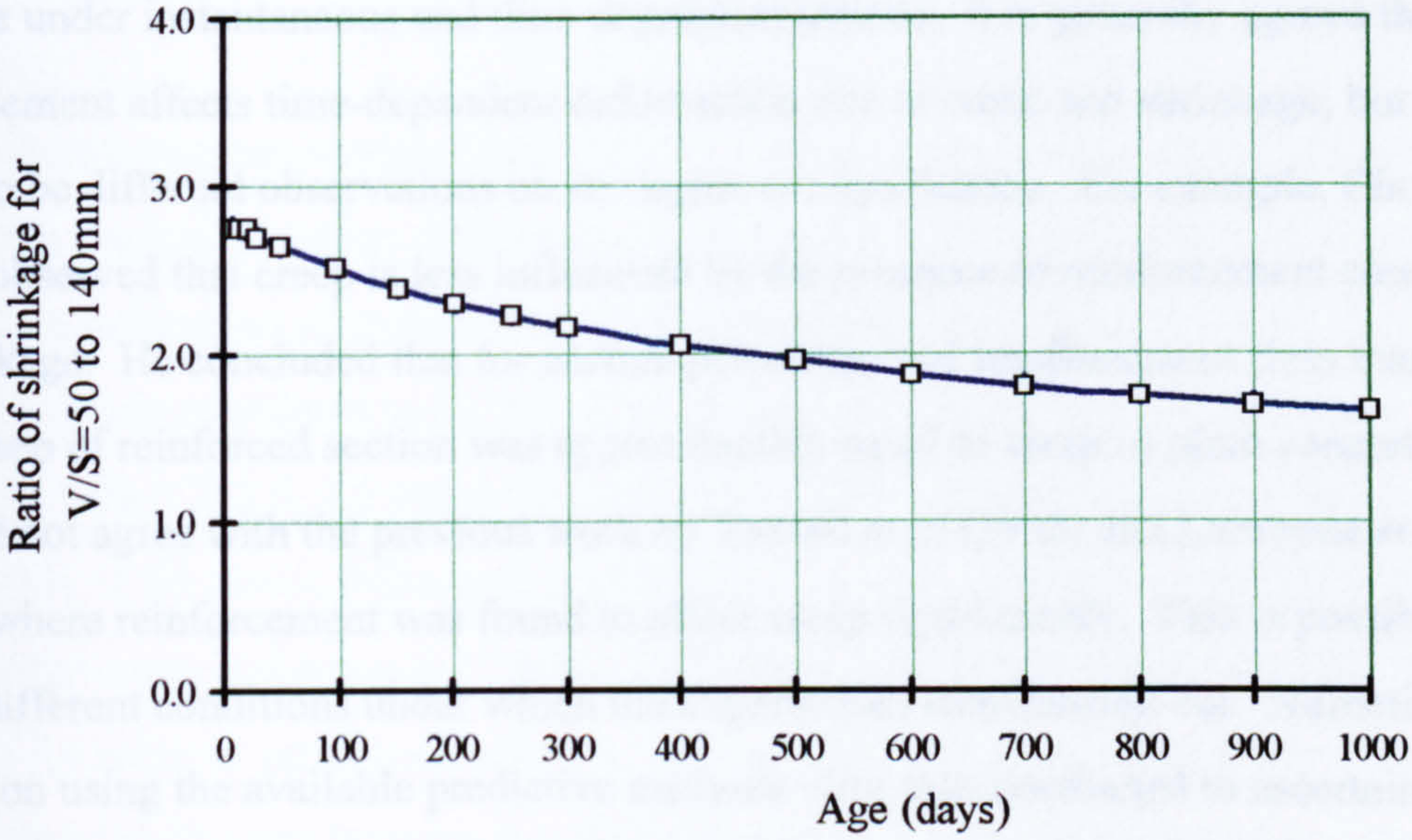

Figure 5.12: Ratio of shrinkage for *V/S*=50mm and 140mm under any combination of other parameters

5.3 Parameters Affecting Deformation of Reinforced Sections

The presence of reinforcement in concrete increases sectional stiffness, thus affecting its deformation under load. Reinforced sections have less deformation compared to plain concrete under instantaneous and time-dependent actions. It is generally agreed that reinforcement affects time-dependent deformation due to creep and shrinkage, but there seems to be different observations on its degree of significance. For example, Chouman (1990) observed that creep is less influenced by the presence of reinforcement compared to shrinkage. He concluded that for normal percentages of reinforcement (less than 3%), creep of reinforced section was approximately equal to creep of plain concrete. This did not agree with the previous work by Troxell *et al* (1958) and Lambotte *et al* (1983) where reinforcement was found to affect creep significantly. This is possibly due to different conditions under which the experiments were carried out. Numerical evaluation using the available predictive methods were thus conducted to ascertain the effects of reinforcement on the deformation of reinforced concrete sections.

The elastic, creep and shrinkage deformations of reinforced concrete sections subject to different combinations of parameters were evaluated in a similar way to those for the plain concrete. These deformations as well as the change in concrete and steel stresses were evaluated for the two different combinations of parameters where concretes were expected to display maximum and minimum deformation. In each combination, the sections contained 0.0, 0.5, 1.0, 2.0 and 3.0% reinforcement. The effects of the reinforcement on time-dependent deformation for both combinations of parameters are shown in Figures 5.13-5.15. Tables 5.4 and 5.5 summarise the calculations for the elastic, creep, shrinkage and total strains under combinations of parameters yielding maximum and minimum deformation respectively.

5.3.1. Elastic deformation

In plain concrete, it was shown that the parameters affecting the elastic strain were the age at loading and the characteristic strength of concrete. These parameters were directly related to the values of the elastic modulus, hence affecting the elastic deformation. It was calculated that concrete with any characteristic strength and loaded

at 3 days displayed about 29% greater instantaneous deformation than the corresponding concrete loaded at 28 days. It was also calculated that, for any age at loading, concrete of 30MPa strength displayed about 26% greater instantaneous deformation than that of 60MPa strength.

For reinforced concrete sections subjected to an axial stress, the calculation showed a decrease in the instantaneous deformation as the percentage of reinforcement increased. Under the combination of parameters yielding maximum deformation (Table 5.4), the deformation was calculated to be 202, 196, 185 and 175 microstrain for sections reinforced with 0.5, 1.0, 2.0 and 3.0% steel respectively. These represent about 96, 94, 89 and 84% of the elastic deformation of the plain section. Under the combination yielding minimum deformation (Table 5.5), the percentages calculated were 98, 95, 91 and 87% for sections reinforced with 0.5, 1.0, 2.0 and 3.0% steel respectively. Based on the calculated difference between the elastic strains of plain and reinforced sections, it can be concluded that sections reinforced with up to 2.0% reinforcement do not significantly affect the elastic deformation under any combination of parameters. For the combination of parameters yielding minimum deformation, a percentage of reinforcement up to 3.0% does not significantly affect elastic deformation.

The decreasing level of elastic deformation associated with an increasing amount of the reinforcement was also accompanied by a decreasing level of concrete stress. This clearly has an effect on the analysis of prestressed sections containing bonded reinforcement, as is the case for prestressed bridge beams. It was calculated that the initial stress in the concrete was reduced to 4.84 and 4.19MPa for sections containing 0.5 and 3.0% reinforcement respectively (Table 5.7). For sections reinforced with 3.0% steel, this constituted a reduction of about 17% in the applied initial stress of 5MPa.

Ignoring the presence of bonded reinforcement (or underestimating its effect) will overestimate the elastic deformation and stress in the concrete. This will lead to an overestimation of stress loss in the prestressing steel due to elastic shortening of the concrete. While this appears to be acceptable because it is on the conservative side, the higher compressive stress assumed to be present in the concrete may result in a non-

conservative estimate of the cracking load. This is made worse if the concrete stress is further reduced over time due to the effects of creep and shrinkage. The high initial elastic stress will further overestimate creep and the time-dependent loss of stress in the prestressing steel. It is therefore, necessary to consider the presence of reinforcement for the analysis of sections under instantaneous load for sections having appreciable amounts of reinforcement over 2.0%.

5.3.2. Deformation due to creep

The effects of reinforcement on the creep characteristics of reinforced sections under the combinations of parameters yielding maximum and minimum deformations are shown in Figures 5.13-5.15. The figures show comparisons for the time-dependent deformations between concretes containing different percentages of reinforcement.

Figure 5.13(a) shows that, under the combination of parameters yielding maximum deformation, the deformations due to creep were significantly affected for all the reinforced sections considered. The effect increased as the percentage of the reinforcement increased. The 28 and 10,000 day creep values for plain sections were calculated to be 373 and 835 microstrain respectively, whereas equivalent for sections reinforced with 0.5% steel were 332 and 654 microstrain respectively. These creep values represent about 89 and 86% of those of the plain section, Table 5.4. Sections reinforced with 3.0% steel were even more significantly affected by creep where the 10,000 day deformation was calculated to be 155 microstrain which represented only about 19% of the plain section. This indicates that creep deformation for sections subjected to a moderate axial stress of 5MPa can be significantly affected by 0.5% or more of reinforcement.

A similar comparison for creep under the combination of parameters yielding minimum deformation shows that creep deformation is not significantly affected by steel reinforcement (Figures 5.14). Under this combination of parameters, the 28 and 10,000 day creep values for plain concrete were calculated to be 41 and 146 microstrain respectively; for sections reinforced with 3.0% steel, these values 39 and 101 microstrain respectively. The small difference between the creep values for the plain

concrete and reinforced sections indicates that creep is not significantly affected by steel reinforcement (see also Figures 5.15(a)).

A comparison for creep expressed as a percentage of the total deformation shows that the percentage of deformation due to creep is greatly affected by the reinforcement, Figure 5.15(b). Under the combination of parameters yielding maximum deformation, it was calculated that the final creep represented about 51, 46, 41, 30 and 19% of the final total deformation for sections having 0.0, 0.5, 1.0, 2.0 and 3.0% reinforcement respectively.

It can also be observed that the development of creep occurred earlier for sections with higher levels of reinforcement. It was calculated that, under the combination yielding maximum deformation, plain sections took about 900 days (after loading) to reach 90% of the final creep, compared to 600, 300, and 50 days for sections reinforced with 0.5, 1.0 and 2.0% reinforcement respectively. The section with 3.0% reinforcement displayed maximum creep after about 100 days of loading where the maximum creep was calculated to be 218 microstrain. The deformation due to creep then reduced to 155 microstrain at 10,000 days after loading. The decreasing amount of creep for highly reinforced sections is possibly reduced from the peak values at later ages by tensile stress developed in the concrete due to the continuing action of shrinkage. This observation indicates that the reinforcement does not only affect creep deformation, but also its rate of development.

It has been noted earlier that the deformation due to creep in plain concrete sections was directly proportional to the applied concrete stress where it remained unchanged with time. In the case of the reinforced sections, the concrete stress is expected to change with time, hence the creep deformation is no longer proportional to the initially applied stress level. A comparison for the effect of applied stress on the creep of plain and reinforced sections is shown in Figures 5.16 where concretes were subjected to initial stresses of 5 and 10MPa. The sections were all subject to the combination of parameters yielding maximum deformation.

For the plain sections, the ratios between creep values due to applied stress levels of 10 and 5MPa remained constant at 2.0 at any time after loading. The ratios between the creep of sections reinforced with 1.0% steel due to similar levels of applied were calculated to be 2.06 at 28 days and 2.22 at 10,000 days. Similar calculations for sections with 3.0% reinforcement yielded the ratios at 2.19 and 3.70 at 28 and 10,000 days respectively. This indicates that, the level of applied stress affects the creep of reinforced sections significantly when reinforcement is greater than 1.0%.

5.3.3. Deformation due to shrinkage

The effects of reinforcement on shrinkage deformation of reinforced sections are shown in Figures 5.13-5.15 and Tables 5.4-5.5.

Figure 5.13(b) shows that under the combination of parameters yielding high deformation, steel reinforcement does affect shrinkage significantly. It was calculated that the shrinkage for sections reinforced with 0.5, 1.0, 2.0 and 3.0% steel at 28 days were 166, 153, 133, and 117 microstrain respectively. These values represent about 91, 84, 73, and 64% of the shrinkage deformation of similar plain sections. The equivalent percentages were less for the long term shrinkage where, at 10,000 days, they were calculated to be 86, 75, 60 and 50%. Therefore, as for creep, the presence of reinforcement of any proportion needs to be considered to compute the deformation of reinforced sections due to shrinkage.

The presence of reinforcement, however, does not significantly affect the deformation due to shrinkage for the combination of parameters yielding minimum deformation (Figure 5.14(b)). In the presence of high average relative humidity, the shrinkage of any reinforced sections can be considered equal to that of plain sections.

5.3.4. Stresses in steel and concrete

The reduction in creep as the ratio of reinforcement increases is accompanied by a decrease in concrete stress but an increase in compressive stress in the reinforcement. Figures 5.17-5.18 show time-dependent stresses in concrete and steel for concrete

sections reinforced with 0.5, 1.0, 2.0 and 3.0% steel for the combinations of parameters yielding maximum and minimum values of deformation, respectively. Table 5.6 shows the distribution of compressive stress in the reinforcement due to creep, shrinkage, and total deformation under the combination of parameters yielding maximum deformations.

Under a moderate initial compressive stress of 5MPa, stress due to creep represents a very significant percentage of the total stress in the reinforcement. Stresses developed in the steel reinforcement due to creep were calculated to be 67, 61, 47 and 41 MPa at 28 days for sections reinforced with 0.5, 1.0, 2.0 and 3.0% steel respectively. These values represent about 51.1, 50.8, 45.6 and 45.0% of the total stress in the reinforcement. A similar calculation at 10,000 days yielded percentages of 49.3, 48.1, 44.9 and 42.9% for the same reinforcement ratios.

The stress increase in the reinforcement due to creep for the combination of parameters yielding minimum deformation was less pronounced. The 10,000 day steel stress due to creep was calculated to be 27, 25, 22 and 20MPa for section reinforced with 0.5, 1.0, 2.0 and 3.0% steel respectively.

The percentages of steel stress due to shrinkage actions were calculated to be nearly constant for all levels of reinforcement subject to any combination of parameters. The percentages due to shrinkage were calculated to be about 26 and 40% of the total stress at 28 and 10,000 days respectively under the combination of parameters yielding maximum deformation. Under the combination of parameters yielding minimum deformation the percentage were calculated to be 7 and 30% at 28 and 10,000 days respectively.

The increase of compressive stress in the reinforcement must be accompanied by a decrease in the compressive stress in the concrete in order to maintain equilibrium of forces. Table 5.7 and Figure 5.17(a) show that the presence of the reinforcement could be very significant in reducing the compressive stress of the concrete. Figure 5.17(a) shows that the applied compressive stress in the concrete is drastically reduced as the

percentage of steel reinforcement is increased. The 10,000 day compressive concrete stress reduced to 3.59, 2.53, 1.07 and 0.11MPa from the initially applied stress of 5MPa for sections reinforced with 0.5, 1.0, 2.0 and 3.0% steel respectively. This indicates that it is possible, under the combination of parameters yielding maximum deformation, that a highly reinforced section subjected to a moderate initial compressive stress could even result in tensile stress in the concrete.

Under the combination of parameters yielding minimum deformation, the stress reduction in the concrete can also be considered significant in a highly reinforced section. Table 5.7 shows that the final compressive stress in the concrete reinforced with 3.0% steel was reduced to 3.21MPa from the initially applied stress of 5.0MPa.

The calculation for concrete stress shows that a high reinforcement content results in a higher tensile stress due to shrinkage actions. The 10,000 day values for sections reinforced with 0.5, 1.0, 2.0 and 3.0% steel were calculated to be -0.54, -0.99, -1.58, and -1.97MPa respectively. This indicates that highly reinforced sections are unlikely to crack due to the action of shrinkage alone under any combination of parameters. The compressive and tensile stresses developed in the steel and concrete were less significant for the combination of parameters yielding minimum deformation. The 10,000 day stress due to shrinkage actions was calculated to be -0.53MPa for the concrete reinforced with 3.0% steel.

A comparison between the effects of creep and shrinkage on the steel is shown in Figures 5.19. Figure 5.19(a) shows time-dependent stress due to creep. Figures 5.19(b) and (c) show the percentage of the stress developed due to creep and shrinkage respectively. The figures show that, under a moderately applied stress of 5MPa, and subject to combination of parameters yielding maximum deformation, creep has a more significant effect on the compressive stress in the steel than does shrinkage for sections containing any degree of reinforcement. The effect is expected to be more significant under a higher level of applied stress.

Table 5.4: Microstrain values in reinforced concrete sections under combinations of parameters yielding maximum deformations

Deformation	plain [1]	A_s=0.5% [2]	A_s=1.0% [3]	A_s=2.0% [4]	A_s=3.0% [5]	A_s=0.5% [2]÷[1]	A_s=1.0% [3]÷[1]	A_s=2.0% [4]÷[1]	A_s=3.0% [5]÷[1]
ε_c(elastic)	208	202	196	185	175	0.962	0.942	0.889	0.841
ε_{cr28}	373	332	297	242	199	0.890	0.796	0.649	0.534
ε_{cr252}	635	532	440	304	209	0.838	0.693	0.479	0.329
ε_{cr1000}	764	612	485	303	179	0.801	0.635	0.396	0.234
$\varepsilon_{cr10000}$	835	654	505	295	155	0.856	0.605	0.353	0.186
ε_{sh28}	182	166	153	133	117	0.912	0.841	0.731	0.643
ε_{sh252}	432	381	341	281	239	0.882	0.789	0.650	0.553
ε_{sh1000}	574	498	439	355	298	0.868	0.765	0.618	0.519
$\varepsilon_{sh10000}$	656	563	493	394	329	0.858	0.751	0.600	0.502
$\varepsilon_{tot.28}$	715	653	601	517	454	0.913	0.840	0.723	0.634
$\varepsilon_{tot.252}$	1215	1080	963	790	670	0.889	0.792	0.650	0.551
$\varepsilon_{tot.1000}$	1483	1295	1138	916	765	0.873	0.767	0.618	0.516
$\varepsilon_{tot.10000}$	1634	1413	1233	982	815	0.860	0.754	0.601	0.499

Table 5.5: Microstrain values in reinforced concrete sections under combinations of parameters yielding minimum deformations

Deformation	plain [1]	A_s=0.5% [2]	A_s=1.0% [3]	A_s=2.0% [4]	A_s=3.0% [5]	A_s=0.5% [2]÷[1]	A_s=1.0% [3]÷[1]	A_s=2.0% [4]÷[1]	A_s=3.0% [5]÷[1]
ε_c(elastic)	128	125	122	116	111	0.977	0.953	0.906	0.867
ε_{cr28}	41.2	40	39	36	34	0.97	0.947	0.874	0.825
ε_{cr252}	77.5	74.0	71	66	61	0.955	0.916	0.852	0.787
ε_{cr1000}	108	102	97	88	80	0.944	0.898	0.815	0.741
$\varepsilon_{cr10000}$	146.5	137	129	113	101	0.935	0.880	0.771	0.689
ε_{sh28}	13	13	12	12	11	1.0	0.92	0.92	0.846
ε_{sh252}	37.8	36	35	33	31	0.952	0.926	0.88	0.827
ε_{sh1000}	66.6	64.5	62	57	53.5	0.968	0.931	0.856	0.803
$\varepsilon_{sh10000}$	115.3	110	105	96	89	0.954	0.911	0.833	0.772
$\varepsilon_{tot.28}$	178	176	171	161	152	0.989	0.961	0.904	0.854
$\varepsilon_{tot.252}$	233	233	225	210	196	1.00	0.966	0.901	0.841
$\varepsilon_{tot.1000}$	291	291	279	258	239	1.00	0.959	0.886	0.821
$\varepsilon_{tot.10000}$	376	371	354	324	298	0.987	0.941	0.862	0.792

Table 5.6: Stresses in steel under combinations of parameters yielding maximum deformations.

Percentage of	Stress (MPa)				Ratio to final (10,000 days) values				Ratio to total values			
reinforcement	0.5%	1.0%	2.0%	3.0%	0.5%	1.0%	2.0%	3.0%	0.5%	1.0%	2.0%	3.0%
σ_s(elastic)	31	30	29	27	0.110	0.121	0.148	0.166	N/A.	N/A.	N/A.	N/A.
σ_{s28}(total)	131	120	103	91	0.464	0.486	0.526	0.558	N/A.	N/A.	N/A.	N/A.
σ_{s252}(total)	216	193	158	134	0.766	0.781	0.806	0.822	N/A.	N/A.	N/A.	N/A.
σ_{s1000}(total)	259	228	183	153	0.918	0.923	0.934	0.939	N/A.	N/A.	N/A.	N/A.
σ_{s10000}(total)	282	247	196	163	1.00	1.00	1.00	1.00	N/A.	N/A.	N/A.	N/A.
σ_{s28}(creep)	67	61	47	41	0.482	0.513	0.534	0.586	0.511	0.508	0.456	0.450
σ_{s252}(creep)	109	95	72	59	0.784	0.798	0.818	0.843	0.505	0.492	0.456	0.440
σ_{s1000}(creep)	128	110	83	66	0.921	0.924	0.943	0.943	0.494	0.482	0.454	0.431
σ_{s10000}(creep)	139	119	88	70	1.00	1.00	1.00	1.00	0.493	0.481	0.449	0.429
σ_{s28}(shrink.)	33	31	27	23	0.295	0.456	0.342	0.348	0.253	0.258	0.258	0.253
σ_{s252}(shrink.)	76	68	57	48	0.678	0.694	0.721	0.727	0.352	0.352	0.361	0.358
σ_{s1000}(shrink.)	100	88	71	60	0.893	0.898	0.899	0.909	0.386	0.386	0.388	0.392
σ_{s10000}(shrink.)	112	98	79	66	1.00	1.00	1.00	1.00	0.397	0.397	0.403	0.405

Table 5.7: Stresses in concrete under combinations of parameters yielding maximum and minimum deformations.

Deformation	plain [1]	A_s=0.5% [2]	A_s=1.0% [3]	A_s=2.0% [4]	A_s=3.0% [5]	[2]÷[1]	[3]÷[1]	[4]÷[1]	[5]÷[1]
	f'_c=30MPa, *RH*=40%, *V/S*=50mm, t_o=t_s=3 days								
σ_c(elastic)	5	4.84	4.70	4.43	4.19	0.968	0.940	0.886	0.838
σ_{c28}	5	4.35	3.80	2.93	2.28	0.870	0.760	0.586	0.456
σ_{c252}	5	3.92	3.07	1.84	0.98	0.784	0.614	0.368	0.196
σ_{c1000}	5	3.71	2.72	1.34	0.41	0.74	0.544	0.268	0.082
σ_{c10000}	5	3.59	2.53	1.07	0.11	0.718	0.506	0.214	0.022
	f'_c=60MPa, *RH*=90%, *V/S*=140mm, t_o=t_s=28 days								
σ_c(elastic)	5	4.88	4.76	4.54	4.33	0.976	0.952	0.908	0.866
σ_{c28}	5	4.82	4.65	4.36	4.09	0.964	0.93	0.87	0.818
σ_{c252}	5	4.77	4.54	4.16	3.82	0.954	0.908	0.83	0.764
σ_{c1000}	5	4.71	4.43	3.97	3.57	0.942	0.886	0.79	0.714
σ_{c10000}	5	4.63	4.28	3.71	3.21	0.926	0.856	0.738	0.642

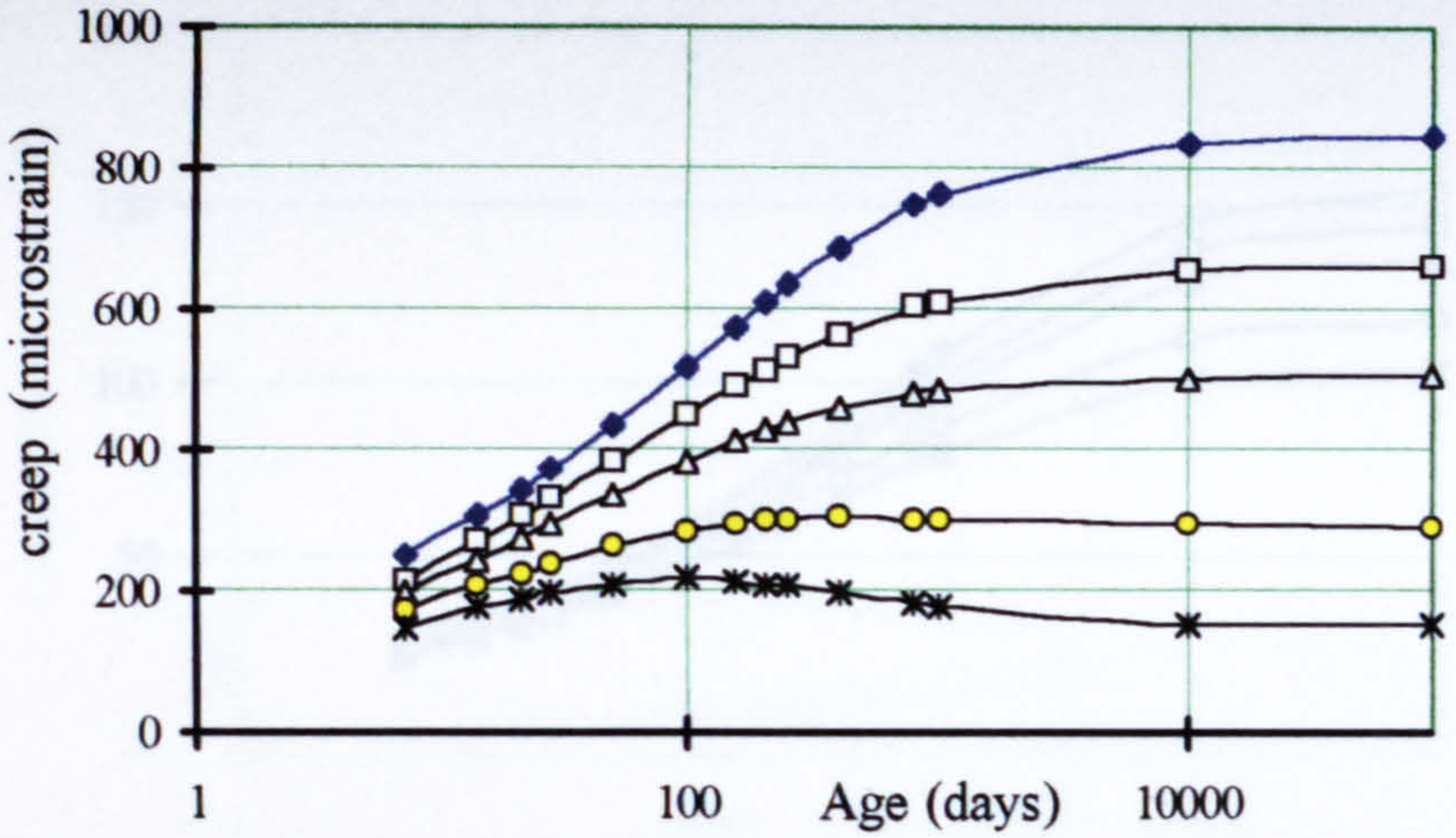

(a) Deformation due to creep for reinforced concrete sections

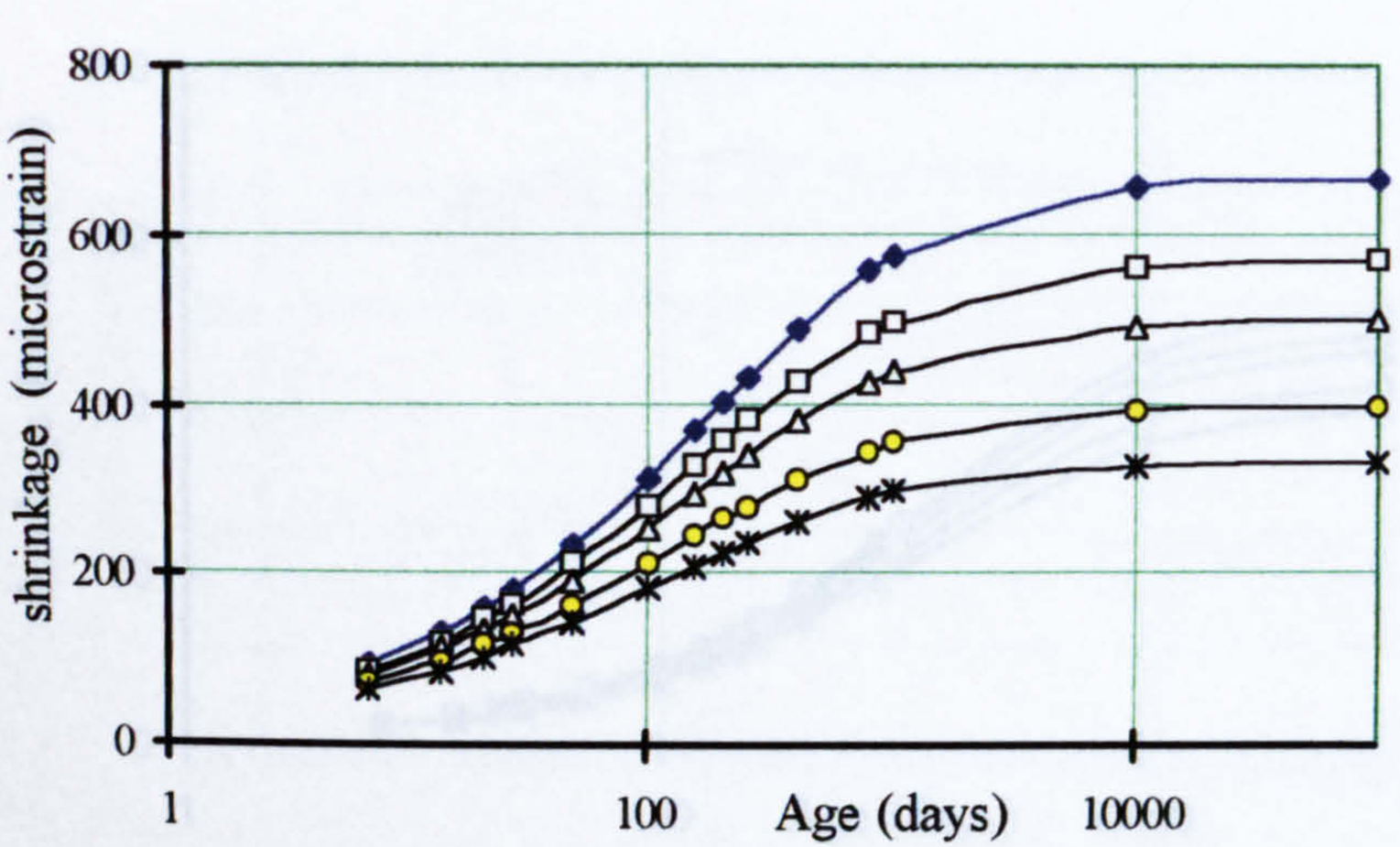

(b) Deformation due to shrinkage for reinforced concrete sections

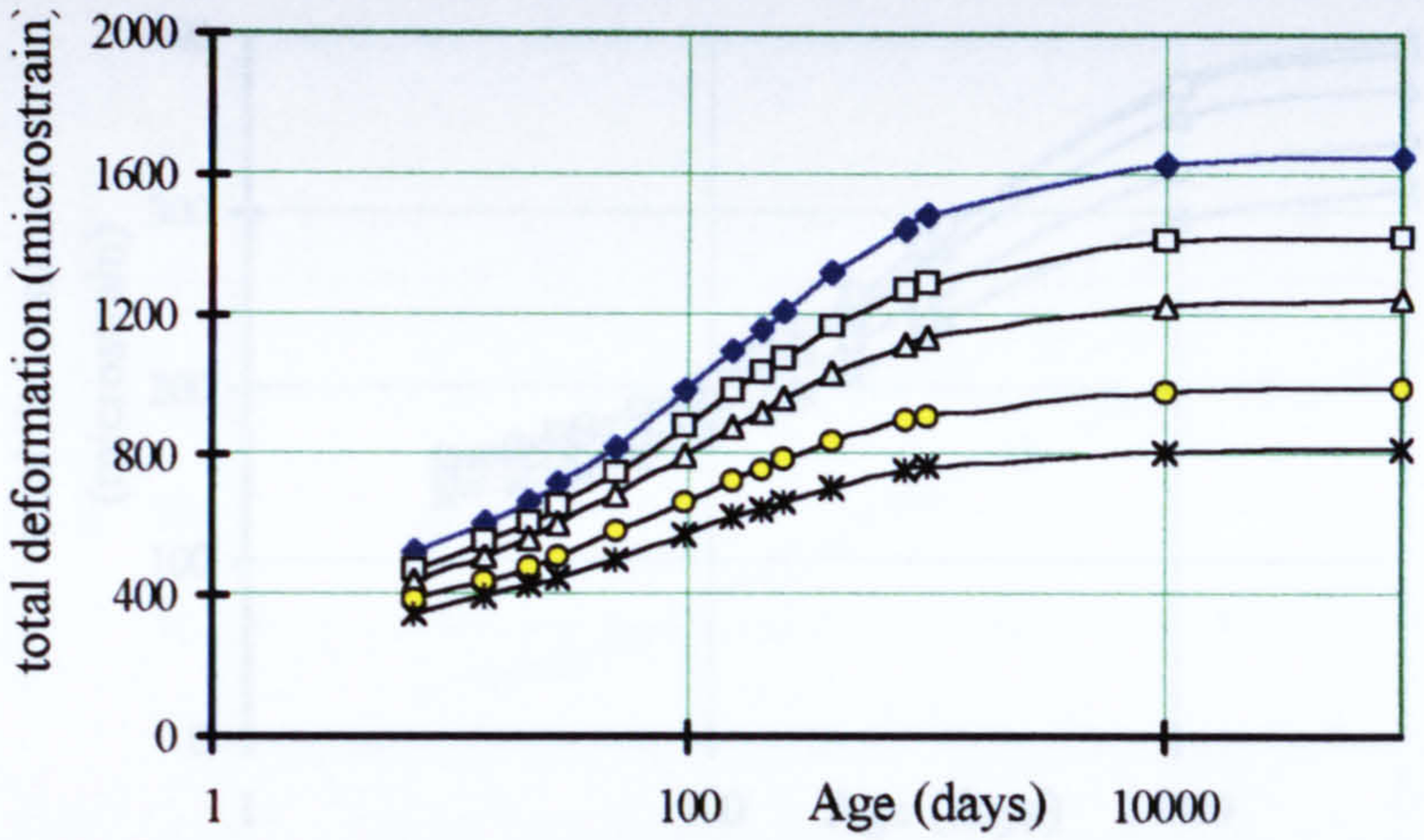

(c) Total deformation for reinforced concrete sections

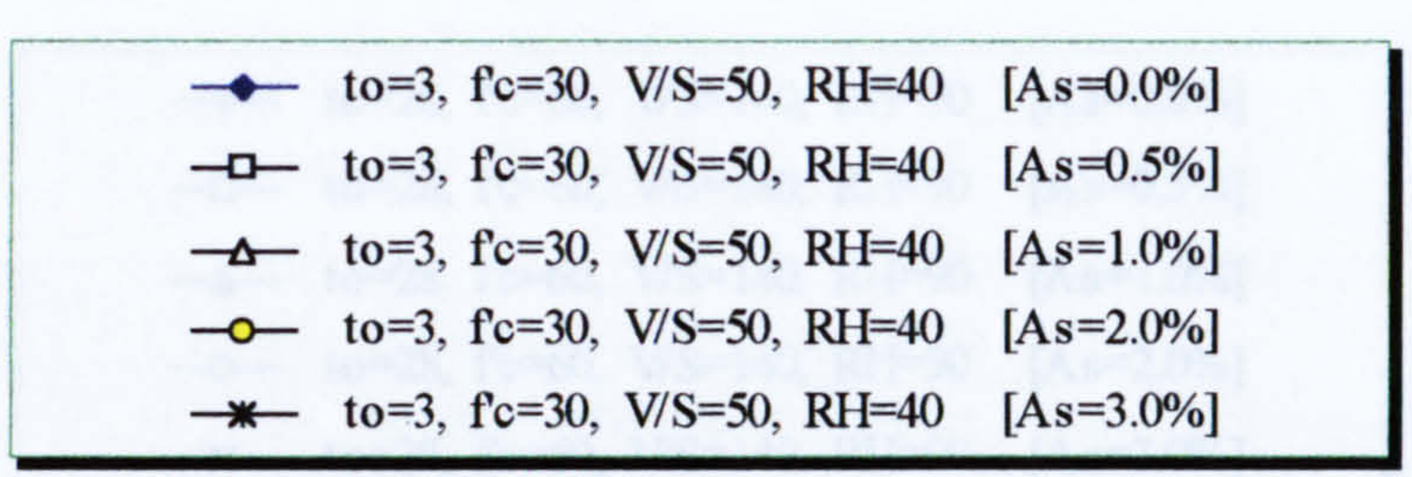

Figure 5.13: Time-dependent deformations of reinforced concrete sections subject to a combination of parameters yielding maximum deformation.

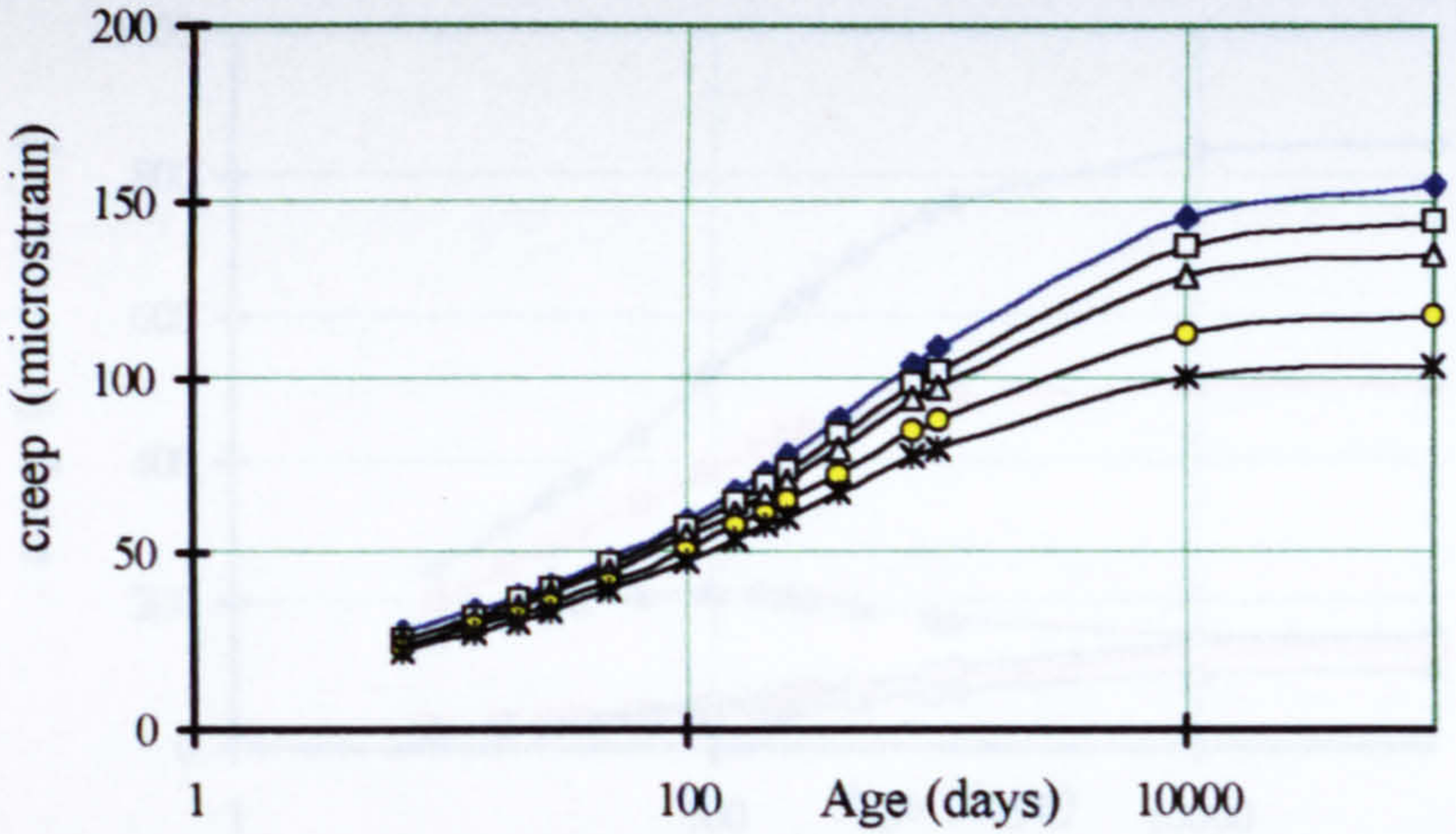

(a) Deformation due to creep for reinforced sections

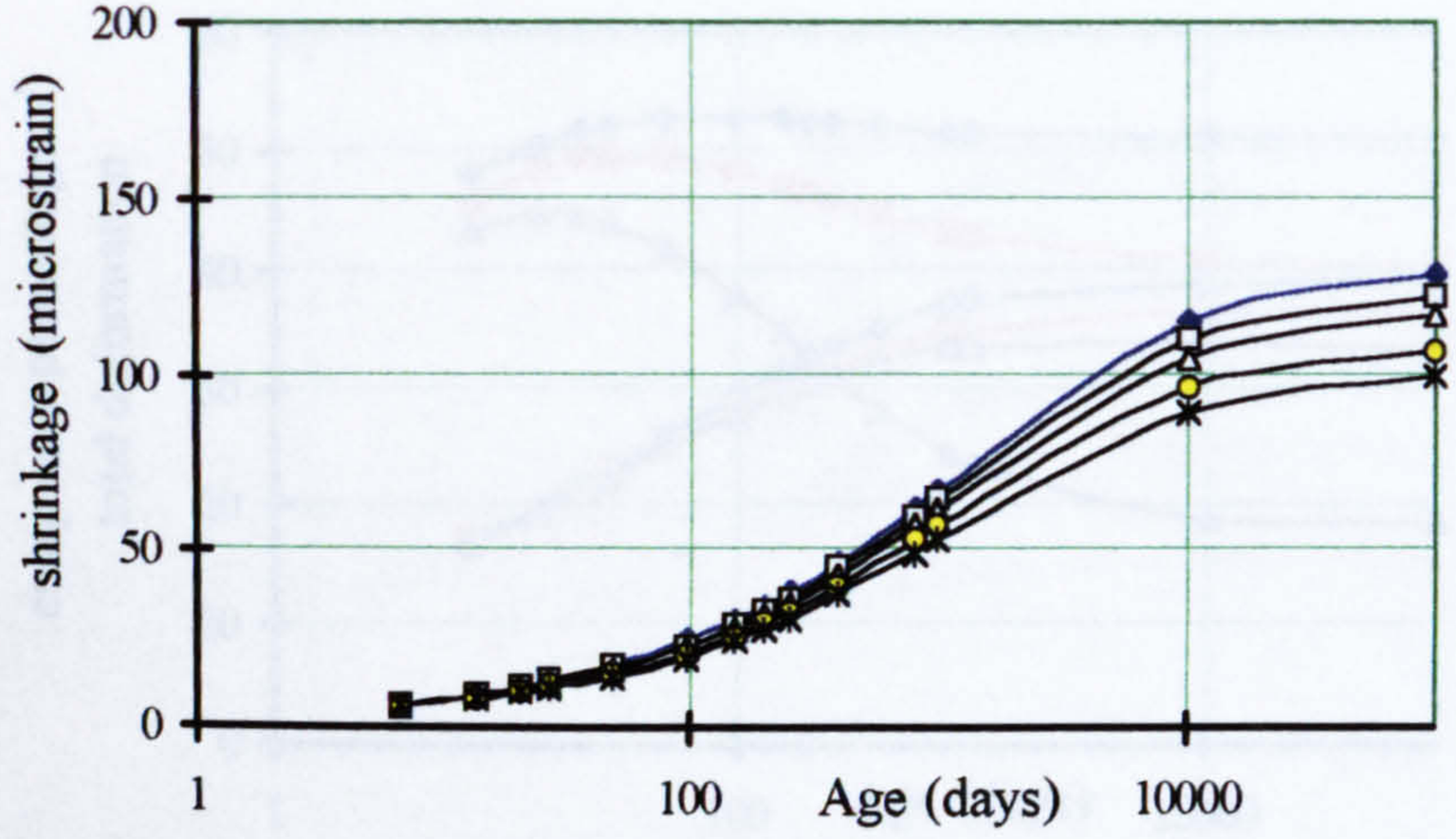

(b) Deformation due to shrinkage for reinforced concrete sections

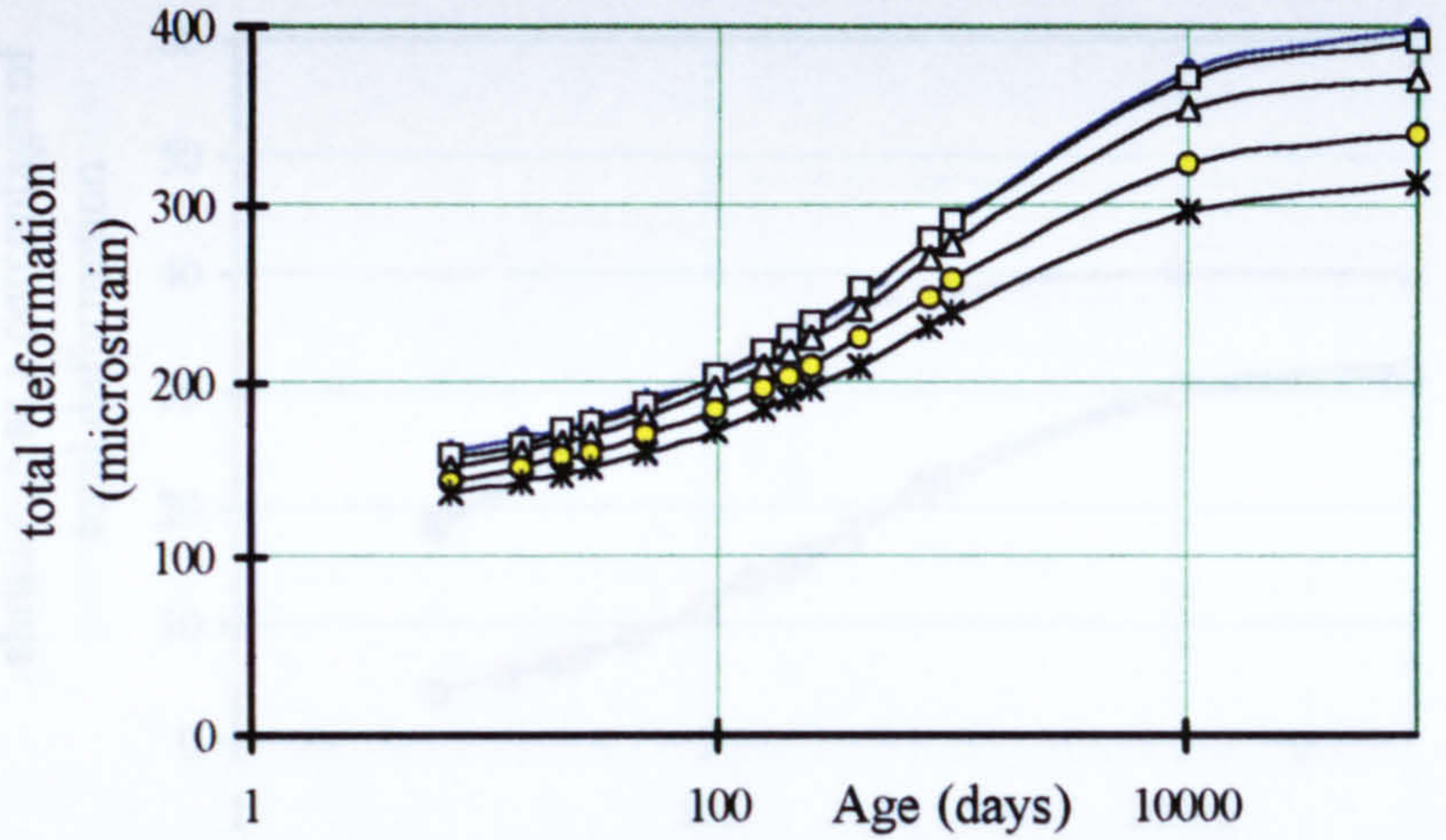

(c) Total deformation for reinforced concrete sections

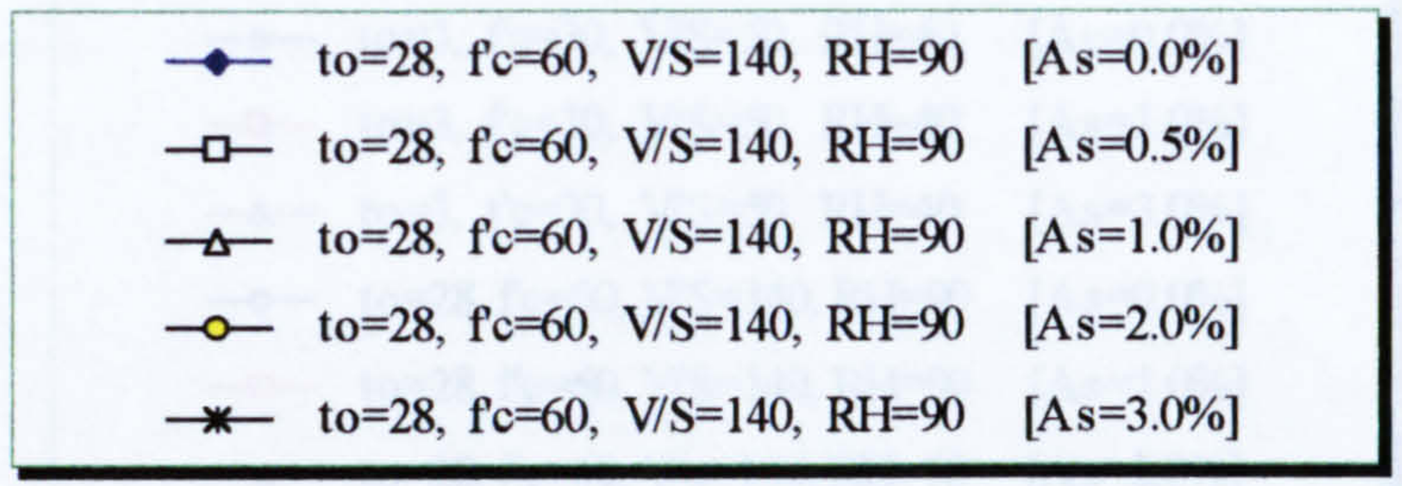

Figure 5.14: Time-dependent deformations for reinforced concrete sections under a combination of parameters yielding minimum deformation.

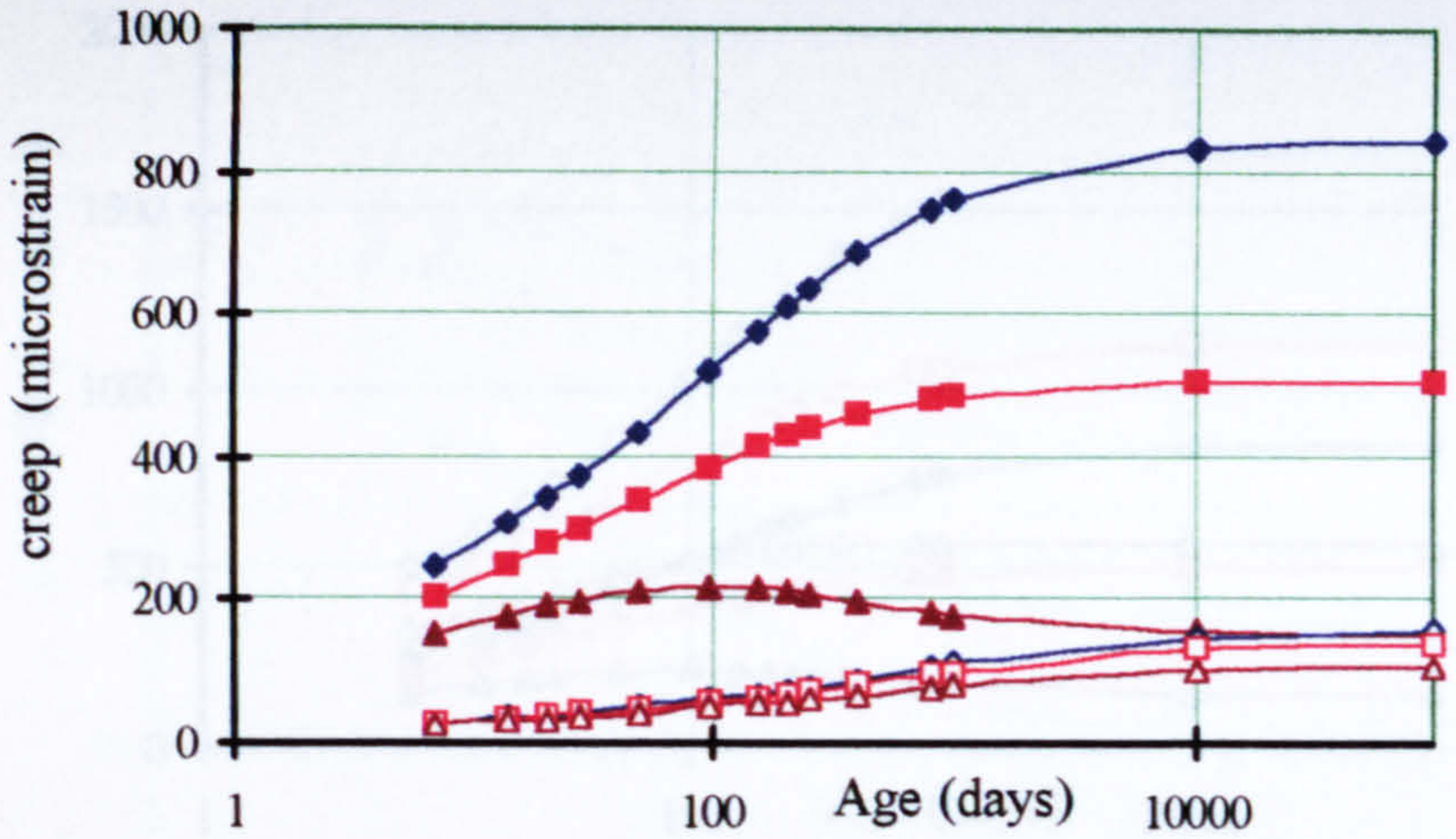

(a) Effect of reinforcement on creep

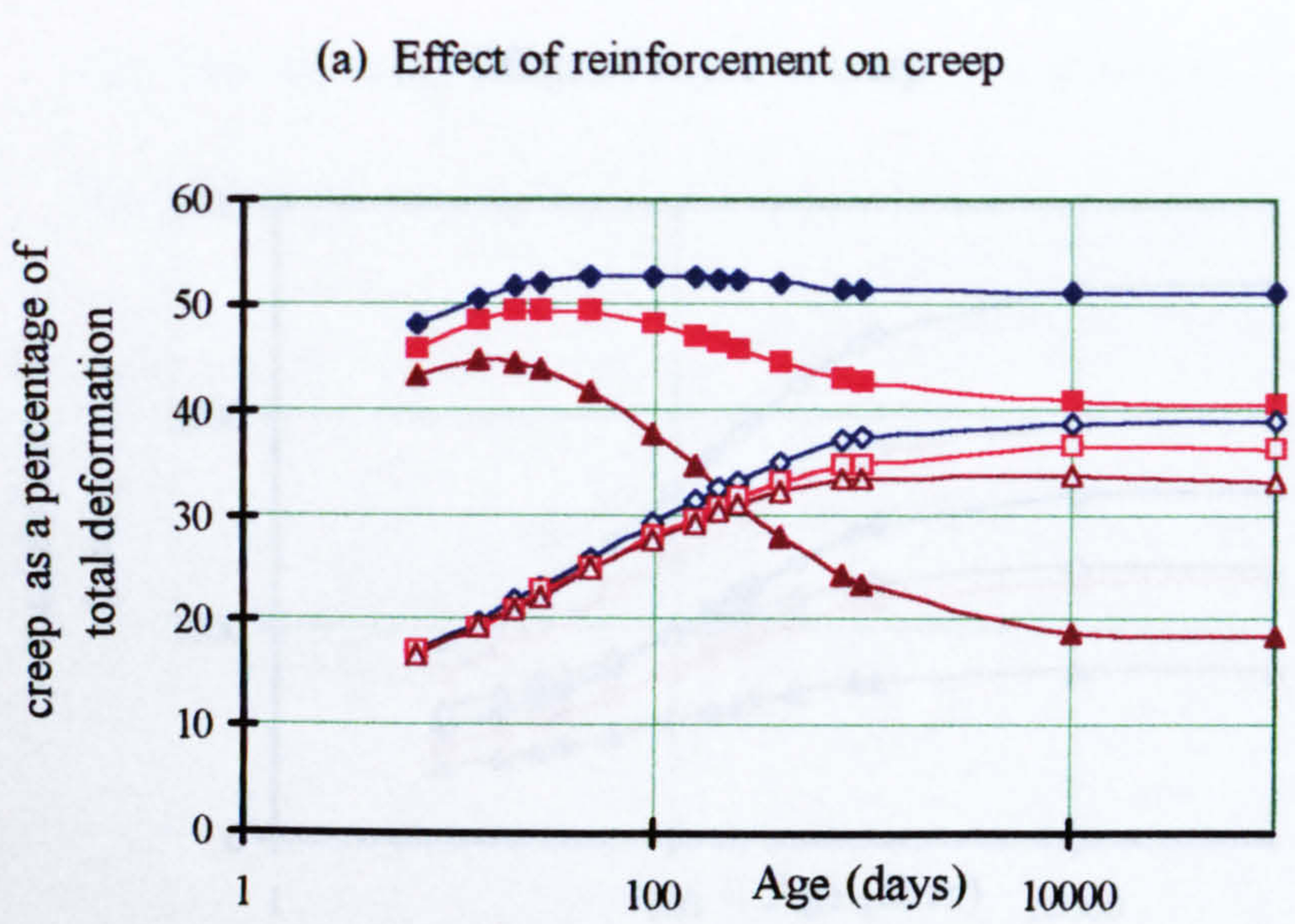

(b) Effect of reinforcement on creep as a percentage to total deformation

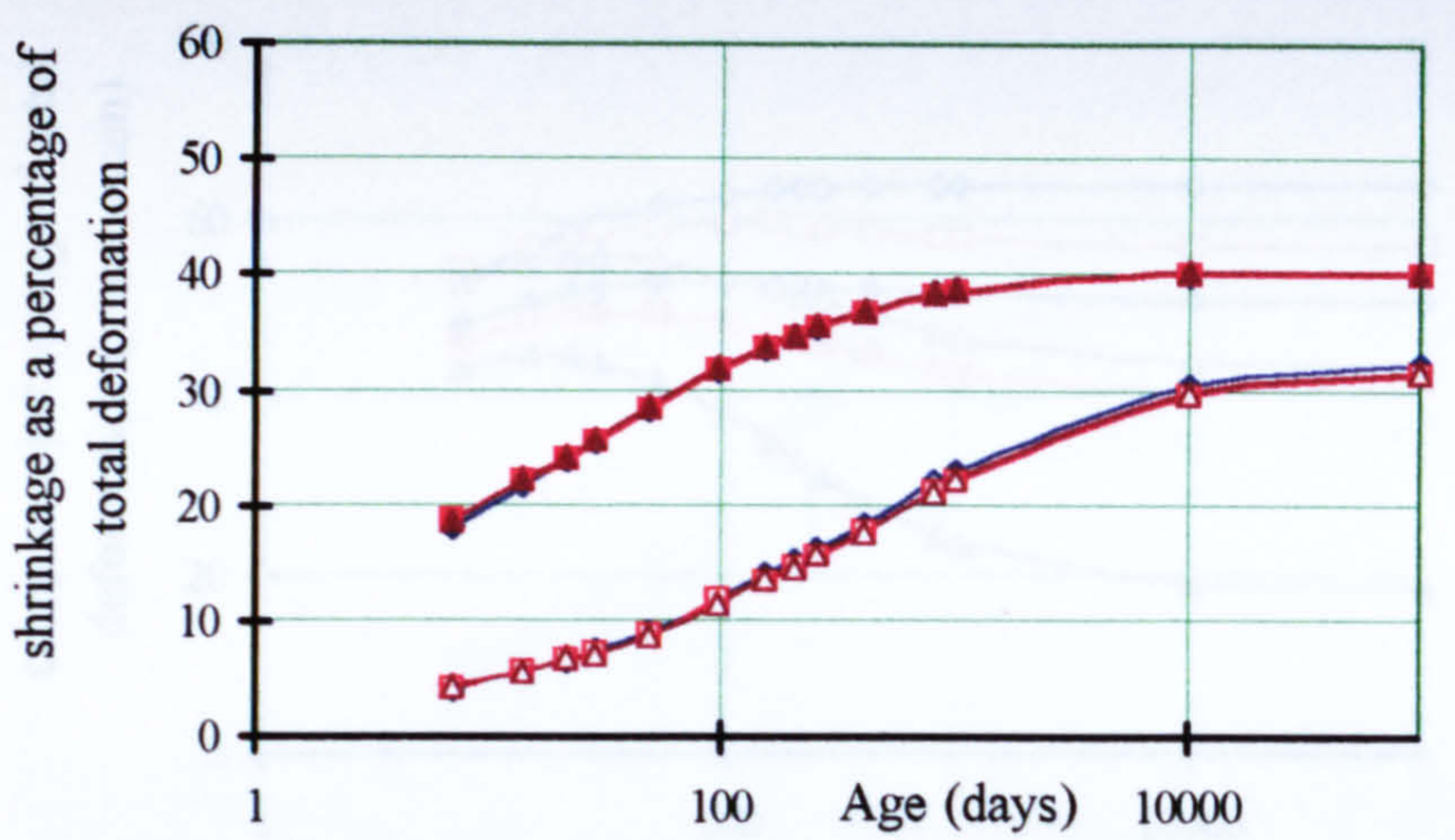

(c) Effect of reinforcement on shrinkage

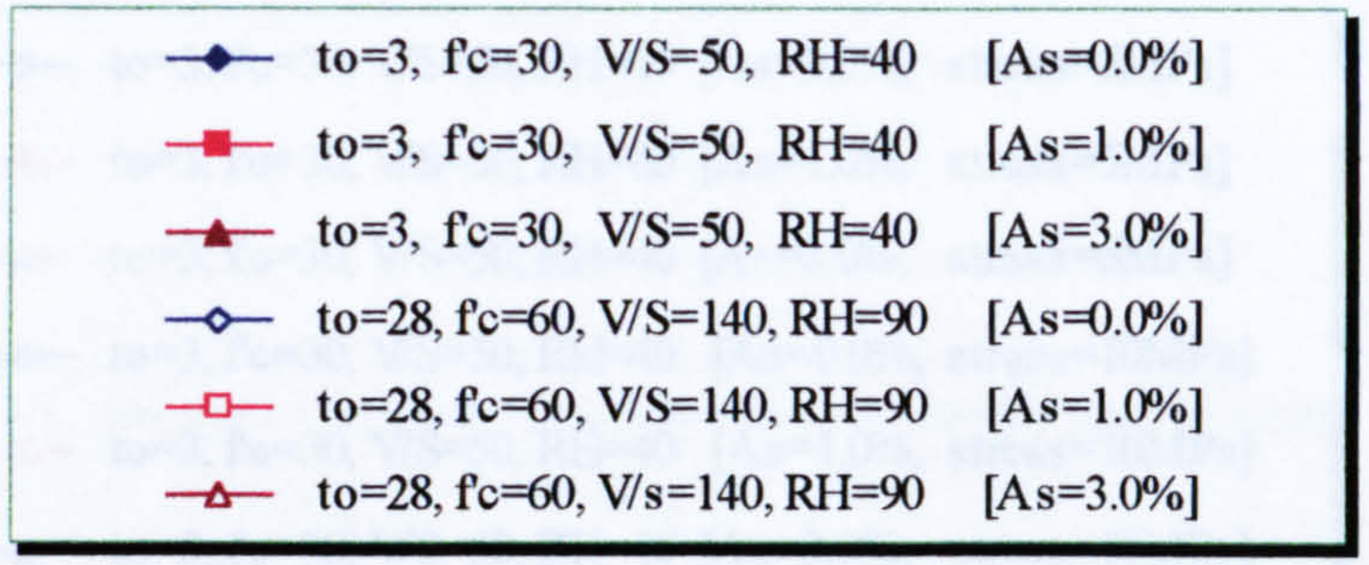

Figure 5.15: Effect of reinforcement on creep and shrinkage of reinforced sections subject to combinations of parameters yielding maximum and minimum deformation

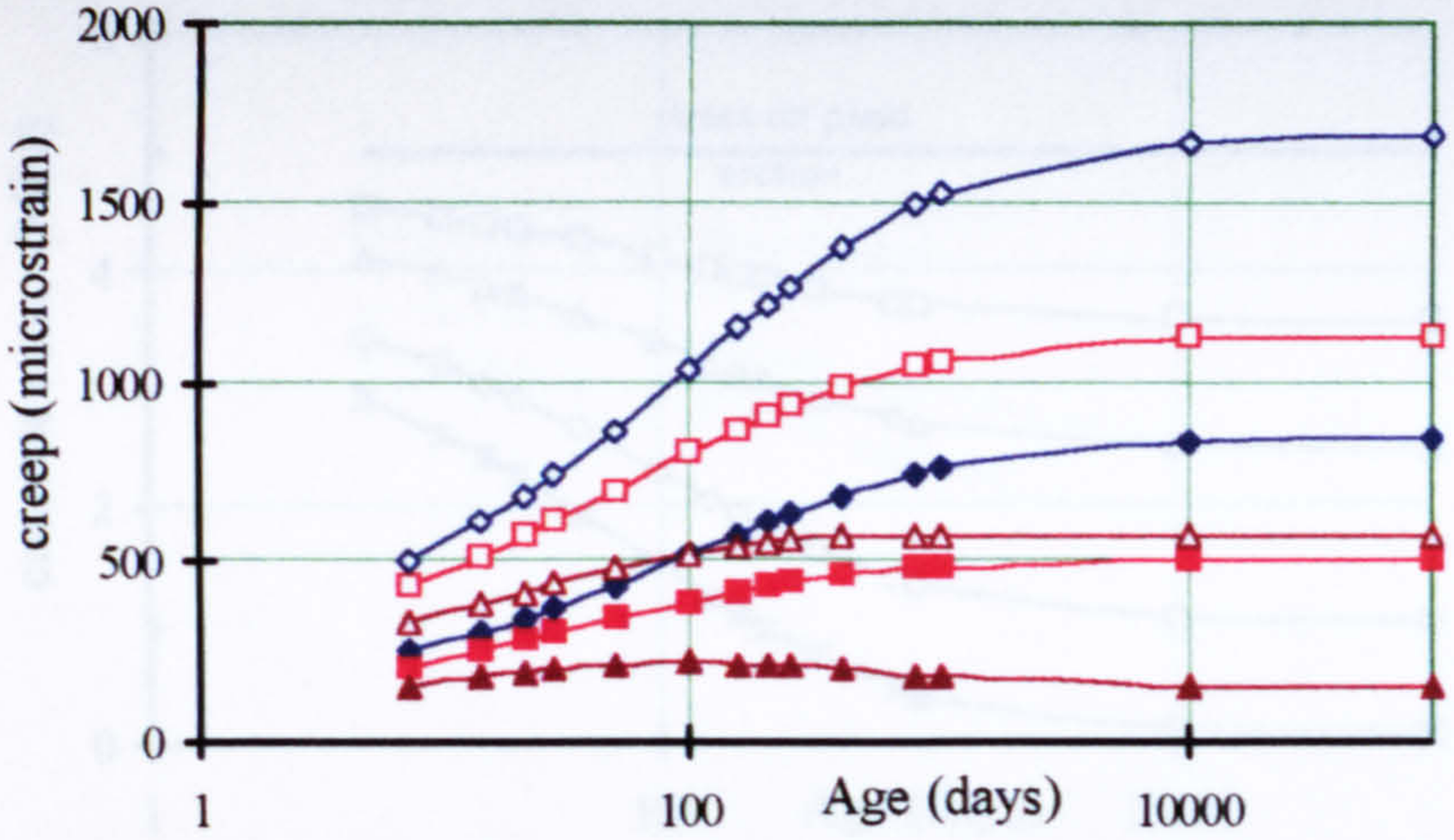

(a) Effect of stress on creep

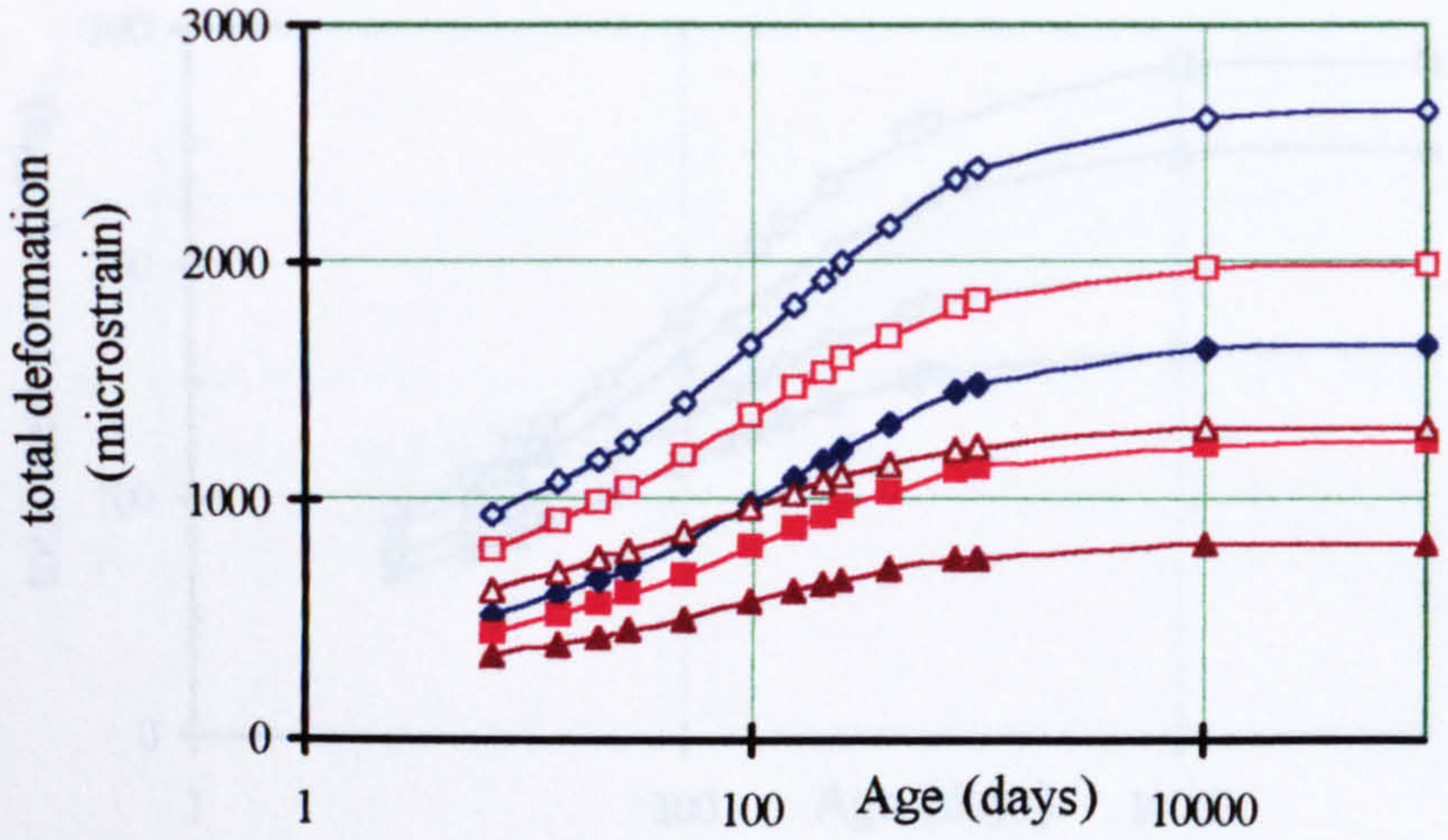

(b) Effect of stress on total deformation

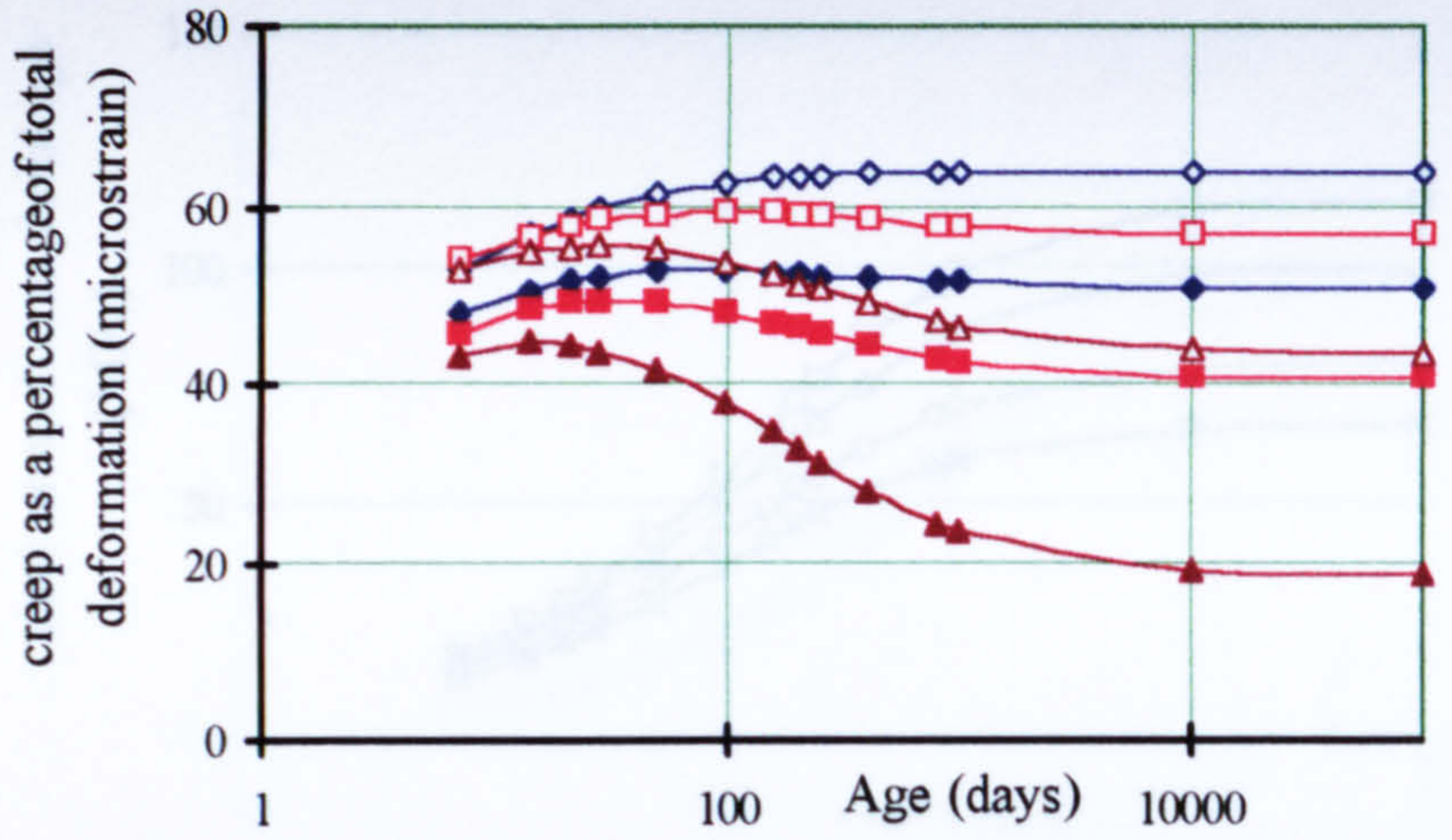

(c) Effect of stress on creep expressed as percentage to total deformation

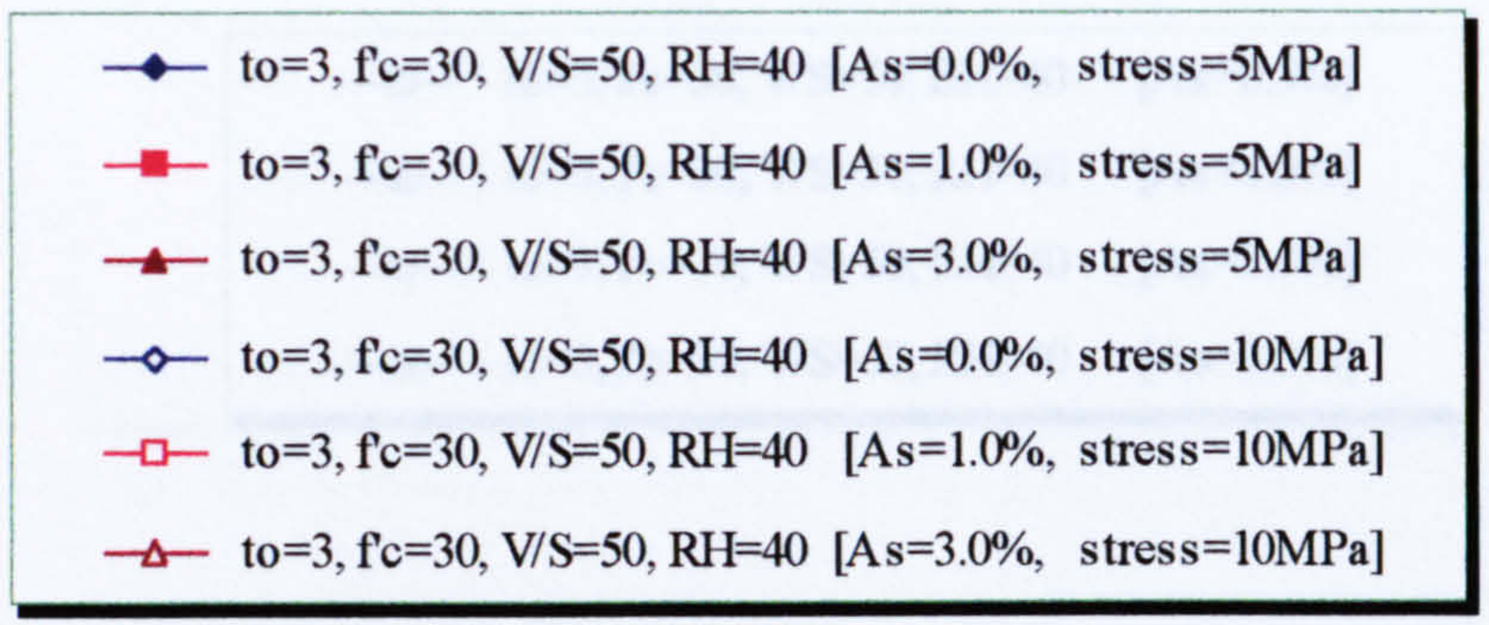

Figure 5.16: Effect of stress on creep characteristics of plain and reinforced concrete sections.

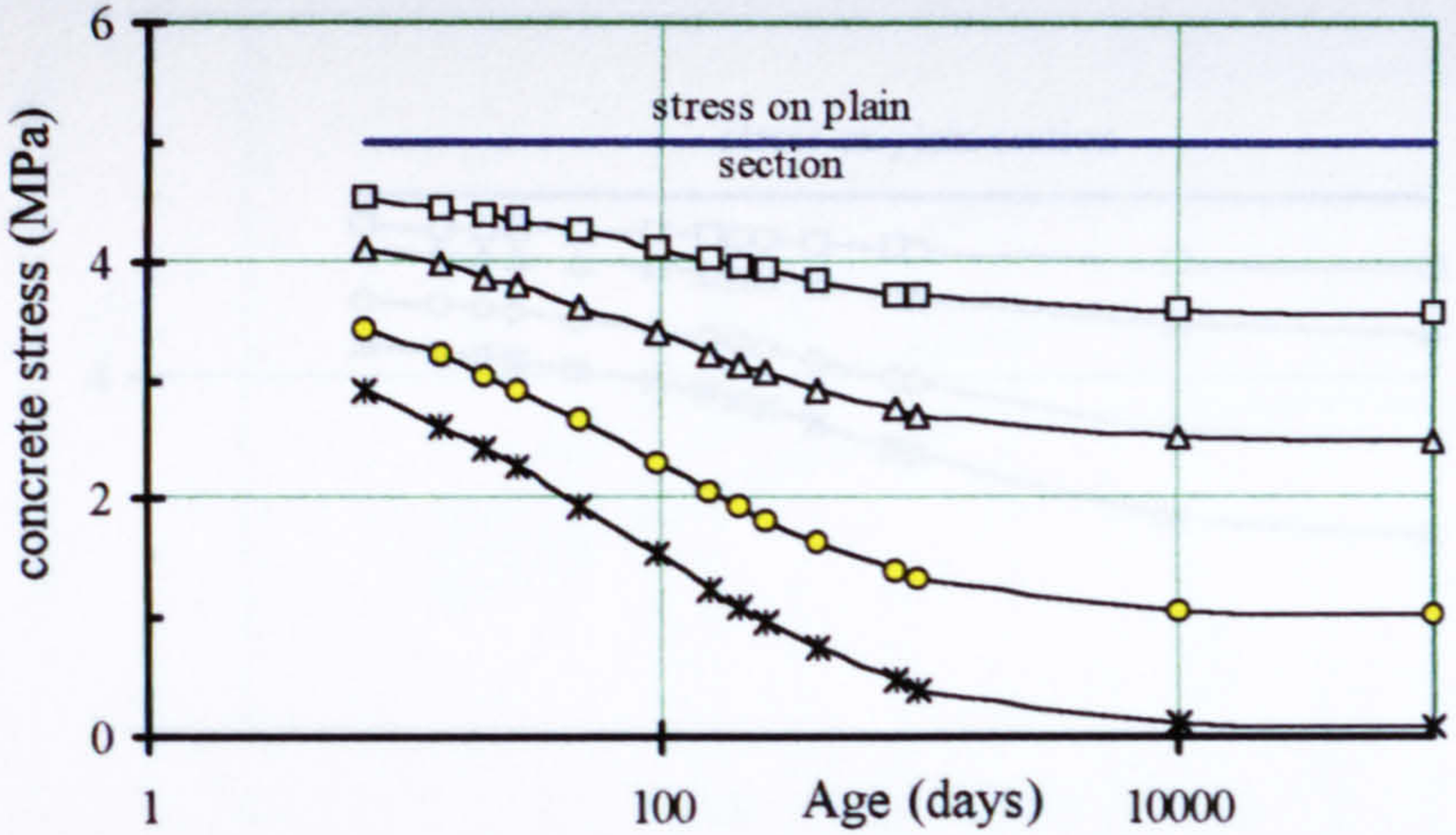

(a) Time-dependent stress in concrete for reinforced sections

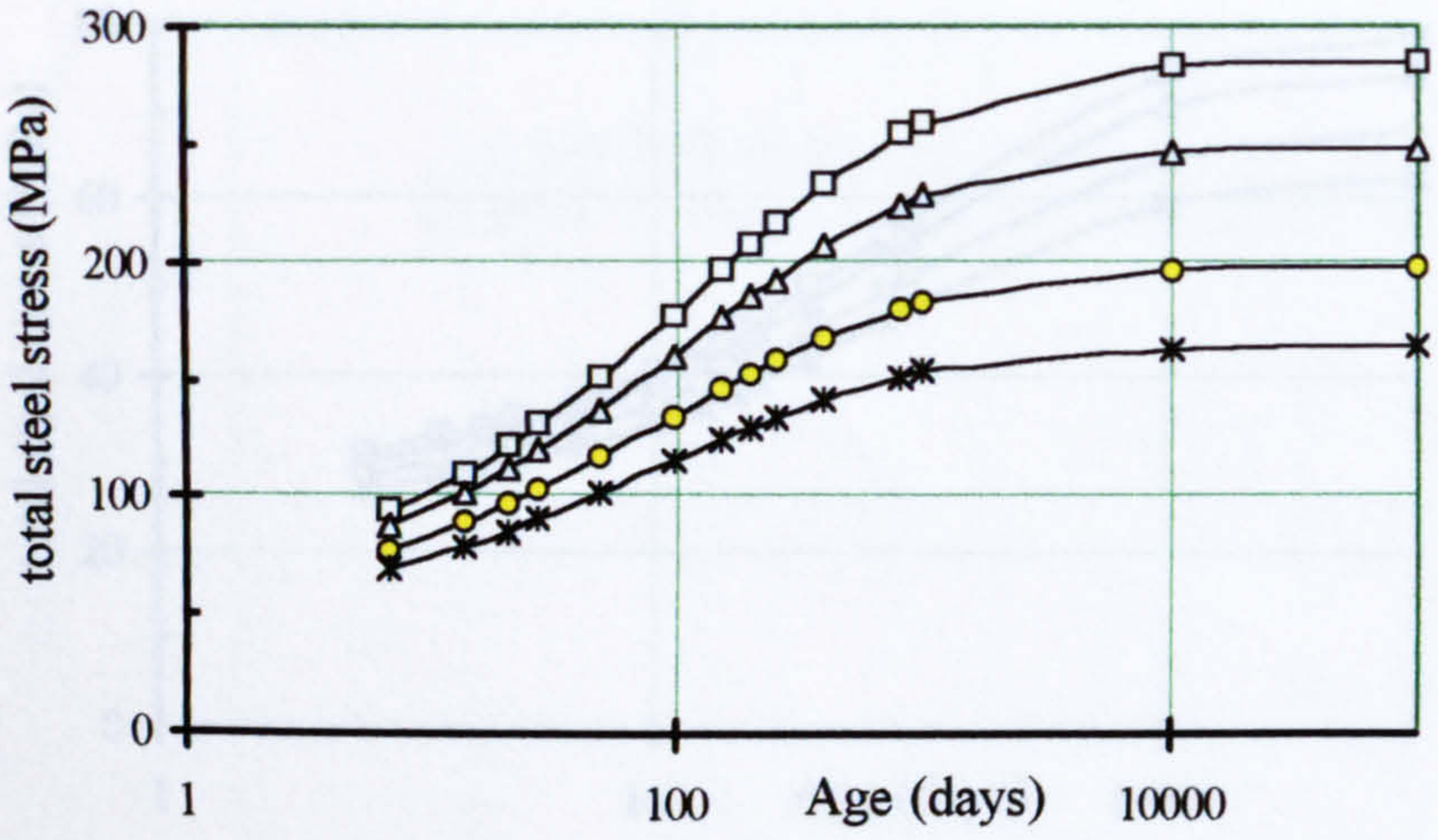

(b) Time-dependent stress in steel for reinforced sections

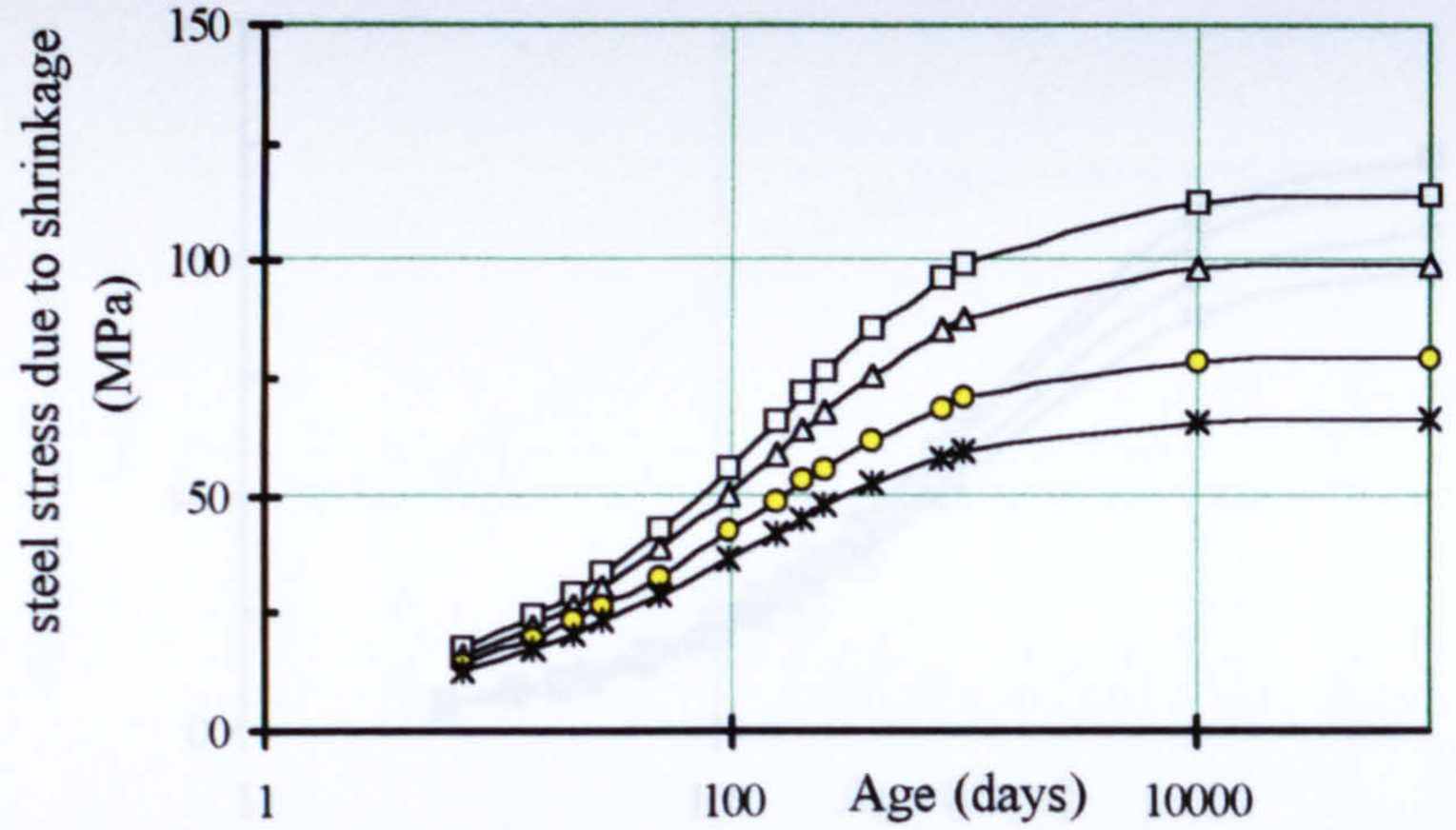

(c) Time-dependent stress in steel due to shrinkage

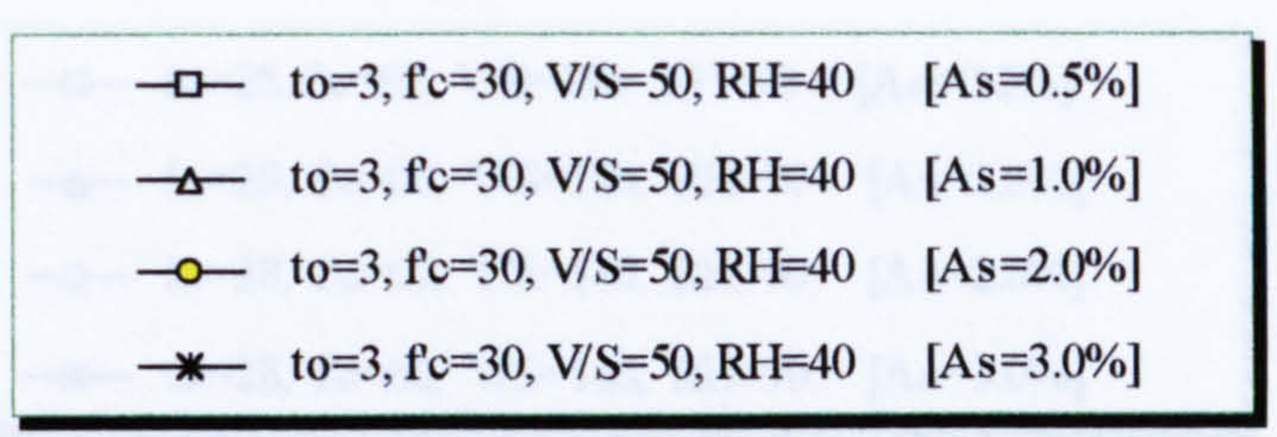

Figure 5.17: Time-dependent stresses in concrete and steel for reinforced sections under a combination of parameters yielding maximum deformation

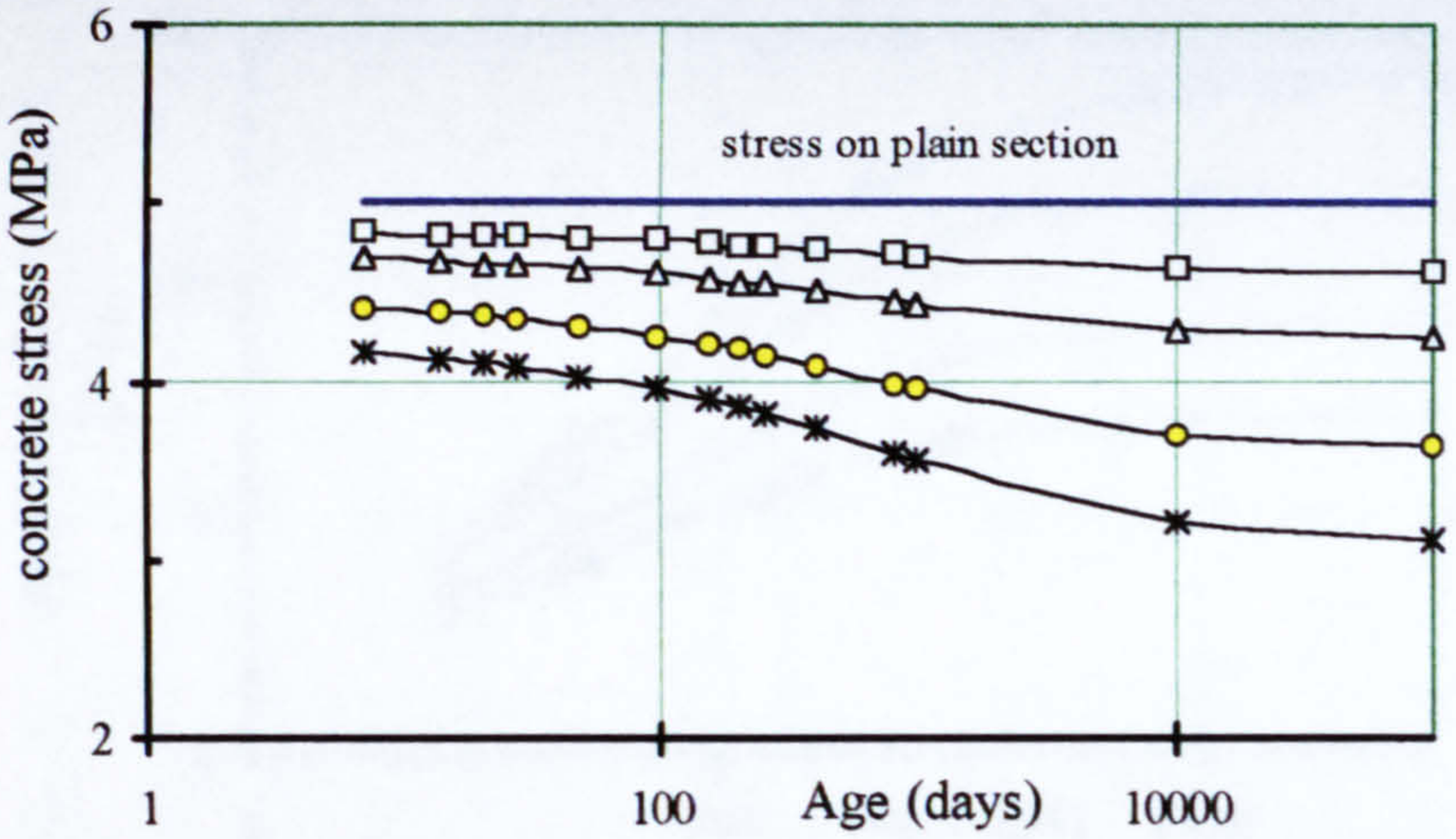

(a) Time-dependent stress in concrete for reinforced sections

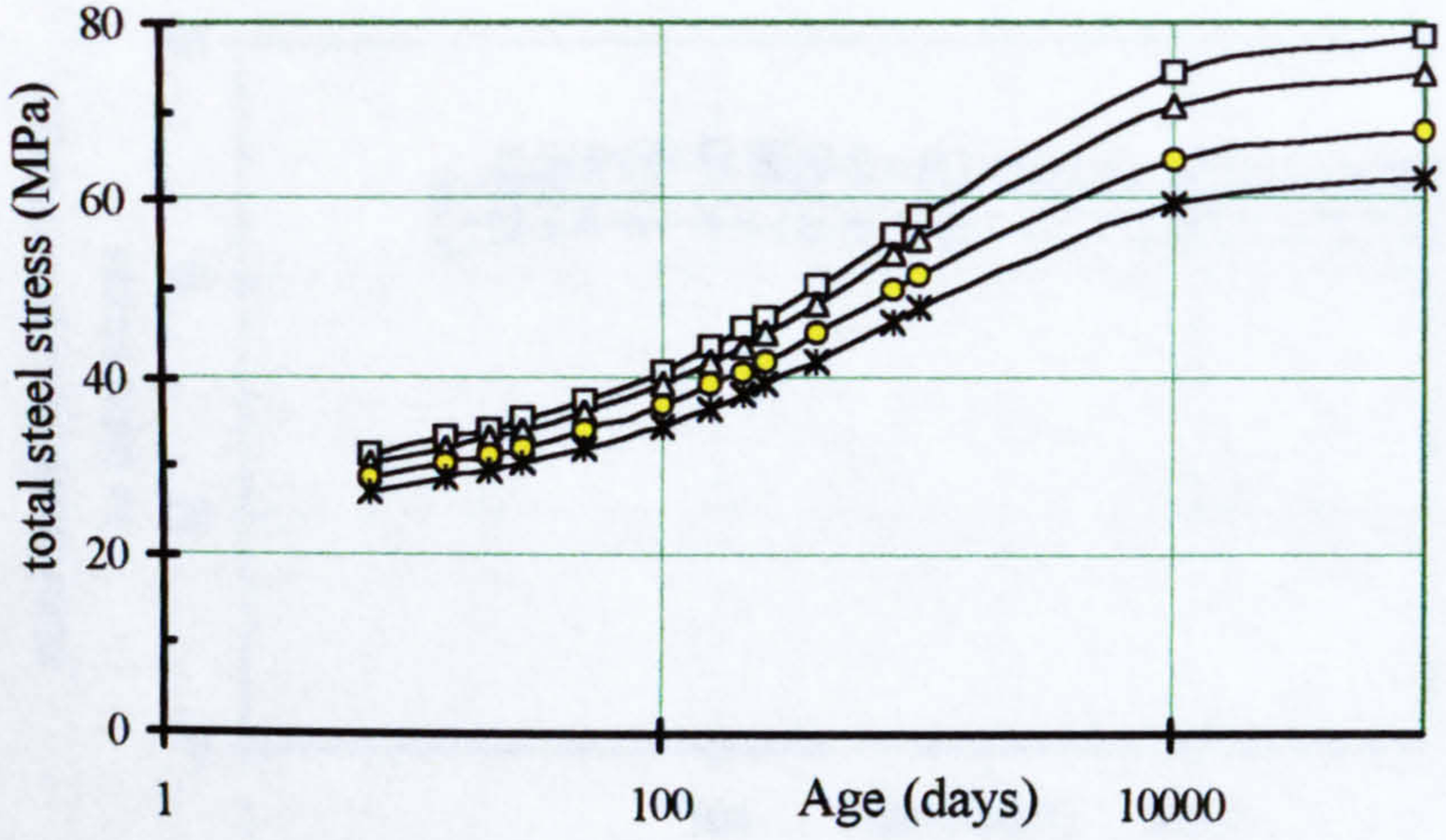

(b) Time-dependent stress in steel for reinforced sections

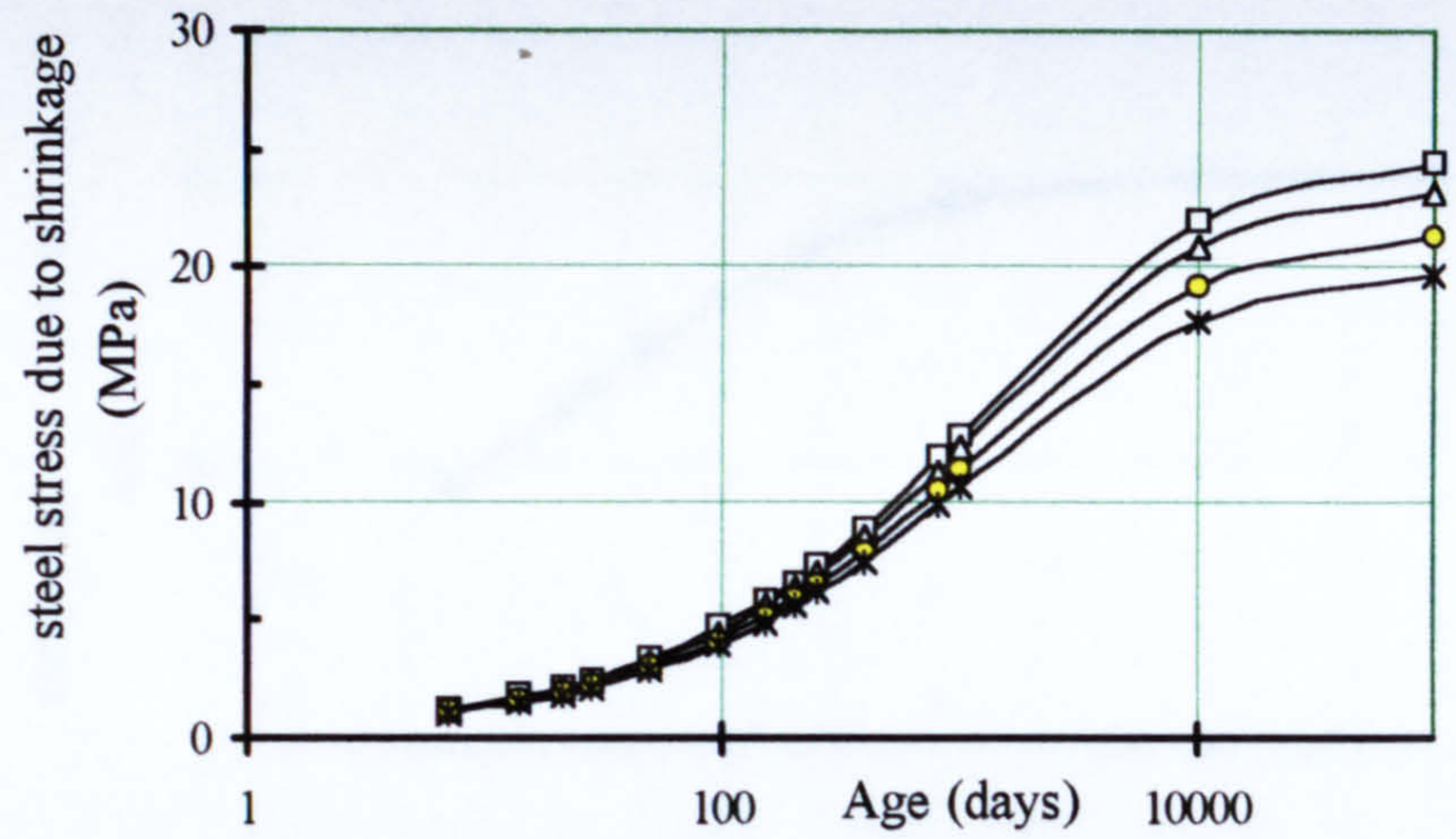

(c) Time-dependent stress in steel due to shrinkage

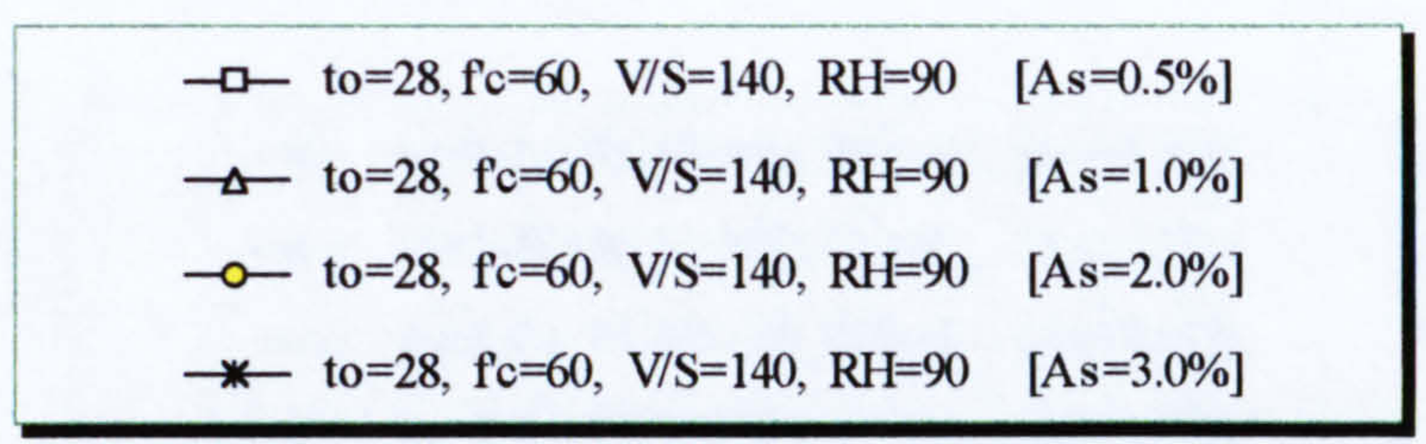

Figure 5.18: Time-dependent stresses in concrete and steel for reinforced sections under a combination of parameters yielding minimum deformation

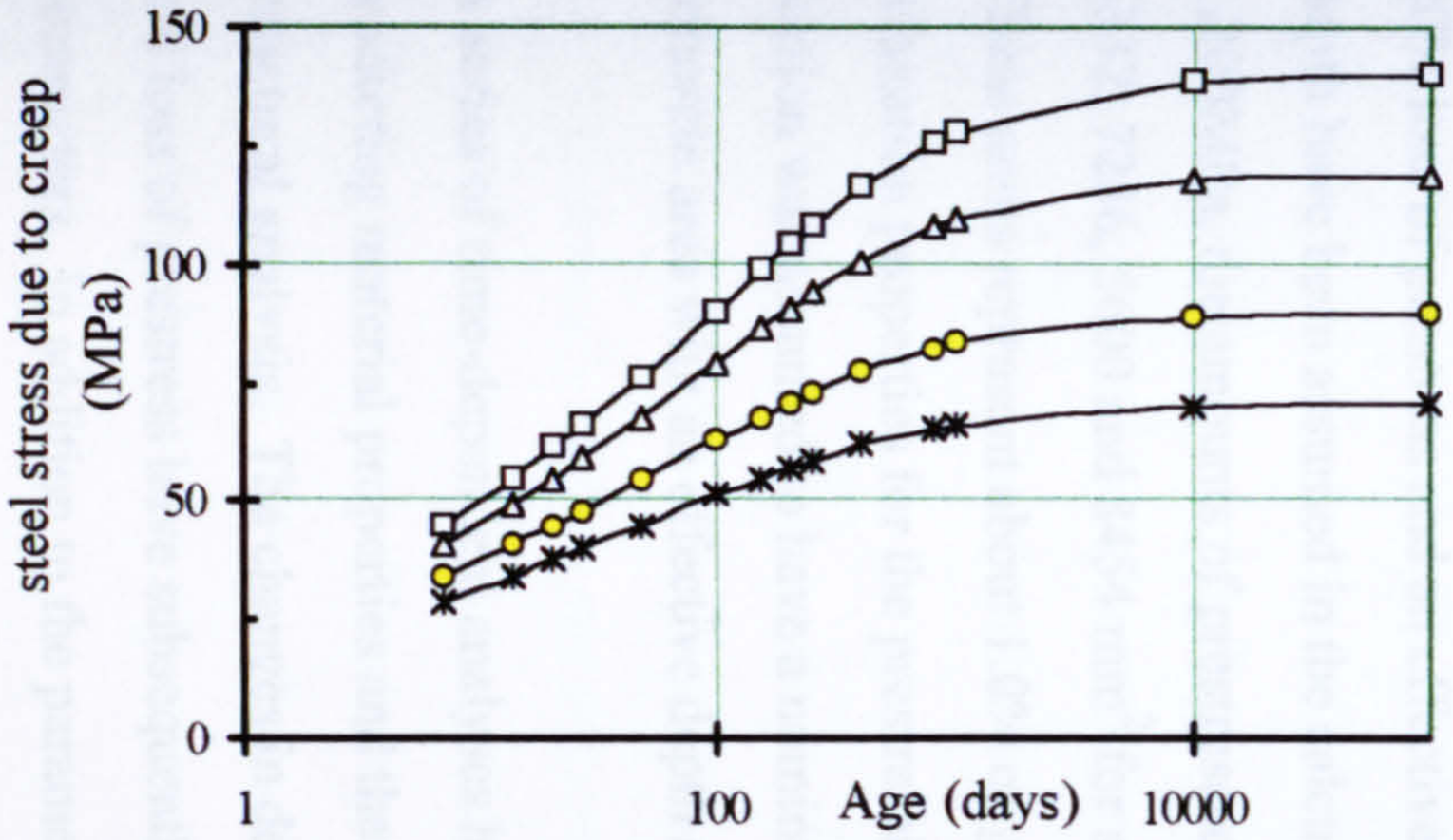

(a) Time-dependent stress in steel reinforcement due to creep

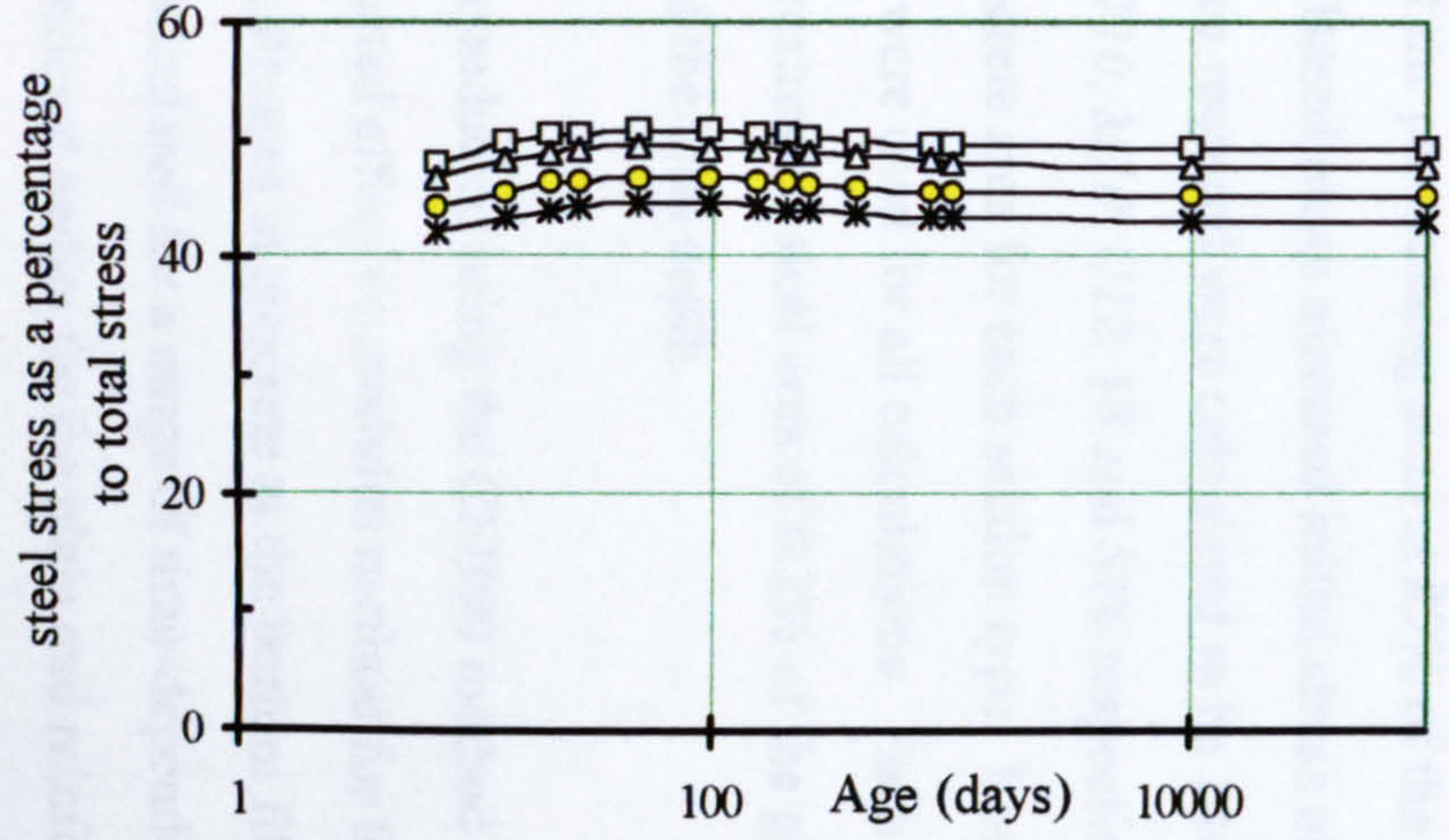

(b) Stress in steel due to creep expressed as a percentage of total stress

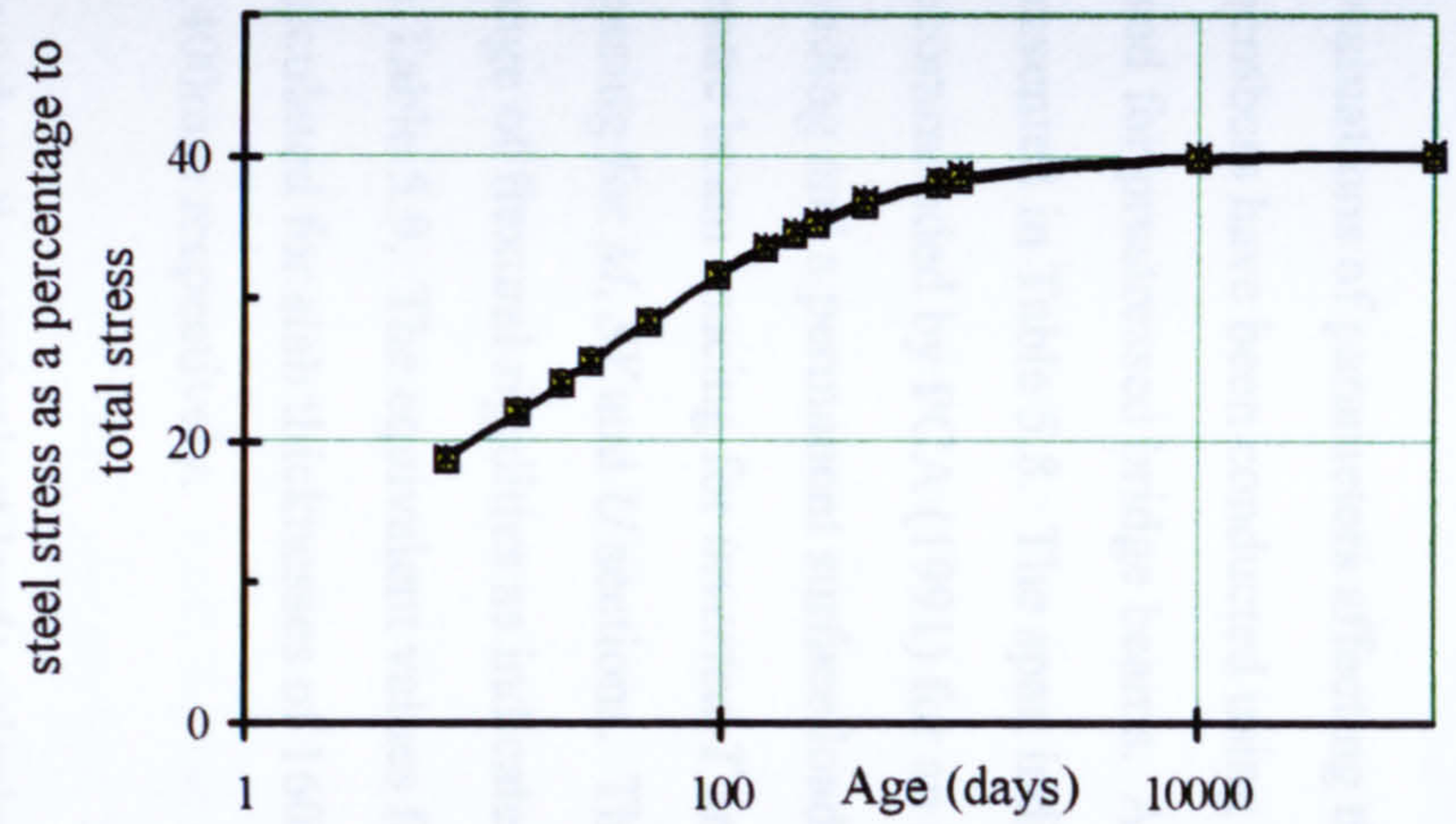

(c) Stress in steel due to shrinkage expressed as a percentage of total stress

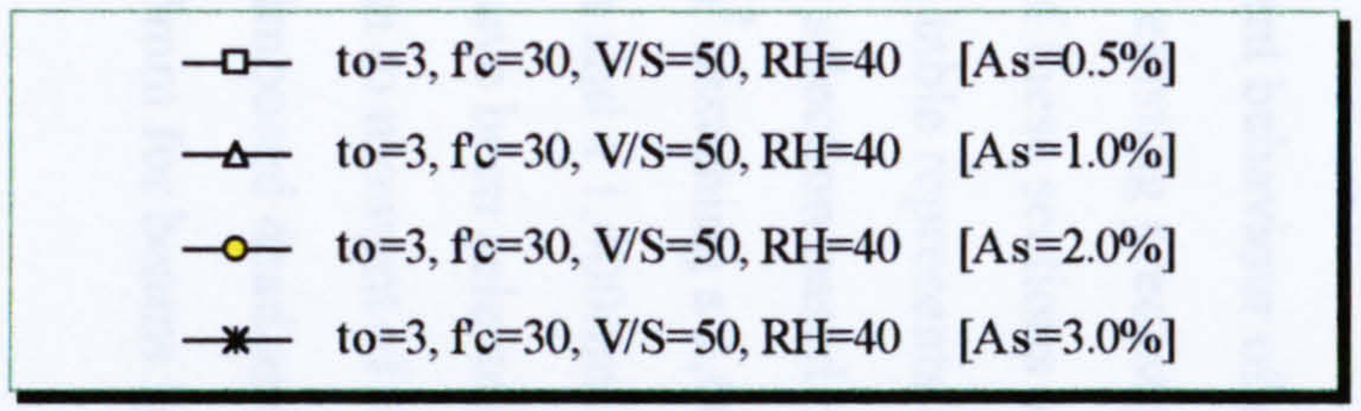

Figure 5.19: The effect of creep and shrinkage on time-dependent stress in steel reinforcement under the combination of parameters yielding maximum deformation

5.4 Time-dependent Behaviour of Simple Flexural Members

Evaluations of parameters affecting time-dependent behaviour of simple flexural members have been conducted using some of the existing precast prestressed sections used for prestressed bridge beams. A summary of these sections and their properties is presented in Table 5.8. The span indicated in the table represents the maximum length recommended by PCA (1991) for an initial beam selection based on 45 units HB loading and a permanent surface load of 2.4kN/m^2 assuming a 1,000mm centre-to-centre beam spacing for *inverted-T* and *Y* sections and a 1,400mm centre-to-centre spacing for *M*, *SY* and *U* sections. The sections have been selected to represent a wide range of flexural rigidities as indicated by the span to moment of inertia ratios calculated in Table 5.9. The equivalent values for the superimposed dead and live loads have been calculated for slab thicknesses of 160mm and 195mm for beams spaced at 1,000mm and 1,400mm respectively.

Based on the equivalent loads calculated and shown in Table 5.8, a combination of prestressing force and steel areas have been calculated for each section, Table 5.9. The combinations have been calculated based on the assumption of zero tensile stress at service (a total of selfweight, superimposed dead load and superimposed live load). A 20% loss of prestress and an effective depth of the prestressing steel at 85% of the total depth have been assumed in the calculations. Based on an assumed initial stress of 1,200MPa, the amounts of prestressed steel area required were calculated to be 1845, 5332, 7236, 5600 and 8454 mm^2 for sections *T10*, *M10*, *U12*, *Y8* and *SY6* respectively. These areas represent about 1.0% of gross concrete area for each section type. Low relaxation properties for the prestressing steel were used for all calculations. Each section was assumed to have a nominal non-prestressed steel area of 0.2% of the gross concrete area with an effective depth at 90% of the total depth.

A series of time-dependent analyses has been conducted using the CEB90 method for predicting material properties and the age-adjusted effective modulus method for the structural analysis. The changes in deflection, stresses in concrete at the bottom fibres and loss of prestress have subsequently been calculated for a range of time-dependent parameters. In addition to the parameters considered earlier for the plain and reinforced

sections subjected to axial stress, the following parameters have been considered in order to evaluate their effects on the time-dependent behaviour of simple flexural members:

(a) flexural rigidity;
(b) the ratio between prestressing and load; and
(c) the age of precast beams at first loading.

Although the span to depth ratio is frequently used in design to ensure adequate performance against the serviceability limit for deflection, flexural rigidity was found to be a more suitable parameter for this parametric evaluation. Table 5.9 shows that, for the whole range of available sections, the values of span to depth ratio remain between 20 to 25. On the other hand, the flexural rigidity range from 1.4 ($x10^{-7}mm^{-3}$) for section *SY6* to 72.3 ($x10^{-7}mm^{-3}$) for section *T1*. Lower values indicate lower degrees of flexural rigidity, thus reflecting larger deflections under equivalent loads. Figures 5.20 indicate that there is a clear relationship between beam deflection and flexural stiffness, whereas no meaningful relationship can be seen between deflection and span to depth ratios.

The ratio between the hogging bending moment due to the prestressing and the sagging moment due to other loads needs to be considered because it indicates whether the beam is undergoing downward deflection or camber under a given ratio. Due to the fact that the initial prestressing force changes due to the actions of creep and shrinkage, the ratio is also expected to change with time.

The age of precast beams at first loading needs to be considered because it affects the time-dependent behaviour of prestressed beams significantly. An unloaded prestressed beam is generally high in precompression at the bottom fibres, thus resulting in increasing creep. This will inevitably yield bigger negative curvature apparent in the form of a large camber. The time at which insitu slabs are cast and permanent surface load is applied will have an effect on the scale of this camber because these additional loads reduce the initial precompression (thus reducing creep) at the bottom fibres.

The first series of analyses have been conducted on the maximum recommended span which represent the minimum flexural rigidity value for each section in order to evaluate the overall time-dependent behaviour. Each beam has been analysed under four different combinations of parameters representing two different values of concrete strength (f'_c) and the average relative humidity (RH). The beams were prestressed at 3 days and left unloaded. Time dependent deflections for each beam under all four combinations of parameters are shown in Figures 5.21-23 and a summary of the analyses for loss of prestress, camber and stress at the bottom fibres is presented in Table 5.10.

5.4.1 Overall time-dependent behaviour flexural members

For sections subjected to an axial stress, the combination of parameters that results in the maximum axial deformation was similar to that yielding maximum creep and shrinkage values as expected. It was shown that the combination of parameters with the minimum values of t_o, f'_c, RH and V/S yielded maximum axial deformation, regardless of the stress level applied to the section. In the case of simple prestressed members subjected to flexural loading, the same observation cannot be expected. In a simply supported prestressed beam, prestressing and creep actions result in a continuing camber, whereas the beam selfweight and its creep, loss of prestress and shrinkage actions result in a continuing downwards deflection. The shrinkage action is not expected to yield any deflection if the beam is symmetrically reinforced at the top and bottom regions of the section. However, this is not generally the case for prestressed beams where bonded reinforcement is generally concentrated at the bottom of the section, hence resulting in continuing deflection due to shrinkage.

The interactions between the effects causing upwards and downwards deflection are continuously changing throughout the service life of the beams. Depending on the combination of conditions such as the ratio between the bending due to prestressing and other loads as well as the creep and shrinkage actions, the deflection of the beam may change its direction. Figures 5.21- 5.23 show that although the level of prestressing are similar for all five of the selected beams, the members subjected to Combination 1 conditions change the direction of deflection. Sections *M10*, *SY6*, *Y8* and *U12* can be

seen to experience a reduction in camber with time, while section *T10* continues to increase or maintain its camber to the final value. The reduction in the ratio of bending moment due to the effective prestressing force and the beam selfweight indicates that it is possible for a simple unloaded prestressed beam to change from negative to positive curvature and for it to undergo downwards deflection instead of continuing in camber. Lower level of prestress at transfer will result in more chances of this phenomena occurring. The level of prestress at transfer, therefore, has to properly account for the effect of creep and shrinkage so that the beam can remain in camber, as is normally required, before superimposed dead and live loads are applied.

From Figures 5.21 and 5.22, it can be seen that all sections display the biggest camber at any time under combination of parameters with minimum values of f'_c and *RH* (Combination 1), except for sections *SY6* and *Y8* where the maximum long term cambers were slightly greater under Combination 3. All other sections display a maximum long term camber under Combination 1. A comparison of the time-dependent loss of prestress and the stress at the bottom fibres for all conditions indicates that Combination 1 resulted in the largest values. Therefore, despite the observation of camber for sections *SY6* and *Y8*, it can still be concluded that, for beams subjected to the given level of prestress, the combination of parameters with the minimum values of f'_c and *RH* yielded maximum deformation. Figures 5.21-22 also indicate that the combination of parameters with the maximum values of f'_c and *RH* (Combination 4) yielded minimum deformation at any time after transfer. Any other combination of f'_c and *RH* is expected to yield results within these two extreme cases.

5.4.2 Effect of concrete strength

To evaluate the effect of concrete strength on the time-dependent behaviour of flexural members, comparisons were made between Combinations 1 & 2 and 3 & 4 (Table 5.10).

Calculations for the loss of prestress due to elastic shortening show that the sections with a concrete strength of 30MPa display about 23% greater losses than those of 60MPa. An almost similar percentage was also calculated for the initial camber. Comparison of the long term values shows that, for beams exposed at 40% *RH*, sections

with a concrete strength of 30MPa display about 40% greater prestress loss than those of 60MPa. The equivalent loss for beams exposed at 90% *RH* was calculated to be 46%. This is in accordance with larger creep and shrinkage values for sections with lower characteristic strength of concrete, as discussed in Sections 5.2 and 5.3.

A comparison of the resulting cambers shows that, for beams exposed at 40% *RH*, sections *T10*, *M10*, *U12*, *Y8* and *SY6* with a concrete strength of 30MPa displayed about 31, 21, 14, 14, and 12% greater camber respectively than those of 60MPa. Equivalent percentages were calculated to be 38, 35, 33, 31, and 30% for sections exposed to 90%*RH*.

This indicates that the long term camber may be overestimated by about 38% if the concrete strength is assumed to be 60MPa, whereas the actual value is only 30MPa. Similarly, the loss of prestress could be underestimated by about 46% if the same assumption applies.

5.4.3 Effect of the average relative humidity

To evaluate the effect of RH on the time-dependent behaviour of flexural members, comparisons were made between Combinations 1 & 3 and 2 & 4 (Table 5.10).

Unlike concrete strength, the average relative humidity will only affect the time-dependent behaviour of prestressed beams. In axially loaded plain concrete, it was shown that for any concrete strength, concretes at 40% *RH* displayed about 3.5 times greater shrinkage than those at 90% *RH*. Long term deformation due to creep for concrete exposed at 40% *RH* displayed between 74 to 90% greater deformation (depending on the *V/S* ratios), than those at 90% *RH*.

Comparisons of long term cambers of flexural members for the same values of *RH*, however, did not arrive at similar orders of magnitude. Calculations show that the final camber for sections with a concrete strength of 30MPa and exposed to 40% *RH* were 22, 8, 1, 0, and -2% greater than those at 90% *RH* for sections *T10*, *M10*, *U12*, *Y8* and *SY6*

respectively. Equivalent percentages were calculated to be 29, 21, 18, 15, and 14% for sections with a concrete strength of 60MPa.

Calculations for the time-dependent loss of prestress show that, for sections with a concrete strength of 30MPa, the beams exposed to 40% *RH* displayed prestress losses between 60-66% greater than those at 90% *RH*. For sections with a concrete strength of 60MPa, the percentages were calculated to be between 67-74%.

Evaluation of the overall behaviour, the effect of concrete strength and average relative humidity indicate that Combinations 1 and 4 provide the upper and lower boundaries for the extent of deformation experienced by each section investigated. Members subjected to any other combination of parameters within this range are expected to behave within these boundaries. A comparison of cambers also suggests that sections *T10* and *SY6* provide an upper and lower limit in the change of the flexural behaviour due to the time-dependent effects. For the given level of initial prestressing, other sections whose flexural rigidity fall within those of these two sections are expected to display a change in behaviour between these extreme conditions.

5.4.4 Effect of non-prestressed steel

In a prestressed beam containing zero non-prestressed steel, any loss of force in the prestressed steel is equivalent to the reduction of force on the concrete section. However, when the presence of non-prestressed steel needs to be considered, as in the case of prestressed bridge beams, this reduction of force is equal to the loss of prestress force plus the force transferred to the non-tensioned steel. The compressive force transferred to the additional bonded non-prestressed steel results in the reduction of stress in the concrete. This net effective stress remaining in the concrete is of primary importance because it reduces the rate of creep increase at the bottom fibres as well as affecting the behaviour under service loads i.e. the deflection and the extent of cracking.

The presence of non-prestressed steel at the bottom of the section reduces compressive force the in concrete (due to the prestressing force), thus reducing creep and camber. Its presence at the top of the concrete section, likewise, reduces the compressive force (due

to selfweight and external loads), thus reducing creep and downwards deflection. It has been recognised, therefore, that non-prestressed steel can be used to control downward deflection as well as camber, depending on its location in the section.

Earlier evaluation for the reinforced sections subjected to an axial stress showed that the sections reinforced with up to 2.0% of steel are not significantly affected by elastic deformation. It was found, however, that sections reinforced by 0.5% or more steel could be significantly affected by creep and shrinkage. The extent of the effect is expected to be different on flexural members. This was, therefore, subsequently evaluated using the same PCA beams used in the previous evaluation. Sections *SY6* and *T10* were selected for this purpose because they represented the maximum and minimum flexibility respectively. A series of analyses has been conducted where each section contained 0.0, 0.5, 1.0, and 2.0% of the non-prestressed steel at either the top or bottom of the sections. The non-prestressed steel at the top of the sections was assumed to be located at 10% of the total depth of the sections. Each section was subjected to Combinations 1 and 4 to ascertain the maximum and minimum effects respectively.

Figures 5.24-25 show the effect of bottom and top non-prestressed steel on time-dependent camber at the mid-span for beams *T10* and *SY6* subjected to Combination 1, and Tables 5.11 and 5.12 show a summary of the analysis where the initial and final values are presented for all degrees of reinforcement. When the effect of the bottom steel was calculated, no top steel was provided. Similarly, the analysis for the effect of the top steel assumed zero non-prestressed steel at the bottom of the section.

Calculations indicated that both elastic and time-dependent loss of prestress decreased with increases in the amount of non-prestressed steel. The presence of the bottom non-prestressed steel does not reduce the elastic loss significantly, but it has a greater effect on the time-dependent value. Table 5.11 shows a small reduction in the elastic loss of prestress where, for section *T10*, the loss reduced from 12.3% for the section without non-prestressed steel to 10.4% for the section with 2.0% steel. Equivalent percentages for section *SY6* were calculated to be 11.6 and 9.9%. Time-dependent loss reduces from 46.7% for the *T10* section without the non-prestressed steel to 23.8% for sections when

2.0% of steel is included. Similar calculation for the section *SY6* yielded the reduction in the time-dependent loss from 39.2% to 21.7%. This reduction is due the transfer of some of the compressive force from concrete to the non-prestressed steel. This can be seen from the decrease in the concrete compressive stress at the bottom fibres as the amount of bottom steel increase (Table 5.11).

Figures 5.24 show that the presence of bottom steel significantly affects the time-dependent camber of both sections. Section *SY6* can be seen to be more significantly affected since the presence of the non-prestressed steel at the bottom of the section reduced the final (10,000 days) camber from 196mm (zero bottom non-prestressed steel) to 130, 84 and 29mm for sections reinforced with 0.5, 1.0 and 2.0% of steel respectively. These represent about 66, 43, and 15% of the final camber for the section without non-prestressed steel. The reduction in the final camber for the T10 section was reduced from 161mm (zero non-prestressed steel) to 124, 98 and 68mm for sections reinforced with 0.5, 1.0 and 2.0% of steel. These final three values represent about 77, 61, and 42% of the final camber for the section without reinforcement.

It should be noted that, under similar conditions, section *T10* will always display greater creep and shrinkage values compared to section *SY6* due to a smaller volume to surface ratio. However, this was not necessarily the case for the time-dependent camber where, for an equivalent content of non-prestressed steel, the section *SY6* developed greater change in the camber. This seems to suggest that an equivalent level of reinforcement affects slender members more significantly. It is also possible that members with a lower ratios of bending due to prestress and beam selfweight (shown as Mps/Msw in Table 5.11) display greater change in the time-dependent deformation. The initial values of these ratios are 3.553 and 1.69 for section *T10* and *SY6* respectively. The corresponding final values were calculated to be 1.455 and 0.831 for sections without non-prestressed steel. These effects i.e. the flexural rigidity (slenderness) and the Mps/Msw ratios, are subsequently discussed in the forthcoming sections.

It can also be seen that *T10* sections containing more than 1.0% non-prestressed steel display a reduction in camber with time, Figure 5.24(b). Hence, all sections containing

more than 1.0% non-prestressed steel and whose flexural rigidities or Mps/Msw ratios are less than that of section *T10* may also be expected to undergo a reduction in camber over time due to the effect of prestress and the selfweight of the beam.

The presence of the bottom non-prestressed reinforcement is shown to reduce the compressive stress in the concrete for both sections, Table 5.11. For section *T10*, the table shows that the final compressive stress reduces from 9.07MPa for the section without non-prestressed steel to 5.24, 2.64 and -0.58MPa for sections reinforced with 0.5, 1.0 and 2.0% steel respectively. For section *SY6*, the final stress at the bottom fibres reduces from 7.53MPa for the section with zero non-prestressed steel to -0.81MPa for the section reinforced with 2.0% steel. The stresses for the most highly reinforced sections are obviously very small and may result in cracking at service where tensile stress at the bottom fibres may well exceed the limit once other external loads are applied.

The presence of the top reinforcement, as has been noted earlier, will reduce the downwards deflection. Figures 5.25 show the effect of non-prestressed steel at the top of the section under Combination 1 (yielding maximum deformation) and subjected to only prestressing and beam selfweight. In the absence of external loading, its presence has the effect of increasing camber. This is similar to the effect of the bottom steel where the rate of creep is altered, albeit in the opposite direction. The corresponding effect on time-dependent camber, however, is shown to be less significant compared to that arising from the presence of bottom steel.

A comparison of Figures 5.25 shows that the effect of top reinforcement is only significant for the slender section (*SY6*). The final camber was about 160mm for all levels of reinforcement for section *T10*, whereas the values for section *SY6* were calculated to be 196, 241, 262 and 279mm for sections reinforced with 0.0, 0.5, 1.0 and 2.0% steel respectively, Table 5.12. The final cambers for section *SY6* indicate that, for the most flexible members subjected to the combination of parameters yielding maximum deformation, the presence of top reinforcement may increase long term

camber by about 23, 34 and 42% for sections reinforced with 0.5, 1.0 and 2.0% steel respectively.

Comparisons of the time-dependent loss of prestress and stress at the bottom fibres show that the top reinforcement does not have a very significant effect. The long term loss of prestress remained between 44-47% and 37-39% for sections *T10* and *SY6*, respectively. The value of the compressive stress at the bottom fibre remained virtually unchanged for section *T10*, but there was a slight increase for section *SY6* where the final stress was calculated to be 7.53MPa for section without top steel compared to 8.66MPa for section containing 2.0% top steel.

The concrete stress at the top fibre reduced, as expected, due to the presence of the top reinforcement. The reduction, however, was found to be small and the stresses were calculated to be still less than the tensile strength of concrete. The stress at the top fibre for section *T10* reduced from 1.28MPa for the section without top reinforcement to -2.97MPa for the section reinforced with 2.0% steel. Equivalent stresses for section *SY6* were calculated to be 7.29 and -1.89MPa. In an actual structure, the beam may not experience these tensile stresses because other loads would have been applied (causing compressive stress at the top fibre) before the tensile stress could develop to the maximum values indicated here.

The presence of the top reinforcement, can be seen to be very beneficial especially for slender members or members with low Mps/Msw ratios. The reduction in camber of the unloaded prestressed beams experienced by some of the sections without top reinforcement can worsen the overall downward deflection once other loads are applied. Top reinforcement has been shown to reduce possible excessive deflections.

Figures 5.26 compare the effects of top and bottom steel for sections *T10* and *SY6* under Combination 4 yielding minimum deformation. A summary of the analyses under this combination for sections reinforced with 0.0 and 2.0% of either top or bottom non-prestressed steel is presented in Table 5.13. Figure 5.26(a) shows that the time-dependent cambers are significantly affected by the presence of the bottom non-

prestressed steel. The final cambers for section *T10* reduced from 88mm for the section containing zero bottom non-prestressed steel to 62mm for the section reinforced with 2.0% steel. Equivalent values for sections *SY6* were calculated to be 137mm and 87mm. However, it can be seen that, under Combination 4, all sections reinforced with up to 2.0% of the bottom non-prestressed steel are not expected to experience a reduction in camber, as those under Combination 1 (Figure 5.26(a)). A similar evaluation of the presence of top non-prestressed steel indicates that any percentage of top reinforcement does not affect time-dependent cambers significantly, Figure 5.26(b).

Table 5.13 shows a significant reduction in the time-dependent loss of prestress and compressive stress at the bottom fibres for sections containing bottom reinforcement. The loss of prestress reduced from 18.4 to 12.4% for section *T10* and 16.3 to 11.4% for section *SY6*. The compressive stress reduced from 17.3MPa to 10.25MPa for section *T10* and from 15.07 to 8.99MPa for section *SY6*.

The loss of prestress and compressive stress at the bottom fibres are not significantly affected by the presence of top reinforcement.

5.4.5 Effect of initial stress level

In the previous series of analyses, the maximum possible prestress has been employed to comply with the zero tensile stress condition at the middle of the simply supported span for full service loading. In the case where precast beams are made continuous, the levels of prestressing required for the beams are less because part of the dead load and the whole live load are applied to the more efficient continuous beam. The lower level of initial prestress is expected to affect the time-dependent behaviour of the prestressed beam.

To ascertain the extent of this effect, another series of analyses has been conducted where the required areas of prestressing steel have been calculated assuming zero tensile stress (at the bottom fibres) for members subjected to selfweight and superimposed dead load only. The required amounts of prestressed steel area were calculated to be 880, 3084, 5399, 3601, and 4653mm^2 for sections *T10*, *M10*, *SY6*, *Y8* and *U12* respectively.

These steel areas represent 0.51, 0.67, 0.75, 0.62 and 0.64% of the corresponding gross concrete areas. The initial forces associated with these areas were calculated to be about 48, 58, 64, 64 and 77% of those from the previous analyses for sections *T10*, *M10*, *SY6*, *Y8* and *U12* respectively.

Every section has been analysed under the four combinations of parameters, as in the previous analyses. Time-dependent camber and deflection for all beams are shown in Figures 5.27 and 5.28. Table 5.14 presents a summary of the analyses for sections *T10* and *SY6* subjected to Combinations 1 and 4. Comparisons between the results of the analyses for the higher and the reduced levels of initial prestress are also given in this table as well as in Figure 5.29.

The initial compressive stresses at the bottom fibres of the beam subjected to only the prestressing force and beam selfweight were calculated to be 8.55, 8.53, 9.27, 7.45 and 8.19MPa for sections *T10*, *M10*, *SY6*, *Y8* and *U12* respectively. These stresses represent about 40, 46, 48, 47 and 49% of the initial stresses in the previous analyses.

Comparisons for the initial cambers, however, displayed smaller percentages. For example, the initial cambers for sections subjected to the reduced prestress were calculated to be 32 and 29% of those for the higher prestress for sections *T10* and *SY6* respectively, Table 5.14.

Comparisons for time-dependent camber, as in the previous evaluation, show that the beams had the largest change in the time-dependent behaviour under Combination 1, and smallest under Combination 4, Figures 5.27 and 5.28. For the reduced level of initial prestressing, all sections continue to display an increase in camber under Combination 4, but indicate a reduction in camber at some point in time under Combination 1. Under Combination 1, sections *M10*, *SY6*, *Y8* and *U12* are shown to experience substantial changes in the time-dependent behaviour. Section *SY6*, for example, was calculated to display a final downward deflection of 10mm after reaching a maximum camber of 36.6mm at about 30 days after prestressing. Figures 5.27 and 5.28, however, suggest that members under Combinations 2 and 3 do not display substantial changes in the behaviour as those under Combination 1.

Calculations for the long term stresses on the concrete suggest that their levels corresponded with the levels of reduction in the initial prestressing force. The final stresses at the bottom fibres were calculated to be 3.6, 3.2, 2.9, 2.3 and 2.5MPa for sections *T10*, *M10*, *SY6*, *Y8* and *U12* respectively, compared to the final stresses of 7.3, 6.5, 6.1, 5.5 and 5.4MPa (Combination 1) in the previous analyses.

This evaluation indicates that, while the lower level of initial prestressing may satisfy the zero stress requirement at service, the serviceability limit on deflection may not be satisfied. This is due to the fact that the stress on the concrete is section dependent, hence any change of actions in a section (such as the prestress level) will correspond to that particular section only. Maximum deflection is member dependent since a change in deformation at a particular section depends on the overall change of actions in other part of the member. Therefore, proper account of creep and shrinkage characteristics as well as the structural properties needs to be taken when a reduction in the initial prestressing is envisaged.

5.4.6 Effect of the age at loading

Whether the pre-camber of the precast units increases or decreases when the insitu slab is cast and continuity is established is an important indicator as to whether positive or negative restrained bending would be developed at the intermediate support. A simply supported prestressed beam which is increasing in camber when continuity is established results in a development of a positive (sagging) restrained bending moment at the intermediate support. Conversely, a beam with a decreasing camber or increasing downward deflection results in the development of negative (hogging) restrained bending moment.

Previous evaluations have shown that, depending on the combinations of material and structural properties as well as the level of initial prestressing, some of the unloaded prestressed flexural members did not display a behaviour of increasing camber with time as generally expected. For some members, the loss of prestressing force significantly contributes to this phenomenon. A high level of stress on the concrete at

the bottom fibre of unloaded members resulted in a high rate of creep which reduced the prestressing force to such an extent that its contribution to the negative bending moment was less than that of the positive bending moment due to beam selfweight. An application of additional loads before a large percentage of the prestressing force is lost due to creep is expected to change this behaviour. The concrete compressive stress at the fibre will be significantly reduced, hence reducing the rate of creep which subsequently causes a smaller loss of prestressing force.

A series of analyses have been conducted to ascertain the effect of the age of precast beams at the application of load on their time-dependent behaviour. Similar beams to those evaluated in Section 5.4.1 have been used, except additional dead loads representing the slab and surfacing loads have been applied to the precast beams when the beams were 30 and 100 days old. These represent the range of ages within which precast beams are normally erected and the insitu slabs are cast. Sample results of the analyses for sections *T10* and *SY6* are shown in Figures 5.30 and 5.31.

Figures 5.30 show that all unloaded members generally display a continuing increase in camber under Combinations 1 and 4. Section *T10* displays nearly constant values of camber after the load application under both combinations of parameters. Section *SY6*, however, displays near constant camber only for Combination 4, whereas, under Combination 1, the section shows a substantial reduction in camber for both ages at loading, Figure 5.30(a).

Before the load application, the cambers for section *SY6* at 30 and 100 days were calculated to be 154 and 171mm, respectively. These subsequently reduced to 119.5 and 138.0mm immediately after loading. The corresponding final (10,000 days) cambers were calculated to be 54.6 and 83.6mm. This indicates that members loaded at an earlier age displayed greater reduction in camber where the long term reduction in camber for the beam loaded at 30 days was calculated to be 64.9mm compared to 54.4mm for the beam loaded at 100 days.

A comparison of the compressive stress at the bottom fibre shows that an early application of additional load results in a smaller reduction in the final compressive stress, Figures 5.31. For sections *T10* (under Combination 1), the final concrete stresses at the bottom fibre were calculated to be 1.6 and -0.8MPa for members loaded at 30 and 100 days respectively. Equivalent stresses were calculated to be 1.6 and 0.4MPa for section *SY6*. Load application at ages greater than 100 days may clearly result in tensile strength of the concrete being exceeded. This is due to the continuing transfer of the concrete compressive stress to the reinforcing steel over time due to the action of creep, figure 5.31(a). Members subjected to Combination 4, however, may not experience tensile stress at the bottom fibre due to the smaller reduction of the initial concrete compressive stress over time, Figure 5.31(b).

The final values for the loss of prestress for loaded members were, as expected, smaller than those for the unloaded members. For section *T10*, the final losses for members loaded at 30 and 100 days were calculated to be 16.2 and 8.0% respectively, whereas the percentage was calculated to be 42.8% for unloaded members (under Combination 1). Equivalent losses were calculated to be 18.2, 12.6 and 36.6% for section *SY6*. The reduction in the losses was largely due to the reduction in the creep component due to the reduction in the compressive stress at the bottom of the section, and due to the loss recovery of the prestressing steel after the additional loads are applied.

Evaluation of the time-dependent deflection and compressive stress at the bottom fibre suggests that the differences between the beams loaded at 30 and 100days are not significant. It can also be seen that, for the given combination of parameters and level of prestress, the cambers are greatly reduced after the application of loads. More slender members, as represented by section *SY6*, may even display a continuing deflection under total dead load alone. There is more chance of this occurring for members subjected to lower level of initial prestress (as discussed in the previous section). This suggests that if the insitu slabs are cast prior to continuity being established, the positive restrained bending moment developed at the support may be very small or non-existent. Negative restrained bending moment due to a continuing

reduction in camber may turn out to be more significant, especially for slender members or for members with lower levels of initial prestress.

This evaluation also indicates that, apart from the combination of material and structural properties and the level of initial prestressing, the sequence of construction such as the ages of both the slab casting and the establishment of continuity may be critical as to whether the resulting restrained bending moments at the intermediate support are positive or negative. The magnitude of these moments needs to be ascertained and this is consequently dealt with in Chapter 6.

5.4.7 Effect of different parameters on beam deflection

It has been noted earlier that the prestressing force and the consequential creep action affect the flexural behaviour of a simply supported beam in the opposite direction to that due to the selfweight and shrinkage of the beam. Previous analyses have combined all these effects into single analyses, as it necessary to capture the interactive nature of these parameters. However, in order to ascertain the contribution of these individual components on the time-dependent behaviour of flexural members, separate (independent) analyses for each component have been conducted. These have also been conducted to study the difference between the combined and independent analyses. The total effects of the independent analyses have been calculated by superimposing deformations due to prestressing, selfweight and shrinkage acting independently. The resultant deflections were then compared with those from the combined analyses.

Analysis for the effect of prestressing force has assumed zero selfweight, and likewise, the analysis for the effect of beam selfweight has assumed zero prestressing force. Subsequently, the analysis for the effect of shrinkage has assumed zero prestressing and selfweight. All beams were prestressed with the lower level of initial prestressing, as referred to in Section 5.4.5, and subjected to the combination of parameters yielding maximum deformation (Combination 1).

Figures 5.32 show the time-dependent camber and deflection for these three components for all sections with the maximum recommended span. The figures show that, under the

separate actions of prestressing, beam selfweight and shrinkage, sections *T10* and *SY6* display the smallest and greatest changes in time-dependent deflections, respectively. The initial downward deflections due to the beam selfweight for sections *T10*, *M10*, *U12*, *Y8* and *SY6*, were calculated to be 14, 42, 58, 62 and 77mm, respectively, with the corresponding long term deflections were 76, 213, 286, 293 and 366mm. The long term values being 5.4, 5.1, 4.9, 4.7 and 4.8 times greater than the initial deflections for sections *T10*, *M10*, *U12*, *Y8* and *SY6* respectively. These correspond with the final creep coefficients which were calculated to be 4.97, 4.60, 4.60, 4.32 and 4.34. The ratios between the final and the initial deflections are slightly greater than the creep coefficients due to the effect of bonded bottom reinforcement. The bonded steel at the bottom of the section (both the prestressed steel and nominal non-prestressed steel) slightly increased the long term deflection between 6-10%. It should be noted that the amount of bonded steel in these analyses was less than 1.0%.

The fact that the ratios between the final and initial deflections for all the five sections evaluated corresponded closely with the creep coefficients suggests that the flexural rigidity does not affect the time-dependent deformation of flexural members. The flexural rigidity seems only to be reflected in the extent of the initial deflection, but the time-dependent deflection is shown to be directly related to the creep coefficient.

The initial upward deflections due to the prestressing force were calculated to be 29, 58, 78, 79 and 100mm for sections *T10*, *M10*, *U12*, *Y8* and *SY6* respectively. The corresponding long term cambers were calculated to be 105, 203, 261, 265 and 331mm that is 3.6, 3.5, 3.34, 3.35 and 3.31 times greater than the initial cambers for sections *T10*, *M10*, *U12*, *Y8*, and *SY6* respectively. These ratios are smaller than the creep coefficients due the reduction of the prestressing force and the effect the bonded steel at the bottom of the section.

Time dependent deflection due to the action of shrinkage is shown in Figure 5.32(c) where sections *SY6* and *T10* are shown to display the greatest and smallest long term deflections, respectively. The final downward deflections were calculated to be 12.4, 20.7, 27.6, 25.8 and 30.5mm for sections *T10*, *M10*, *U12*, *Y8*, and *SY6* respectively.

These values represent between 8 to 10% of the final deflection due to selfweight. The percentages will be less if the deflections due to other loads are taken into consideration. This indicates that the components of deflection contributed by the action of shrinkage are not significant compared to those due to other factors.

Figures 5.33 show the time-dependent creep and shrinkage characteristics for all sections considered in these analyses. It can be seen that the smallest section (*T10*) displays the largest creep and shrinkage values and the largest sections (*SY6* and *Y8*) display the smallest values. A comparison of the rate of increase in deflection, however, indicates that the rates are nearly the same for all sections, Figures 5.34. It should be noted that this observation is only relevant for conditions where members are subjected to uni-directional loads and remain uncracked. In other words, it is only applicable for lightly reinforced uncracked, non-prestressed beams where only loads causing downwards deflection are applied. In the case of prestressed beams where the interactions between the negative and positive curvatures are present, this observation is not applicable.

Figure 5.35 shows a comparison of time-dependent deflections between the combined and independent analyses of *T10* and *SY6* sections. The graph shows that time-dependent deflections may be wrongly estimated if independent analyses are considered. The final deflections from the combined analyses were calculated to be -5 and 41mm for sections *SY6* and *T10* respectively, compared to -66 and 17mm for the corresponding sections using the independent analyses. The superposition of deflections overestimates the long term downward deflections by about 61 and 24mm for sections *SY6* and *T10* respectively. The rule of superposition of deflections is only valid for the initial values, but once the nonlinearity is introduced from the actions of creep and shrinkage, the validity ceases. Therefore, care should be taken when time-dependent deflections are estimated using superposition from different load effects, especially for members subjected to combination of parameters yielding maximum deformation.

In the case of composite construction of road bridges, the differential shrinkage between precast and cast insitu units need to be considered because they may cause substantial bending moments. However, the potentially large difference in shrinkage due to different values of *RH* (as calculated earlier) is simply non-existent because the structures will always be subjected to similar atmospheric conditions. The differential shrinkage which may subsequently cause bending moments in composite beams is possible only due to different casting ages, volume to surface area ratios and material characteristics of the concrete. The differential shrinkage will generally cause downward deflection, thus contributing to the hogging restrained moment at the support if the structures are formed into continuous members. This adds to an earlier observation where it was shown that a hogging moment was more likely to be developed at the intermediate support than a sagging moment.

The overall effects of creep and differential shrinkage on the development of restrained bending moment at the support are subsequently evaluated in the next Chapter.

5.5 Brief Comparisons Between CEB90 and ACI

The difference in the material properties of concrete predicted by CEB90 and ACI has been discussed in Chapter 3. It was shown that the prediction given by CEB90 generally displayed greater creep but lower shrinkage values than those given by ACI. However, the difference between the total deformation predicted by the two methods i.e. due to the elastic, creep and shrinkage deformations together, was smaller. The difference between the individual predictions for creep and shrinkage, together with the difference in their rates of development, is expected to show different time-dependent responses of flexural members. This is due the counteracting effects from the creep and shrinkage actions as previously discussed in Section 5.4. A brief comparison has subsequently been conducted to ascertain the effect of the different material predictions on the time-dependent behaviour of simple prestresssed beams. The structural analyses have used the age adjusted effective modulus method as in the previous Sections.

To enable a comparison to be drawn, the material parameters for the concrete were assumed to be similar to those adopted in Chapter 3. Analyses of beams in Section

5.4.5 have been extended to include the effects of the material properties according to ACI. Material characteristics and time-dependent camber for sections *SY6* and *T10* subjected to Combinations 1 and 4 are shown in Figures 5.36-5.38. A summary of the analyses is presented in Table 5.15 where creep per unit stress, shrinkage and total axial deformation represented the material characteristics, while the loss of prestress, camber and stress on the concrete bottom fibre represented the structural characteristics of the beams.

Figures 5.36(a) and 5.37(a) show that for both sections *SY6* and *T10*, ACI displays lower creep values under Combination 1, but higher values under Combination 4. A comparison of shrinkage, however, shows that ACI generally displays greater deformation for both sections under both combinations of parameters, Figures 5.36(b) and 5.37(b). For sections *SY6* and *T10* under Combination 1, ACI displays greater shrinkage for up to 800 days, after which CEB90 predicts greater values. According to ACI, both sections display greater shrinkage at any time under Combination 4. It can be seen that, while the rates of creep development are nearly similar between CEB90 and ACI, the rates of shrinkage development are higher for ACI than CEB90.

The variations in the prediction of material characteristics are not correspondingly reflected in the flexural members. For example, greater creep values predicted by CEB90 for section *SY6* (under Combination 1) do not necessarily result in greater camber. Greater creep values cause greater change in the flexural deflection where the final value was calculated to be -5.2mm (net downwards deflection, Table 5.15). The equivalent value using ACI was calculated to be 11.8mm (net camber). On the other hand, although the creep values given by CEB90 are smaller under Combination 4, the final camber displayed a greater value than that given by ACI. The final cambers for section *T10* and *SY6* given by CEB90 were calculated to be 27.3 and 30.1mm, respectively. The corresponding cambers given by ACI were 24.2 and 22.9mm.

Comparisons of prestress loss and concrete compressive stress at the bottom fibres also show similar patterns to those for the cambers. Calculations using CEB90 display a greater loss of prestress under Combination 1, but a smaller loss under Combination 4.

Similarly, calculations according to CEB90 for the concrete compressive stress at the bottom fibres display smaller values under Combination 1, but greater values under Combination 4 (Table 5.15).

This brief comparison demonstrates that the time-dependent analysis of prestressed flexural members using the material predictions by CEB90 are not necessarily more conservative than those of ACI. They depend on various combinations of material and structural properties. Therefore, it is necessary to exercise some care when assessing the time-dependent behaviour of prestressed concrete beams using either CEB90 or ACI. The results yielded by different material predictions need to be interpreted qualitatively rather than quantitatively.

Table 5.8: A summary of sections used for the evaluation of time-dependent behaviour of simple flexural members.

Section	Depth (mm)	Area (mm^2)	*Yb* (mm)	*Yt* (mm)	*I* ($10^9 mm^4$)	*V/S* (mm)	Span (mm)	*SW* (kN/m)	*SDL* (kN/m)	*SLL* (kN/m)
T1	380	98000	140	240	1.24	50.0	9000	2.31	6.16	11.2
T10	815	171560	356	459	12.4	62.0	17000	4.05	6.16	11.2
M2	720	316650	265	455	16.2	88.0	18000	7.47	9.78	15
M10	1360	457450	568	792	102.0	94.0	29500	10.8	9.78	15
SY1	1500	549158	598	902	120.0	126.0	30000	12.96	9.78	15
SY6	2000	709158	855	1145	284.0	132.0	40000	16.74	9.78	15
Y1	700	309202	255	445	11.1	114.0	16500	7.42	6.16	11.2
Y8	1400	584708	639	761	119.0	135.0	32000	14.02	6.16	11.2
U1	800	466450	355	445	29.9	96.0	18000	11.01	9.78	15
U12	1600	730450	738.5	862.5	203.0	90.0	34000	17.24	9.78	15

Notes: *Yb* and *Yt* are distance to bottom and top fibres respectively; *I* is moment of inertia; and *SW*, *SDL* and *SLL* are loads due to selfweight, superimposed dead load and superimposed live loads.

Table 5.9: A summary of the instantaneous stress, deflection and prestressing required for each section used in the time-dependent analysis.

Section	Span/ Depth	Span/ Inertia ($x10^6 mm^3$)	Stress at bottom fibre (MPa)			Deflection at mid-span (mm)			Fpi (kN)	Aps (mm^2)
			SW	*SDL*	*SLL*	*SW*	*SDL*	*SLL*		
T1	23.7	72.3	2.63	7.02	12.76	5.3	14.1	25.6	1433	1194
T10	20.9	13.7	4.20	6.39	11.62	11.8	18.0	32.8	2214	1845
M2	25.0	11.1	4.96	6.49	9.95	21.0	27.4	42.2	4667	3889
M10	21.7	2.9	6.55	5.93	9.10	34.8	31.5	48.4	6398	5332
SY1	20.0	2.5	7.30	5.50	8.45	38.1	28.7	44.1	7198	5999
SY6	20.0	1.4	10.09	5.89	9.04	65.6	38.3	58.7	10144	8454
Y1	23.6	14.9	5.82	4.83	8.78	21.6	17.9	32.6	3630	3025
Y8	22.9	2.7	9.65	4.24	7.71	53.7	23.6	42.9	6720	5600
U1	22.5	6.0	5.30	4.71	7.22	16.8	14.9	22.9	4362	3635
U12	21.3	1.7	9.06	5.14	7.88	49.3	28.0	42.9	8683	7236

Table 5.10: Summary of time-dependent analysis for sections with the maximum recommended span under four different conditions

Sections	Comb.	Loss of prestress (%)		Mps/Msw ratio		Camber at mid-span (mm)			Stress at bottom fibre (MPa)		Final	Final
		Elastic	Time-dep.	Initial	Final	initial	maximum (day)	Final	Initial	Final	Creep	Shrinkage
T10	1	12.1	42.8	3.55	1.60	45.1	144 (10000)	144	21.3	7.3	4.97	650
M10	1	11.0	38.7	1.99	1.00	57.1	150 (1000)	146	18.5	6.5	4.605	630
U12	1	10.0	35.4	1.74	0.951	62.3	154 (400)	144	16.8	5.4	4.605	630
Y8	1	9.5	32.9	1.64	0.943	59.3	142 (400)	131	15.9	5.5	4.321	596
SY6	1	11.4	36.3	1.69	0.883	78.2	181 (400)	166	19.1	6.1	4.338	598
T10	2	9.8	30.8	3.55	2.11	36.3	110 (10000)	110	21.8	12.0	3.515	438
M10	2	9.0	27.6	1.99	1.26	45.8	121 (10000)	121	18.9	10.6	3.256	424
U12	2	8.2	25.3	1.74	1.16	50.2	126 (1000)	126	17.2	9.2	3.256	424
Y8	2	7.7	23.5	1.64	1.13	47.8	116 (1000)	115	16.3	9.0	3.055	401
SY6	2	9.3	26.1	1.69	1.09	63	149 (1000)	148	19.5	10.4	3.067	403
T10	3	12.1	25.8	3.55	2.20	45.1	118 (10000)	118	21.3	13.0	2.644	188
M10	3	11.0	23.6	1.99	1.30	57.1	135 (10000)	135	18.5	11.4	2.554	182
U12	3	10.0	21.5	1.74	1.19	62.3	142 (10000)	142	16.8	10.0	2.554	182
Y8	3	9.5	20.3	1.64	1.15	59.3	131 (10000)	131	15.9	9.6	2.472	172
SY6	3	11.4	22.7	1.69	1.11	78.2	169 (10000)	169	19.1	11.1	2.477	173
T10	4	9.8	17.7	3.55	2.58	36.3	85 (10000)	85	21.8	16.3	1.870	127
M10	4	9.0	16.0	1.99	1.49	45.8	100 (10000)	100	18.9	14.2	1.806	123
U12	4	8.2	14.7	1.74	1.34	50.2	107 (10000)	107	17.2	12.7	1.806	123
Y8	4	7.7	13.9	1.64	1.28	47.8	99.8 (10000)	99.8	16.3	12.1	1.748	116
SY6	4	9.3	15.6	1.69	1.27	63	130 (10000)	130	19.5	14.2	1.752	117

Note: Combination 1 [f'_c=30, *RH*=40]; Combination 2 [f'_c=60, *RH*=40]; Combination 3 [f'_c=30, *RH*=90]; Combination 4 [f'_c=60, *RH*=90];Msw=Moment due to selfweight

Table 5.11: Summary of analysis on the effect of bottom non-prestressed steel for sections *T10* and *SY6* under combinations of f'_c=30 and *RH*=40% (Combination 1).

Calculation	Section *T10*				Section *SY6*			
	As=0.0%	As=0.5%	As=1.0%	As=2.0%	As=0.0%	As=0.5%	As=1.0%	As=2.0%
Initial loss of prestress (%)	12.3	11.8	11.3	10.4	11.6	11.1	10.7	9.9
Final time-dependent loss of prestress(%)	46.7	38.0	31.8	23.8	39.2	32.7	28.0	21.7
Initial camber (mm)	45.7	44.3	43.1	41.0	79.2	76.8	74.6	71.1
Maximum camber (mm), and the age at the maximum camber(day)	161 (10000)	124 (10000)	101 (600)	78 (100)	204 (1000)	156 (300)	129 (100)	102 (30)
Final camber (mm)	161	124	98	68	196	130	84	29
Initial stress at bottom fibre (MPa)	21.6	20.7	19.9	18.4	19.4	18.6	17.9	16.7
Final stress at bottom fibres (MPa)	9.07	5.24	2.64	-0.58	7.53	4.32	2.07	-0.81
Initial stress at top fibre (MPa)	-1.55	-1.78	-1.99	-2.41	4.1	3.8	3.5	2.96
Final stress at top fibre (MPa)	1.28	2.19	2.68	3.02	7.29	8.06	8.47	8.71
Span/$E_c(t_o)I_t$ (x10^{-9})	54.26	52.63	51.19	48.76	5.542	5.374	5.225	4.975
Span/ $E_c(28)I_t$ (x10^{-9})	41.97	40.71	39.59	37.71	4.287	4.156	4.041	3.848
Mps/Msw (initial)	3.553	3.553	3.553	3.553	1.69	1.69	1.69	1.69
Mps/Msw (final)	1.455	1.785	2.021	2.336	0.831	0.95	1.037	1.157

Table 5.12: Summary of analysis on the effect of top non-prestressed steel for sections *T10* and *SY6* under combinations of f'_c=30 and *RH*=40% (Combination 1).

Calculation	Section *T10*				Section *SY6*			
	As=0.0%	As=0.5%	As=1.0%	As=2.0%	As=0.0%	As=0.5%	As=1.0%	As=2.0%
Initial loss of prestress (%)	12.3	12.0	11.7	11.2	11.6	11.2	10.9	10.4
Final time-dependent loss of prestress (%)	46.7	46.0	45.3	43.9	39.2	39.0	38.4	37.2
Initial camber (mm)	45.7	42.6	40.1	36.1	79.2	73.2	68.3	61.0
Maximum camber (mm), and the age at maximum camber (day)	161 (10000)	165 (10000)	166 (10000)	165 (10000)	204 (1000)	241 (10000)	262 (10000)	279 (10000)
Final camber (mm)	161	165	166	165	196	241	262	279
Initial stress at bottom fibre (MPa)	21.6	20.9	20.3	19.3	19.4	18.7	18.1	17.1
Final stress at bottom fibres (MPa)	9.07	9.22	9.23	9.1	7.53	8.27	8.55	8.66
Initial stress at top fibre (MPa)	-1.55	-0.69	-0.03	0.9	4.1	4.58	4.92	5.3
Final stress at top fibre (MPa)	1.28	-0.51	-1.62	-2.97	7.29	3.0	0.65	-1.89
Span/ $E_c(t_o)I_t$ ($x10^{-9}$)	54.26	50.596	47.588	42.94	5.542	5.124	4.785	4.271
Span/ $E_c(28)I_t$ ($x10^{-9}$)	41.97	39.134	36.808	33.214	4.287	3.963	3.701	3.304
Mps/Msw (initial)	3.553	3.553	3.553	3.553	1.69	1.69	1.69	1.69
Mps/Msw (final)	1.455	1.492	1.528	1.597	0.831	0.842	0.857	0.886

Table 5.13: Summary of analysis on the effect of top and bottom non-prestressed steel for sections *T10* and *SY6* under combinations of f'_c=60 and *RH*=90% (Combination 4).

Calculation	Section *T10*				Section *SY6*			
	Bottom As=0.0%	Bottom As=2.0%	Top As=0.0%	Top As=2.0%	Bottom As=0.0%	Bottom As=2.0%	Top As=0.0%	Top As=2.0%
Initial loss of prestress (%)	10.0	8.7	10.0	9.2	9.4	8.3	9.4	8.6
Final time-dependent loss of prestress (%)	18.4	12.4	18.4	17.5	16.3	11.4	16.3	15.7
Initial camber (mm)	36.7	33.6	36.7	30.4	63.6	58.2	63.6	51.6
Final camber (mm)	88.4	62.4	88.4	78.8	136.6	86.8	136.6	134
Initial stress at bottom fibre (MPa)	22.1	19.40	22.1	20.11	19.79	17.55	19.79	17.9
Final stress at bottom fibres (MPa)	17.3	10.25	17.3	16.2	15.07	8.99	15.07	14.58
Initial stress at top fibre (MPa)	-1.4	-2.08	-1.4	0.65	4.31	3.39	4.31	5.33
Final stress at top fibre (MPa)	-0.33	0.52	-0.33	-0.68	5.58	6.19	5.58	2.31
Span/ $E_c(t_o)I_t$ (x10^{-9})	43.56	39.878	43.56	36.128	4.455	4.073	4.455	3.615
Span/ $E_c(28)I_t$ (x10^{-9})	33.692	30.844	33.692	27.943	3.446	3.150	3.446	2.796
Mps/Msw (initial)	3.553	3.553	3.553	3.553	1.69	1.69	1.69	1.69
Mps/Msw (final)	2.543	2.802	2.543	2.604	1.256	1.358	1.256	1.283

Table 5.14: Summary of analyses on the effect of initial stress level for sections *T10* and *SY6* under combinations 1 (f'_c=30MPa and *RH*=40%) and 4 (f'_c =60MPa and *RH*=90%)

Calculation	Section *T10*				Section *SY6*			
	Combination. 1 High stress	Combination. 1 Low stress	Combination. 4 High stress	Combination. 4 Low stress	Combination. 1 High stress	Combination. 1 Low stress	Combination. 4 High stress	Combination. 4 Low stress
Initial prestressing force (kN) and area of prestressing steel (mm^2)	2214 (1844.8)	1056 (879.8)	2214 (1844.8)	1056 (879.8)	10140 (8453)	6479 (5399)	10140 (8453)	6479 (5399)
Ratio of initial moment due to prestressing and selfweight, Mps/Msw (final)	3.55 (1.60)	1.69 (1.14)	3.55 (2.58)	1.69 (1.45)	1.69 (0.833)	1.08 (0.733)	1.69 (1.27)	1.08 (0.914)
Initial loss of prestress (%)	12.1	5.1	9.8	4.1	11.4	6.1	9.3	4.9
Final time-dependent loss of prestress (%)	42.8	27.4	17.7	10.2	36.3	26.0	15.6	10.4
Initial camber (mm)	45.1	14.6	36.3	11.7	78.2	22.9	63.0	18.4
Maximum camber (mm), and the age at maximum camber(day)	144 (10000)	42.5 (400)	84.7 (10000)	27.3 (10000)	181 (400)	36.6 (28)	129.5 (10000)	30.1 (10000)
Final camber (mm)	144	41.4	84.7	27.3	166	-5.2	129.5	30.1
Initial stress at bottom fibre (MPa)	21.3	8.55	21.76	8.66	19.1	9.27	19.54	9.42
Final stress at bottom fibres (MPa)	7.34	3.58	16.33	6.95	6.1	2.92	14.24	7.03
Initial stress at top fibre (MPa)	-1.64	2.16	-1.47	2.22	3.98	7.5	4.21	7.63
Final stress at top fibre (MPa)	1.71	3.41	-0.16	2.65	7.66	9.34	5.71	8.31

Note: High stress is applied to counter total service load and Low stress is applied to counter only selfwieght and superimposed dead loads

Table 5.15: Summary of simple prestressed beam analyses using CEB90 and ACI predictions for material characteristics and AEM method for time-dependent analyses for sections *T10* and *SY6*.

Calculation	Section *T10*				Section *SY6*			
	CEB90 f'c=30, RH=40	CEB90 f'c=60, RH=90	ACI f'c=30, RH=40	ACI f'c=60, RH=90	CEB90 f'c=30, RH=40	CEB90 f'c=60, RH=90	ACI f'c=30, RH=40	ACI f'c=60, RH=90
Initial stress from prestressing (MPa)	6.15	6.15	6.15	6.15	9.14	9.14	9.14	9.14
Creep per unit stress at 28, 252, 1,000 and 10,000 days (microstrain/MPa)	69.9 120.1 145.6 160.2	15.9 29.4 39.2 47.8	51.8 89.7 105.4 117.5	26.0 44.8 52.8 58.8	54.8 97.3 122.7 139.9	12.8 24.0 33.5 44.9	45.3 78.4 92.2 102.7	22.8 39.3 46.2 51.4
Shrinkage strain at 28, 252, 1,000, and 10,000 days(microstrain)	148 377 538 650	29 74 105 127	208 506 584 613	104 253 292 307	71 204 359 598	14 40 70 117	166 404 467 490	83 202 233 245
Total axial deformation at 28, 252, 1,000 and 10,000 days (microstrain)	835 1373 1690 1893	331 458 550 625	856 1386 1561 1664	496 762 849 901	953 1475 1861 2257	433 561 678 829	1068 1608 1796 1916	635 906 1000 1060
Initial loss of prestress (%)	5.1	4.1	6.5	4.7	6.1	4.9	7.6	5.6
Time-dependent loss of prestress 10,000 days (%)	27.4	10.2	19.4	11.8	26.0	10.4	17.1	10.7
Initial camber (mm)	14.4	11.7	18.5	13.3	22.9	18.4	28.9	20.8
Camber at 10,000 days (mm)	41.4	27.3	30.2	24.2	-5.2	30.1	11.8	22.9
Initial stress at bottom fibres (MPa)	8.55	8.66	8.4	8.6	9.27	9.42	9.08	9.34
Stress at bottom fibres at 10,000 days (MPa)	3.58	6.95	4.9	6.5	2.92	7.03	4.9	6.8

Note: Prestressing and load are similar to those in Section 5.4.5 and assumptions for concrete composition as similar to those in Section 3.6.2

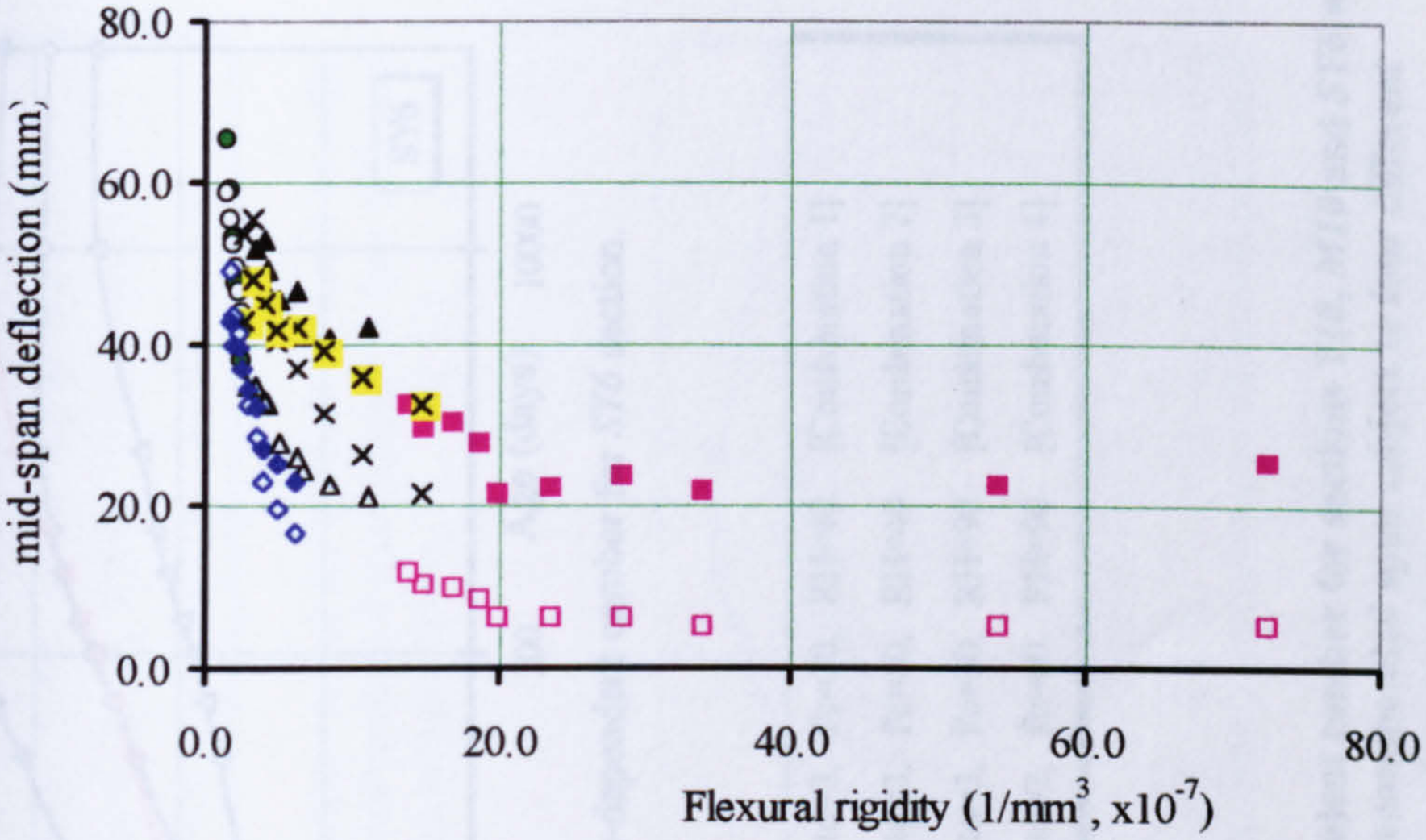

(a) Relationships between flexural rigidity and deflection

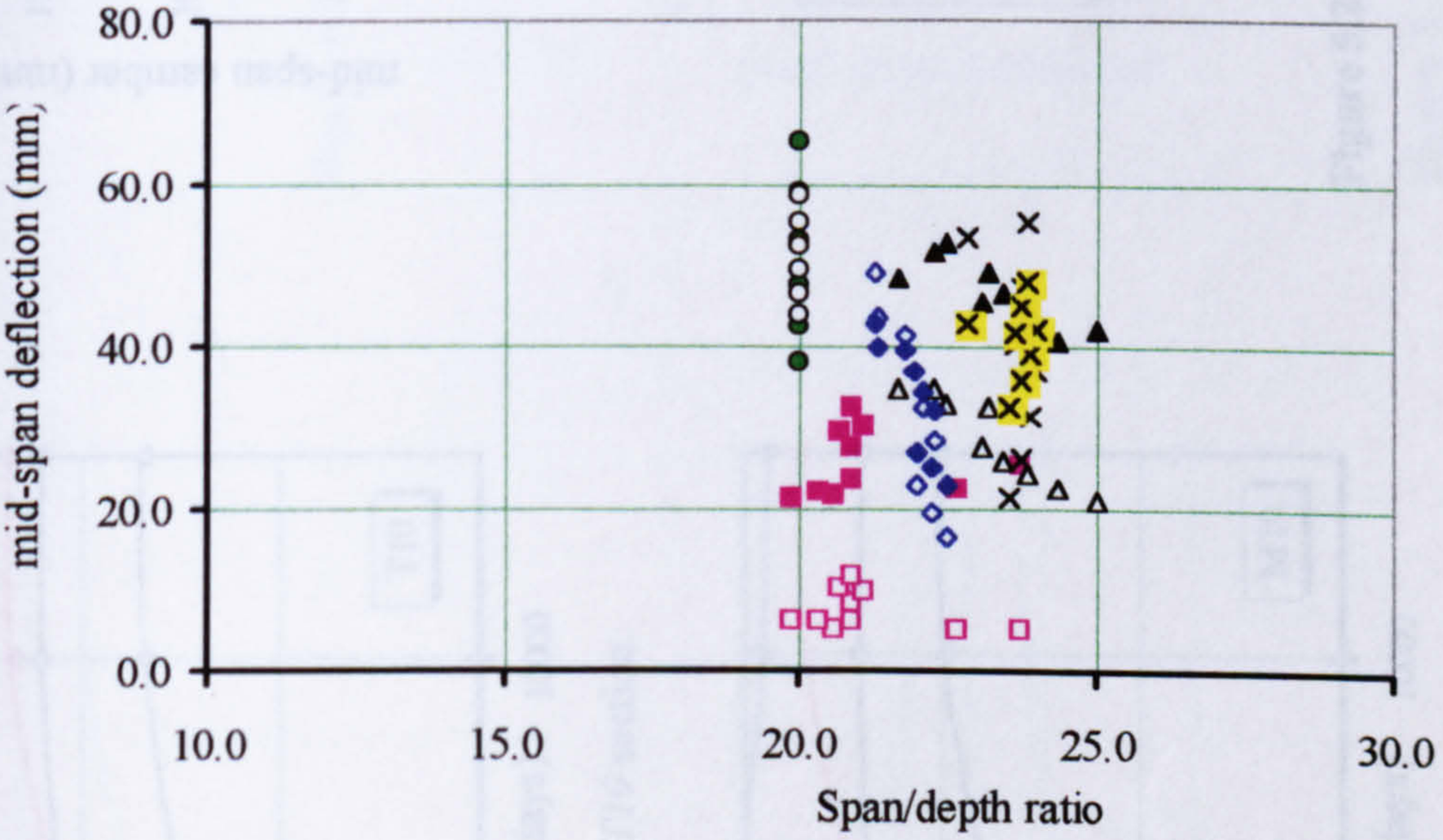

(b) Relationships between span/depth ratio and deflection

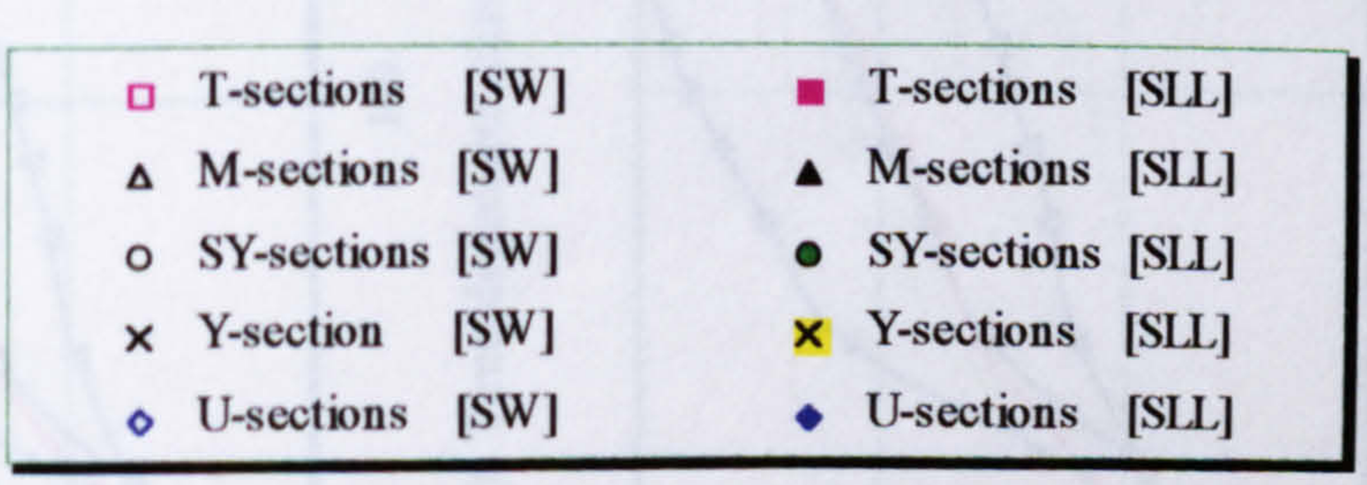

Figure 5.20: A comparison between span/depth ratio and flexural rigidity to deflections due beam selfweight (SW) and superimposed live load (SLL)

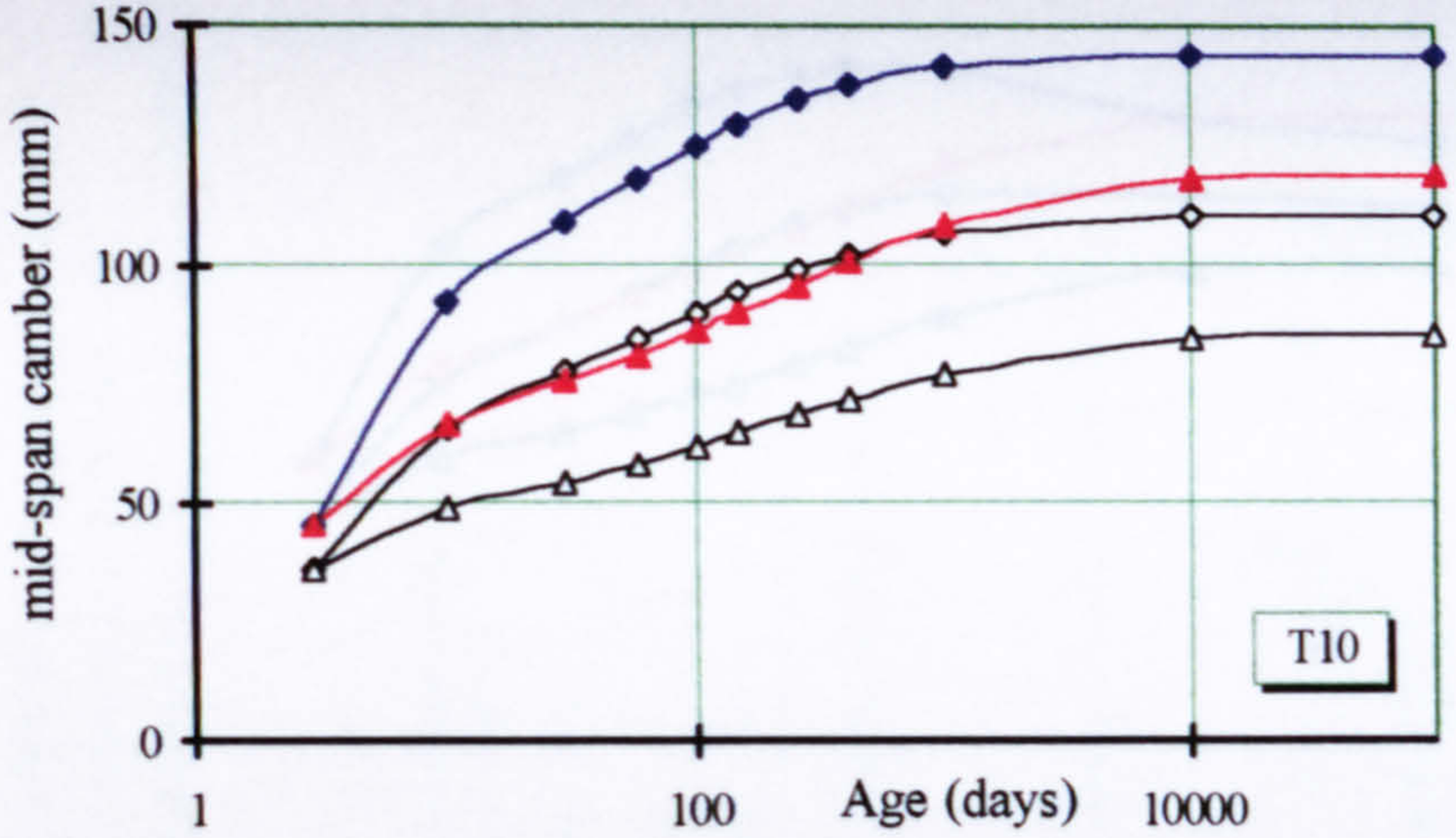

(a) Time-dependent camber for *T10* section.

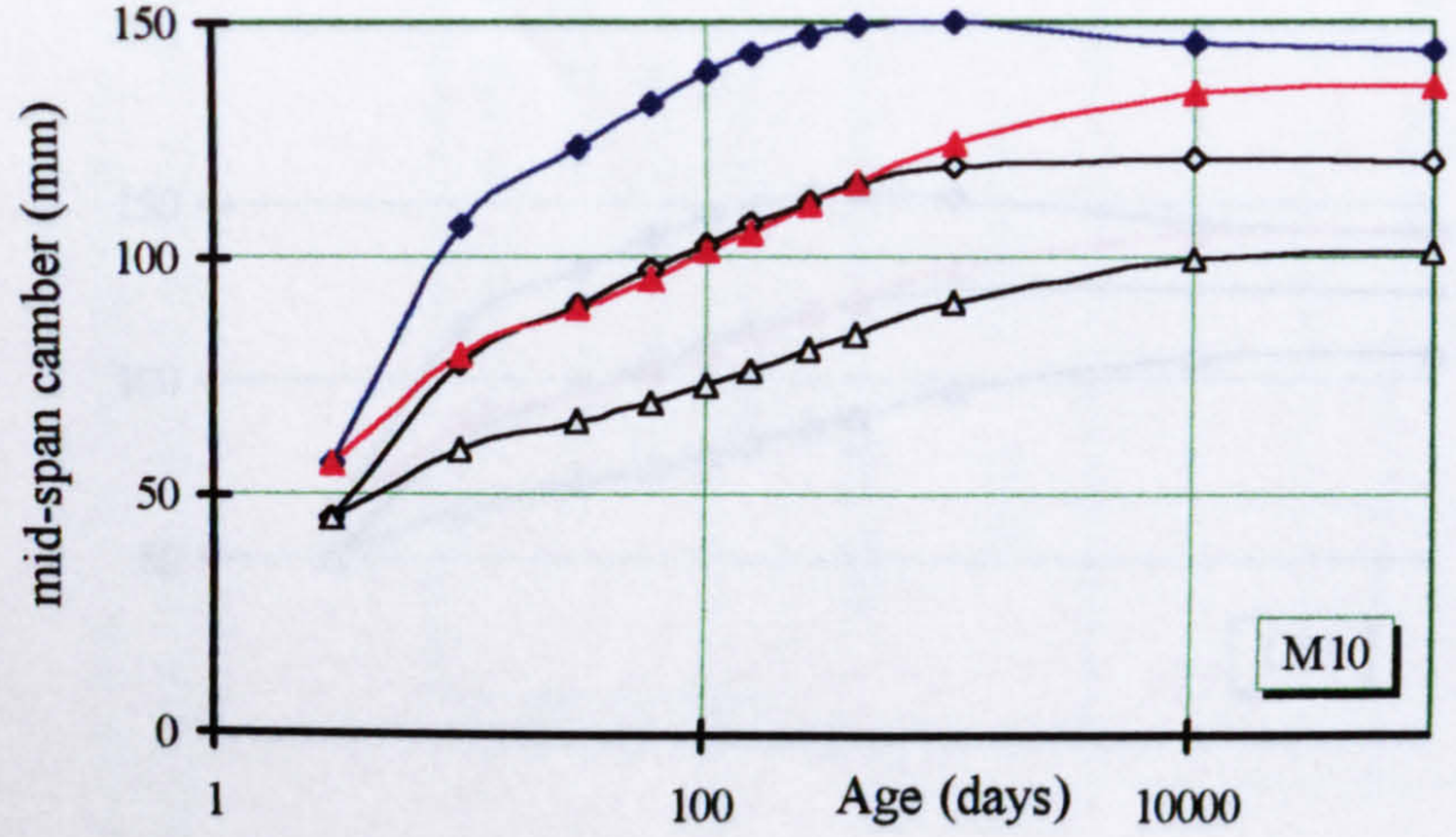

(b) Time-dependent camber for *M10* section.

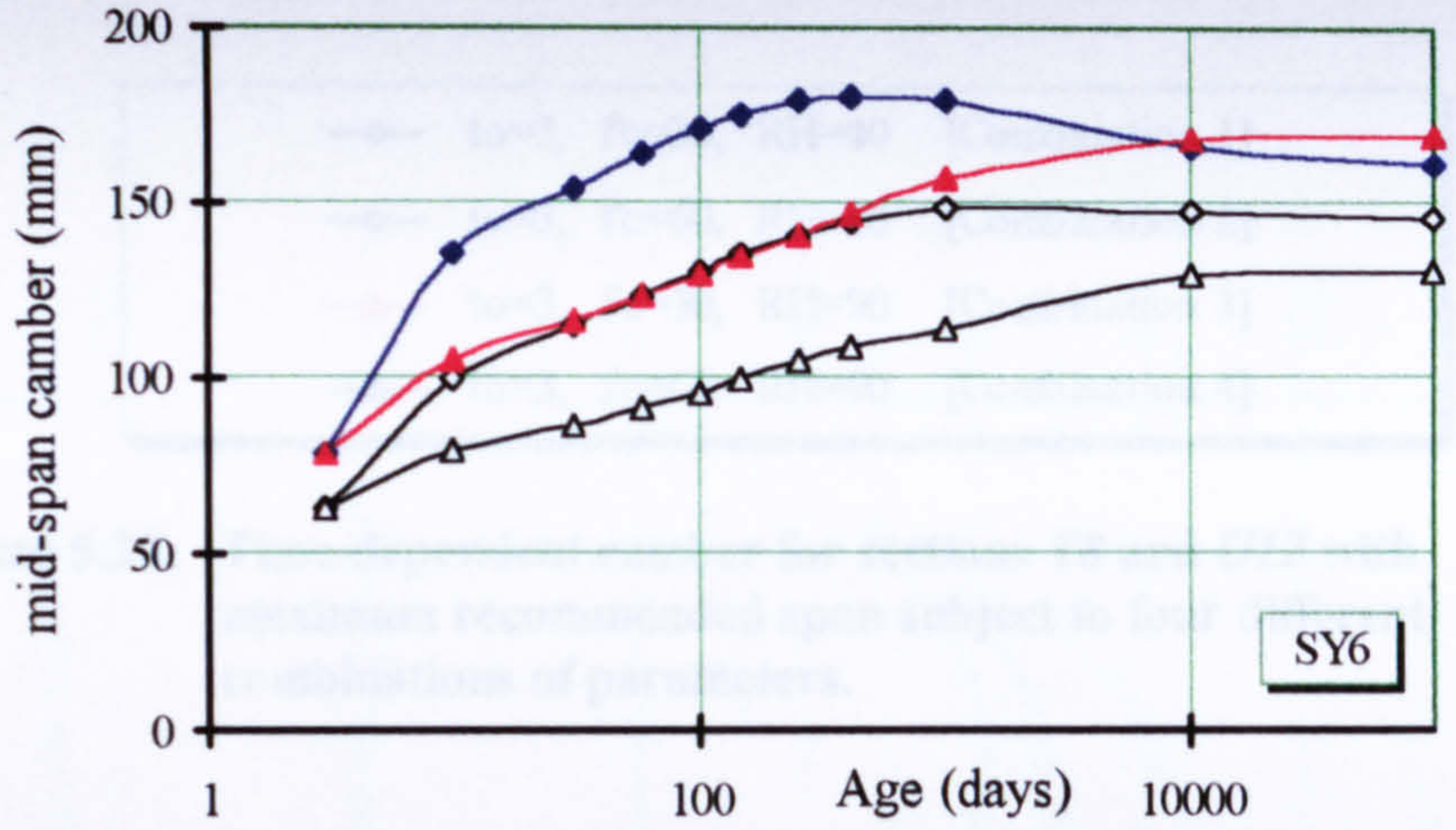

(c) Time-dependent camber for *SY6* section.

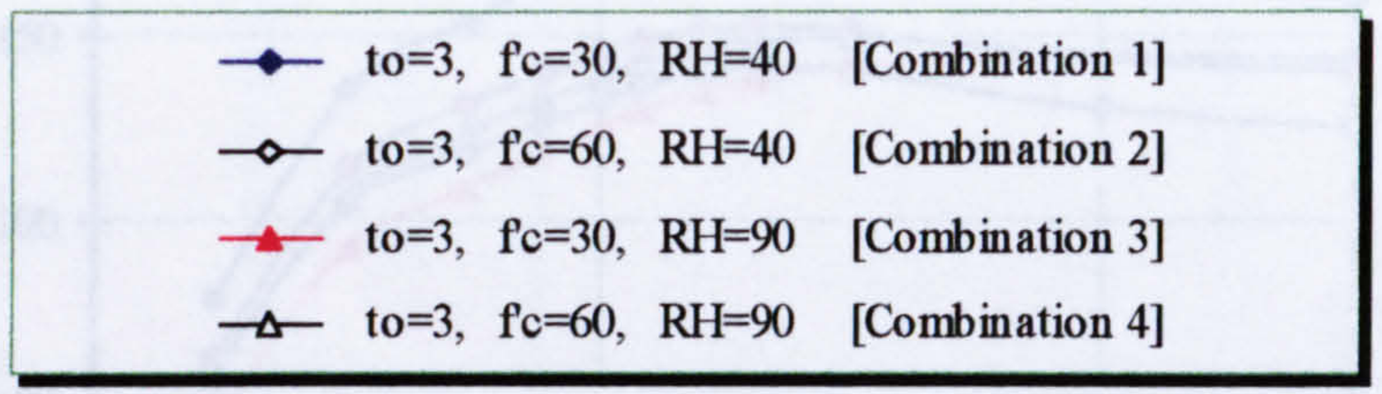

Figure 5.21: Time-dependent camber for sections *T10*, *M10* and *SY6* with maximum recommended span subject to four different combinations of parameters.

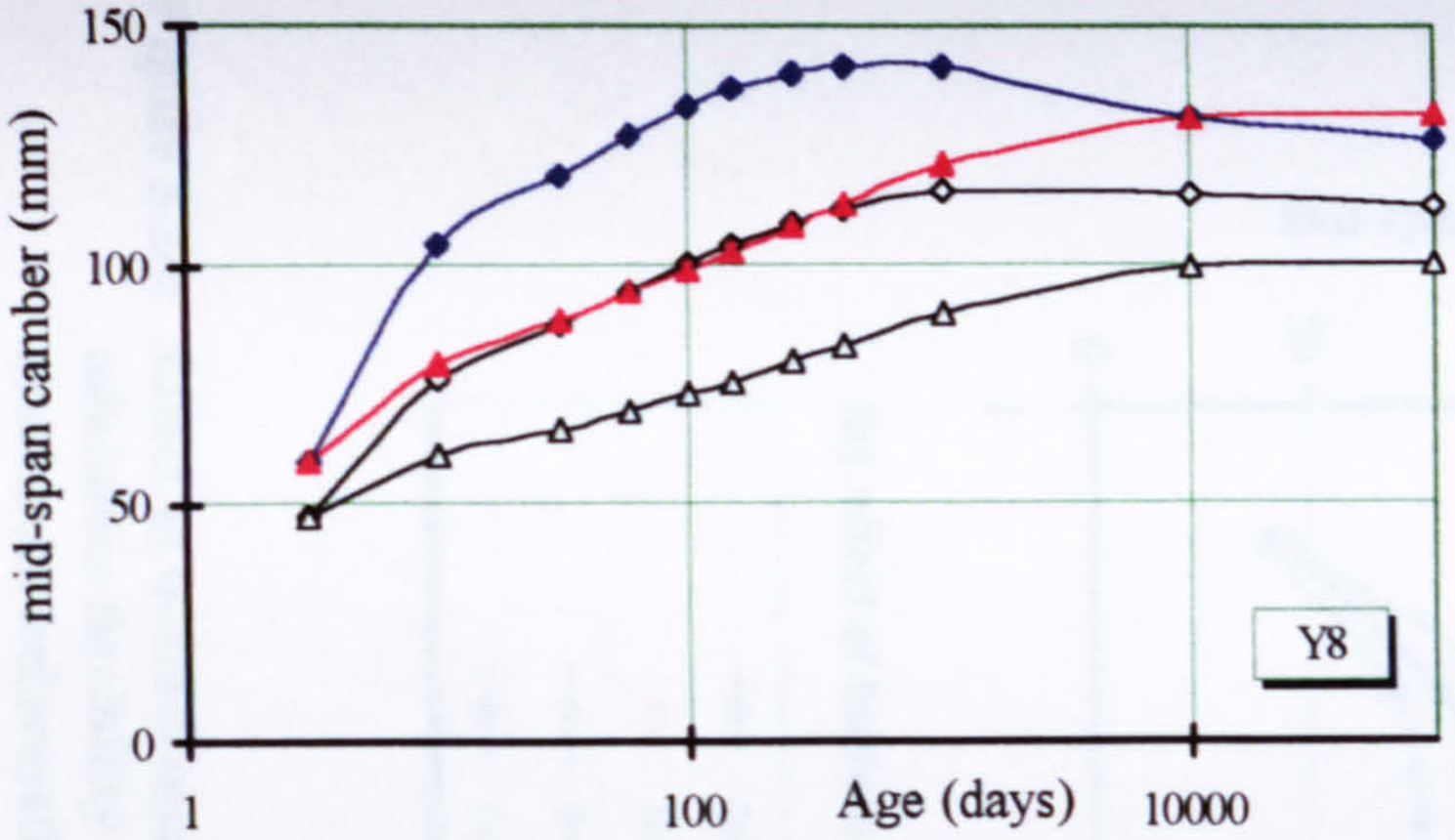

(d) Time-dependent camber for *Y8* section.

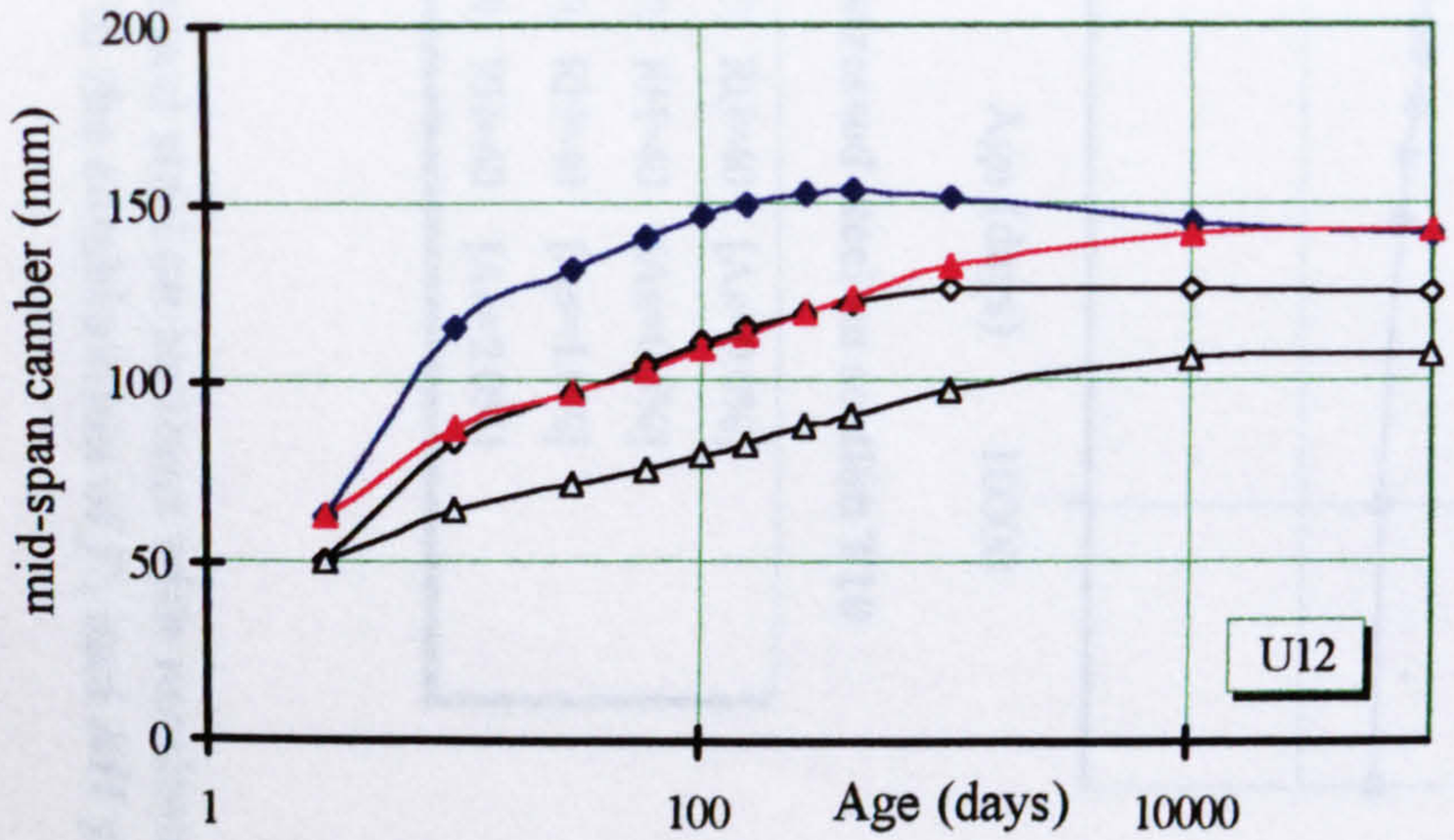

(e) Time-dependent camber for *U12* section.

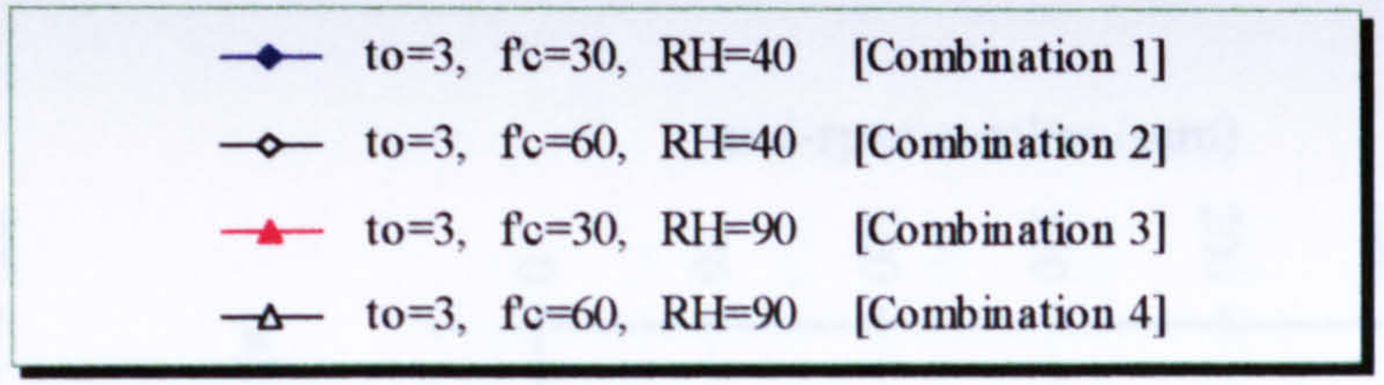

Figure 5.22: Time-dependent camber for sections *Y8* and *U12* with maximum recommended span subject to four different combinations of parameters.

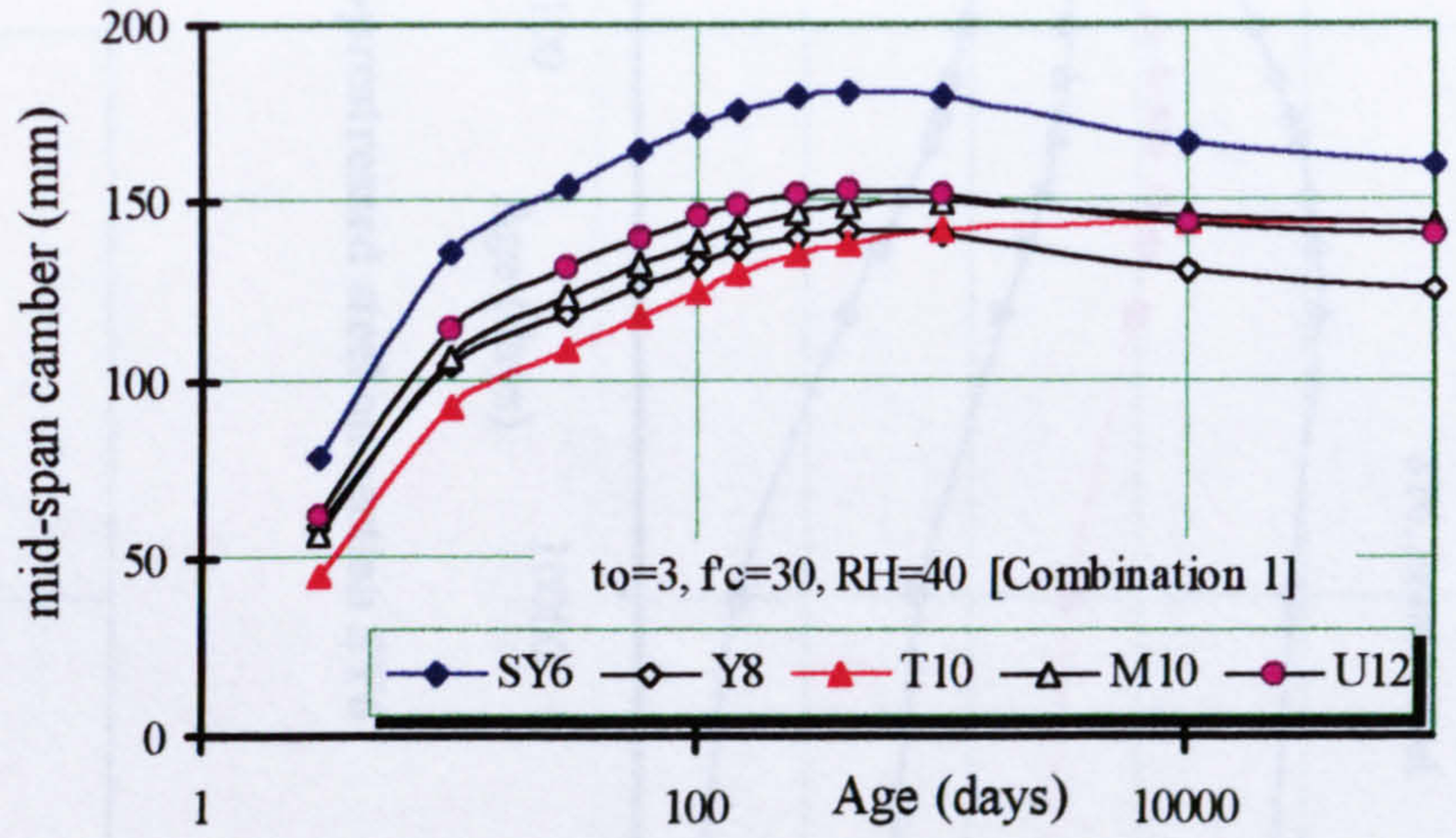

Figure 5.23: Camber of prestressed section with maximum recommended span.

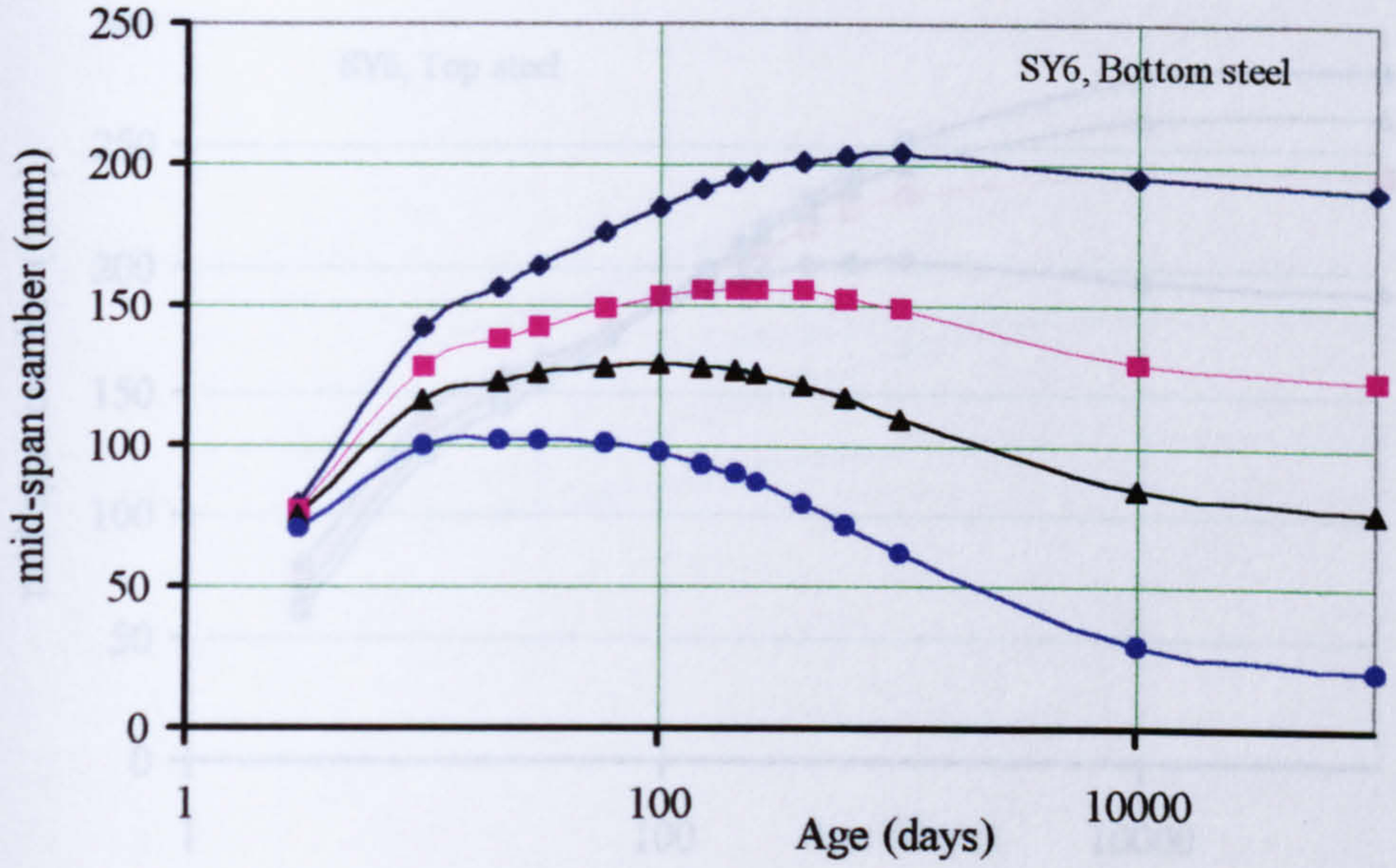

(a) Effect of bottom non-prestressed steel on section SY6

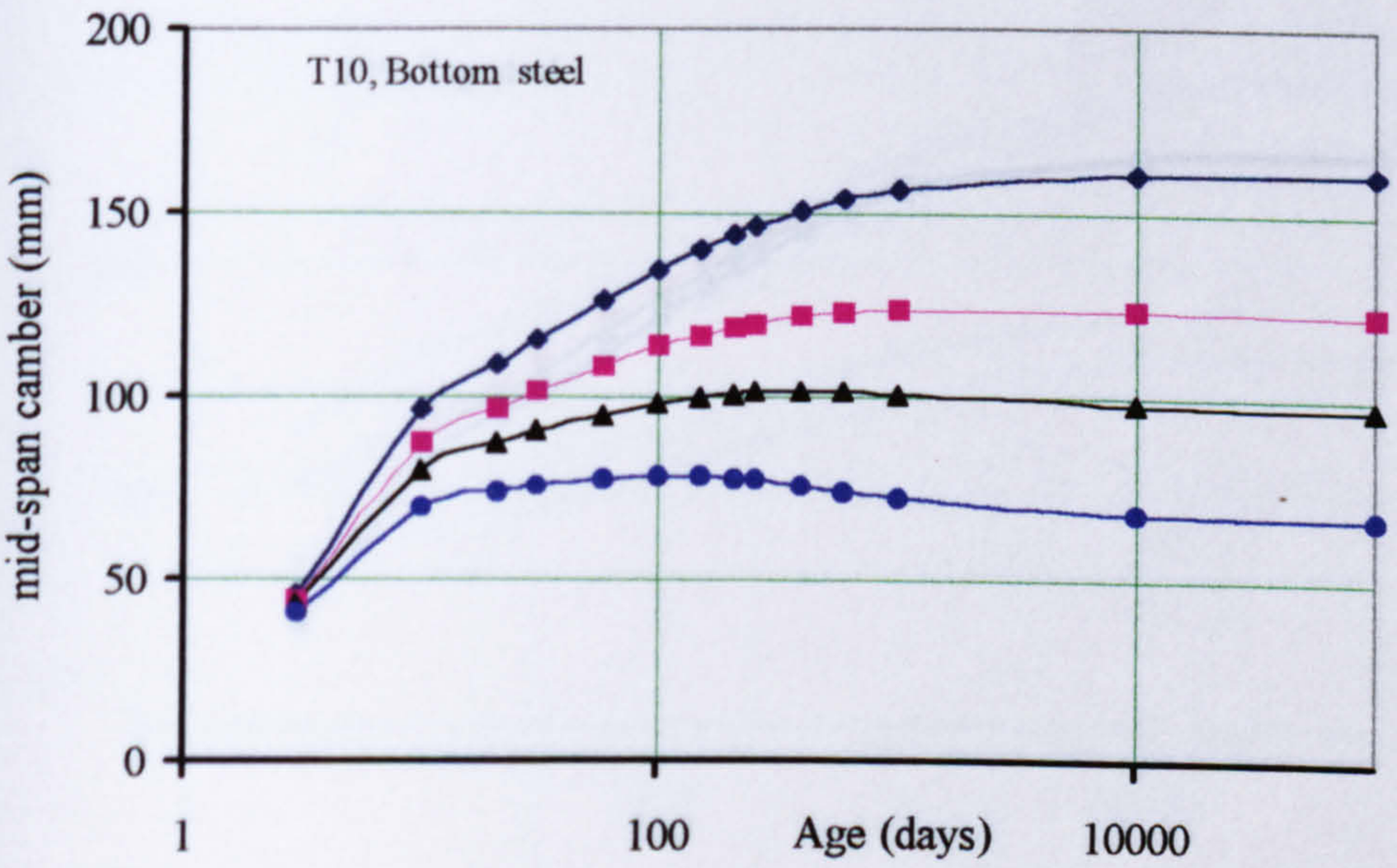

(b) effect of bottom non-prestressed steel on section T10

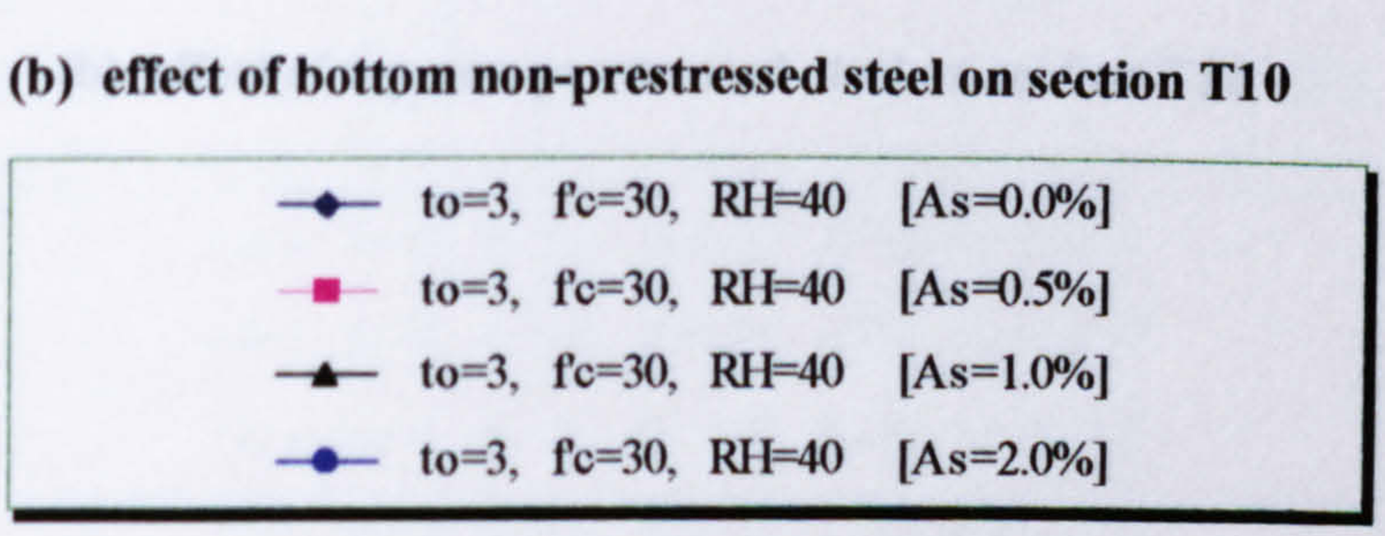

Figure 5.24: Effect of bottom non-prestressed steel on sections with maximum and minimum flexibility subject to the combination of f'_c and *RH* yielding maximum deformation

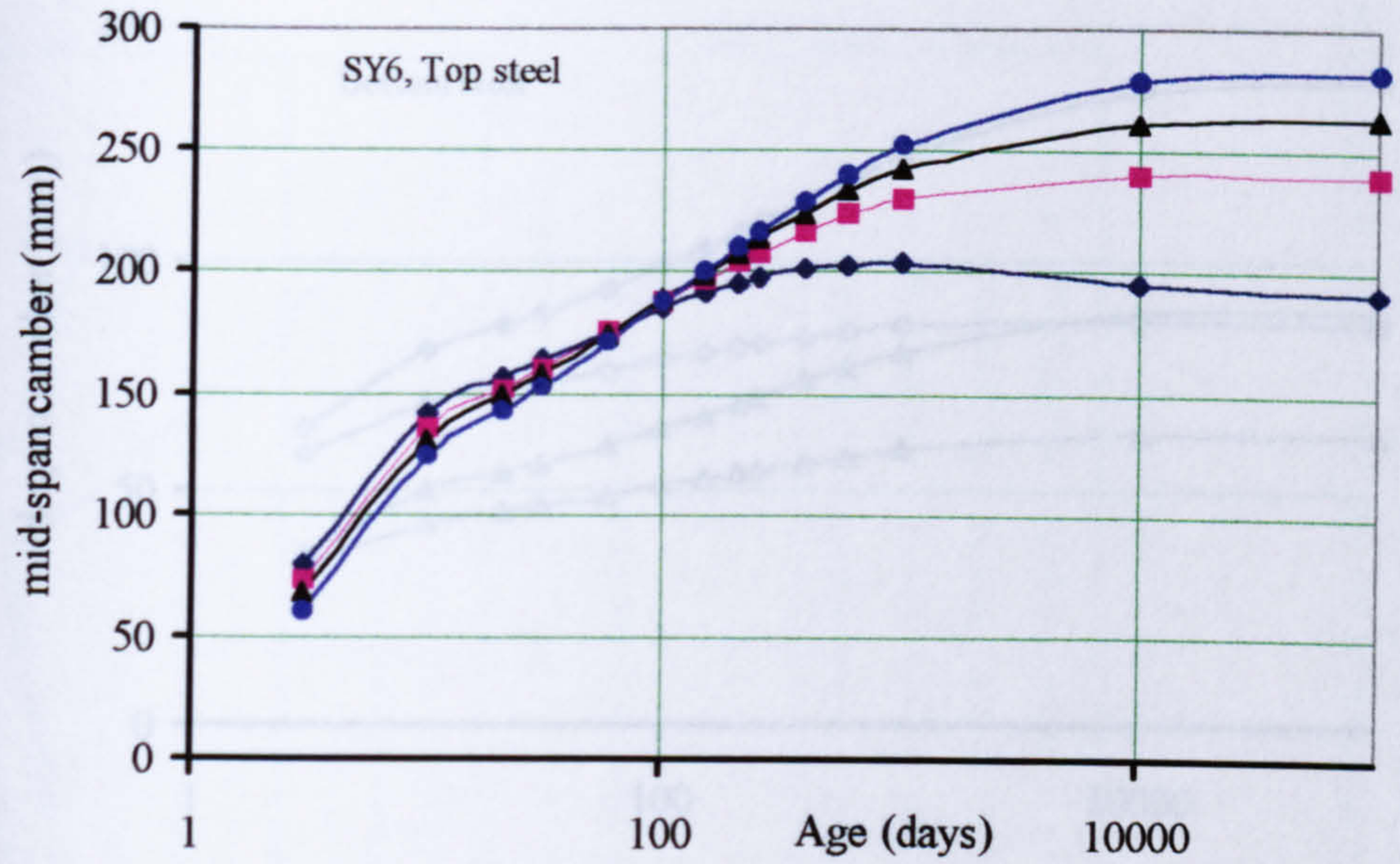

(a) Effect of top non-prestressed steel on section SY6

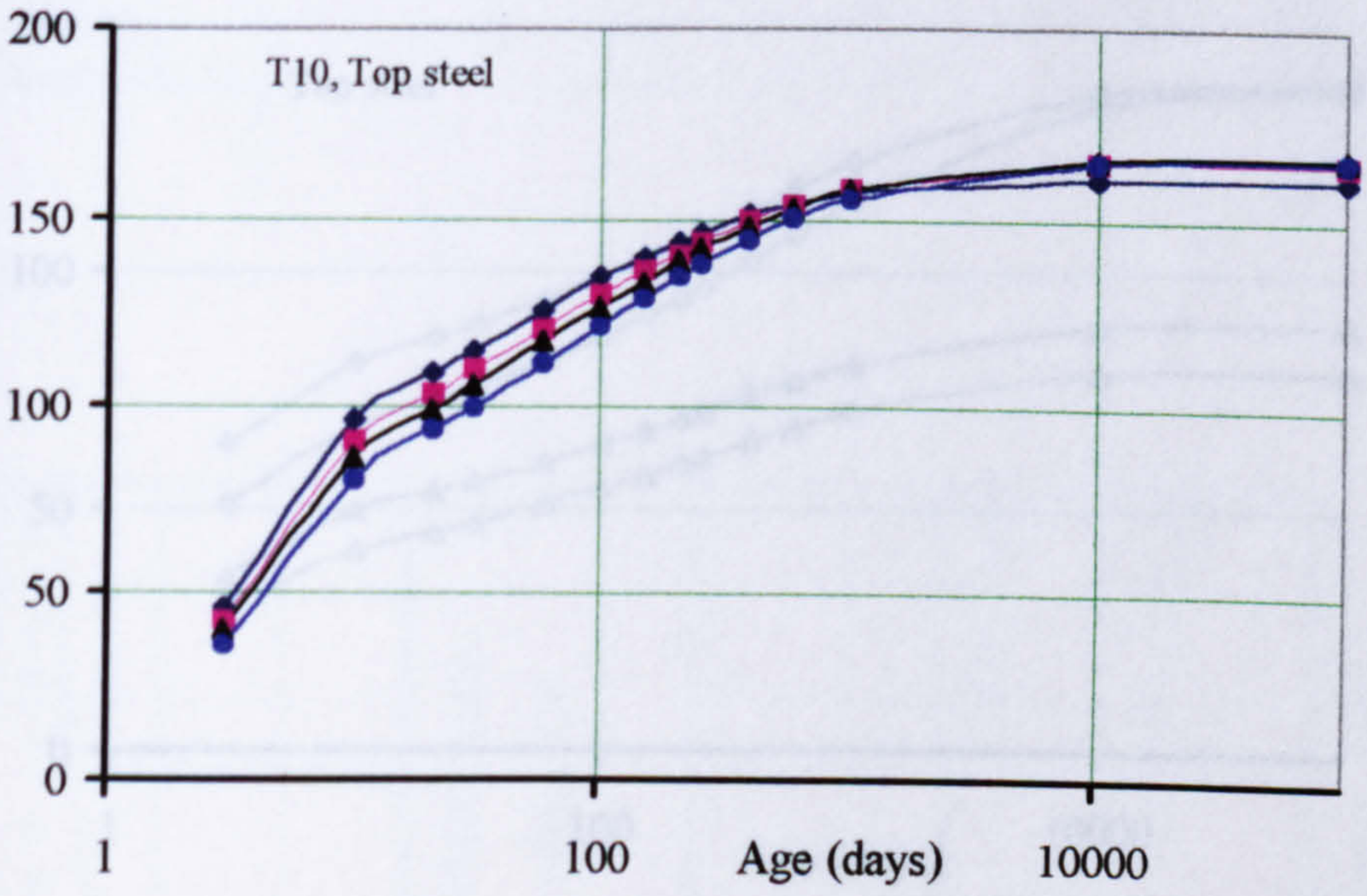

(b) effect of top non-prestressed steel on section T10

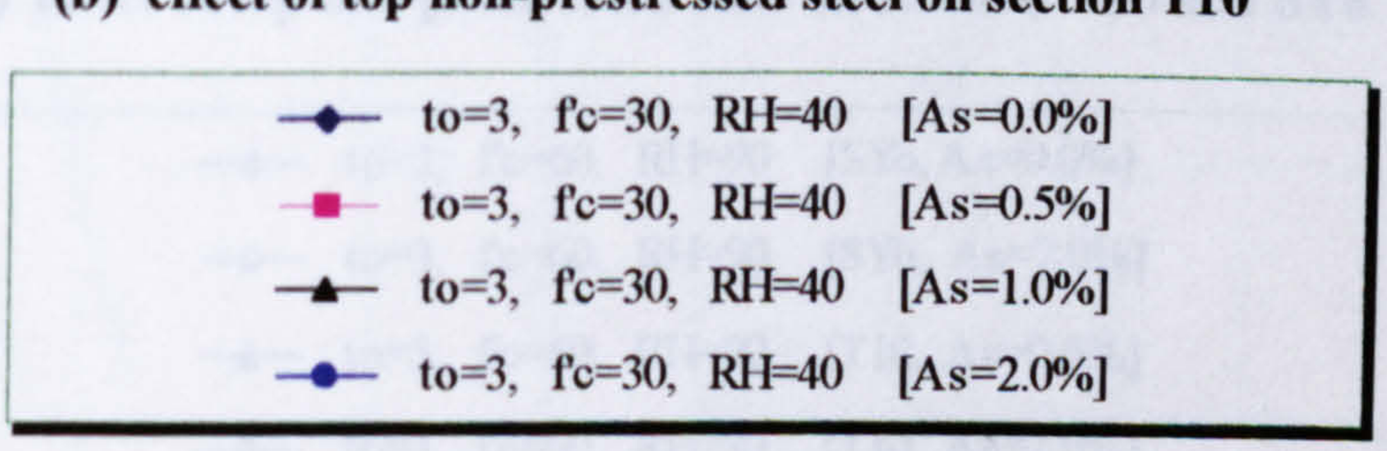

Figure 5.25: Effect of top non-prestressed steel on sections with maximum and minimum flexibility subject to the combination of f'_c and *RH* yielding maximum deformation

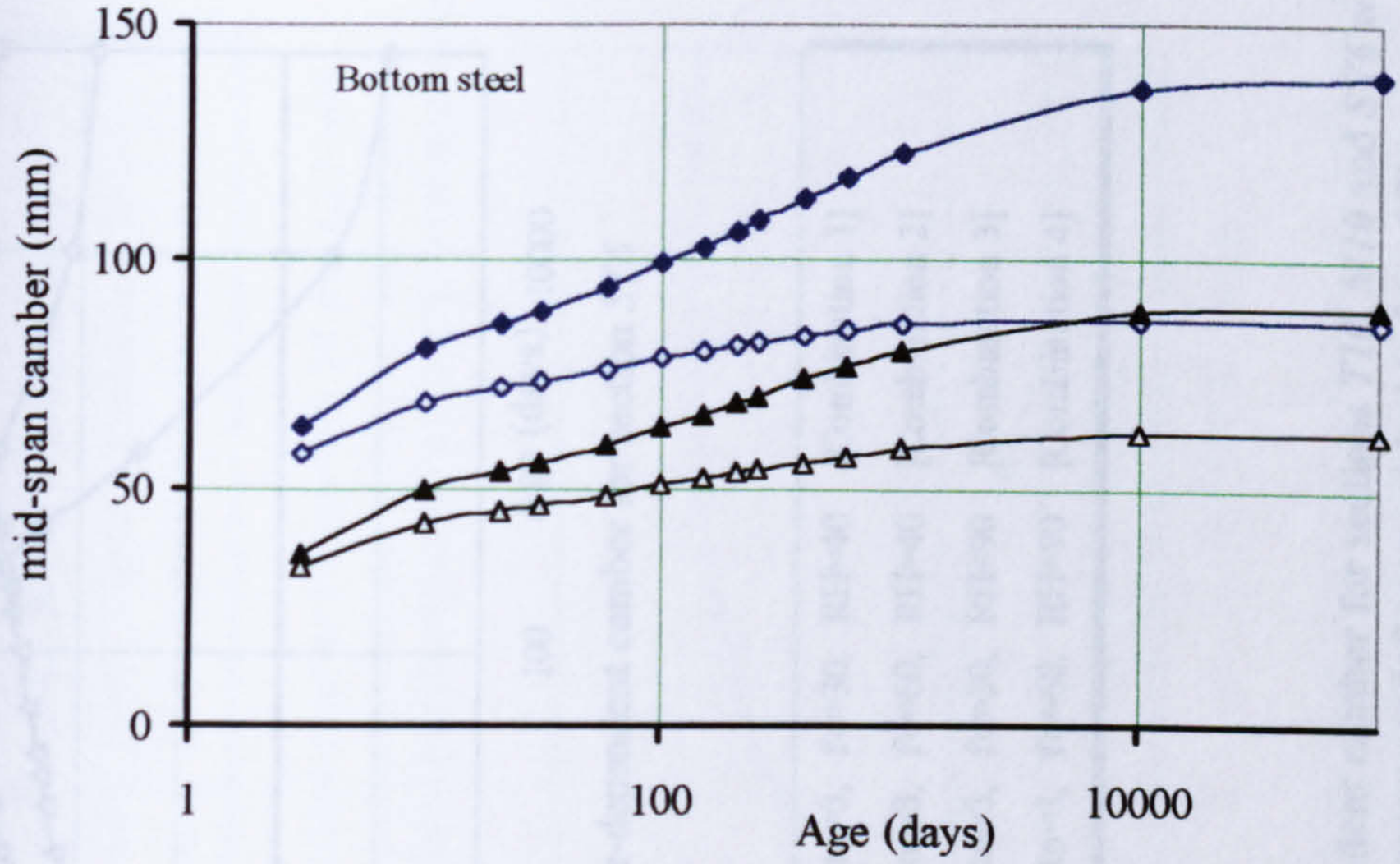

(a) effect of bottom non-prestressed steel on sections T10 and SY6

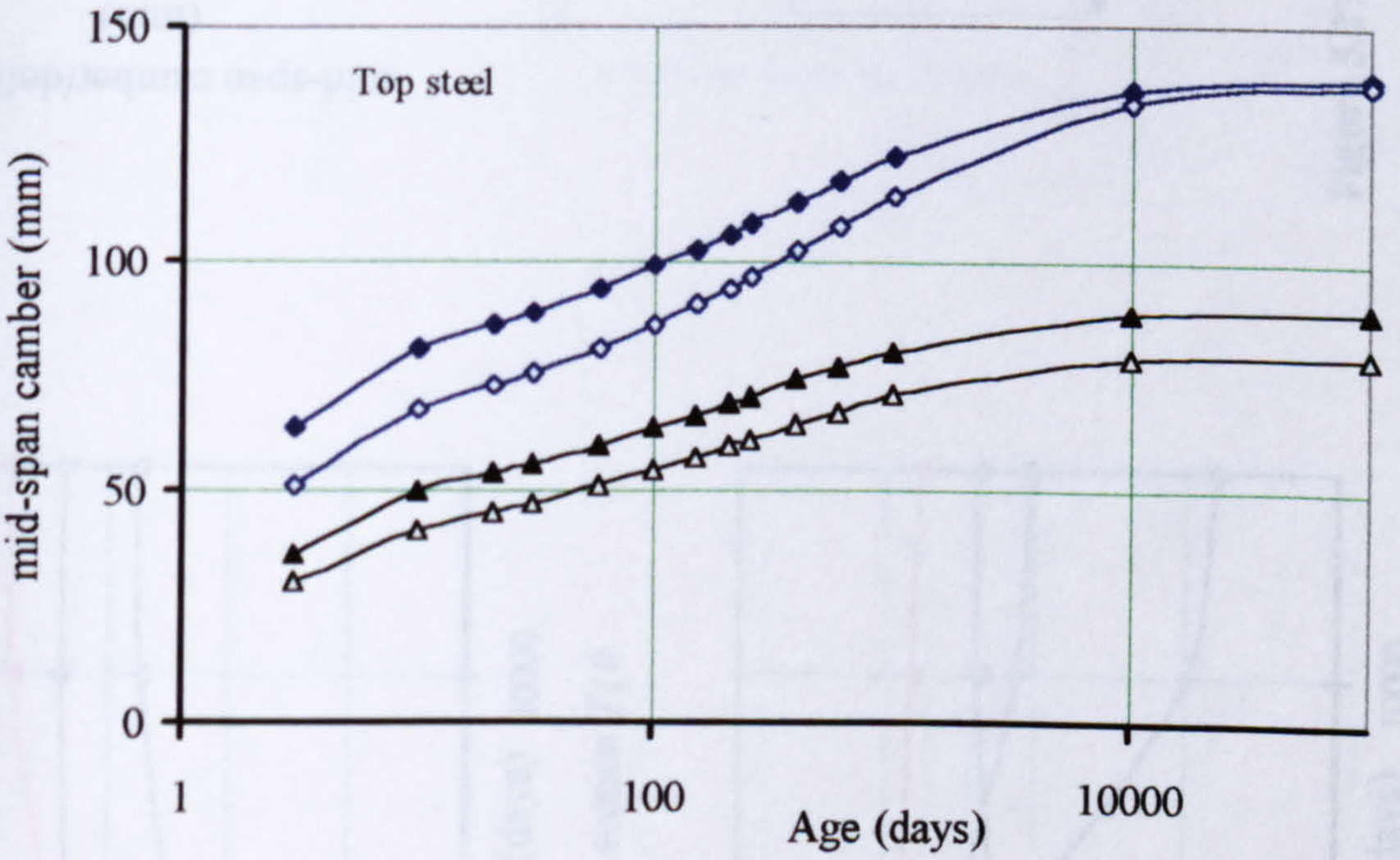

(b) effect of top non-prestressed steel on sections T10 and SY6

Figure 5.26: Effect of top and bottom non-prestressed steel on sections with maximum and minimum flexibility subject to the combination of f'_c and *RH* yielding minimum deformation.

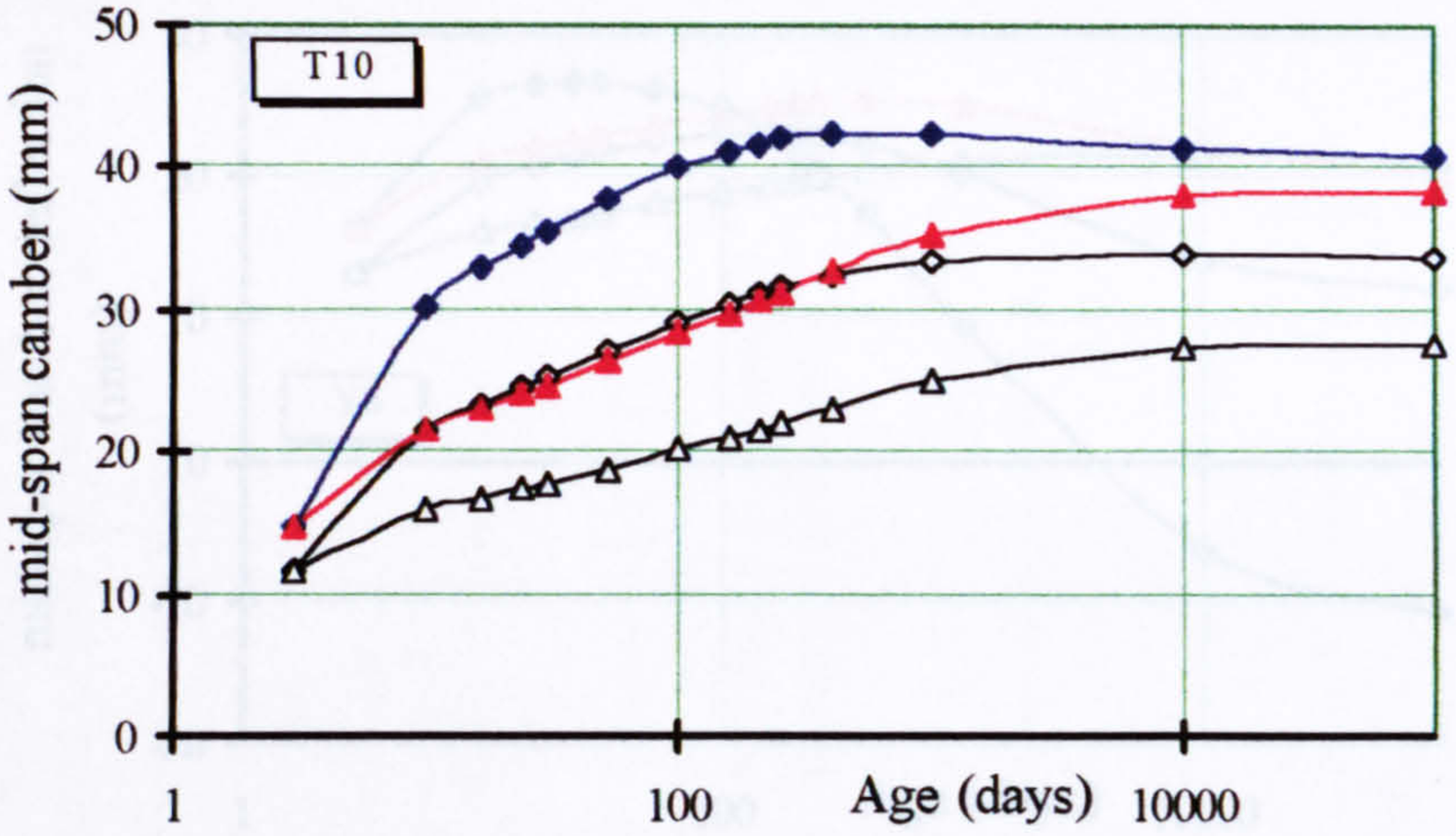

(a) Time-dependent camber for section *T10*

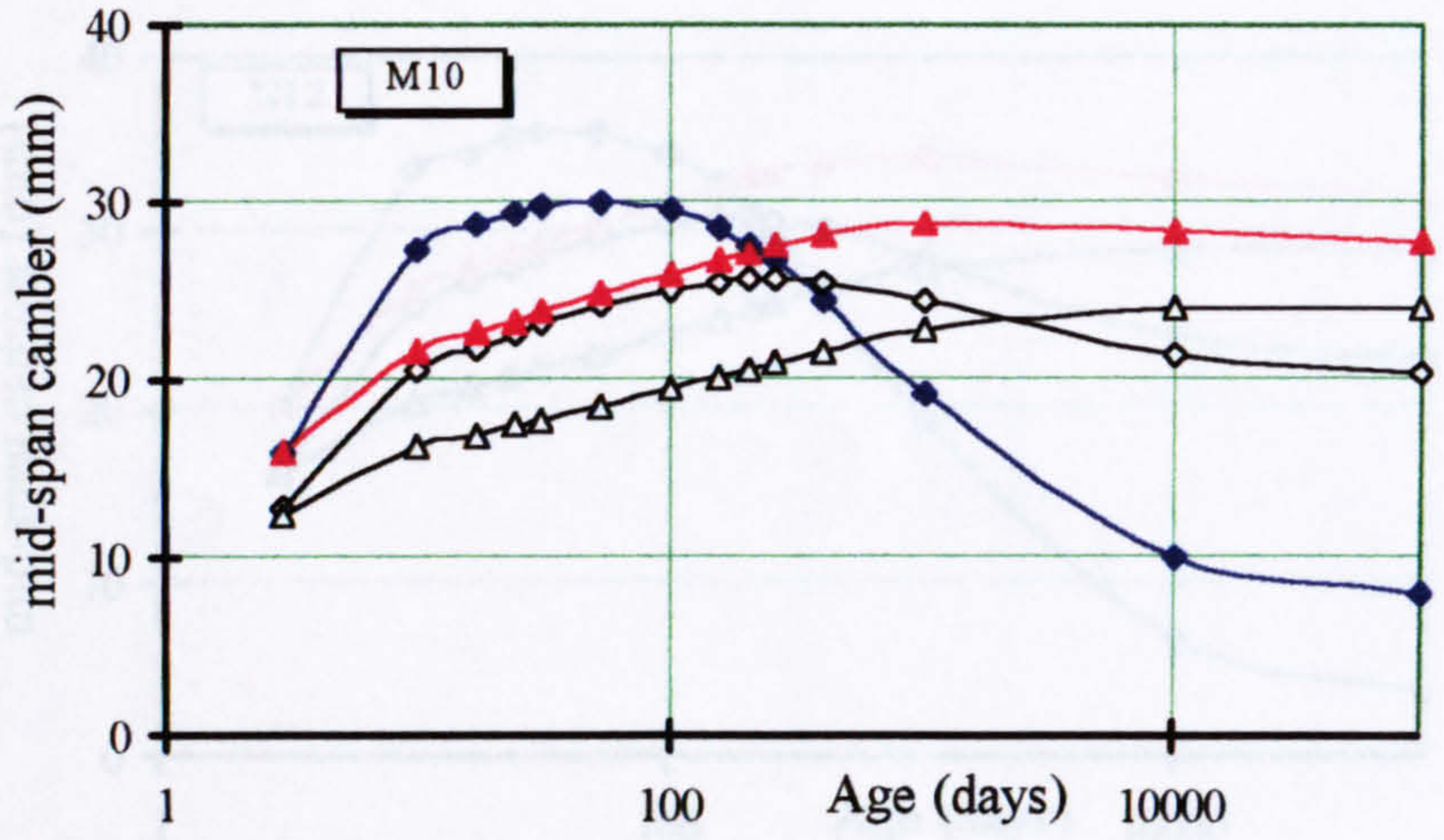

(b) Time-dependent camber for section *M10*

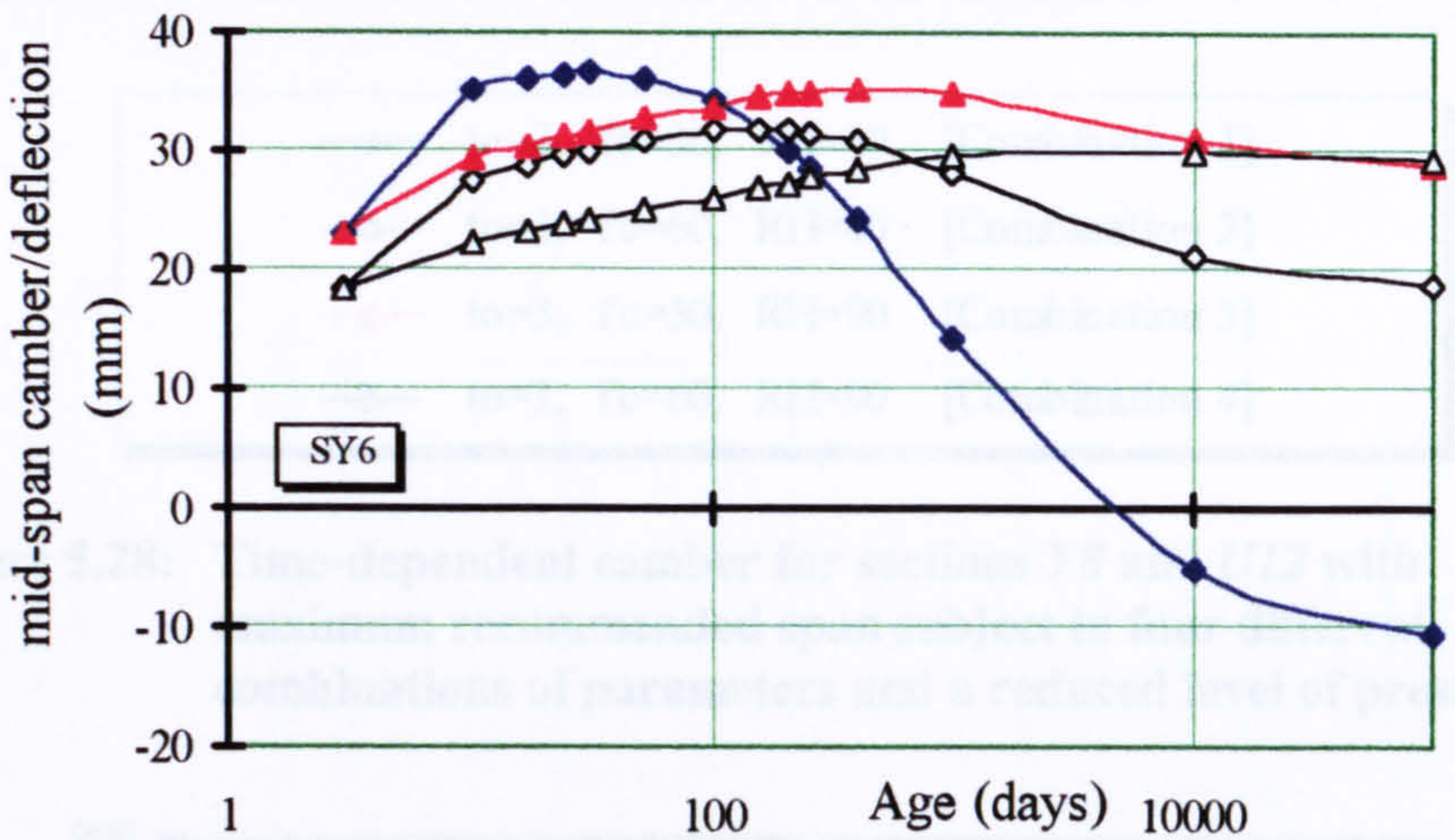

(c) Time-dependent camber for section *SY6*

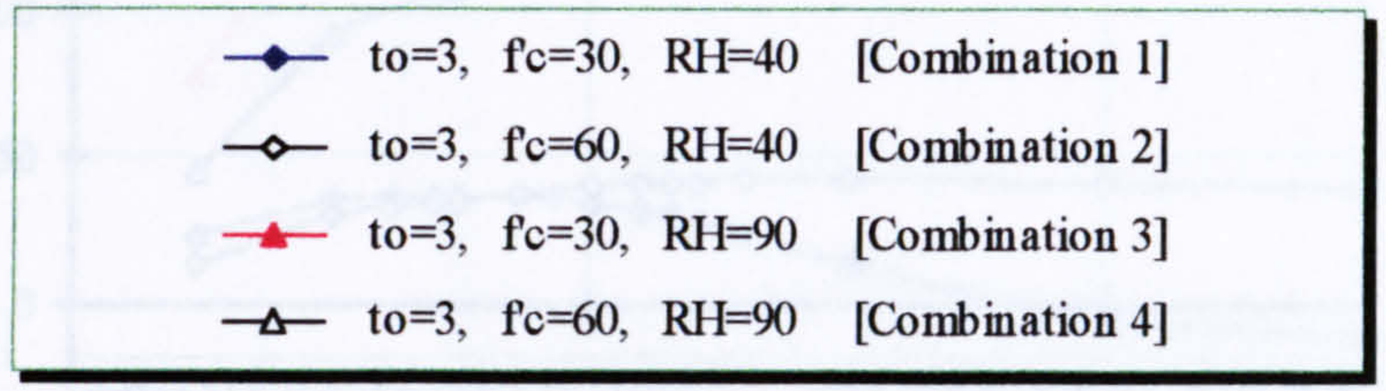

Figure 5.27: Time-dependent camber for sections *T10*, *M10* and *SY6* with maximum recommended span subject to four different combinations of parameters and a reduced level of prestress

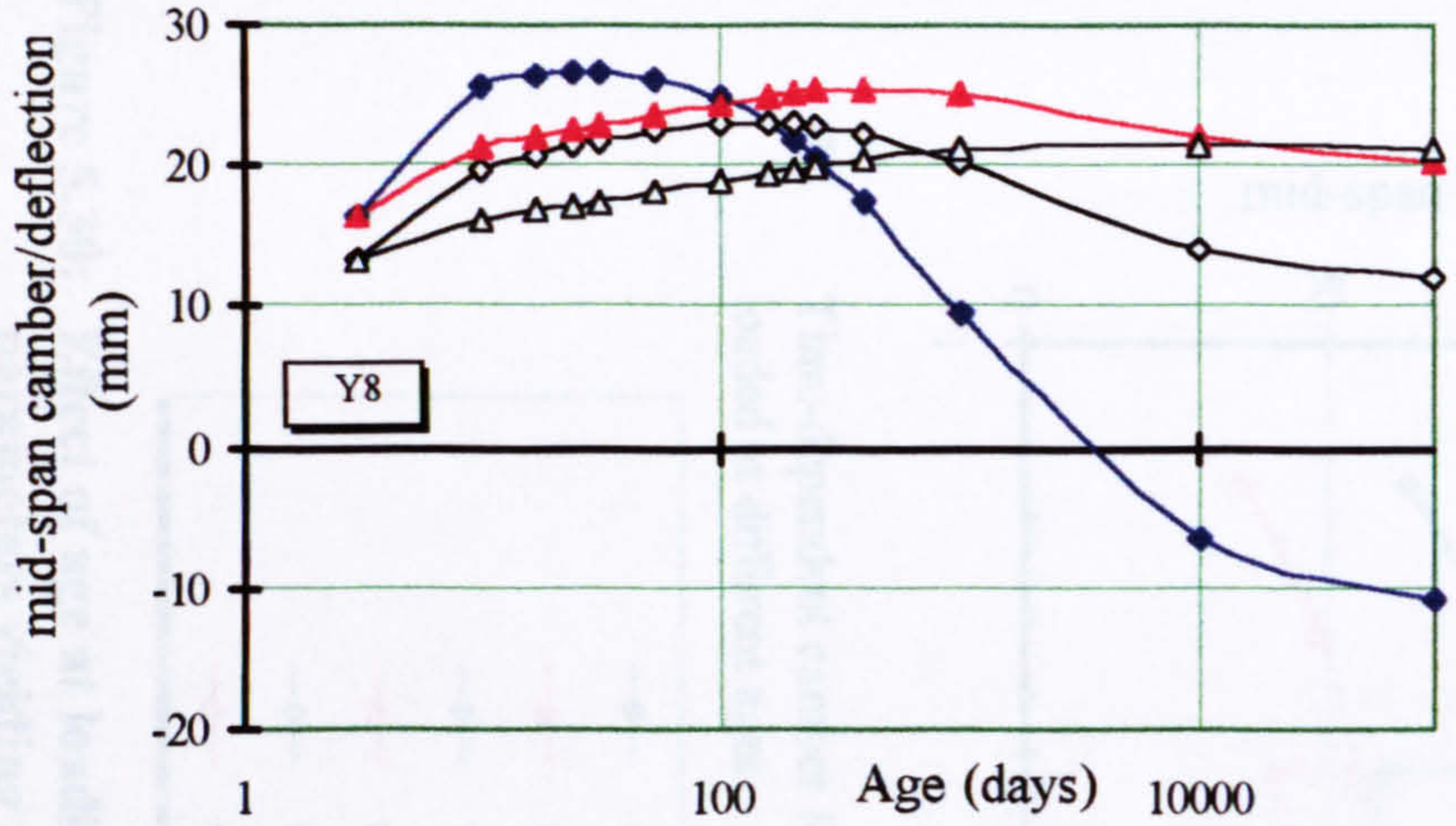

(a) Time-dependent camber for section *Y8*

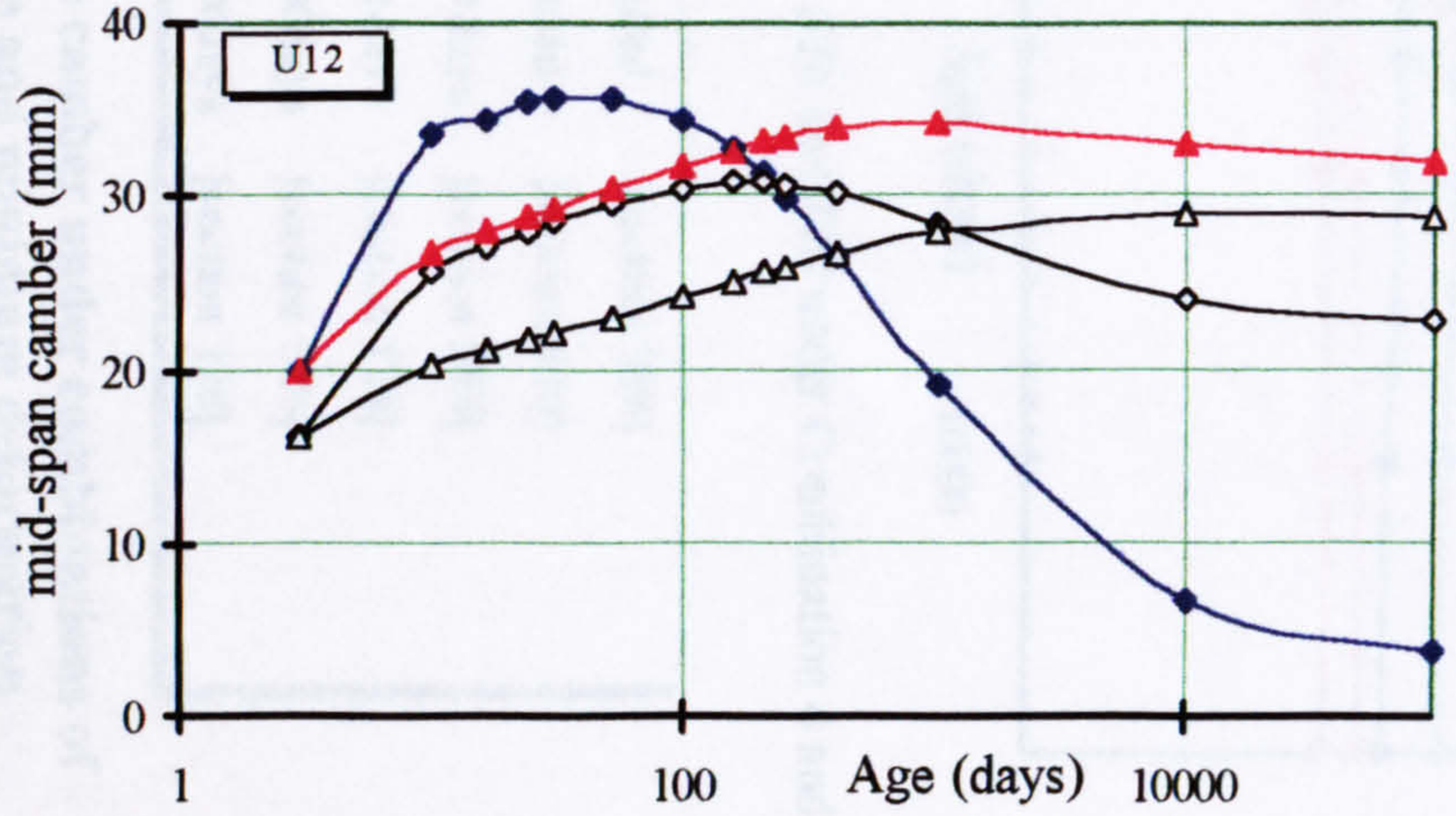

(b) Time-dependent camber for section *U12*

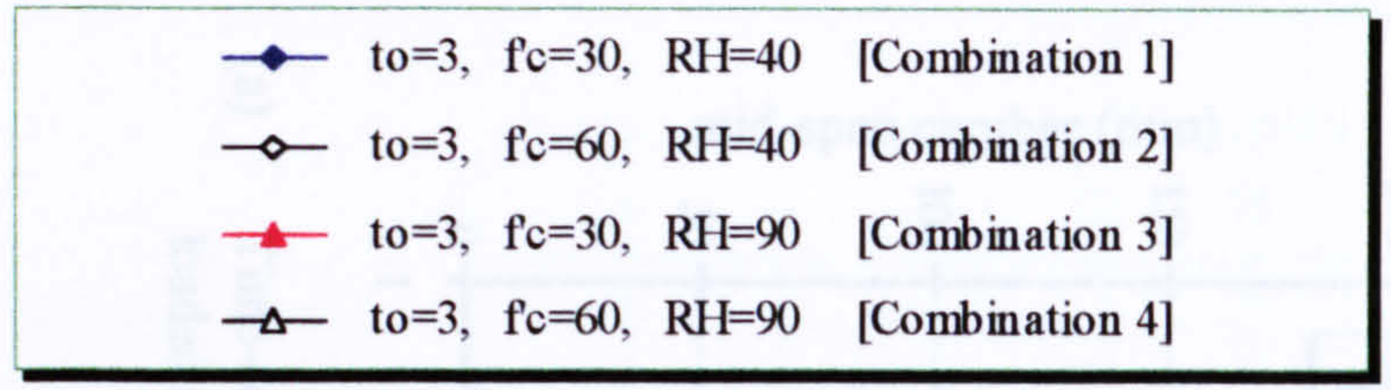

Figure 5.28: Time-dependent camber for sections *Y8* and *U12* with maximum recommended span subject to four different combinations of parameters and a reduced level of prestress.

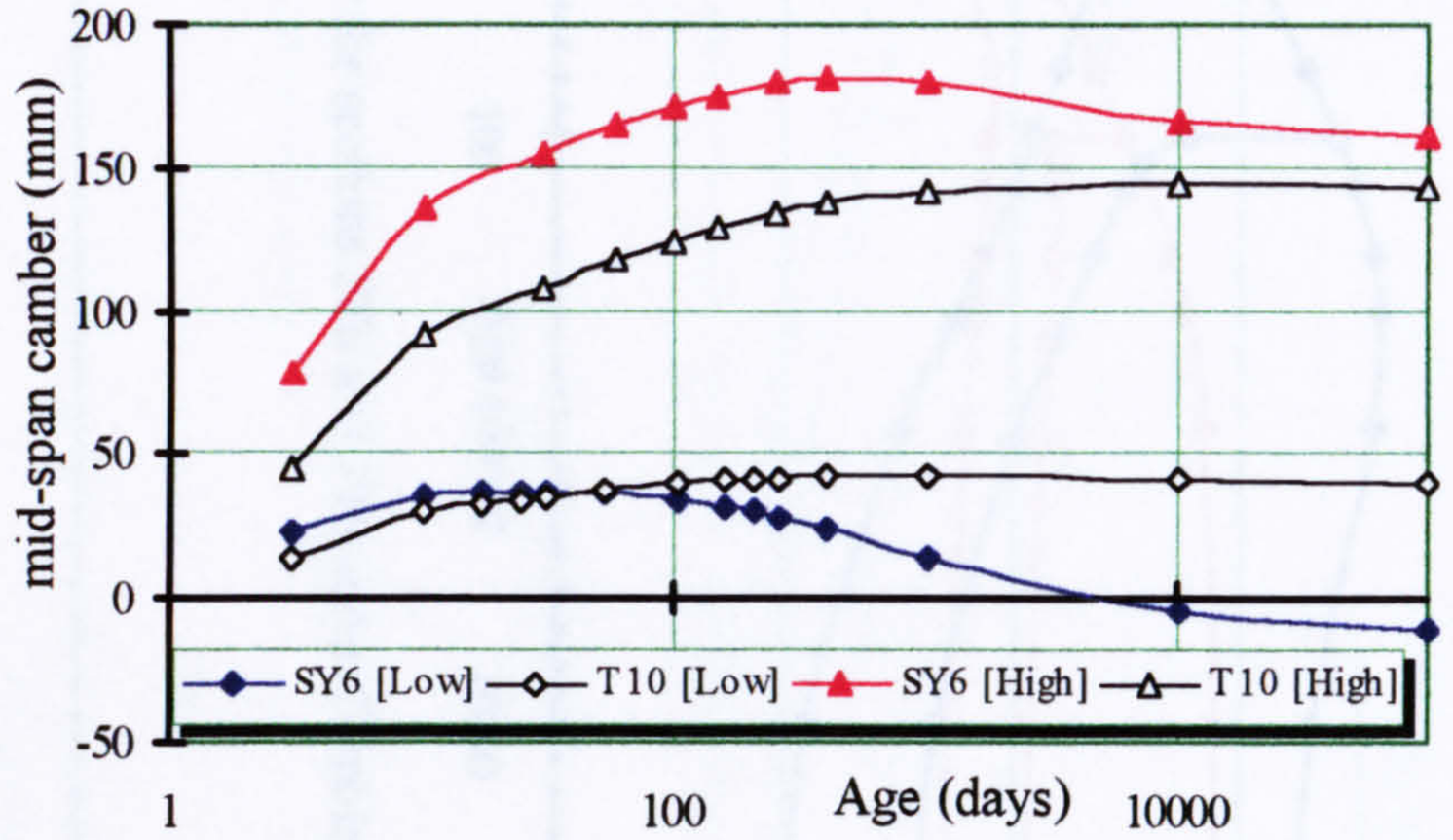

Figure 5.29: Camber of prestressed section with maximum recommended span subjected to the higher and the reduced initial stress

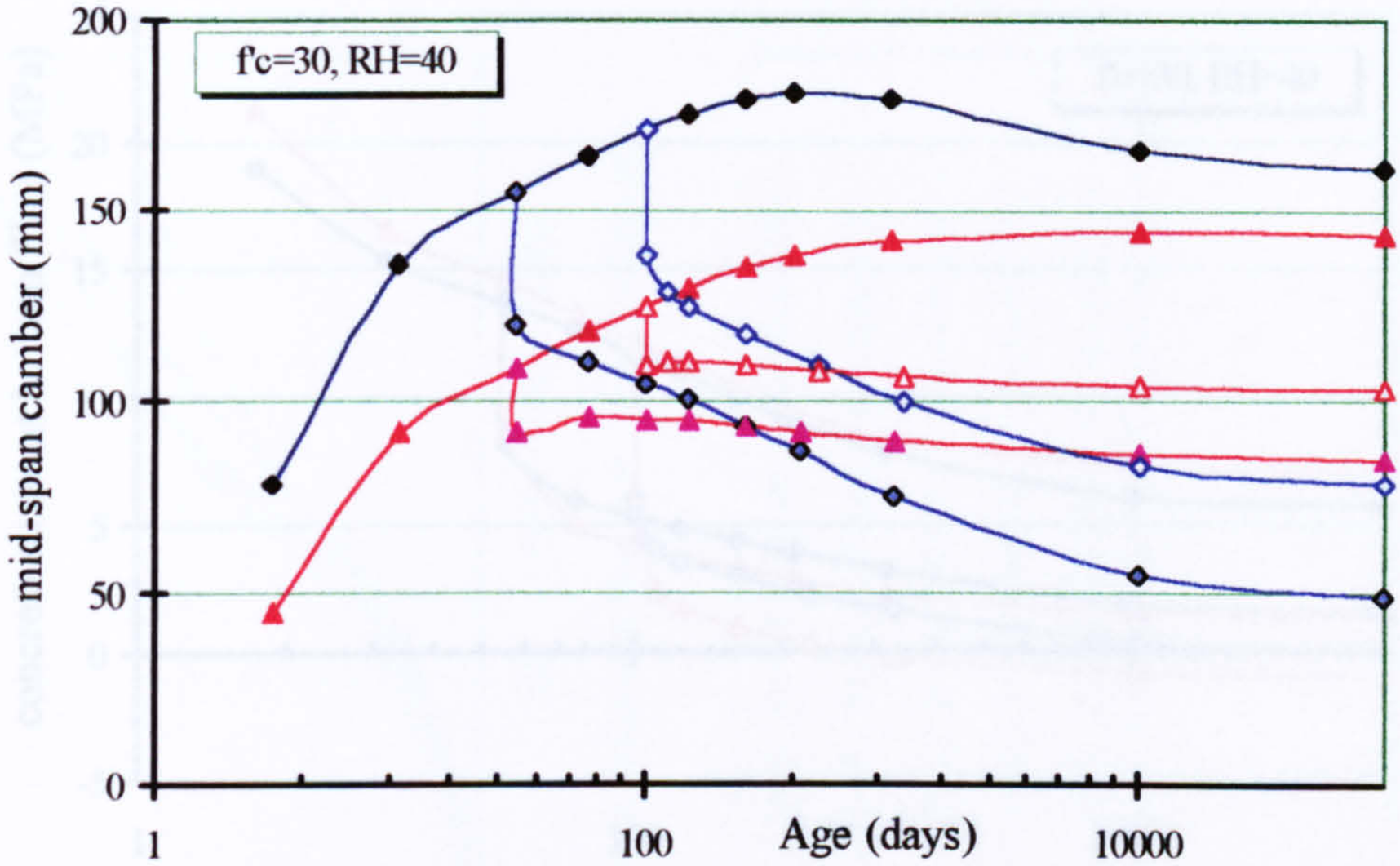

(a) Time-dependent camber for sections *SY6* and *T10* under Combination 1 and loaded at different ages.

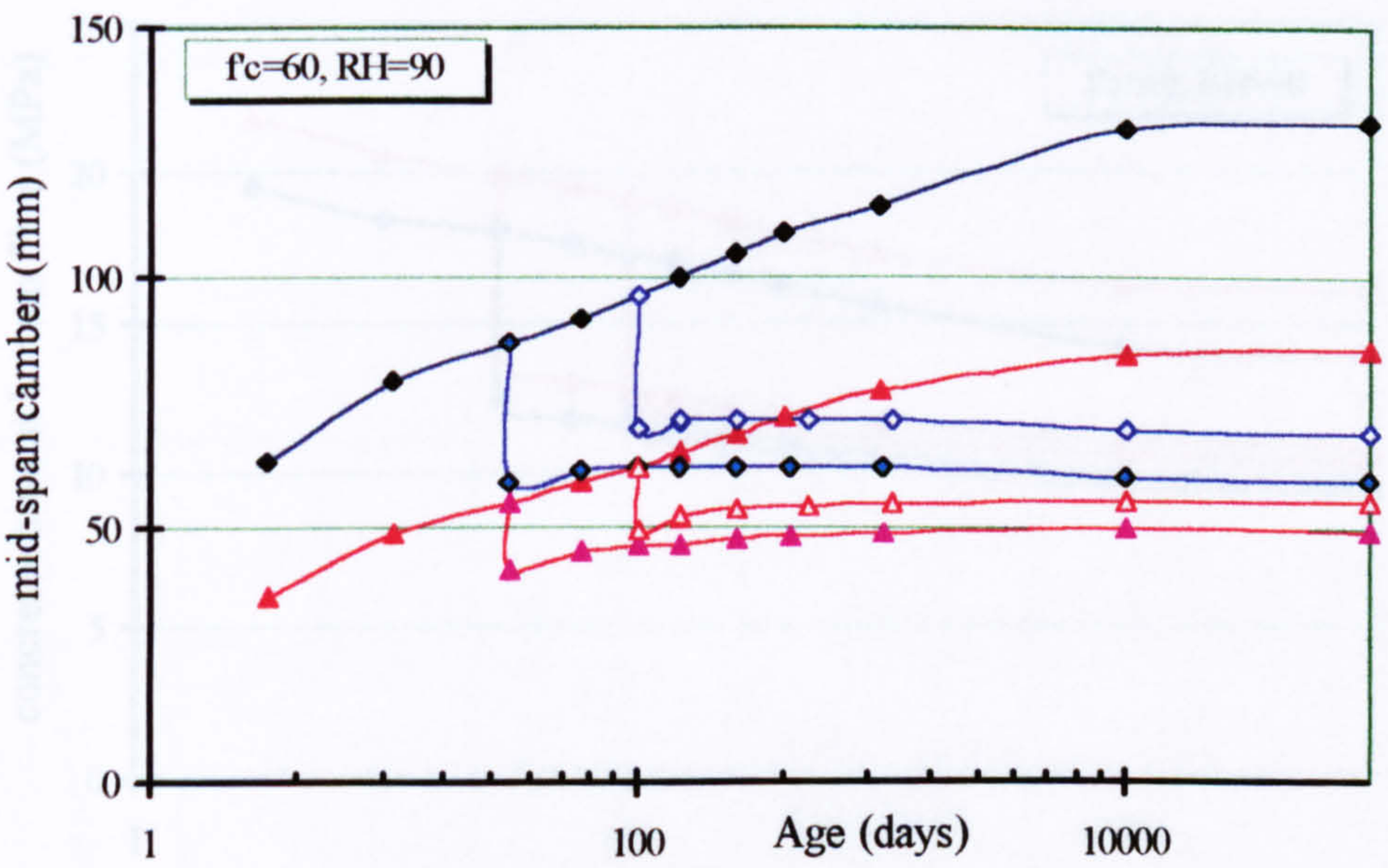

(b) Time-dependent camber for sections *SY6* and *T10* under Combination 4 and loaded at different ages.

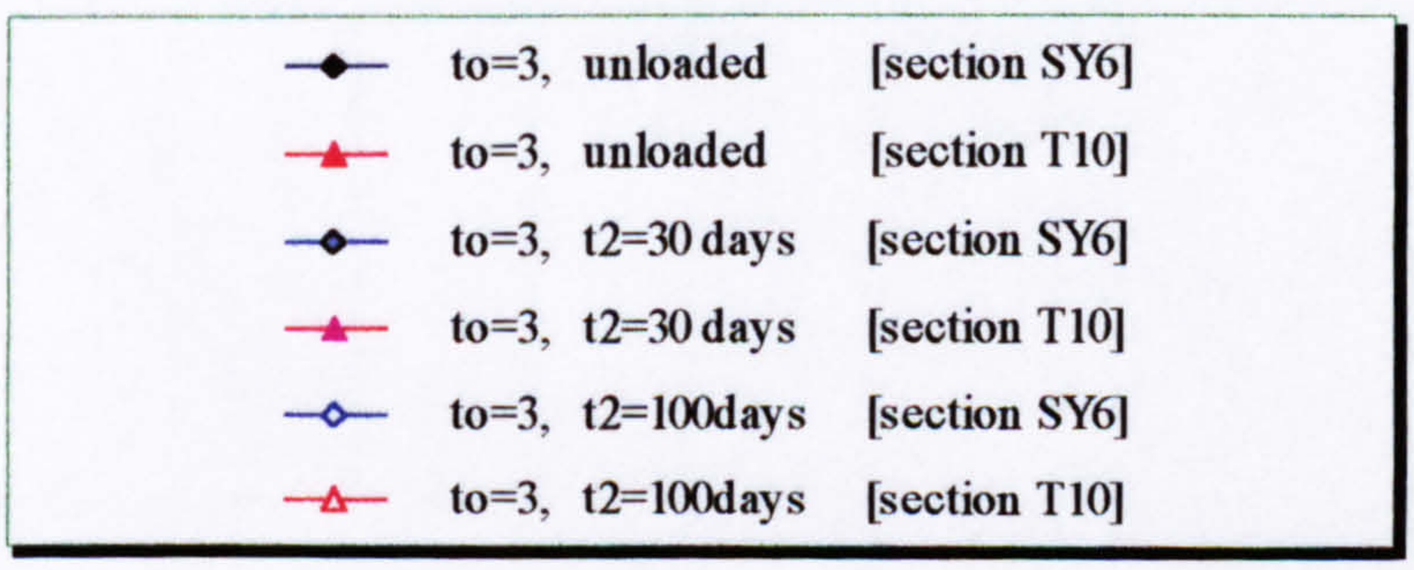

Figure 5.30: Effect of age at loading on the camber under combinations of parameters yielding maximum and minimum deformation.

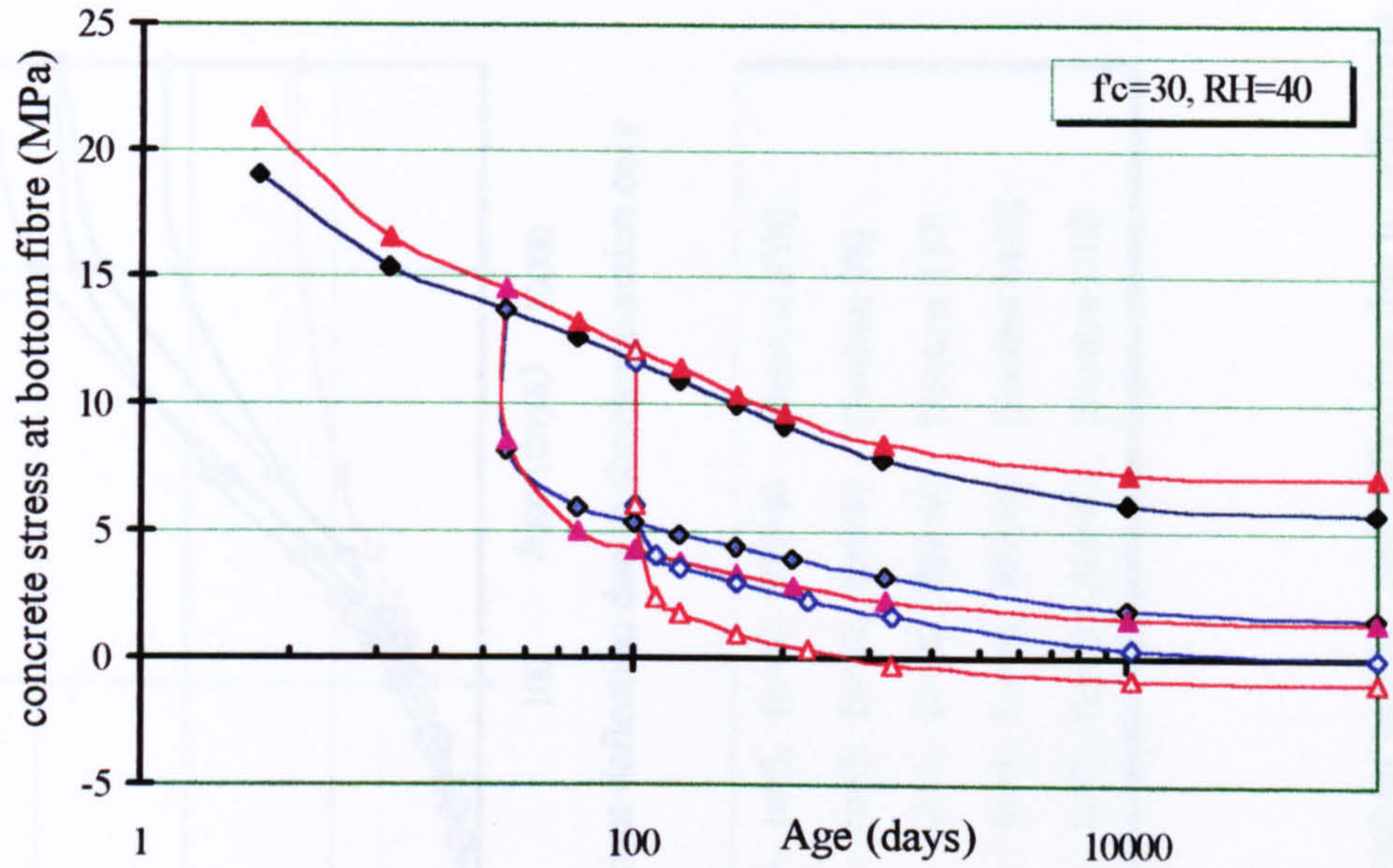

(a) Time-dependent stresses at the bottom fibre for sections *SY6* and *T10* under Combination 1 and loaded at different ages.

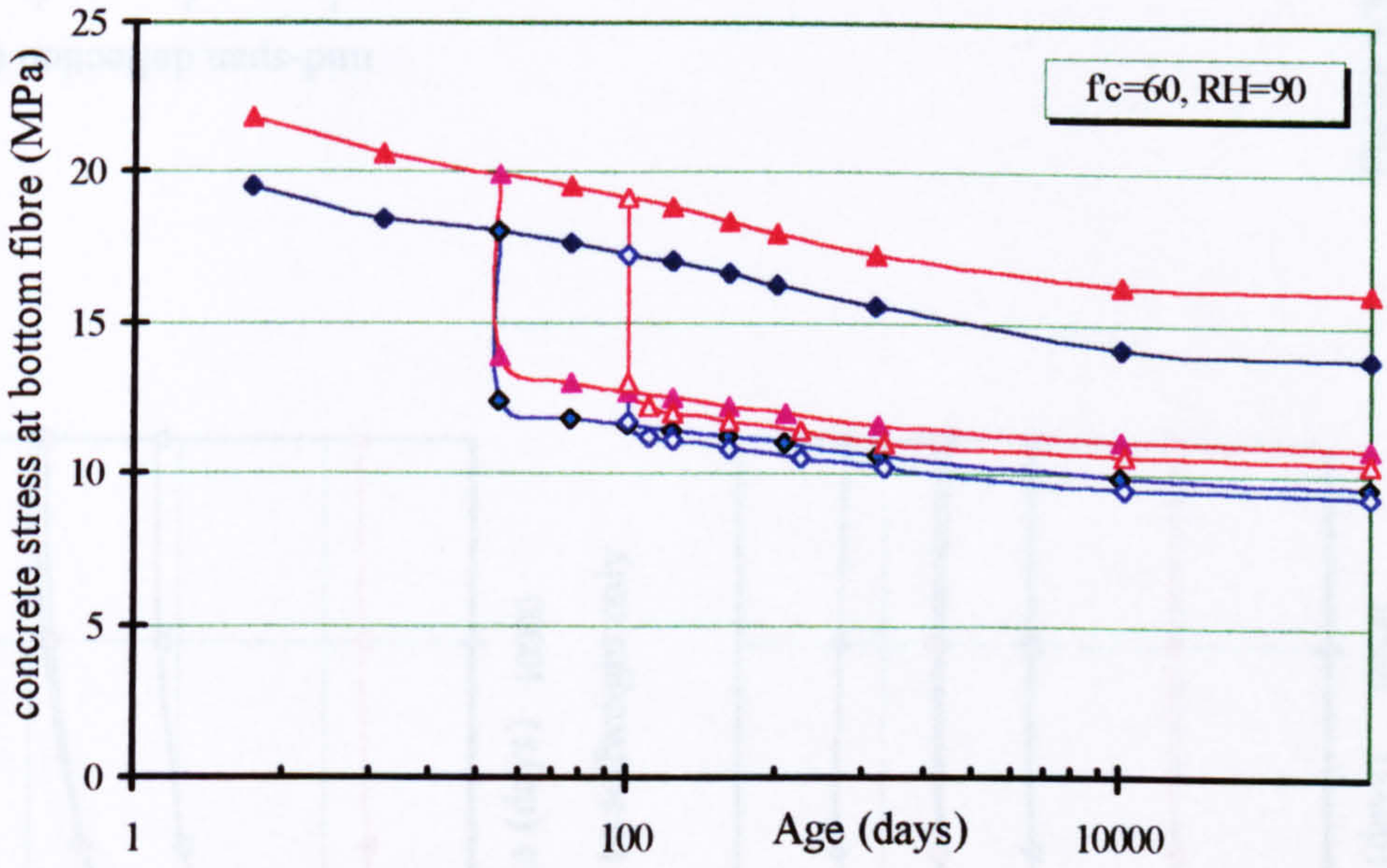

(b) Time-dependent stresses at the bottom fibre for sections *SY6* and *T10* under Combination 4 and loaded at different ages.

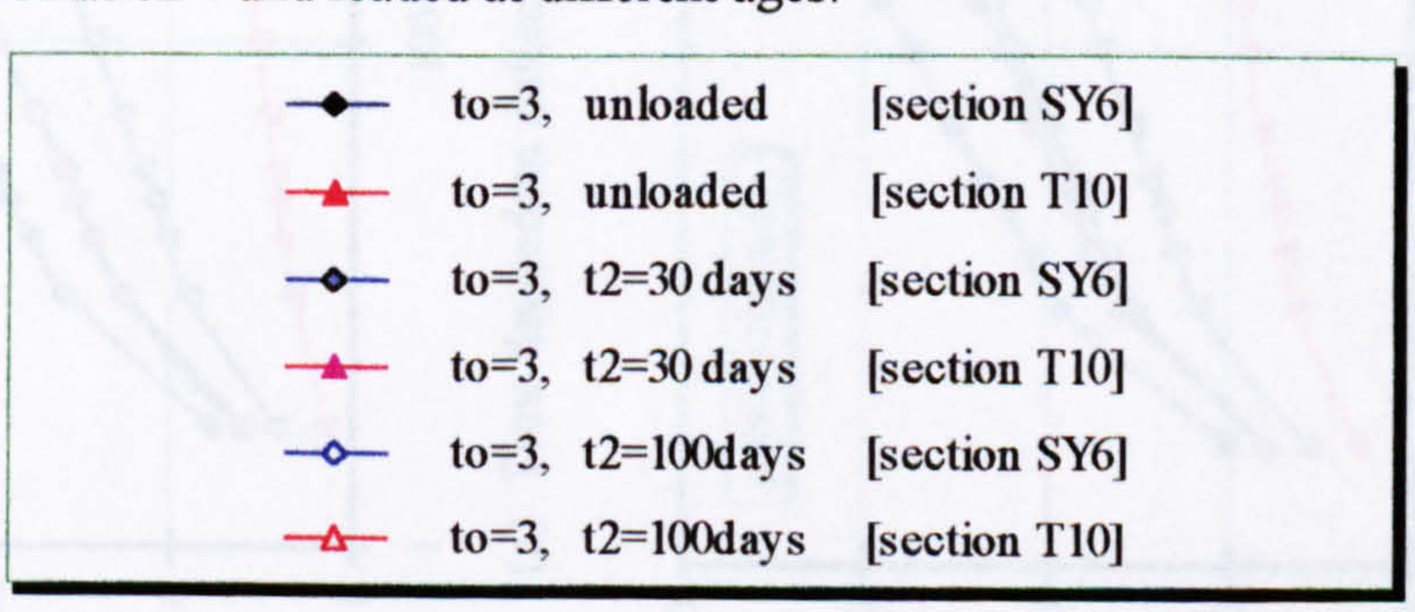

Figure 5.31: Effect of age at loading on stresses at the bottom fibre under the combinations of parameters yielding maximum and minimum deformation.

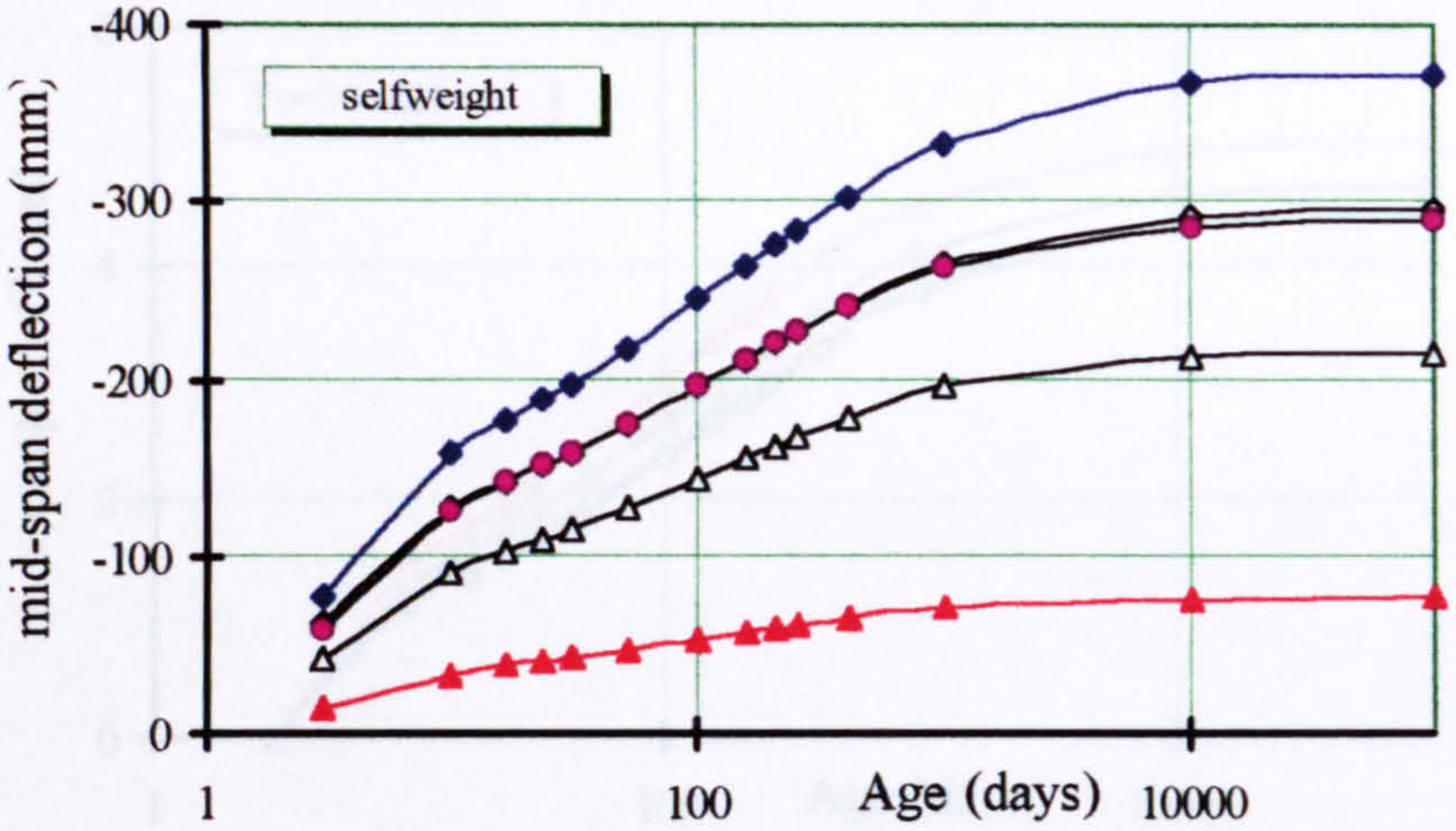

(a) Time dependent deflection due to selfweight only

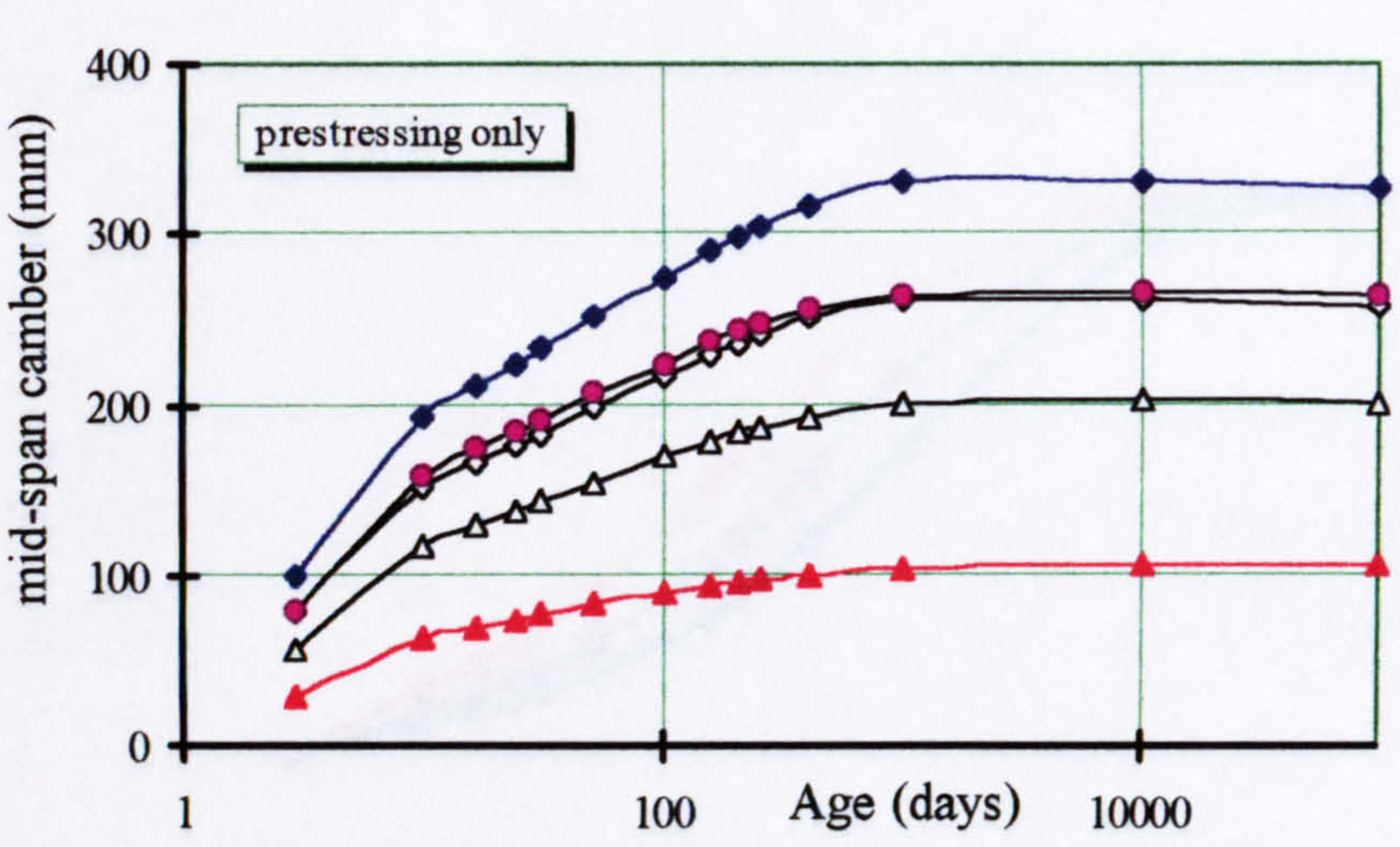

(b) Time-dependent camber due to prestressing only

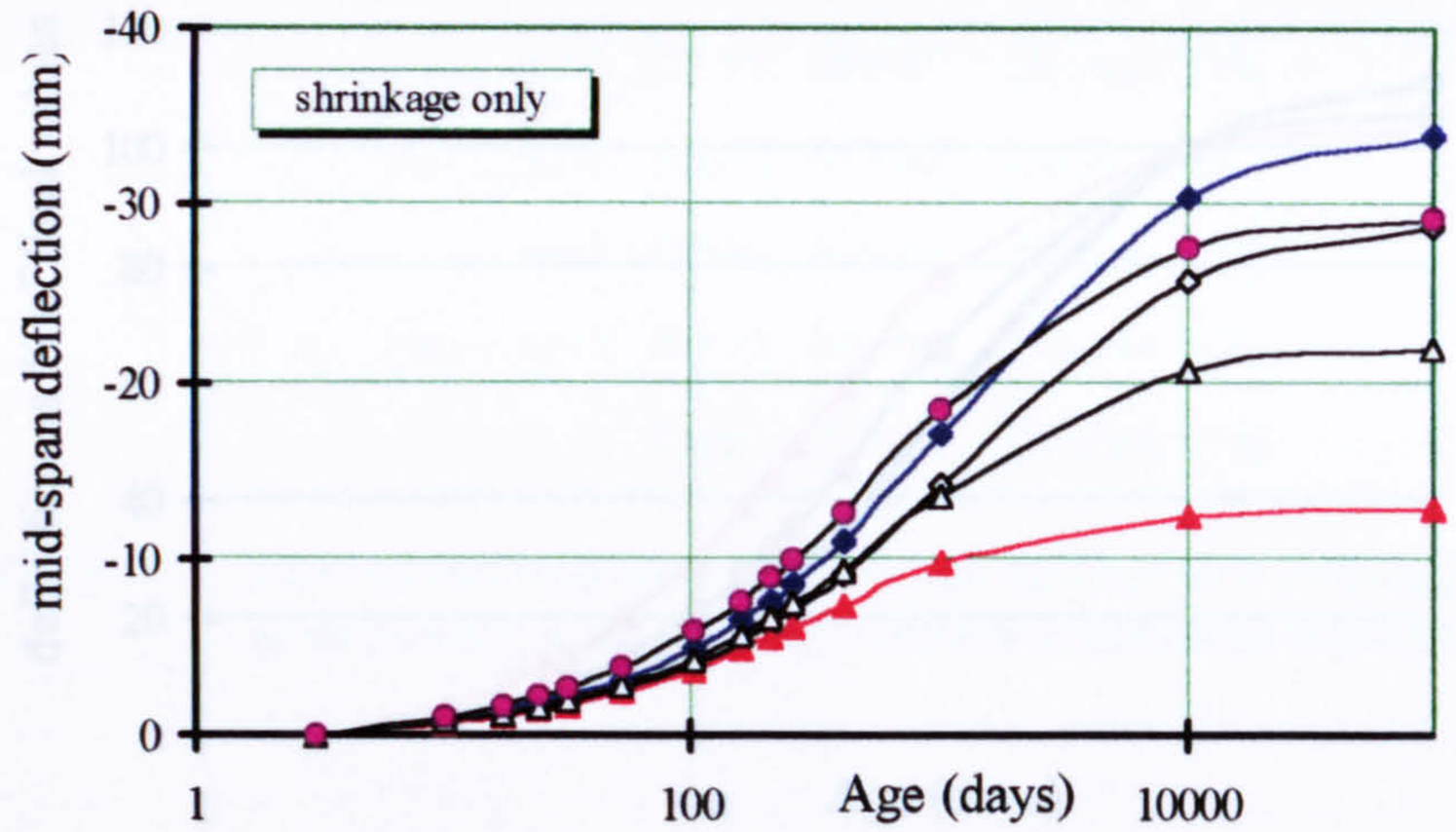

(c) Time-dependent deflection due to shrinkage action only

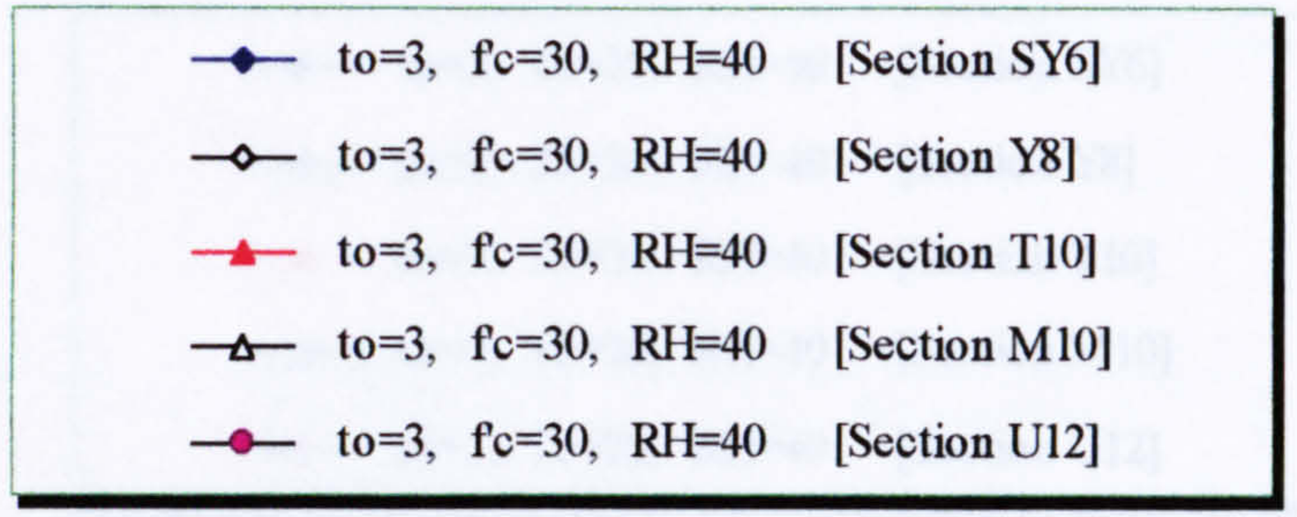

Figure 5.32: Time-dependent camber and deflection due to selfweight, prestressing and shrinkage actions considered separately

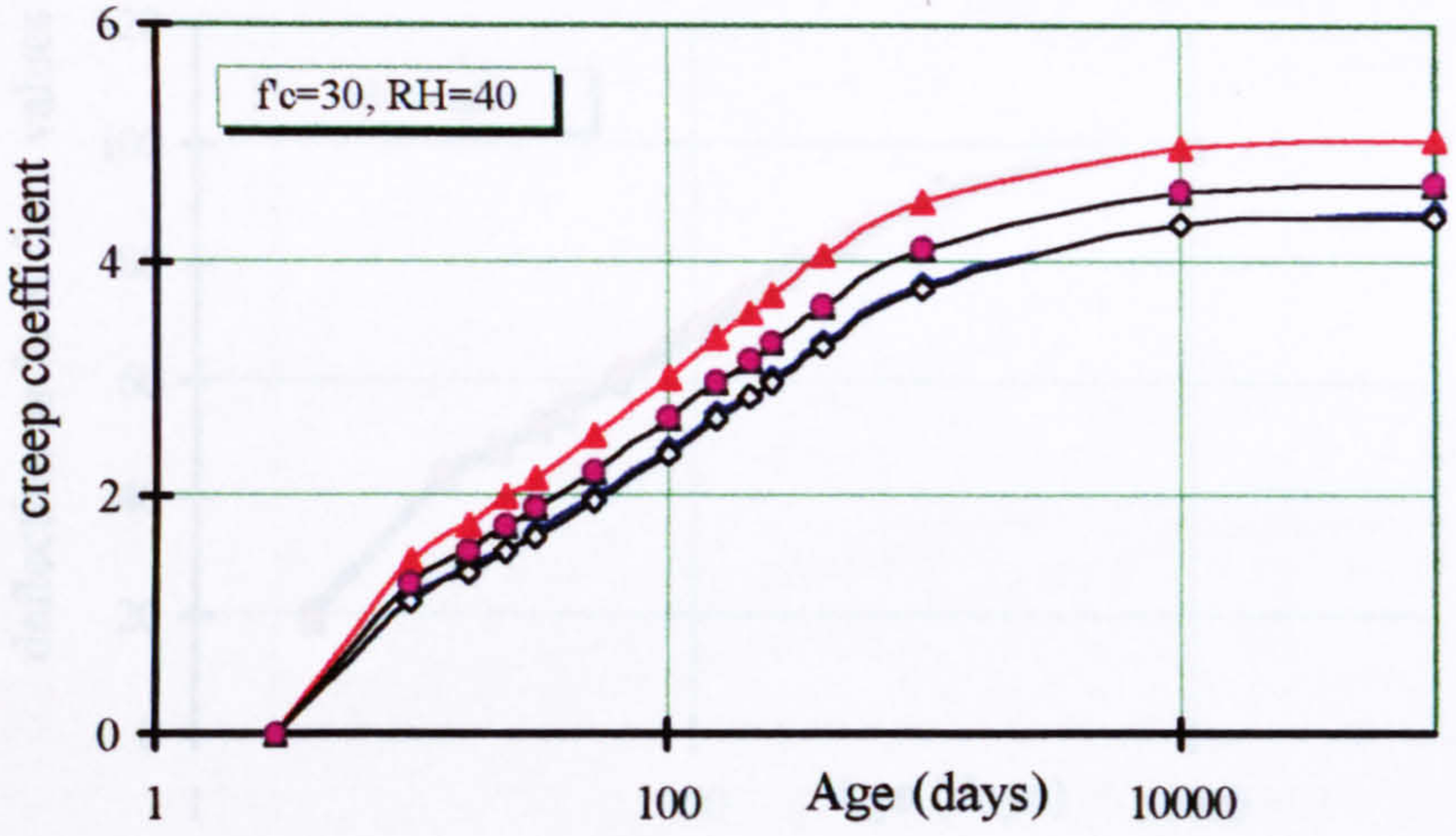

(a) creep coefficient for different sections

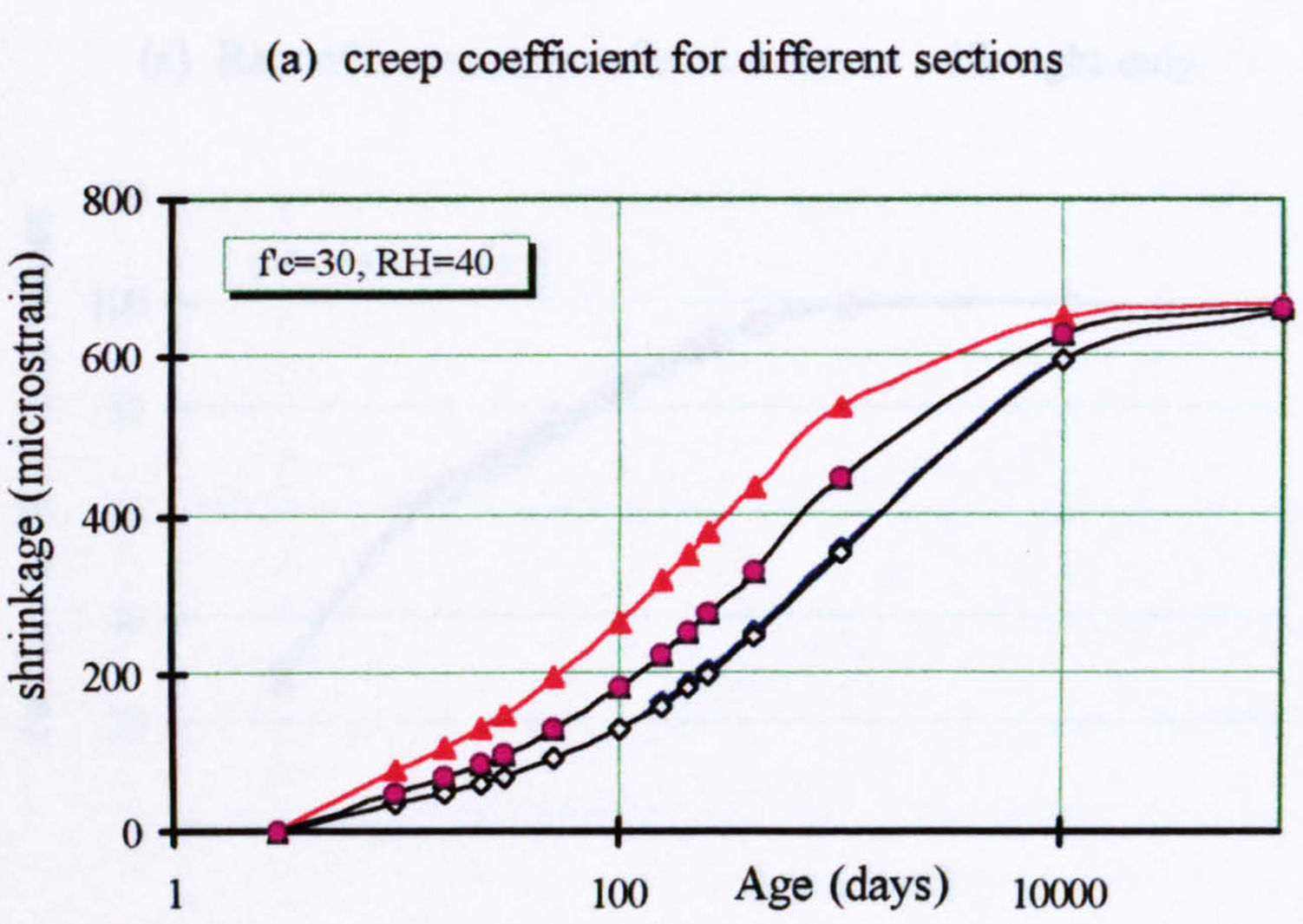

(b) shrinkage deformation for different sections

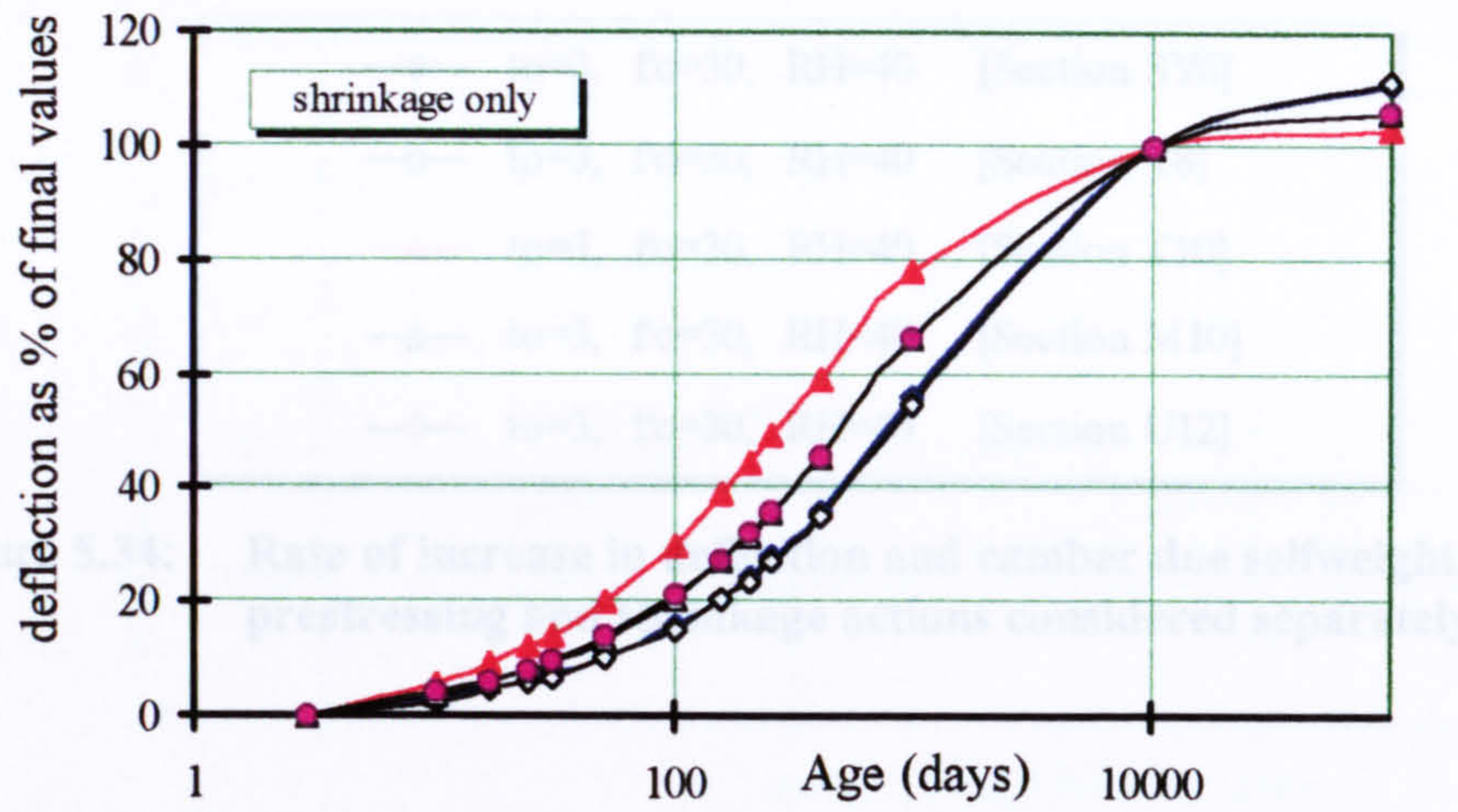

(c) Rate of increase in deflection due to shrinkage only

to=3, f'c=30, RH=40 [Section SY6]
to=3, f'c=30, RH=40 [Section Y8]
to=3, f'c=30, RH=40 [Section T10]
to=3, f'c=30, RH=40 [Section M10]
to=3, f'c=30, RH=40 [Section U12]

Figure 5.33: Creep and shrinkage properties for different sections

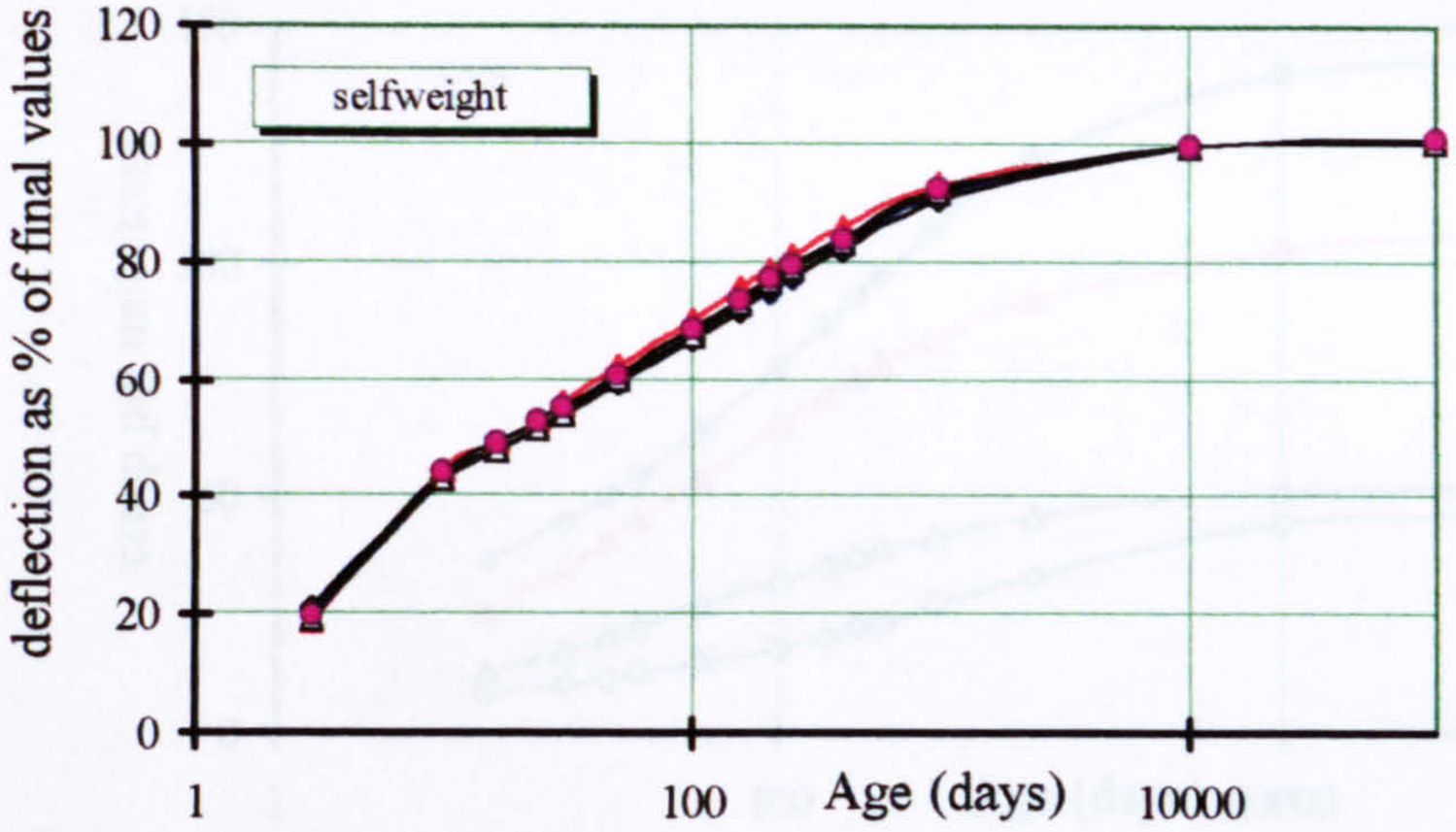

(a) Rate of increase in deflection due to selfweight only

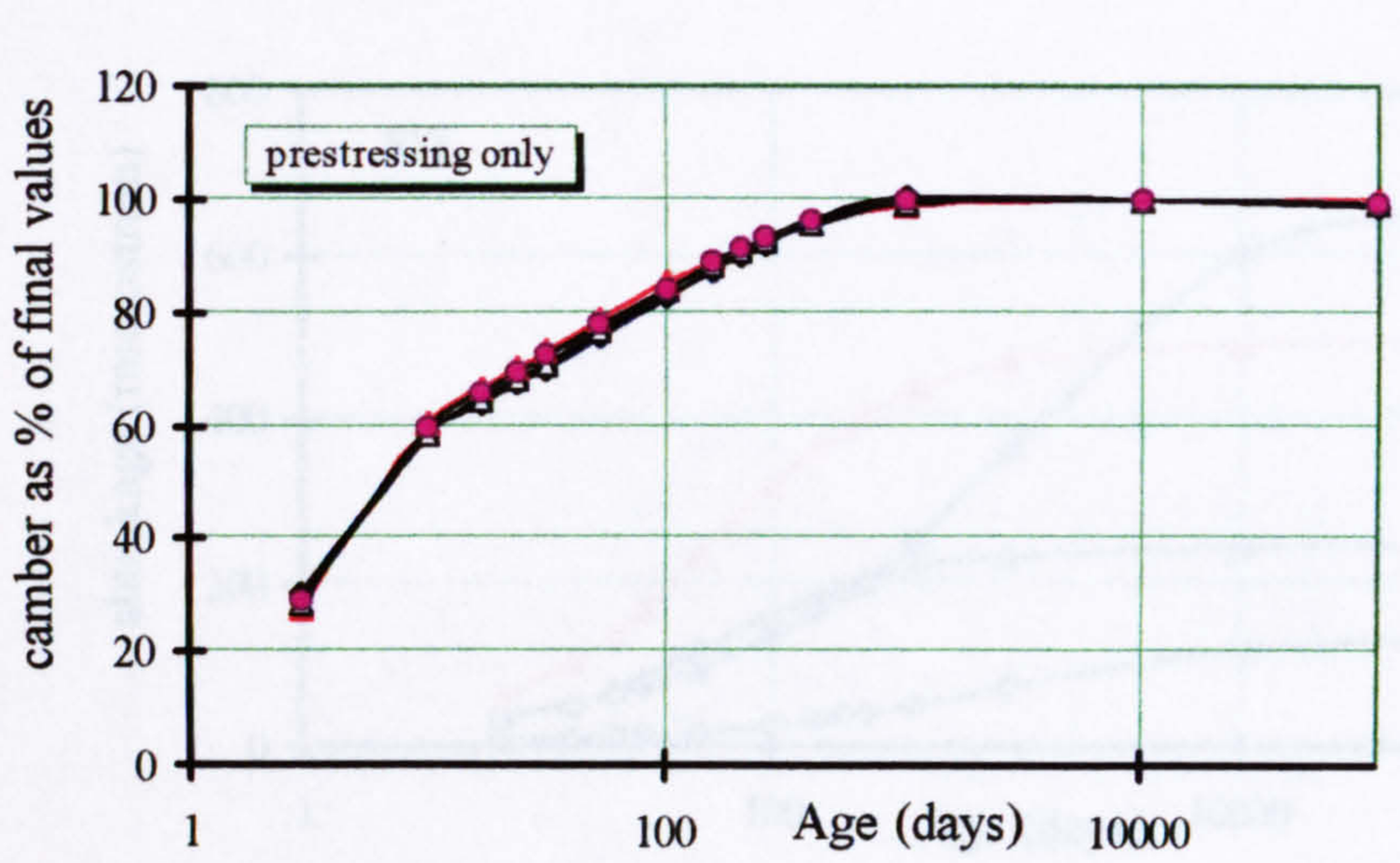

(b) Rate of increase in camber due to prestressing only

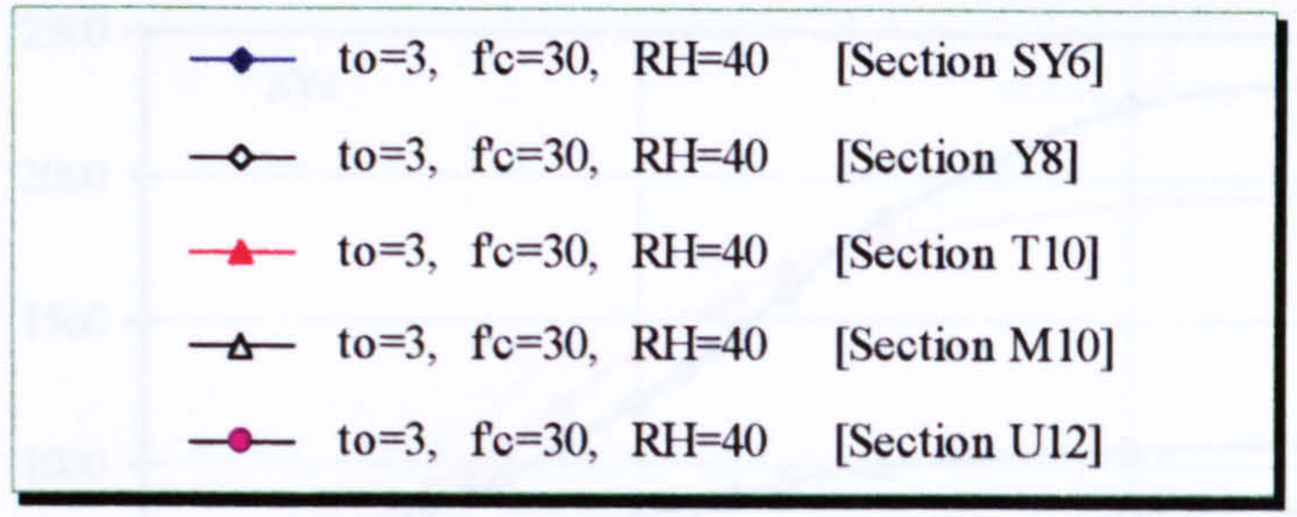

Figure 5.34: Rate of increase in deflection and camber due selfweight, prestressing and shrinkage actions considered separately

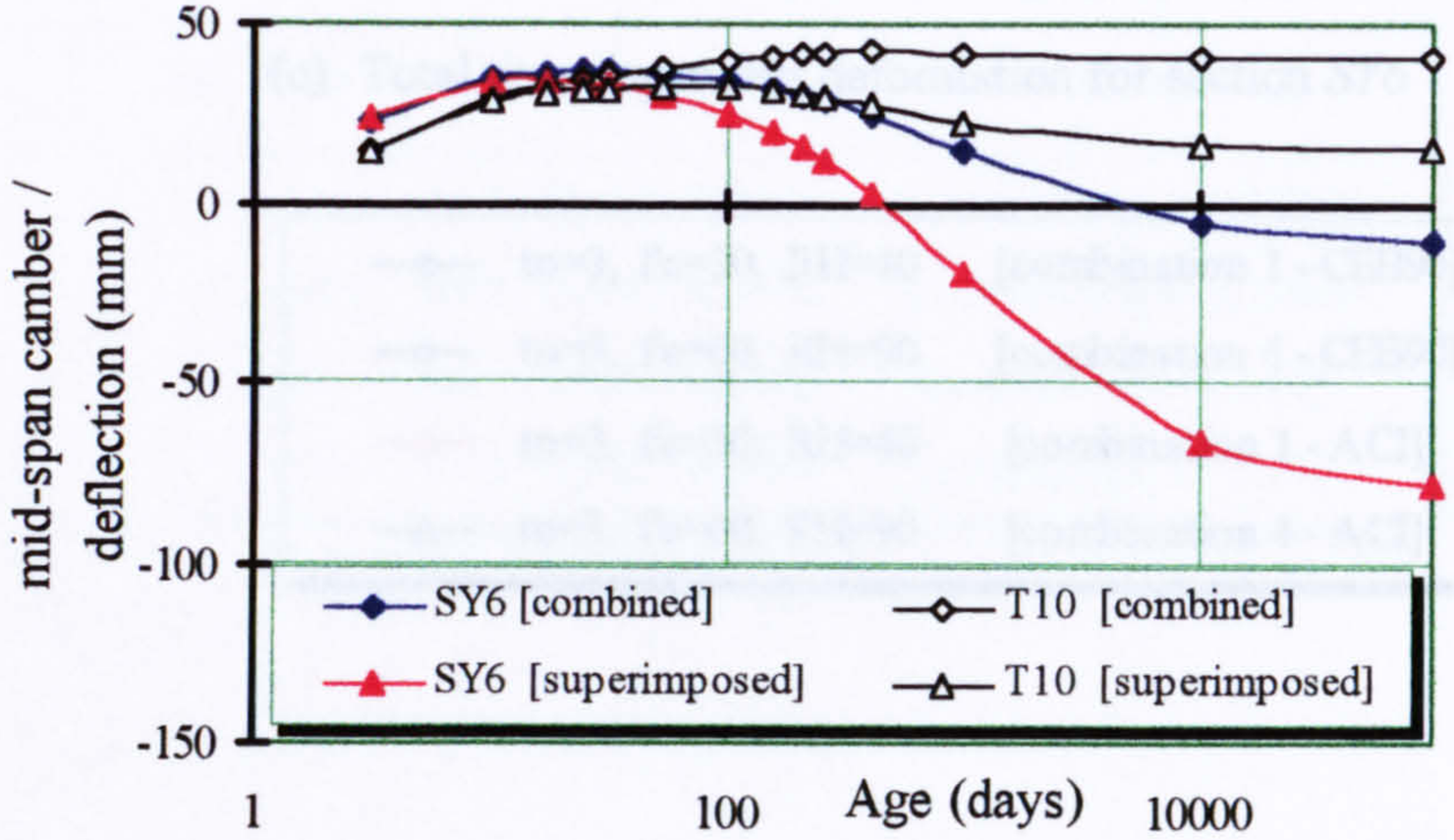

Figure 5.35: Comparison for time-dependent deflections between combined and separate analyses.

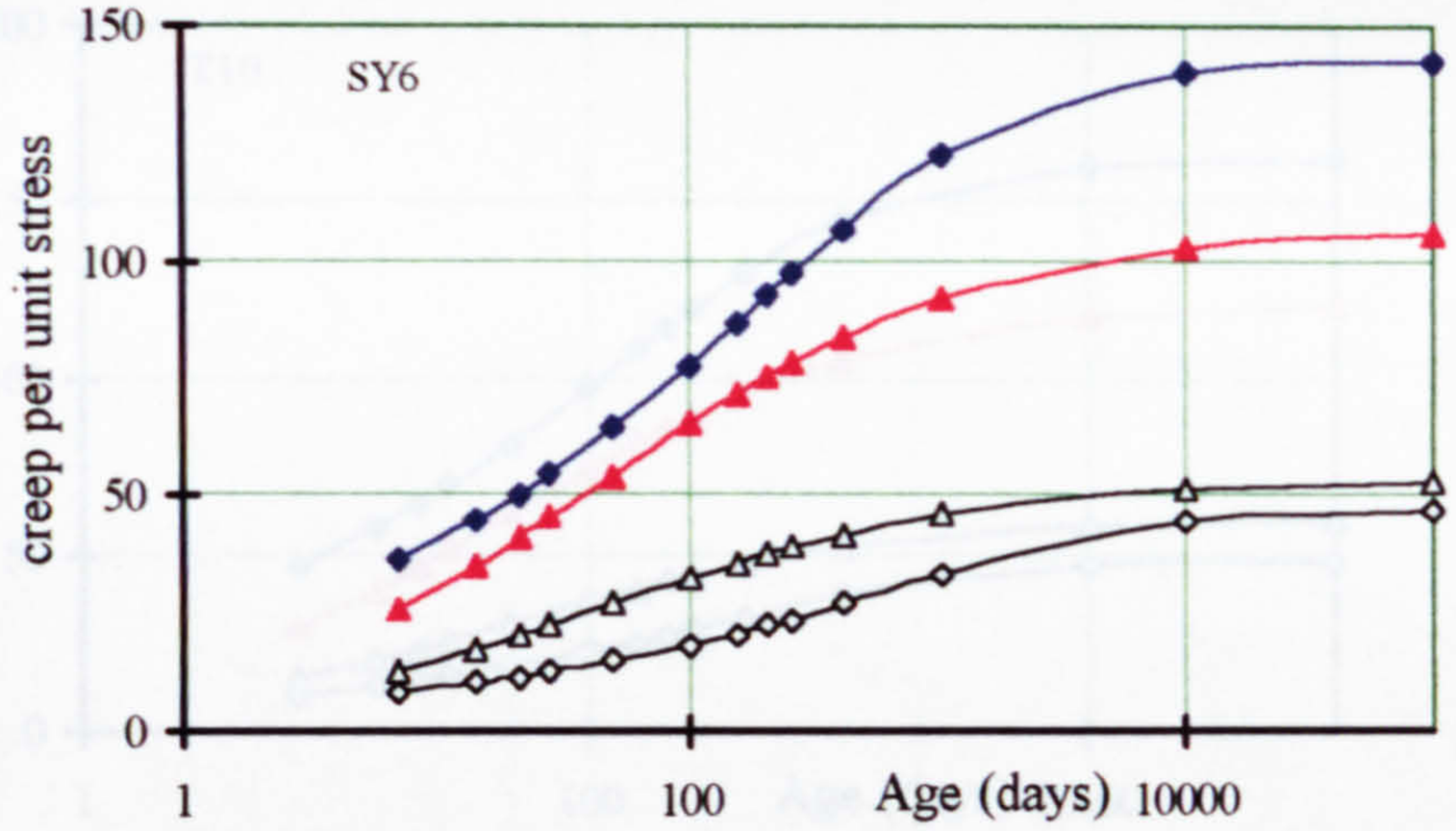

(a) Time-dependent creep characteristic for section *SY6*

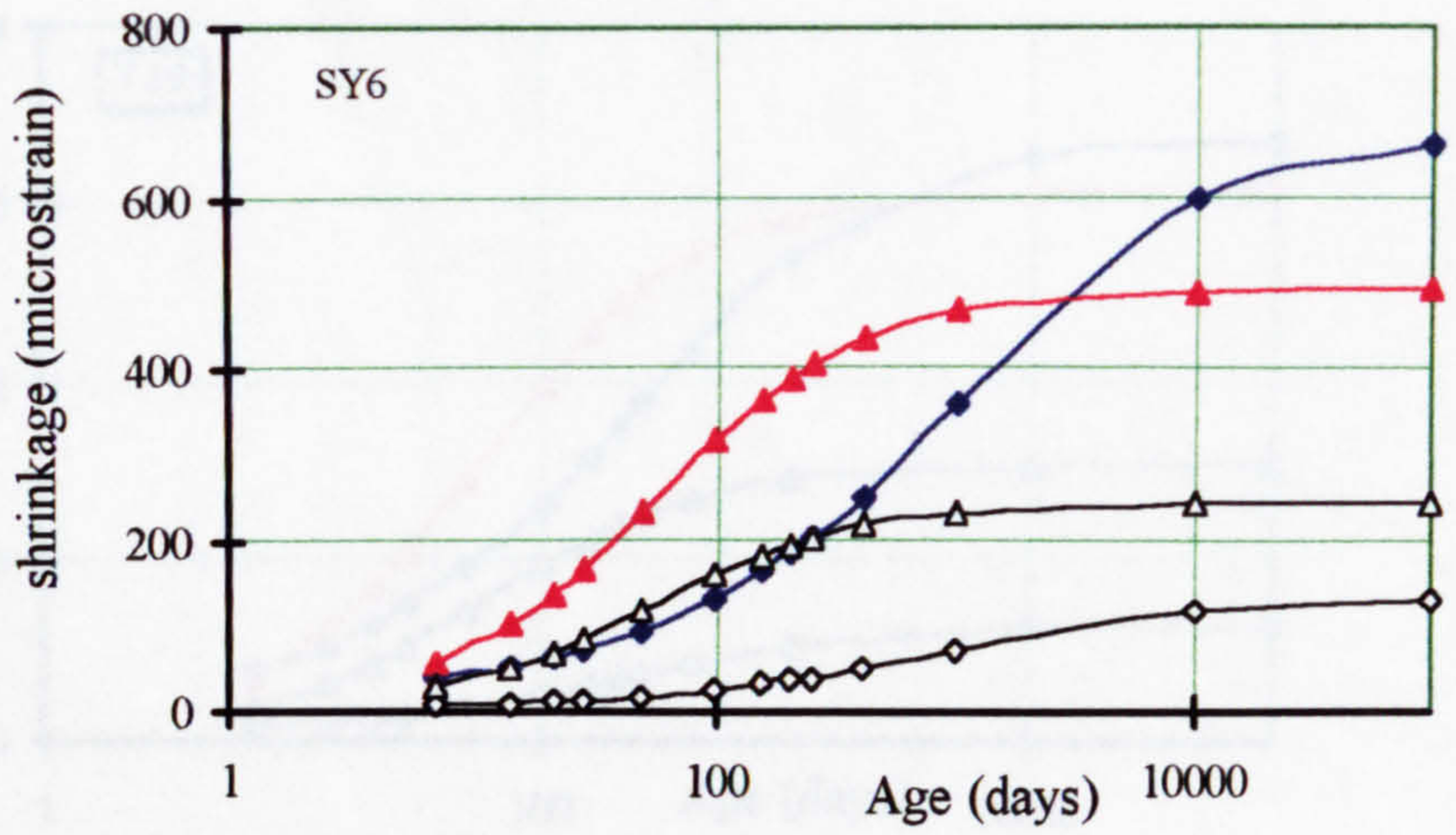

(b) Time-dependent shrinkage for section *SY6*

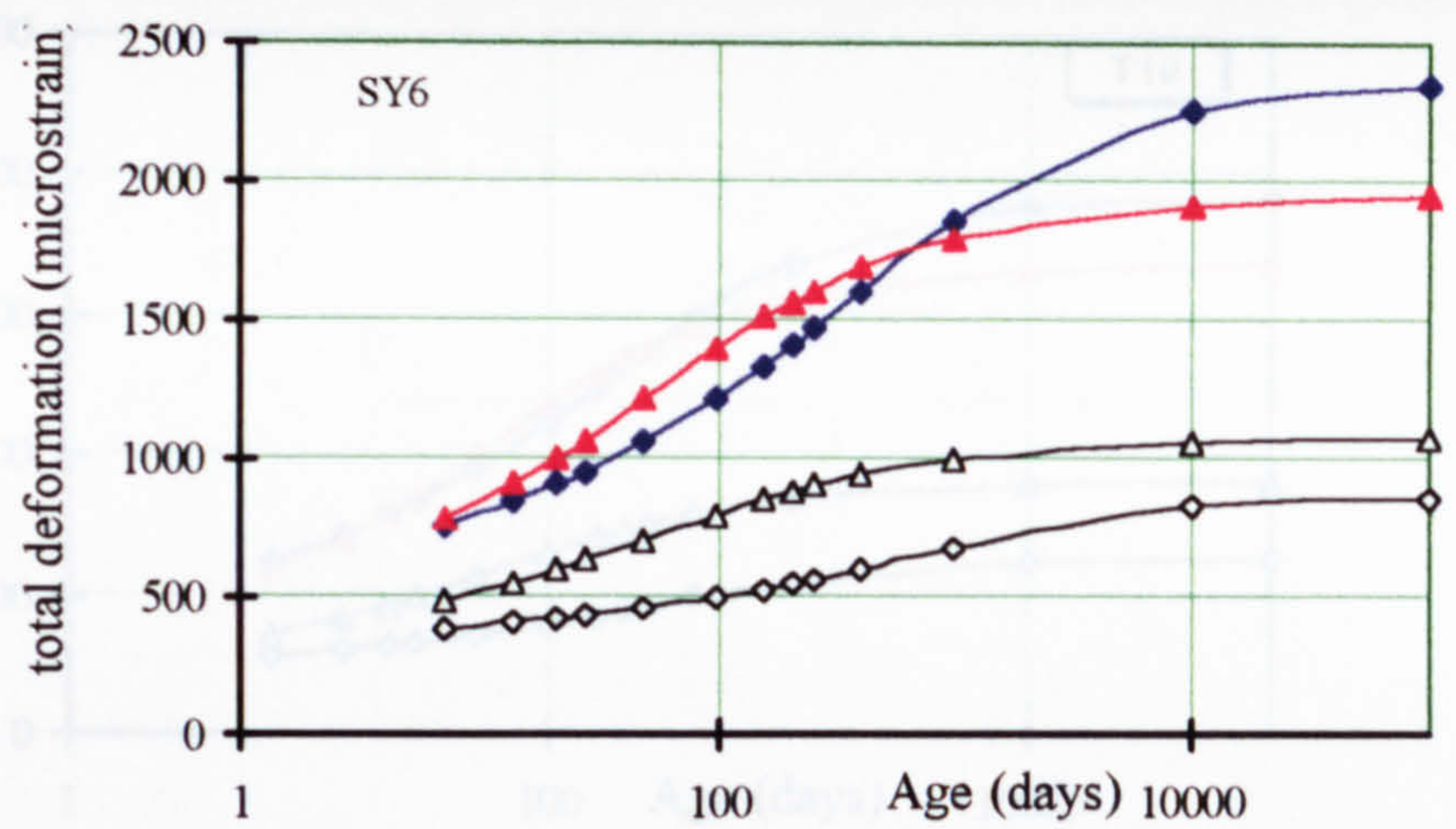

(c) Total time-dependent deformation for section *SY6*

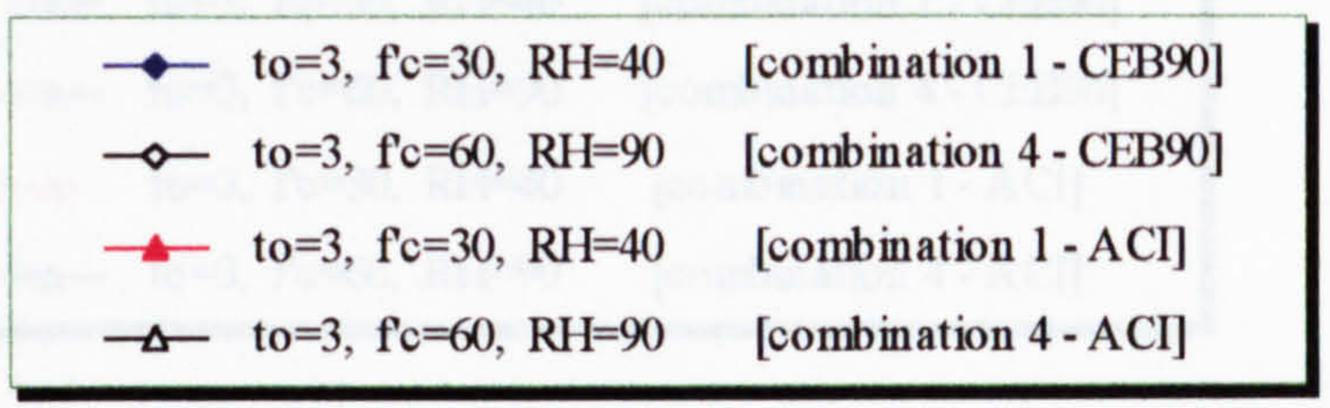

Figure 5.36: Comparison of time-dependent material characteristics according to CEB90 and ACI for section *SY6*

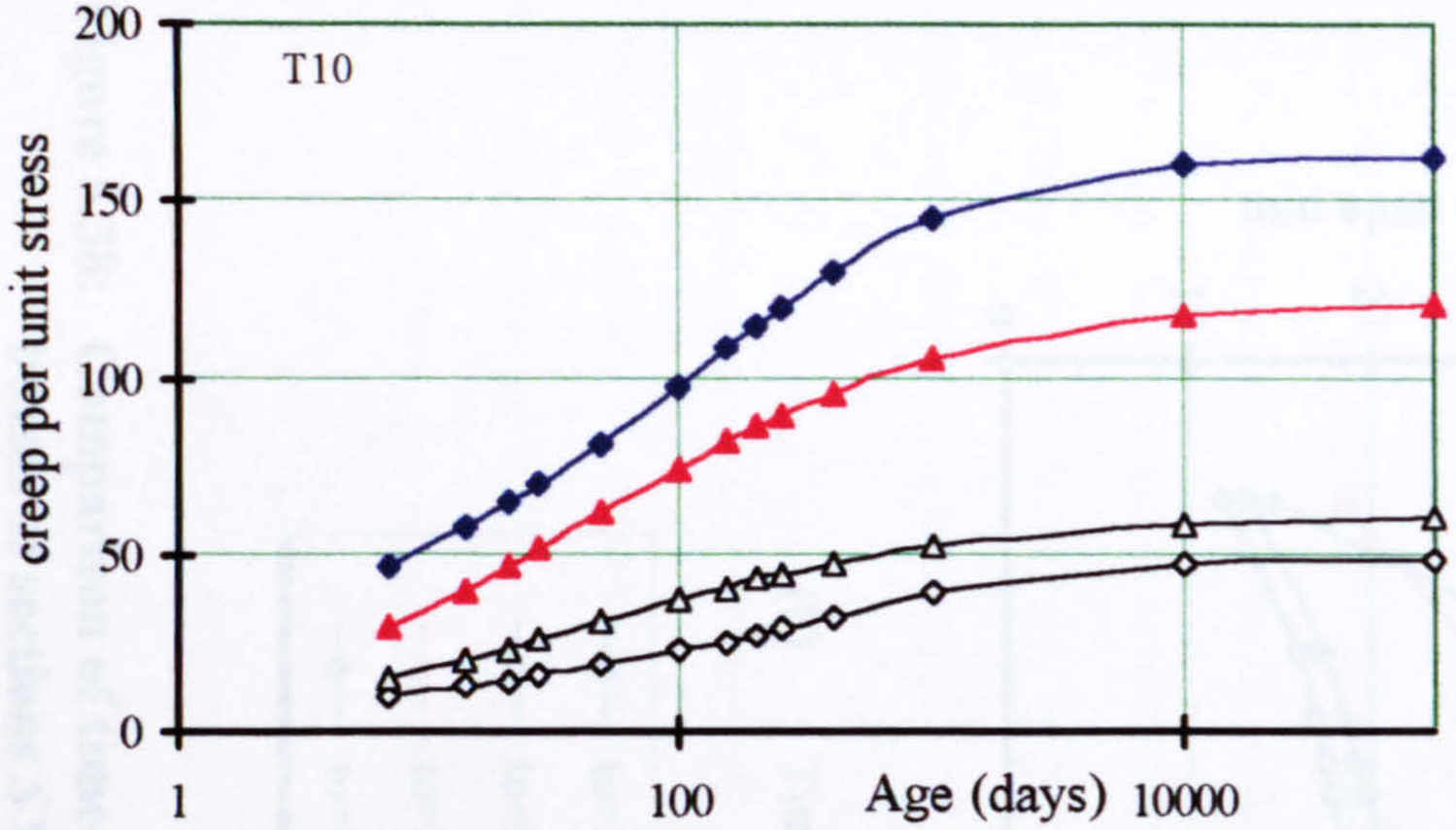

(a) Time-dependent creep characteristic for section *T10*

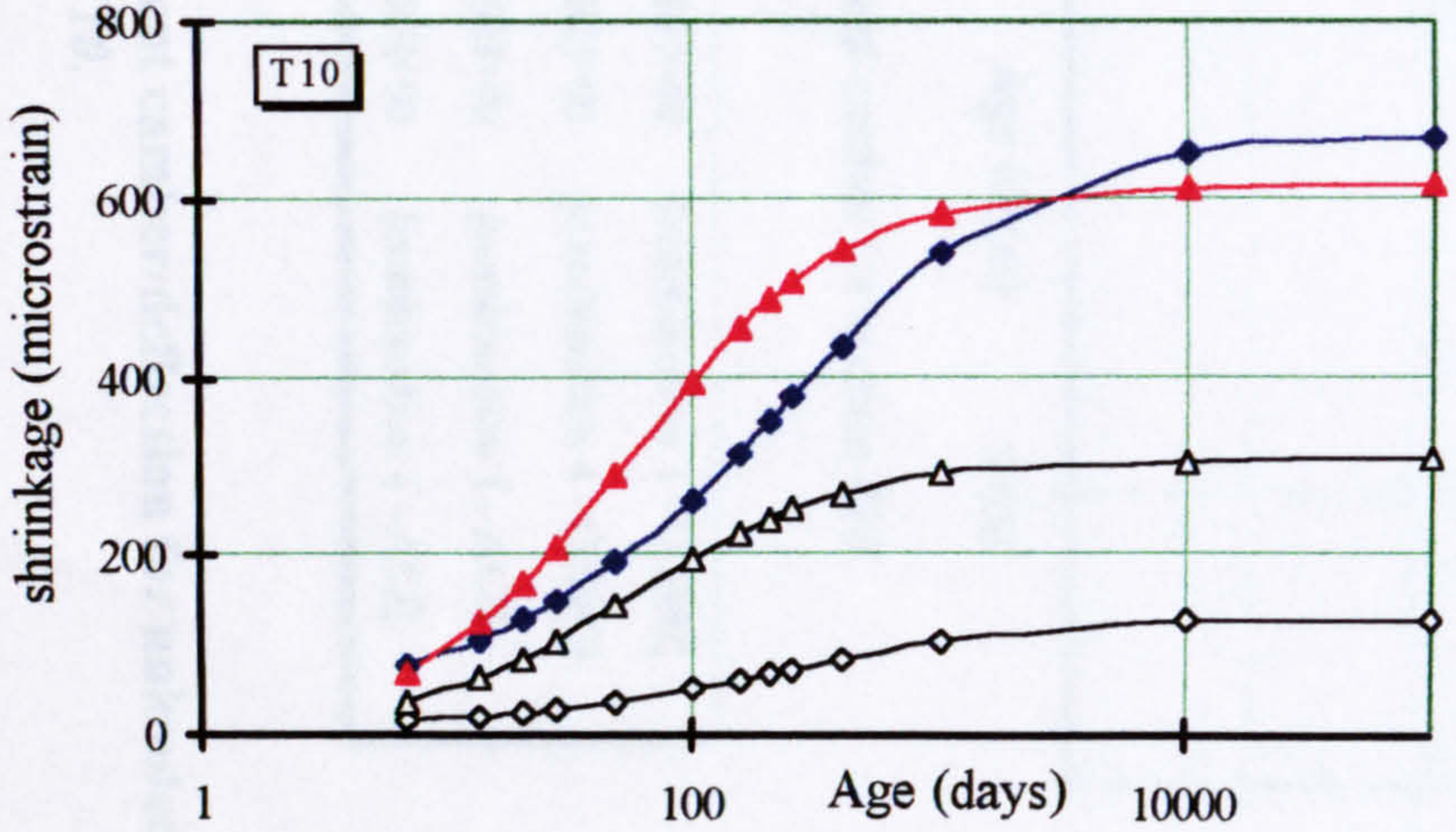

(b) Time-dependent shrinkage for section *T10*

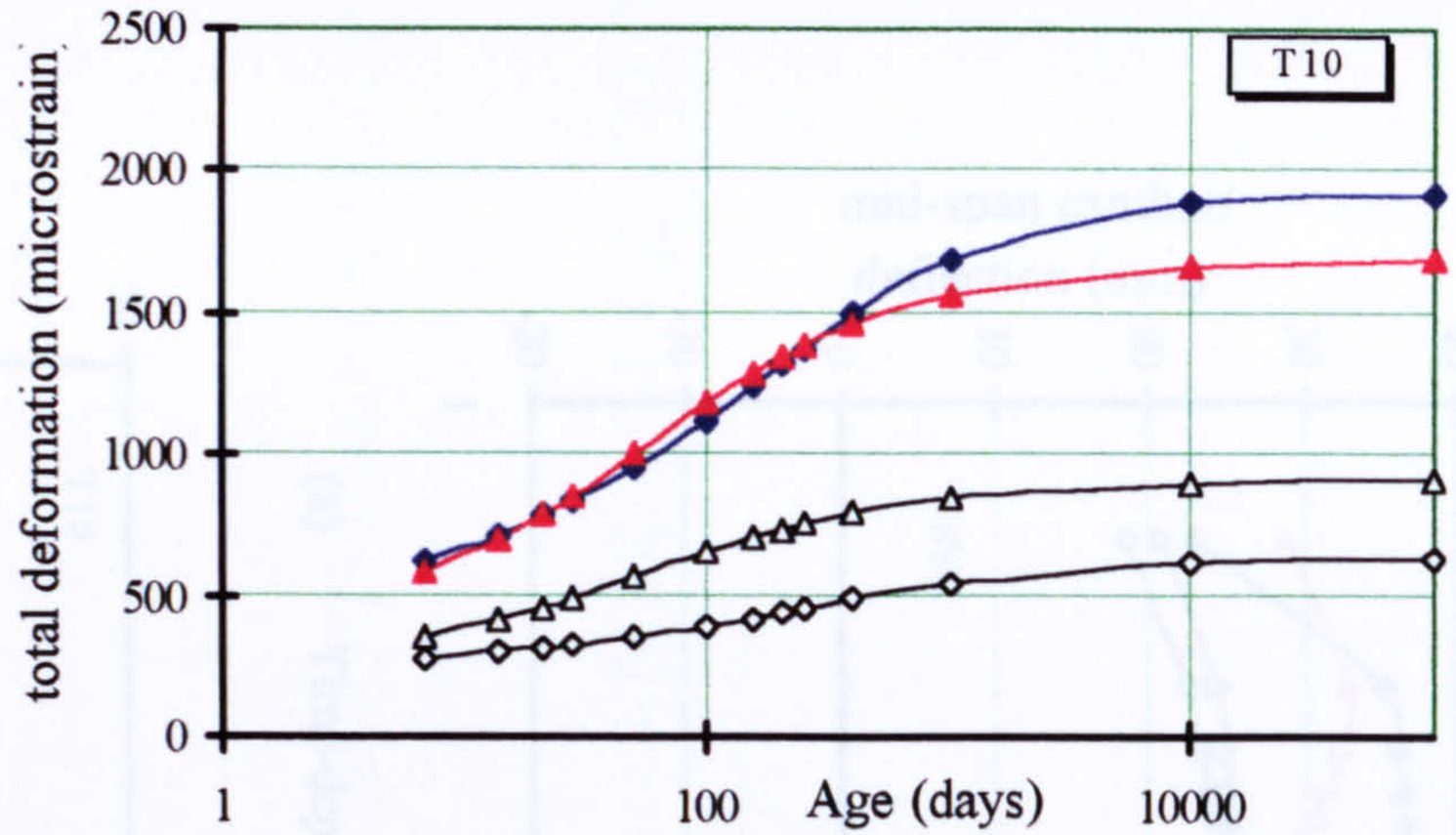

(c) Total time-dependent deformation for section *T10*

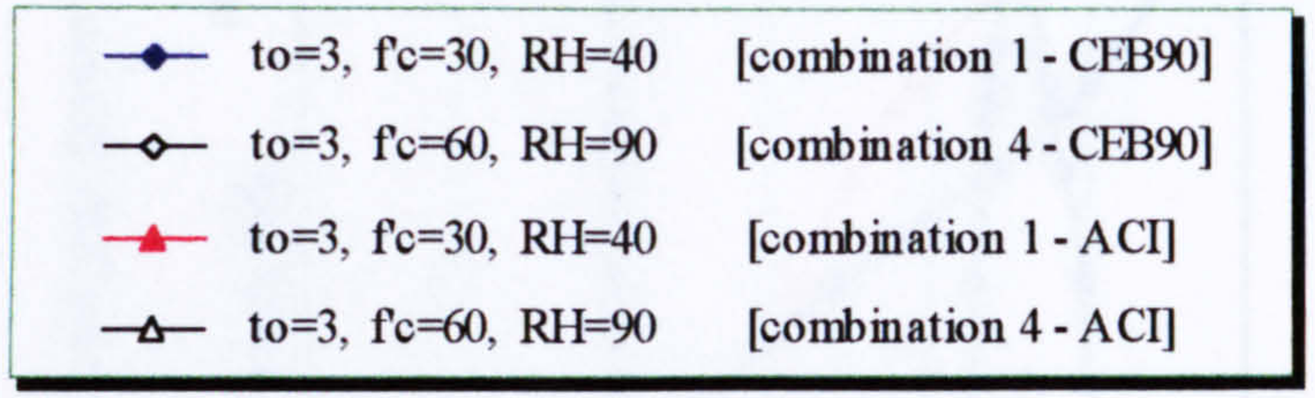

Figure 5.37: Comparison of time-dependent material characteristics according to CEB90 and ACI for section *T10*

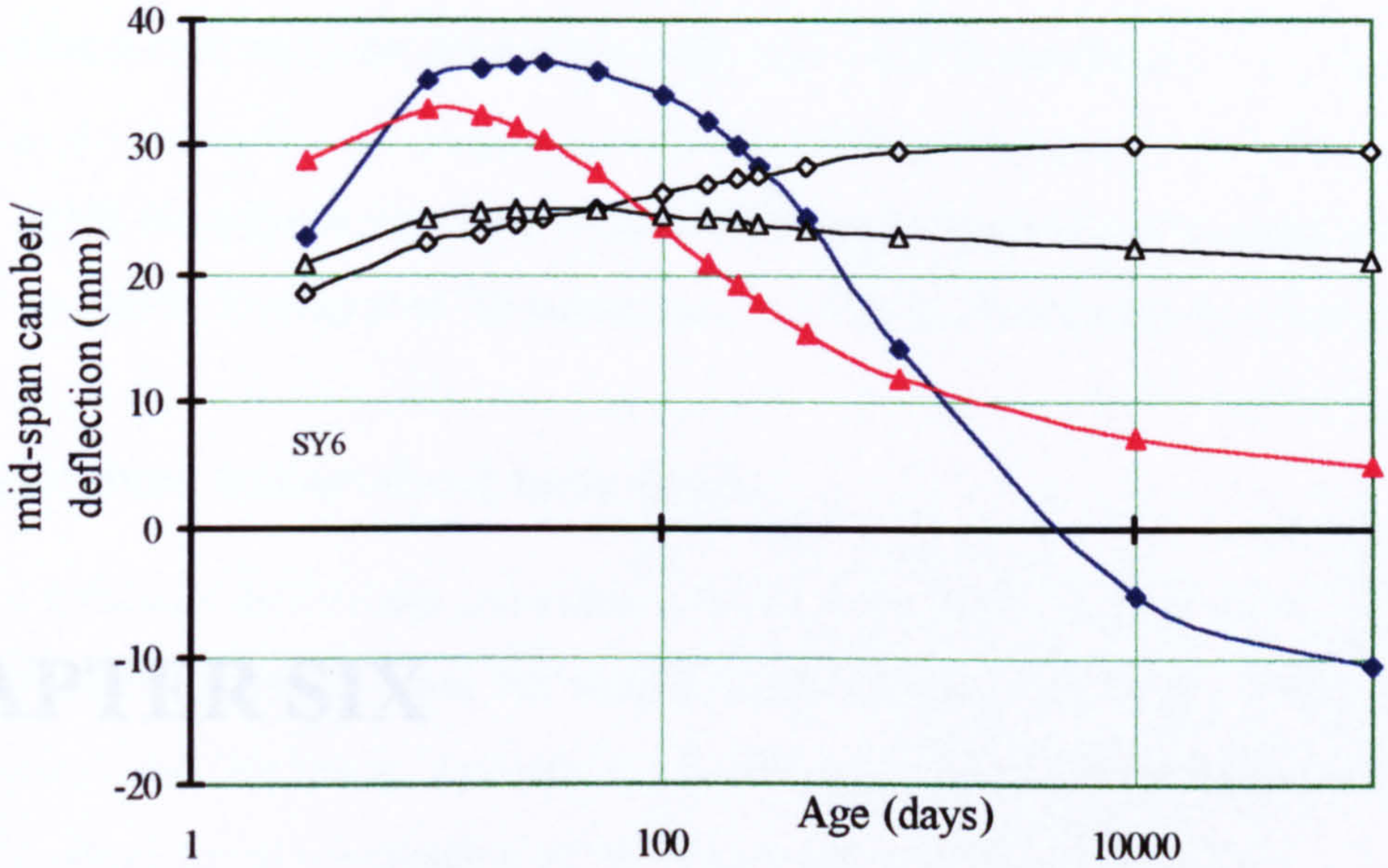

(a) Time-dependent camber/deflection for sections *SY6*

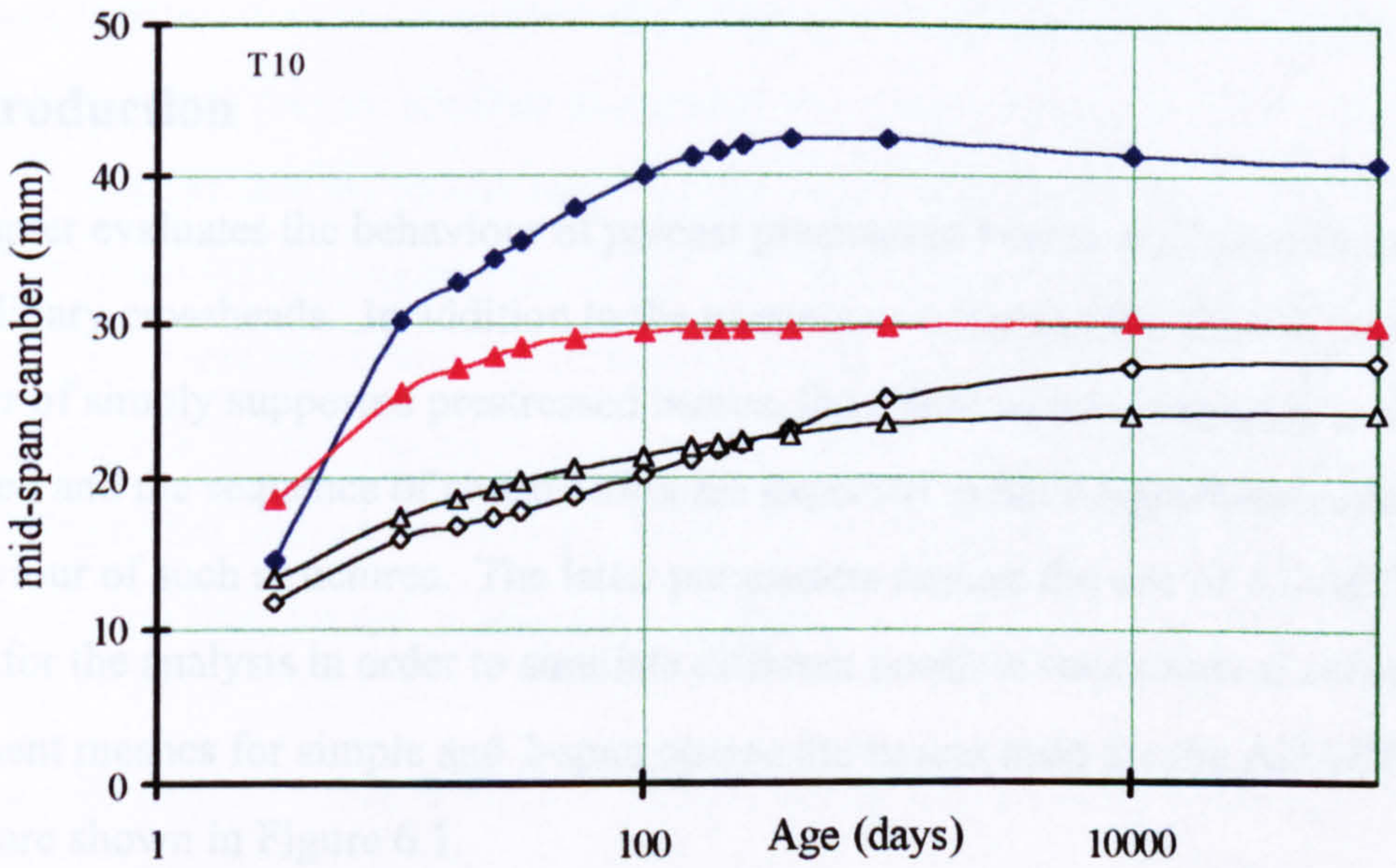

(b) Time-dependent camber for section *T10*

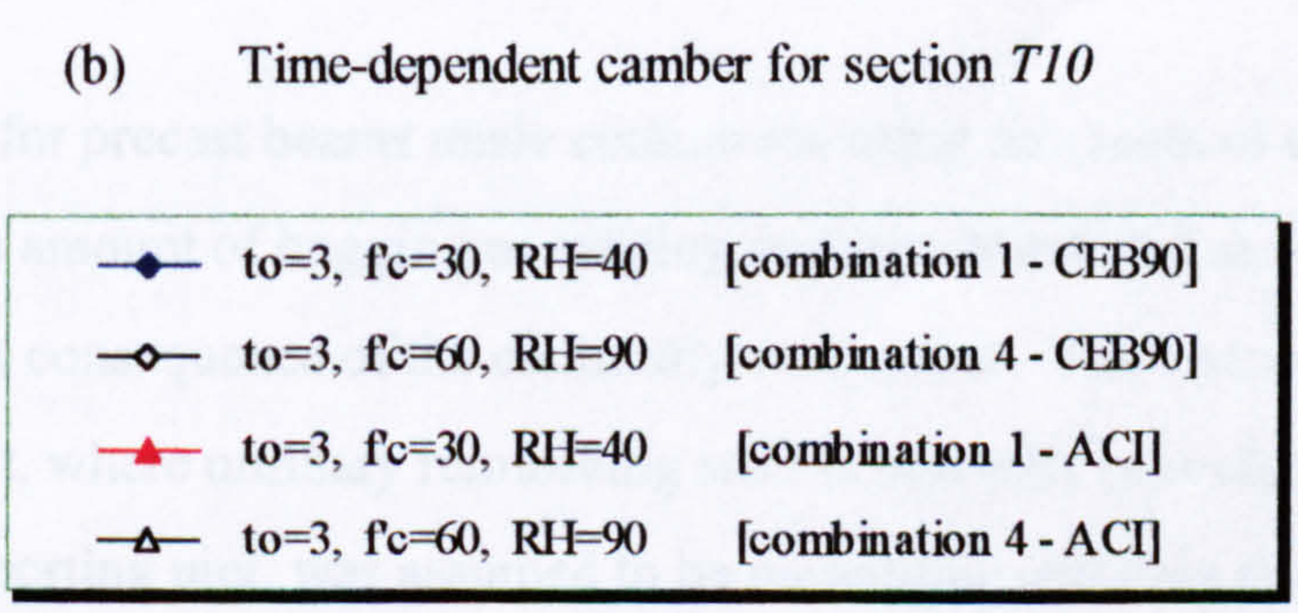

Figure 5.38: Comparison of time-dependent camber/deflection for unloaded beams of sections *SY6* and *T10*.

CHAPTER SIX

ORDINARY CROSSHEADS FOR CONTINUITY

6.1 Introduction

This Chapter evaluates the behaviour of precast prestressed beams made continuous using ordinary crossheads. In addition to the parameters affecting the time-dependent behaviour of simply supported prestressed beams, the age at which continuity is first established and the sequence of construction are expected to have significant effects on the behaviour of such structures. The latter parameters require the use of ADAPT software for the analysis in order to simulate different possible sequences of construction. The element meshes for simple and 2-span composite beams used for the ADAPT analyses are shown in Figure 6.1.

The analyses conducted for precast beams made continuous using this method were aimed at establishing the amount of hogging or sagging moment developed at the intermediate support as a consequence of the continuity connection. The connection established at the support, where ordinary reinforcing steel is normally provided in the deck slab across the supporting pier, was assumed to be monolithic and thus able to resist rotational deformation due to creep and shrinkage actions. There are several possible

sequences of construction that can be adopted, and each sequence will have a varying effect on the elastic and time-dependent behaviour of such structures.

Several series of analyses have been conducted to study the levels of hogging and sagging moments developed at the support under both short and long term loading.

6.2 Behaviour under short term loads

Table 6.1 indicates the stresses generated at the extreme fibres of a composite beam for each component of precast beam self weight, insitu concrete self weight, surfacing load and superimposed live loads. The values of stresses at each fibre are notional values in which the stress due to prestressing of the precast beam needs to be added.

For simply supported composite beams, the maximum tensile stress at the bottom fibre of a mid-span section occurs in members using unpropped construction. Calculations for each of the available precast sections supported over their maximum recommended span (Table 6.1) indicate that the tensile stress for the unpropped members can be 2-3MPa greater than those for the propped members. The difference is greatest for the lightest members (the *T1* section) where the selfweight amounts to only about 12% of the total service loads. For heavier members (such as the *SY* sections whose selfweight amounts to about 40% of the total service loads), the tensile stress at the bottom fibre is only about 1-1.5MPa greater than for the unpropped members.

For 2-span composite beams, besides differences arising from the propped and unpropped construction procedures, the sequence of construction is also expected to yield different levels of elastic stress on the members. The levels of tensile stress at the bottom fibre of the mid-span regions and at the top fibre of the intermediate support regions have been calculated for three different possible sequences of construction. In Sequence 1, deck slabs and insitu crossheads are assumed to have been cast simultaneously using unpropped construction. The weight of the slabs was considered to be supported entirely by the simply supported precast beams and continuity can be assumed to have been established to transform the structure into a continuous structure before other loads such as the surfacing and superimposed live loads are applied. In Sequence 2, the insitu

crossheads are assumed to be cast first and the insitu deck slab then cast on the unpropped structure. The weight of the insitu slab was considered to be supported by the continuous precast members. In Sequence 3 the whole insitu deck slabs and crossheads are assumed to have been cast simultaneously using propped construction.

For each sequence of construction, alternative insitu diaphragms of 0.2 and 2.0m thickness have been selected to represent narrow and wide insitu crossheads respectively. For the purpose of this evaluation, the analyses assumed homogenous, uncracked sections and the crossheads had similar properties as those for the precast beams. A summary of stresses at mid-span and the intermediate support is given in Tables 6.2 and 6.3 for the narrow and wide insitu crossheads respectively.

The stresses at the top fibre at the support indicate that the insitu crossheads may crack under service loads for all three construction sequences in case of both the narrow and the wide insitu crossheads. For the *T1* section, the smallest tensile stress occurred at this section in Sequence 1 using the narrow insitu crossheads ($\sigma 4$=-3.56MPa, Table 6.2) and the greatest hypothetical tensile developed in Sequences 2 and 3 for the wide insitu crossheads ($\sigma 4$=-5.53MPa, Table 6.3). The tensile stresses at the support are greater for longer spans such as the *SY6* sections where the stress was calculated to be $\sigma 4$=-8.79MPa for Sequences 2 and 3 using the wide insitu crossheads (Table 6.3). The calculated hogging moment will reduce by about 10-15% if the cracked stiffness is adopted for the insitu crossheads in the analyses, but the section would still be subjected to tensile stress at the top fibre at this section. This indicates that, under short term loading, the requirement for zero tensile stress under live load for Class 1 bridges designed according to BS5400 is inevitably violated, irrespective of the sequence of construction or the thickness of the crossheads.

Further comparison of results shows that the sagging moments at the mid-span for Sequences 2 and 3, are about 10-20% less than those for Sequence 1. Although the sagging moments at the mid-span regions are the same for Sequences 2 and 3, the tensile stress at the bottom fibre for Sequence 3 is less by about 1-2MPa than that of the Sequence 2. If the tensile stress at mid-span governs the design requirement for

continuous precast prestressed beams, it can be seen that Sequence 3 clearly offers the better option as it results in the least tensile stress at this section, which in turn can result in minimum amount of prestressing steel in the pre-tensioned beams. This can result in the least amount of prestressing steel in the pre-tensioned beams. Sequence 2, however, offers some savings where no props are required in the construction. The choice is clearly open for bridge designers to select the best economic and practical solution.

A comparison of the equivalent tensile stresses at the mid-span regions between the simple composite beams (σ1 unpropped, Table 6.1) and two-span composite beams (σ1, Tables 6.2 and 6.3 for Sequence 3) shows reductions to an extent of about 5MPa in the tensile stresses in the latter cases. As the stresses at the bottom fibre in the mid-span regions are less for the continuous members built using propped construction, this reduces the amount of prestressing required in the precast sections. The long term effects of this reduced level of prestressing, however, needs to be properly evaluated, as discussed in the previous Chapter.

Analyses have also been conducted to ascertain the effects of different elastic moduli for precast beams and the insitu slabs. The structure chosen for this investigation incorporated a wide insitu crosshead and the analysis carried out under full superimposed dead loads. A concrete strengths of 60MPa for both the precast beams and the insitu slabs was assumed in the first analysis. The moments at mid-span and the intermediate support were calculated to be 133.3 and -280.8kNm respectively. Subsequent analyses where the concrete characteristic strengths were assumed to be 30MPa for the cast insitu slab and 60MPa for precast beams, resulted in sagging and hogging moments of 136.2 and -274.6kNm for the mid-span and intermediate support, respectively. Thus, under short term loads, the difference in calculated moments is less than 3%. This indicates that the difference in the elastic modulus, associated with the difference in the strength properties, does not significantly affect the distribution of sagging and hogging moments.

6.3 Time-dependent Analysis

6.3.1 Creep and shrinkage effects

Time-dependent analyses of simply supported prestressed beams evaluated in the previous chapter have shown that, apart from the combination of material and structural properties, the level of initial prestressing and the age of the precast beams when an external load was applied were important factors to determine the long term behaviour of such beams. It has been found that a prestressed beam under its own weight with a reduced level of initial prestressing might undergo a reduction in camber (it is always expected that such beams would continue to camber with time). This may occur under a combination of parameters yielding high creep and shrinkage whereby the loss of prestress is large enough so that the hogging moment due to prestressing force becomes smaller than the sagging moment due the beam's selfweight. If the beams are made continuous at any time before the creep and shrinkage effects cease to make a significant contribution to the time-dependent deformation, a restraint moment is expected to develop at the intermediate support. The level of the restraint moment and its directions i.e. either sagging or hogging also depends on the ages at which the slab was cast and the continuity was established.

To assess the significance of the restraint moment, a total of more than 300 time-dependent analyses have been conducted on 40 different beams consisting of the *inverted-T*, *M*, *Y*, *U* and *SY* sections. Each beam has been assessed for 8 different cases of construction sequence or time-dependent material properties. The required amount of the pre-tensioned steel and its layout for each beam have been determined so that all the limiting stress criteria at transfer and service at both the mid-span and the support regions were satisfied. From these calculations, it has been observed that the tensile stress at the top fibre in the support regions at transfer and the tensile stress at the bottom fibre in the mid-span regions at service generally govern the choice of prestressing steel areas and the tendon eccentricities. To satisfy the tensile stress requirements at transfer in the support regions, tendons were either inclined and/or debonded as permitted by the sectional properties of each section. The choice of having deflected tendons is likely to be more costly than debonded tendons, but it may help in resisting some of shear stresses

which are generally high in the support regions of continuous beams. Clearly, there are many possible different combinations of prestressing steel layout satisfying the stress requirements especially for those sections which allow greater flexibility for having inclined tendons at the ends of the beams such as the *T*, *M* and *U* sections.

A summary of the pre-tensioned steel areas, their eccentricities at mid-span and beam ends adopted for the time-dependent analyses is given in Table 6.4. The terms ep_1 and ep_2 are the resultant tendon eccentricities at the mid-span and support sections, respectively. A general layout for the pre-tensioned steel used for all the precast sections is shown in Figure 6.2.

The required amount of pre-tensioned steel in all cases was found to be between 0.64 to 1.06% of the gross concrete area of the precast sections. If continuity is taken into consideration, the amount of pre-tensioned steel will be reduced accordingly. This, however, is rarely achieved in practice. Designers of continuous precast prestressed beams often do not take advantage of continuity when they design members as simply supported structures, and then provide ordinary reinforcing steel across the deck slab at the intermediate support to satisfy the ultimate strength requirement (NCHRP 1985).

The material properties adopted for these analyses are similar to those described in Section 5.5. Besides the effect of construction sequence, the analyses have also been carried out to ascertain the effects of the age when continuity is first established on the hogging or sagging restraint moments at the intermediate support. For this series of analyses, only the effect of creep and shrinkage on the precast beams has been considered. The effect of differential shrinkage on the restraint moment has not been included in these analyses this effect has been studied separately (Section 6.3.2). This is to enable a proper evaluation of their respective effects on the level of restraint moment at the intermediate support.

For each of the available precast sections, analyses have been conducted for eight different cases as follows:

(a) Case 1: Slabs and insitu crossheads are cast simultaneously on the unpropped beams and continuity was assumed to come into effect after 7

days of slab casting. Precast beams are aged 24 days when the insitu concrete is cast.

(b) Case 1a: Similar to Case 1 except that the precast beams are assumed to be aged 100 days when the insitu concrete is cast.

(c) Case 2: Slabs and insitu crossheads are cast using propped construction when precast beams are 24 days old.

(d) Case 2a: Similar to Case 2 except the precast beams are 100 days old.

(e) Case 3: Slabs are cast unpropped at 24 days, and the crossheads are cast later at 100 days.

(f) Case 4: Crossheads are first cast at 24 days, and slabs are cast unpropped at 100 days.

(g) Case 5: A hypothetical case where only crossheads are cast at 24 days.

(h) Case 6: Similar to Case 1, except using the combination of parameters yielding minimum creep and shrinkage values.

Cases 1 and 2 are the most common sequences adopted in the construction of bridges of this type. Cases 1a and 2a have been included to assess the possible effect of the delay in construction where the slabs are cast when the precast beams are about 3 months old. Cases 3 and 4 represent alternatives sequence of construction where some benefits may be obtained from such sequences depending on the design requirements. The slight delay in the casting of the insitu crossheads (Case 3) for example, can reduce sagging restraint moment at the intermediate support. This may be beneficial if combinations of material and structural parameters result in potentially high sagging restraint moments. The hypothetical situation represented by Case 5, where only continuity connection is assumed with no additional load (e.g. from cast insitu slabs), has been included to ascertain the highest possible restraint moment developed at the support. It should be noted that although such a case is hypothetical for the composite bridge construction investigated in this study, it may be a realistic situation for precast prestressed structural floor systems. In such a system, the pre-tensioned floor slabs may be made continuous and left unloaded or only lightly loaded permanently by surfacing loads.

In the analyses for Cases 1-5, the combination of parameters yield high creep and shrinkage values. However, it has been earlier shown in Chapter 5 that the combination of parameters yielding maximum creep and shrinkage values may not necessarily result in maximum camber. Depending on the structural properties and the initial stress level, the cambers for structures containing materials with high creep and shrinkage characteristics have been shown to reduce with time. This reduction may result in the reduction of sagging restraint moments that are expected to develop at the intermediate support. In other words, the levels of the restraint moment are not characterised only by material creep and shrinkage values, but reflect the combined effect of material and structural properties of each member. To assess the significance of the material properties on the restraint moment, analyses for Case 6 have been conducted for each of the sections analysed for Case 1. Case 6 is similar to Case 1 but used the combination of parameters yielding minimum creep and shrinkage values. A summary of the restraint moments developed at the intermediate support in Cases 1-6 is presented in Table 6.5; and the corresponding stresses at the top and bottom fibre of the insitu crossheads at the intermediate support are presented in Table 6.6.

A comparison of restraint moment between those of Cases 1 and 1a (Table 6.5) indicates that a delay in slab casting results in a reduction of sagging restraint moment at the intermediate support. In some of the beams, the delay in slab casting transformed the restraint moment from sagging to hogging. The reduction has been calculated to be quite substantial in most cases, the largest reduction being 625.2kNm for the *SY6* section. However, observation of the corresponding tensile stress at the bottom fibre of the insitu crossheads (Table 6.6) shows that the largest reduction occurs in *SY3* section, calculated to be 1.53MPa. It can be seen in Table 6.6 that in all *SY* sections, a tensile stress reduction in excess of more than 1.0MPa occurs and most of the larger sections for other beam types also show similar levels of reduction.

A similar comparison of the restraint moments at the intermediate support for the propped construction (Cases 2 and 2a) also shows reductions in the sagging restraint moments. The largest reduction has been found in Section *SY6* where a sagging restraint moment changes from a value of 735.4kNm (Case 2) to a hogging moment value of

-28.5kNm (Case 2a). Since the sagging restraint moments for propped construction (Case 2) are smaller than those for unpropped construction (Case 1), the reduction in the sagging restraint moments due to the delay in the slab casting for the propped construction (Case 2a) generally transformed the restraint moment from sagging to hogging. In fact, comparisons with all other Cases shows that Case 2a displayed the greatest hogging restraint moments (or the smallest restrained sagging moments as in the case of the *Y6*, *Y7* and *Y8* sections).

A comparison between results of the analyses of propped and unpropped construction (Case 1 & 2 and 1a & 2a, respectively) clearly shows that unpropped construction results in larger sagging restraint moments or smaller hogging restraint moments. The sagging restraint moments for the *SY6* section using unpropped construction, for example, has been calculated to be 66% greater than that for propped construction. The comparison suggests that an early slab casting using unpropped construction displayed the largest sagging restraint moments. The levels of the sagging restraint moment due to the early slab casting in unpropped construction are only exceeded by those of Case 5. From the typical construction sequences (Cases 1, 1a, 2 and 2a), it can be seen that the tensile stress at the bottom fibre ($\sigma 1$) of the insitu crossheads caused by the sagging restraint moments are generally very small. The values of $\sigma 1$ for Case 1 in Table 6.6 show that the majority of the sections display such low levels of tensile stress that the tensile strength of concrete is unlikely to be exceeded. All beams develop levels of tensile stress less than -2.5MPa except the SY3 beam in which a tensile stress of -3.31MPa develops. Beams of the *inverted-T*, *M* and *U* sections generally display smaller levels of tensile stress compared to those of the *SY* and *Y* sections. Case 6 (where concrete with lower creep and shrinkage values were used in the analyses) generally shows lower levels of tensile stress at the bottom fibre of the insitu crossheads. The greatest tensile stress for this case has been found for the *SY3* section at -3.06MPa.

The low levels of tensile stress that have been observed to develop at the bottom fibres of the insitu crossheads suggest that this requires no provision of positive reinforcement at the bottom section of the insitu crossheads. Only the analyses given by the hypothetical Case 5 indicates a need to provide positive reinforcement. Generally the sagging

restraint moments determined in Case 5 are about twice those of Case 1. In the former case, it can be seen that the levels of the sagging moment could be sufficiently large that the tensile strength of the insitu crossheads may well be exceeded. The notional tensile stress is greatest for the *SY3* section with a value of -6.17MPa. This, however, cannot justify the need to provide positive reinforcement at the bottom section of the insitu crossheads in more realistic designs.

It has been argued that the tensile stress at the bottom fibres of the insitu crossheads is more critical at the interface between the precast beams and the insitu crossheads than that at the intermediate support (Clark, 1997). This is explained by the fact that the maximum sagging moment calculated due to the long term creep and shrinkage effects at the intermediate support are subsequently reduced by maximum short term hogging moments due to the slab weight (in case of propped construction) and permanent surfacing loads. The resultant sagging moment i.e. the summation of the short term hogging moment and the time-dependent sagging moment, therefore, is greater at some distance away from the intermediate support. This is illustrated in Figure 6.3 where it can be seen that resultant moments at section D (interface between precast beam and insitu concrete) is greater than that at section E (at the intermediate support).

A summary of the levels of sagging moment at the interface between the precast and cast insitu concretes for Cases 1 and 2 and their corresponding stresses at the top and bottom fibres is presented in Table 6.7. A comparison of the sagging moments for Cases 1 and 2 in Table 6.5 and those of Table 6.7 shows that moments at the interface are greater although for most of the beams, this increase in less than 20%. The corresponding tensile stress at the interface has been calculated to be greatest for the *SY3* section of Case 1 (-3.41MPa). Stresses in other cases can still be considered to be sufficiently low as to not justify the need for the positive reinforcement at the bottom sections of the insitu crossheads at the interface with the beam ends.

It should be noted that the levels of the tensile stress given by Case 1 can be expected to reduce if the action of differential shrinkage is taken into account. Slab casting at later ages and the generally higher shrinkage values for the insitu slab (compared with those of

the precast beams) result in a hogging moment at the intermediate support which in turn causes compressive stress at the bottom fibre of the insitu crossheads. This reduces the tensile stress due to the sagging restraint moment.

The results for the other cases (Cases 3 and 4) show that the restraint moment developed at the support are less than those for Case 1 but greater than those for Case 2a. The levels of stress at the top or bottom fibre of the insitu crossheads are unlikely to cause any concern. It can be concluded that Case 1 yields the greatest possible sagging restraint moments while Case 2a can be expected to yield the greatest hogging restraint moments. The greatest hogging restrain moment has been calculated to be -195kNm in case of M5 section. Calculations for corresponding stress at the top fibre of the insitu crossheads show that *M2* section develops the greatest tensile stress at -0.89MPa. This level of tensile stress may increase if the effect of the differential shrinkage is taken into account, or a reduced level of prestressing is adopted.

It should also be noted that the prestressing force that principally causes the development of the sagging restraint moment at the support to occur, has been applied without considering the effect of transfer length. Full prestressing force has been used in the analyses starting from the beam ends or from the end of the debonded length. The effect of the transfer length will reduce the prestressing effects at the beam ends, thus reducing the sagging restraint moment. The level of the initial prestressing force could further be reduced if the advantages of propped construction and continuity are taken into consideration when provision for the prestressing force is made. Taking these into consideration, together with the low level of tensile stress calculated under Case 1, it is clear that it is very unlikely that the sagging restraint moment will be of significance and cause cracking at the bottom fibre of the cast insitu crossheads.

Finally, it should be noted that suggestions for the need to provide the positive reinforcement arose from the experimental and analytical work conducted at the Precast Concrete Association, USA (Mattock *et al* 1960). The experimental work consisted of two 2-span continuous precast beams (Chapter 2). The analytical prediction assumed that prestressing and its creep effect (which is the principal cause of the sagging restraint

moment) acted independently (or separately) to those of the beam and slab self weights (which are the principal causes of hogging restraint moment). The same analytical assumption has continued to be adopted up to this date (Freyermuth, 1969, Hambly and Nicholson, 1992 and Clark, 1997). This assumption, as has been pointed out in Chapter 5, overestimates the effects of the prestressing force and its associated deformation due to the action of creep. This is because prestressing effects never act alone, but always in the presence of the beam and slab self weights. Since the creep effects are stress dependent, the deformations due to creep in beams that consider prestressing and the beam self weights separately will always be greater than those where prestressing force and beam self weight are assumed to act simultaneously.

It is understood that the suggestion of providing positive reinforcement at the bottom sections is more precautionary rather than an absolute requirement. This is because most analyses rely on predictions rather than known material characteristics. The maximum tensile stress as calculated for section *SY3*, for example, may or may not exceed the tensile strength of the insitu crossheads. This uncertainty has so far justified the need to provide positive reinforcement. Based on the analyses carried out in this study, however, it may be concluded that it is not necessary to provide positive reinforcement. If positive reinforcement is provided, it may be generally justified only for bridges constructed using unpropped construction and where the insitu concrete is cast at an early age (as shown for Case 1). For other cases, the need for positive reinforcement is difficult to justify.

6.3.2 Effects of differential shrinkage

It has been noted earlier that the shrinkage of the precast and cast insitu concretes and hence the level of differential shrinkage is only due to the difference in sectional and material properties. The sectional properties are represented by the *V/S* ratio, while the material properties are represented by the characteristic strength f'_c (for the CEB90 prediction). Earlier calculations in Section 5.2 show that the greatest difference in the final (10,000 day) shrinkage for the sections with the maximum and the minimum *V/S* ratios (135 and 50mm, respectively) is 65 microstrain (Conditions 25 and 29). The corresponding value for f'_c varying from 60 and 30MPa is 214 microstrain. This

indicates that the greatest possible difference in the final shrinkage between precast beams and cast insitu slab is less than 300 microstrain.

It is almost always assumed that cast insitu slabs have greater shrinkage values than precast beams. This is because the insitu component of concrete is invariably of a lower characteristic strength than concrete used for the factory made precast units and also due to the fact that a significant portion of the total shrinkage is likely to have already taken place in the precast beams at the time of casting the insitu slab. Figure 6.4a shows shrinkage development with time of various sections which have been previously evaluated for the creep and shrinkage effects. All other things being equal, slab sections which have volume to surface area ratios of between 80-100mm are expected to have shrinkage development curves close to that of the *U* and *M* sections. Figure 6.4b shows the magnitude of potential difference in the final shrinkage for slabs cast at beam ages of 24 and 100 days.

To evaluate the effects of differential shrinkage on the restraint moment at the insitu crossheads at the intermediate support, a series of analyses considering the slab cast at different beam ages has been conducted. Three cases each for beams of sections *T10* and *SY6* have been considered. Cases 7 and 8 ascertain the effects of casting of slab at beam ages 24 and 100 days respectively. Both cases consider the structures to be exposed to 40% *RH*. Case 8a ascertains the effects of slab being cast at beam age of 100 days and exposed to 70% *RH*. ADAPT has been used for the analyses using the element mesh adopted for 2-span beams as shown in Figure 6.1. A summary of the results of the analyses for the resulting restraint moment and the corresponding stress is shown in Table 6.8.

A comparison of restraint moment developed at the intermediate support for Cases 7 and 8 shows that the moments for Case 8 are about 40 and 50% greater than those for Case 7 at 1,000 and 10,000 days, respectively for both *T10* and *SY6* sections. The final (10,000 days) moments calculated for Case 8 represent about 35 and 15% of the sagging restraint moments calculated for Case 1 in the previous section (Table 6.5). This shows that the hogging moments resulting from differential shrinkage will reduce the sagging moments

resulting from the creep and shrinkage effects by similar percentages. In other words, the tensile stress at the bottom fibre calculated for section *T10* in the previous evaluation will be reduced from -1.56MPa (Case 1, Table 6.6) to -1.04MPa. This demonstrates that superimposing effect of differential shrinkage on creep and shrinkage effects reduces the level of tensile stress at the bottom fibre of the insitu crossheads resulting from time-dependent alone restraint moment.

The final tensile stress at the top fibre of the insitu crossheads for Case 8 are found to be about -0.3MPa for both *T10* and *SY6* sections. This level of stress is lower than the value which develops due to the hogging restraint moments calculated for Case 2a in the previous section. It can be said that the stresses developed at the top and bottom fibre of the insitu crossheads due to differential shrinkage effects are less significant compared to those arising from the creep and shrinkage effects of the precast beams. The effects are even less significant if shrinkage of concrete under more typical levels of relative humidity is considered as shown by calculations for Case 8a, Table 6.8.

6.4 Comparisons with Current Design Method

Current design practice to calculate the restraint moment at the intermediate support due to time dependent effects still adopts the PCA method which was first suggested in 1969 (Freyermuth). The procedure is based on the investigations conducted in the PCA Laboratory, USA from 1960-61 (Chapter 2). Relevant equations are reproduced below as Equations 6.1and 6.2 to facilitate further discussion.

The final restraint moment, M_r, at the intermediate support can be calculated as:

$$M_r = \left(M_{ps} - M_d\right)\left(1 - e^{-\phi}\right) - M_{sh}\left(\frac{1 - e^{-\varphi}}{\phi}\right) + M_{LL} \qquad (6.1)$$

where M_r = final restraint moment

M_{ps} = restraint moment due to prestress force

M_d = restraint moment at the intermediate support due to dead load

M_{sh} = restraint moment at the intermediate support due to differential shrinkage between precast beams and cast insitu slabs

M_{LL} = positive moments due to live loads applied at remote spans

ϕ = creep coefficient from the time continuity is established.

The moments due to the prestressing force and dead loads are computed in such a way that assume the beams to be already continuous. The calculations for M_{ps}, M_d and M_{LL} can use any standard structural analysis procedure for indeterminate structures. The moment due to the differential shrinkage (M_{sh}) can be computed as:

$$M_{sh} = \varepsilon_{diff} E_s A_s (a_{cent}) \tag{6.2}$$

where, ε_{diff} = the differential shrinkage strain

E_s , A_s = Elastic modulus and cross sectional area of slabs

a_{cent} = the distance of the centroid of the concrete flange from the centroid of the composite section.

In the light of the PCA method, the BS5400: Part 4 (1990) clause 7.4.3.5 states that:

> ..."*The restraint moment, M_{cs}, will be modified with time by creep due to dead load and creep due to any prestress in the precast units. The restraint moment due to prestress may be taken as the restraint moment which would have been set up if the composite section as a whole had been prestressed, multiplied by a creep coefficient...*".

The creep coefficients referred to in the BS5400 are actually the creep correction factors referred to in Equation 6.1 which is represented by $\left(1-e^{-\phi}\right)$ and $\left(\frac{1-e^{-\phi}}{\phi}\right)$.

BS5400 is not clear as to how different construction sequences and procedures are to be treated. From the design examples given by Freyermuth (1969), Hambly and Nicholson (1990 and 1992) and Clark (1997), slab self weight is considered together with that of the precast beams in the calculation of M_d (Equation 6.1). It should be noted that this is only strictly true if the structures are built using unpropped method of construction.

Consequently, if the slab is cast using propped construction, the additional self weight is applied to the continuous beam, hence the application of the correction factor is not valid. This is also true if permanent surfacing loads which are normally applied to the continuous beam which requires no modification to the moment incurred at the intermediate support. Therefore, if propped construction is adopted and surfacing loads are considered in the calculation, Equation 6.1 should suitably be modified to become:

$$M_r = \left(M_{ps} - M_{bd}\right)(1 - e^{-\phi}) - M_{sh} + M_{LL} - M_{pd} - M_{sd} \qquad (6.3)$$

where M_{bd} = moment due to precast beams at the intermediate support

M_{pd} = moment due permanent surfacing loads at the intermediate support

M_{sd} = moment due to cast insitu slabs at the intermediate support.

If unpropped construction is adopted, and the permanent surfacing load is considered, the restraint moment given by Equation 6.1 should be reduced by the value of M_{pd}.

The PCA method of analysis for the restraint moment calculations has been programmed on *Excel 5* worksheet and the results of the analyses have then been compared with those given by ADAPT analyses. The worksheet is capable of analysing members having up to four continuous spans of equal length. Sections with debonded and deflected tendons have also been incorporated within the analyses. Similar material properties and prestressing steel layouts to those for the ADAPT analyses (Section 6.2) have been adopted. Comparisons of the final restraint moment and the corresponding stresses at the bottom fibres of the insitu crossheads for Sections *T10*, *M10*, *Y8*, *SY6* and *U11* are presented in Table 6.13.

Results of the analyses from the PCA method show that the tensile stress at the bottom fibre of the insitu crossheads for slabs cast at 24 days using unpropped construction will probably exceed the modulus of rupture of concrete. All sections considered develop tensile stresses of 4.93MPa or more. Greater tensile stresses can be expected if the slabs are cast at earlier ages, thus requiring provision of positive reinforcement , as previously discussed. The high level of tensile stress predicted by the PCA method leads to an

expectation of large cracks occurring at the bottom fibre of the insitu crossheads. Based on this prediction of large cracks, the study by NCHRP (1985) suggested that the analysis of the structures under live loads should not take the advantage of the continuity.

A comparison of the results with those from the ADAPT analyses, shows that the restraint moment from the PCA method are overestimated by more than 100%. These ADAPT results are of similar magnitude to those calculated by PBEAM analyses (NCHRP, 1985). Since this leads to lower levels of tensile stress at the bottom fibre of the insitu crossheads, as has been shown and discussed in Section 6.2, the structure rarely requires positive reinforcement to be provided. Results of other cases (i.e. propped construction at 24 days, propped or unpropped constructions at 100 days) calculated by the PCA method suggest that the tensile strength of concrete is very unlikely to be exceeded, thus requiring no positive reinforcement.

6.5 Effects of cracked insitu crossheads on sagging restraint moments

In the theoretical analysis for the restraint moment calculations both in the present study and by the PCA method, it is assumed that the sections remain uncracked throughout the service life of the structures. However, it has also been shown that the insitu slab over the intermediate crossheads may crack under full service loads. Since the insitu slab over the intermediate crossheads contains only ordinary reinforcing steel, cracks may remain open even after the live load is removed, thus reducing the stiffness of the joints. This will obviously affect the time-dependent behaviour of such structures.

Analyses of 2-span beams with reduced stiffness at the continuity connections have been conducted for five different sections i.e. sections *T10*, *M10*, *Y8*, *SY6* and *U10*. Each section has been analysed assuming propped and unpropped methods of construction as has been done for the earlier cases (Cases 1 – 6). Cases 9 and 10 are similar to Cases 1 and 2 respectively (Section 6.2.2), except that the reduced stiffness for the insitu crosshead over the intermediate support has been included for Cases 9 and 10. The inclusion of the reduced stiffness at cracked sections into the analysis is similar to that discussed in Chapter 4 where an average stiffness between the fully cracked and

uncracked sections has been adopted. A summary of the results for the restraint moment and the notional stress is presented in Table 6.10.

Results from Table 6.10 show that positive restraint moments are developed at the support for all the sections investigated. In a comparison of the restraint moments for cracked and uncracked crossheads (Table 6.5), it is generally observed that the sagging restraint moments of cracked insitu crossheads are less than those for the uncracked sections. This is not totally unexpected as the ability to transfer the action across the cracked joints is less that that for the uncracked sections. This effect is also acting in tandem with due to short term loading where the level of hogging moment across cracked sections at the support can be 10-20% smaller than that for uncracked sections.

A comparison of methods of construction shows that unpropped construction results in higher positive restraint moments than propped construction. A similar pattern has also been observed for uncracked sections (Cases 1 and 2, Table 6.5). The levels of restraint moment, however, are insignificant when considered for design purposes regardless of the method of construction adopted. This reaffirms the earlier finding (for the uncracked section) that the presence of the positive restraint moment may be ignored. This is especially so for cracked insitu crossheads.

All analyses carried out in this chapter have shown the levels of restraint moment developed at the support due to long term effects. It is clear that the tensile stresses predicted by the PCA method are shown to be high and the suggestion to provide positive reinforcement at the support does not apply in most circumstances. The recommendation that continuity be neglected in the analyses, as a result of the possible formation of cracks at the soffit of the insitu crossheads, (NCHRP, 1985 and Hambly and Nicholson, 1992) does not enable the full economic benefit of continuity to be achieved. This needs to be urgently addressed if continuous precast concrete beams are to provide an attractive alternative to steel composite beams in modern bridge construction. The behaviour of beams considering full continuity using non-conventional methods for continuity is addressed in the next chapter.

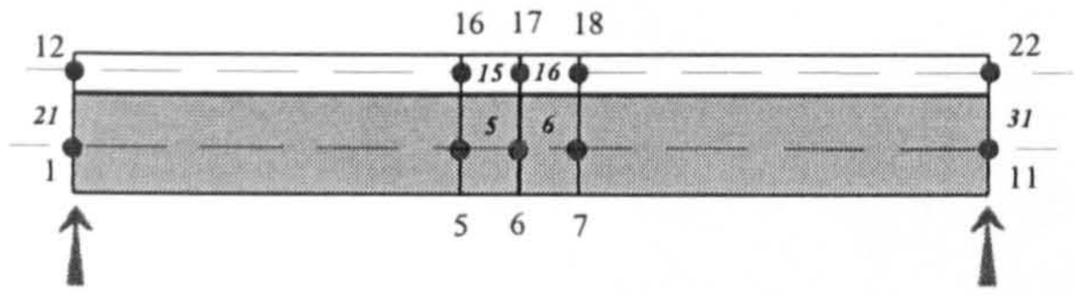

(a) element mesh for simply supported beams

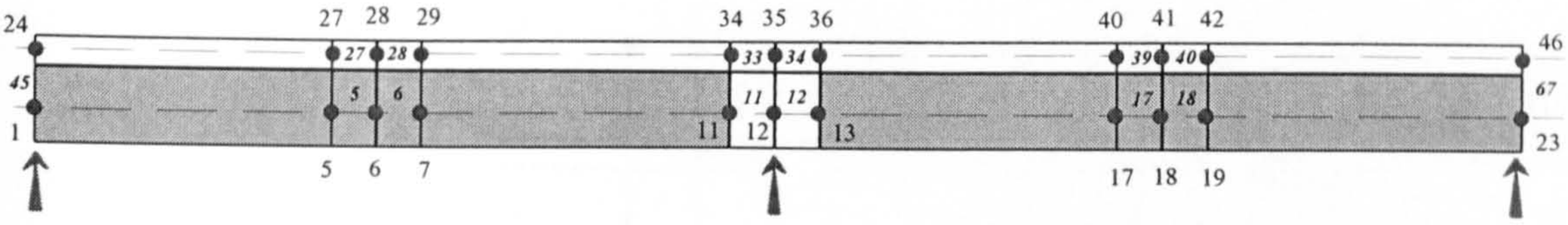

(b) element mesh for 2-span beams

Figure 6.1: Element mesh used for composite beams

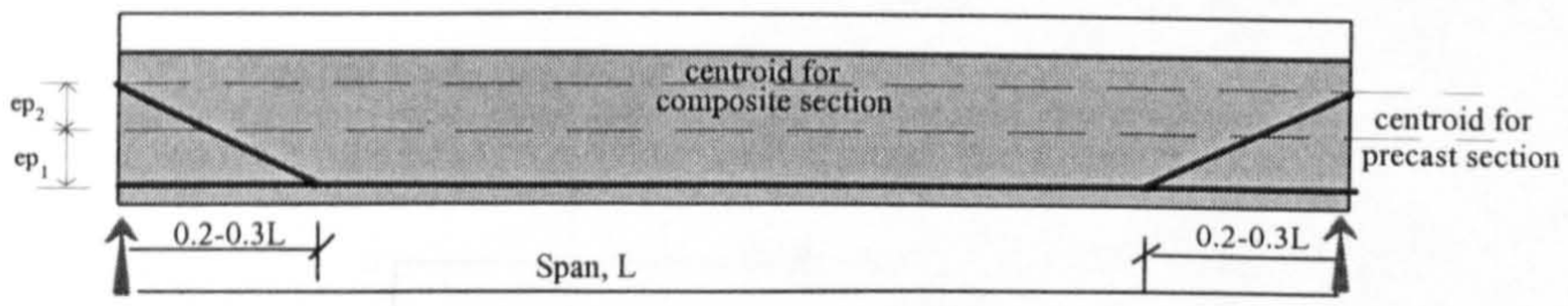

Figure 6.2: General tendon layout for pretensioned steel in precast beams

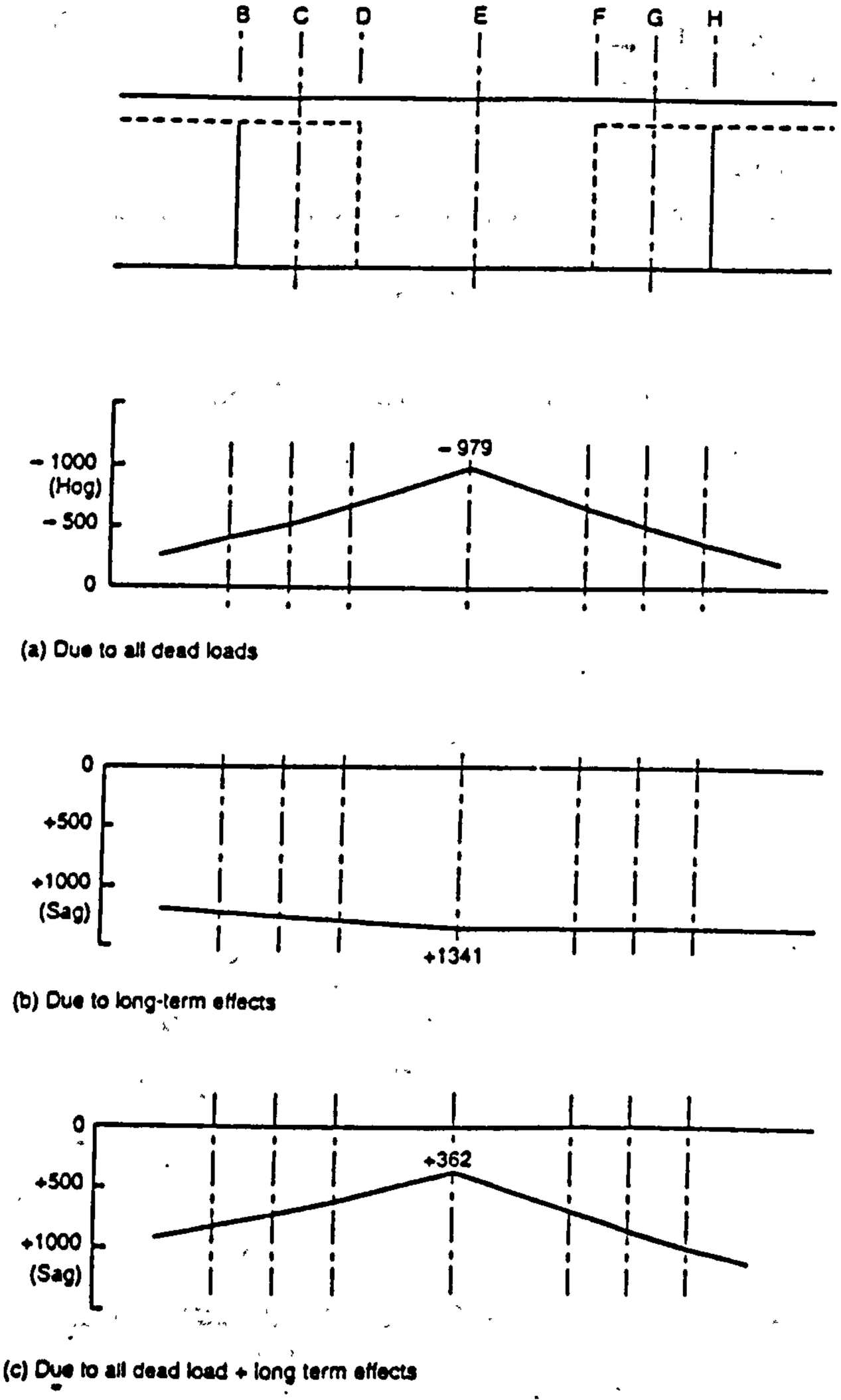

(a) Due to all dead loads

(b) Due to long-term effects

(c) Due to all dead load + long term effects

Figure 6.3: Bending moments (kNm) in the region of an internal support in the absence of live load (Clark, 1997)

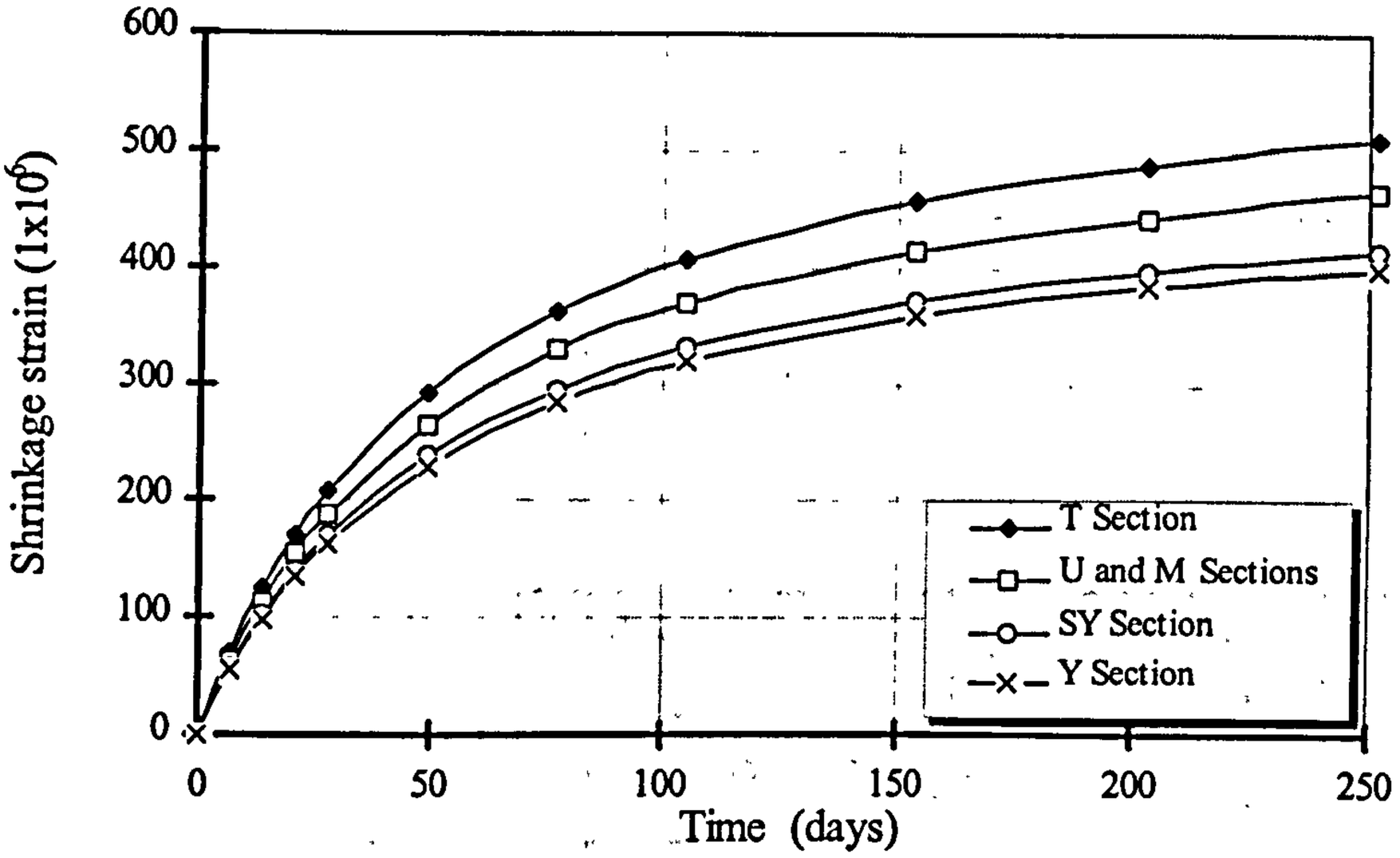

(a) Development of shrinkage for each section type

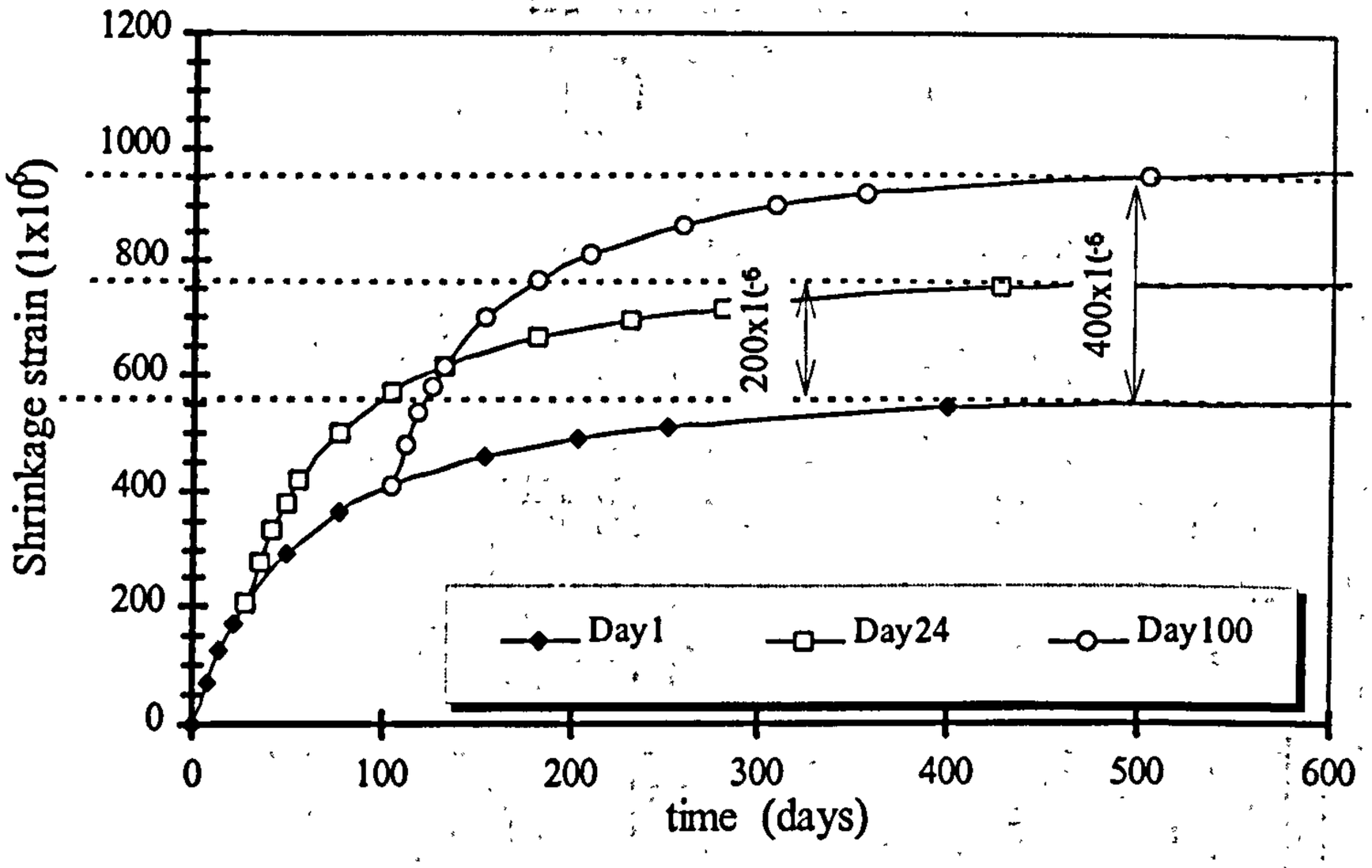

(b) Differential shrinkage for concrete casting at different times

Figure 6.4: Development of shrinkage and its differential strain

Table 6.1: Components of elastic stress in simply supported beams constructed using propped and unpropped procedures at mid-span (Node 6)

PCA Section	Depth(mm	Span (mm)	Moments on simple (Nmm)				Stress for unpropped construction (MPa)				Stress for propped construction (MPa)			
			Selfweight	Slab	Surfacing	SILL	σ1	σ2	σ3	σ4	σ1	σ2	σ3	σ4
T1	380	9000	2.34E+07	3.93E+07	2.43E+07	1.13E+08	-12.93	12.73	0.65	3.48	-10.19	5.34	0.83	4.48
T2	420	9500	2.82E+07	4.37E+07	2.71E+07	1.26E+08	-12.37	11.46	0.82	3.42	-10.05	5.22	1.05	4.40
T3	535	11000	4.07E+07	5.86E+07	3.63E+07	1.69E+08	-11.87	11.57	1.19	3.36	-9.99	5.78	1.52	4.32
T4	575	12000	5.20E+07	6.98E+07	4.32E+07	2.02E+08	-12.72	11.63	1.41	3.64	-10.91	6.17	1.81	4.68
T5	615	12500	6.02E+07	7.57E+07	4.69E+07	2.19E+08	-12.61	10.99	1.51	3.63	-10.96	6.14	1.95	4.67
T6	655	13000	6.91E+07	8.19E+07	5.07E+07	2.37E+08	-12.57	10.62	1.62	3.63	-11.02	6.20	2.08	4.66
T7	695	14500	9.12E+07	1.02E+08	6.31E+07	2.94E+08	-14.50	12.06	1.98	4.19	-12.80	7.30	2.54	5.38
T8	735	15500	1.10E+08	1.16E+08	7.21E+07	3.36E+08	-15.48	12.63	2.21	4.46	-13.75	7.90	2.84	5.73
T9	775	16000	1.23E+08	1.24E+08	7.68E+07	3.58E+08	-15.44	12.48	2.31	4.44	-13.78	8.03	2.96	5.71
T10	815	17000	1.46E+08	1.40E+08	8.67E+07	4.05E+08	-16.38	13.14	2.54	4.71	-14.68	8.68	3.26	6.05
M2	720	18000	3.03E+08	2.60E+08	1.36E+08	6.08E+08	-15.48	18.22	2.40	4.74	-13.41	11.74	3.23	6.40
M3	800	19500	3.91E+08	3.05E+08	1.60E+08	7.13E+08	-15.83	17.45	2.64	4.86	-13.98	11.88	3.56	6.55
M4	880	21000	4.95E+08	3.54E+08	1.85E+08	8.27E+08	-16.32	17.34	2.87	4.98	-14.59	12.32	3.88	6.72
M5	960	22500	5.30E+08	4.06E+08	2.13E+08	9.49E+08	-16.17	18.85	3.09	5.10	-14.51	13.09	4.16	6.88
M6	1040	24000	6.57E+08	4.62E+08	2.42E+08	1.08E+09	-16.67	18.12	3.27	5.20	-15.16	13.14	4.41	7.02
M7	1120	26000	8.36E+08	5.42E+08	2.84E+08	1.27E+09	-18.01	18.62	3.59	5.52	-16.52	13.96	4.84	7.45
M8	1200	27000	8.47E+08	5.85E+08	3.06E+08	1.37E+09	-17.37	20.09	3.71	5.51	-15.88	14.69	5.00	7.44
M9	1280	28500	1.02E+09	6.51E+08	3.41E+08	1.52E+09	-17.92	19.32	3.84	5.59	-16.56	14.63	5.19	7.54
M10	1360	29500	1.17E+09	6.98E+08	3.66E+08	1.63E+09	-18.00	18.42	3.86	5.49	-16.75	14.34	5.20	7.41
Y1	700	16500	2.53E+08	1.32E+08	8.17E+07	3.81E+08	-13.76	18.38	2.92	4.77	-12.12	13.91	3.76	6.13
Y2	800	19000	3.67E+08	1.75E+08	1.08E+08	5.05E+08	-14.61	18.87	3.41	5.23	-13.17	14.86	4.39	6.72
Y3	900	21500	5.17E+08	2.24E+08	1.39E+08	6.47E+08	-15.55	19.34	3.85	5.63	-14.27	15.76	4.95	7.23
Y4	1000	24000	7.07E+08	2.79E+08	1.73E+08	8.06E+08	-16.59	19.74	4.24	5.97	-15.44	16.56	5.45	7.67
Y5	1100	26000	9.11E+08	3.28E+08	2.03E+08	9.46E+08	-17.07	19.49	4.41	6.03	-16.07	16.76	5.67	7.75
Y6	1200	28500	1.20E+09	3.94E+08	2.44E+08	1.14E+09	-18.30	20.03	4.71	6.29	-17.38	17.58	6.06	8.09
Y7	1300	31000	1.54E+09	4.66E+08	2.88E+08	1.35E+09	-19.60	20.64	4.98	6.51	-18.74	18.43	6.40	8.37
Y8	1400	32000	1.79E+09	4.96E+08	3.07E+08	1.43E+09	-19.13	19.42	4.75	6.11	-18.40	17.60	6.11	7.86
U1	800	18000	4.46E+08	2.60E+08	1.36E+08	6.08E+08	-13.46	12.75	2.24	4.02	-12.14	9.66	3.02	5.42
U3	900	20000	5.90E+08	3.21E+08	1.68E+08	7.50E+08	-14.20	13.47	2.52	4.22	-12.96	10.49	3.40	5.70
U5	1000	22000	7.60E+08	3.88E+08	2.03E+08	9.08E+08	-14.80	14.06	2.77	4.40	-13.64	11.22	3.74	5.94
U7	1100	24500	1.00E+09	4.81E+08	2.52E+08	1.13E+09	-16.16	15.38	3.14	4.78	-15.01	12.50	4.24	6.45
U8	1200	26500	1.24E+09	5.63E+08	2.95E+08	1.32E+09	-16.86	16.13	3.38	4.95	-15.75	13.33	4.57	6.69
U9	1300	28500	1.51E+09	6.51E+08	3.41E+08	1.52E+09	-17.58	16.88	3.61	5.12	-16.51	14.15	4.87	6.92
U10	1400	30500	1.82E+09	7.46E+08	3.91E+08	1.74E+09	-18.31	17.60	3.83	5.29	-17.27	14.94	5.16	7.14
U11	1500	32000	2.11E+09	8.21E+08	4.30E+08	1.92E+09	-18.47	17.82	3.91	5.29	-17.48	15.28	5.28	7.13
SY1	1500	30000	1.46E+09	7.22E+08	3.78E+08	1.69E+09	-17.26	20.33	3.89	5.22	-15.87	16.25	5.25	7.05
SY2	1600	32000	1.76E+09	8.21E+08	4.30E+08	1.92E+09	-18.05	20.86	4.12	5.43	-16.71	16.97	5.56	7.32
SY3	1700	34000	2.09E+09	9.27E+08	4.86E+08	2.17E+09	-18.87	21.48	4.34	5.63	-17.56	17.73	5.86	7.59
SY4	1800	36000	2.47E+09	1.04E+09	5.44E+08	2.43E+09	-19.72	22.17	4.56	5.82	-18.43	18.54	6.16	7.86
SY5	1900	38000	2.88E+09	1.16E+09	6.06E+08	2.71E+09	-20.58	22.90	4.78	6.01	-19.31	19.37	6.45	8.12
SY6	2000	40000	3.35E+09	1.28E+09	6.72E+08	3.00E+09	-21.45	23.67	4.99	6.20	-20.20	20.23	6.73	8.37

Stress notations for Tables 6.1-6.13

Compressive: +ve

Tensile: -ve

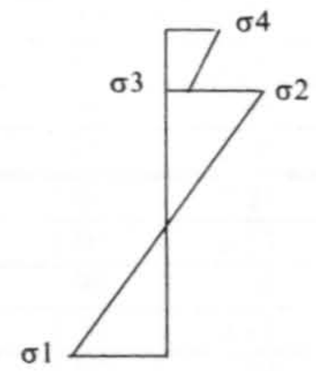

Stresses at mid-span

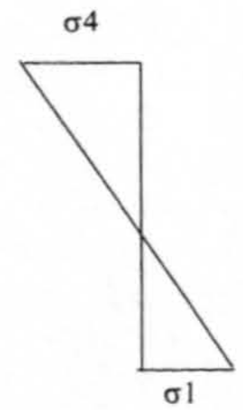

Stresses at support

Table 6.2: Components of elastic stress for two-span beams constructed using three different sequences of construction using narrow insitu crossheads

PCA Section	Sequence 1- unpropped construction						Sequence 2- unpropped, continuity first						Sequence 3 - propped construction					
	stress at mid-span				stress at support		stress at mid-span				stress at support		stress at mid-span				stress at support	
	σ1	σ2	σ3	σ4	σ1	σ4	σ1	σ2	σ3	σ4	σ1	σ4	σ1	σ2	σ3	σ4	σ1	σ4
T1	-10.05	12.41	0.33	1.78	6.01	-3.56	-7.90	8.71	0.33	1.78	7.73	-4.58	-6.50	4.94	0.43	2.29	7.73	-4.58
T2	-9.52	11.06	0.42	1.75	5.94	-3.49	-7.57	7.90	0.42	1.75	7.64	-4.49	-6.39	4.71	0.54	2.25	7.64	-4.49
T3	-8.99	10.98	0.60	1.71	5.97	-3.42	-7.25	7.98	0.60	1.71	7.67	-4.40	-6.29	5.03	0.78	2.20	7.67	-4.40
T4	-9.58	10.94	0.72	1.85	6.49	-3.71	-7.80	8.06	0.72	1.85	8.34	-4.76	-6.88	5.29	0.92	2.38	8.34	-4.76
T5	-9.47	10.24	0.77	1.85	6.48	-3.69	-7.76	7.65	0.77	1.85	8.33	-4.74	-6.92	5.18	0.99	2.37	8.33	-4.74
T6	-9.43	9.83	0.82	1.84	6.47	-3.68	-7.78	7.42	0.82	1.84	8.31	-4.73	-6.99	5.17	1.05	2.37	8.31	-4.73
T7	-10.89	11.08	1.00	2.12	7.43	-4.24	-9.02	8.46	1.00	2.12	9.54	-5.45	-8.16	6.05	1.29	2.73	9.54	-5.45
T8	-11.63	11.54	1.12	2.26	7.90	-4.52	-9.68	8.89	1.12	2.26	10.15	-5.80	-8.80	6.50	1.44	2.90	10.15	-5.80
T9	-11.62	11.34	1.17	2.25	7.83	-4.50	-9.71	8.82	1.17	2.25	10.07	-5.78	-8.87	6.57	1.50	2.89	10.07	-5.78
T10	-12.35	11.89	1.29	2.38	8.25	-4.76	-10.36	9.33	1.29	2.38	10.61	-6.12	-9.50	7.07	1.65	3.06	10.61	-6.12
M2	-12.38	17.03	1.21	2.40	6.34	-4.80	-10.28	13.42	1.21	2.40	8.55	-6.47	-9.23	10.15	1.64	3.24	8.55	-6.47
M3	-12.63	16.14	1.33	2.45	6.52	-4.91	-10.60	12.93	1.33	2.45	8.80	-6.62	-9.67	10.12	1.80	3.31	8.80	-6.62
M4	-13.04	15.92	1.45	2.51	6.69	-5.02	-11.04	12.93	1.45	2.51	9.02	-6.78	-10.17	10.40	1.96	3.39	9.02	-6.78
M5	-12.78	17.32	1.56	2.57	6.90	-5.15	-10.78	13.93	1.56	2.57	9.31	-6.94	-9.94	11.03	2.10	3.47	9.31	-6.94
M6	-13.18	16.50	1.65	2.62	7.10	-5.24	-11.21	13.46	1.65	2.62	9.58	-7.08	-10.45	10.95	2.22	3.54	9.58	-7.08
M7	-14.27	16.84	1.81	2.78	7.59	-5.57	-12.23	13.90	1.81	2.78	10.25	-7.51	-11.48	11.55	2.44	3.76	10.25	-7.51
M8	-13.70	18.25	1.87	2.78	7.46	-5.55	-11.68	14.93	1.87	2.78	10.06	-7.49	-10.93	12.21	2.52	3.75	10.06	-7.49
M9	-14.15	17.41	1.94	2.81	7.66	-5.63	-12.15	14.41	1.94	2.81	10.34	-7.60	-11.46	12.05	2.61	3.80	10.34	-7.60
M10	-14.24	16.50	1.94	2.76	7.61	-5.53	-12.31	13.81	1.94	2.76	10.27	-7.46	-11.68	11.75	2.62	3.73	10.27	-7.46
Y1	-11.34	16.94	1.48	2.41	4.96	-4.83	-9.84	14.32	1.48	2.41	6.38	-6.20	-9.01	12.06	1.90	3.10	6.38	-6.20
Y2	-11.95	17.18	1.73	2.64	5.45	-5.29	-10.48	14.72	1.73	2.64	7.00	-6.79	-9.75	12.69	2.22	3.40	7.00	-6.79
Y3	-12.66	17.43	1.94	2.84	5.88	-5.68	-11.20	15.11	1.94	2.84	7.56	-7.30	-10.56	13.30	2.50	3.65	7.56	-7.30
Y4	-13.49	17.64	2.14	3.01	6.30	-6.02	-12.04	15.47	2.14	3.01	8.10	-7.74	-11.46	13.86	2.75	3.87	8.10	-7.74
Y5	-13.90	17.30	2.22	3.04	6.45	-6.08	-12.50	15.32	2.22	3.04	8.28	-7.81	-11.99	13.94	2.86	3.90	8.28	-7.81
Y6	-14.93	17.69	2.37	3.17	6.83	-6.34	-13.52	15.81	2.37	3.17	8.77	-8.14	-13.05	14.58	3.05	4.07	8.77	-8.14
Y7	-16.05	18.17	2.50	3.28	7.18	-6.56	-14.62	16.37	2.50	3.28	9.23	-8.43	-14.19	15.26	3.22	4.21	9.23	-8.43
Y8	-15.74	17.06	2.39	3.08	6.85	-6.15	-14.42	15.48	2.39	3.08	8.81	-7.91	-14.05	14.56	3.07	3.95	8.81	-7.91
U1	-10.95	11.65	1.13	2.03	5.13	-4.06	-9.43	9.73	1.13	2.03	6.92	-5.48	-8.76	8.17	1.52	2.74	6.92	-5.48
U3	-11.55	12.22	1.27	2.13	5.42	-4.27	-10.00	10.31	1.27	2.13	7.31	-5.76	-9.38	8.81	1.72	2.88	7.31	-5.76
U5	-12.03	12.69	1.40	2.22	5.65	-4.44	-10.49	10.80	1.40	2.22	7.62	-5.99	-9.90	9.36	1.89	3.00	7.62	-5.99
U7	-13.15	13.82	1.58	2.41	6.13	-4.82	-11.52	11.85	1.58	2.41	8.27	-6.50	-10.95	10.40	2.14	3.25	8.27	-6.50
U8	-13.74	14.45	1.70	2.50	6.33	-4.99	-12.10	12.48	1.70	2.50	8.54	-6.74	-11.54	11.07	2.30	3.37	8.54	-6.74
U9	-14.36	15.08	1.82	2.58	6.53	-5.16	-12.70	13.10	1.82	2.58	8.81	-6.96	-12.16	11.73	2.45	3.48	8.81	-6.96
U10	-14.99	15.70	1.93	2.66	6.73	-5.32	-13.32	13.71	1.93	2.66	9.08	-7.18	-12.79	12.37	2.60	3.59	9.08	-7.18
U11	-15.16	15.87	1.97	2.66	6.70	-5.32	-13.51	13.93	1.97	2.66	9.04	-7.18	-13.02	12.66	2.66	3.59	9.04	-7.18
SY1	-14.11	18.40	1.96	2.63	6.39	-5.26	-12.31	15.69	1.96	2.63	8.63	-7.10	-11.61	13.64	2.64	3.55	8.63	-7.10
SY2	-14.77	18.81	2.07	2.73	6.64	-5.46	-12.96	16.16	2.07	2.73	8.96	-7.37	-12.28	14.20	2.80	3.68	8.96	-7.37
SY3	-15.47	19.32	2.18	2.83	6.87	-5.66	-13.64	16.70	2.18	2.83	9.27	-7.64	-12.98	14.82	2.95	3.82	9.27	-7.64
SY4	-16.21	19.90	2.29	2.93	7.10	-5.85	-14.34	17.30	2.29	2.93	9.58	-7.90	-13.70	15.48	3.10	3.95	9.58	-7.90
SY5	-16.96	20.52	2.40	3.02	7.32	-6.05	-15.06	17.94	2.40	3.02	9.87	-8.16	-14.43	16.17	3.24	4.08	9.87	-8.16
SY6	-17.72	21.19	2.51	3.12	7.53	-6.23	-15.80	18.61	2.51	3.12	10.16	-8.41	-15.17	16.89	3.38	4.21	10.16	-8.41

Table 6.3: Components of elastic stress for two-span beams constructed using three different sequences of construction using wide insitu crossheads

PCA Section	Sequence 1 - unpropped construction						Sequence 2 unpropped, continuity first						Sequence 3 - propped construction					
	stress at mid-span				stress at support		stress at mid-span				stress at support		stress at mid-span				stress at support	
	σ1	σ2	σ3	σ4	σ1	σ4	σ1	σ2	σ3	σ4	σ1	σ4	σ1	σ2	σ3	σ4	σ1	σ4
T1	-10.68	12.48	0.40	2.15	7.26	-4.30	-8.99	9.58	0.40	2.15	9.33	-5.53	-7.30	5.02	0.51	2.76	9.33	-5.53
T2	-10.11	11.15	0.50	2.09	7.11	-4.18	-8.56	8.63	0.50	2.09	9.14	-5.37	-7.14	4.81	0.64	2.69	9.14	-5.37
T3	-9.49	11.09	0.71	2.00	6.98	-4.00	-8.06	8.60	0.71	2.00	8.97	-5.14	-6.94	5.16	0.91	2.57	8.97	-5.14
T4	-10.08	11.05	0.83	2.14	7.49	-4.28	-8.58	8.63	0.83	2.14	9.63	-5.50	-7.52	5.43	1.06	2.75	9.63	-5.50
T5	-9.95	10.36	0.88	2.12	7.44	-4.24	-8.50	8.16	0.88	2.12	9.56	-5.44	-7.54	5.33	1.13	2.72	9.56	-5.44
T6	-9.89	9.94	0.94	2.10	7.39	-4.21	-8.48	7.89	0.94	2.10	9.49	-5.40	-7.58	5.32	1.20	2.70	9.49	-5.40
T7	-11.36	11.21	1.13	2.39	8.37	-4.78	-9.74	8.93	1.13	2.39	10.76	-6.15	-8.77	6.21	1.45	3.07	10.76	-6.15
T8	-12.10	11.67	1.25	2.53	8.83	-5.05	-10.39	9.35	1.25	2.53	11.35	-6.49	-9.41	6.67	1.61	3.25	11.35	-6.49
T9	-12.07	11.47	1.30	2.51	8.73	-5.02	-10.39	9.25	1.30	2.51	11.22	-6.45	-9.45	6.74	1.67	3.22	11.22	-6.45
T10	-12.80	12.03	1.42	2.64	9.14	-5.28	-11.03	9.75	1.42	2.64	11.75	-6.78	-10.08	7.25	1.83	3.39	11.75	-6.78
M2	-12.70	17.15	1.34	2.64	6.98	-5.29	-10.82	13.92	1.34	2.64	9.42	-7.13	-9.67	10.31	1.80	3.57	9.42	-7.13
M3	-12.94	16.26	1.46	2.68	7.14	-5.37	-11.10	13.36	1.46	2.68	9.63	-7.24	-10.08	10.29	1.97	3.62	9.63	-7.24
M4	-13.33	16.04	1.58	2.73	7.27	-5.46	-11.50	13.32	1.58	2.73	9.81	-7.37	-10.56	10.57	2.13	3.69	9.81	-7.37
M5	-13.06	17.45	1.68	2.78	7.46	-5.56	-11.22	14.34	1.68	2.78	10.06	-7.51	-10.32	11.20	2.27	3.75	10.06	-7.51
M6	-13.45	16.63	1.77	2.82	7.64	-5.64	-11.63	13.82	1.77	2.82	10.31	-7.62	-10.81	11.12	2.39	3.81	10.31	-7.62
M7	-14.54	16.96	1.93	2.98	8.13	-5.96	-12.64	14.24	1.93	2.98	10.97	-8.04	-11.84	11.73	2.61	4.02	10.97	-8.04
M8	-13.95	18.37	1.99	2.96	7.96	-5.93	-12.07	15.28	1.99	2.96	10.74	-8.00	-11.27	12.38	2.69	4.00	10.74	-8.00
M9	-14.39	17.53	2.06	2.99	8.15	-5.99	-12.52	14.73	2.06	2.99	11.00	-8.08	-11.79	12.22	2.78	4.04	11.00	-8.08
M10	-14.48	16.62	2.06	2.94	8.08	-5.87	-12.67	14.09	2.06	2.94	10.90	-7.92	-12.00	11.91	2.78	3.96	10.90	-7.92
Y1	-11.62	17.10	1.64	2.68	5.52	-5.37	-10.29	14.78	1.64	2.68	7.09	-6.90	-9.36	12.27	2.11	3.45	7.09	-6.90
Y2	-12.21	17.35	1.89	2.90	5.97	-5.80	-10.88	15.13	1.89	2.90	7.67	-7.45	-10.09	12.90	2.43	3.72	7.67	-7.45
Y3	-12.91	17.60	2.11	3.08	6.38	-6.16	-11.58	15.48	2.11	3.08	8.20	-7.92	-10.88	13.52	2.71	3.96	8.20	-7.92
Y4	-13.73	17.81	2.30	3.24	6.78	-6.48	-12.39	15.80	2.30	3.24	8.72	-8.33	-11.77	14.07	2.96	4.16	8.72	-8.33
Y5	-14.12	17.45	2.38	3.25	6.90	-6.50	-12.82	15.62	2.38	3.25	8.87	-8.36	-12.28	14.14	3.06	4.18	8.87	-8.36
Y6	-15.15	17.85	2.52	3.37	7.26	-6.74	-13.83	16.08	2.52	3.37	9.33	-8.66	-13.33	14.77	3.24	4.33	9.33	-8.66
Y7	-16.26	18.32	2.65	3.47	7.60	-6.94	-14.92	16.62	2.65	3.47	9.77	-8.92	-14.46	15.45	3.41	4.46	9.77	-8.92
Y8	-15.94	17.19	2.53	3.25	7.24	-6.50	-14.69	15.71	2.53	3.25	9.31	-8.36	-14.30	14.74	3.25	4.18	9.31	-8.36
U1	-11.21	11.76	1.25	2.24	5.65	-4.47	-9.85	10.05	1.25	2.24	7.63	-6.04	-9.11	8.32	1.68	3.02	7.63	-6.04
U3	-11.79	12.34	1.39	2.33	5.91	-4.66	-10.40	10.60	1.39	2.33	7.98	-6.28	-9.71	8.96	1.87	3.14	7.98	-6.28
U5	-12.26	12.81	1.51	2.41	6.11	-4.81	-10.85	11.08	1.51	2.41	8.25	-6.49	-10.22	9.52	2.04	3.25	8.25	-6.49
U7	-13.38	13.94	1.70	2.59	6.59	-5.18	-11.88	12.12	1.70	2.59	8.89	-6.99	-11.25	10.56	2.30	3.49	8.89	-6.99
U8	-13.96	14.57	1.82	2.67	6.77	-5.33	-12.43	12.73	1.82	2.67	9.13	-7.20	-11.84	11.22	2.46	3.60	9.13	-7.20
U9	-14.57	15.20	1.93	2.75	6.95	-5.49	-13.02	13.35	1.93	2.75	9.38	-7.41	-12.44	11.88	2.61	3.70	9.38	-7.41
U10	-15.20	15.81	2.04	2.82	7.13	-5.64	-13.62	13.95	2.04	2.82	9.62	-7.61	-13.06	12.53	2.75	3.81	9.62	-7.61
U11	-15.35	15.98	2.08	2.81	7.08	-5.62	-13.80	14.16	2.08	2.81	9.55	-7.59	-13.27	12.81	2.81	3.79	9.55	-7.59
SY1	-14.30	18.52	2.08	2.79	6.78	-5.58	-12.62	15.98	2.08	2.79	9.15	-7.53	-11.87	13.80	2.80	3.76	9.15	-7.53
SY2	-14.96	18.93	2.19	2.89	7.01	-5.77	-13.25	16.43	2.19	2.89	9.47	-7.79	-12.54	14.36	2.96	3.89	9.47	-7.79
SY3	-15.66	19.43	2.30	2.98	7.24	-5.96	-13.92	16.96	2.30	2.98	9.77	-8.04	-13.22	14.97	3.11	4.02	9.77	-8.04
SY4	-16.39	20.01	2.41	3.07	7.46	-6.15	-14.62	17.55	2.41	3.07	10.06	-8.30	-13.94	15.64	3.25	4.15	10.06	-8.30
SY5	-17.13	20.64	2.52	3.17	7.67	-6.33	-15.33	18.18	2.52	3.17	10.34	-8.55	-14.66	16.32	3.39	4.27	10.34	-8.55
SY6	-17.89	21.30	2.62	3.26	7.87	-6.52	-16.06	18.84	2.62	3.26	10.62	-8.79	-15.40	17.04	3.53	4.40	10.62	-8.79

Table 6.4: Prestressing mid-span and end beams to satisfy initial and service limiting stress requirements according to BS5400

PCA	Span	At mid-span					At support: areas of deflected and debonded wires (mm^2)					Moment	Ratios of moments	
Section	(mm)	ep1 (mm)	Ap1(mm^2)	Fpi (kN)	Mps (kNm)	Ap (%)	ep2 (mm)	deflected	debonded	Mpse	Ape/Ap1	Msw (kNm	Mps/Msw	Mpse/Mps
T1	9000	50	1036	1272	63.60	1.06	50	0	0	63.60	100.00	23.39	2.72	1.000
T2	9500	65	1036	1272	82.68	0.98	65	0	0	82.68	100.00	28.20	2.93	1.000
T3	11000	90	1130	1387	124.86	0.99	90	0	0	124.86	100.00	40.69	3.07	1.000
T4	12000	125	1130	1387	173.42	0.92	90	188	377	83.20	66.64	52.02	3.33	0.480
T5	12500	140	1130	1387	194.23	0.86	102	188	377	94.30	66.64	60.16	3.23	0.485
T6	13000	150	1224	1503	225.41	0.88	150	0	754	86.56	38.40	69.08	3.26	0.384
T7	14500	180	1319	1619	291.49	0.90	134	188	565	124.05	57.16	91.20	3.20	0.426
T8	15500	200	1319	1619	323.88	0.85	144	377	0	233.19	100.00	109.91	2.95	0.720
T9	16000	220	1413	1735	381.66	0.86	163	377	0	282.77	100.00	123.20	3.10	0.741
T10	17000	238	1664	2043	485.21	0.97	183	277	832	186.93	50.00	146.31	3.32	0.385
M2	18000	167	3190	3917	654.06	1.01	119	555	832	344.51	73.92	302.54	2.16	0.527
M3	19500	198	3468	4258	843.05	0.99	149	555	555	532.89	84.00	391.18	2.16	0.632
M4	21000	251	3745	4598	1154.08	0.98	172	555	1110	556.44	70.36	495.02	2.33	0.482
M5	22500	264	3468	4258	1124.07	0.98	178	555	1110	515.32	67.99	530.30	2.12	0.458
M6	24000	306	3745	4598	1406.96	0.97	210	555	1110	679.38	70.36	657.36	2.14	0.483
M7	26000	378	4161	5109	1931.08	0.99	236	555	1387	803.76	66.67	835.71	2.31	0.416
M8	27000	368	4161	5109	1879.99	1.06	230	555	1387	783.33	66.67	846.55	2.22	0.417
M9	28500	428	4161	5109	2186.51	0.98	268	555	1387	912.75	66.67	1019.37	2.14	0.417
M10	29500	477	4330	5316	2535.81	0.95	300	555	1387	1083.98	67.97	1174.84	2.16	0.427
SY1	30000	479	4854	5959	2854.60	0.88	256	832	1110	1176.75	77.13	1458.00	1.96	0.412
SY2	32000	513	5132	6301	3232.32	0.88	273	832	1110	1348.08	78.37	1756.16	1.84	0.417
SY3	34000	581	5271	6471	3759.92	0.86	331	832	1110	1690.97	78.94	2090.92	1.80	0.450
SY4	36000	622	5825	7152	4448.32	0.90	294	832	1110	1701.92	80.94	2467.26	1.80	0.383
SY5	38000	672	6103	7493	5035.27	0.90	346	832	1110	2121.03	81.81	2884.39	1.75	0.421
SY6	40000	718	6519	8004	5746.66	0.92	397	832	1110	2636.44	82.97	3348.00	1.72	0.459
Y1	16500	149	2449	3007	448.01	0.79	74	377	754	154.00	69.21	252.51	1.77	0.344
Y2	19000	206	2543	3122	643.17	0.75	79	377	942	155.28	62.96	367.32	1.75	0.241
Y3	21500	247	2826	3470	857.00	0.76	127	377	942	293.76	66.67	517.14	1.66	0.343
Y4	24000	293	3203	3932	1152.22	0.78	180	377	942	499.67	70.59	707.04	1.63	0.434
Y5	26000	344	3485	4279	1471.88	0.78	196	754	1036	589.32	70.27	910.91	1.62	0.400
Y6	28500	415	4161	5109	2120.10	0.85	55	377	1664	168.61	60.01	1196.04	1.77	0.080
Y7	31000	465	5132	6301	2929.88	0.96	374	555	3051	955.55	40.55	1544.81	1.90	0.326
Y8	32000	528	5132	6301	3326.83	0.88	437	555	3051	1116.51	40.55	1794.56	1.85	0.336
U1	18000	246	3109	3817	939.00	0.67	143	377	754	413.46	75.75	445.91	2.11	0.440
U3	20000	309	3202	3931	1214.76	0.64	197	377	942	546.62	70.58	589.50	2.06	0.450
U5	22000	354	3391	4163	1473.81	0.64	222	377	942	667.50	72.22	760.49	1.94	0.453
U7	24500	413	4300	5279	2180.36	0.76	241	555	1664	779.96	61.30	1000.92	2.18	0.358
U8	26500	455	4577	5619	2556.83	0.76	276	555	1942	892.89	57.57	1239.47	2.06	0.349
U9	28500	497	4993	6130	3046.69	0.79	314	555	2358	1015.83	52.77	1512.82	2.01	0.333
U10	30500	540	5271	6471	3494.59	0.79	321	555	2358	1148.04	55.26	1823.29	1.92	0.329
U11	32000	583	5548	6812	3971.14	0.80	377	555	2358	1476.53	57.50	2106.88	1.88	0.372

Table 6.5: Summary of restraint moments (kNm) at the intermediate support

Section	Case 1	Case 1a	Case 2	Case 2a	Case 3	Case 4	Case 5	Case 6
T1	-5.35	-14.6	-17.6	-31.6	-10.05	-15.6	49.89	-4.29
T2	6.02	-8	-7.74	-27	-31.6	-5.05	68.15	6.25
T3	21.32	-1.26	2.75	-26.86	4.75	6.89	105.6	20.9
T4	15.73	-8.21	-6.45	-38.7	-0.529	-2.07	113.6	21
T5	46.2	11.61	21.96	-21.6	18.72	27.9	153.9	26.7
T6	35.78	2.5	9.66	-33.38	11	15.5	151.5	19.9
T7	75.15	41.99	65.38	-3.18	49.34	9.3	245.3	43.6
T8	82.49	26.76	44.47	-24.97	36.6	54.3	248	84.2
T9	115.8	48.3	-6.89	-6.98	57.45	98.3	293.5	121.9
T10	93.9	29.7	48.38	-32.2	93.92	59.63	290	98.3
M2	48.6	-25.5	-31.5	-140.1	-3.56	-42.8	361.5	28.7
M3	122.4	16.6	29.1	-118	38	14	490.7	91.9
M4	235.7	85.7	127.9	-71	104.6	107.6	660.3	195.2
M5	107.4	-15.3	-18.3	-195.2	15.8	-36.9	592.6	76.7
M6	210.7	45.5	68.4	-160	74.9	44.7	763.2	169.3
M7	419.9	177.4	253.4	-64.2	198.6	220.2	1064.9	362
M8	302.1	86	121.7	-174.4	117.6	90.2	998.1	258
M9	371.1	120.7	169.6	-170.1	153.6	133.5	1144.9	316.9
M10	513.8	211.4	299.1	-100.1	239.4	257.1	1343.5	445.1
SY1	647.2	293.5	412.5	-38.8	319.7	368.9	1495	610
SY2	667.7	289	400	-89.5	319.1	352.1	1632.2	636.2
SY3	1285	690.6	974.3	250	696.9	910.2	2396	1189
SY4	934.1	436.8	596	-45.6	459.9	532.3	2151	896.4
SY5	1038.4	489.2	661	-49.02	536.8	590.2	2394	1002.5
SY6	1221.9	596.7	735.4	-28.5	639.5	719.6	2723.2	1127.8
Y1	30.4	-13.6	-11.01	-71.8	-3.8	-17.04	198.7	21.2
Y2	54.9	-7.03	-0.2	-84.9	47.3	-8.6	276.7	41
Y3	83.6	1.45	13.1	-98.4	14.8	-49.7	367.6	65.6
Y4	136.4	26.1	49.1	-98.3	39.1	34.1	490.2	111.8
Y5	206.2	64.2	104.4	-81.6	75.6	85.5	621.1	172.2
Y6	383	175.4	262.8	0.8	177.3	235.9	880.2	327.3
Y7	499.3	246.5	359.8	40.6	238.2	325.3	1083.7	436.7
Y8	574.1	291.5	423.1	67.3	281.6	385.1	1168	502
U1	143.6	40.1	63.6	-75.08	57.34	49.9	457.6	141.1
U3	198.3	65.2	99.5	-77	84.9	81.8	583.1	194
U5	206.2	81	86	-115.3	81.03	65.6	671.5	206
U7	387.9	168.8	241.2	-44.2	185	211.3	961.1	383.4
U8	351.7	115.3	180.3	-133.7	134.9	146.6	1064.5	354
U9	381.8	119.6	184.4	-167.7	139.8	145.6	1203.6	443.5
U10	553.4	222.4	328.2	-109.4	233.8	280.2	149.8	621.5
U11	571.3	239.4	322.5	-126.1	257.2	273	1544.5	591.1

Note: sagging moment = +ve, and hogging moment = -ve

Case 1: Slabs and insitu cross heads are cast unpropped and the continuity was assumed to come into effect after 7 days of slab casting. Wet concrete is supported by precast beams alone. The ages of precast beams at 24 and 100 days were considered

Case 2: Slabs and insitu cross heads are cast using propped construction and the wet concrete is supported by the indeterminate beams. The ages of precast beams at 24 and 100 days were considered.

Case 3: Slabs are cast unpropped at 24 days and the weight is supported by the simple precast beams. Cross heads insitu is later cast at 100 days.

Case 4: Cross heads are first cast at 24 days. Slabs are cast unpropped at 100 days and the wet concrete is supported by the indeterminate beams

Case 5: A hypothetical condition where only the insitu cross heads are cast at 24 days leaving the interactions for the restrained moments to the prestressing and beam selfweight alone.

Case 6: Similar to Case1 except combination of parameters yielding minimum creep and shrinkage are used

Table 6.6: Stresses (MPa) at the bottom (σ1) and top (σ4) fibres of the insitu crossheads at the intermediate support resulting from restraint moments

PCA	Case 1		Case 1a		Case 2		Case 2a		Case 3		Case 4		Case 5		Case 6	
Section	σ1	σ4	σ1	σ4	σ1	σ4	σ1	σ4	σ1	σ4	σ1	σ4	σ1	σ4	σ1	σ4
T1	0.23	-0.14	0.62	-0.37	0.75	-0.45	1.35	-0.80	0.43	-0.25	0.67	-0.39	-2.13	1.26	0.18	-0.11
T2	-0.23	0.13	0.30	-0.18	0.29	-0.17	1.02	-0.60	1.20	-0.70	0.19	-0.11	-2.59	1.52	-0.24	0.14
T3	-0.61	0.35	0.04	-0.02	-0.08	0.04	0.77	-0.44	-0.14	0.08	-0.20	0.11	-3.01	1.72	-0.60	0.34
T4	-0.41	0.23	0.21	-0.12	0.17	-0.10	1.01	-0.58	0.01	-0.01	0.05	-0.03	-2.96	1.69	-0.55	0.31
T5	-1.11	0.63	-0.28	0.16	-0.53	0.30	0.52	-0.30	-0.45	0.26	-0.67	0.38	-3.70	2.10	-0.64	0.37
T6	-0.79	0.45	-0.06	0.03	-0.21	0.12	0.74	-0.42	-0.24	0.14	-0.34	0.20	-3.36	1.91	-0.44	0.25
T7	-1.54	0.88	-0.86	0.49	-1.34	0.77	0.07	-0.04	-1.01	0.58	-0.19	0.11	-5.03	2.87	-0.89	0.51
T8	-1.57	0.90	-0.51	0.29	-0.85	0.49	0.48	-0.27	-0.70	0.40	-1.04	0.59	-4.73	2.71	-1.61	0.92
T9	-2.06	1.18	-0.86	0.49	0.12	-0.07	0.12	-0.07	-1.02	0.59	-1.75	1.00	-5.22	3.00	-2.17	1.24
T10	-1.56	0.90	-0.49	0.28	-0.80	0.46	0.53	-0.31	-1.56	0.90	-0.99	0.57	-4.81	2.78	-1.63	0.94
M2	-0.41	0.31	0.21	-0.16	0.27	-0.20	1.18	-0.89	0.03	-0.02	0.36	-0.27	-3.05	2.31	-0.24	0.18
M3	-0.91	0.68	-0.12	0.09	-0.22	0.16	0.87	-0.66	-0.28	0.21	-0.10	0.08	-3.63	2.73	-0.68	0.51
M4	-1.54	1.16	-0.56	0.42	-0.84	0.63	0.46	-0.35	-0.68	0.51	-0.70	0.53	-4.32	3.25	-1.28	0.96
M5	-0.63	0.47	0.09	-0.07	0.11	-0.08	1.15	-0.86	-0.09	0.07	0.22	-0.16	-3.49	2.60	-0.45	0.34
M6	-1.12	0.83	-0.24	0.18	-0.36	0.27	0.85	-0.63	-0.40	0.29	-0.24	0.18	-4.06	3.00	-0.90	0.67
M7	-2.04	1.49	-0.86	0.63	-1.23	0.90	0.31	-0.23	-0.96	0.71	-1.07	0.78	-5.17	3.79	-1.76	1.29
M8	-1.34	1.00	-0.38	0.28	-0.54	0.40	0.77	-0.57	-0.52	0.39	-0.40	0.30	-4.42	3.29	-1.14	0.85
M9	-1.51	1.11	-0.49	0.36	-0.69	0.51	0.69	-0.51	-0.63	0.46	-0.54	0.40	-4.67	3.43	-1.29	0.95
M10	-1.94	1.41	-0.80	0.58	-1.13	0.82	0.38	-0.28	-0.91	0.66	-0.97	0.71	-5.08	3.69	-1.68	1.22
SY1	-1.99	1.64	-0.90	0.74	-1.27	1.04	0.12	-0.10	-0.98	0.81	-1.13	0.93	-4.60	3.78	-1.88	1.54
SY2	-1.87	1.54	-0.81	0.67	-1.12	0.92	0.25	-0.21	-0.90	0.74	-0.99	0.81	-4.58	3.77	-1.79	1.47
SY3	-3.31	2.72	-1.78	1.46	-2.51	2.07	-0.64	0.53	-1.79	1.48	-2.34	1.93	-6.17	5.08	-3.06	2.52
SY4	-2.22	1.83	-1.04	0.85	-1.41	1.17	0.11	-0.09	-1.09	0.90	-1.26	1.04	-5.10	4.21	-2.13	1.75
SY5	-2.28	1.88	-1.07	0.89	-1.45	1.20	0.11	-0.09	-1.18	0.97	-1.30	1.07	-5.26	4.34	-2.20	1.82
SY6	-2.49	2.06	-1.22	1.01	-1.50	1.24	0.06	-0.05	-1.30	1.08	-1.47	1.22	-5.55	4.60	-2.30	1.90
Y1	-0.32	0.31	0.14	-0.14	0.12	-0.11	0.76	-0.74	0.04	-0.04	0.18	-0.18	-2.11	2.05	-0.22	0.22
Y2	-0.48	0.47	0.06	-0.06	0.00	0.00	0.75	-0.72	-0.42	0.40	0.08	-0.07	-2.43	2.36	-0.36	0.35
Y3	-0.62	0.60	-0.01	0.01	-0.10	0.09	0.73	-0.70	-0.11	0.11	0.37	-0.36	-2.73	2.63	-0.49	0.47
Y4	-0.87	0.83	-0.17	0.16	-0.31	0.30	0.63	-0.60	-0.25	0.24	-0.22	0.21	-3.13	2.99	-0.71	0.68
Y5	-1.15	1.08	-0.36	0.34	-0.58	0.55	0.45	-0.43	-0.42	0.40	-0.48	0.45	-3.46	3.26	-0.96	0.90
Y6	-1.88	1.75	-0.86	0.80	-1.29	1.20	0.00	0.00	-0.87	0.81	-1.16	1.07	-4.32	4.01	-1.61	1.49
Y7	-2.18	1.99	-1.08	0.98	-1.57	1.43	-0.18	0.16	-1.04	0.95	-1.42	1.30	-4.73	4.32	-1.91	1.74
Y8	-2.25	2.02	-1.14	1.02	-1.66	1.49	-0.26	0.24	-1.10	0.99	-1.51	1.35	-4.57	4.10	-1.96	1.76
U1	-0.98	0.78	-0.27	0.22	-0.43	0.34	0.51	-0.41	-0.39	0.31	-0.34	0.27	-3.12	2.47	-0.96	0.76
U3	-1.16	0.91	-0.38	0.30	-0.58	0.46	0.45	-0.35	-0.50	0.39	-0.48	0.38	-3.41	2.68	-1.13	0.89
U5	-1.04	0.82	-0.41	0.32	-0.43	0.34	0.58	-0.46	-0.41	0.32	-0.33	0.26	-3.38	2.66	-1.04	0.82
U7	-1.71	1.35	-0.75	0.59	-1.06	0.84	0.20	-0.15	-0.82	0.64	-0.93	0.73	-4.24	3.33	-1.69	1.33
U8	-1.37	1.08	-0.45	0.35	-0.70	0.55	0.52	-0.41	-0.53	0.41	-0.57	0.45	-4.15	3.27	-1.38	1.09
U9	-1.33	1.05	-0.42	0.33	-0.64	0.51	0.58	-0.46	-0.49	0.38	-0.51	0.40	-4.19	3.31	-1.54	1.22
U10	-1.73	1.37	-0.70	0.55	-1.03	0.81	0.34	-0.27	-0.73	0.58	-0.88	0.69	-0.47	0.37	-1.95	1.54
U11	-1.62	1.29	-0.68	0.54	-0.91	0.73	0.36	-0.28	-0.73	0.58	-0.77	0.61	-4.37	3.47	-1.67	1.33

Table 6.7: Restraint moments and concrete stresses at the interface between precast beams and insitu cross heads

Section	Moments (kNm)		Stress (MPa), Case 1		Stress (MPa), Case 2	
	Case 1	Case 2	σ1	σ4	σ1	σ4
T1	-1.43	-13.6	0.06	-0.04	0.58	-0.34
T2	10.1	-3.48	-0.38	0.23	0.13	-0.08
T3	26.1	7.6	-0.74	0.43	-0.22	0.12
T4	21.1	-0.9	-0.55	0.31	0.02	-0.01
T5	51.6	27.6	-1.24	0.71	-0.66	0.38
T6	41.7	15.8	-0.92	0.53	-0.35	0.20
T7	81.7	72	-1.67	0.96	-1.48	0.84
T8	89.7	51.9	-1.71	0.98	-0.99	0.57
T9	123.2	1.17	-2.19	1.26	-0.02	0.01
T10	102.1	56.9	-1.70	0.98	-0.94	0.54
M2	63.9	-15.8	-0.54	0.41	0.13	-0.10
M3	139.3	46.4	-1.03	0.78	-0.34	0.26
M4	254.2	146.9	-1.66	1.25	-0.96	0.72
M5	127.3	2.17	-0.75	0.56	-0.01	0.01
M6	232.5	90.7	-1.24	0.91	-0.48	0.36
M7	443.8	278	-2.16	1.58	-1.35	0.99
M8	326.6	146.9	-1.44	1.08	-0.65	0.48
M9	398	197.2	-1.62	1.19	-0.80	0.59
M10	542.4	328.3	-2.05	1.49	-1.24	0.90
SY1	679.2	326.5	-2.09	1.72	-1.00	0.83
SY2	703.1	436.2	-1.97	1.62	-1.22	1.01
SY3	1322.8	1012.6	-3.41	2.80	-2.61	2.15
SY4	976.4	639.2	-2.32	1.91	-1.52	1.25
SY5	1084.5	708.1	-2.38	1.97	-1.55	1.28
SY6	1271.7	786.5	-2.59	2.15	-1.60	1.33
Y1	41.3	0.18	-0.44	0.43	0.00	0.00
Y2	68.1	13.3	-0.60	0.58	-0.12	0.11
Y3	99.3	29.1	-0.74	0.71	-0.22	0.21
Y4	154.9	67.9	-0.99	0.94	-0.43	0.41
Y5	227.2	125.8	-1.26	1.19	-0.70	0.66
Y6	407	287.2	-2.00	1.85	-1.41	1.31
Y7	526.9	387.9	-2.30	2.10	-1.69	1.55
Y8	604.4	453.8	-2.36	2.12	-1.78	1.59
U1	161.5	81.9	-1.10	0.87	-0.56	0.44
U3	218.9	120.6	-1.28	1.01	-0.70	0.55
U5	229.8	110.1	-1.16	0.91	-0.55	0.44
U7	414.5	268.5	-1.83	1.44	-1.19	0.93
U8	382.7	211.9	-1.49	1.18	-0.83	0.65
U9	416.3	219.6	-1.45	1.14	-0.76	0.60
U10	591.1	140.6	-1.85	1.46	-0.44	0.35
U11	611.4	363.3	-1.73	1.38	-1.03	0.82

Table 6.8: Restraint moments (kNm) and the corresponding stresses (MPa) over the intermediate support due to differential shrinkage.

Moment (kNm) / Stress (MPa)	Section *T10*			Section *SY6*		
	Case 7	Case 8	Case 8a	Case 7	Case 8	Case 8a
1000 days (kNm)	-20.5	-28.8	-16.1	-113	-156	-107.8
σ_1 (MPa)	0.34	0.48	0.27	0.23	0.32	0.22
σ_4(MPa)	-0.20	-0.28	-0.15	-0.19	-0.26	-0.18
10000 days (kNm)	-21.8	-32.8	-22.5	-120	-178.3	-123.2
σ_1(MPa)	0.36	0.54	0.37	0.24	0.36	0.25
σ_4(MPa)	-0.21	-0.31	-0.22	-0.20	-0.30	-0.21
Note: σ_1 and σ_4 are stresses at bottom and top fibre of the insitu cross heads, respectively						

Table 6.9: Comparisons of the restraint moments (kNm) and the corresponding stresses (MPa) determined from PCA method and ADAPT analyses

Precast Sections	PCA method (24 days)				ADAPT analyses (24 days)			
	Unpropped		Propped		Unpropped		Propped	
	Moment	Stress	Moment	Stress	Moment	Stress	Moment	Stress
T10	374	-6.22	64.1	-1.06	93.9	-1.56	48.3	-0.80
M10	1480	-5.61	533.0	-2.02	513.8	-1.94	299.4	-1.13
Y8	1620	-6.32	1010	-3.97	574.1	-2.25	423.1	-1.66
SY6	2700	-5.50	1300	-2.66	1221.9	-2.49	735.4	-1.50
U11	1740	-4.93	738	-2.09	571.3	-1.62	322.5	-0.91
	PCA method (100 days)				ADAPT analyses (100 days)			
	Unpropped		Propped		Unpropped		Propped	
	Moment	Stress	Moment	Stress	Moment	Stress	Moment	Stress
T10	4.3	-0.07	-500	8.29	29.7	-0.49	-32.2	0.53
M10	291.0	-1.10	-1200	4.61	211.4	-0.80	-100.1	0.38
Y8	729	-2.85	-210	0.84	291.5	-1.14	67.3	-0.26
SY6	880	-1.79	-1300	2.64	596.7	-1.22	-28.5	0.06
U11	518	-1.47	-1100	3.04	239.4	-0.68	-126.1	0.36

Table 6.10: Effects of cracked insitu crossheads on time-dependent restraint moments and stresses

Sections	Case 9			Case 10		
	Restraint moment (kN-m)	Notional stress at bottom fibre, σ1 (MPa)	Notional stress at top fibre, σ4 (MPa)	Restraint moment (kN-m)	Notional stress st bottom fibre, σ1 (MPa)	Notional stress at top fibre, σ4 (MPa)
T10	99.6	-1.65	0.96	54.8	-0.91	0.53
M10	439.2	-1.66	1.2	227.7	-0.86	0.62
Y8	568.2	-2.22	1.99	354.5	-1.38	1.24
SY6	1211.7	-2.48	2.05	729.3	-1.49	1.23
U10	507.5	-1.59	1.26	273.4	-0.86	0.68

CHAPTER SEVEN

NON-CONVENTIONAL METHODS FOR CONTINUITY

7.1 Introduction

Results from the previous chapter indicate that problems may arise in satisfying serviceability requirements in the case of continuous precast prestressed structures using the conventional method of achieving continuity (use of ordinary reinforcing steel over the intermediate insitu crossheads). This Chapter attempts to address the problem by evaluating the behaviour of precast prestressed beams made continuous using non-conventional methods of achieving continuity. From several methods of achieving continuity discussed in Chapter Two, continuity achieved through the use of prestressing steel and the forced support settlement technique will be investigated. The two methods are capable of obviating the tensile stress at the top fibre of insitu crossheads as well as increasing the effective continuity across the joints. The effectiveness of the continuity methods is evaluated both under instantaneous and time-dependent actions.

7.2 Continuity Using Prestressing Steel

It has been shown that the presence of concrete tensile stresses at the top fibre of insitu crossheads is inevitable. In some circumstances, the time-dependent effects due to the prestressing force in the precast beams and the superimposed dead loads may cause tensile stress at the top fibre of the insitu crossheads to develop. Combined with the

tensile stress due to superimposed live loads, the top sections of the insitu crossheads may well experience cracking. This possible durability problem is one of the concerns that has led to the call for the construction of jointless concrete bridges in the UK. And it is apparent that the concern may not be fully addressed if only ordinarily reinforced crossheads are used. Depending on circumstances, the use of other methods may be necessary, not only to satisfy the BS5400 requirement for Class 1 bridges, but also to avoid any future durability problem that will inevitably be encountered.

The use of prestressing steel (post-tensioned) over the intermediate support is one of the suggestions that has been proposed to overcome the problem. This procedure may not only ensure tensile free regions in the upper surfaces of concrete road bridges, but will also increase rigidity across the connected members. There are several different profiles that may be adopted for the post-tensioned steel. This section evaluates three possible profiles as shown in Figure 7.1. Prestressing in Profiles A and B limit the post-tensioned steel to the region over the intermediate support only, while Profile C post-tensions the entire beam length. These tendons may be located between the beams, thus requiring little or no modifications to the existing precast sections. To anchor the post-tensioned steel, insitu slabs may be used in case of Profile A while for Profile B, an intermediate diaphragm may be provided as normally done for long span bridges.

To evaluate the effectiveness of each of the tendon profiles, a series of elastic and time-dependent analyses have been conducted. For the purpose of this evaluation, the required amount of post-tensioned steel has been calculated based on the superimposed live loads alone. The required amount of prestressing steel has been obtained by assuming that composite beams were continuous at the time of application of the live loads, and the post-tensioned steel has been located at the mid-depth of the cast insitu slabs. The prestressing force is provided to satisfy the zero concrete tensile stress requirement at the top fibre at the intermediate support. A 20% loss of prestress in the post-tensioned steel has been assumed. Table 7.1 shows the concrete stress at top fibre at the intermediate support, the eccentricity and the required amount of the prestressing for the largest and smallest cross-sections for each of the available precast sections. The required area of the

prestressing steel has been found to be about 0.2% of the total concrete area for all sections.

The elastic and time-dependent analyses for each of the tendon profiles assumes that the prestressing steel has been post-tensioned when the precast beams were 30 days of age and 7 days after casting of the insitu concrete, at which stage full composite actions between the cast insitu slab and the precast beams could be assumed. The presence of the prestressed and non-prestressed steel in the precast beams has been modelled accordingly, but the prestressing force (from the pre-tensioned steel) has been de-activated. In other words, the elastic and time-dependent responses for these analyses are entirely due to the interactions between the load from the self weight of the composite beams and the prestressing force of the post-tensioned steel.

A summary of the elastic and time-dependent responses for the support reactions, secondary and resultant moments and the concrete stresses for the *T10* section is presented in Table 7.2. The notional results for the beams containing the same levels of post-tensioned steel but with zero prestress force are also included to provide a benchmark for the respective responses to be evaluated. The analyses assume uncracked concrete sections for all beams and the resulting moments and the associated stresses are only due to the permanent dead loads. Any change of moment or stress resulting from the application of prestressing for Profiles A, B and C are then calculated from the moments and stresses from the non-prestressed reference beams. The stresses shown in the table refer to the bottom fibre of the precast sections at mid-span and top fibre of the insitu crossheads at the intermediate support.

The provision of prestressing steel across the intermediate support requires careful consideration due to the presence of parasitic (secondary) moments arising from such provision. If the profiles are not properly chosen, the benefits of pre-compression from the prestressing steel may be significantly reduced by the effects of its secondary moment. For the tendon layout represented by Profile A for example, the beneficial effect of pre-compression is reduced by 54% due to the secondary moments if the post-tensioned steel is spread over 20% of the span length on either side of the intermediate

support. This reduction reduces to about 12.5% if the tendon length is extended up to 50% of the span length from the intermediate support.

A comparison of Profiles A and B clearly shows that the prestressing layout of Profile B, extending over a similar distance from the intermediate support, displays smaller values of the secondary moments. The secondary moments at the intermediate support were calculated to be -153.3 and -42.8kNm for the Profiles A and B respectively (Table 7.2). Furthermore, if the eccentricity of the ends of the Profile B tendons is increased below the beam centroid this could result in zero secondary moments, thereby alleviating the members completely from the effects of the secondary moments. The resultant instantaneous concrete stresses at the top fibre of the insitu crossheads have been subsequently found to be -0.31 and 1.38MPa representing an increase in the compressive stress of 2.68 and 4.37MPa for Profiles A and B respectively with reference to the beams with zero prestress. It can be seen that, although both profiles have similar levels of initial prestressing force, the compressive stress transferred to the concrete is more effective if Profile B is selected over Profile A. Profile A, however, displays a greater reduction in the tensile stress at the bottom fibre at mid-span where the instantaneous stress reduces from 2.62MPa to 1.50MPa. Profile A apparently relieves the tensile stress at the mid-span due to the permanent loads rather better. This could mean requirement of less prestressing steel in the precast beams.

For the prestressing tendon Profile C, although it displays the greatest secondary moment at the support (-338kNm), the resultant instantaneous concrete stress at the top fibre over the intermediate support is found to be 4.82MPa. This represents an increase in the concrete compressive stress of 7.81MPa with reference to the beam with zero prestressing. Although the secondary moment arising from this profile is the greatest, the equivalent uplifting forces in the spans are large enough to create a sagging moment at the support. It can be seen that, although the profile chosen uses greater length of prestressing steel, the cross-sectional areas of the tendons may be halved and yet this could still yield greater compressive force at the top fibre over the intermediate support. A further reduction in the pre-tensioned wires is still possible as it is seen that the post-

tensioned steel has increased the stress at the bottom fibre at mid-span from -2.62 to 3.59MPa. This represents an increase in the compressive stress component by 6.21MPa.

The results for the time-dependent analyses for the beams without post-tensioning show that the concrete tensile stress at mid-span decreases from -2.62 to -2.84MPa. The equivalent values over the intermediate support are found to be -2.99 and -3.24MPa. This indicates that the shrinkage and creep actions from the concrete and its self weight (alone) yield an insignificant decrease in the concrete tensile stress as calculated to be about 0.22MPa. The decrease in the concrete tensile stress at the two critical sections for the beams with the tendon Profiles A and B are found to be about 0.6MPa or less. There is, however, a greater significant change in the levels of concrete stress for the beams with the tendon Profile C. In this case, the concrete compressive stress decreased by about 2MPa at mid-span and by 1.5MPa over the intermediate support.

This evaluation indicates that each profile is an improvement over the beneficial effects of the conventional methods for providing continuity. For as little as 0.2% of prestressing steel, the possibility of structural cracks developing under service loads at the top section of the insitu crossheads can be overcome. Each profile, however, seems to offer some advantages and disadvantages. It is clear that Profile B could only help in reducing the tensile stress at the top section, and is not able to alleviate any tensile stress at the bottom section of the beams in mid-span regions. It can also be expected that Profile B poses some restriction on the construction procedure as it is very difficult to anchor the prestressing steel between the beams if the beams are closely spaced, as has been observed with existing bridges which have been designed with zero spacing between the beams.

Profile C can be seen to be the best choice to overcome the tensile stress at both the top of the insitu crossheads and the soffit of the mid-span regions. The amount of prestress required to improve the conditions at the top section of the insitu crossheads can be less than half of that required by either Profile A and B. The profile, however, requires long prestressing tendons, deviators in the middle-third of the beam length and anchorages at

the beam ends. It is thus obvious that the solution provided by Profile C is likely to be more expensive than the other two alternatives.

Profile A can be seen to be able to counter the tensile stress at the top of the insitu crossheads and at the soffit of mid-span sections, albeit with a smaller effect compared with that for the Profile C. Profile A does not pose restrictions on construction aspects as the stressing and anchoring are to be carried out in the slab sections. The beams can thus be placed touching each other if this profile is adopted. The only possible problem that may arise by use of this profile is the close proximity of the tendons to the road surface, thus exposing them to corrosive agents. This possibility, however, is considered remote because the sections are ensured to remain in compression by prestressing and thus should remain crack free.

7.3 Continuity Using Forced Support Settlement

Support movements such as those due to the settlement of soil in actual structures develop gradually over a period of time. For statically indeterminate structures, different amounts of settlements at each support results in the development of secondary moments. If differential settlements of this nature are applied to the structure in a controlled way, the problem of tensile stresses developing in the top slabs of continuous precast prestressed beams may be overcome. The compressive stresses resulting from the forced support settlements decrease with time due to creep, as shown in Figure 7.2. Adopting the analytical procedure proposed by Ghali (1986), effectiveness of applying the forced support settlement to continuous precast prestressed beams, has been evaluated.

A series of forced displacements of 0.1, 0.2, 0.3, 0.4 and 0.5% of the span length (downward) has been applied at the central support of the two span beams for each section previously considered. The amounts of forced displacement and their associated instantaneous effects on reduction in the central support reactions and stresses at the top fibre over the intermediate support are tabulated in Table 7.3. It can be seen that the stresses yielded by the 0.2% of span length forced settlement are very similar in all cases to those produced by the post-tensioning of the continuous precast prestressed beams

using Profile B. The compressive stress in the extreme fibres over the intermediate support resulting from the post-tensioned steel of Profile B has been reported earlier to be 4.37MPa whereas the resulting stress for the same beam (section *T10*) due to 0.2% support settlement is 4.43MPa. Based on these elastic calculations for the induced compressive stress at the top fibre of the insitu crossheads, 0.2 % support settlement is thus deemed to be sufficient to overcome the tensile stress arising from superimposed live loads. However, considering the creep effects which reduce the instantaneous stresses, a forced displacement of 0.3% of the span length is probably a more realistic option if this procedure has to be adopted to overcome tensile stresses in the crossheads over the intermediate supports of continuous beams.

A comparison of stresses calculated at the top and bottom fibres of the insitu crossheads due to 0.3% forced differential settlement of the intermediate support and those due to superimposed live loads is made in Table 7.4. It can be seen that on average, the compressive stress due to the support settlement is about 50% greater than the tensile stress due to the superimposed live loads. The tensile stress at the bottom fibre of the insitu crossheads due to the support settlement, however, is also about 50% greater than the compressive stress due to the superimposed live loads. This indicates that, if forced support settlement is adopted as a measure to overcome tensile stresses at the intermediate supports, it is essential to estimate accurately and provide for any tension which may develop at the bottom fibres.

A typical time dependent reduction of the induced forces for continuous members subjected to the forced differential support settlement at the age of 30 days and exposed to RH of 70% is shown in Figure 7.3. The forces at the age of 10,000 days are found to be about 40% of the initial values. It is also seen in the figure that 50% of the induced force is lost after about 200 days. This indicates the need to carry out the forced settlement on the members for 2 or 3 times throughout the lifetime of the structures in order to maintain a tensile free region over the intermediate support

It thus obvious that the beneficial effect of this method to induce pre-compression at the top fibre of the insitu crossheads is off-set by the resulting tensile stress at the bottom

fibre of the section. It has been found that a forced differential settlement of 0.2% of the span length could result in tensile stress at the bottom fibre of the insitu crossheads of -4.0MPa or more. If there is no pre-compressive stress already present before forcing the displacement, it is very likely that cracks will appear at the bottom fibres of the insitu crossheads. And once such cracks appear, the hogging moment due to applied live loads at the intermediate support gets effectively reduced, resulting in greater sagging moment along the span. The continuous beam will thus require greater amount of prestressing for the safety of the mid-span regions of the precast beams. The design process is thus not only in less economic but also becomes iterative.

7.4 Further evaluations on the use of post-tensioned deck slabs for continuity.

Evaluations in earlier sections indicate that continuity achieved by post-tensioned tendons in the deck slab can be effective and sufficient to satisfy the Class 1 bridge design requirement where no tension is permitted anywhere in the concrete at service. For reasons mentioned earlier, providing continuity through the use of cable Profile A has been further examined to ascertain its effectiveness for bridges having different construction sequences and methods of construction. In addition to the sequences considered for conventional methods for continuity, Profile A introduces an additional step in the construction sequence where the slab casting and post-tensioning are carried out at different times. For slab casting, it is possible to stagger the casting depending on the effects desired by the designer. The whole slab may be cast in one instance, or portions of the slab to be post-tensioned may be first cast, followed by other portions after prestressing is carried out. The former sequence may be expected to display less sagging restraint moment compared to the latter. Both of these sequences may adopt either propped or unpropped construction methods.

Five different cases of analyses have been considered for T10 sections in order to study the effects of different sequences of construction on the time-dependent behaviour of continuous beams. The cases considered are similar to Case 1 (unpropped) and Case 2 (propped) discussed in Chapter 6 except that an additional step in the construction

sequence (post-tensioning) has been introduced. The content and layout of the prestressing steel are similar to those considered in Section 7.2. The cases considered for analyses are:

Case 11: Unpropped construction, portion of the deck slab to be post-tensioned first cast at 24 days, the remaining slabs are cast after prestressing at 100 days.

Case 12: Unpropped construction, the whole deck slabs are cast at 24 days and post-tensioned are carried out at 100 days.

Case 13: Propped construction, portion of the deck slab to be post-tensioned first cast at 24 days, the remaining slabs are cast after prestressing at 100 days.

Case 14: Propped construction, the whole deck slabs are cast at 24 days and post-tensioned are carried out at 100 days.

Case 15: Similar to Case 1, except no post-tensioning for continuity has been carried out.

Results of the analyses are summarised in Table 7.5, where the actions (bending moments and axial forces) and stresses at the top and bottom fibres of the insitu crossheads are shown. It may be noted that Case 15 (in Table 7.5) is similar to Case 1 (in Table 6.5, Chapter 6), except that the slab in Case 15 is assumed to have been cast in two stages, whereas the slab in Case 1 (in Table 6.5) is cast in one operation. As discussed in the previous chapter, the prestressing in the precast beams is principally responsible for the high sagging restraint moment at the intermediate support. These potentially high sagging restraint moments due to prestressing get reduced by the slabs which are cast on unpropped beams at 24 days (Case 1, Table 6.5). In Case 15, casting of the slab in two stages has increased the sagging restraint moment at the intermediate support from 93.9 kN/m (Table 6.5) to 134.8kN/m (Table 7.5). This increase is equivalent to increasing the tensile stress at the bottom fibre of insitu crossheads from 1.55MPa to 2.23MPa. Similarly, the compressive stress at the top fibre of the insitu crossheads also increases from a value of 0.9 to 1.29MPa value. This can be very beneficial as it can delay the presence of tensile stress at the top fibre of the insitu crossheads due to live loads.

It should be noted, however, that this sequence of construction might result in cracking at the bottom section of the insitu crossheads for some beams. Some of the beams (Case 1, Table 6.6 Chapter 6) display large tensile stress at the bottom fibres of the insitu crossheads. Adopting the sequence of construction as in Case 15 increases the possibility of development of soffit cracks, thus requiring provision of positive reinforcement. It can be concluded that if the slab is cast in two stages (as Case 15), it is necessary to provide positive steel reinforcement at the intermediate supports and the full continuity must be considered while analysing for live loads effects.

Casting of slabs in two stages becomes a feasible solution if prestressing is carried out in the deck slabs over the intermediate support, as in Cases 11 and 13. A comparison of theoretically obtained results for Cases 11 and 15 shows that the sagging moments at the insitu crossheads are subsequently increased due to the prestressing in the deck slab. This results in greater tensile stress at the bottom fibre of the insitu crossheads. However, the tensile stress (for Case 11) is countered by the axial force from the prestressing, hence keeping the stresses in the section well outside cracking limits. It can be seen that the tensile stress reduce from 2.23 to 0.79MPa (Table 7.5).

A comparison of results between Cases 11 and 13 and between Cases 12 and 14 shows that unpropped construction leads to greater compressive stresses at the top fibre, or smaller tensile stresses at the bottom fibre of the insitu crossheads. This observation is useful in that the need for the prestressing in the deck slab to overcome the tensile stresses at the top fibre of the insitu crossheads due to the live loads may be obviated or considerably reduced by adopting the unpropped method construction.

Comparisons between results of analyses for Cases 11 and 12 and Cases 13 and 14 shows that the sequence of slab construction and prestressing affects the amount of sagging moment at the insitu crossheads. It can be seen that bridges in which the slab was cast in one operation (Cases 12 and 14) display greater sagging moment at the insitu crossheads compared to those for which the slab was cast in two stages (Cases 11 and 13). The resultant compressive stress at the top fibre increases from 3.92MPa (for Case 11) to 4.27MPa (for Case 12), and from 3.62MPa (for Case 13) to 4.12MPa (for Case 14). The

increases are of the order of 9-14%. This indicates that in the case of prestressed deck slabs, slabs cast in one operation provide a better solution for continuous beams. It should be noted that this is in direct contrast with an earlier observation that the two-stage slab casting is a better solution. It is clear that the introduction of prestressing in the deck slab has changed the situation observed earlier.

It may be concluded that in the case of continuity being achieved through the use of conventional crossheads, two-stage slab casting may be preferred, whereas if continuity is achieved through use of a post-tensioned slab, single stage casting of the slab is recommended.

7.5 Further evaluations on the use of forced differential settlement for continuity.

For the case of forced support settlement, it has been stated earlier that the procedure does not provide an attractive solution as it resulted in reasonably high sagging moments which may cause the beam soffit to crack. In the earlier analyses (Section 7.3), the effects of forced support settlement was ascertained in isolation of other effects e.g. the effect of prestressing in the precast beams. Since it has also been found that the prestressing effect for most design conditions results in sagging restraint moments, cracking at the soffit of the insitu crossheads is inevitable. The shortcomings of forced support settlement, however, may be overcome if the procedure is combined with that of prestressing the deck slabs.

To examine the effect of this combination, further analyses have been conducted. Four cases have been considered in which two cases are related to Case 12 (unpropped) and the other two are related to Case 14 (propped). For unpropped construction, two analyses were conducted where one is for the combined effects of restraint moment and forced support settlement (Case 16) and the other is the combined effects of restraint moment, forced support settlement and prestressing of the deck slabs (Case 17). Two similar analyses were also conducted for propped construction (Cases 18 and 19). Forced support settlement of 0.2% of span length has been assumed for all cases. From these analyses, it

was found that high tensile stress was still present at the soffit of the insitu crossheads. For the unpropped case (where it was earlier found to display higher sagging restraint moment than for the propped case), the provision of 0.2% prestressed steel in the deck slab was still insufficient to avoid cracks at the bottom fibre of the insitu crossheads. In fact, the analyses showed that the notional tensile stress remained at 3.8MPa for prestressed (Case 17) and unprestressed (Case 16) cases. The tensile stress may be reduced if higher percentage of prestressing steel is used in the deck slabs. For the propped case, the provision of prestressing steel in deck slab improved the tensile stress by lowering it from 3.6MPa to 2.3MPa. The level of tensile stress i.e. 2.3 MPa is, however, greater than that if only prestressed deck slab is used, where the tensile stress was calculated to 1.13MPa (Case 14, Table 7.5).

Based on the overall analyses that have been conducted in this chapter, it is reasonable to expect that the solution provided by the forced support settlement is less attractive because it only serves to alleviate the tensile stress at the top fibre of the insitu crossheads, but it increases the chances of cracks occurring at the soffit of the insitu crossheads.

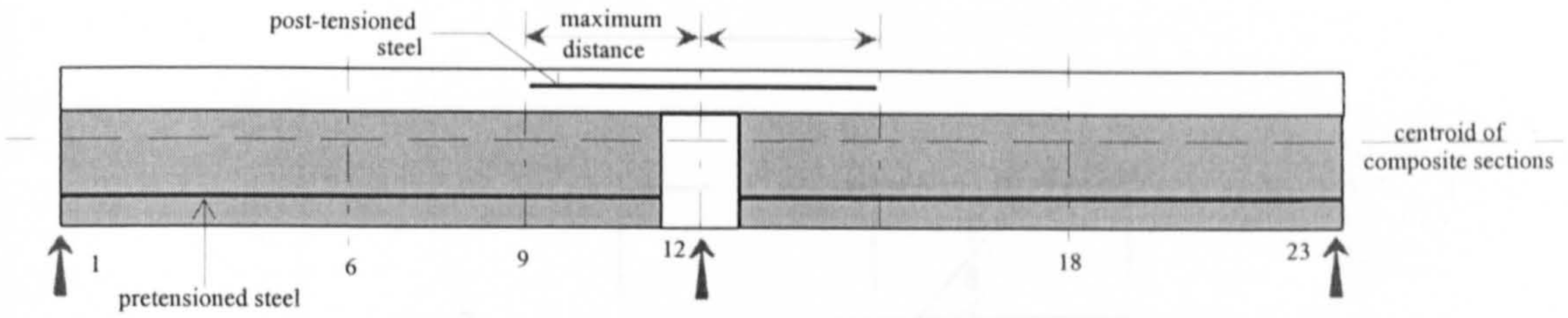

(a) Profile A

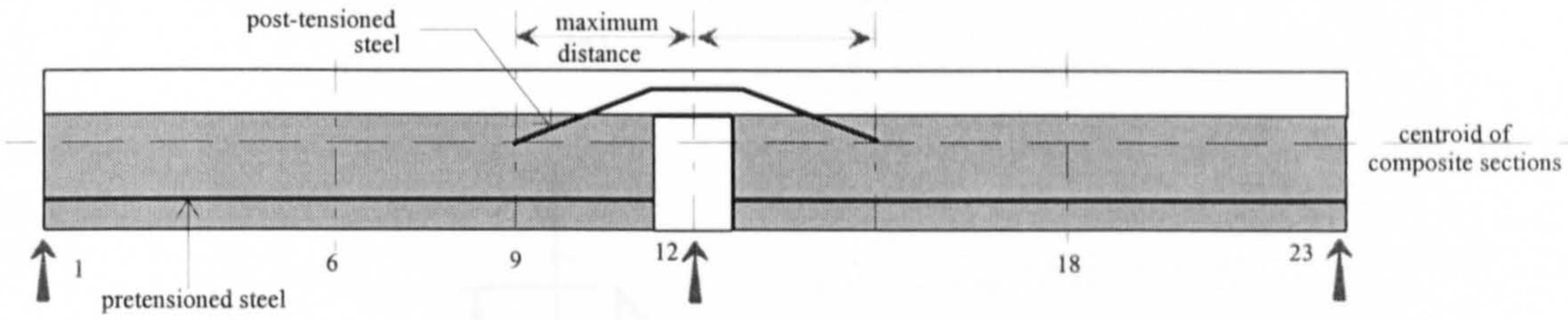

(b) Profile B

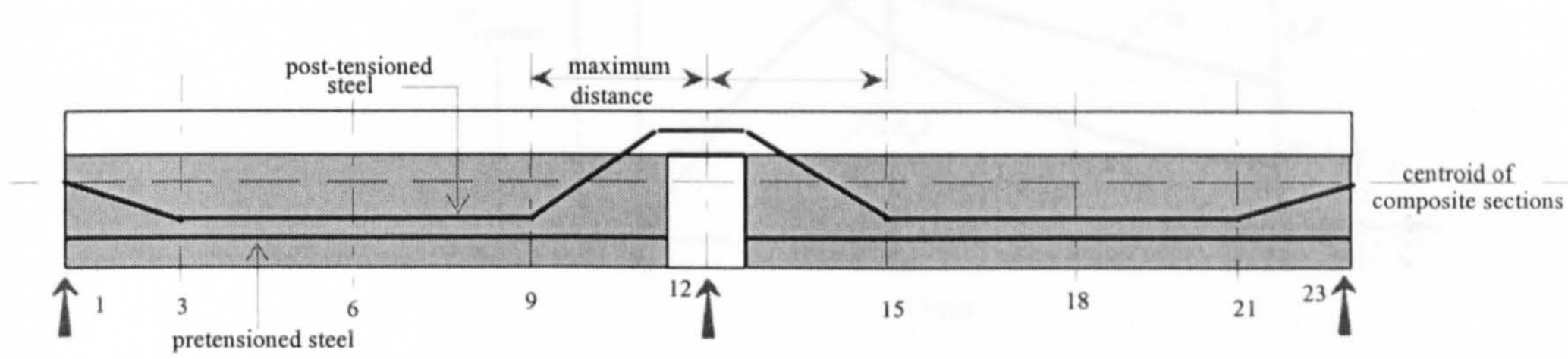

(c) Profile C

Figure 7.1: Three different prestressing profiles evaluated to counter hogging stress over the support

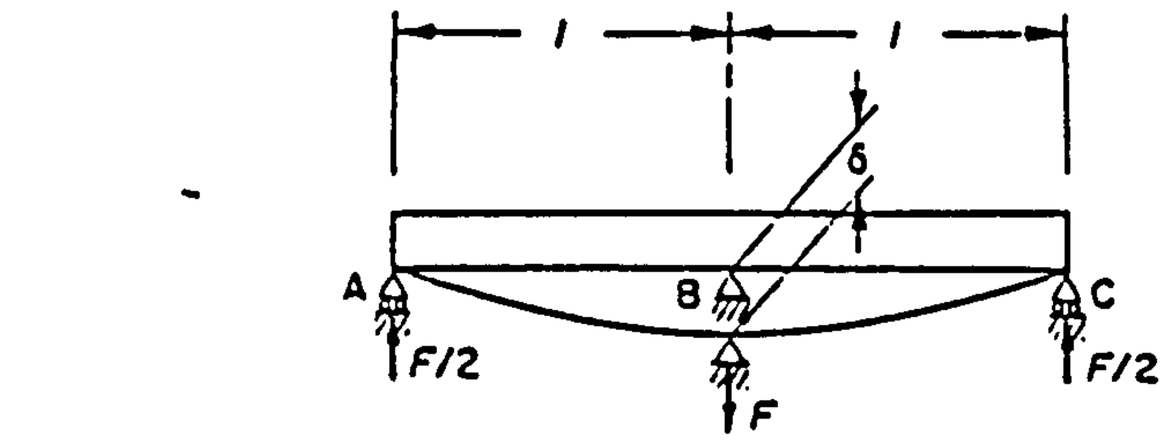

(a)

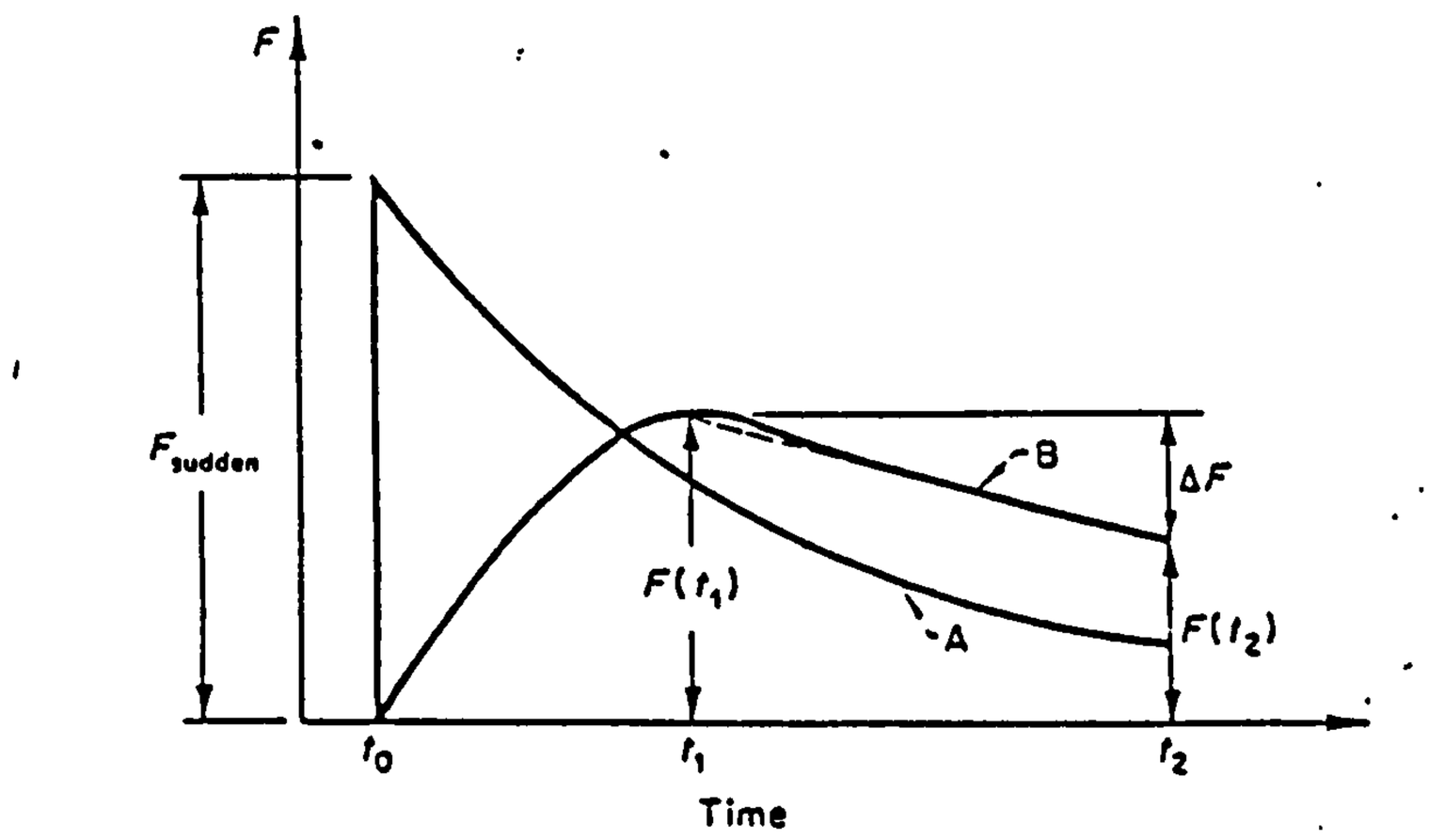

(b)

Fig. 4.6 Time dependent forces caused by support settlement in a continuous beam: (a) continuous beam; (b) reaction at central support versus time; A, sudden settlement; B, progressive settlement

Figure 7.2: Effects of differential support settlement in a continuous beam on the development of forces (Ghali, 1986).

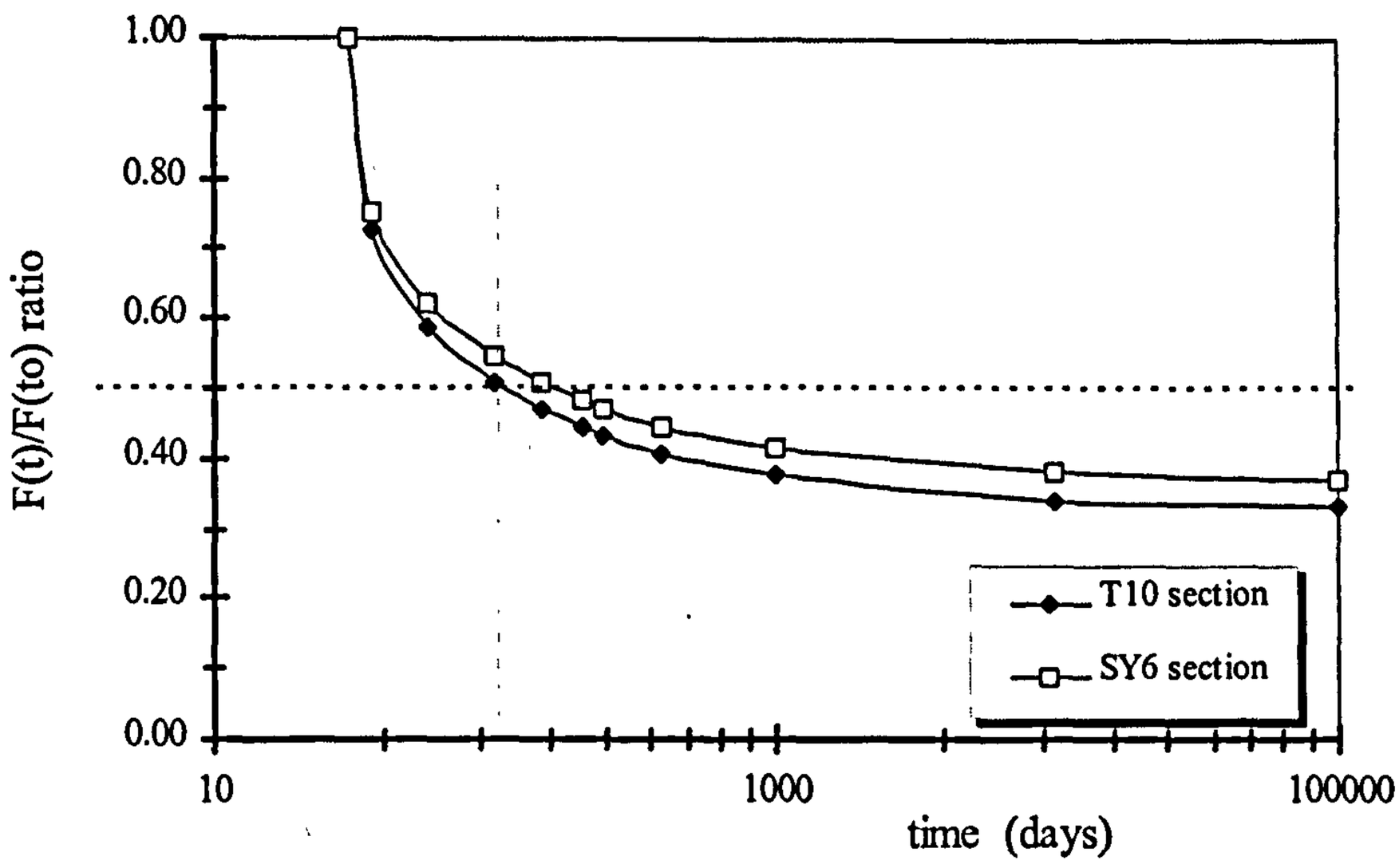

Figure 7.3: Typical reduction in the induced forces due to the action of creep

Table 7.1: The required level of prestressing to satisfy the zero concrete tensile stress condition under superimposed live loads

Sections	Composite Area ($mm^2 x10^5$)	Second moment of inertia ($mm^4 x10^9$)	Concrete stress at the top fibre (MPa)	Initial prestressing force (kN)	Area of post-tensioned steel (mm^2)	Eccentricity (mm)
T1	2.630	8.014	2.87	524	437	120
T10	3.365	37.43	3.88	863	719	276
M2	5.896	56.85	3.97	1385	1154	289
M10	7.304	228.8	4.49	1952	1627	548
Y1	4.742	41.38	3.93	868	724	344
Y8	7.497	210.8	5.04	1727	1439	658
SY1	8.222	291.5	4.28	1856	1547	657
SY6	9.822	574.0	5.06	2518	2098	886
U1	7.394	75.74	3.33	1311	1092	333
U12	10.03	375.3	4.45	2309	1924	688

Note: Calculations based on composite sections for beams with the maximum recommended spans (as per Chapter 5)

Table 7.2: A summary of results from the short term and time-dependent analyses for Sections *T10* made continuous using post-tensioned steel

Results	zero prestressing force		Profile A		Profile B		Profile C	
	mid-span	support	mid-span	support	mid-span	support	mid-span	support
Secondary moment (kNm)	-	-	-72.4.1	-153.3	-20.2	-42.8	-159.6	-338
Reactions (kN) -Instantaneous	-	177	-	195	-	182.8	-	142.9
-255 days	-	179.6	-	197.1	-	185.6	-	149.5
-Final	-	180.3	-	197.7	-	186.4	-	151.6
Moment(kNm) -Instantaneous	161.7	-311.8	92.2	-233.2	139.9	-123.7	-69.9	235.3
-255 days	166.7	-332.8	103.6	-263.1	144.7	-161.3	-39.1	143.5
-Final	167.9	-338.8	106.9	-271.9	146	-172.5	-29.9	115.6
Stress (MPa) -Instantaneous	-2.62	-2.99	-1.50	0.33	-2.22	1.38	3.59	4.82
-255 days	-2.72	-3.19	-1.81	-0.07	-2.49	0.89	1.64	3.78
-Final	-2.84	-3.24	-1.91	-0.20	-2.58	0.74	1.60	3.46
Prestressing force (kN)-Initial	-	-	-	86.28	-	86.28	86.28	86.28
-255 days	-	-	-	82.28	-	81.71	81.47	80.87
-Final	-	-	-	80.97	-	80.22	79.98	79.21

Table 7.3: Calculations for instantaneous reduction in centre support reaction and stress due to forced differential settlement of the central support

PCA Section	Span (mm)	Displacement based on a % of span length (mm)					Instantaneous force due to forced displacement (N)					Stress over the intermediate support, σ4 (MPa)				
		0.10%	0.20%	0.30%	0.40%	0.50%	0.10%	0.20%	0.30%	0.40%	0.50%	0.10%	0.20%	0.30%	0.40%	0.50%
T1	9000	9	18	27	36	45	20776	41552	62328	83103	103879	2.36	4.73	7.09	9.46	11.82
T2	9500	9.5	19	28.5	38	47.5	22595	45191	67786	90382	112977	2.39	4.79	7.18	9.58	11.97
T3	11000	11	22	33	44	55	27097	54194	81291	108388	135485	2.43	4.87	7.30	9.74	12.17
T4	12000	12	24	36	48	60	26338	52675	79013	105350	131688	2.35	4.71	7.06	9.41	11.76
T5	12500	12.5	25	37.5	50	62.5	27812	55624	83436	111248	139060	2.38	4.75	7.13	9.51	11.88
T6	13000	13	26	39	52	65	29290	58580	87870	117160	146449	2.40	4.81	7.21	9.61	12.02
T7	14500	14.5	29	43.5	58	72.5	26676	53352	80028	106704	133380	2.26	4.53	6.79	9.06	11.32
T8	15500	15.5	31	46.5	62	77.5	26222	52444	78666	104888	131110	2.22	4.44	6.66	8.87	11.09
T9	16000	16	32	48	64	80	27556	55112	82668	110224	137780	2.25	4.50	6.75	9.00	11.25
T10	17000	17	34	51	68	85	27200	54400	81601	108801	136001	2.21	4.43	6.64	8.86	11.07
M2	18000	18	36	54	72	90	40051	80102	120152	160203	200254	2.30	4.60	6.90	9.20	11.50
M3	19500	19.5	39	58.5	78	97.5	42386	84771	127157	169543	211928	2.30	4.60	6.90	9.20	11.50
M4	21000	21	42	63	84	105	44657	89314	133971	178628	223285	2.31	4.61	6.92	9.22	11.53
M5	22500	22.5	45	67.5	90	112.5	46631	93262	139893	186524	233155	2.30	4.61	6.91	9.21	11.52
M6	24000	24	48	72	96	120	48622	97244	145865	194487	243109	2.30	4.59	6.89	9.18	11.48
M7	26000	26	52	78	104	130	48532	97064	145597	194129	242661	2.25	4.49	6.74	8.98	11.23
M8	27000	27	54	81	108	135	52058	104117	156175	208234	260292	2.32	4.63	6.95	9.26	11.58
M9	28500	28.5	57	85.5	114	142.5	53869	107738	161607	215476	269345	2.30	4.60	6.90	9.21	11.51
M10	29500	29.5	59	88.5	118	147.5	57435	114870	172305	229740	287175	2.33	4.66	6.99	9.32	11.65
SY1	30000	30	60	90	120	150	70574	141148	211723	282297	352871	2.68	5.35	8.03	10.71	13.39
SY2	32000	32	64	96	128	160	71965	143930	215895	287861	359826	2.66	5.32	7.98	10.63	13.29
SY3	34000	34	68	102	136	170	73321	146642	219963	293284	366605	2.64	5.29	7.93	10.57	13.21
SY4	36000	36	72	108	144	180	74651	149303	223954	298605	373257	2.63	5.26	7.89	10.52	13.15
SY5	38000	38	76	114	152	190	75967	151933	227900	303867	379834	2.62	5.24	7.86	10.48	13.10
SY6	40000	40	80	120	160	200	77272	154544	231816	309088	386360	2.61	5.22	7.83	10.44	13.05
Y1	16500	16.5	33	49.5	66	82.5	31917	63834	95751	127669	159586	2.71	5.43	8.14	10.86	13.57
Y2	19000	19	38	57	76	95	32441	64882	97324	129765	162206	2.63	5.25	7.88	10.51	13.13
Y3	21500	21.5	43	64.5	86	107.5	33190	66379	99569	132759	165948	2.56	5.11	7.67	10.22	12.78
Y4	24000	24	48	72	96	120	34029	68058	102088	136117	170146	2.49	4.98	7.47	9.96	12.45
Y5	26000	26	52	78	104	130	36338	72675	109013	145350	181688	2.48	4.96	7.44	9.92	12.39
Y6	28500	28.5	57	85.5	114	142.5	37284	74567	111851	149135	186418	2.42	4.84	7.26	9.68	12.10
Y7	31000	31	62	93	124	155	38322	76644	114966	153289	191611	2.37	4.74	7.11	9.47	11.84
Y8	32000	32	64	96	128	160	43229	86458	129688	172917	216146	2.43	4.86	7.29	9.72	12.15
U1	18000	18	36	54	72	90	52768	105536	158305	211073	263841	2.56	5.13	7.69	10.26	12.82
U3	20000	20	40	60	80	100	55055	110111	165166	220221	275277	2.53	5.07	7.60	10.13	12.67
U5	22000	22	44	66	88	110	57619	115237	172856	230474	288093	2.51	5.02	7.53	10.05	12.56
U7	24500	24.5	49	73.5	98	122.5	57470	114939	172409	229879	287348	2.44	4.88	7.33	9.77	12.21
U8	26500	26.5	53	79.5	106	132.5	59826	119651	179477	239302	299128	2.44	4.87	7.31	9.75	12.18
U9	28500	28.5	57	85.5	114	142.5	62058	124115	186173	248230	310288	2.43	4.86	7.29	9.72	12.16
U10	30500	30.5	61	91.5	122	152.5	64205	128409	192614	256818	321023	2.43	4.85	7.28	9.70	12.13
U11	32000	32	64	96	128	160	68416	136831	205247	273662	342078	2.46	4.92	7.39	9.85	12.31

Table 7.4: Comparison between stresses due to forced sttlement of 0.3% of span length and those from superimposed live loads

PCA Section	Span (mm)	disp. (mm)	stress due settlement		Stress due live loads	
			σ4	σ1	σ4	σ1
T1	9000	27	7.09	-11.98	-4.58	7.74
T2	9500	28.5	7.18	-12.21	-4.39	7.47
T3	11000	33	7.30	-12.74	-4.04	7.05
T4	12000	36	7.06	-12.37	-4.23	7.41
T5	12500	37.5	7.13	-12.53	-4.15	7.29
T6	13000	39	7.21	-12.66	-4.08	7.17
T7	14500	43.5	6.79	-11.89	-4.52	7.92
T8	15500	46.5	6.66	-11.64	-4.71	8.23
T9	16000	48	6.75	-11.75	-4.64	8.08
T10	17000	51	6.64	-11.52	-4.82	8.36
M2	18000	54	6.90	-9.11	-4.95	6.54
M3	19500	58.5	6.90	-9.18	-4.95	6.58
M4	21000	63	6.92	-9.21	-4.97	6.61
M5	22500	67.5	6.91	-9.26	-4.99	6.69
M6	24000	72	6.89	-9.32	-5.01	6.78
M7	26000	78	6.74	-9.19	-5.22	7.12
M8	27000	81	6.95	-9.33	-5.16	6.93
M9	28500	85.5	6.90	-9.40	-5.17	7.04
M10	29500	88.5	6.99	-9.61	-5.04	6.94
SY1	30000	90	8.03	-9.77	-4.78	5.81
SY2	32000	96	7.98	-9.69	-4.78	5.81
SY3	34000	102	7.93	-9.63	-4.79	5.81
SY4	36000	108	7.89	-9.57	-4.79	5.81
SY5	38000	114	7.86	-9.51	-4.80	5.81
SY6	40000	120	7.83	-9.45	-4.81	5.80
Y1	16500	49.5	8.14	-8.37	-4.93	5.07
Y2	19000	57	7.88	-8.12	-5.18	5.33
Y3	21500	64.5	7.67	-7.94	-5.38	5.57
Y4	24000	72	7.47	-7.82	-5.55	5.81
Y5	26000	78	7.44	-7.89	-5.49	5.83
Y6	28500	85.5	7.26	-7.82	-5.61	6.05
Y7	31000	93	7.11	-7.78	-7.43	8.13
Y8	32000	96	7.29	-8.12	-6.85	7.63
U1	18000	54	7.69	-9.72	-4.19	5.29
U3	20000	60	7.60	-9.65	-4.27	5.42
U5	22000	66	7.53	-9.58	-4.34	5.51
U7	24500	73.5	7.33	-9.32	-4.58	5.83
U8	26500	79.5	7.31	-9.27	-4.66	5.91
U9	28500	85.5	7.29	-9.23	-4.74	6.00
U10	30500	91.5	7.28	-9.20	-4.79	6.06
U11	32000	96	7.39	-9.30	-4.66	5.87

Note: σ1 = stress at the bottom fibre of the insitu crossheads

σ4 = stress at the top fibre of the insitu crossheads

Table 7.5: Actions and stresses for different sequences and methods of construction for beams with Profile A tendons.

Actions and Stress (MPa)	Case 11	Case 12	Case 13	Case 14	Case 15
100 days					
Moment (kNm)	43.6	100.6	-7.1	76.7	-14.6
Axial Force (kN)	816	807	823	809	0
σ_1 (MPa)	1.68	0.73	2.51	1.13	0.24
σ_4(MPa)	2.81	3.36	2.33	3.13	-0.4
10,000 days					
Moment (kNm)	180	216	148.2	200.8	134.8
Axial Force (kN)	744	733	749	735	0
σ_1 (MPa)	-0.79	-1.4	-0.26	-1.13	-2.23
σ_4(MPa)	3.92	4.27	3.62	4.12	1.29

Note: σ_1 and σ_4 are stresses at bottom and top fibre of the insitu cross heads, respectively

CHAPTER EIGHT

CONCLUSIONS AND FURTHER RECOMMENDATIONS

8.1 Conclusions

Time-dependent behaviour of continuous precast prestressed concrete beams has been investigated. An extensive evaluation of the time-dependent properties of the concrete material and the structural behaviour of both reinforced and prestressed concrete structures have been conducted. Factors affecting the time-dependent behaviour of the concrete material and structures have been evaluated considering many different combinations of parameters selected to be within the ranges that are being used in practice.

Predictions for the time-dependent behaviour of the concrete material from major international codes have been incorporated in conducting the numerical evaluations. Suitably verified analytical procedures have been used to investigate the behaviour of reinforced and prestressed concrete structures. Conclusions drawn from this study are applicable within the range of the parameters considered, but some can be suitably generalised for other conditions. However, the generalisations should be made with some care and are always best supported by experimental data.

The main conclusions that can be drawn from this study are summarised as follows:

1. Predictions for the elastic modulus of concrete have a direct effect on the predictions for creep. ACI-209 predicts slower development of the elastic modulus compared with those of the CEB. For concrete subjected to stress at early age, ACI yields greater instantaneous deformation, hence resulting in smaller creep coefficients. The instantaneous strains at 28 days are more uniformly predicted by the codes.

2. ACI predicts the greatest values for shrinkage, but the smallest values for creep. Both CEB78 and CEB90 predict low shrinkage strains, but high creep values. The difference between the maximum and minimum predictions for creep and shrinkage strains were calculated to be 29 and 18% of the maximum creep and shrinkage values, respectively. The difference between maximum and minimum values drastically reduced to 6.5% for total strain.

3. For concrete loaded at an early age, the change in the elastic modulus with time needs to be considered when the instantaneous deformation is calculated. The elastic modulus for concrete at 3 days can be up to 25% less than that at 1,000 days.

4. Application of the methods of prediction for the concrete properties need to be used consistently i.e. if ACI is used for the shrinkage calculation, then it needs to be used for the elastic modulus and creep calculations.

5. The superposition method is the most accurate method for predicting the time-dependent deformation of concrete structures. The age-adjusted effective modulus method which requires less computational effort provides results of sufficient accuracy for many design purposes.

6. Bonded reinforcement exceeding 1.5% of the cross-sectional area needs to be modelled appropriately when using ADAPT to predict the time-dependent behaviour of concrete structures. For lightly reinforced structures, transformed section properties yield solutions to a sufficient level of accuracy for most design purpose.

7. Uncracked section stiffness can be used in ADAPT to predict time-dependent behaviour of cracked or uncracked prestressed concrete beams. The use of cracked stiffness is required to predict the time-dependent behaviour of cracked reinforced concrete beams.

8. The features available in ADAPT can readily be used to model the construction sequence of continuous precast prestressed concrete beams. It is thus possible to conduct parametric studies for this type of structure.

9. Based on the CEB90 predictions for concrete behaviour, the rate of creep development is independent of the concrete characteristic strength and age at loading. Curing duration neither affects the level of shrinkage nor its development. The shrinkage of concrete having f'_c=30MPa is always 50% greater than that for f'_c=60MPa but the concrete strength does not affect the rate of shrinkage development. Shrinkage strain of concrete exposed at 40% *RH* is always about 3.5 times greater than that exposed at 90% *RH*.

10. Any given combination of parameters yields unique creep and shrinkage values. However, the consistent patterns that correlate these values make it possible to further simplify the methods of predicting the creep and shrinkage properties of concrete.

11. For concrete sections reinforced with up to 2.0% of bonded steel, any combination of parameters does not significantly affect the elastic deformation. For the combination of parameters yielding minimum deformation, up to 3.0% of bonded steel does not significantly affect the elastic deformation.

12. For sections reinforced with up to 3.0% of steel and subjected to combinations of parameters yielding minimum deformation, creep values can be considered to be similar to those for plain sections. Under the combination of parameters yielding maximum deformation, however, 0.5% or more steel reinforcement does

significantly affect the deformation due to the creep action. The level of applied stress significantly affects deformation due to creep for sections reinforced with 1.0% or more steel.

13. Greater levels of tensile stress are developed in sections having higher reinforcement content due to the action of shrinkage. The action of shrinkage alone, however, will not lead to concrete cracking for sections reinforced with up to 3.0% steel.

14. Under a moderately applied compressive stress of 5MPa, the action of creep has a more significant effects on stress development in the reinforcement than that of shrinkage. More significant effects due to the action of creep are expected under higher levels of applied stress.

15. For sections subjected to an axial stress, the combination of parameters yielding maximum creep and shrinkage will lead to maximum time-dependent deformation. The case, however, is not necessarily true for prestressed members subjected to flexural loads. High creep and shrinkage values result in higher loss of prestress force, which may cause a greater reduction in camber with time.

16. The presence of bonded non-prestressed steel at the bottom section of prestressed beams significantly affects the time-dependent loss of prestress. The loss could be reduced by about 20% for sections containing 2.0% of non-prestressed steel.

17. The presence of non-prestressed steel at the bottom of the section also affect the time-dependent camber significantly. Sections containing 2.0% of non-prestressed steel could experience a reduction in the final camber of up to about 85% of that for those sections without zero non-prestressed steel. Sections containing more than 1.0% of non-prestressed steel may display a reduction in camber with time.

18. The presence of top reinforcement is beneficial especially for slender members or members with low ratios of prestressing to dead load bending. Top reinforcement can reduce excessive deflections under service loads.

19. Proper account of creep and shrinkage characteristics as well as the structural properties needs to be taken when a reduction in the initial level of prestressing is envisaged to take advantage of continuity under service loads. The lower level of initial prestressing may satisfy the service stress requirement, but the serviceability limit on deflection may not be satisfied.

20. The rule of superposition for determining the behaviour of prestressed beams is only valid under short-term loads but, once nonlinearity is introduced from the actions of creep and shrinkage, the validity ceases. Time-dependent deflections of prestressed beams may be greatly overestimated if the superposition rule is used. When the serviceability limit for deflection is critical, combined analyses considering the continuos interaction between prestressing and permanent loads need to be conducted.

21. Although CEB predictions yield greater values of creep than those of the ACI, the time-dependent deformations of prestressed beams predicted using the CEB methods are not necessarily more conservative.

22. Tensile stress at the top fibre of the insitu crossheads violates the service stress requirement for Class1 bridges designed according to the BS5400 and may crack under service loads for all sequences of construction using either narrow or wide insitu crossheads.

23. The effect of different elastic moduli for the concrete in the precast beams and insitu crossheads is not significant for the distribution of hogging or sagging moments in continuous beams.

24. Unpropped construction procedures were found to yield the greatest sagging restraint moment at the intermediate support. Slab casting and the establishment of continuity when the unpropped precast beams are still young may yield a sagging restraint moment that causes the bottom insitu crosshead to crack.

25. For unpropped construction, it was shown that for the majority of circumstances, the tensile stress at the bottom of the insitu crosshead did not exceed the modulus of rupture of the concrete. The provision of a positive moment connection, therefore, is not necessary in the majority of cases to carry the tensile stress (in excess of the concrete tensile strength) that the time-dependent effects may cause.

26. The positive moment connection is not required for all sequences of propped construction. It is also not required in unpropped construction if the slabs and the insitu crossheads are cast when the precast beams are more than 3 months old.

27. The current PCA method of analysis and design for the time-dependent effects of continuous precast prestressed concrete beams greatly overestimates the sagging restraint moment at the intermediate support.

28. The formulations for the restraint moment at the intermediate support given by the current PCA method, are only applicable to bridges constructed using unpropped construction. For structures using propped construction, the effect of the slab selfweight and the differential shrinkage need not be corrected by the creep correction factor. They are treated in a similar way as the permanent surfacing loads which are applied after continuity is established.

29. Suitably verified computer analyses which consider continuous interactions between the prestressing and permanent loads i.e. the likes of ADAPT, can be used to give better predictions of the restraint moment due to the time-dependent effects.

30. For typical precast sections commonly used in bridges, the effect of differential shrinkage between the precast beams and the insitu slabs on the restraint moment is less significant than that of the creep and shrinkage actions in the precast beams.

31. The levels of restraint moment developed across cracked insitu crossheads are not significant to be considered, regardless of the method of construction

32. In the case of continuity being achieved through the use of ordinary crossheads, two-stage slab casting may be preferred, whereas if continuity is achieved through the use of post-tensioned slab, single stage casting of the slab is recommended.

33. The use of overall post-tensioning is most effective in enhancing the state of stress under service loads.

34. The solution provided by the forced support settlement is less attractive because it only serves to alleviate the tensile stress at the top fibre of the insitu crossheads, but it increases the chances of cracks occuring at the soffit of the insitu crossheads.

8.2 Recommendations for Further Work

1. The majority of the data used in the present investigations has been obtained from controlled laboratory experiments. Continuous collection of field data where concrete is exposed to actual cyclic environmental and loading conditions is recommended.

2. Most of the information on the material properties has been obtained from either European or American sources. More widespread application of the time-dependent analysis can only be achieved if investigations of the other material and environmental conditions are conducted.

3. Simpler methods for predicting the material properties need to be formulated based the use of short-term data.

4. More experimental work needs to be carried out to ascertain the ductility of continuous prestressed beams at ultimate. This is strongly recommended for structures for which the ultimate load capacity governs the design.

5. With the advantages of continuity and possibly the additional use of prestressing over the support, it is possible to design more slender beams to satisfy flexural stress

and strength requirements for prestressed concrete bridges. This, however, may result in potential problems with respect to shear design for sections close to the intermediate support. Further studies, therefore, are recommended to include the performance for this type of structure with respect to shear.

REFERENCES

Abdel-Karem, A.M. and Tadros, M.K. (1993): Computer analysis of spliced girders bridges. American Concrete Institute Structural Journal Jan.-Feb., pp. 21-31.

ACI Committee 209 (1982): Prediction of creep, shrinkage and temperature effects in concrete structures. Designing for Creep and Shrinkage in Concrete Structures American Concrete Institute: SP-76, pp. 193-300.

ACI Committee 435 (1966): Deflections of reinforced concrete flexural members, American Concrete Institute Journal, June, pp 637-673.

ADAPT (1993): Software Manual for Incrementally Constructed Bridges and Frames, Redwood City, California.

Al-Khaja, W.A.A (1986): Time-dependent losses in post-tensioned prestressed concrete. Ph.D. Dissertation, University of Leeds, Leeds. 317 p.

Al-Zaid, R.Z., Naaman, A.E. and Nowak, A.S (1988): Partially prestressed composite beams under sustained and cyclic loads, Journal of Structural Engineering, ASCE, Vol. 114 No. 2, pp 269-291.

Ayyub, B.M., Sohn, Y.G. and Saadatmanesh, H (1992): Prestressed composite girders II: analytical study for negative moment. Journal of Structural Eng. 118, No.10, pp. 2743-2761.

Ayyub, B.M., Sohn, Y.G. and Saadatmanesh, H (1992): Prestressed composite girders I: experimental study for negative moment. Journal of Structural Eng. 118, No.10, pp. 2743-2761.

Bakos, S.L., Gilbert, R.I., Faulkers, K.A. and Pulmano, V.A. (1982): Long term deflections of reinforced concrete beams. Magazine of Concrete Research Vol. 34, No.121, Dec., pp. 203-211.

Basu, P.K., Sharif, A.M. and Ahmed, N.U. (1987): Partially prestressed continuous composite beams I&II. ASCE Structural Journal 113 Sept. 1987, pp. 1909-1937.

Bazant Z.P. (1972): Predictions of concrete creep effects using age-adjusted effective modulus method, American Concrete Institute Journal, Proceedings Vol. 69, No. 4, April, pp 212-217.

Bazant, Z.P. and Whitman, F.H. (Eds.) (1982): Creep and shrinkage in concrete structures. John Wiley and Sons, New York, 363 pp.

Bishop, E.D. (1962): Continuity connection for precast prestressed concrete bridges. Journal of the American Concrete Institute April 1962, pp. 585-598.

Bradford, M.A. (1991): Deflections of composite steel-concrete beams subjected to creep and shrinkage. American Concrete Institute Structural Journal 88 No.5, pp. 610-614.

Bradford, M.A. and Gilbert, R.I. (1991): Time-dependent behaviour of simply supported steel-concrete composite beams. Magazine of Concrete Research 43, No.157, pp. 265-274.

Branson, D.E (1977): Deformation of Concrete Structures, McGraw-Hill International Book Company.

Branson, D.E and Trost, H (1982): Application of I-effective method in calculating deflections of partially prestressed members. Prestressed Concrete Institute Journal 27 (Sept.-Oct.), pp.62-77.

Branson, D.E. and Ozell, A.M (1961): Camber in prestressed concrete beams, American Concrete Institute Journal Vol. 57 No. 68, pp 1549-1574.

Branson, D.E. and Trost, H (1982): Unified procedures for predicting the deflection and centroidal axis location of partially cracked nonprestressed and prestressed concrete members. American Concrete Institute Journal Mar-April, pp. 119-130.

Breckenridge, R.A. and Bugg, S.L. (1964): Effects of long-time loads on prestressed concrete beams. Prestressed Concrete Institute Journal, Dec. pp75-89.

British Standard BS5400 (1990): Steel, concrete and composite bridge, Part 4. Code of practice for design of concrete bridges.

Brooks, J.J. (1984): Accuracy of estimating long-term strains in concrete. Magazine of Concrete Research 36 no. 128, Sept., pp. 131-145.

Brooks, J.J., Gamble, A.E.; and Chouman, M.M. (1992): Assessment of methods of predicting time-dependent deformations of plain and reinforced concrete. The Structural Engineer 70 no.1, 7 Jan, pp. 8-13.

Burke, M.P. (1990): The integrated construction and conversion of single and multiple span bridges. First International Conference on Bridge Management University of Surrey, March, pp. 667.

Burns, N.H. (1966): Development of continuity between precast concrete beams. Prestressed Concrete Institute Journal June, pp. 23-36.

Campbell, T.I.; and Batchelor, B. (1977): Load testing of a model two-span continuous prestressed concrete trapezoidal bridge girder. Prestressed Concrete Institute Journal Nov.-Dec. 1977, pp. 62-79.

Chiorino, M.A., Napoli, P., Mola, F. and Koprna, M. (Eds.) (1984): CEB Design Manual on Structural Effects of Time-Dependent Behaviour of Concrete. Georgi Publishing Company Saint-Saphorin, Switzerland. 391 pp.

Chouman, MM (1990): The effect of additional reinforcement on time-dependent behaviour of partially prestressed concrete. Ph.D. Dissertation, University of Leeds, Leeds. 285 pp.

Clark, L.A. (1983): Concrete Bridge Design to BS5400. Construction Press, London. 186 pp.

Clark, L.A. (1997): Serviceability limit state aspects of continuous bridges using precast beams, The Structural Engineer, Vol. 75 No. 11 (June), pp 185-190.

Cohn, M.Z. and Lounis, Z (1991): Moment redistribution in structural concrete codes. Canadian Journal of Civil Engineering 18, pp. 97-108.

Comite Euro-International du Beton (1978): Bulletin D'Information N.124/125-E-CEB-FIP, CEB-FIP Model Code for Concrete Structures, English Translation, April.

Comite Euro-International du Beton (1993): CEB-FIP Model Code 1990.

Corley, W.G. and Sozen M.A. (1972): Time-dependent deflections of reinforced concrete beams, American Concrete Institute Journal 63 (3), pp 373-386

Cottingham, W.S, Fluck, P.G and Washa, G.W (1961): Creep of prestressed beams, American Concrete Institute Journal, February, pp 929-935.

Department of Transport (1992): Standards for post-tensioned prestressed concrete bridges to be reviewed, Press Notice No. 260, 25 September.

Dilger, W.H. (1982): A simple method to analyse time-dependent forces developed in continuous concrete structures. Designing for Creep and Shrinkage in Concrete Structures American Concrete Institute SP-76, pp. 325-339.

Dilger, W.H. (1982): Creep analysis of prestressed concrete structures using creep-transformed section properties. Prestressed Concrete Institute Journal 27 (Jan-Feb.), pp. 98-118.

Dixon, A.S. and O'Brien, E.J. (1991): Prestressing of concrete bridge decks by vertical jacking at supports. FIP notes 1991/4, pp. 18-21.

Ficence, J.A., Kneip, S.D., Tadros, M.K. and Fischer (1993): Prestressed spliced I-Girders: Tenth street viaduct project, Lincoln-Nebraska. Prestressed Concrete Institute Journal Sept.-Oct. 1993, pp. 40-48.

Freyermuth, C.L. (1969): Design of continuous highway bridges with precast prestressed concrete girders. Prestressed Concrete Institute Journal, April, pp. 14-39.

Gee, A (1987): Bridge winners and losers. The Structural Engineer 65A no.4 April, pp. 141-145.

Gesund, H. (1962): Shrinkage and creep influence of deflections and moments of reinforced concrete beams, American Concrete Institute Journal, May pp 687-703.

Ghali, A (1986): A unified approach for serviceability design of prestressed and non prestressed reinforced concrete structures. Prestressed Concrete Institute Journal March-April, pp. 118-137.

Ghali, A (1989): Stress and strain analysis in prestressed concrete: A critical review. Prestressed Concrete Institute Journal Nov.-Dec., pp. 80-97.

Ghali, A (1993): Deflection of reinforced concrete members: A critical review. American Concrete Institute Structural Journal July-Aug. 1993, pp. 364-373.

Ghali, A and Elbadry, M (1987): Cracking of composite prestressed concrete sections. Canadian Journal of Civil Engineering 14, pp. 314-319.

Ghali, A and Elbadry, M (1989): Serviceability design of continuous prestressed concrete structures. Prestressed Concrete Institute Journal Jan.-Feb., pp. 54-91.

Ghali, A and Favre, R (1986): Concrete Structures: Stresses and Deformations. Chapman Hall, 352 pp.

Gilbert, R.I (1988): Time Effects in Concrete Structures. Elsevier, Oxford. 321 pp.

Gilbert, R.I (1992): Shrinkage cracking in fully restrained concrete members. American Concrete Institute Structural Journal March-April, pp. 141.

Grant, A (1966): Naches River Bridge. Prestressed Concrete Institute Journal August, pp. 40-48.

Hambly, E.C and Nicholson, B (1992): Prestressed Beam Integral Bridges, Prestressed Concrete Association, 31pp.

Hambly, E.C and Nicholson, B.A (1990): Prestressed beam integral bridges. The Structural Engineer 63, Dec., pp. 474-481.

Hansen, T.C and Mattock, A.H (1966): Influence of size and shape of member on shrinkage and creep of concrete, American Concrete Institute Journal Proceedings Vol. 63, No. 2 pp 267-289.

Hanson, N.W (1960): Precast-prestressed concrete bridges 2. Horizontal connections. Journal of the PCA Research and Development Laboratories, May, pp. 38-58.

Harajli, M.H. and Hijazi, S.A. (1991): Evaluation of the ultimate steel stress in partially prestressed concrete members, Prestressed Concrete |Institute Journal, Sept. - Oct., pp 91-95.

Herbert, T.J (1990): Computer analysis of deflections and stresses in stage constructed concrete bridges. Prestressed Concrete Institute Journal 35, May-June, pp. 52-62.

Huber, A. (1986): Effect of hyperstatic prestressing moment and the carrying capacity of continuos beams, American Concrete Institute Journal, Proceedings V. 83 No. 4, July, pp 561-566.

Hutton, S.G and Loov, R.E (1966): Flexural behaviour of prestressed, partially prestressed and reinforced concrete beams, American Concrete Institute Journal, Dec., pp 1401-1408.

Illston, J.M and Stevens, R.F (1972): Long-term cracking in reinforced concrete beams. Proceedings Institution of Civil Engineers (London) Part 2 vol.53 December, pp. 445-459.

Inomata, S (1987): An approach for creep analysis of cracked partially prestressed concrete members. Prestressed Concrete Institute Journal Jan-Feb., pp. 104-125.

Jayanandana, A.D.C (1989): Continuity Development Between Precast Beams Using Prestressed Slabs. Ph.D. Dissertation, University of Leeds. 296 pp.

Johnson, R.P (1987): Shrinkage-induced curvature in composite beams with a cracked concrete flange. The Structural Engineer 65B no.4 Dec., pp. 72-77

Kaar, P.H, Kriz, L.B and Hognestad (1960): Precast-prestressed concrete bridges 1. Pilot tests of continuous girders. Journal of PCA Research and Development Laboratories May, pp. 21-37.

Kajfasz, S., Sommerville, G. And Rowe, R.E. (1963): An investigation of the behaviour of composite concrete beams, Cement and Concrete Association Research Report 15, November, 44pp.

Kang, Y.J. and Scordelis, F. (1980): Non-linear time-dependent analysis of reinforced and prestressed concrete frames, ASCE Structural Journal, Vol. 106 No. ST2, pp 445-463.

Kennedy, J.B and Grace, N.F (1982): Prestressed decks in continuous composite bridges. Journal of the Structural Division, ASCE 108, no.11, pp. 2394-2411

Kumar A. (1993): Locally separated deck slab continuity in composite bridges, Continuous and Integral Bridges, E & FN SPON, pp 239-246.

Kumar, A (1986): Continuity in composite bridge construction. International Symposium on Medium and Short Span Bridges 2, Ottawa, Canada, pp. 93-106.

Kumar, A (1988): Composite Concrete Bridge Superstructure. Wexham Spring, British Cement Association.

Lawther, R and Gilbert, R.I (1992): Deflection analysis of composite structures using the rate of creep method. The Structural Engineer 70 no.12 16 June, pp. 220-223.

Lin, T.Y. and Burns, N.H. (1981): Design of Prestressed Concrete Structures, Third Edition, John Wiley & Sons, 646pp.

Lin, T.Y. and Thornton, K. (1972): Secondary moment and moment redistribution in continuous prestressed concrete beams, Prestressed concrete Institute Journal Vol. 17 Jan.-Feb. pp 8-20.

Loveall, C.L (1985): Jointless Bridge decks. Civil Engineering (ASCE) November, pp. 64-67.

Martin, L.D (1977): A Rational method for estimating camber and deflection of precast prestressed members. Prestressed Concrete Institute Journal Jan-Feb., pp. 100-108.

Mattock, A and Kaar, P.H (1960): Precast-prestressed concrete bridges 3. Further tests of continuous girders. Journal of PCA Research and Development Laboratories September, pp. 51-77.

Mattock, A.H (1961): Precast-prestressed concrete bridges 5. Creep and shrinkage studies. Journal of PCA Research and Development Laboratories May, pp. 32-63.

Mattock, A.H and Kaar, P.H (1960): Precast-prestressed concrete bridges 4. Shear tests of continuous girders. Journal of PCA Research and Development Laboratories January, pp. 19-47.

Mattock, A.H and Kaar, P.H (1961): Precast-prestressed concrete bridges 6. Test of half-scale highway bridge continuous over two spans. Journal of PCA Research and Development Laboratories Sept., pp. 30-69.

Meyers, B.L, Branson, D.E and Schumann, C.G (1972): Prediction of creep and shrinkage for design from short term test. Prestressed Concrete Institute Journal 1972, pp. 29.

Muller, H.S and Hilsdorf, H.K (1990): Evaluation of the time-dependent behaviour of concrete. CEB Bulletin no. 199.

NCHRP-322 (1985): Design of precast prestressed bridge girders made continuous, Transportation Research Board, Washington D.C. 97 pp.

Neville, A.M (1970): Creep of concrete: plain, reinforced and prestressed. North Holland, Amsterdam. 622 pp.

New Civil Engineer (1996): Grouted tendons cleared for bridge use, 26 September, pp 5.

Noor, F.A. and Boswell, L.F. (Ed.) (1992): Small Scale Modelling of Concrete Structures, Elsevier Applied Science, 349pp.

Ojdrovic, R.P and Zarghamee, M.S (1996): Concrete creep and shrinkage prediction from short term tests. American Concrete Institute Materials Journal vol. 93 no. 2, March-April, pp. 169-177.

Paterson, G.P. (1993): The UK Department of Transport view on continuity/integral bridges, Continuous and Integral Bridges, E & FN SPON, pp 161-166.

PCI Committee on Losses (1975): Recommendations for estimating losses. Prestressed Concrete Institute Journal July-Aug., pp. 44-74.

Pritchard, B.P (Ed.) (1994): Continuous and Integral Bridges. E&FN Spon, London. 285 pp.

Pritchard, B.P and Smith, A.J (1991): A Survey of Composite concrete bridge decks made continuous. Contractor Report 294, TRRL, Department of Transport, 17pp.

Pritchard, B.P and Smith, A.J (Eds.) (1991): Investigation of methods of achieving continuity in composite concrete bridge decks. TRRL Contractor Report 247. Department of Transport, London.

Rao, A.S.P and Jayaraman, R (1987): Creep and shrinkage analysis of partially prestressed concrete members. Journal of Structural Eng. 115, May, pp. 1169-1189.

Rao, S.V, Rao, A.S and Dilger, W.H (1993): Time-dependent analysis of cracked partially prestressed concrete members. Journal of Structural Eng. 119, Dec., pp. 3571-3589.

Rodrigues Lopes, S.M. (1990): Moment Redistribution in Partially Prestressed Composite Concrete Beams. Ph.D. Dissertation, University of Leeds. 230 p.

Saadatmanesh, H., Albrecht, P. And Ayyub, B.M. (1989): Experimental study of prestressed composite beams, Journal of Structural Engineering, ASCE, 115 (9), pp 2349-2364.

Samra, R.M. (1989): Predicting deflections of reinforced concrete beams analytically, Journal of Structural Engineering, ASCE, Vol. 115 No. 5, May pp 1158-1167.

Scholz (1990): ductility, redistribution, and hyperstatic moments in partially prestressed members, American Concrete Institute Journal, Vol. 87 No. 3, pp 341-349.

Scordelis, A (1982): Analytical models for Non-linear material, geometric and time-dependent effects. International Symposium on nonlinearity and continuity in prestressed concrete, University of Waterloo, Canada, pp. 25-43.

Seible, F (1986): Problems with coupling joints of prestressing tendon in continuous post-tensioned concrete bridges. Second International Symposium on Short and Medium Span Bridges, pp. 93-106.

Shaikh, A.F and Branson, D.E (1970): Non-tensioned steel in prestressed concrete beams, Prestressed Concrete Institute Journal Vol. 15 No. 1, pp 14-36.

Sinno, R and Furr, HL (1972): Computer program for predicting prestress loss and camber. Prestressed Concrete Institute Journal Sept.-Oct., pp. 27-38.

Smallowitz, H (1985): Bridging the gaps in bridges. Civil Engineering (ASCE) November 1985, pp. 43-45.

Srikandan, K (1989): Prestressed concrete road bridges in Great Britain: A historical survey. Proceeding Institution of Civil Engineers, Part 1, 86, April, pp. 269-303.

Stevens, R.F (1972): Deflections of reinforced concrete beams. Proceedings Institution of Civil Engineers (London) Part 2 Vol.53 Sept., pp. 207-224.

Sturrock, R.D (1974): Tests on model bridge beams in precast to in situ concrete construction. Technical Report 488, Cement and Concrete Association, London 17pp.

Suter, R (1981): The design of a continuous structure made up of precast units. IABSE Proceedings P-42/81, pp. 61-80.

Suttikan, C (1978): A Generalised Solution for Time Dependent Response and Strength of Non-Composite and Composite Prestressed Beams. Ph.D. Dissertation, University of Texas, Austin.

Tadros, M.K, Ficenec, J.A, Einea, A and Holdsworth, S (1993): A new technique to create continuity in prestressed concrete members. Prestressed Concrete Institute Journal Sept.-Oct.1993, pp. 30-37.

Tadros, M.K, Ghali, A and Dilger, W.H (1975): Time-dependent loss and deflection in prestressed concrete members. Prestressed Concrete Institute Journal 1975.

Tadros, M.K, Ghali, A and Dilger, W.H (1977): Time-dependent analysis of composite frames. Journal of the Structural Division (ASCE) 103 ST4 (April), pp. 871-884.

Taylor H.P.J. (1993): Continuity in decks with precast beams - practical issues, Continuous and Integral Bridges, E & FN SPON, pp 65-71.

Taylor, H.P.J, Clark, L.A and Banks, C.C (1990): The Y-Beam: A replacement for the M-beam in beam and slab bridge decks. The Structural Engineer 68 no.23 4 Dec., pp. 459-465.

Teng, S (1991): Time-step Analysis of the Initial and Time-dependent Deformations of Reinforced and Partially prestressed Concrete Structures. Ph.D. Dissertation, University of Iowa.

Teng, S and Branson, D.E (1993): Initial and time-dependent deformation of progressively cracking non-prestressed and partially prestressed concrete. American Concrete Institute Structural Journal Sept.-Oct., pp. 480-488.

Tilly G.P. (1993): Historical review of the development of continuity and expansion joints in bridges, Continuous and Integral Bridges, E & FN SPON, pp 45-54.

Tong, W and Saadatmanesh, H (1992): Parametric study of continuous prestressed composite girders. Journal of Structural Eng. 118, no.1, pp. 186-205.

Trost, H (1982): Effects of the time-dependent behaviour of concrete in prestressed concrete members. Designing for Creep and Shrinkage in Concrete Structures American Concrete Institute:SP-76, pp. 301-308.

Washa, G.W. and Fluck, P.G. (1956): Plastic flow of reinforced concrete continuous beams, American Concrete Institute Journal 52(5), pp 549-561

Wyche, P.J., Uren, J.G. and Reynolds, G.C (1992): Interactions between prestress secondary moments, moment redistribution, and ductility - a treatise on the Australian Concrete Codes, American Concrete Institute Structural Journal, Vol. 89 No. 1, pp 57-70.

Yamane, T, Tadros, M.K and Arumugusamy, P (1994): Short to medium span precast prestressed concrete bridges in Japan. Prestressed Concrete Institute Journal March-April 1994, pp. 74-100.

Yu, W and winter, G (1960): Instantaneous and long-time deflections of reinforced concrete beams under working loads, Journal of American Concrete Institute Vol. 57, No. 1 July, pp 29-50.

APPENDIX A

DETAILS OF EXPERIMENTAL BEAMS

CONTENTS

A1.1 Washa , G.W and Fluck, P.G. (1956)

A1.2 Yu and Winter (1960)

A1.3 Cottingham, W.S., Fluck, P.G. and Washa, G.W. (1961)

A1.4 Breckenridge and Bugg (1964)

A1.5 Hutton, S.G and Loov, R.E. (1966)

A1.6 Shaikh and Branson, D.E. (1970)

A1.7 Choumann, M.M. (1990)

A1.8 Al-Khaja, W.A. (1986)

A1.9 Bakos, S.L. *et al* (1982)

A1.1 Washa GW and Fluck PG (1956)

The experimental data have been obtained from three different publications i.e. from Washa and Fluck (1956), Yu and Winter (1960) and ACI Committee 435 Report (1966).

Rectangular reinforced concrete beams were tested under sustained uniformly distributed loads. All beams were loaded at 14 days and exposed to an average relative humidity of 50%. Section details are shown in Table A1. Concrete strength, ratio of superimposed loads to selfweight, immediate and time-dependent deflections are shown in Table A2. Concrete has an ultimate shrinkage of 500 microstrains and a creep coefficient of 2.5. The concrete mix used Portland Cement Type I and sand gravel aggregate of 19mm maximum size.

Table A1: Beam details for single span rectangular beams

Beam No.	Span (m)	Cross section, DXB(mm)	Area x10⁴(mm²)	As1 (ds1) mm² (mm)	As2 (ds2) mm² (mm)	Inertia x10⁸(mm⁴)
A1,A4	6.09	305x203	6.19	851 (30.5)	851 (274.5)	4.80
B1,B4	6.09	203x152	3.097	400 (20.0)	400 (183.0)	1.06
C1,C4	6.34	127x305	3.871	516 (38.1)	516 (88.9)	0.521
D1,D4	3.81	127x305	3.871	516 (38.1)	516 (88.9)	0.521
E1,E4	5.33	76x305	2.3226	284 (24.0)	284 (52.0)	0.1116
A2,A5	6.09	305x203	6.19	400 (30.5)	851 (274.5)	4.80
B2,B5	6.09	203x152	3.097	200 (30.5)	400 (183.0)	1.06
C2,C5	6.34	127x305	3.871	258 (20.0)	516 (88.9)	0.521
D2,D5	3.81	127x305	3.871	258 (38.1)	516 (88.9)	0.521
E2,E5	5.33	76x305	2.3226	142 (38.1)	284 (52.0)	0.1116
A3,A6	6.09	305x203	6.19	0	851 (274.5)	4.80
B3,B6	6.09	203x152	3.097	0	400 (183.0)	1.06
C3,C6	6.34	127x305	3.871	0	516 (88.9)	0.521
D3,D6	3.81	127x305	3.871	0	516 (88.9)	0.521
E3,E6	5.33	76x305	2.3226	0	284 (52.0)	0.1116

Table A2: Instantaneous and long term deflections

Beam No.	f'_c(28) (MPa)	Dead load (kN/m)	SL (kN/m)	Instant. Deflect. (mm)	900-day deflection (mm)	Total deflection (mm)
A1,A4	28.1	1.45	4.06	13.5	10.2	23.6
B1,B4	23.6	0.73	0.803	23.4	27.7	51.1
C1,C4	22.7	0.91	0.273	40.1	39.9	80.0
D1,D4	24.3	0.91	2.46	11.9	15.7	27.7
E1,E4	25.2	0.54	0.0	59.4	64.5	123.9
A2,A5	28.1	1.45	4.06	15.7	16.5	32.2
B2,B5	23.6	0.73	0.803	24.9	40.1	65.0
C2,C5	22.6	0.91	0.273	43.4	57.1	100.5
D2,D5	24.3	0.91	2.46	14.2	18.8	33.0
E2,E5	25.2	0.54	0.0	55.9	72.9	128.8
A3,A6	28.1	1.45	4.06	17.0	27.7	44.7
B3,B6	23.6	0.73	0.803	26.4	59.9	86.3
C3,C6	22.7	0.91	0.273	47.6	93.0	140.6
D3,D6	24.3	0.91	2.46	17.8	30.7	48.5
E3,E6	25.2	0.54	0.0	63.0	122.0	185.0

A1.2 Yu, W and Winter, G (1960)

T-shape reinforced concrete beams were tested under sustained uniformly distributed loads. The beams were exposed to an average relative humidity of 34% and temperature of 79°F. Fresh concrete had a slump between 60mm-90mm. Table A3 shows the beam details and Table A4 shows the 28 days strength, loading and age at first loading and deflection readings.

Table A3: Beam properties

Beam No.	Span/ depth (m)	Area $x10^2(mm^2)$	As1 (ds1) mm^2 (mm)	As2(ds2) mm^2 (mm)	Inertia $x10^8$ mm^4	C.A from top, yg mm
A-2	6.09/0.305	5.6	0	400(259)	4.76	131.3
B-2	6.09/0.305	5.6	200(40.0)	400(259)	4.76	131.3
C-2	6.09/0.305	5.6	400(40.0)	400(259)	4.76	131.3
D-2	6.09/0.305	7.53	0	774(246)	6.26	105.8
E-2	4.27/0.305	5.6	0	400(249)	4.76	131.3
F-2	6.09/0.25	3.86	0	400(157)	1.43	86.1

Table A4: Concrete strength, loading and deflection readings

Beam No.	$f_c(28)$ (MPa)	age at loading, t_o (days)	load (udl) kN/m	immediate deflection (mm)	180-day deflection (mm)
A-2	25.4	30	5.1	30.2	67.3
B-2	26.8	29	5.1	29.9	56.6
C-2	24.4	28	5.1	30.0	51.6
D-2	25.4	31	9.95	32.7	67.0
E-2	29.4	29	11.0	14.7	29.2
F-2	29.4	34	2.9	51.8	100.0

A1.3 Cottingham, W.S., Fluck, P.G. and Washa G.W. (1961)

Three fully prestressed beams of 133x254mm cross section with spans of 6.09m were tested under three different load levels. Each beam was tested under 50, 75 and 100% of the service loads (2.08kN/m, 3.12kN/m and 4.16kN/m) for 120 days.

The beams had a concrete cylinder strength of 41.4N/mm^2 and prestressing steel of 181.9mm in diameter. The prestressing steel had an ultimate strength of 1917MPa and elastic modulus of 176.6MPa. The initial stress of 965 MPa was transferred after 3 days and the beams were loaded after 60 days. They were kept under sustained load for 120 days under a relative humidity of 70%. Instantaneous and long term deflections are shown in Table A5.

Table A5: Instantaneous and long term deflection

Beams	Beam 1	Beam 2	Beam 3
applied loads (kN/m)	4.16	3.13	2.08
instantaneous deflections (mm)	17.0	11.9	7.9
after 2500 days	29.5	17.3	9.6

A1.4 Breckenridge and Bugg (1964)

A total of 8 grouted post-tensioned full size beams were tested for 7 years under changing environmental conditions. The beams were of I-shape with a span length of 40ft (12.19m) between supports. The beams were post-tensioned with 2-1.125 inch diameter high strength steel bars. The section was 609.9mm deep with cross sectional area and second moment of area of 116451mm^2 and 5.143318x10^9 mm^4 respectively. The sections had a prestressing steel area of 1282mm^2 and were initially stressed 876.3kN. The centroid of the section and the position of prestressing bars from the top fibre were 328.7mm and 520mm respectively.

Beams were moist cured for 22 days, stressed after 8 days, grouted on day 9 and loads were applied on day 22. Portland Cement Type III was used with a water-cement ratio of 0.4, and mix design of 1:1.71:1.75. The average 28 days cylinder strength was 6,000 psi (41.3 MPa) and elastic modulus was 3500 ksi (24MPa). The prestressing bars had ultimate stress of 146 ksi (1000 MPa) and elastic modulus of 24,500 ksi (169 MPa).

Beams were left in outdoor conditions and average relative humidity was recorded all year round. The minimum average *RH* was 45% during winter, and 65% during summer. The maximum average *RH* was 86% during winter and 95% during summer. The maximum shrinkage were 320 and 390 at top and bottom fibres respectively. Two beams were left unloaded, 2 were loaded to 50% of design loads (7,600 lbf or 33.8kN), 2 were loaded to 100% (15,200 lbf or 67.6kN) and the remaining two were loaded at 150% (101.4kN). Loads were applied at quarter points and results are shown in Table A6.

Table A6: Instantaneous and time-dependent deflection

Beams	loading ratio /service load	Instantaneous deflection (mm)	time-dependent deflection (mm)	total long term deflection (mm)
Beam 1&2	0.0/ 0.0	-17.5	-16.8	-34.3
Beam 3&4	0.5/ 33.8	12.7	12.7	25.4
Beam 5&6	1.0/ 67.6	25.6	37.4	63.0
Beam 7&8	1.5/ 101.4	46.0	65.2	111.2

A1.5 Hutton, S.G and Loov, R.E (1966)

Four simply supported beams ranging from fully prestressed to ordinarily reinforced sections were tested under their own weight for four months. The beams had cross sections of 152mmx127mm and 3.05m spans. All beams were stressed at 7 days at an initial stress of 1169N/mm^2. Average 28 day strength of concrete was 46N/mm^2. The beams were stored under 75% relative humidity. Details of beam reinforcement and final deflection readings are shown in Table A7.

Table A7: Beam reinforcements and final deflections

Beams	3P-0R	2P-1R	1P-2R	0P-3R
Ap (mm^2)	148	99.0	49.5	0.0
As (mm^2)	0.0	198.0	396.0	594.0
final deflection (mm)	-11.9	-2.3	1.8	9.4
number of days	121	111	114	143

A1.6 Shaikh and Branson (1970)

The camber of 12 simply supported prestressed beams with varying degrees of non-tensioned steel were measured. The beams were 15 feet (4.57m) long with cross sections of 6x8inches (152x203mm). They were left unloaded in order to observe their time-dependent cambers. At the end of the tests, the beams were loaded to failure to observe the behaviour after cracking.

All beams and shrinkage specimens were moist cured for seven days after which they were kept under laboratory conditions of a temperature varying between 70-80°F. The beams were stressed at 7 days. Other details as shown in Table A8 and experimental results are shown in Table A9.

Table A8: Concrete strength and cross section details for each beam

Beam	$f_{ci}(28)$ (MPa)	Ap (mm^2)	As (mm^2)	ds (mm)	Fpi (kN)	age (days)
I-1	37.2	112.5	129	152	132.5	172
I-3	37.2	112.5	387	152	133.9	172
II-2	40.6	75.0	129.0	189	89.0	140
II-3	40.6	75.0	258.0.0	171	87.6	140
III-1	45.3	112.5	0.0	-	135.7	124
III-2	45.3	154.8	0.0	-	132.6	124
III-3	45.3	154.8	200	152	132.6	124
IV-1	40.6	103.2	51.6	189	112	123
IV-2	40.6	103.2	200	189	114.8	123
IV-3	40.6	103.2	387.0	180	108.5	123
Note: depth of prestressing steel was maintained at189mm for all beams, section 152x203mm.						

Table A9: Experimental results

Beam	I-1	I-3	II-2	II-3	III-1	III-2	III-3	IV-1	IV-2	IV-3
As/Ap	1.15	3.46	1.73	3.46	0.0	0.0	1.3	0.5	1.94	3.76
Initial camber (mm)	6.3	6.4	3.6	3.6	5.7	5.7	5.6	5.2	5.2	4.7
Time-dependent camber (mm)	6.5	4.0	1.9	1.1	6.3	5.4	2.7	3.3	2.7	1.04
Total camber (mm)	12.8	10.4	5.5	4.7	12.0	11.1	8.3	8.5	7.9	5.74
age (days)	172	172	140	140	124	124	124	123	123	123

E9. Chouman, M.M. (1990)

Concrete was designed for 7-day cube strength 50MPa with proportions of 1:1.81:3.02 and a water/cement ratio of 0.49. The mix used Portland Cement Type I and maximum aggregate size of 10mm. All beams had single prestressing wire areas of 38.5mm^2 with an ultimate strength and elastic modulus of 1793 MPa and 206.4 MPa respectively. The initial prestressing force was 49.3kN (1280N/mm^2) and was transferred on day 8 to the beams. Beams were of rectangular cross section (100x180mm). Reinforcements details of are shown in Table A10 and concrete properties are shown in Table A11.

Beams were cured under moist conditions for 5 days and kept under a room temperature of 20°C. A single point load to produce zero stress at bottom fibre was applied on day 8 and sustained for the desired duration for beams GLR1,0 and GLR1,2. Beam GNR1,3 was left unloaded. Corresponding sections of similar sizes but with different degrees of reinforcement i.e. 0, 0.63, 1.62, 1.74, 3.66 and 4.47% (symmetrical and unsymmetrical reinforcement) were tested for creep under a constant axial stress of 5MPa and for shrinkage under average relative humidities of 45-55%.

Experimental results for creep and shrinkage tests are shown in Table A12. Time-dependent losses of prestress strains at the centroid of the sections for beams GLR1,0, GLR1,2 and GNR1,3 are shown in Table A13.

Table A10: Section properties

Section prop\Beams	GLR1,0	GLR1,2	GNR1,3
Tension steel area Ans1 (mm^2)	0.0	235	603
Compression steel area, Ans2 (mm^2)	0.0	56.5	56.5
Transformed area (mm^2)	18209	19807	21640
Transformed Second moment (mm^4)	48.94 (10^6)	56.4 (10^6)	62.52 (10^6)
eps (mm)	39.5	36.2	31.1
ens1 (mm)	-	65.2	57.1

Table A11: Cube strength (MPa) and Elastic modulus (GPa)

day	GLR1,2 and GNR1,3		GLR1,0	
	f_{cu}	E_c	f_{cu}	E_c
7	49.7	32.99	47.8	32.16
28	63.1	35.77	61.7	32.99
90	69.3	35.94	64.7	31.63
180	65.3	36.8	63.5	34.48
365	69.1	36.62	65.57	31.00

Table A12: Total time-dependent deformation (microstrain) of rectangular sections

day	plain	0.63%Sym	1.62%Unsy	1.74%Sym	3.66Unsym	4.47%Sym
0	200	200	200	200	200	200
28	520	500	460	450	420	340
53	710	670	610	580	540	450
83	790	750	680	640	600	490
113	830	770	690	660	620	480
143	870	820	730	690	650	510
173	920	850	760	720	680	520
203	930	870	770	730	690	540
233	940	880	780	740	700	540

Table A13: Total losses and time-dependent axial strains

prestress loss (%)				Average axial strains at centroid of the section (microstrain)			
day	GLR1,0	GLR1,2	GNR1,3	day	GLR1,0	GLR1,2	GNR1,3
21	7.0	4.9	6.0	21	360	300	280
53	8.7	6.1	6.5	53	470	440	400
83	9.5	6.5	7.0	83	590	460	420
113	10.2	7.0	7.3	113	610	490	450
143	11.0	7.6	7.5	143	690	560	480
173	12.0	7.6	7.5	173	680	550	470
233	12.5	9.5	8.3	233	750	560	470

A1.8 Al-Khaja, W.A.A. (1986)

The test program had two concrete mixes. Mix 1 used rapid hardening Portland cement with a 28 days strength of 45.0 MPa and Mix 2 used ordinary Portland cement with 28 days strength of 41.0 MPa. Mix 1 had a 12mm slump and mix two had a 30mm slump. Prestressing steel and operations and other experimental conditions were similar to those of Chouman, (1990)

Beams of rectangular section 100x180mm, had a gross area of $1.8x10^4(mm^2)$ second moment of $4.86x10^7(mm^4)$, volume to surface area ratio of 31.4mm, and distance to top fibre of 90mm. Beams of I-section had a gross area of $1.26x10^4(mm^2)$ second moment of $4.4955x10^7(mm^4)$ and volume to surface area ratio of 21.8mm.

Test results for time-dependent camber and prestress losses are shown in Table A14 and A15.

Table A14: Time dependent camber (mm)

Day	NGI/c1	NGR/c1	NGI/c2
7	1.3	1.1	1.04
28	2	1.76	2.36
90	2.4	2.15	3.01
180	2.6	2.32	3.3
365	2.76	2.45	3.51

Table A15: Time dependent loss of prestress (%)

day	NGI/C1	NGI/V1	NGI/C2	NGI/V2	NGR/C1	NGR/V1
7	82	80	75	70	72	67
28	137	117	144	123	125	90
90	177	140	187	143	160	114
180	197	161	206	163	185	140
365	227	182	235	187	221	166

A1.9 Bakos, S.L., Gilbert, R.I., Faulkes, K.A and Pulmano, V.A. (1982).

Two simply supported beams (1B1 and 1B2) and two continuous beams (2B1 and 2B2) were tested under sustained load of more than 500 days. The cross-sections of the beams were 100x150mm and were reinforced with 2-12mm diameter deformed bars at an effective depth of 130mm. The beams were moist-cured for 14 days after casting and thereafter were kept in a climate controlled laboratory. The simply supported beams had span of 3.75m and the continuous beams had 3.5m span length.

Beam 1B1 was subjected to sustained load consisting of two point loads, each 2.6kN, applied at the third-points of the span. The load was applied at 28 days. The other simply supported beam was left loaded under its own weight. The load on the continuous beams was applied at 23 days after casting. The loading for theses beams consisted of a point load of 6kN applied at the mid-point of each of the two equal spans.

The concrete compressive strength and the elastic modulus for the simply supported beams at 28 days were measured at 39MPa and 31.2GPa respectively. The strength and elastic modulus for the continuous beams at 22 days were measured at 33.1MPa and 27.3GPa. The long term (about 580 days) values for the creep coefficient and shrinkage were measured at 2.5 and 700 microstrains. The long term (550 days) deflection for the unloaded simply supported beam was measured at 8mm and the time-dependent deflection for the loaded beams are given in Table A16.

Table A16: Time dependent deflection at mid-spans

Simply supported		Continuous	
time under loads (days)	deflections (mm)	time under loads (days)	deflections (mm)
0	8.94	0	4.92
25	13.9	12	6.89
95	18.16	60	9.66
260	21.83	130	12.34
500	25.02	400	14.97

APPENDIX B:

Statistical evaluation of time-dependent deformation of flexural beams.

Statistical evaluations for creep and shrinkage have been conducted on the CEB material models (CEB Bulletin No. 199, 1990). The time-dependent behaviour of structural members is thus evaluated adopting a similar approach which is reproduced here.

To characterize the accuracy of the predictions of long term deformations, the following statistical values are evaluated:

$$\bar{m} = \frac{1}{N}\sum m_i \tag{B1}$$

$$F = \sqrt{\frac{1}{N}\sum F_i^2} \tag{B2}$$

$$\bar{V} = \sqrt{\frac{1}{N}\sum V_i^2} \tag{B3}$$

Equations B1-B3 are determined from the following relations:

$$m_i = \frac{calX}{obsX} \tag{B4}$$

$$F_i = \frac{calX - obsX}{obsX}100 \tag{B5}$$

$$V_i = \frac{S_i}{\bar{Y}_i}100 \tag{B6}$$

$$S_i = \sqrt{\frac{1}{n-1}\sum\left(\Delta Y_{ij}\right)^2} \tag{B7}$$

$$\bar{Y}_i = \frac{1}{n}\sum Y_{ij} \tag{B8}$$

where:

calX predicted values

obsX experimental values

N Total number of experiments

i indicates the number of the experiment considered

ΔY_{ij} differences between observed strains or deflections or losses of prestress and predicted values at time j of the experiment i

Y_{ij} observed strain or deflections or losses of prestress at time j of experiment i

n total number of values j of experiment i considered at a fixed time.

The term $\overline{m}$ indicates systematic over or underestimates of predicted values, whereas $\overline{F}$ is an indication of the overall error. Both values are determined for a fixed time. The term $\overline{V}$ corresponds to a mean coefficient of variation for the method of prediction, which characterizes the mean error over the entire duration of loading (Figure B1)

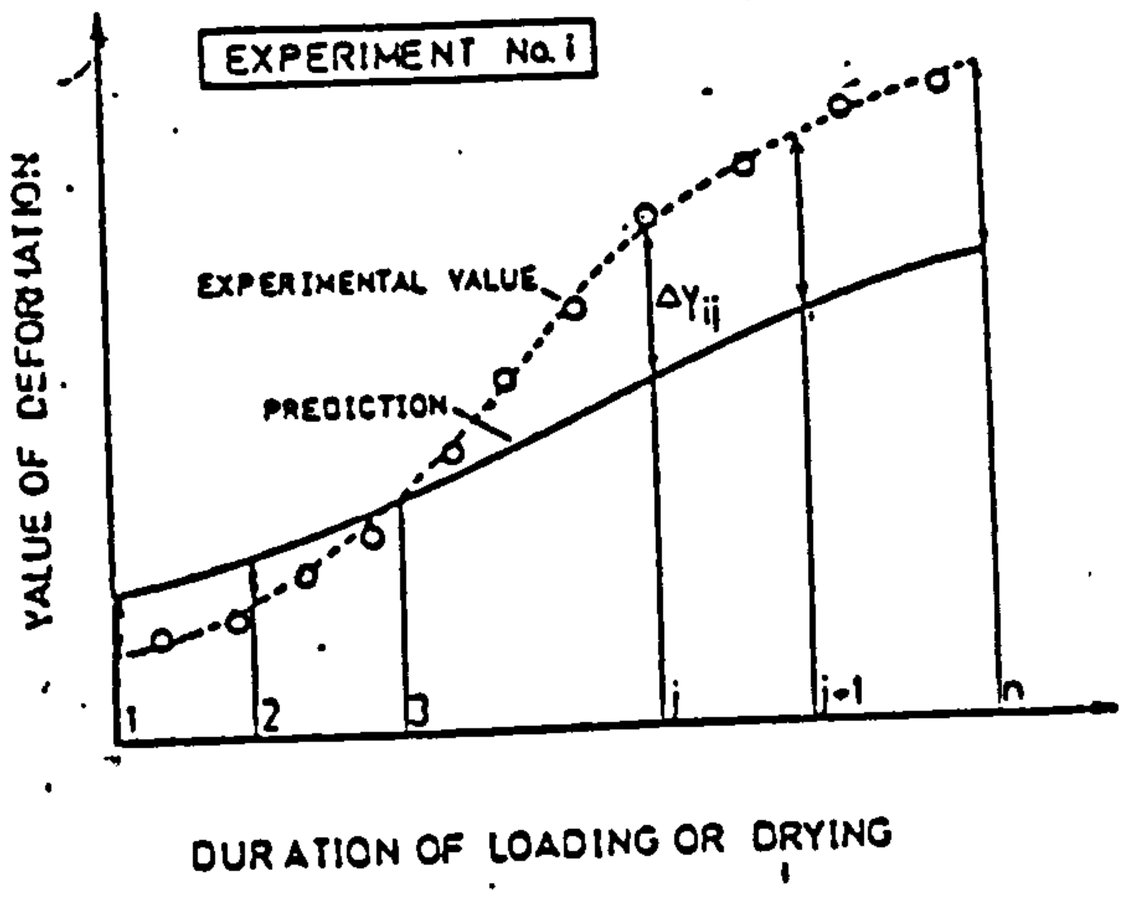

Figure B1: Statistical evaluation of experimental data

APPENDIX C:

Typical Cross Sections Used for Evaluation.

C-1 Inverted Tee Beams

C-2 Y Beams

C-3 SY Beams

C-4 M Beams

C-5 U Beams

INVERTED TEE BEAMS

PRESTRESSED
CONCRETE
ASSOCIATION

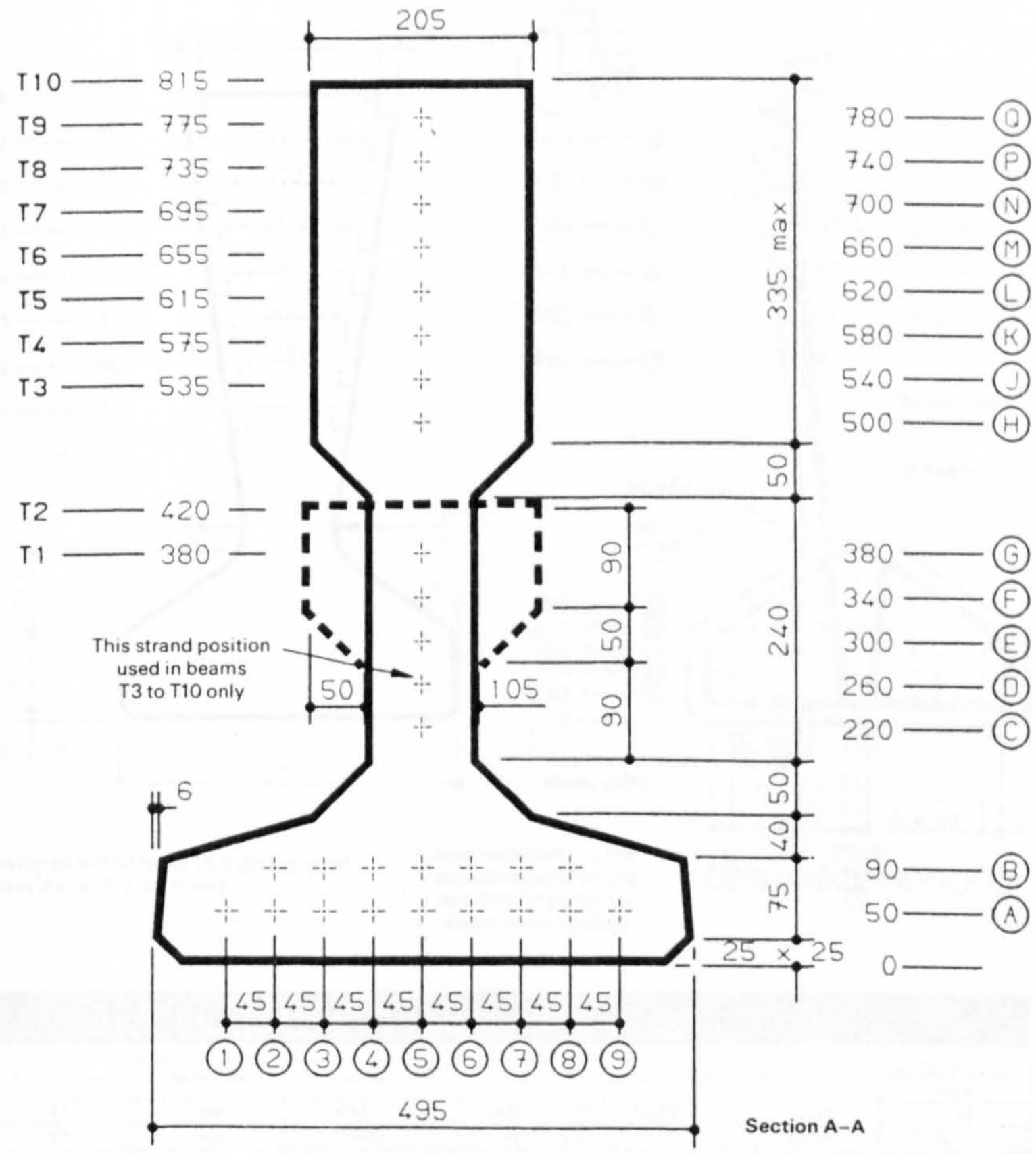

Section A–A

Preferred strand to be 12.5 dia standard class 2.

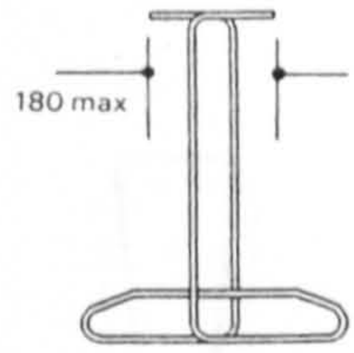

One piece web and flange stirrup

Stirrup detail where bent bar
at top exceeds 180mm

For skewed beams, the links are perpendicular to the beam axis except at the end where they follow the skew.
End skews should be in increments of 5°.

SECTION PROPERTIES

Section No	Depth mm	Area mm^2	Yb mm	Zt $mm^3 \times 10^6$	Zb $mm^3 \times 10^6$	App self weight KN/m
T1	380	98000	140	5.18	8.89	2.31
T2	420	106200	160	6.76	10.38	2.50
T3	535	114275	196	9.57	16.55	2.69
T4	575	122475	220	11.92	19.23	2.89
T5	615	130675	244	14.30	21.81	3.08
T6	655	138875	267	16.73	24.36	3.27
T7	695	147075	289	19.20	26.91	3.47
T8	735	155160	312	21.73	29.46	3.66
T9	775	163360	334	24.31	32.10	3.85
T10	815	171560	356	26.97	34.82	4.05

Design self weight per unit volume has been taken as 23.6 kN/m^3

Y BEAMS

PRESTRESSED
CONCRETE
ASSOCIATION

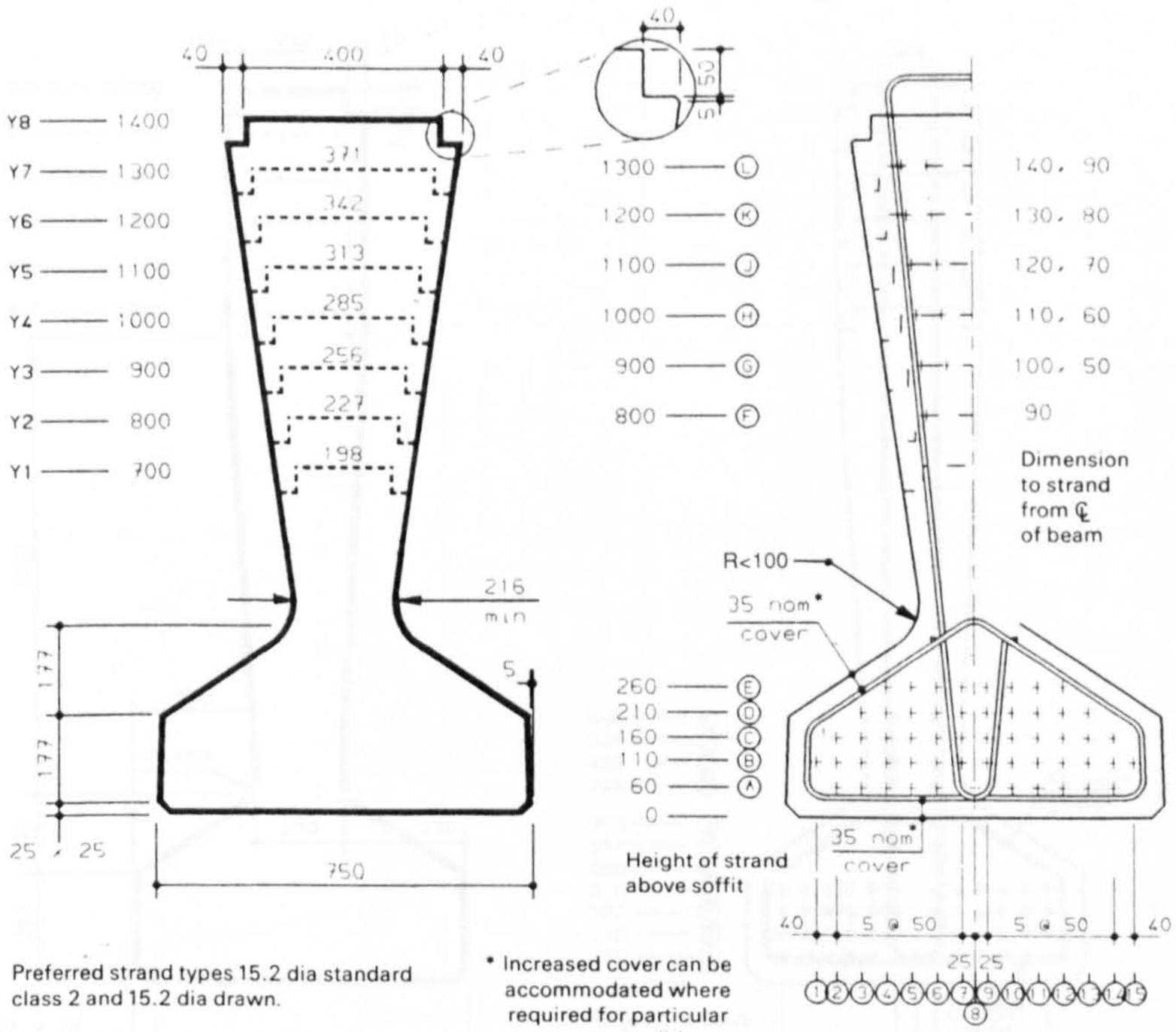

Preferred strand types 15.2 dia standard class 2 and 15.2 dia drawn.

* Increased cover can be accommodated where required for particular exposure conditions

SECTION PROPERTIES

Section No	Depth mm	Area mm^2	Yb mm	Zt $mm^3 \times 10^6$	Zb $mm^3 \times 10^6$	App self weight KN/m
Y1	700	309202	255	24.85	43.40	7.42
Y2	800	339882	299	35.02	58.78	8.14
Y3	900	373444	347	47.88	76.27	8.95
Y4	1000	409890	400	63.53	95.41	9.82
Y5	1100	449220	456	82.06	116.02	10.78
Y8	1200	491433	515	103.58	138.00	11.78
Y7	1300	536530	576	128.15	161.31	12.86
Y8	1400	584708	639	155.98	186.01	14.02

Design self weight per unit volume has been taken as 23.6 kN/m^3

Additional advice may be obtained direct from PCA member companies, who will assist at the earliest stages of planning, or from the Prestressed Concrete Association.

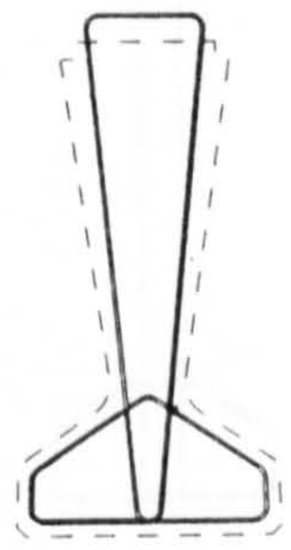

Split stirrup

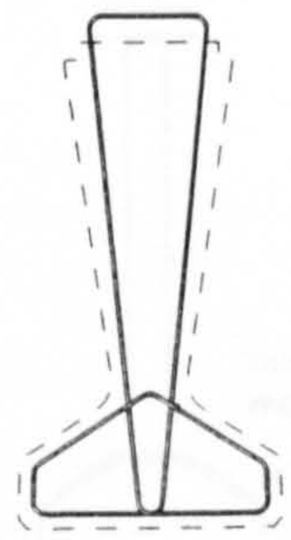

One piece web and flange stirrup

For skewed beams, the links are perpendicular to the beam axis except at the end where they follow the skew. End skews should be in increments of 5°.

SY BEAMS

PCA

PRESTRESSED
CONCRETE
ASSOCIATION

Additional advice may be obtained direct from PCA member companies, who will assist at the earliest stages of planning, or from the Prestressed Concrete Association.

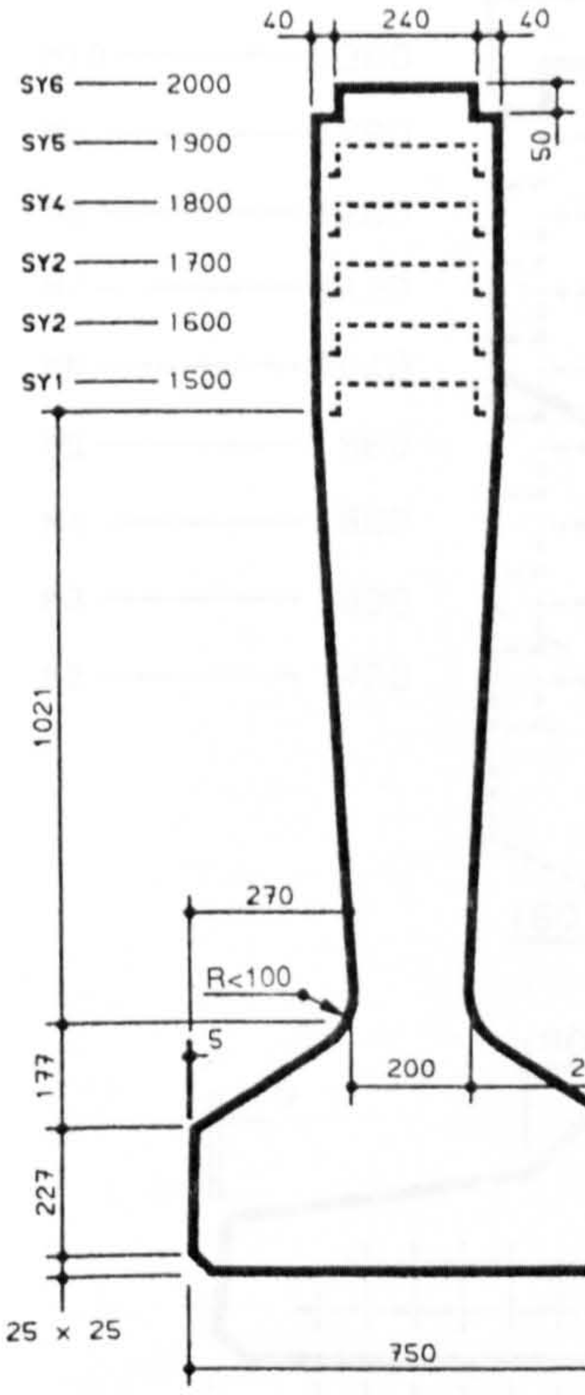

Preferred strand types 15.2 dia standard class 2 and 15.2 dia drawn

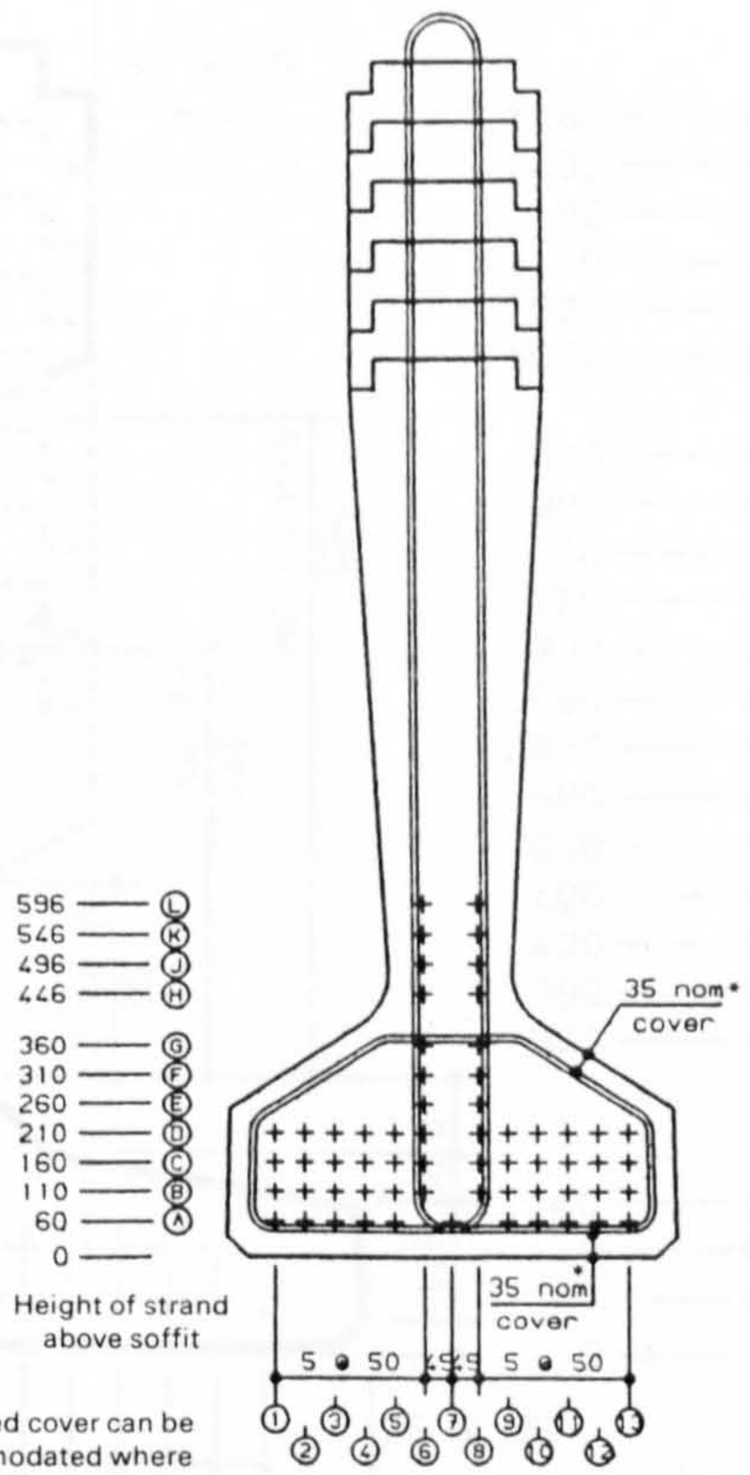

* Increased cover can be accommodated where required for particular exposure conditions

SECTION PROPERTIES – PRECAST SECTION

Section No	App self weight KN/m	Depth mm	Area mm^2	Yb mm	Zt $mm^3 \times 10^6$	Zb $mm^3 \times 10^6$
SY1	12.96	1500	549158	598.35	132.59	199.81
SY2	13.72	1600	581158	650.06	153.97	225.00
SY3	14.47	1700	613158	701.59	176.16	250.69
SY4	15.23	1800	645158	752.98	199.16	276.98
SY5	15.98	1900	677158	804.23	223.09	303.97
SY6	16.74	2000	709158	855.36	247.89	331.72

Design self weight per unit volume has been taken as 23.6 kN/m^3

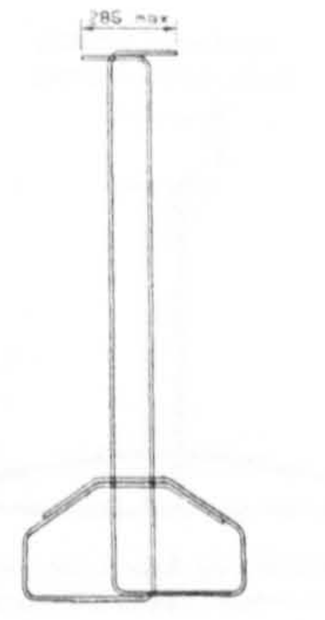

Split stirrup

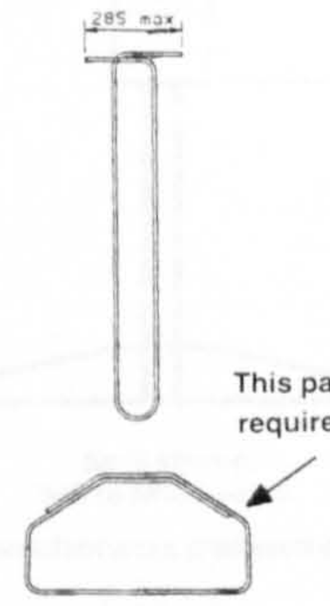

Reinforcement over transverse holes where required

For skewed beams, the links are perpendicular to the beam axis except at the end where they follow the skew. End skews should be in increments of 5°.

M BEAMS

PRESTRESSED
CONCRETE
ASSOCIATION

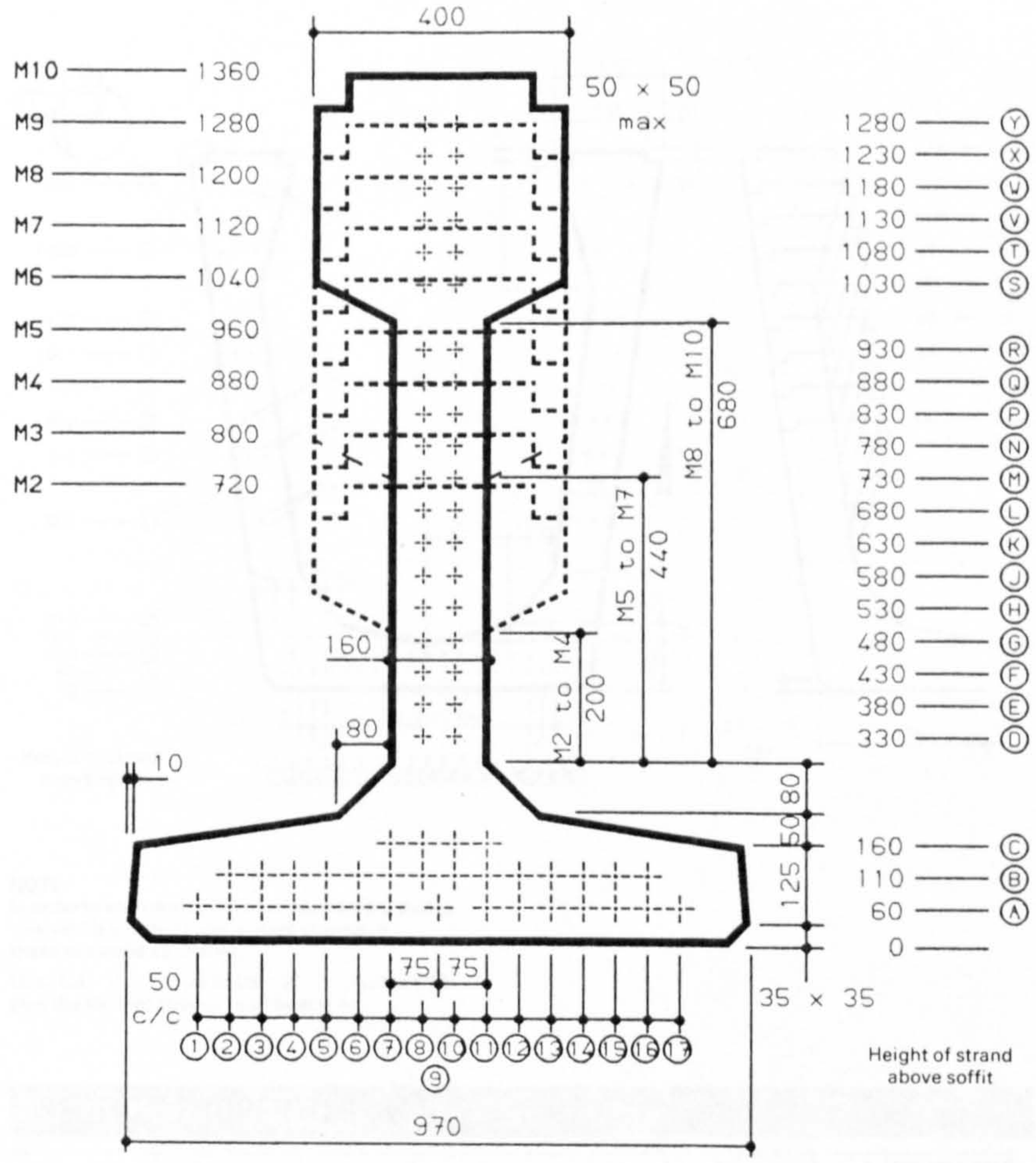

Preferred strand types 15.2 dia standard class 2 and 15.2 dia drawn

SECTION PROPERTIES

Section No	Depth mm	Area mm^2	Yb mm	Zt $mm^3 \times 10^6$	Zb $mm^3 \times 10^6$	App self weight KN/m
M2	720	316650	265	35.64	61.04	7.47
M3	800	348650	310	46.96	74.31	8.23
M4	880	380650	353	58.77	87.57	8.98
M5	960	355050	357	59.39	100.33	8.38
M6	1040	387050	409	75.39	116.23	9.13
M7	1120	419050	460	91.53	131.54	9.89
M8	1200	393450	454	87.39	143.57	9.29
M9	1280	425450	512	108.09	161.96	10.04
M10	1360	457450	568	128.65	179.36	10.80

Design self weight per unit volume has been taken as 23.6 kN/m^3

Additional advice may be obtained direct from PCA member companies, who will assist at the earliest stages of planning, or from the Prestressed Concrete Association.

One piece web and flange stirrup M2 to M4 beams only

To manufactures preferred detail

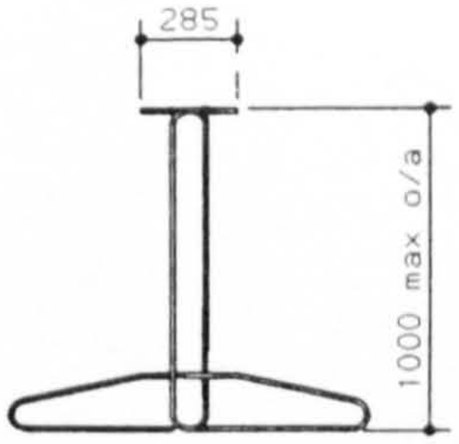

Split stirrup M5 to M10 beams

To manufacturers preferred detail

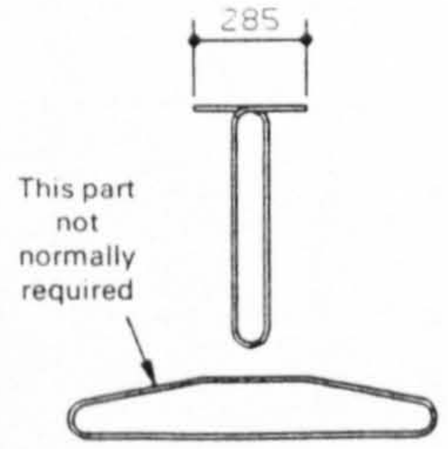

Reinforcement over transverse holes where required

For skewed beams, the links are perpendicular to the beam axis except at the end where they follow the skew. End skews should be in increments of 5°.

U BEAMS

PRESTRESSED
CONCRETE
ASSOCIATION

Additional advice may be obtained direct from PCA member companies, who will assist at the earliest stages of planning, or from the Prestressed Concrete Association.

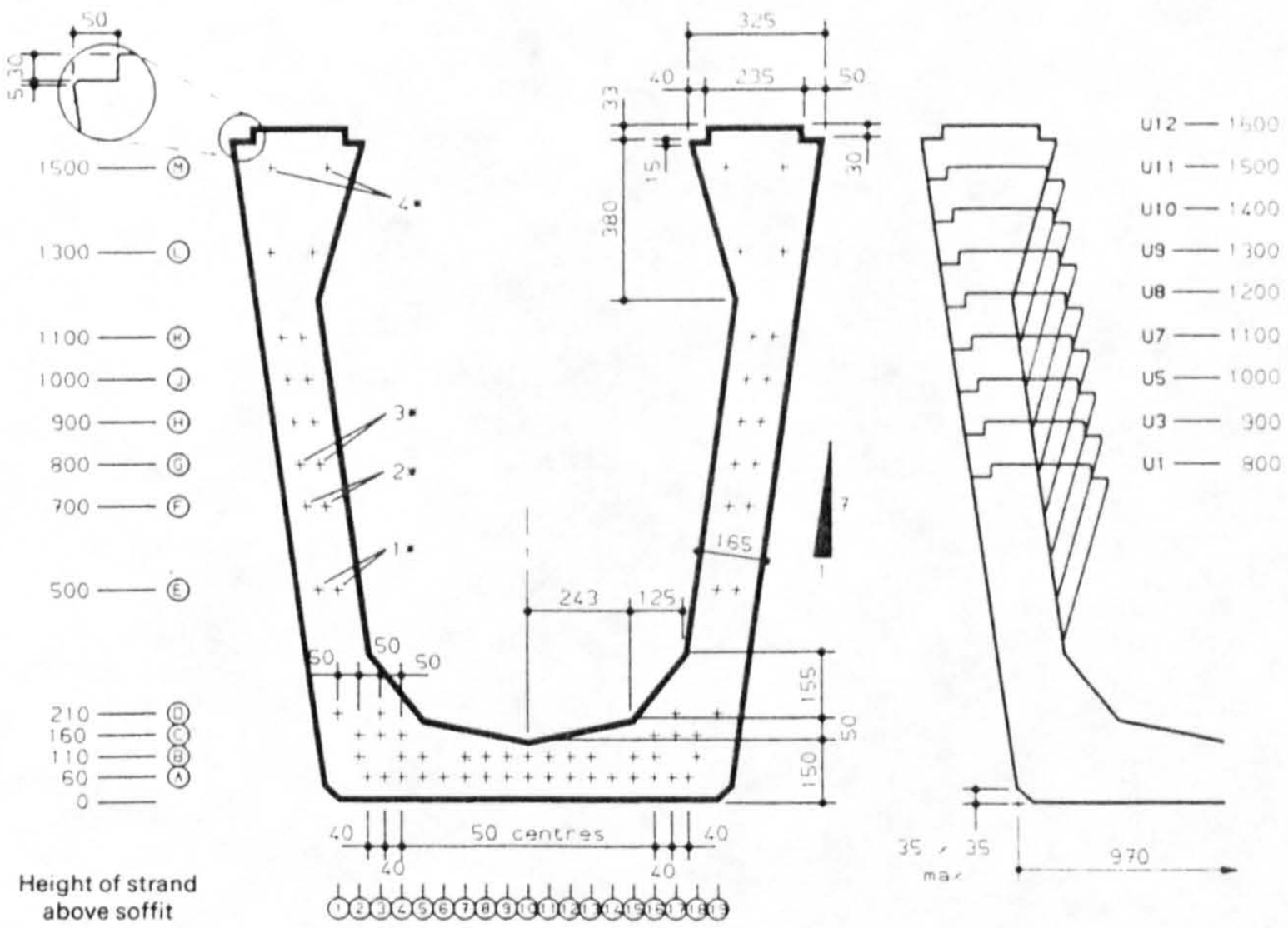

Height of strand above soffit

NOTE:
In order to ensure stability of reinforcement during concreting it is desirable to have strands in these positions as follows:

U1 to U4 1• U5 to U8 2• U9 to U12 3•
also the top two strands in all beams 4•

SECTION PROPERTIES

Section No	Depth mm	Area mm^2	Yb mm	Zt $mm^3 \times 10^6$	Zb $mm^3 \times 10^5$	App self weight KN/m
U1	800	466450	355	67.18	84.13	11.01
U3	900	499450	402	83.75	103.00	11.79
U5	1000	532450	449	101.70	124.80	12.57
U7	1100	565450	497	121.00	147.00	13.34
U8	1200	598450	544	141.50	170.50	14.12
U9	1300	631450	592	163.30	195.10	14.90
U10	1400	664450	641	186.30	220.90	15.68
U11	1500	697450	689	210.50	247.90	16.46
U12	1600	730450	737.5	235.90	275.00	17.24

Design self weight per unit volume has been taken as 23.6 kN/m^3